CHARLES PANKOW
FOUNDATION
Building Innovation through Research

Development and Splice Lengths for High-Strength Reinforcement

Volume I: General Bar Development

Purdue University

Robert J. Frosch, PhD, PE, FACI, FASCE

Eric T. Fleet

Rebecca Glucksman

Sponsored by:

The Charles Pankow Foundation

The Concrete Reinforcing Steel Institute

The American Concrete Institute Foundation

May 2020

Development and Splice Lengths for High-Strength Reinforcement

Volume I: General Bar Development

CPF Research Grant No. 02-17

by:

Eric T. Fleet

Rebecca Glucksman

Graduate Research Assistants

Robert J. Frosch, PhD, PE, FACI, FASCE

Professor of Civil Engineering

Senior Associate Dean of Engineering

Bowen Laboratory

Lyles School of Civil Engineering

Purdue University

May 2020

ACKNOWLEDGEMENTS

This investigation was conducted in the Bowen Laboratory for Large-Scale Civil Engineering Research at Purdue University and was made possible through the support of the Charles Pankow Foundation (Research Grant No. 02-17). Support provided by the ACI Foundation and the Concrete Reinforcing Steel Institute are also gratefully acknowledged. Thanks are also extended to Nucor Steel, Harris Rebar, MMFX Technologies (Commercial Metals Company), and Dayton Superior for providing the necessary reinforcing bars and beam casting components used in the experimental program. Finally, thanks are extended to Mark Perniconi who has been a champion for the development of high-strength reinforcement, Anne Ellis for taking over this championship role, and our advisory committee (Dominic Kelly, Ron Klemencic, and Jack Moehle) for their valuable advice.

TABLE OF CONTENTS

LIST OF FIGURES

LIST OF TABLES

CHAPTER 1. INTRODUCTION

1.1 History of High-Strength Reinforcement

In the past decade, high-strength reinforcement (f_y>60 ksi) has become more prevalent and widely accepted. Building codes such as ACI 318-14 (ACI Committee 318 2014) lack adequate guidance for the use of high-strength reinforcement. In 2004, ASTM A1035 was developed and addressed the use of Grade 100 bars. Grade 120 bars were added in 2007. In 2009, ASTM A615 was expanded to include provisions for Grade 80 reinforcement. Because of increasing use, in 2014, the Applied Technology Council (ATC) developed a "roadmap" for the adoption of high-strength reinforcement (ATC 115). With the expansion of these standards, high-strength reinforcement is becoming more readily available and implemented in construction. Additionally, Grade 100 reinforcing bars have been approved for use in column reinforcement by the New York City Department of Buildings (ATC 2014).

1.2 Advantages of High-Strength Reinforcement

The use of Grade 80, Grade 100, and Grade 120 reinforcement is being considered specifically for gravity, wind, and seismic loading (ATC 2014). The benefits of using high-strength reinforcement include reducing congestion within members, providing better consolidation, and speeding up construction time (ATC 2014).

Because of the cost premium associated with high-strength reinforcement, there is a need for an overall reduction in the volume of reinforcement to allow for overall project savings. As a result, cost effectiveness of high-strength reinforcement is dependent on minimum spacing, minimum reinforcement ratios, and other detailing requirements specified in ACI 318 (ATC 2014). Although longer splice lengths may be required, using less reinforcement at larger spacings means that construction and cost efficiencies are achieved through lower placement costs, less congestion, and better consolidation of the concrete during placement. According to a cost study reported in the National Institute for Standards and Technology GCR 14-917-30 (NIST 2014), it was determined that cost savings associated with the substitution of Grade 80 reinforcement for Grade 60 reinforcement was approximately 4% of the cost of the concrete structure (ATC 2014).

1.3 Bar Development

In reinforced concrete structures, bars must be properly developed to take advantage of their strengths and to avoid (brittle) bond failures. Stresses must be transferred from the steel reinforcement to the surrounding concrete to ensure a safe design. Stress is transferred between the steel bars and the surrounding concrete by three mechanisms: chemical adhesion, surface friction, and mechanical interlock (Tepfers 1973). Stresses are first transferred through the chemical adhesion that is formed during the curing process. As the bar slips, chemical adhesion is lost, and force is transferred through surface friction arising from the roughness of the concrete interface and bearing against bar deformations. After initial slip of the bar, most of the force is transferred by bearing of the reinforcement ribs against the concrete (ACI Committee 408 2003, Orangun et al. 1977). Friction also transfers force as demonstrated by the lower bond capacities of bars with no deformations and bars with epoxy coatings, which have lower coefficients of friction (ACI Committee 408 2003). These friction and bearing forces are balanced by compressive and shear stresses in the surrounding concrete (Tepfers 1973). The compressive stresses in the surrounding concrete serve to tighten the concrete around the reinforcing bar, thus increasing frictional resistance. Tensile forces are also caused by the inclined force exerted by the bar deformation on the concrete. The radial component of the tensile force causes splitting of the surrounding concrete at failure (Tepfers 1973). The forces acting on the reinforcing bar and concrete are shown in Figure 2.1.

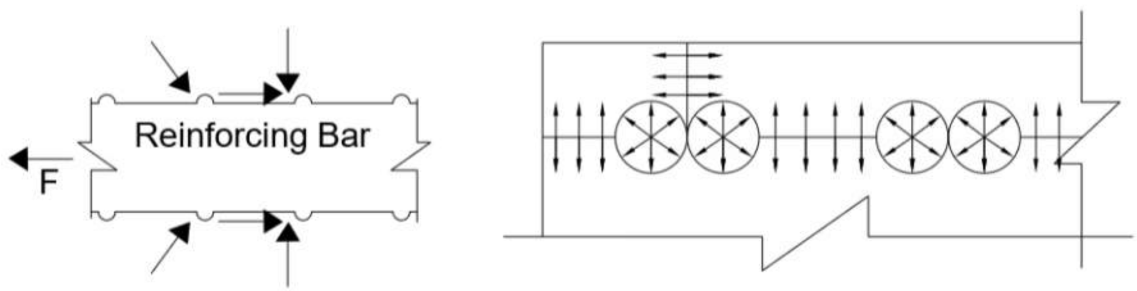

a) Compressive Forces on Longitudinal Bar **b) Tensile Forces on Concrete**

Figure 2.1: Forces Acting on Reinforcement and Concrete

The capacity of the concrete to resist splitting is dependent on the tensile strength of the concrete (Orangun et al. 1977). If concrete cover and spacing between bars is small, splitting cracks can eventually cause a splitting failure (Tepfers 1973).

1.4 <u>Nonuniform Bond Stress</u>

Although it is more convenient to treat bond stress as if it were uniform over the splice length (ACI Committee 408 2003), bond stresses over the development length are not uniform (Kluge and Tuma 1945). Axial tensile stress in the reinforcement varies from high values at cracks to lower values between cracks where the concrete shares the tensile resistance with the reinforcing steel. While assuming a linear relationship of bar force development is conservative for shorter splice lengths, the assumption becomes unconservative with increasing splice length (ACI Committee 408 2003).

Failures start at the end of the splice where there is the highest bond force per unit length (ACI Committee 408 2003) and the strain is the largest. As the relative deformation capacity between the reinforcing bar and concrete exceeds the deformation corresponding to the peak bond strength, local bond damage occurs, which causes the bond stress to decrease (Hwang and Yi 2017). The use of transverse reinforcement has been shown to reduce the variation of stress along splices (Ferguson and Krishnaswamy 1971).

1.5 Factors Influencing Bond Behavior

The different variables that impact bond behavior are described in the following sections.

1.5.1 Casting Position

Top casting, defined in ACI 318-14 as placing more than 12 in. of fresh concrete below the bars, has been shown to reduce bond strength by 3 – 8% (Chinn, Ferguson, and Thompson 1955). This phenomenon is likely because of bleeding and settlement of the concrete below the bars (Zuo and Darwin 1998). The larger the depth of concrete below the bar, the larger the settlement and accumulation of bleed water. As the concrete settles, it leaves a void beneath the rigid reinforcing bars. The effects of settlement and bleeding on bond strength are magnified by a higher concrete slump and decreased top cover. Thorough vibration of the concrete helps to combat the effects of settlement and bleeding by restoring uniformity within the concrete and removing trapped air (ACI Committee 408 2003).

1.5.2 Bar Size

According to Mathey and Watstein (1961), bond strength has been shown to decrease with an increase in bar diameter for a consistent splice length to bar diameter ratio (l_s/d_b). For specimens with comparable l_s/d_b and cover in terms of bar diameter, No. 3 bars showed a 19% increase in bond strength compared to No. 6 bars, while the No. 11 bars showed a 16% decrease in bond strength (Chinn et al. 1955).

1.5.3 Splice Length

Although splice strength increases with increasing splice length, the effectiveness of increasing the splice length decreases as the length increases. Mathey and Watstein (1961) have shown that the unit bond strength decreases with increasing splice length for a given bar size. This finding was based on experimental testing with relatively short splice lengths up to $40d_b$. Therefore, doubling the splice length from 18 in. to 36 in. results in a 41% increase in bar stress. Studies conducted by Chinn et al. (1955) show that compared with an 11-in. splice length of No. 6 bars, a 16-in. splice length (45% increase) was 19-28% stronger, while a 24-in. splice length (118% increase) was 60-80% stronger.

Canbay and Frosch (2005) found the influence of splice length on bond strength to be proportional to the square root. Findings from Seliem et al. (2009) support the notion that bond strength is proportional to the square root of l_s/d_b. Additionally, tests conducted by Richter (2012) support that achieving a higher bond strength by increasing splice length is inefficient because bond stress distribution across long splice regions causes the additional contribution from larger embedment to be less effective in increasing bond strength. Azizinamini et al. (1993) found that the nonlinear relationship between splice length and bond strength also holds true regardless of concrete strength. Nonlinearity in splice length and bond strength was observed when using fiber reinforced polymer (FRP) reinforcing bars (Pay 2005).

1.5.4 Concrete Strength

The tensile and bearing strength of the concrete impacts the bond strength (ACI Committee 408 2003). The traditionally accepted relationship between concrete and bond strength is represented by the square root of the concrete compressive strength (Ferguson and Thompson 1962, Tepfers 1973, Orangun et al. 1977, Darwin et al. 1992). Esfahani and Rangan (1998) observed that the extent of crushing in front of the ribs, and thus the bond strength, was dependent on the concrete strength. In specimens with normal-strength concrete, crushing of the concrete occurred regardless of the size of the concrete cover. For 7250-psi concrete, crushing only occurred for large covers, and for 10,880-psi concrete, no crushing occurred (Azizinamini et al. 1993). Because of the reduced crushing in high-strength concrete, local slip was reduced (Zuo and Darwin 1998). When crushing occurred in front of the ribs, fewer ribs participated in resisting the applied forces in the bars. When crushing around the bar deformations was coupled with a smaller concrete cover, the result was a splitting failure in concrete prior to achieving a uniform bond stress distribution (Zuo and Darwin 1998).

Additionally, increasing the coarse aggregate content increased the splice strength. For specimens without transverse reinforcement within the splice length, increasing the coarse aggregate content produced a higher splice strength characterized by ${f_c'}^{0.25}$. Likewise, for specimens with transverse reinforcement within the splice length, increasing the coarse aggregate content produced a higher splice strength characterized by ${f_c'}^{0.75}$ (Zuo and Darwin 1998).

The quarter root, $\sqrt[4]{f_c'}$, has been shown to provide a more accurate representation of the relationship between concrete strength and developed reinforcement strength (Darwin et al. 1996, Zuo and Darwin 2000). Canbay and Frosch (2005) analyzed a total of 203 unconfined beams with f_c' ranging from 2600 psi to 15,600 psi and concluded that the use of the quarter root provided a better representation of spliced bar strength as compared to the use of the square root.

1.5.5 Concrete Cover and Bar Spacing

Concrete cover and bar spacing determine the type of bond failure and influence bond behavior of the specimen. Chamberlin (1956) and Orangun et al. (1977) found that increasing the side cover (c_{so}) or clear spacing ($2c_{si}$) also increased splice strength. Thompson et al. (1975) found that increasing the ratio of clear cover to clear spacing ($c_{so}/2c_{si}$) could provide a 10% increase in splice strength.

In experiments conducted by Chinn et al. (1955), doubling the cover from 0.75 in. to 1.50 in. increased the strength of shorter splices by 7 – 15%. Chinn et al. (1955) found that increasing the concrete cover increased the splice strength, but only for shorter splices. The same trend between concrete cover and splice strength was also observed for both uncoated black bars and epoxy-coated bars (Hadje-Ghaffari et al. 1994).

Orangun, Jirsa, and Breen (1977) initially found that although the minimum of bottom cover, side cover, and bar spacing is important in determining the type of failure mode, the value of c_{so}/d_b or c_{si}/d_b has a stronger correlation to the stress achieved in the longitudinal reinforcement, as long as this ratio is less than three or four. Orangun et al. (1977) also observed that as side cover or inner bar spacing increased, bond capacity increased. Thompson et al. (1975) found that bond strength can be improved by increasing the ratio of side cover to bar spacing. Tests showed that a 10% increase in bond strength could be achieved by increasing the ratio of side cover to bar spacing.

1.5.6 Transverse Reinforcement (Confinement)

The use of transverse reinforcement has been shown to increase splice strength. Chinn, Ferguson, and Thompson (1955) observed that the use of ties around the splice region increased bond strength by almost 50%. Ferguson and Breen (1965) observed a similar outcome when conducting tests with varying amounts of confinement steel within the splice region. Bond capacities were increased by 20% when the minimum number of stirrups was present ($\rho_t = 0.15\%$) and up to 50% when ρ_t was increased to 1.23%. Transverse reinforcement has also been found to cause a more ductile failure than comparable unconfined specimens (Ferguson and Krishnaswamy 1971, Morita and Fujii 1982). The use of transverse reinforcement allows larger deformations of the longitudinal reinforcement prior to failure by minimizing the distress caused by concrete splitting (Zekany, Neumann, Jirsa, and Breen 1981). Transverse reinforcement adds to bond strength by resisting tension where the concrete has split (Ferguson and Krishnaswamy 1971, Orangun, Jirsa, and Breen 1977, Seliem et al. 2009) and decreasing the effective crack length between bars (ACI Committee 408 2003). In this way, the transverse reinforcement helps to slow the spread of splitting (Ferguson and Krishnaswamy 1971). Rezansoff, Konkankar, and Fu (1992) showed that the contribution to bond strength provided by confining stirrups is greater than the contribution of increasing concrete cover on an unconfined section. Transverse reinforcement has been shown to be more effective for larger bars as larger bars induce higher strains and stresses when they slip (ACI Committee 408 2003). The use of transverse reinforcement in MMFX specimens (ASTM A1035) allowed the failure stresses in No. 8 and No. 11 bars to reach 150 ksi, enabling the full capability of the high-strength reinforcement to be utilized (Seliem et al. 2009).

Thompson et al. (1975) found that transverse reinforcement resists tension by noticing an increase in strain in the transverse reinforcement after cracking of concrete in the plane of the splice. It was also observed that strain in the transverse reinforcement increased before failure of the specimen. Additionally, the stirrups located closest to the ends of the splice were observed to have the highest strains (Thompson et al. 1975). This observation supports the finding that bond stress is nonlinear across the embedded length and reaches a maximum at the ends (Canbay and Frosch 2005). In fact, tests conducted by Azizinamini et al. (1999) showed that the strain in stirrups located at the ends of splices can reach their yield strength. Sim (2014) found that stirrups placed in the middle of the splice region resulted in essentially no increase in bond strength; however, when stirrups were placed at the ends of the splice, bond strength was increased by either 20% or 30%, depending on splice length.

1.5.7 Relative Rib Area

The relative rib area, R_r, for ribbed steel reinforcing bars is calculated using the expression specified in ACI 408R-03 Section 6.6 (Equation 1-1). Figure 2.2 shows the variables used to calculate R_r.

$$R_r = \left(\frac{h_r}{s_r}\right)\left(1 - \frac{\sum gaps}{p}\right) \tag{1-1}$$

where:

$\sum gaps$ = *a sum of gaps between ends of transverse deformations, plus the width of any continuous longitudinal lines used to represent the grade of the bar multiplied by the ratio of the height of the line, h_r (in.)*

h_r = *average height of deformations (ACI 408R-03 Section 6.6.1) (in.)*

$$= \frac{\frac{a_1 + a_5}{2} + a_2 + a_3 + a_4}{4}$$

p = *nominal perimeter of bar (in.)*

s_r = *average spacing of deformations (in.)*

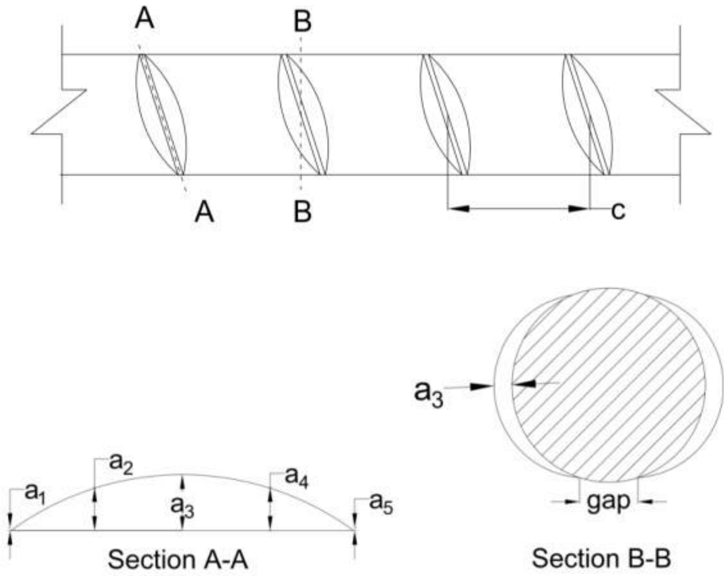

Figure 2.2: Relative Rib Area Calculation

Zuo and Darwin (1998) found that splice strength is not affected by the relative rib area, R_r, for bars not confined by transverse reinforcement. For splices confined by transverse reinforcement, results show an increase in splice strength with an increase in bar size and R_r (Zuo and Darwin 1998).

1.6 Failure Modes

Bond failures can occur in two ways: bar pullout or concrete splitting. A splitting failure occurs if the concrete cover and/or spacing of the bars are small enough for a splitting plane to develop (Tepfers 1993). If the concrete cover, bar spacing, and transverse reinforcement are sufficient, but the development length is not, the specimen will fail in a pullout mode. A pullout failure occurs when concrete splitting is prevented, but the splice length is inadequate to develop the forces.

Splitting failures occur in two ways: side-splitting and face-splitting. A third face-and-side-splitting mode can also occur. According to Tepfers (1973), splitting failures depend on whether the bottom clear cover, c_b, is smaller than either the concrete side cover, c_{so}, or half of the bar clear spacing, c_{si} (Figure 2.3). If c_{so} or c_{si} is smaller than c_b, the splitting crack forms through the side cover or between the reinforcing bars (side-splitting, as shown in Figure 2.3(a)). If c_b is smaller than c_{so} and c_{si}, the splitting crack occurs through the cover to the tension face (face splitting, as shown in Figure 2.3(b)). Cracks initiate at the end of the splice where the bond stress is the highest and propagate toward the center.

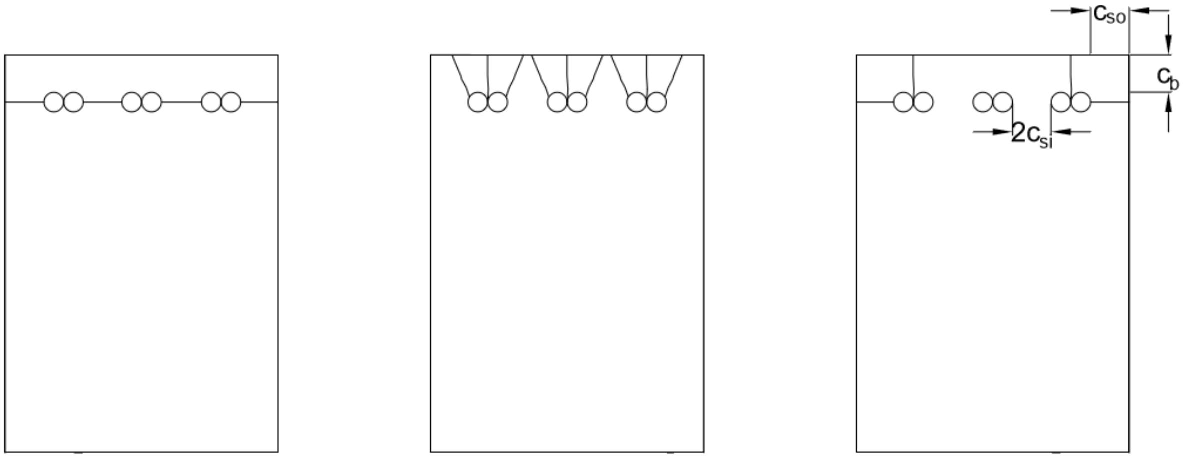

a) Side-Splitting **b) Face-Splitting** **c) Face-and-Side-Splitting**

Figure 2.3: Splitting Failure Modes

For face-and-side-splitting (Figure 2.3(c)), initial splitting occurs in the clear cover over the splices on the sides. If the distances between the reinforcing bars are large and the concrete side cover is smaller than the bottom cover, the side cover will longitudinally crack. When the ultimate tensile stress of the concrete is reached, a block of concrete bordering the edge lap splices will spall off due to the failure of the bottom cover (Tepfers 1973).

1.7 Past High-Strength Reinforcement Research

Limited splice tests have been conducted using high-strength reinforcement, and these tests were conducted with ASTM A1035 (MMFX) bars rather than ASTM A615 bars. The two materials have similar stress-strain curves, but the shape of the post-yield response is different. Past research has been conducted comparing the splice strength of MMFX bars to conventional Grade 60 bars and determining the reliability of the current code equations. Ansley (2002) first evaluated this reinforcement and tested four pairs of splice-beam specimens to compare the impact of replacing Grade 60 reinforcement with MMFX. He warned of "blind substitution" of MMFX for Grade 60 because although the strength of the beam was increased, the ductility of the beam was inadequate. Ansley also concluded that the use of reinforcing bars without a well-defined yield point, like MMFX, needs to be addressed before adoption. In 2006, El-Hacha et al. (2006) tested eight splice-beam specimens reinforced with MMFX. He found that the bond behavior of Grade 60 specimens and MMFX specimens was similar up to the proportional limit of 80 ksi; however, at higher stress levels, the bond strength of MMFX changes. El-Hacha et al. (2006) also concluded that the ACI 318-02 equation was unconservative for use with MMFX. Extensive research was conducted at the University of Kansas, North Carolina State University, and the University of Texas at Austin. Sixty-nine (69) splice-beam specimens were tested, of which 64 specimens failed in bond (Briggs 2008). Based on these tests, they also concluded that ACI 318-05 is unconservative and recommended that a high-strength reinforcement factor of 1.48 be included when bar stresses exceed 80 ksi; however, they concluded that ACI 408R-03, with $\varphi = 0.82$, is safe for use with high-strength reinforcement. They also recommended the use of confining transverse reinforcement as it increased the splice strength and beam deformation capacity. Currently, high-strength reinforcement splice tests have been conducted using specimens with splice lengths ranging from 10 in. to 91 in. Of the tests, only confined specimens failed in flexure. Additionally, all the unconfined specimens failed in bond before yield, except one of El-Hacha's specimens which failed at the yield stress calculated from the 0.2% offset method. Although limited research has been conducted on the splice strength of high-strength reinforcement, no known splice research has been conducted using ASTM A615 Grade 100 bars.

1.8 Objective and Scope

The objective of this research program is to evaluate the development of high-strength reinforcing steel and establish a design expression for the development and splicing of this steel. Research was conducted in two parts by Glucksman (2018) and Fleet (2019) and focused on the following:

1. Influence of splice length on bond strength

2. Influence of transverse reinforcement on bond strength

3. Effectiveness of high-strength (100 ksi) transverse reinforcement on bond strength

4. Bar development in slabs. Slabs are of specific concern as they are unconfined and are constructed with small covers (0.75 in.)

5. Influence of high-strength concrete (10,000 psi) on bond strength

6. Effect of different stress-strain relationships of the high-strength steel (ASTM A615 vs. ASTM A1035) on bond strength

7. Influence of transverse reinforcement location on bond strength

CHAPTER 2. SERIES I – IV: BEAM TESTS

2.1 Introduction

Twenty-two (22) beams with tension lap splices were tested to evaluate the effect of splice length, transverse reinforcement, and bar spacing on bond strength. The beams were constructed in four series.

2.2 Specimen Design

The specimens were designed to investigate the bond behavior of high-strength steel reinforced concrete beams. Grade 100 longitudinal bars were used for all specimens. Each of the specimens was designed to fail in bond when tested in four-point bending. The concrete strength targeted for these specimens was 5000 psi.

All specimens were rectangular in cross section with a height of 20 in. Three No. 8 Grade 100 longitudinal bars were spliced at midspan, in a region of constant moment. Cross sectional details for both unconfined and confined specimens are shown in Figure 2.1. Unconfined specimens are defined as having no transverse reinforcement in the splice region, while confined specimens are defined as having transverse reinforcement in the splice region. Confinement configurations and splice lengths were varied to determine the effect of these variables on the capacity of the splice.

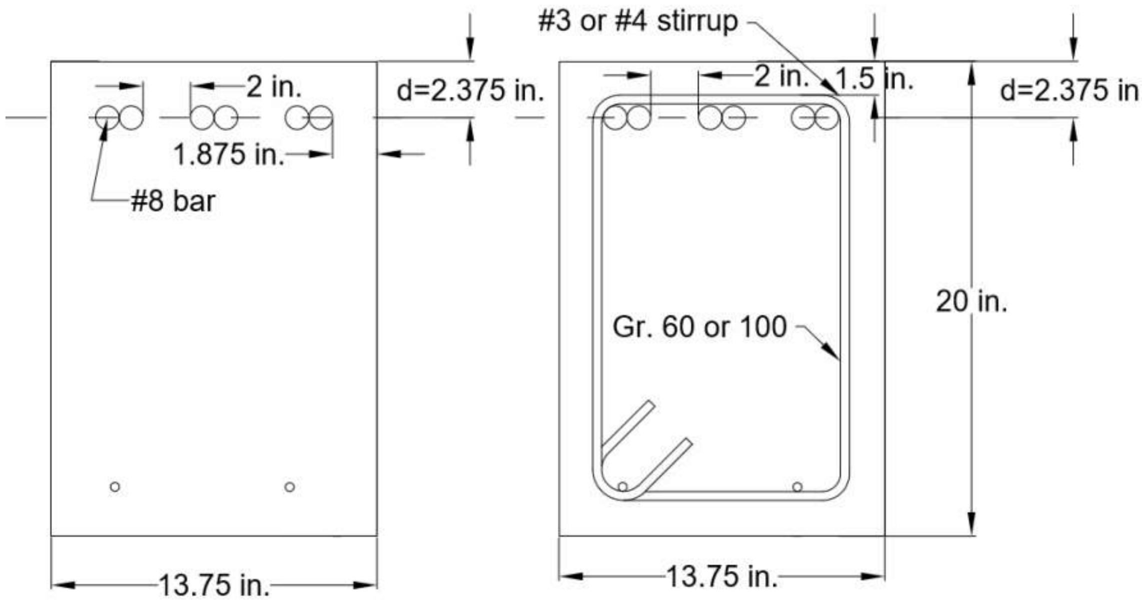

Figure 2.1: Typical Cross Section

The specimens with transverse reinforcement had a cover of 1-1/2 in. (the minimum cover specified by ACI 318-14 for beams). To keep the effective depth the same for all specimens, the cover for specimens without transverse reinforcement was designed to be 1-7/8 in. It is important to keep the effective depth constant to eliminate its effect in the study.

Nineteen (19) out of 22 specimens had a 2-in. clear spacing between longitudinal bars. This resulted in the confined specimens, with a minimum clear side cover of 1-1/2 in., having an overall beam width of 13-3/4 in. The confined and unconfined specimens were designed to have the same width. The 2-in. clear spacing between longitudinal bars was selected as it represented a lower bound dimension for a typical beam design. Three (3) specimens had 1-in. clear spacing between longitudinal bars. The 1-in. clear spacing is the minimum clear spacing specified in ACI 318-14 Section 25.2. The specimens with a 1-in. spacing represent the worst-case scenario for bar spacing. As-built dimensions for Series I through IV are provided in Appendix A.

Confined specimens were designed with varied spacings, grades, and sizes of transverse reinforcement in the splice region. Both No. 3 and No. 4 stirrups were used; however, the width of the specimen and effective depth remained the same. Additionally, both Grade 60 and Grade 100 stirrups were selected to understand the influence of transverse reinforcement yield strength.

The length of the beam was controlled by two factors: the longest splice length to be tested and the spacing of tie-down holes in the Bowen Laboratory strong floor. The longest splice length was selected as 120 in. According to St. Venant's principle, stresses due to bending approach a linear distribution at a distance equal to the overall height of the specimen. To be conservative, the supports were placed at least 1.5 times the overall height of the specimen away from the end of the 120-in. splice. This distance was rounded to 36 in. so that the loading points would line up with the holes in the strong floor. Although the length of the splice varied from specimen to specimen, the length of the beam was maintained constant for all specimens in Series I through IV so that the same test setup could be utilized, as well as to allow for a direct comparison between results.

The specimens were tested in four-point bending to produce a realistic stress-state in the region of the bars. Additionally, the majority of data used to establish current design provisions for development and lap splice lengths were tested in four-point bending (ACI Committee 408 2003). A constant shear region of 4 ft was selected, and the load was placed 1 ft from the end of the beam. The shear regions of the beam were reinforced with No. 4 Grade 60 stirrups at 4-1/4 in. center-to-center. These stirrups were included to prevent failure outside the constant moment region. The specimens were designed for the load to be applied downward to each end of the beam so that the top of the specimen was in tension, allowing for easier crack mapping and measuring of crack widths. Although the specimens were tested with the reinforcement near the top face, all specimens were cast with reinforcement near the bottom face. Therefore, the beams were flipped prior to testing because casting position has been shown to influence the bond strength of the specimen, and elimination of this factor was desired. Figure 2.2 shows the test setup used for the testing of all the beams in Series I through IV. Two (2) No. 3 longitudinal bars were included in the compression zone of the specimen to assist with fabrication and to prevent the specimen from falling in the case of a brittle failure.

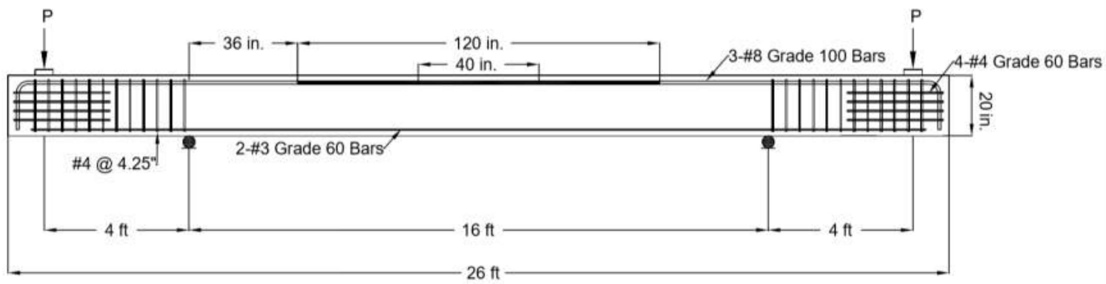

a) Unconfined

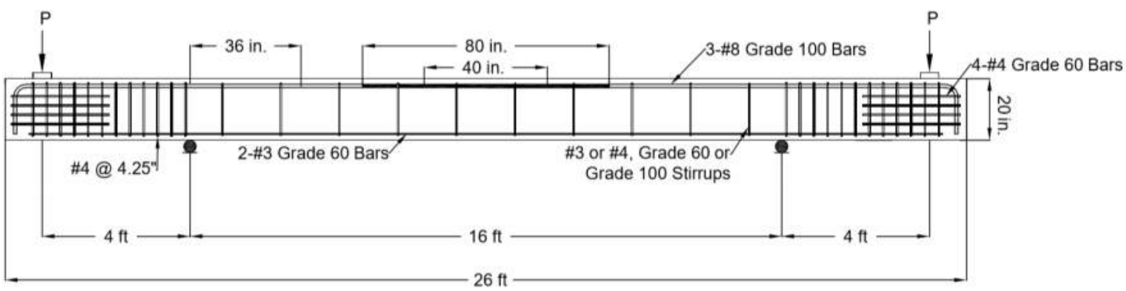

b) Confined

Figure 2.2: Typical Specimen Configuration

2.3 Test Variables

Investigated variables include splice length, spacing of bars, grade of transverse reinforcement, and transverse reinforcement spacing. Each of the experimental variables is described in detail in Table 2.1.

The selected concrete mix was maintained constant throughout all specimens. Additionally, the bar cover and bar spacing were also constant in the majority of specimens. All specimens had No. 8 Grade 100 longitudinal bars from the same heat and had an effective depth, *d*, of 17-5/8 in.

Unconfined specimens are labeled using the notation in Figure 2.3 while confined specimens are labeled using the notation in Figure 2.4. Note that for two specimens in Series IV, the letter "*a*" following the target compressive strength term indicates a duplicate specimen from Series I.

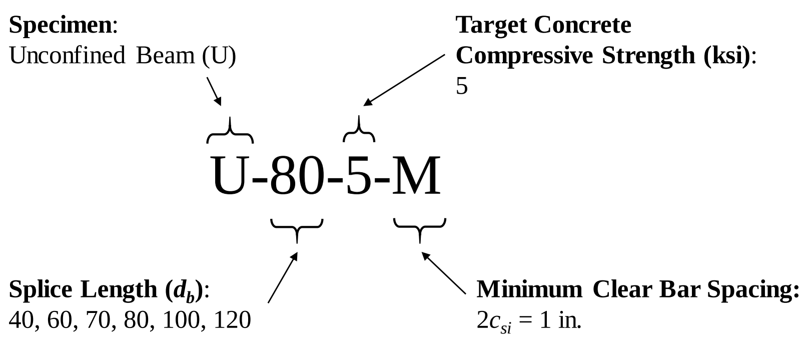

Figure 2.3: Unconfined Specimen Identification Label

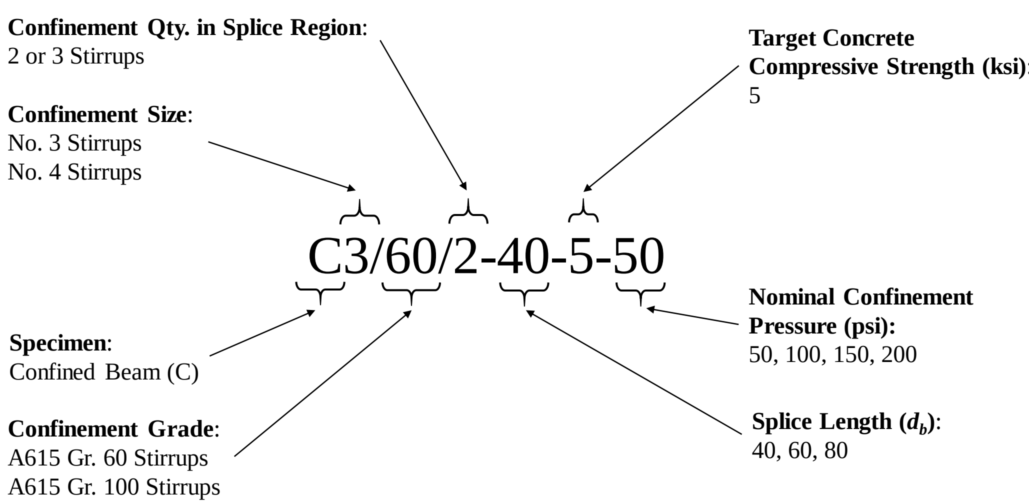

Figure 2.4: Confined Specimen Identification Label

Table 2.1: Specimen Variables

Series	Specimen Name	Splice Length (d_b)	Target Concrete Strength (ksi)	Bar Spacing (d_b)	Trans. Reinf. Bar Size (No.)	Trans. Reinf. Gr. (ksi)	Spacing of Trans. Reinf. (in.)
I	U-40-5	40	5	2	-	-	-
	U-60-5	60	5	2	-	-	-
	U-80-5	80	5	2	-	-	-
	U-100-5	100	5	2	-	-	-
	U-120-5	120	5	2	-	-	-
	U-80-5-M	80	5	1	-	-	-
	U-100-5-M	100	5	1	-	-	-
	U-120-5-M	120	5	1	-	-	-
II	C3/60-60-5-50	60	5	2	3	60	19
	C3/60-60-5-100	60	5	2	3	60	9.5
	C3/60-60-5-150	60	5	2	3	60	6.375
	C3/60-60-5-200	60	5	2	3	60	4.75
	C4/60-60-5-100	60	5	2	4	60	9.5
	C3/100-60-5-100	60	5	2	3	100	9.5
	C4/60-60-5-150	60	5	2	4	60	6.375
	C3/100-60-5-150	60	5	2	3	100	6.375
III	C3/60-80-5-50	80	5	2	3	60	19
	C3/60-80-5-100	80	5	2	3	60	9.5
	C3/60-80-5-150	80	5	2	3	60	6.375
	C3/60-80-5-200	80	5	2	3	60	4.75
	C4/60-80-5-100	80	5	2	4	60	9.5
	C3/100-80-5-100	80	5	2	3	100	9.5
	C4/60-80-5-150	80	5	2	4	60	6.375
	C3/100-80-5-150	80	5	2	3	100	6.375
IV	U-40-5a	40	5	2	3	-	-
	U-60-5a	60	5	2	3	-	-
	U-70-5	70	5	2	3	-	-
	C3/60/2-40-5-50	40	5	2	3	60	19
	C3/60/3-40-5-50	40	5	2	3	60	19
	C3/100/3-40-5-50	40	5	2	3	100	19
	C3/60-40-5-100	40	5	2	3	60	9.5
	C3/100-40-5-100	40	5	2	3	100	9.5

2.3.1 Splice Length

Mathey and Watstein (1961) have shown that the relationship between splice length and bar stress is not linear. Because of the lack of data for longer splice lengths (greater than $40d_b$), longer splice lengths that would be required for high-strength reinforcement were of primary interest in Series I through IV.

Splice lengths were varied as follows:

Unconfined Specimens: $40d_b$ to $120d_b$

Confined Specimens: $40d_b$ to $80d_b$

2.3.2 Spacing of Bars

Increasing the clear spacing between bars and the concrete clear cover have both been shown to increase the splice strength. Additionally, concrete clear cover and clear spacing dimensions are important in determining the mode of failure. The clear spacing between spliced bars, based on a typical beam design, was selected as 2 in. for 19 of 22 specimens. To evaluate the lower limit allowed by the code, three specimens (designated by the letter "*M*") included a clear spacing of 1 in. between bars. For these specimens, the specimen width was correspondingly reduced (Figure 2.5(a)), while the side cover remained constant.

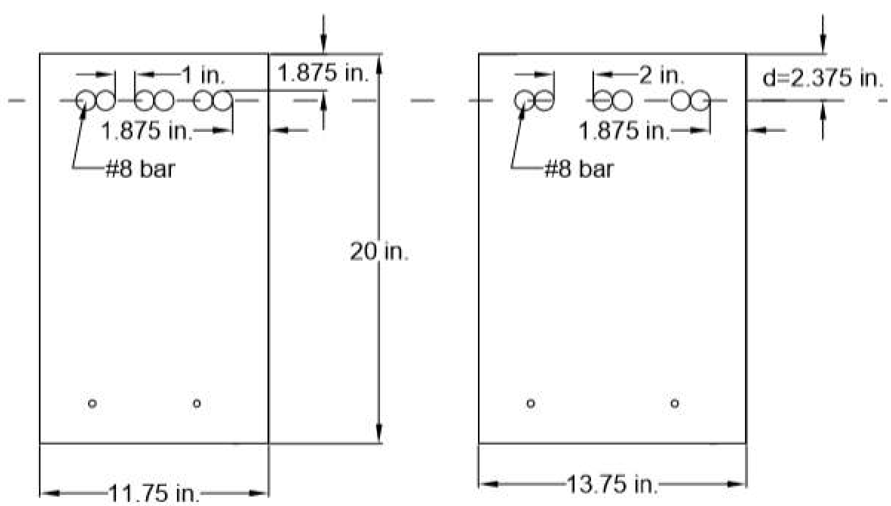

a) 1-in. Clear Spacing **b) 2-in. Clear Spacing**

Figure 2.5: Minimum Cover Cross Section

2.3.3 Transverse Reinforcement Grade

There has been debate whether it is beneficial to use high-strength transverse reinforcement to increase splice strength. It has been reported (ACI 318-14 Section R25.4.2.3, Azizinamini et al.

1995) that transverse reinforcement rarely reaches yield prior to a brittle failure, even for Grade 60 reinforcement. To investigate the effectiveness of high-strength transverse reinforcement, comparable specimens were built with either Grade 60 or Grade 100 transverse reinforcement in the splice region. The same size stirrups and spacings were used so that the effect of the grade of transverse reinforcement could be directly compared.

2.3.4 Transverse Reinforcement Spacing

Transverse reinforcement has been shown to improve the ductility and strength of splices. This study attempts to quantify the increase in splice strength with a given area of transverse reinforcement. Series II through IV varied the spacing of the transverse reinforcement from 4-3/4 in. to 19 in. In addition to evaluating spacings, two specimens were designed with the same stirrup spacing, but a different number of stirrups within the splice region. Specimen C3/60/3-40-5-50 contained three stirrups in the splice region, whereas Specimen C3/60/2-40-5-50 contained only two stirrups. The purpose of these specimens was to investigate if the location of the stirrups within the splice region affected the bond strength of the specimen.

A minimum amount of shear reinforcement is required by the building code (ACI 318-14). Both a minimum spacing ($d/2$, ACI 318-14 Table 10.7.6.5.2) and a minimum area (ACI 318-14 Equation 10.6.2.2) are specified.

The spacing of transverse reinforcement in this study was selected based on the minimum area requirements, which typically produce the largest spacing. Based on Equation 10.6.2.2.b in ACI 318-14, which provides for a minimum nominal stress of 50 psi, the nominal stress that the transverse reinforcement provides was calculated to determine the various spacings of the stirrups within the splice region. The nominal stresses selected were 50, 100, 150, and 200 psi.

$$50\frac{b_w s}{f_{yt}} = A_{v,min} \qquad \text{(ACI 318-14 Equation 10.6.2.2.b)}$$

The spacings calculated for these nominal pressures are based on a beam width (b_w) of 13-3/4 in., a transverse reinforcement area ($A_{v,min}$) of 0.22 in^2 (No. 3 stirrup with 2 legs), and transverse reinforcement yield strength (f_{yt}) of 60 ksi. The "pressure" coefficient in ACI 318-14 Equation 10.5.2.2.b was varied in 50-psi increments to calculate spacings at consistent intervals. The calculated spacings for each of the four confinement cases are shown below.

$A_{v,min} = 0.11\ in.^2 * 2 = 0.22\ in.^2$ (two stirrup legs)

50 psi: $$s = \frac{A_{v,min} f_{yt}}{50 b_w} = \frac{(0.22\ in.^2)(60\ ksi)}{(50\ psi)(13.75\ in.)} = 19.2\ in. \rightarrow 19\ in.$$

100 psi: $$s = \frac{(0.22\ in.^2)(60\ ksi)}{(100\ psi)(13.75\ in.)} = 9.6\ in. \rightarrow 9.5\ in.$$

150 psi: $s = \frac{(0.22\ in.^2)(60\ ksi)}{(150\ psi)(13.75\ in.)} = 6.4\ in. \rightarrow 6.375\ in.$

200 psi: $s = \frac{(0.22\ in.^2)(60\ ksi)}{(200\ psi)(13.75\ in.)} = 4.8\ in. \rightarrow 4.75\ in.$

The spacings were maintained for No. 4 stirrups and Grade 100 stirrups, regardless of the actual nominal pressure that would be calculated. The spacings were maintained to directly compare results.

2.4 <u>Materials</u>

2.4.1 Steel Reinforcement

ASTM A615 deformed steel bars were exclusively used in Series I through IV. All reinforcing bars were manufactured and fabricated at Nucor Kankakee. Bars of each size were obtained from the same heat to ensure consistent material properties. A minimum of three bar coupons were tested for each bar type and size.

2.4.1.1 Longitudinal Bars

Figure 2.6 shows the bar mark for the longitudinal bars in this study. Testing was conducted using a 220-kip MTS universal testing machine according to ASTM E8 (Figure 2.7).

Figure 2.6: Bar Mark for Longitudinal Bars

Figure 2.7: Testing of No. 8 Bars

To determine the stress-strain response, the test machine measured the load applied while an Epsilon 2-in. extensometer measured strain during testing. Stress was calculated by dividing the measured load by the nominal bar area. A representative stress-strain curve is shown in Figure 2.8 and Figure 2.9. The elastic limit of the No. 8 bars was measured as 87 ksi (Figure 2.9). In addition, the yield strength of the No. 8 bars using the 0.2% offset method was determined to be 108 ksi (Figure 2.9). The strength of the No. 8 Grade 100 bars was measured as 140 ksi, and the elongation at failure, 11% (Figure 2.8). The material properties of the Grade 100 No. 8 longitudinal bars are summarized in Table 2.2. The stress-strain curves for the longitudinal bars tested are provided in Appendix B .

Table 2.2: Material Properties of Longitudinal Reinforcement

Bar Size (No.)	Grade (ksi)	Elastic Limit Stress (ksi)	Yield Stress 0.2% Offset (ksi)	Ultimate Strength (ksi)	Elongation at Failure
8	100	87	108	140	11%

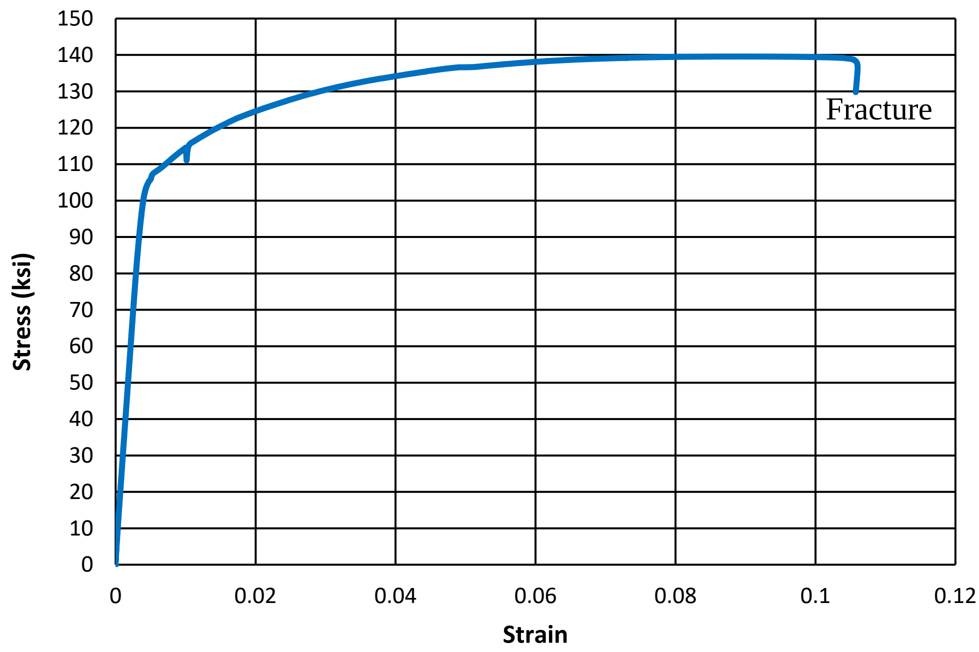

Figure 2.8: Stress-Strain Curve of Representative No. 8 Grade 100 Bar

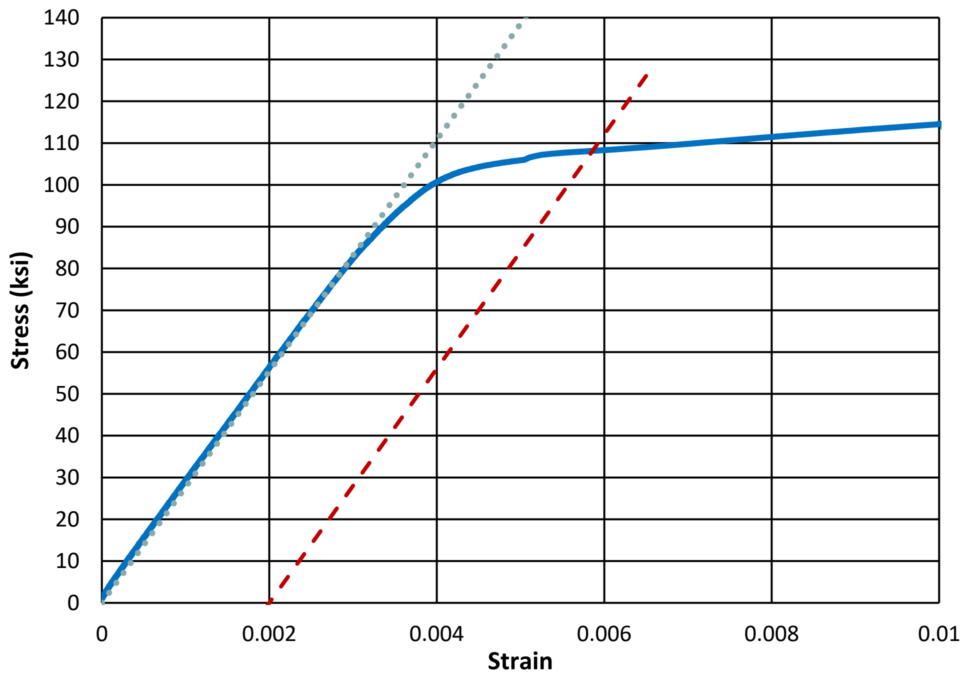

Figure 2.9: Linear Limit and Yield Strength, No. 8 Grade 100 Bar

To measure the elongation at failure, the bars were marked with a punch before testing at approximately 4-in. increments. The spacing of the punches was measured using a micrometer before and after testing to determine the failure strain. No failures occurred at the location of a punch. Additionally, the use of a breakaway extensometer allowed the strain at failure to be captured. The relative rib area for the longitudinal bars is 0.098, calculated according to Equation 1-1.

2.4.1.2 Transverse Reinforcement

Both Grade 60 and Grade 100 ASTM A615 steel were used as transverse reinforcement. In addition to varying the grade of steel, both No. 3 and No. 4 stirrups were selected. All stirrups were fabricated from straight bars rather than coils to minimize residual stresses caused from bending and unbending the coil. A minimum of three samples for each bar size and grade were tested in a 120-kip Baldwin universal testing machine in accordance with ASTM E8. The testing machine measured the stress, while an Epsilon 2-in. extensometer measured the strain during testing.

To determine the elongation at failure, the bars were marked with a punch and measured before and after testing. None of the specimens had the location of rupture coincide with one of the punches. Additionally, the use of a breakaway extensometer allowed the strain at failure to be captured. Representative stress-strain curves for each type of transverse reinforcement used in Series I through IV are shown in Figure 2.10, Figure 2.11, and Figure 2.12. The mean yield and elongation properties at failure are summarized in Table 2.3. The stress-strain curves for the transverse reinforcement tested in Series I through IV are provided in Appendix B.

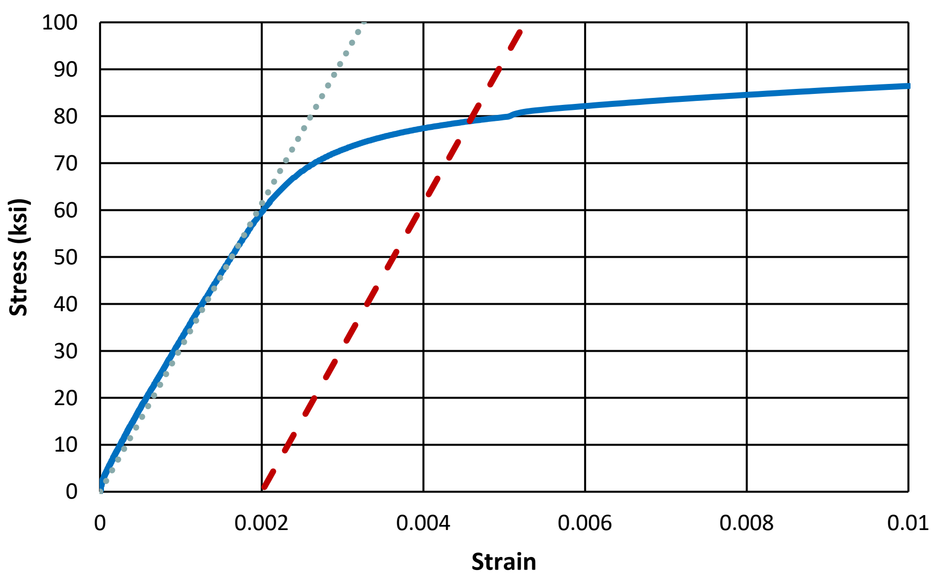

Figure 2.10: Linear Limit and Yield Strength, No. 3 Grade 60 Bar

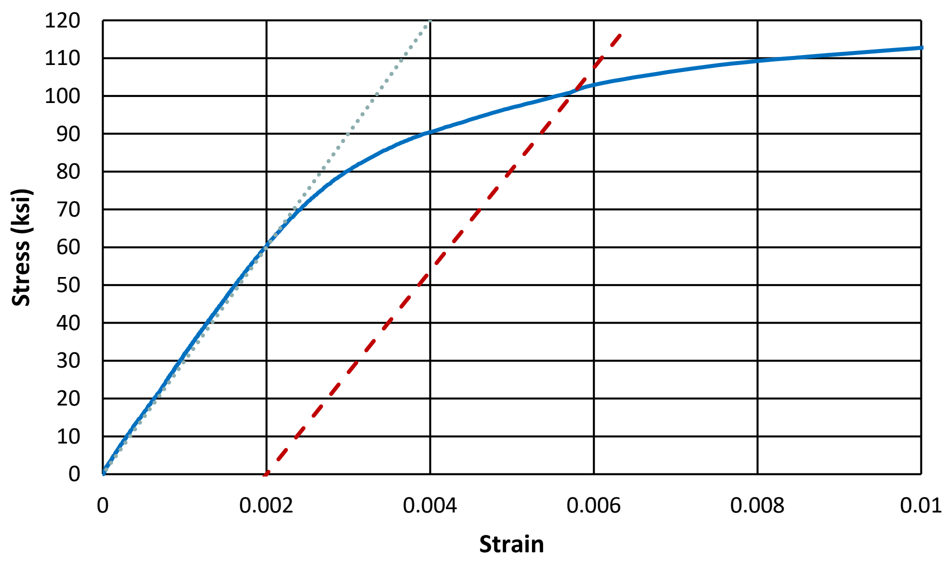

Figure 2.11: Linear Limit and Yield Strength, No. 3 Grade 100 Bar

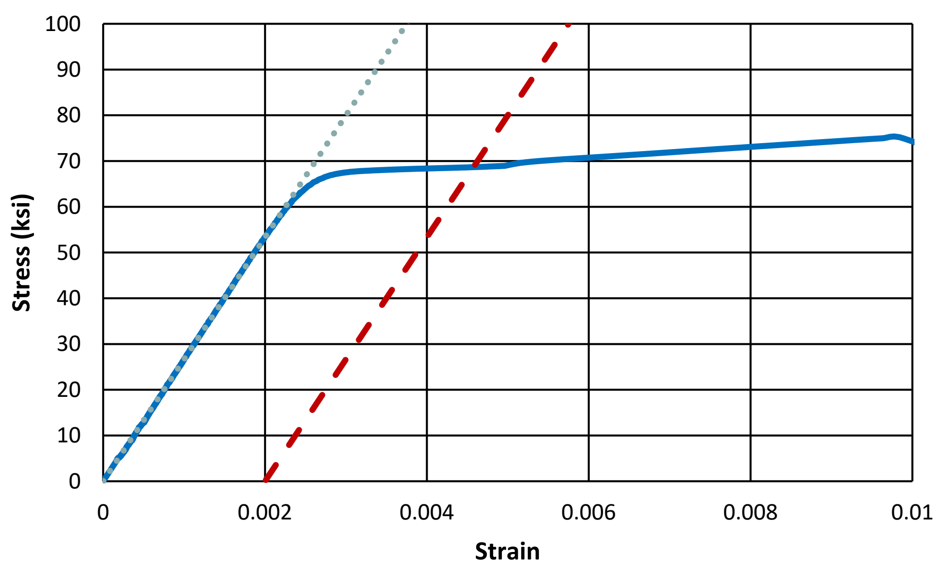

Figure 2.12: Linear Limit and Yield Strength, No. 4 Grade 60 Bar

Table 2.3: Material Properties of Transverse Reinforcement

Bar Size (No.)	Grade (ksi)	Elastic Limit Stress (ksi)	Yield Stress 0.2% Offset (ksi)	Ultimate Strength (ksi)	Elongation at Failure
3	60	62	79	101	11%
	100	72	102	138	8%
4	60	65	69	105	12%

2.4.2 Concrete Strength

Concrete was provided by Irving Materials Inc. (IMI), a ready-mix supplier in West Lafayette, Indiana. The selected mixes were based on previous batch statistics provided by IMI and a target 28-day strength of 5000 psi. After the Series I mix (4101CC) provided lower strengths than desired, the mix design was changed to 4601CC for Series II. Concrete mix 4601CC provided strengths that were much higher than desired. For Series III and IV, mix 4101CC was used.

All specimens in the same series were cast with the same mix design. Both concrete mixes were non-air entrained containing 3/4-in. crushed limestone aggregate. Details of the two mix designs are provided in Table 2.4. Actual mix quantities for each series are provided in Appendix C.

Table 2.4: Concrete Mix Design per Cubic Yard

	Mix Design I 4101CC	Mix Design II 4601CC
Series	I, III, and IV	II
Nominal Strength (psi)	4000	4500
Type I Cement (lb/yd^3)	517	564
#8 Limestone (lb/yd^3)	1875	1850
Fine Aggregate (lb/yd^3)	1475	1450
Water (lb/yd^3)	249.9	249.9
Mid-Range Water Reducer (oz/yd^3)	20.7	11.3
Slump (in.)	6	6

Concrete strength was determined using 6 x 12 in. cylinders that were cured and cast in the same conditions as the specimens. Differences in concrete strengths between series occurred because of time of year, water added, and mix design. Compressive and tensile strengths were determined from testing in a 600-kip Forney testing machine according to ASTM C39 and ASTM C496, respectively. Loading was applied at 35 psi/s for the compression tests and 2.5 psi/s for the split tensile tests. The test setup for the compression and split tensile tests are shown in Figure 2.13. The elastic modulus test was also conducted using the 600-kip Forney testing machine. Load was applied at 35 psi/s in accordance with ASTM C469.

Two trucks were required for the casting of each series in Series I through IV. To minimize the number of cylinders required, only cylinders from Truck 1 were tested at 7 and 14 days. Cylinders were tested at 28 days, the first day of testing, and the last day of testing of each series for each of the two trucks. At 28 days, the first day of testing, and the last day of testing, three cylinders from each truck were tested for each compression and split tensile test. Additionally, the modulus of elasticity test was conducted on either the first or last day of testing for the series. The results from the cylinder tests conducted on days 7, 14, and 28 days, and the first and last days of testing are summarized in Table 2.5. The strength gain of the different concrete series over time is shown in Figure 2.14.

a) Compression **b) Split Cylinder**

Figure 2.13: Concrete Cylinder Testing

Table 2.5: Concrete Strengths

Series	Truck	Day	f_c (psi)	f_t (psi)	E (ksi)
I	1	7	3980	-	-
		14	4350	-	-
		28	4530	490	-
		180	4780	450	3000
		189	4830	470	4000
	2	28	4470	460	-
		56	4660	460	4400
		177	4600	460	-
II	1	10	5680	-	-
		14	5830	-	-
		28	6450	570	-
		100	7250	560	4600
		103	7400	560	-
	2	28	6360	560	-
		107	7400	530	-
		110	7400	590	4900
III	1	7	4510	-	-
		14	5660	-	-
		28	6090	530	-
		38	6310	530	5500
	2	28	6960	610	
IV	1	7	4810	-	-
		14	5360	-	-
		28	5910	460	5100
		48	6110	510	5100
	2	28	6530	500	-
		49	6510	500	5000
		51	6520	520	5000

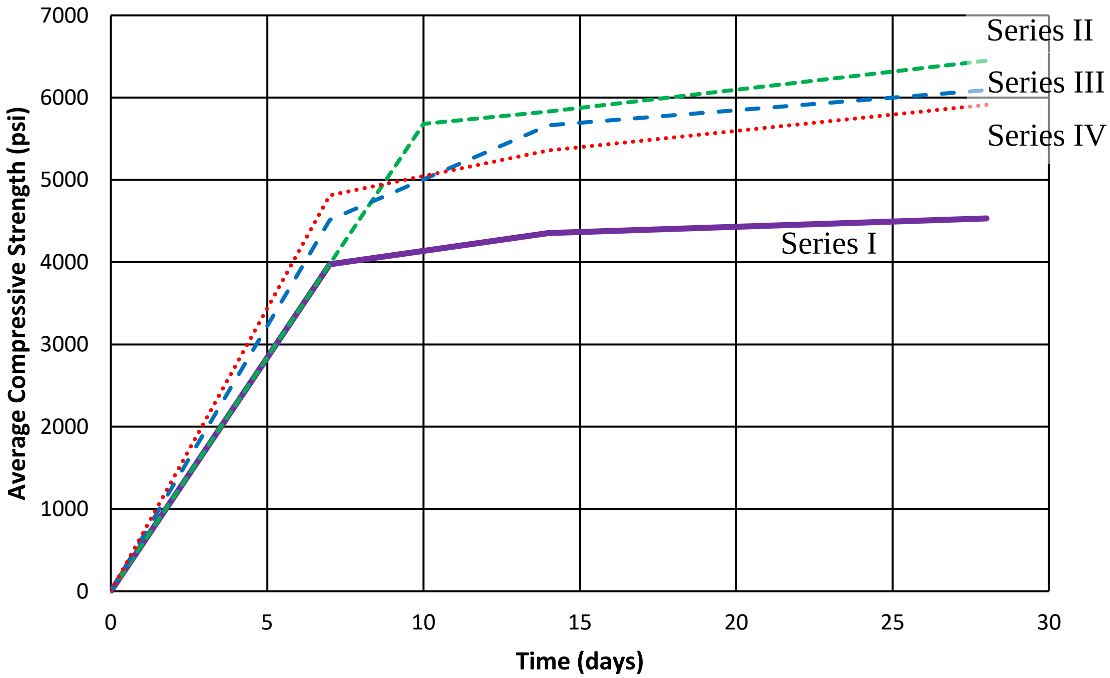

Figure 2.14: Concrete Compressive Strength Gain

2.5 Specimen Construction

2.5.1 Fabrication of Formwork

All series used the same set of wooden formwork. To conserve space and materials, the forms were designed and constructed so that two specimens could be cast side-by-side. Four sets of forms were built so that eight specimens could be cast at once. To build the side forms, stud-wall-like structures were built out of 2x4 lumber and sheathed with 3/4-in. HDO plyform (Figure 2.15). HDO plyform has a resin coating that allows the forms to be reused multiple times. To ensure that the top of the forms did not bulge during casting, a 1/4-in. threaded rod was used in conjunction with wedges at seven points along the beam as shown in Figure 2.16. To prevent the threaded rod from bonding to the concrete, 3/8-in. PEX pipe was included as a barrier between the concrete and threaded rod so that the rod could be removed from the specimen after curing. Both the side forms and end forms were secured to the platform using lag screws for ease of removal.

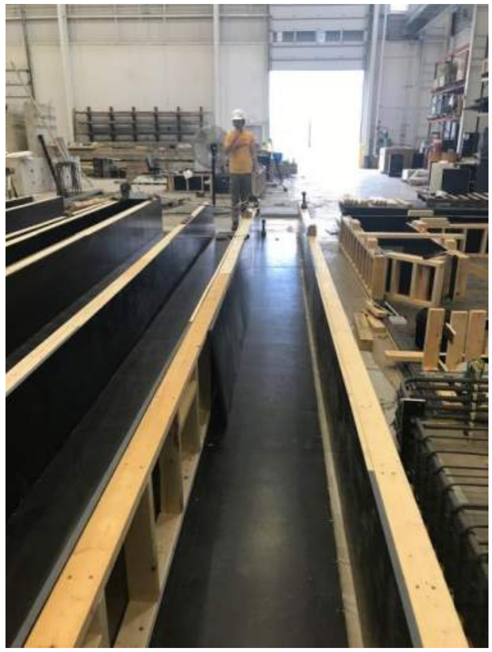

Figure 2.15: Center Side Form

Figure 2.16: Completed Formwork

2.5.2 Construction of Reinforcement Cages

The reinforcement cages contained longitudinal reinforcement both on the tension and compression faces of the specimen (Figure 2.2). All specimens also contained stirrups in the shear span to prevent failure outside of the splice region. The number of stirrups in the splice region varied according to the specimen. The cages were constructed on top of the forms and then lowered with two overhead gantry cranes. Stirrups were secured to the No. 3 compression bars and the No. 8 longitudinal bars using metal rebar ties. The 1-7/8-in. concrete cover to the bars from the bottom of the forms was maintained using 2-in. plastic chairs with 1/8-in. tips that were ground off. The longitudinal bars were tied to the chairs to ensure the spacing between bars remained during casting. Spacer wheels were placed on the ends to ensure that appropriate side cover was maintained (Figure 2.17). Lifting inserts were tied to the stirrups with metal ties approximately 5 ft from the ends of the beam. The location of the lifting inserts was controlled by the minimum 19 ft spacing required to use two overhead cranes simultaneously and the cracking moment of the beam. An unconfined and a confined lap splice are shown in Figure 2.18.

Figure 2.17: Reinforcing Cages Inside Forms

a) Unconfined Splice (Left: U-60-5, Right: U-40-5)

b) Confined Splice (Left: C3/60-60-5-100, Right: C3/60-60-5-150)

Figure 2.18: Lap Splice Construction

2.6 Casting, Curing, and Storage

Specimens in each series were cast at the same time. Because of the volume of concrete required to cast eight beams at once, two trucks were required. For Series I, II, and III, four specimens were cast from the first truck and four specimens from the second truck. For Series IV, five specimens were cast from the first truck and three from the second truck. Appendix C indicates the specific truck from which each specimen was cast. The slump was checked upon arrival of the concrete truck. The design slump was 6 in. If the slump was less than the 1-in. tolerance, water was added to the mixture, and the slump test repeated. Once the mix was accepted, the concrete was transported from the ready-mix truck to the forms using a bucket and overhead crane as shown in Figure 2.19.

The beams were cast in two lifts, alternating specimens on either side of the center form to ensure that the center form did not tilt because of the pressure of the concrete on one side. After each lift, the beams were vibrated to ensure that the concrete was properly consolidated.

Figure 2.19: Casting Procedure for Specimens

From each truck, 6 x 12-in. cylinders were cast in plastic molds simultaneously with the beams in accordance with ASTM C192. The cylinders were consolidated with a mechanical vibrator after each of the two lifts (Figure 2.20). The cylinders were also finished, cured, and stored in the same manner as the beams to ensure a reliable representation of strength. After allowing the concrete to set, the specimens were covered with wet burlap and plastic sheathing for moist curing. Once a day for six days, the burlap on the specimens was watered to maintain moist curing. On day seven after casting, the cylinder molds, burlap, and forms were removed. The beams were stored inside of Bowen Laboratory until testing. The beams were flipped using a crane prior to installation in the test setup so that the bottom-cast bars were in the top testing position.

Figure 2.20: Making of Cylinders

2.7 <u>Test Setup and Procedure</u>

The beams were tested in four-point bending. Two equal, concentrated loads were applied 1 ft from each end of the beam with hydraulic rams connected to a single pump (Figure 2.21).

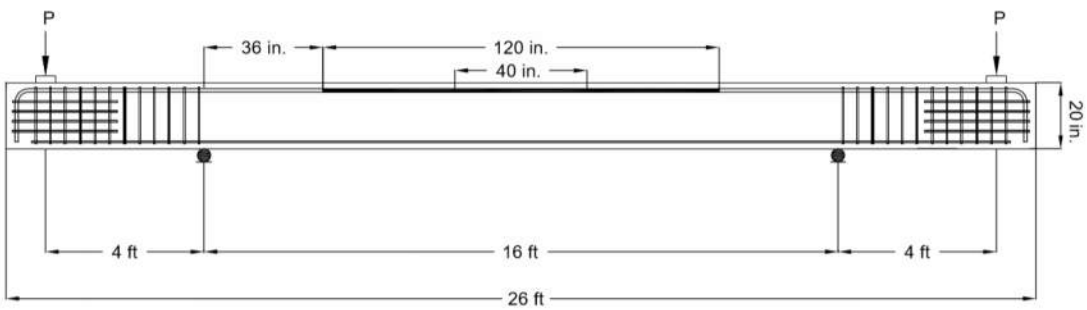

Figure 2.21: Test Setup

Concrete supports with either pin or roller supports were spaced 4 ft from the loading point. The beam was loaded in 5-kip increments. At each load step, the specimen was crack mapped, and crack widths were measured using an Edmund Direct 50x microscope. The specimen was crack mapped and crack widths were measured until it was deemed unsafe to approach the beam. Because these specimens contained some of the longest lap splices that have ever been tested, there was concern regarding maintaining verticality of the load. Different iterations of the test setup were explored as discussed in the following sections.

2.7.1 First Test Setup

The first test setup used a pin support on top of the concrete beam to allow the load to be applied vertically as the end of the beam deflected downward. The pin support was made from a 1-1/4-in. steel roller and two 1 x 6 x 18-in. grooved steel plates. The groove was 1/4-in. deep and 1-1/8-in.

wide to allow the roller to fit partially within the groove. The pin did not work in the manner intended, and the loading rods bent as the end deflection of the beam increased. For Specimen U-40-5, the pin beneath the HSS cross beam was removed to finish the test. Two Enerpac 30-ton hydraulic rams were placed on each of the 1-in. DYWIDAG bars to apply load to the specimen.

The beam was supported by a pin-roller support condition. The pin support was made from a 1-1/4-in. steel roller and two grooved steel plates, while the roller support was made from a 1-1/4-in. steel roller and two flat steel plates. This setup was only used for U-40-5 as the loads and deflections were small enough that the DYWIDAG bars used in the test setup did not yield during testing. The first iteration of test setup is shown in Figure 2.22.

Figure 2.22: First Test Setup (U-40-5)

2.7.2 Second Test Setup

The second iteration of the test setup included a frame and the same pin-roller support conditions as the first test setup. The second test setup was only used to fail Specimens U-60-5 and U-80-5. The same 1-in. DYWIDAG bars and 30-ton hydraulic rams were used along with the rollers described in the first test setup, as well as the same HSS cross beam. To stabilize the system and to prevent bending of the DYWIDAG bars with the deflection of the end of the beam, the hydraulic rams pushed against two HSS cross beams that transferred the load to two 1-1/4-in. DYWIDAG bars. This test setup configuration is shown in Figure 2.23.

Figure 2.23: Second Test Setup (U-60-5)

The second test setup worked well for lower loads. When higher loads were reached while testing U-80-5, the DYWIDAG bars yielded suddenly as shown in Figure 2.24. This behavior was attributed to a lack of centering on the pin under the HSS section. The setup was fixed and Specimen U-80-5 was failed using the same setup. While testing Specimen U-100-5, the second test setup failed again. This failure was because the top of the beam expanded as more cracks developed and opened on the tension face. The pin support on the top of the beam allowed rotation, but did not allow translation, forcing all displacement to one side of the specimen.

Figure 2.24: DYWIDAG Bars Yielding in Testing of U-80-5

2.7.3 Third Test Setup

The setup that was used to fail all specimens except for U-40-5, U-60-5, and U-80-5 (as previously discussed) is shown in Figure 2.25. Cross beams composed of two back-to-back channels and two 1-in. plates were used to suspend a 100-ton Enerpac hydraulic ram. With only one point of loading rather than two, the system could rotate even without a saddle bearing or pin support.

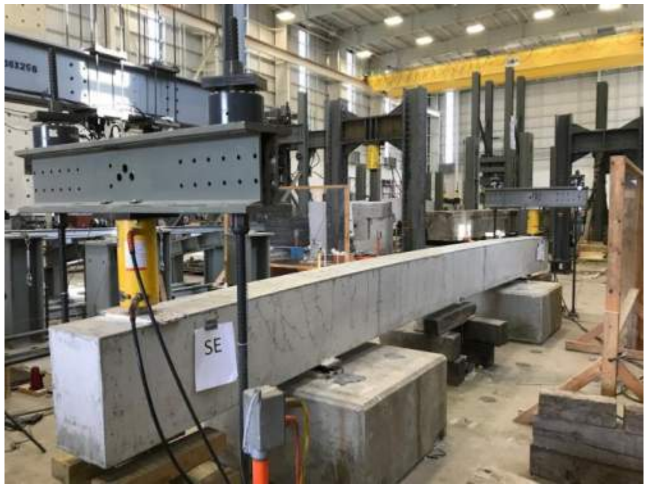

Figure 2.25: Third Test Setup (U-100-5-M)

Additionally, the support conditions were changed from pin-roller to roller-roller to allow for the equal expansion of the top of the specimen (and contraction of the bottom of the beam) at both supports. As shown in Figure 2.26, the rollers allowed for the translation that was required during testing. With two rollers as opposed to one, translation at the loading points was minimized as both ends could translate equally.

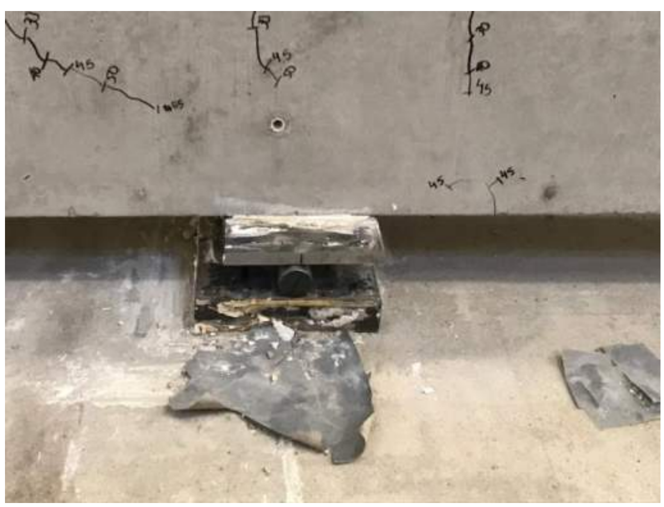

Figure 2.26: Roller-Roller Support (U-120-5-M)

2.7.4 Instrumentation Layout

Four Lebow 50-kip load cells (two on each end of the beam) were selected to measure the load applied to the beam. String potentiometers with a stroke of 10 in. measured the deflection under each load and at midspan. Two string potentiometers were used at midspan, one on each side face of the beam. Only one string potentiometer was placed under each end of the beam at the load point and centered beneath the bottom face. For Specimens U-40-5, U-60-5, and U-80-5, LVDTs were used to measure settlement at the pin support. The support settlements were shown to be negligible from the LVDT readings at the supports taken from the first three tests. With the pin support being changed to a roller, the LVDTs were eliminated because of the LVDT rods shearing when the beam failed suddenly. The instrumentation layouts for the various test setups are shown in Figure 2.27.

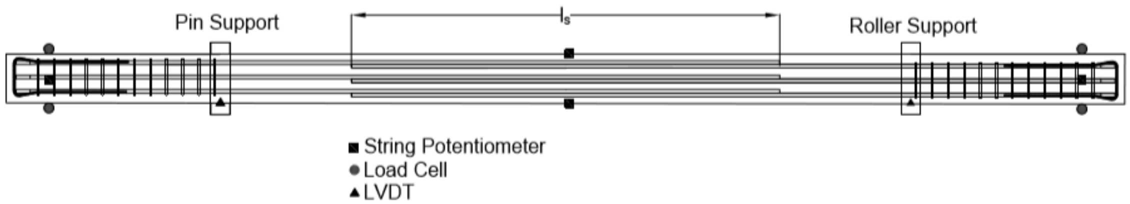

a) First Test Setup

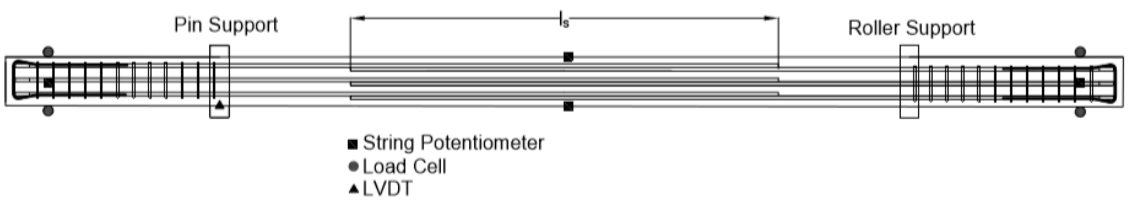

b) Second Test Setup

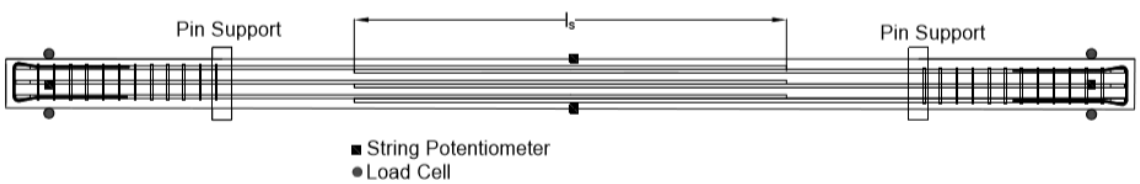

c) Third Test Setup

Figure 2.27: Instrumentation Layout

2.8 Results Introduction

The experimental results from each test in Series I through IV are presented to evaluate the effects of the test variables on the behavior of the specimen and the bond strength of the splice. The failure mechanisms and cracking behavior of the specimen will be presented with an emphasis on failure modes and crack patterns. This chapter presents load-deflection response, crack width measurements, and observations made regarding crack patterns.

2.9 Test Results

A summary of the test results for each specimen are provided in Table 2.6 and the load-deflection responses are provided in Appendix D for Series I through IV. The load at each end of the beam was measured using a total of four load cells. The maximum average load from the two ends of the beam is defined as P_{ult}. The loads were averaged as they were approximately equal at each end. The loads measured at each end were within 2% of each other. The moment within the splice region, M_{ult}, is calculated by multiplying P_{ult} by the distance between the load and the support (4 ft). The bar stress, f_b, was calculated assuming a nonlinear stress distribution in the concrete. The compressive strength of the concrete was characterized by the Hognestad curve described by Equation 2-1. The tensile strength of the concrete was assumed to be zero. Nominal dimensions were used for all calculations.

$$f_c = f'_c \left[\frac{2\varepsilon}{\varepsilon_0} - \left(\frac{\varepsilon}{\varepsilon_0} \right)^2 \right] \qquad (2\text{-}1)$$

where:

ε = *concrete strain*

ε_o = *concrete strain at* f_c'

f_c' = *compressive strength of concrete (psi)*

The concrete strength of the specimen was taken as the average of the first and last day of testing for the two trucks. This was done so that all specimens in a series could be compared. Differences in concrete strengths between the first and last day of testing and each of the two trucks were within the acceptable variation of concrete tests.

The stress, f_b, was also calculated assuming a linear stress distribution in the concrete. This value is presented for comparison purposes. In general, the computed stresses are similar. For this study, the stresses considering the more accurate representation of the concrete stress-strain relationship were used. Both the self-weight of the beam and the contribution of compression steel were ignored in the calculation of bar stress as they were found to be negligible.

The specimens that experienced a splice failure and had a bar stress beyond the linear-elastic limit are indicated by an asterisk (*), while the specimens with a bar stress beyond the yield stress calculated according to the 0.2% offset method are indicated by a cross (†) in Table 2.6. The bar stress at failure and the corresponding location on the longitudinal bar stress-strain curve is shown for each specimen in Appendix D for Series I through IV. It is observed that unconfined specimens fail in bond as soon as the stress-strain curve starts to become inelastic. For confined specimens, the bond failure occurs after more bar deformation occurs. The specimens that failed in flexure are indicated by double asterisks (**) in Table 2.6.

The specimens that were built, but not tested would have experienced a flexural failure based on the results of specimens with less transverse reinforcement and/or a shorter splice length. A flexural failure did not provide useful data in terms of quantifying the increase in splice strength because of different variables.

Table 2.6: Specimen Results

Series	Specimen	Test Age (days)	f_c (psi)	P_{ult} (kip)	M_{ult} (ft-kip)	Linear f_b (ksi)	Hognestad f_b (ksi)
I	U-40-5	56	4740	44.9	180	57.7	58.1
	U-60-5	112	4740	52.7	211	67.8	68.4
	U-80-5	146	4740	77.6	310	99.8	102.2*
	U-100-5	157	4740	78.7	315	101.2	103.7*
	U-120-5	186	4740	78.6	314	101.1	103.5*
	U-80-5-M	180	4740	73.3	293	95.0	97.6*
	U-100-5-M	187	4740	73.2	293	94.9	97.5*
	U-120-5-M	189	4740	71.8	287	93.0	95.5*
II	C3/60-60-5-50	100	7360	80.4	322	102.3	103.3*
	C3/60-60-5-100	101	7360	85.9	344	109.3	110.5†**
	C3/60-60-5-150	103	7360	85.1	340	108.3	109.4†**
	C3/60-60-5-200	NOT TESTED					
	C4/60-60-5-100	107	7360	84.7	339	107.	108.9†**
	C4/60-60-5-150	NOT TESTED					
	C3/100-60-5-100	110	7360	86.3	345	109.8	111.0†**
	C3/100-60-5-150	NOT TESTED					
III	C3/60-80-5-50	38	6310	79.4	318	100.4	101.9**
	C3/60-80-5-100	NOT TESTED					
	C3/60-80-5-150						
	C3/60-80-5-200						
	C4/60-80-5-100						
	C4/60-80-5-150						
	C3/100-80-5-100						
	C3/100-80-5-150						
IV	U-40-5a	43	6260	54.6	218	69.3	69.8
	U-60-5a	28	6260	69.3	277	88.0	88.9*
	U-70-5	31	6260	73.8	295	93.7	94.9*
	C3/60/2-40-5-50	48	6260	63.9	256	81.1	81.8
	C3/60/3-40-5-50	44	6260	70.0	280	88.9	89.8*
	C3/100/3-40-5-50	49	6260	66.4	266	84.3	85.0
	C3/60-40-5-100	49	6260	71.4	286	90.7	91.7*
	C3/100-40-5-100	51	6260	72.5	290	92.1	93.2*

**beyond linear-elastic limit*
†beyond yield stress
***failed in flexure*

2.10 <u>Behavior</u>

2.10.1 Load-Deflection Response

The load-deflection response can be divided into three sections, and an example response is shown in Figure 2.28. The first section is linear where the response occurs until cracking. All beams exhibited approximately the same stiffness here, indicating that the stiffness of the beam at this point is primarily controlled by the concrete and behavior of the concrete remains elastic. The second section of response occurs after reaching the modulus of rupture of the concrete, resulting in flexural cracking. In this stage, stiffness is a function of the axial stiffness of the reinforcing bars, which is based on the modulus of elasticity and area of the bars. Because all the bars are the same throughout all specimens, the slopes in this stage of response are also similar. The final stage of the response represents yielding of the bars. At this point in the curve, deflection increased with relatively small increases in load. Specimens failed before yielding for 18 of 22 specimens. Therefore, the third stage of response does not occur in these specimens. The load-deflection response for all specimens in Series I through IV is provided in Appendix D.

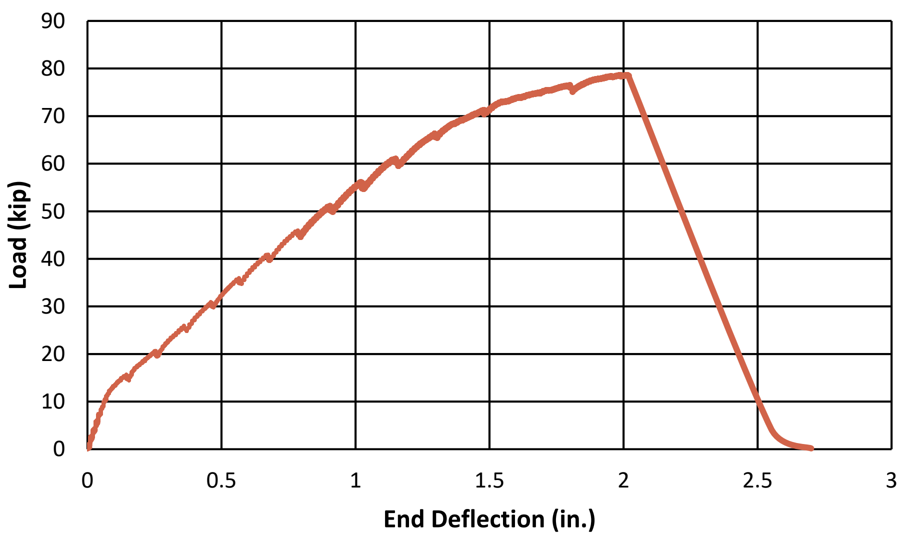

Figure 2.28: Representative Load Deflection Response (U-120-5)

2.10.2 Flexural Cracking of Specimens

Beyond a certain loading point, the full flexural cracking pattern developed and longitudinal cracks in the splice region became more prevalent. Regardless of spacing between bars, confinement, or splice length across all specimens, propagation of the flexural cracks stopped at the beam's neutral axis as shown by the red lines drawn in Figure 2.29 (the red lines are an estimate of the neutral axis based on the cracking profile). The neutral axis at failure varied from 5 in. to 6.5 in. from the bottom of the specimen depending on the stress in the bars, the concrete strength, and the beam width.

a) Specimen U-40-5

b) Specimen U-100-5

c) Specimen C3/100-40-5-100

Figure 2.29: Flexural Cracking

For unconfined specimens, flexural cracking developed across the entire depth of the beam at failure. After failure, large cracks through the entire beam section were observed emanating from the end of the splice (Figure 2.30). Only for the longest unconfined specimen, U-120-5, was a flexural crack also located at midspan (Figure 2.30(b)).

a) Specimen U-40-5a

b) Specimen U-120-5

Figure 2.30: Spacing of Cracks in Unconfined Specimens

For confined specimens, wide cracks emanating from the end of the splice were also observed. However, within the splice region, wide flexural cracks corresponding approximately to the location of the stirrups were also observed. Figure 2.31 shows two specimens with the same splice length, concrete strength, stirrup grade, stirrup size, and stirrup spacing. The only difference is that C3/60/3-40-5-50 (Figure 2.31(a)) has three stirrups within the splice region whereas C3/60/2-40-5-50 (Figure 2.31(b)) only has two stirrups. As shown in Figure 2.31, the locations of the cracks align with the locations of the stirrups (indicated by the red lines).

a) Specimen C3/60/3-40-5-50

b) Specimen C3/60/2-40-5-50

c) Specimen C3/60-60-5-50

Figure 2.31: Spacing of Cracks in 50-psi Specimens

Beams with different stirrup spacings and different splice lengths exhibited this same behavior as shown in Figure 2.32. Figure 2.32 has stirrups spaced at 9-1/2 in., instead of the 19 in. shown in Figure 2.31.

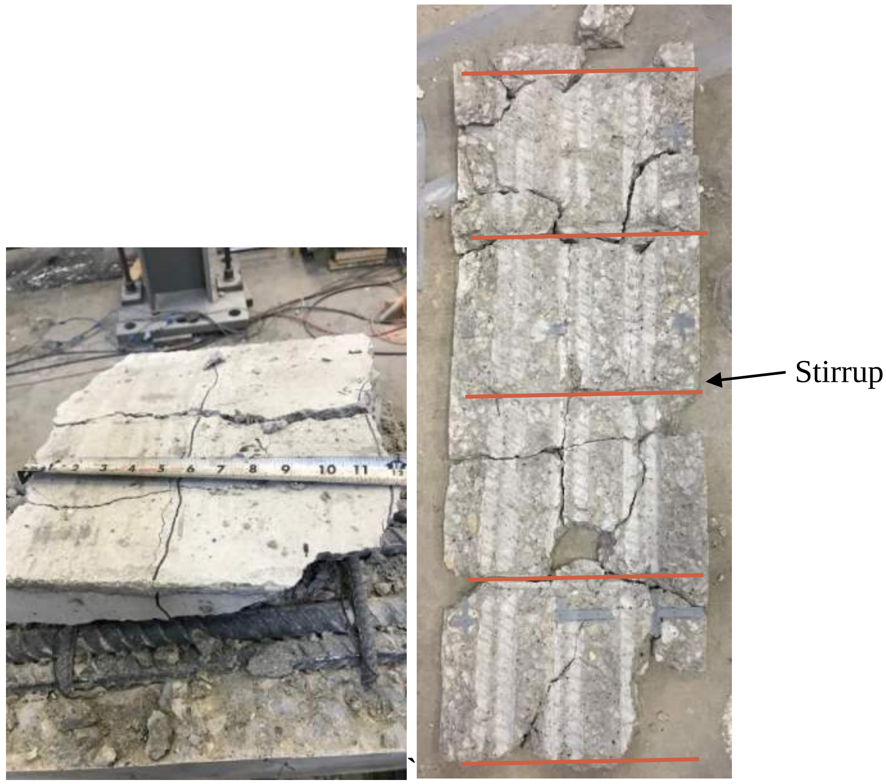

a) Specimen C3/100-40-5-100

b) Specimen C3/60-40-5-100

Figure 2.32: Spacing of Cracks in 100-psi Specimen

The failure mechanism of the beams progressed in a similar manner. At 15 kips, flexural cracks developed at a consistent spacing along the length of the beam. As the load increased, more flexural cracks appeared, and the length of the flexural cracks increased until the neutral axis was reached. Between 30 and 40 kips, longitudinal cracks started to develop along the tension face near the ends of the splice. As additional load was applied to the beam, the longitudinal cracks propagated toward the center of the splice, connecting flexural cracks. The longitudinal cracking continued to propagate toward the center of the splice until the beam failed suddenly. Typically, longitudinal cracking began at the end of the splice and propagated toward the center of the splice. This behavior was observed in both unconfined and confined specimens as shown in Figure 2.33 and Figure 2.34, respectively. For unconfined specimens, horizontal cracking also occurred along the side face. The beams that failed in flexure exhibited similar behavior; however, the beam failed in flexure near the support before the longitudinal cracking fully propagated to cause splice failure.

Figure 2.33(b) shows flexural cracks along the side of the beam that approached the neutral axis as the load increased. Longitudinal cracking became more extensive as loading increased up to failure (Figure 2.33(b) and Figure 2.33(c)).

In Figure 2.34, the end of the splice is indicated by the star, circled in blue. As shown in Figure 2.34(a) for a 40d_b splice, longitudinal cracking propagated about 7 in. from the end of the splice toward the center of the beam at 50 kips. The longitudinal cracking was more extensive (10 in.) for the 60d_b splice. Although longitudinal cracking was observed in all specimens on the top face, longitudinal cracks on the side faces were evident for only a few of the confined specimens.

a) Tension and Side Faces (U-40-5a)

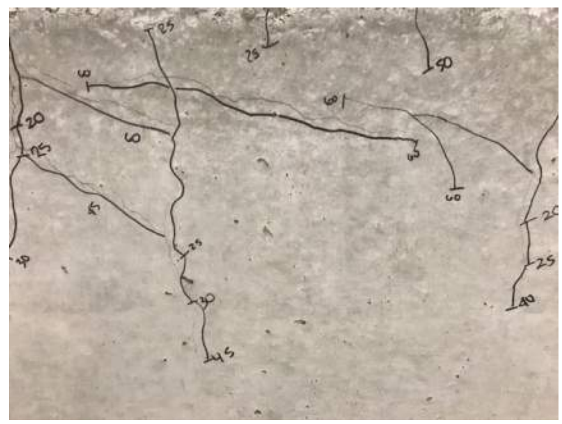

b) Side Face (U-120-5)

c) Tension and Side Faces (U-120-5-M)

Figure 2.33: Longitudinal Cracking in Unconfined Specimens

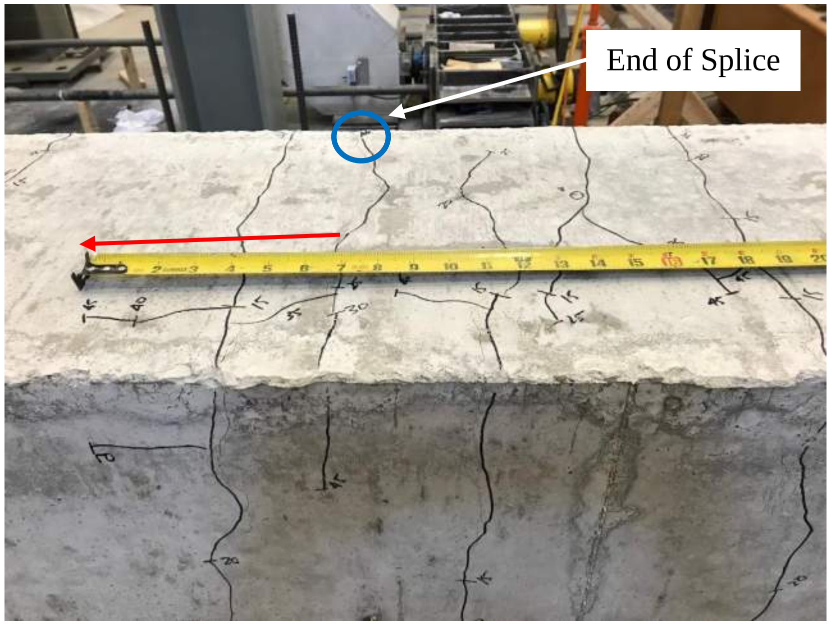

a) Tension Face of Specimen C3/60/3-40-5-50

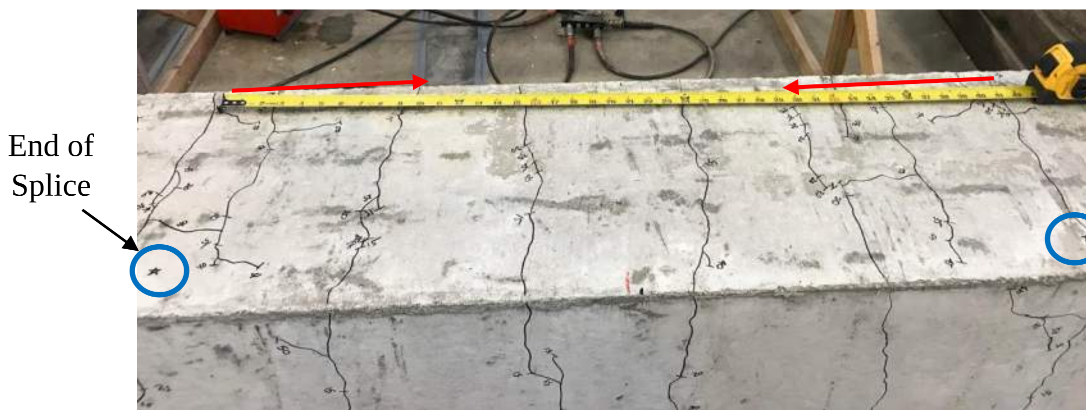

b) Tension Face of Specimen C3/60-60-5-100

Figure 2.34: Longitudinal Cracking in Confined Specimens

2.11 <u>Failure Mode</u>

Bond failures have been observed to initiate from small internal cracks that exist immediately adjacent to the reinforcing bar because of concrete shrinkage that occurs during curing (ACI 408 Committee 2003). The cracks are considered to act as points of crack initiation at relatively low loads. Small splitting cracks begin to develop from the internal cracks formed in front of the ribs. As loading continues, longer longitudinal splitting cracks form (Goto 1971). In regions where transverse reinforcement is limited, splitting cracks open. As the load applied continues to increase, the concrete in front of the reinforcing bar ribs may crush as the bar moves. The specimens that failed in bond seemed to exhibit this progression of behavior.

2.11.1 Unconfined

All unconfined specimens in Series I through IV failed in a brittle manner because of concrete splitting above the splice. Even the specimen with a 120d_b splice exhibited this failure mode. After an unconfined specimen failed, the No. 3 bars in the bottom of the specimen prevented the beam from completely collapsing. In general, the entire top cover split off the beam at the instant of failure (Figure 2.35).

2.11.2 Confined

Depending on the level of confinement, two different failure modes developed. For low levels of confinement, a splice failure with splitting occurred (Figure 2.36).

As confinement increased, a flexural failure occurred (Figure 2.37). A flexural failure occurs when the strength of the splice exceeds the flexural strength (moment capacity) of the beam. Instead of failing in bond within the splice region, the beam failed in compression near one of the supports. With 100 psi of transverse reinforcement in the splice region, the 60d_b splice failed in flexure. For an 80d_b splice, 50 psi of transverse reinforcement was sufficient to result in a flexural failure.

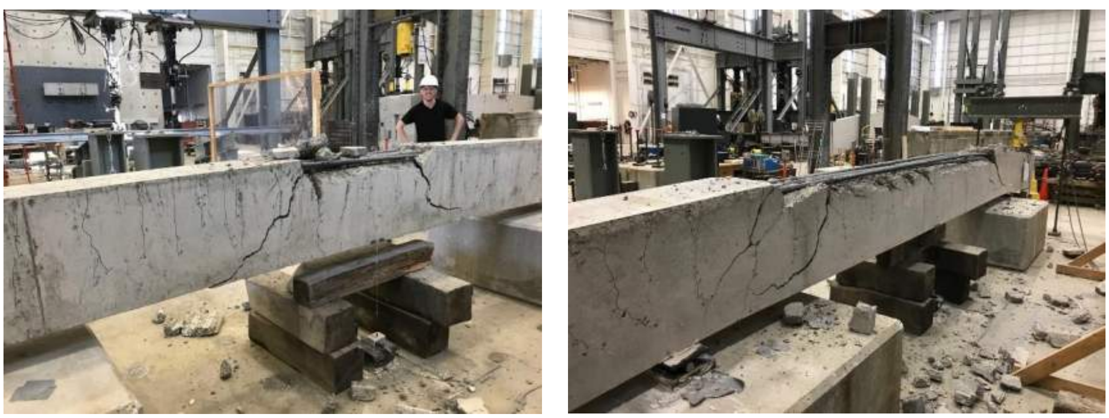

a) U-40-5a **b) U-120-5**

Figure 2.35: Typical Unconfined Specimen Failure

Figure 2.36: Typical Confined Specimen Failure (C3/60-40-5-100)

Figure 2.37: Flexural Failure (C4/60-60-5-100)

2.12 Crack Widths

Cracks were monitored over the course of testing. A specific location of four cracks in each specimen on the top face were selected to enable consistent monitoring (Figure 2.38). At each load step, the crack width at the same location was measured with an Edmund Direct 50X microscope. All cracks selected were located outside of the splice length, but between the supports, in the constant moment region where stress is constant. Two cracks were located north of the end of the splice, and two cracks were located south of the end of the splice. As shown in Figure 2.39(a) and Figure 2.39(b), as the load increased, there was an approximately linear increase in crack width, for both average and maximum crack widths. On average, maximum crack widths were 1.28 times the average crack width (Figure 2.40). The difference remains consistent throughout the range of bar stresses. Appendix E provides detailed information regarding location and crack widths for each specimen in Series I through IV.

Figure 2.38: Example Crack

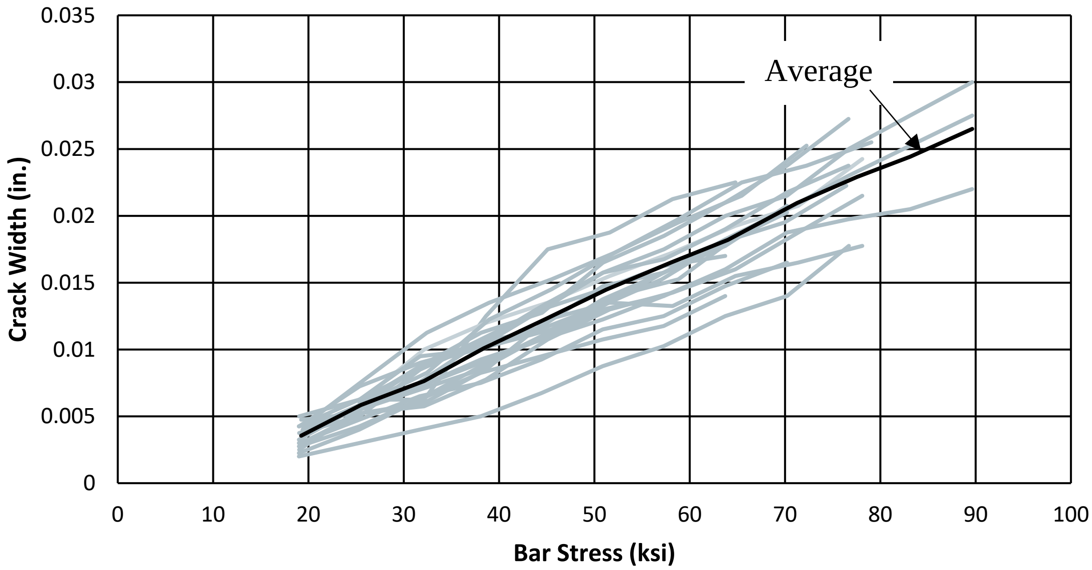

a) Average Crack Widths

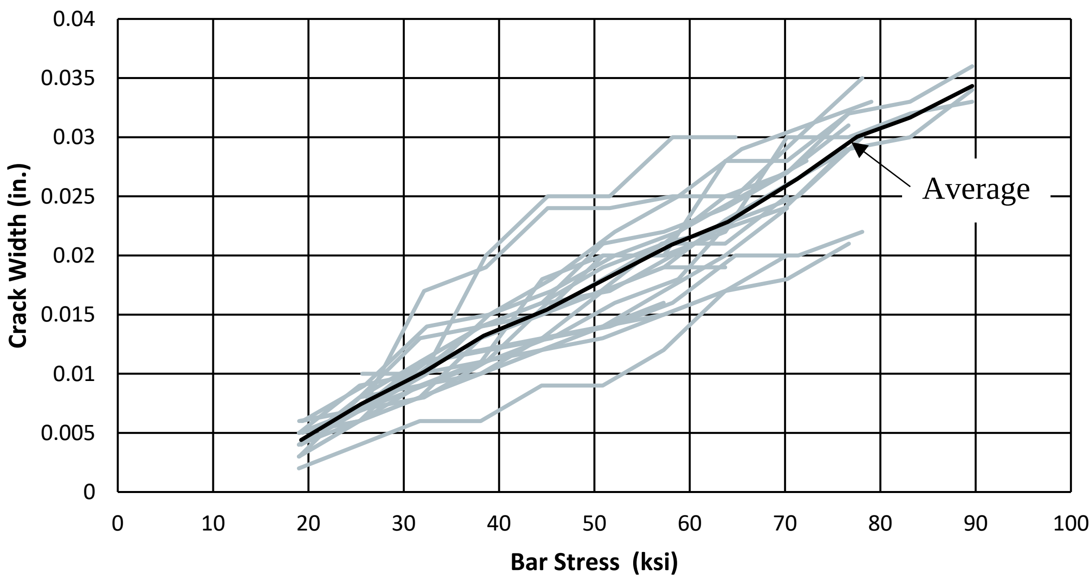

b) Maximum Crack Widths

Figure 2.39: Crack Width Measurements

Figure 2.40: Comparison of Average and Maximum Crack Widths

CHAPTER 3. SERIES V: SLAB TESTS

3.1 Introduction

The objective of Series V was to investigate the development of high-strength reinforcement in slabs. Slabs are considered separately from beams due to several factors: (a) no transverse reinforcement is typically provided, (b) small covers (3/4 in.) are present, and (c) larger bar spacings are typical. Series V contained four reinforced concrete slab specimens. The program for planning, preparing, and conducting these tests is discussed in this chapter.

3.2 Specimen Selection

3.2.1 Slab Design

Series V was implemented to investigate the effect of splice length considering typical slab bar spacings and concrete cover. The rectangular cross-section consisted of a 6-in. thickness typical of building slabs. No. 5 longitudinal reinforcing bars were selected as they are typical in slabs. A minimum bottom cover of 3/4 in. allowed for No. 5 bars in ACI 318-14 (Table 20.6.1.3.1) was selected for all slab specimens. Figure 3.1 shows the cross-section for all slabs in Series V.

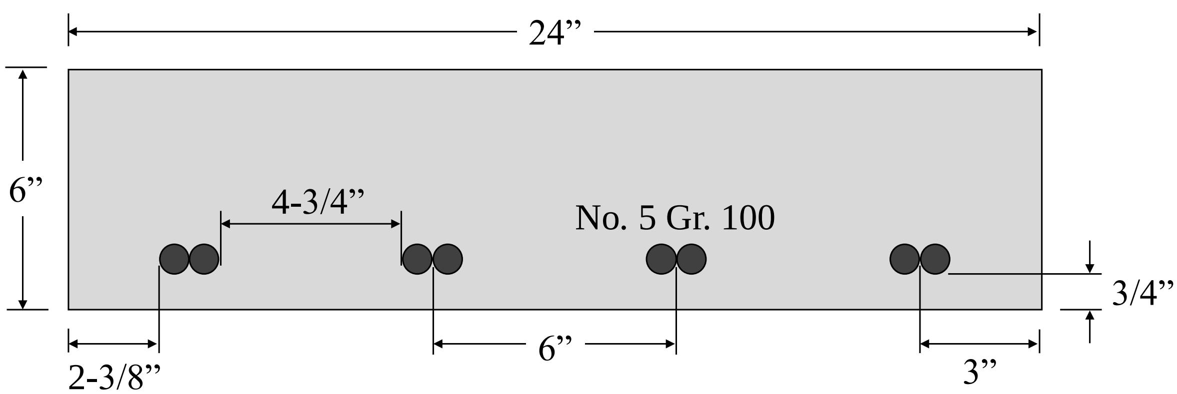

Figure 3.1: Typical Slab Cross-Section

In Series V, four No. 5 Grade 100 longitudinal bars were spliced over a variable distance, with the bar spacing set to 6 in. on-center. With this spacing, the clear bar spacing is 4-3/4 in. The side cover was set equal to half the clear bar spacing (2-3/8 in.). Based on the bar spacings, bar diameters, and cover, the overall slab width totaled 24 in. The primary labeling convention selected for this test series indicates the specimen type, splice length, and target concrete strength. The identification convention implemented in Series V is provided in Figure 3.2.

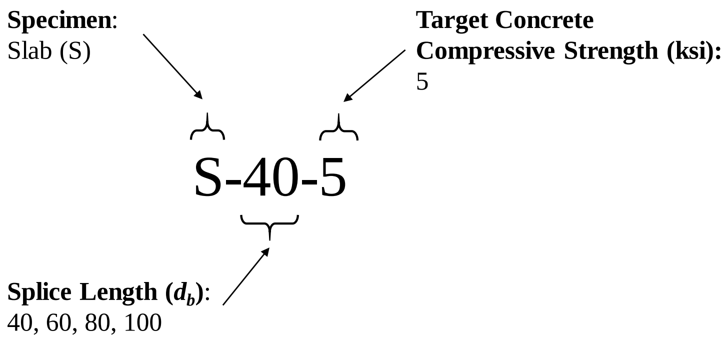

Figure 3.2: Slab Specimen Identification Label

3.2.2 Slab Dimensions

Splice test specimens from previous research programs have been tested in four-point bending to create a tension region at the location of the spliced bars. This four-point bending test setup requires two points of applied loading near the ends of the specimens and two points of support located a distance away from the applied loads (shear span). Due to the 24-in. spacing of the Bowen Laboratory strong floor grid and the need for a symmetric test setup, even dimensions were selected for the spacings between components of the test setup.

A maximum splice length of $100d_b$ (62.5 in.) was selected for Series V slab testing, which directly influenced the size of the constant moment region. A constant moment length of 10 ft (L_M) was maintained between supports for all slabs to accommodate this length. The length of the shear region was selected to be 4 ft (L_V) away from the supports. No transverse reinforcement was required in the shear span considering the shear required to produce a flexural failure. An additional 2 ft overhang (L_O) was included to ensure anchorage of the reinforcement. Overall, the selected dimensions led to a total length of 22 ft (L_T) for all specimens. The slab test configuration is shown in Figure 3.3.

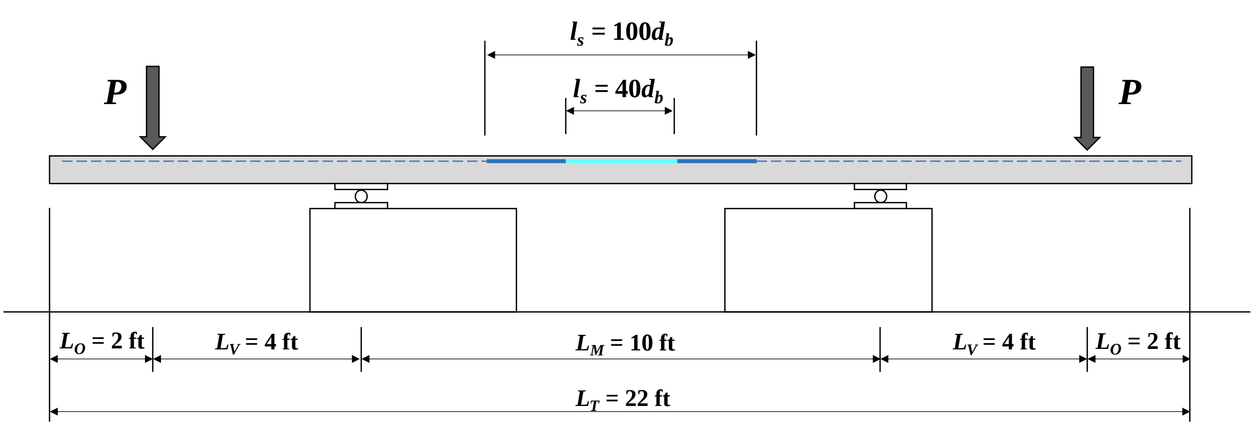

Figure 3.3: Typical Slab Test Specimen

3.2.3 Slab Testing Matrix

Table 3.1 provides the testing matrix for all slab specimens. The splice length is the primary variable, while the cover and bar spacing are fixed. A target concrete compressive strength of 5 ksi was selected based on typical slab design.

Table 3.1: Slab Testing Matrix

Series	Specimen ID	Splice Length (l_s)		Longitudinal Bar Size (No.)	Target Concrete Strength (f'_c)	½ Bar Clear Spacing (c_{si})	Side Cover (c_{so})	Bottom Cover (c_b)
		d_b	in.		ksi	in.	in.	in.
V	S-40-5	40	25	5	5	2.375	2.375	0.75
	S-60-5	60	37.5	5	5	2.375	2.375	0.75
	S-80-5	80	50	5	5	2.375	2.375	0.75
	S-100-5	100	62.5	5	5	2.375	2.375	0.75

3.3 Materials

3.3.1 Concrete

Concrete for Series V was provided by Irving Materials, Inc. (IMI), a local ready-mix concrete supplier with a distribution plant less than one mile away from the casting location. All test specimens were constructed and cast in the Bowen Laboratory for Large-Scale Civil Engineering Research in West Lafayette, Indiana.

The concrete mixture design selected for Series V was consistent with testing conducted in Series I through IV. The concrete had a target compressive strength of 5000 psi and a target slump of 6 in. A breakdown of general casting information for Series V is provided in Table 3.2, and the mix design is provided in Table 3.3 with the batched quantities.

Table 3.2: General Slab Casting Information

Casting Quantities	Series V
Cast Date	4/16/2018
Truck No.	1
Load Size (yd^3)	4
Specimens	S-40-5 S-60-5 S-80-5 S-100-5

Table 3.3: Normal-Strength Concrete – Mix Design Summary

Material	Type	Mix Design 4101CC	Batched
Cement	ASTM C150 - Type I (lb/yd^3)	517	519
Coarse Aggregate	#8 Limestone (lb/yd^3)	1875	1875
Fine Aggregate	#23 Natural Sand (lb/yd^3)	1475	1540
Water-Reducing Admixture	MasterGlenium 7511 (oz/yd^3)	20.7	20.3
Water (lb/yd^3)		250	246
Water/Cement Ratio		0.483	0.475
Slump (in.)		6.0	6.0

3.3.1.1 Concrete Testing

In Series V of this testing program, mechanical properties of the concrete were determined using an ASTM C193 standard cylinder size of 6 x 12 in. Before cylinder testing began, each cylinder was marked with a label indicating series, truck number, designated test, and cylinder number for that test. Figure 3.4 shows an example of the identification label and explains the designations chosen for this testing program.

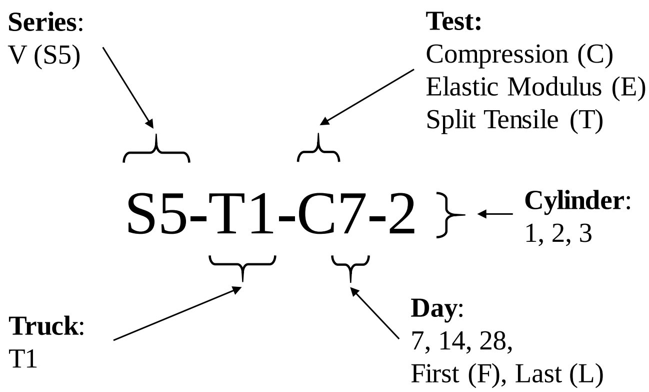

Figure 3.4: Cylinder Testing Identification

3.3.1.2 Compression Testing

To determine the increase in concrete compressive strength as curing took place, several cylinders were tested to failure. This required three (3) cylinders to be tested on days 7, 14, and 28, in addition to the first and last day of specimen testing. The cylinders were placed in a 600-kip Forney compression testing machine with a CA-0396 automatic control system interface. Nominal cylinder diameter and height dimensions were measured with a Fowler 12-in. Dial Caliper and recorded based on the "Standard Test Method for Compressive Strength of Cylindrical Concrete Specimens" in ASTM C39 (2018).

Steel caps lined with a neoprene elastomeric pad were installed on the top and bottom faces of the cylinder to ensure uniform distribution of the compression load and to reduce the chances of edge spalling. Two (2) standard 60-durometer pads were selected for all cylinder testing in Series V consistent with the target compressive strength of the concrete mix. The outer surfaces of the neoprene pads were lined with a polysaccharide powder to prevent frictional forces. With the loading platen installed, the capped cylinder was placed in the machine. The control system was set to a loading rate of 35 psi/s in accordance with ASTM C39 (2018). Once the loading cycle was completed, compressive strength values were recorded and averaged in Table 3.4. A typical compression cylinder test setup before and after failure is shown in Figure 3.5(a) and Figure 3.5(b), respectively. Average concrete compressive strength, f_c, over time is plotted in Figure 3.6 for Series V. It should be noted that Specimen S-100-5 was tested at 102 days. Concrete cylinders were not available for this test; therefore, results are not available and can only be estimated based on previous strength gains for this mix design.

Table 3.4: Series V Compression and Tension Properties

Time (days)	Compressive Strength, f_c (psi)				Fracture Pattern (ASTM C39)			Split Tensile Strength, f_t (psi)			
	Cylinders			Avg.	Cylinders			Cylinders			Avg.
	1	2	3		1	2	3	1	2	3	
7	4680	4870	4690	**4780**	4	3	3	-	-	-	-
14	5960	5950	5830	**5910**	4	2	5	-	-	-	-
28	6260	6030	6230	**6170**	4	2	5	540	525	525	**530**
38[1]	6170	5960	6400	**6180**	1	4	4	510	450	570	**510**
44[2]	6130	6290	6290	**6240**	2	4	4	470	565	435	**490**
102[3]	-	-	-	**(6490)**	-	-	-	-	-	-	-

[1] *First Day of Testing*
[2] *Last Day of Testing*
[3] *Day 102 average strength was estimated by linear interpolation of strengths on Day 28 and Day 44*

a) Before Failure

b) After Failure

Figure 3.5: Typical Compression Cylinder Failure

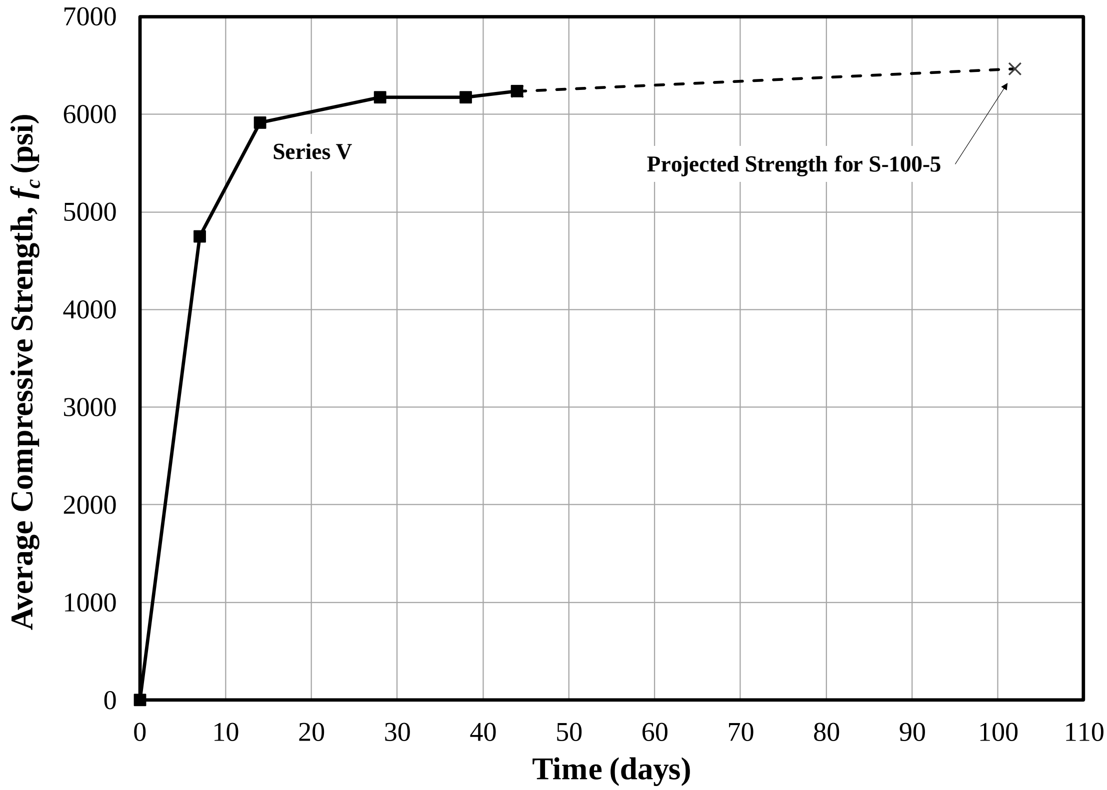

Figure 3.6: Concrete Compressive Strength Variation Over Time

3.3.1.3 Split Cylinder Testing

Split cylinder testing was conducted in accordance with ASTM C496 (2017). Diametrical lines were drawn and measured on each face of the 6 x 12-in. cylinder to assist in test alignment. A split cylinder loading jig was installed before placing the cylinder in the Forney testing machine between two 1/8 x 1-in. plywood bearing strips each approximately 13 in. long. Testing commenced at a loading rate of 2.5 psi/s in accordance with the range permitted by ASTM C496 (2017). Tensile strengths were recorded and averaged in Table 2.4. A typical splitting tensile test setup before and after failure is shown in Figure 3.7(a) and Figure 3.7(b), respectively.

a) Before Failure **b) After Failure**

Figure 3.7: Series V Splitting Tensile Cylinder Failure

3.3.1.4 Elastic Modulus and Poisson's Ratio

Young's modulus and Poisson's ratio were also determined. These properties were tested by mounting a compressometer built with two linear variable differential transformers (LVDT) to the concrete cylinder. Both direct-current LVDT high-sensitivity sensors were installed orthogonally, allowing the change in length to be measured in two directions. As a result, the stress-strain relationships in each direction could be determined, resulting in measurement of the modulus of elasticity and Poisson's ratio.

The concrete cylinder was assembled with steel caps, pads, and polysaccharide powder, similar to the compression test procedure. The compressometer model had an elastic modulus gauge length of 8 in. and a Poisson's gauge length of 6 in. Once the compressometer was secured to the cylinder, the setup was placed in the Forney machine and centered. LVDT sensors were aligned, and the mechanism brackets were removed before testing (Figure 3.8)

Figure 3.8: Series V Modulus Testing Setup

The control system was set to a loading rate of 35 psi/s according to ASTM C469 (2014). Average compressive load from previous testing was used to specify a 40% upper bound for modulus testing (ASTM C469) conducted over three loading cycles. Average values for Young's Modulus and Poisson's Ratio were calculated and provided in Table 3.5.

Table 3.5: Series V Stress-Strain Properties

Time (days)	Young's Modulus, *E* (ksi)			Poisson's Ratio, *v*		
	Cylinders		Avg.	Cylinders		Avg.
	1	2		1	2	
38[1]	4600	5060	**4830**	0.26	0.24	**0.25**
44[2]	5210	4960	**5090**	0.24	0.26	**0.25**
102[3]	-	-	-	-	-	-

[1] *First Day of Testing*
[2] *Last Day of Testing*
[3] *Day 102 data was unavailable due to lack of cast concrete test cylinders*

3.3.2 Reinforcing Steel

ASTM A615 reinforcing steel used in Series V was supplied by Nucor Steel, Kankakee, Illinois and fabricated by Harris Rebar. Only longitudinal reinforcing bars were used in this series. Table 3.6 provides general information for the reinforcing steel used in Series V. All bars were rolled from the same heat.

Table 3.6: Reinforcing Steel Bar Information

Series	Material	Type	Supplier	Fabricator	Grade	Size (No.)	Purpose
V	ASTM A615	Black	Nucor[1]	Harris Rebar[2]	100	5	Longitudinal

[1] *Nucor Steel-Kankakee, IL*
[2] *Harris Rebar-Mooresville, IN*

Bar strength testing was conducted on four bars in a 220-kip MTS universal testing machine. Stress was calculated by dividing applied load by the nominal bar area. A 2-in. extensometer was installed on the bar to measure strain during testing. The stress-strain response of the steel in Series V is provided in Figure 3.9 and Appendix B. From the linear-elastic region of the response, the linear-elastic limit was estimated by determining the point where the linear slope begins to decrease. The 0.2% offset method as specified in ASTM E8-04 (2016) was selected to determine the yield strength of the steel in Series V. The ultimate strength of the steel occurred just before fracture. Material properties are documented in Table 3.7.

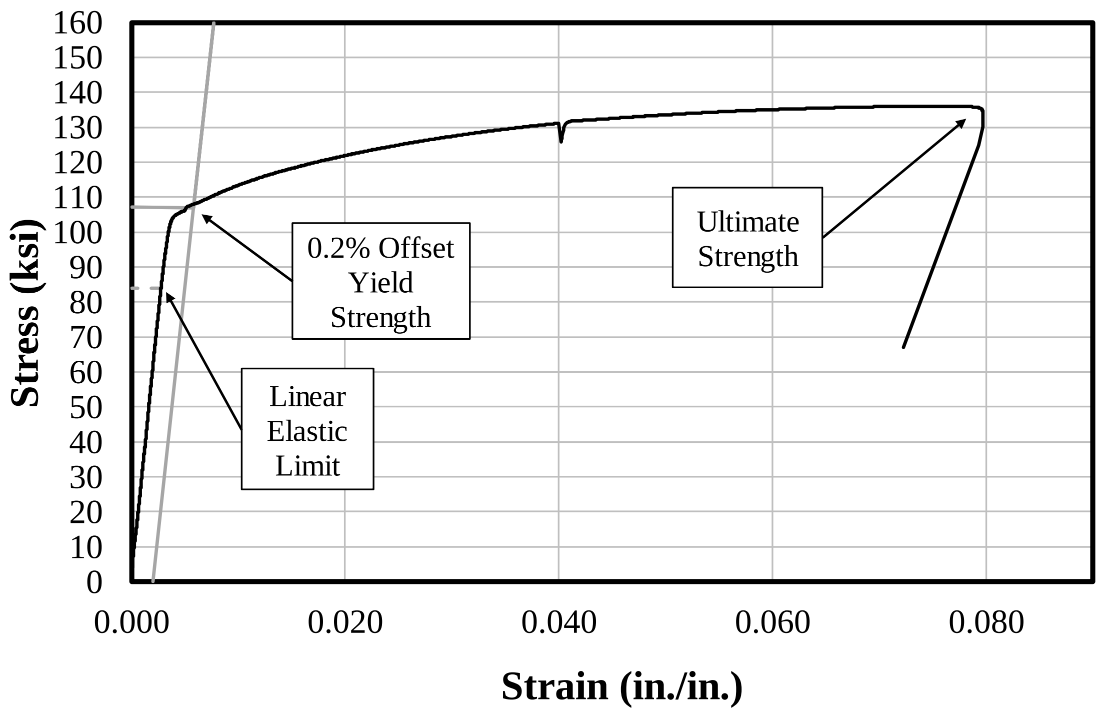

Figure 3.9: Typical Stress-Strain Response for A615 Gr. 100 No. 5 Bars

Table 3.7: Material Properties of Series V Steel

Series	Bar Size (No.)	Grade (ksi)	Linear-Elastic Limit Stress (ksi)	Yield Stress 0.2% Offset (ksi)	Ultimate Strength (ksi)
V	5	100	84	107	137

3.4 Specimen Construction

Four slab specimens were cast by first assembling and securing the appropriate formwork. Once formwork construction was completed, the necessary steel was placed and tied within the forms before casting.

3.4.1 Formwork Assembly

All formwork materials for this series were provided by a local lumber retailer. To accommodate the size of the test specimens in this testing program, base platforms were constructed at a width of 4 ft and a total length of 27 ft - 6 in. The 3/4-in. top plywood was finished with a high-density overlay (HDO) to provide a smooth finish. The HDO plyform was mounted on a series of 4 ft long 2 x 4-in. lumber spaced at 8 in. on-center running in the short direction. This allowed the platforms to be moved and configured into various arrangements for each series while also limiting warping in the plyform. The platforms were used for all seven series in the testing program.

For slab casting, a center form was bolted between two platforms, effectively allowing the two platforms to work as one uniform base. The center form was constructed on a piece of 2 x 4-in. lumber spanning the full slab length of 22 ft, plus an additional 5 in. on each side to accommodate the width of the end forms. Typical 2 x 4-in. wood bracing studs were installed vertically at a 16-in. spacing along the entire length. With the structure of the center form completed, a 6-in. sheet of HDO plyform with a thickness of 3/4 in. was secured to each side by screws. The center form and other main formwork components are shown in Figure 3.10.

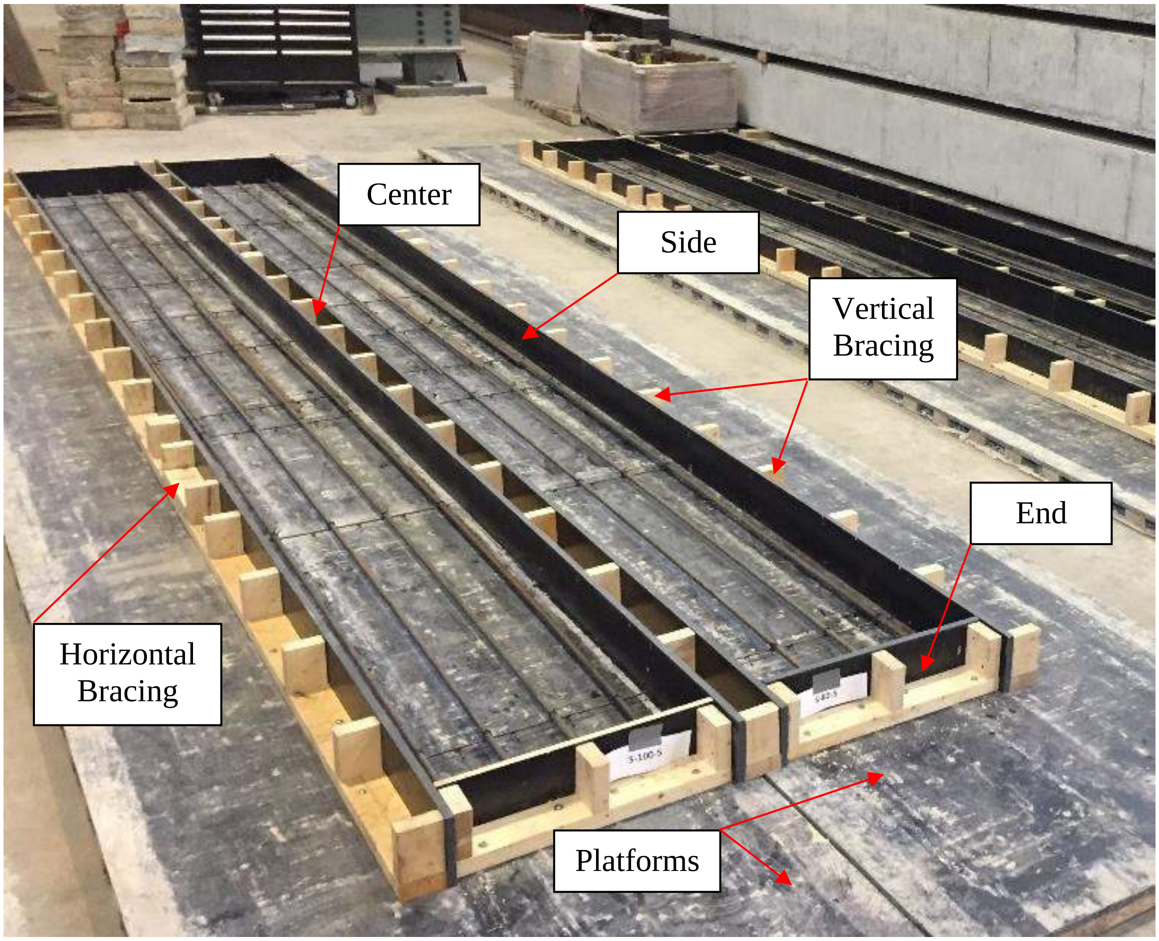

Figure 3.10: Series V Formwork Components

The two side forms were constructed in the same manner as the center form, but only one side sheet of HDO plyform was required for each. Similarly, the end forms were constructed identically to the side forms but with an overall length of 24 in. and a wood brace spacing of approximately 12 in. The locations of all formwork components were first marked with chalk lines before being secured with 1/4-in. lag screws and washers. The completed formwork construction for Series V is shown in Figure 3.11.

Figure 3.11: Series V Completed Formwork

3.4.2 Steel Cage Construction

Once the formwork was secured, the interior surfaces of the plywood were cleaned before cage construction began. The layout of steel for the slabs required eight No. 5 Grade 100 bars to be measured and cut to the appropriate length for each specimen. As shown in Figure 3.12, a 2-in. gap was provided between the end of each bar and the end plyform surface in the shear region.

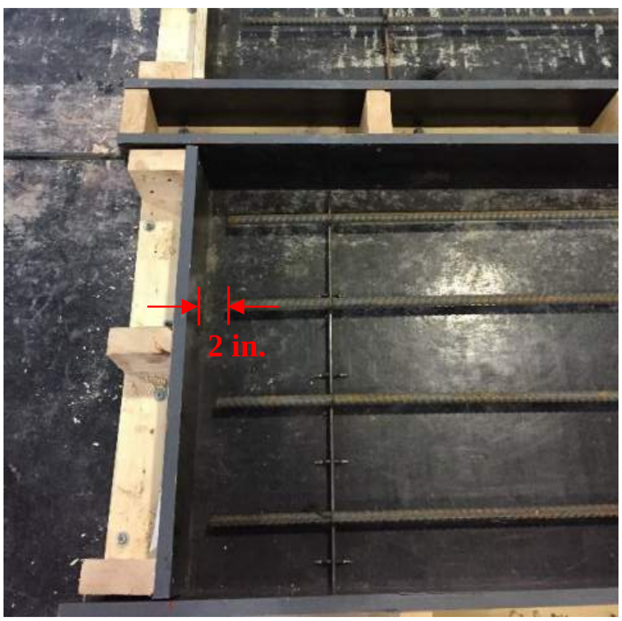

Figure 3.12: Slab Construction – Shear Region

All longitudinal bars were placed on 3/4-in. steel chairs at various points along the length of the slab to ensure a consistent cover across the bottom surface. Annealed steel wire ties were used to secure the bars to the chairs in all locations to prevent any movement or slip during casting.

The intended location of each lap splice termination was marked on the bars. Steel ties were secured to the longitudinal reinforcing steel in the lap splice to prevent a noncontact lap splice from forming during casting. Bar spacing and cover were critical for the splice zone; therefore, care was taken in securing the bars to the steel chairs in this region (Figure 3.13). All four slab specimens were constructed in this manner with the steel reinforcing on the bottom (bottom cast). Immediately after concrete was cast in each specimen, 3-in. plain steel coil loop lifting-inserts were placed 5 ft from the ends of each slab to allow for transporting.

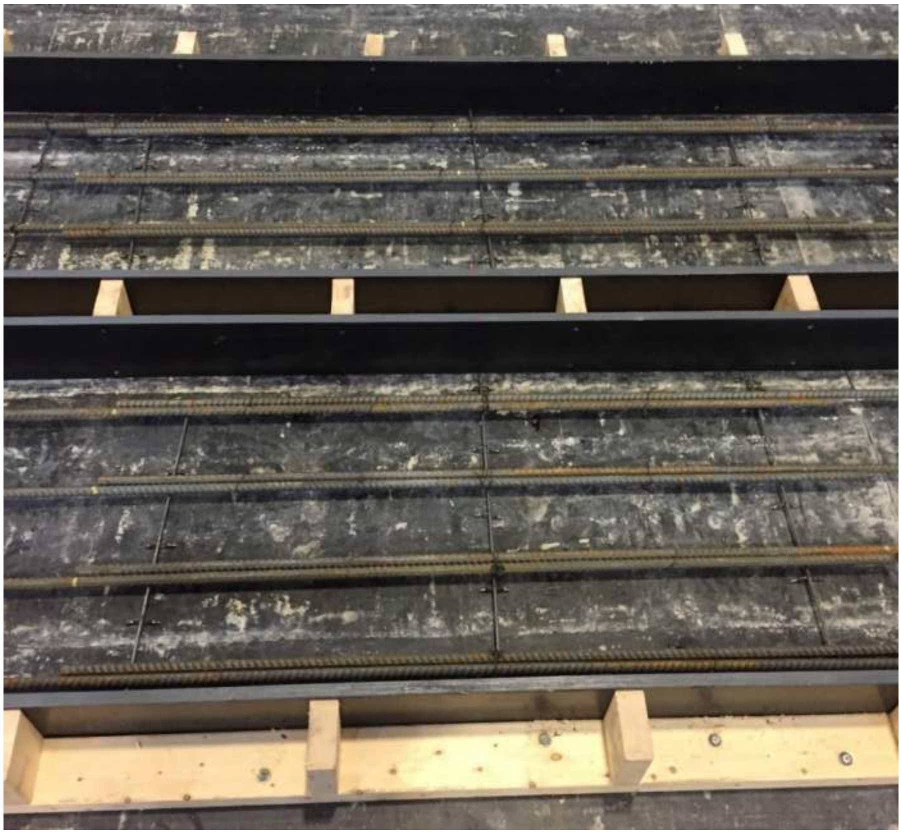

Figure 3.13: Slab Construction – Splice Region

3.5 Casting, Curing, and Storage

3.5.1 Cylinders

Concrete was used to cast cylinder sets (Figure 3.14) for all series in this testing program in accordance with the “Standard for Making and Curing Concrete Test Specimens in the Laboratory” in ASTM C192 (2016).

Figure 3.14: Typical Concrete Cylinder Preparation Space

The molds were filled halfway with a metal scoop before using a low frequency internal vibrator to consolidate the lower layer of concrete. The mold was then filled to the top and vibrated a second time, ensuring that the steel-head vibrator penetrated into the bottom layer of concrete approximately 1 in. to consolidate the concrete. The top surface was finished as shown in Figure 3.15 before sealing the cylinder mold with a flexible, domed plastic lid to prevent loss of moisture and maintain shape during curing.

Figure 3.15: Series V Cylinder Casting

All cylinders in Series V cured in the same location as the specimens to prevent differences in humidity and temperature. Each cylinder was moist cured for seven (7) days in capped plastic containers that sealed moisture. On Day 7, molds were removed and all cylinders were relocated for storage. Cylinders were labeled before being stored until testing.

3.5.2 Casting

All specimens in Series V were cast at the same time from the same delivery of concrete. Series V required one truck of concrete due to the low volume of desired specimens. Concrete was delivered to the specimens using a concrete bucket. Care was taken to ensure that the steel cages in the forms stayed in place while concrete was placed from above. Two external mechanical vibrators operating at 3600 cycles per minute (60 Hz) were inserted following concrete shoveling to ensure proper consolidation. The casting process for Series V was conducted using one lift along the length of each slab specimen. Once concrete had been cast and vibrated within each test specimen (Figure 3.16), the top surface was screeded with a 2 x 4-in. magnesium straight-edge.

Figure 3.16: Series V Consolidation Process

The top surface was evened out through screeding and finished with hand floats. Lifting-inserts were placed by hand within the concrete 5 ft from each end to assist in moving the slab and flipping it over 180 degrees about its longitudinal axis before being placed in the test setup. The lifting-insert location and screeding steel tube used after consolidation are shown in Figure 3.17. The Series V specimens after finishing are shown in Figure 3.18.

Figure 3.17: Series V Casting Process

Figure 3.18: Series V Casting Complete

3.5.3 Curing and Storage

Once all test specimens were finished and cured for approximately one hour, a final finish was conducted with a magnesium float to smooth out any noticeable irregularities in specimen height. To initiate moist curing, all specimens were covered with burlap sheets and watered evenly. Plastic sheathing was placed over the cast specimens to maintain moisture and promote hydration (Figure 3.19). The burlap was watered each day for the following five days, with the final watering period occurring on Day 6.

On Day 7, three (3) compression cylinder tests were performed to evaluate strength gain of the series before removing all side formwork (Figure 3.20). The slabs were then flipped 180° about their longitudinal axis using the crane and lifting-inserts to orient the lap splice on the top face of each member before storing the specimens (Figure 3.21).

Figure 3.19: Series V Moist Curing

Figure 3.20: Series V Side Form Removal

Figure 3.21: Series V Member Stacking and Storage

3.6 <u>Test Setup</u>

3.6.1 Schematic

All specimens in Series V were tested in four-point bending with the load being applied to the top face at the ends of the member and supports provided by rollers on the bottom face. By employing a roller-roller condition, all specimens were allowed to deform equally in the longitudinal direction.

The supports under all slabs were constructed on two 4 x 4 x 2-1/2 ft concrete bearing blocks (Figure 3.22). Roller supports were assembled using a 2-in. diameter steel rod placed between two 1/2-in. thick steel plates measuring 6 x 36 in. The 2-in. rod was selected to allow the Series V slabs to deform at the ends without interfering with the concrete bearing block (Figure 3.23(a)). Hydrostone was used to secure these components to the concrete bearing blocks and the specimens. Wood cribbing was placed below the test specimens in the middle and near the ends to protect string potentiometers (Figure 3.23(b)) and provide a safer testing environment when the concrete member reached failure.

Figure 3.22: Series V Test Setup

a) Roller Support b) End Cribbing

Figure 3.23: Series V Testing Details

Once the test specimens were placed and secured with hydrostone to the roller supports, two bearing plates were positioned on the top face to align with the loading rams. Two (2) 100-ton double-acting hydraulic rams with a maximum stroke of 9.8 in. were secured to the bottom face of a crossbeam built-up from a double channel steel section (Figure 3.24). A 1-in. steel plate and 3/8-in. bolts were used to secure the ram to the crossbeam bottom flange. The crossbeam was threaded through two 1-1/4-in. diameter DYWIDAG force transfer bars that were secured to the strong floor. Center-hole load cells were installed and secured around the DYWIDAG bars above the crossbeam. Once the hydraulic rams were lowered and centered on the bearing plates, the crossbeams were leveled. Figure 3.25 shows an elevation of the test setup for Series V, and Figure 3.26 shows various plan sections of the Series V test setup.

Figure 3.24: Typical Crossbeam Setup

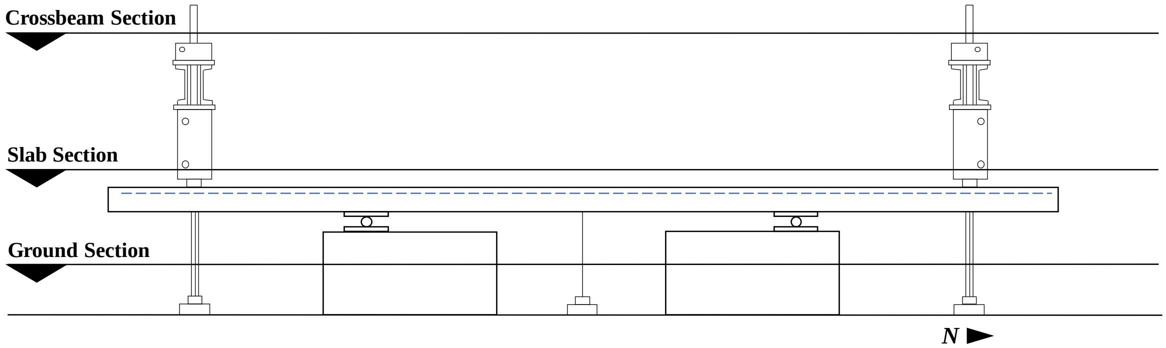

Figure 3.25: Series V Test Setup – East Elevation

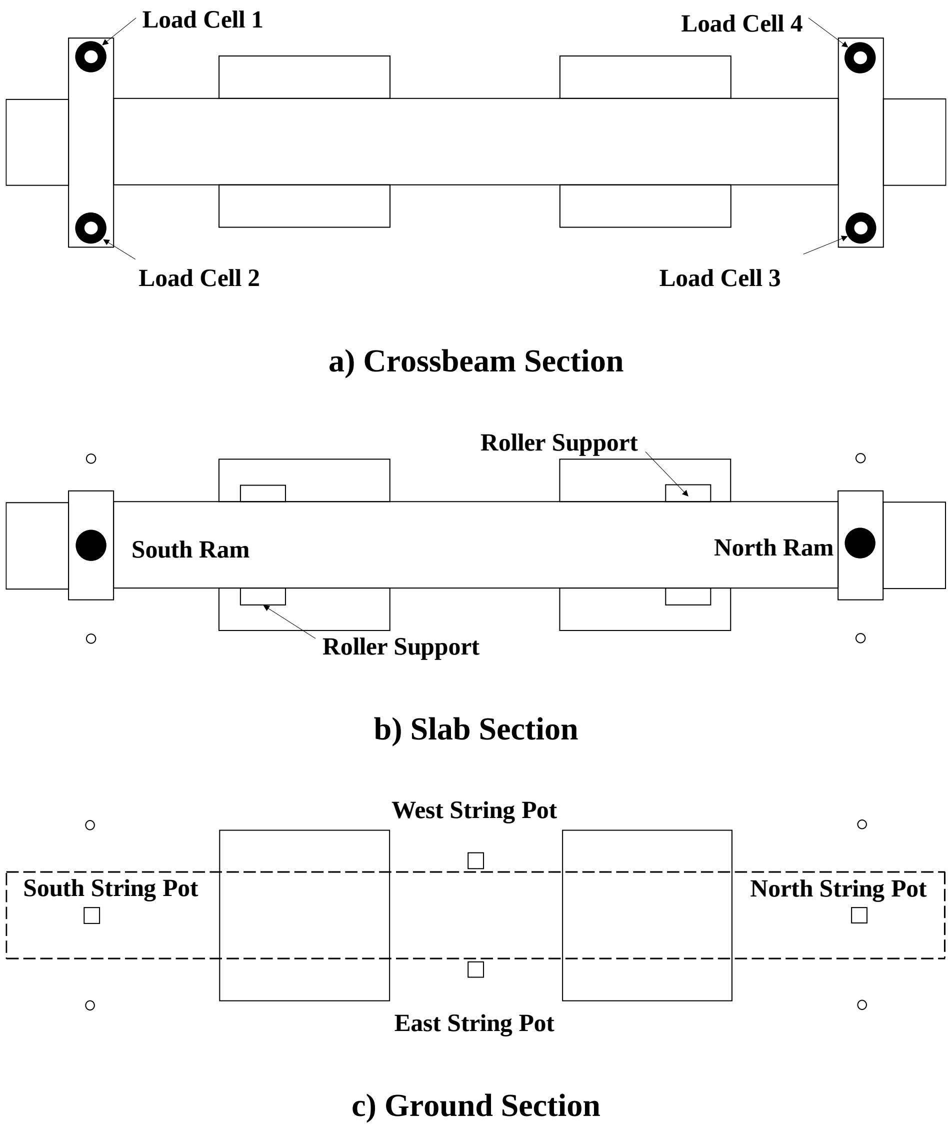

Figure 3.26: Series V Test Setup Schematic Plans

3.6.2 Instrumentation and Equipment

3.6.2.1 Deflection

Four 10-in. UniMeasure digital encoder string potentiometers were secured to the strong floor to measure vertical deflections. Two were located at midspan, aligning with the east and west faces of the slab, while the other two were placed directly below the hydraulic loading rams on the north and south ends of the slab. The two midspan string potentiometers were connected to the test specimen through epoxied steel brackets as shown in Figure 3.27(a), while the north and south brackets were secured with concrete screws (Figure 3.27(b)). The use of concrete screws provided a stronger, more reliable bracket connection as opposed to the epoxied brackets; however, the screws were not installed at midspan to avoid potentially interfering with the stress distribution within the splice region during testing. Calibration was performed using a Fowler Trimos electronic height gauge for all four units.

a) Midspan **b) End of Member**

Figure 3.27: String Potentiometer Connections

3.6.2.2 Loading System

Two 50-kip center-hole load cells were secured above each crossbeam, requiring a total of four load cells for the test setup. A 1-1/2-in. steel plate and 1-1/4-in. threaded steel nut were used as a reaction point against the loading rams (Figure 3.28). The four load cells were calibrated on a 120-kip Baldwin universal testing machine using an Instron data acquisition system.

Figure 3.28: Typical Load Cell Configuration

A manual hand pump was selected to pump hydraulic fluid into a three-outlet manifold. Two of the outlets fed hydraulic fluid to each of the double-acting hydraulic rams (Figure 3.29(a)) while a stainless steel pressure transducer was attached to the third outlet. For three specimens in Series V, the same 10,000-psi pressure transducer was used from Series I through IV testing. Because the pressures required for the slab tests to reach failure were generally lower, it was difficult to obtain accurate data with this high capacity transducer; therefore, a 2000-psi pressure transducer was selected for the S-100-5 slab specimen to provide better resolution at lower pressures. Hydraulic fluid was returned from the loading rams to the hand pump reservoir through a two-outlet manifold. All hoses used in this test setup were rated for 10,000 psi. Figure 3.29(b) shows the layout of the supply and return system.

a) Ram Supply and Return **b) Manifolds and Pump**

Figure 3.29: Typical Pump System for Testing

3.6.2.3 Concrete Cracking

Cracks along the sides and tension face of each specimen were mapped and measured using an Edmund Industrial Optics Crack Width Direct Measuring Microscope with a 50x magnification, allowing concrete crack widths to be identified and measured to 1/1000 in. (Figure 3.30). Four cracks were selected for each specimen outside of the splice region but between the supports. These locations ensured that the measured cracks were in the constant moment region and were not influenced by the splice. The four cracks were observed at each loading interval, and widths were manually recorded.

For some test specimens, a crack was selected early in the testing procedure and over time, another crack formed adjacent to this original crack. It was observed that this close proximity of cracks caused the original crack to reduce in size from shifting of the surrounding concrete.

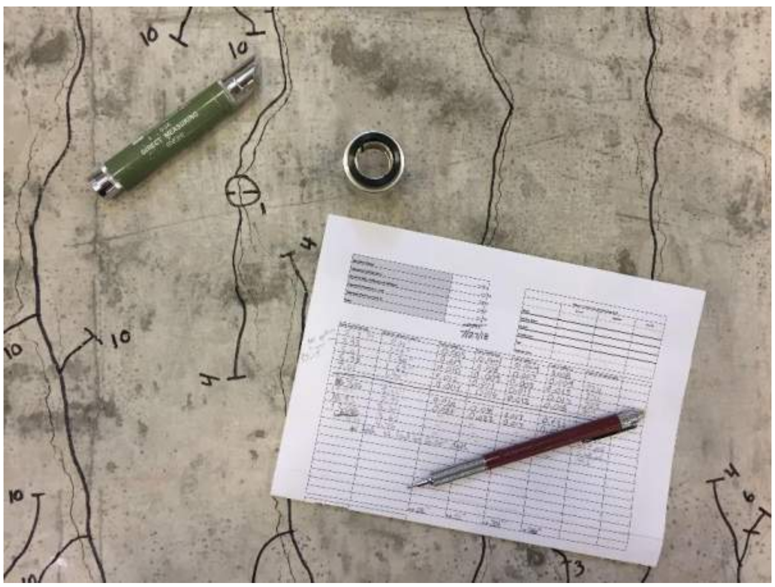

Figure 3.30: Crack Width Microscope and Mapping Process

3.6.2.4 Testing Documentation and Media

A Vishay Precision Group, Inc. System 7000 Digital Data System was selected to collect data from the testing equipment using StrainSmart Version 5.3 (Figure 3.31). The data acquisition software recorded test data at a time interval of 0.1 seconds for all specimens in Series V.

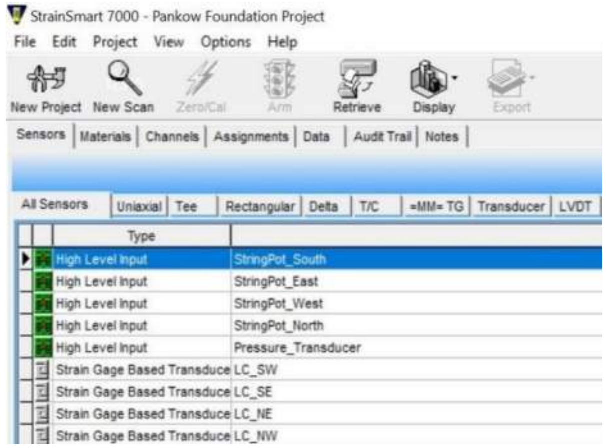

a) System 7000 **b) StrainSmart Version 5.3 Layout**

Figure 3.31: StrainSmart Data Acquisition

A GoPro, Inc. Hero 5 video recording camera was mounted to a nearby steel column and used to capture all load steps during testing, as well as final failure of each specimen. By using a wide lens, most of the specimen was captured; however, a focus was placed on the splice region. Photographs were taken of each specimen before, during, and after failure. During testing, photos were taken to document changes in the splice region, propagation of established cracks, formation of new cracks, and deflections along the member.

3.6.3 General Testing Procedure

Before applying load to each of the specimens, the top surface was inspected for any minor cracks caused by flipping or transporting the specimen to the test setup. No perceptible cracks were found on any of the four specimens. The initial pressure reading was recorded at the beginning of each test. Load was applied to the slabs in 1-kip intervals up to failure of the specimen.

Cracks were mapped (Figure 3.32) and measured in 1-kip increments across the tension face and sides of each specimen. This process was repeated throughout testing until failure was reached. As-built dimensions were measured after failure within the splice region to document cover and bar spacing and are provided for all slabs in Appendix F.

Figure 3.32: General Slab Test – Crack Mapping (S-80-5)

3.7 Results Introduction

The experimental results of each test in Series V are presented to evaluate the effect of splice length on bond strength. Series V consisted of four slab specimens, each tested in four-point bending. The test results are summarized in Table 3.8. Two specimens experienced failure of the splice while two specimens failed in flexure at a support.

3.8 Experimental Results

The applied load at failure, P_{ult}, was determined by doubling the most accurate of the four load cell readings for each slab. Prior to loading, approximately 1 kip was applied to each end of Specimens S-40-5, S-60-5, and S-80-5 from direct bearing of the crosshead assembly. This initial loading is believed to have caused increased readings for various load cells, with some specimens exhibiting a difference between the north and south end loads of up to 20%. The difference in recorded end load may also be attributed to excessive concrete cracking and rotation of the test frame. The ultimate moment at failure, M_{ult}, was calculated by multiplying the failure load, P_{ult}, by the shear span for each slab. The increased moment due to self-weight was neglected.

The stress achieved in the longitudinal reinforcing bars, f_b, was calculated using moment-curvature analysis and the failure load reached for each slab. All cross-sectional dimensions in this calculation were design values. The tensile capacity of the concrete was neglected. The stress-strain relationship for the longitudinal steel was determined from experimental lab testing of the material, while the stress-strain relationship for concrete was represented using the Hognestad (1951) model.

Table 3.8: Slab Test Results

Series	Specimen	Test Age (days)	f_c (psi)	l_s (in.)	P_{ult} (kip)	M_{ult} (ft-kip)	f_b (ksi)	Failure Mode
V	S-40-5	44	6240	25	11.1	44.6	97.9[1]	Splitting
	S-60-5	40	6200	37.5	13.6	54.4	121.0[2]	Splitting
	S-80-5	38	6180	50	13.4	53.6	119.2[2]	Flexure
	S-100-5	102	6490	62.5	13.2	52.8	117.0[2]	Flexure

[1] *Beyond linear-elastic limit (84 ksi)*
[2] *Beyond yield strength (107 ksi)*

As included in Table 3.8, the test age was recorded for all specimens with test dates ranging from 38 days to 102 days. The variation in concrete strength, f_c, between Day 28 and Day 44 of testing was negligible for this test series. Compressive strength data after Day 44 was not obtained; therefore, the S-100-5 slab specimen compressive strength was conservatively approximated. The strength of this specimen, however, was not considered vital to the analysis as the failure mode was flexure.

3.8.1 Self-Weight

Although the slab specimens are subjected to a loading configuration that creates constant moment between supports, self-weight provides for moment variation. When self-weight is acknowledged, moment across the splice increases slightly in the slab specimens. The moment diagrams for loading and self-weight are shown in Figure 3.33 and Figure 3.34, respectively. In general, the maximum moment which occurs at the support is calculated by Equation 3-1:

$$M_{ult\ (slab)} = M_{load} + M_{Self-Weight\ (slab)} \tag{3-1}$$

where:

L_V = $4\ ft$

M_{load} = $(L_V)(P_{ult})$

P_{ult} = *applied load at failure (kip)*

For all slab specimens, the maximum moment at the support due to self-weight is calculated by Equation 3-2:

$$M_{Self-Weight\ (slab)} = \frac{{L_s}^2 w_s}{2} \tag{3-2}$$

where:

L_s = *length of slab from support to closest end,* 6 *ft*

w_s = *slab self-weight*

$$= \left(\frac{0.150\ kips}{ft^3}\right)(24\ in.)(6\ in.)\left(\frac{1\ ft^2}{144\ in.^2}\right) = 0.15\frac{k}{ft}$$

Therefore:

$$M_{ult\ (slab)} = (4\ ft)(P_{ult}) + \frac{(6ft)^2\left(0.15\frac{k}{ft}\right)}{2}$$

$$M_{ult\ (slab)} = (4\ ft)(P_{ult}) + 2.7\ ft\text{-}k$$

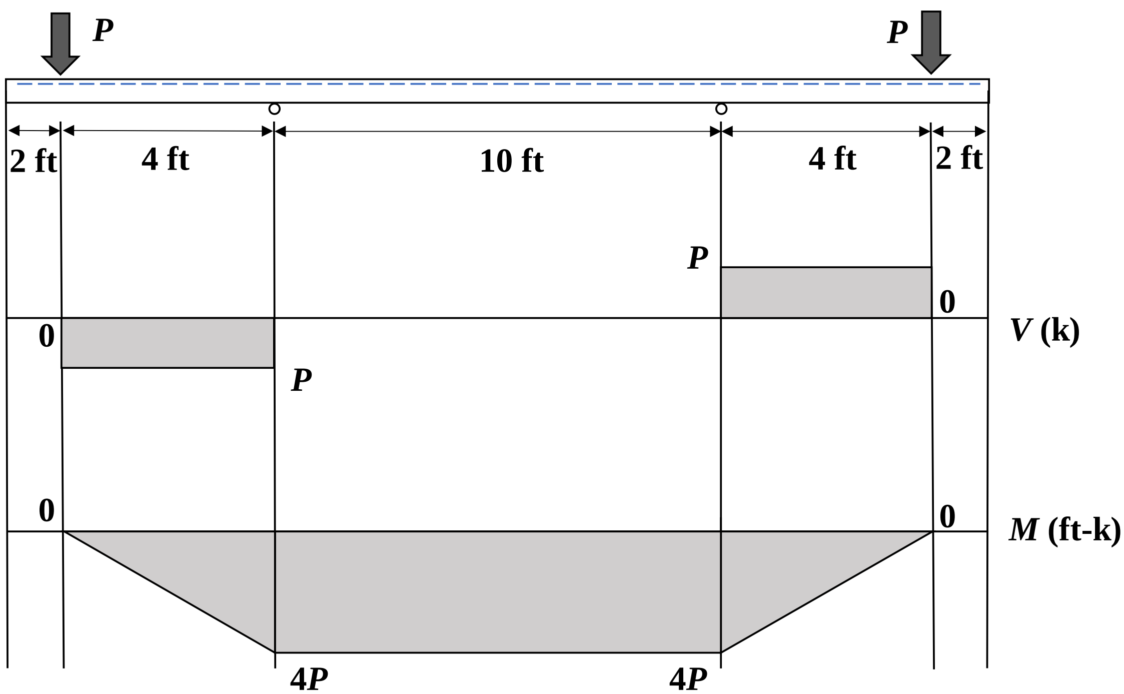

Figure 3.33: Shear and Moment Diagrams for Slabs from Loading

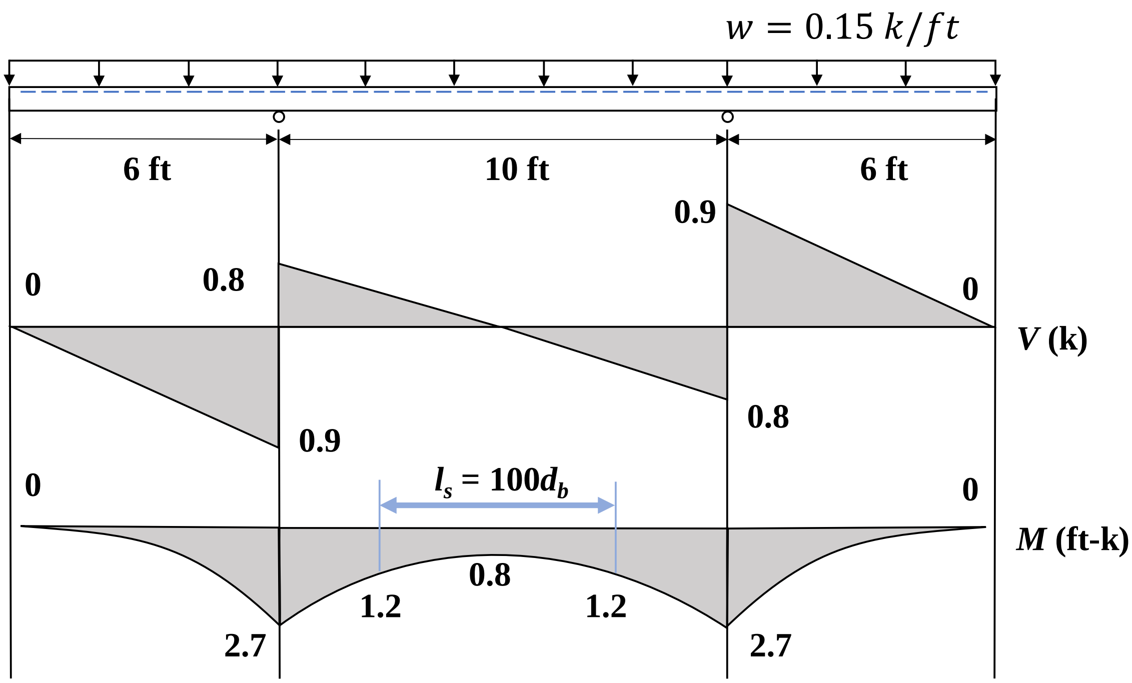

Figure 3.34: Shear and Moment Diagrams for Slab Self-Weight

Because the constant negative moment from the applied load occurs between the supports while the negative moment due to the slab's self-weight peaks at each support, the ultimate moment occurs near the supports. The largest variation in moment across the splice is 0.4 ft-k for the 100d_b specimen resulting from an additional negative moment of 0.8 ft-k in the center and 1.2 ft-k at the ends of the splice.

Considering the applied loads, the self-weight acts as a small percentage of the resisted moment. The greatest influence occurs in the S-40-5 slab, where a 6% increase in ultimate moment occurs due to self-weight. This difference is considered negligible; therefore, the self-weight contribution is conservatively ignored.

3.8.2 Specimen Observations

Cracking moment occurred at approximately 1.8 kips of applied load for all slabs. Large deflections and an abundance of cracking were observed in all slab specimens as shown in Figure 3.35 and Figure 3.36, respectively. The hydraulic ram for Specimens S-80-5 and S-100-5 reached the maximum stroke while loading. To continue testing for the S-80-5 specimen, load was entirely removed from the slab, and the crossbeam was lowered before applying load again until failure was reached. For the S-100-5 specimen, the test was concluded early based on the load reached and considering the results of S-80-5.

Figure 3.35: Slab Deformation during Testing (S-100-5)

Figure 3.36: Typical Flexural Cracking – West Side and Tension Face (S-80-5)

3.9 Load-Deflection Response

Load-deflection behavior was monitored for all slab specimens. Although each curve was unique, the underlying mechanics and regions within the responses were similar. Before reaching the cracking moment for each slab, the stiffness of the specimen was primarily governed by the concrete as shown in Region 1 of Figure 3.37. Once cracking occurred, the stiffness of the member immediately decreased as evidenced in Region 2. The overall response in this region is approximately linear due to the elastic response of the steel. The final region (Region 3) demonstrates yielding of the longitudinal bars. Region 3 only occurred in specimens where the splice strength exceeded the yield strength of the steel. This region provides the lowest member stiffness observed during testing.

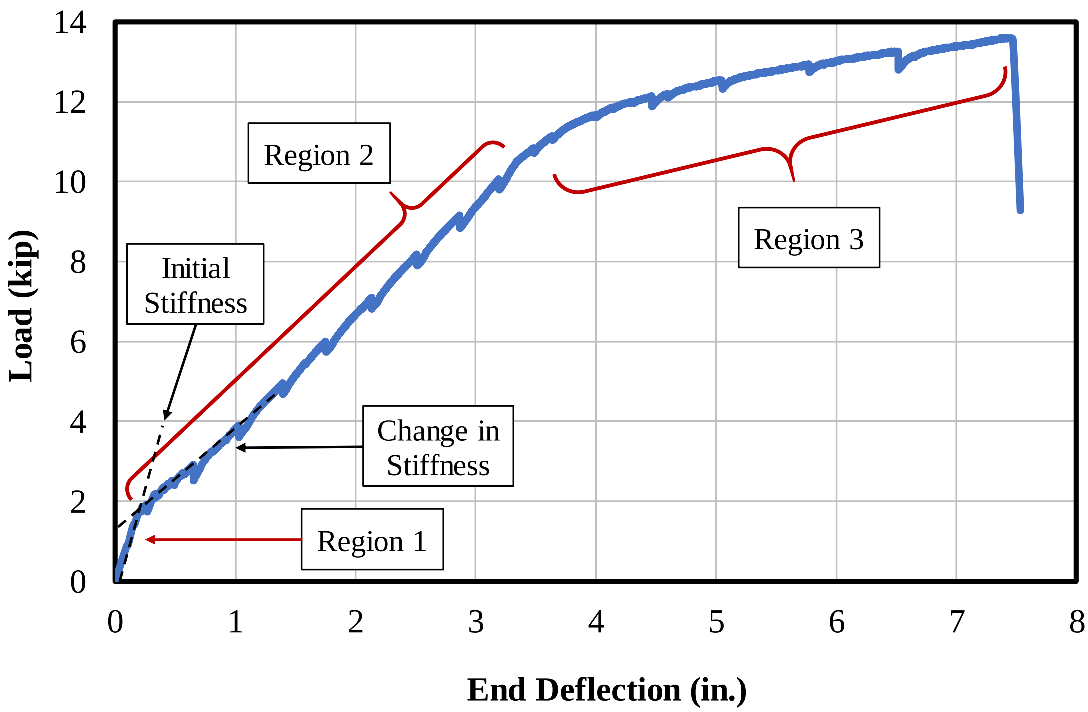

Figure 3.37: General Load-Deflection Behavior (S-60-5)

As shown in Figure 3.38, Specimen S-40-5 did not yield but did begin to exhibit inelastic behavior. Yielding occurred for all other slabs. While S-60-5 provided significant inelastic response, it ultimately failed in splitting. Specimen S-80-5 and S-100-5 failed in flexure initiated by crushing of the concrete. The load-deflection response for all specimens in Series V is provided in Appendix G. Note that the slight increase in cracked stiffness of the specimens (Region 2) may be attributed to the increase in steel within the cross-section as the splice length increased.

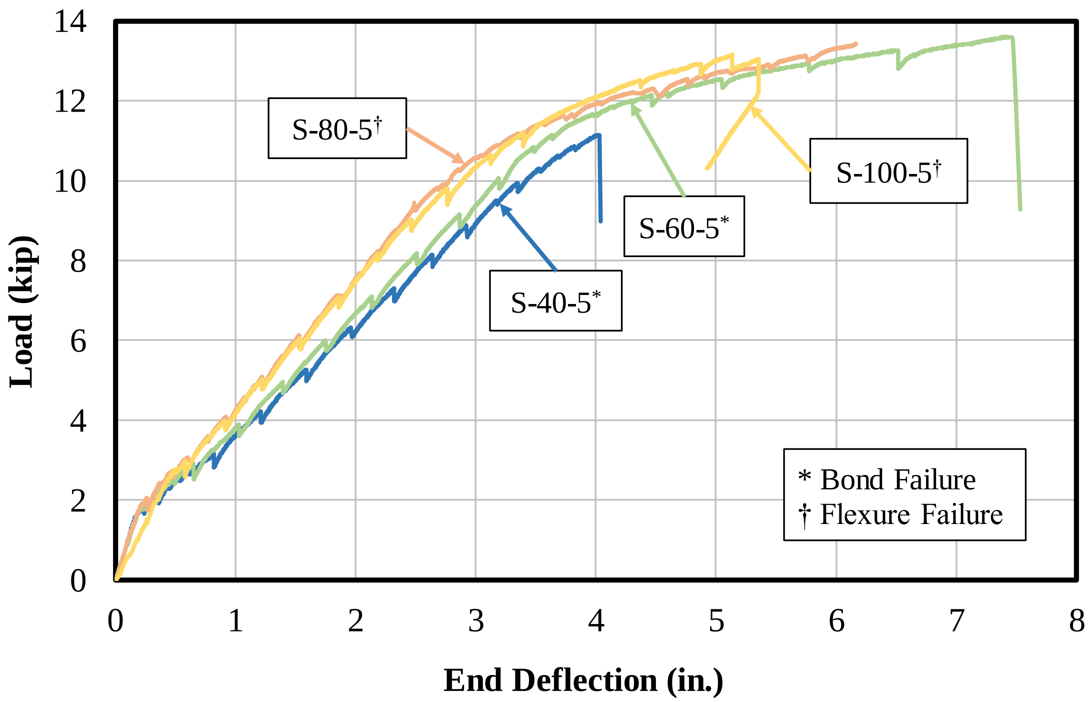

Figure 3.38: Series V Load-Deflection Response

3.10 Concrete Cracking Behavior

Four cracks were selected in the constant moment region, two past the north end of the splice region and two past the south end. Crack widths were monitored at each load step and recorded. Throughout testing within the linear range of the reinforcing steel, crack widths consistently increased linearly. Average and maximum crack width measurements for all slabs in Series V are provided in Figure 3.39. All transverse cracks initiated at a spacing of approximately 1 in. to 4 in. along the entire length of the slab, including throughout the splice region. Fewer new cracks formed across the full width of the slab at each additional load step after cracking moment was reached; however, any established cracks experienced large amounts of branching in all directions (Figure 3.40). Transverse flexural cracking tended to initiate in the middle of the slab at multiple locations outside of the splice region and spread toward the edges as load increased. The region above both supports appeared to have a slightly smaller spacing of cracks along the tension face. The growth pattern of flexural crack widths as bar stress increased is provided in Appendix H for all slabs.

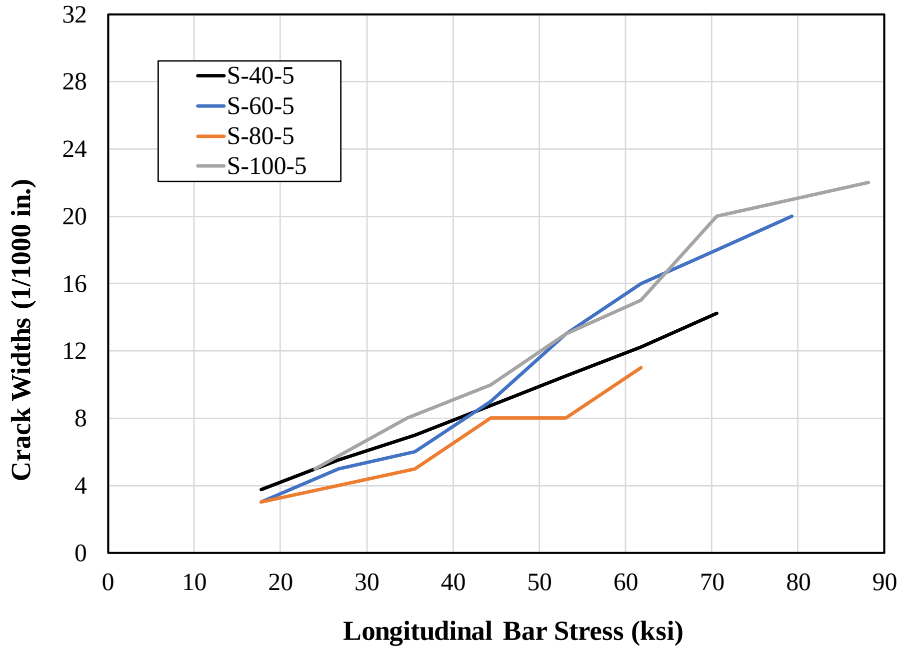

a) Average Crack Widths

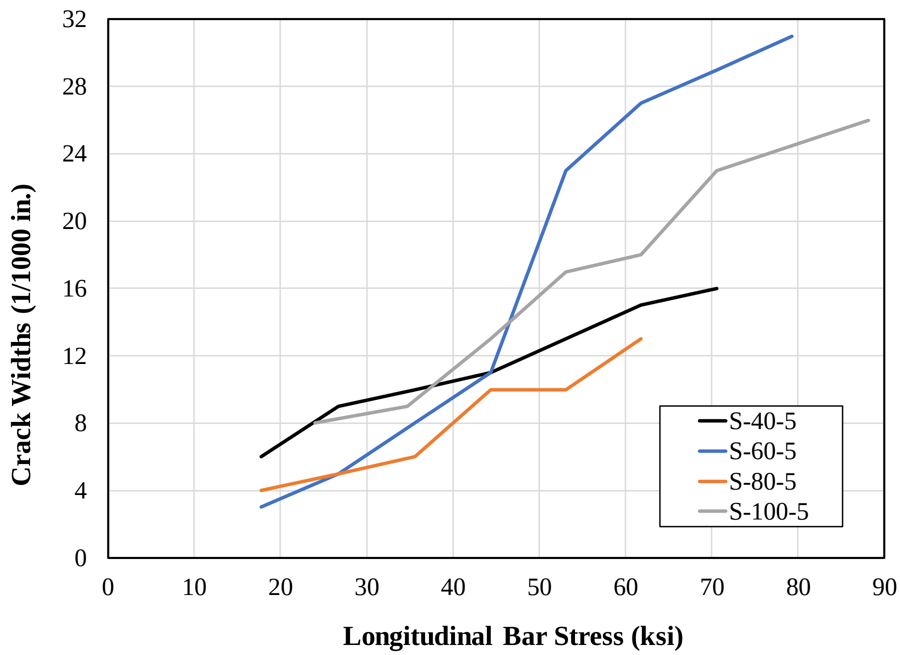

b) Maximum Crack Widths

Figure 3.39: Series V Crack Width Measurements

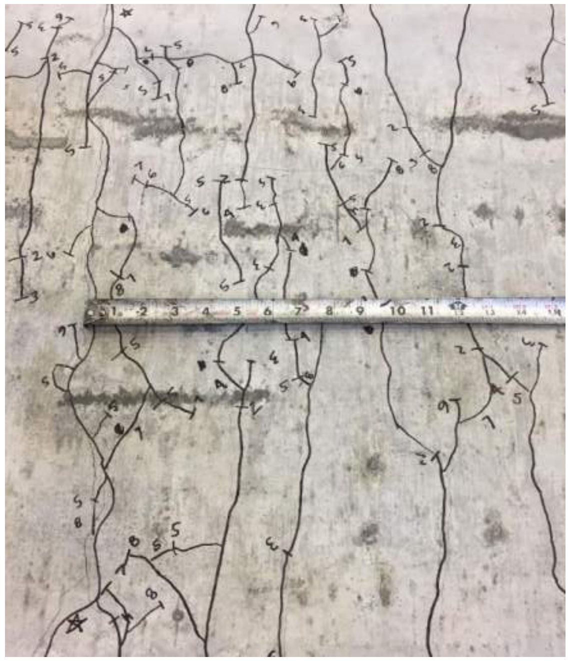

Figure 3.40: Observed Crack Branching Near End of Splice (S-60-5)

Side cracking propagated down along the depth of the slabs at a slow rate, often starting at a depth of 2 in. from the tension face and reaching a maximum depth of approximately 4 in. from the tension face before failure. This depth was indicative of the neutral axis of the cross-section. An example of the propagation of this side cracking at approximately half the full load capacity is shown in Figure 3.41 for Specimen S-100-5.

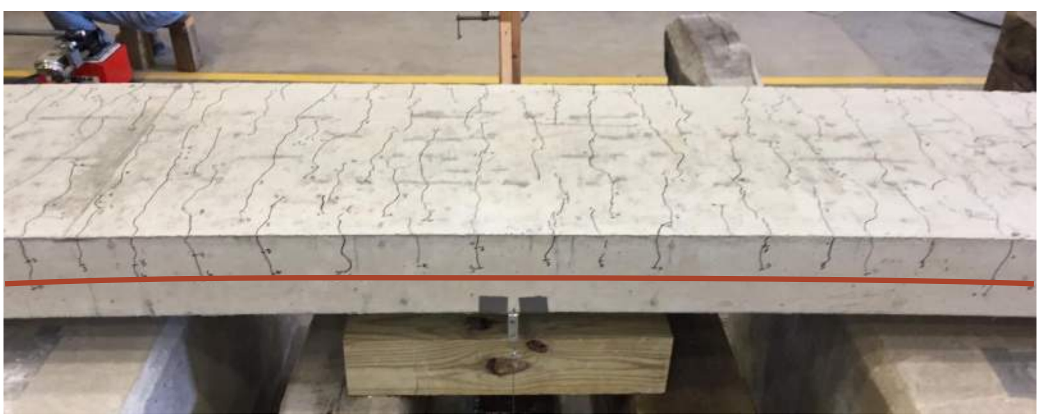

Figure 3.41: Side Crack Propagation (S-100-5)

Branching cracks were less present within the shear spans of each slab. Spacing between transverse flexural cracks in this region was noticeably larger than in the constant moment region and is shown in Figure 3.42. The presence of diagonal cracking across the member depth in this region was minimal due to the small overall depth of the slab specimens.

Figure 3.42: Post-Failure Shear Span Cracking (S-60-5)

Longitudinal cracking occurred above each of the four lap splices as shown in Figure 3.43 and was present in all slab specimens, independent of the failure mode. Longitudinal cracking initiated near splice ends on the tension face after approximately 3 kips were applied to each slab. As load increased, longitudinal cracks slowly propagated toward the middle of the specimen. In the specimens with shorter splices, crack branching occurred near the splice ends and seemed to be localized closer to the sides of the slabs. It was observed that slabs experiencing a side-splitting failure had a greater concentration of longitudinal cracking near the edges and sides before failure.

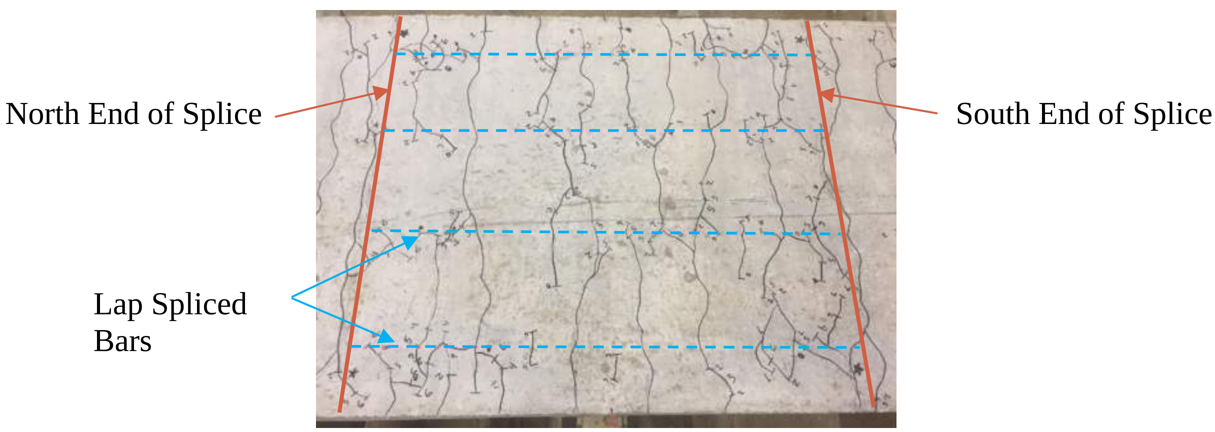

(a) S-40-5

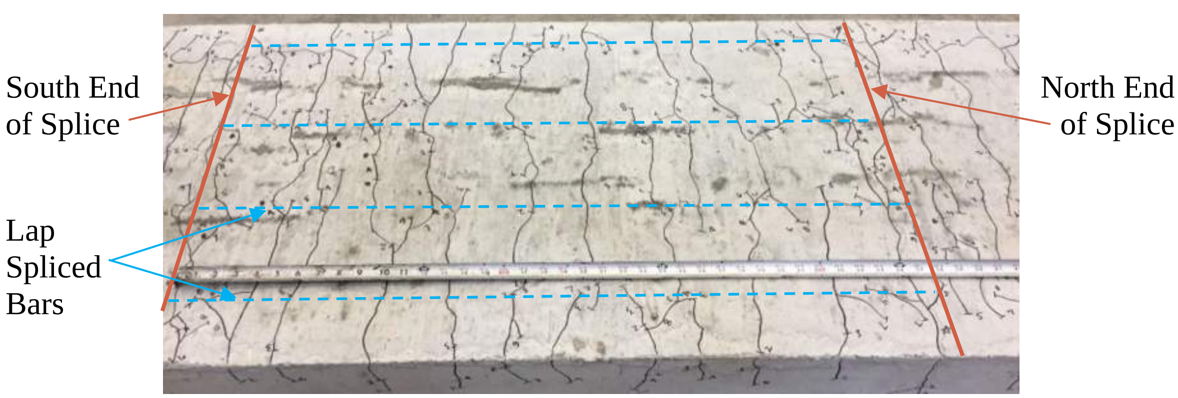

(b) S-60-5

Figure 3.43: Splice Region Crack Observations

3.11 <u>Failure</u>

As splice length was increased from 40d_b to 100d_b in Series V, the failure mode changed. Specimens S-40-5 and S-60-5 failed in splitting of the bottom and side cover in the splice region. Specimens S-80-5 and S-100-5 developed sufficient bond strength along the splice to transition the failure from bond to flexure.

3.11.1 Bond Failure

Longitudinal cracking was present above all four splices. In both slabs (S-40-5 and S-60-5), longitudinal cracking was present along the east, west, and top faces of the specimens, initiating at the ends of the splice and propagating toward the middle. Upon failure, the bottom cover remained relatively intact over the inner two splices while the side cover spalled off entirely. Due to the small bottom cover, concrete spalling was not extensive.

Based on analysis of the maximum longitudinal bar stress achieved, Specimen S-40-5 did not reach yielding of the bars before splice failure. The yield strength of the longitudinal reinforcement, however, was exceeded for the S-60-5 slab. A decrease in slope in the load-deflection plot confirms this behavior with a larger increase in deformation occurring as the applied load increases. Table 3.9 provides the maximum results for each specimen that failed in bond at the conclusion of testing. The load-deflection response for these specimens is provided in Figure 3.44. Load-deflection plots for all slabs are provided in Appendix G.

Table 3.9: Test Results for Series V Bond Failures

Specimen	Load (kip)	Avg. End Deflection (in.)	Avg. Midspan Deflection (in.)	Bar Stress (ksi)
S-40-5	11.1	4.1	2.2	97.9
S-60-5	13.6	7.5	3.7	121.0

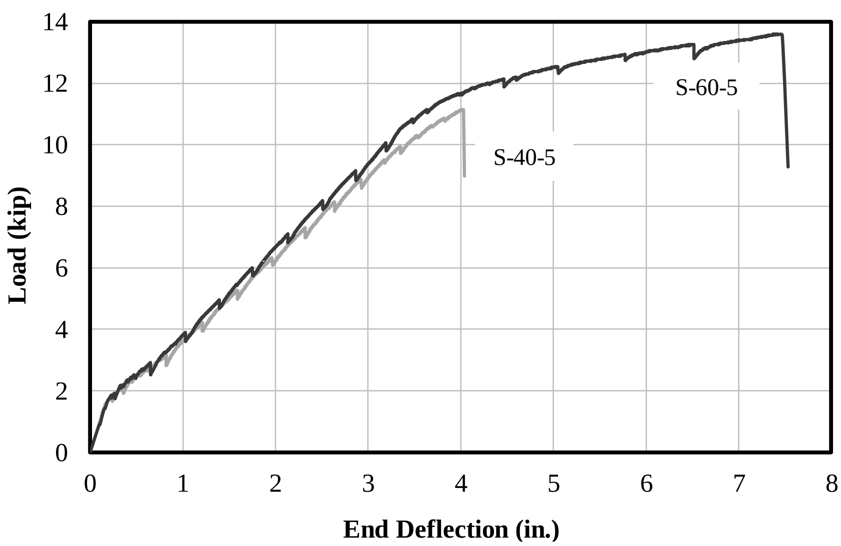

Figure 3.44: Load-Deflection Response of Series V Bond Failures

Failure of S-40-5 occurred in a single event where all splices failed simultaneously while the side cover completely spalled. The bottom cover remained slightly intact for the two inner splices but heavy longitudinal cracking occurred on the tension face as shown in Figure 3.45.

Figure 3.45: S-40-5 Face- and Side-Splitting Failure

Failure of S-60-5 was not a single event. Failures of individual splices occurred twice while loading the slab. The west splice failed first, exhibiting large amounts of cracking while load continued to be carried (Figure 3.46). As more load was applied, the east splice failed and large amounts of cracking were present (Figure 3.47). In both cases, load was maintained and no spalling was observed. Final failure occurred when both inner splices failed and the side cover spalled off entirely (Figure 3.48). It should be noted that a similar failure progression was observed by Seliem et al. (2009) while conducting bond strength testing on MMFX steel in splice specimens.

a) Before

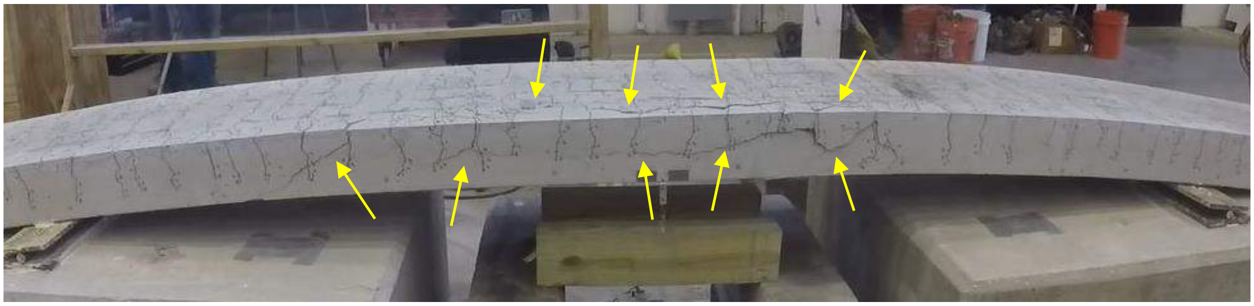

b) After

Figure 3.46: S-60-5 Partial Failure 1

a) Before

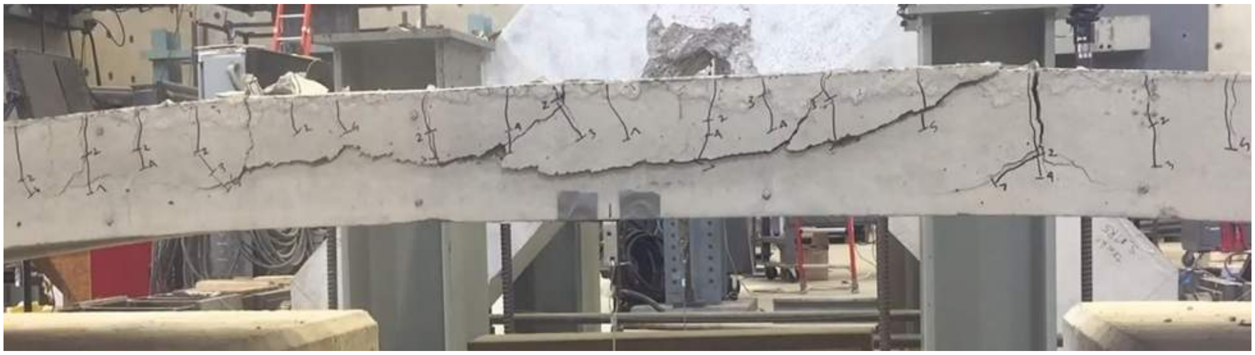

b) After

Figure 3.47: S-60-5 Partial Failure 2

Figure 3.48: S-60-5 Final Failure

3.11.2 Flexural Failure

When splice length was sufficient in developing the reinforcement, a flexural failure was observed. Longitudinal and transverse cracking was observed along the tension face and sides, but a splitting failure was precluded. Final bar stresses indicate that the reinforcing steel exceeded the yield capacity for Specimens S-80-5 and S-100-5.

Table 3.10 provides the maximum results for each specimen that failed in flexure. Load-deflection response for these specimens is provided in Figure 3.49. Note that for Specimen S-100-5, the initial high stiffness region is slightly lower than that of Specimen S-80-5. This may be attributed to possible minor cracking of the concrete prior to testing from flipping and transporting.

Table 3.10: Test Results for Series V Flexural Failures

Specimen	Load (kip)	Avg. End Deflection (in.)	Avg. Midspan Deflection (in.)	Bar Stress (ksi)
S-80-5	13.4	6.2	2.9	119.2
S-100-5	13.2	5.4	2.2	117.0

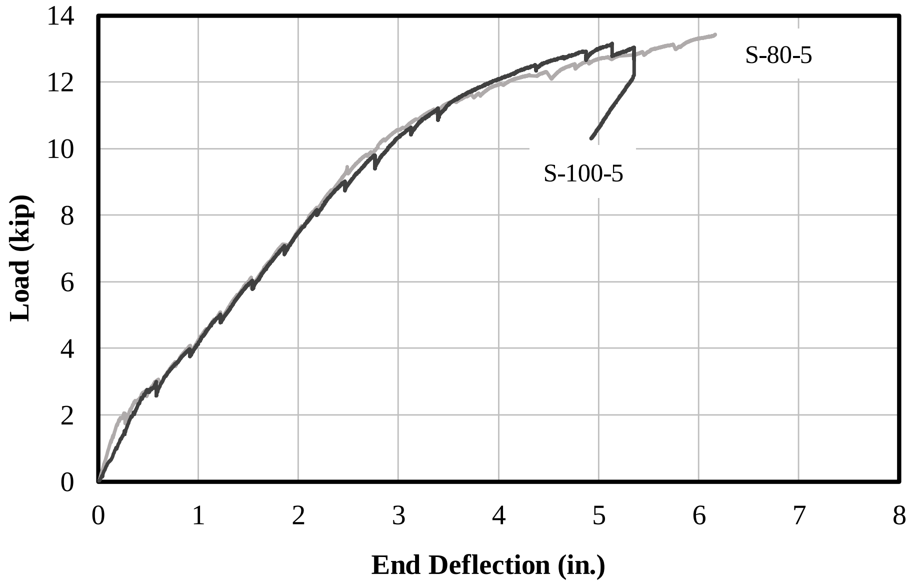

Figure 3.49: Load-Deflection Response of Series V Flexural Failures

Specimen S-80-5 experienced a flexural failure near the north support as evidenced by crushing of the concrete along the compression face of the member (Figure 3.50). As the applied load increased, crushing became more apparent (Figure 3.51).

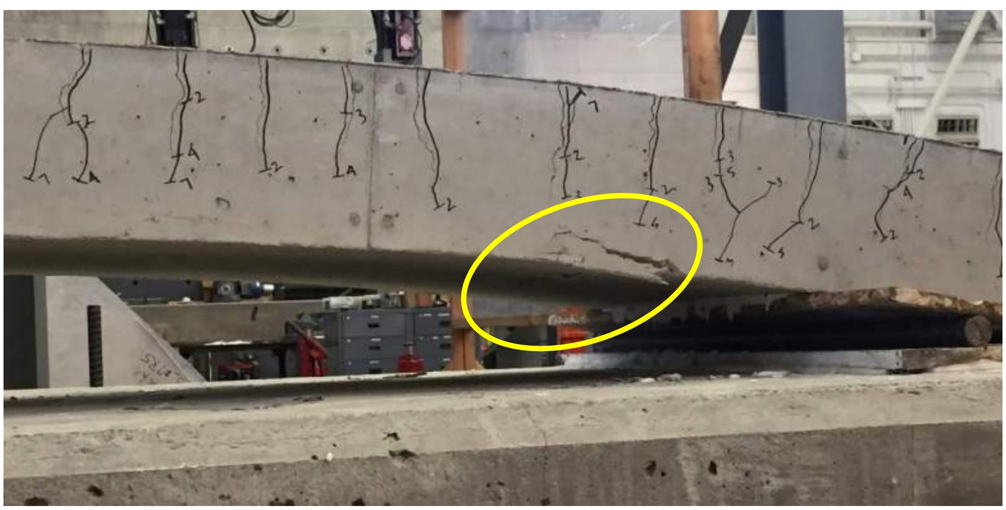

Figure 3.50: Initiation of S-80-5 Failure – East Elevation

Figure 3.51: Final S-80-5 Failure – East Elevation

Load was applied to Specimen S-100-5 until it nearly matched the failure load of Specimen S-80-5. The bar stress achieved in Specimen S-100-5 was nearly equal to the bar stress achieved in Specimen S-80-5, however, failure did not occur. Because the maximum stroke of the loading rams was reached (Figure 3.52), testing was concluded before a flexural failure was observed at the supports. While a flexural failure had not initiated at the supports, it was previously observed in the 50-in. lap splice specimen (S-80-5) that sufficient development length had been provided to prevent a splitting failure.

Figure 3.52: S-100-5 End of Testing

CHAPTER 4. SERIES VI-VII: BEAM TESTS

4.1 Introduction

The objective of Series VI and VII was to investigate the bond strength of high-strength steel reinforcement. Selected variables included splice length, concrete compressive strength, high-strength steels, and transverse reinforcement location. All four parameters were investigated in Series VI by testing eight (8) beams, while the influence of splice length and transverse reinforcement location on bond strength was further investigated in Series VII by testing four (4) additional beams. The program for planning, preparing, and conducting these tests is discussed in this chapter.

4.2 Specimen Selection

4.2.1 Beam Design

For consistency, all specimens tested in Series VI and VII were selected primarily based on specimens designed in Series I through IV. Beams with splices confined by transverse reinforcing stirrups are called confined specimens, while beams without transverse reinforcement are called unconfined specimens. Series VI consisted of three confined beams and five unconfined beams, while Series VII contained four confined beams.

Cross-section dimensions are the same for all confined (Figure 4.1(a)) and unconfined (Figure 4.1 (b)) beams. Specimen height was selected to be 20 in. No. 8 bars were selected to be the primary longitudinal reinforcement. The confined specimen was designed first using the minimum bottom cover of 1-1/2 in. allowed for No. 8 bars in ACI 318-14 (Table 20.6.1.3.1). For confinement, No. 3 Grade 60 stirrups were selected. The effective depth from the compression face was therefore calculated to be 17-5/8 in. To maintain this effective depth parameter throughout the unconfined beam specimens and maintain the same cover to the longitudinal reinforcement, a bottom cover of 1-7/8 in. was required for the unconfined cross-section. No. 3 longitudinal bars were included at a distance of 1-7/8 in. from the compression face to aid in steel cage construction, stirrup alignment, and failure containment after testing.

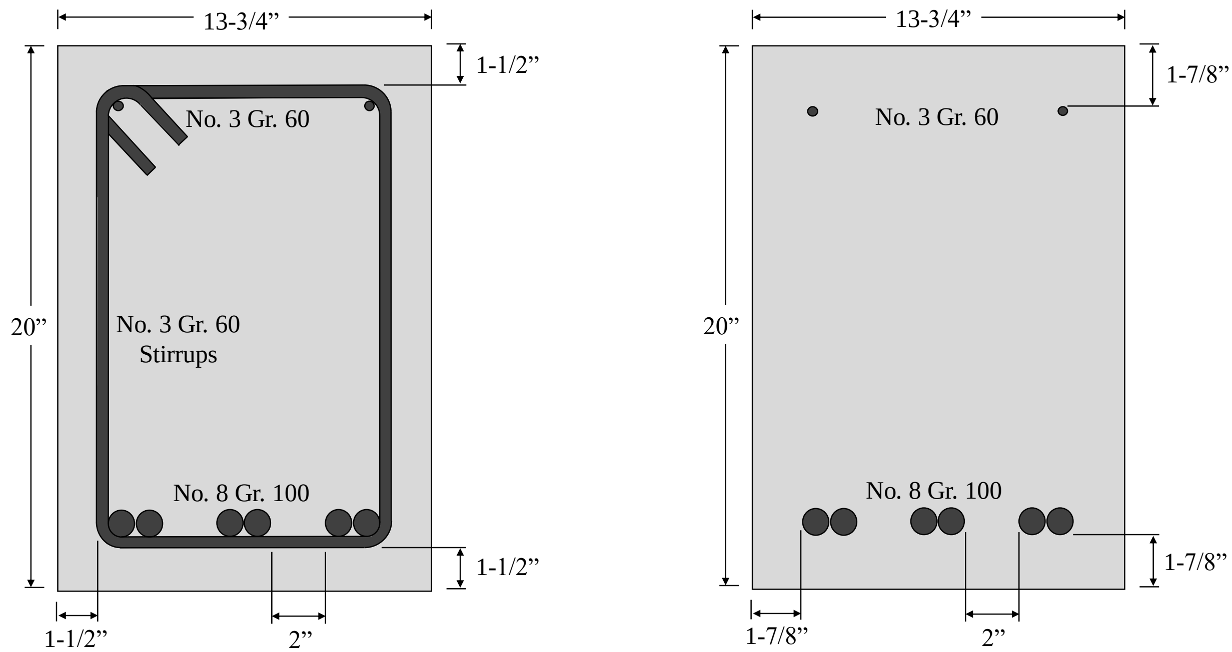

a) Confined Specimen **b) Unconfined Specimen**

Figure 4.1: Typical Beam Cross-Sections

Three (3) No. 8 Grade 100 longitudinal bars were spliced over a variable length with the clear bar spacing between splices fixed at 2 in. Because of the presence of transverse steel in confined beams, the clear side cover was selected to be 1-1/2 in. to achieve the same side cover of 1-7/8 in. over the longitudinal bars. The resulting overall width was 13-3/4 in. for the confined and unconfined specimens. A total beam length of 26 ft was selected for Series I through IV and implemented in Series VI and VII for specimen consistency.

The unconfined beam specimens were designed with various splice lengths, concrete strengths, and types of high-strength steel. Figure 4.2 discusses the general labeling convention for the unconfined specimens in Series VI.

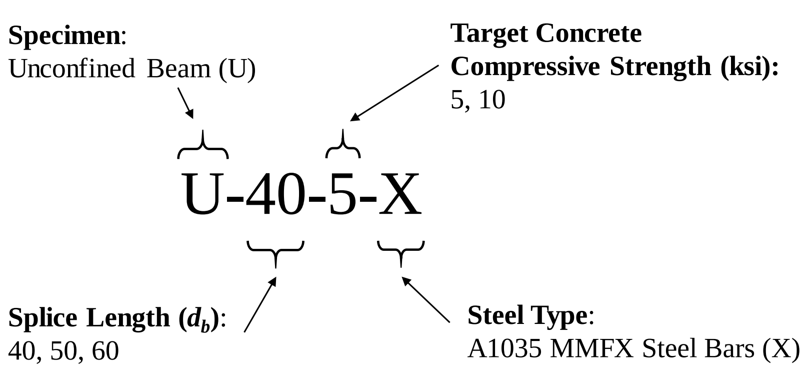

Figure 4.2: Unconfined Specimen Identification Label

For confined beams, a nominal confinement pressure was assigned to give an indication of stirrup spacing based on ACI 318-14. The nominal pressure was also implemented in Series II through IV of this testing program:

$$A_{v,min} = 50\frac{b_w s}{f_{yt}} \tag{4-1}$$

where:

50	=	*coefficient; represents pressure developed by transverse reinforcement (psi)*
$A_{v,min}$	=	*minimum area of shear reinforcement within spacing s (in.^{2})*
b_w	=	*beam width (in.)*
f_{yt}	=	*specified yield strength of transverse reinforcement (psi)*
s	=	*center-to-center spacing of transverse reinforcement (in.)*

The coefficient 50 represents the tensile-resisting pressure produced by the presence of transverse reinforcement. By rearranging Equation 4-1 to solve for the transverse reinforcement spacing s, various nominal pressures (p_c) can be substituted into Equation 4-1. Table 4.1 provides a summary of the nominal pressures and stirrup spacings selected for Series VI and VII. The identification label for confined beams is expanded to include this information in Figure 4.3.

Table 4.1: Nominal Confinement Pressure and Spacing

Nominal Pressure, p_c (psi)	**Bar Size (No.)**	**$A_{v,min} = A_t N_l$ (in.^{2})**	**f_{yt} (ksi)**	**b_w (in.)**	**$s = \frac{A_{v,min} f_{yt}}{p_c b_w}$ (in.)**	**Spacing used (in.)**
25	3	0.22	60	13.75	38.4	38
50	3	0.22	60	13.75	19.2	19
150	3	0.22	60	13.75	6.4	6.375
200	3	0.22	60	13.75	4.8	4.75

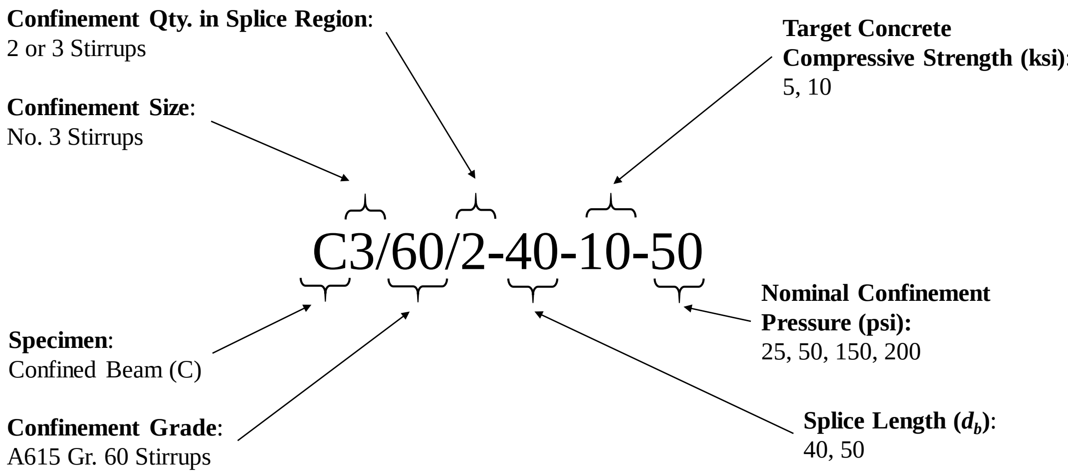

Figure 4.3: Confined Specimen Identification Label

4.2.2 Beam Dimensions

Splice test specimens from previous research programs have been tested in four-point bending to create a tension region at the location of the spliced bars. The four-point bending test setup requires two points of applied loading near the ends of the specimen and two points of support located a distance away from the applied loads (shear span). Due to the 24-in. spacing of the Bowen Laboratory strong floor grid and the need for a symmetric test setup, even dimensions were selected for all spacings between components of the test setup.

Splice length testing requirements of $120d_b$ from Series I through IV testing directly influenced the specimen length for Series VI and VII. A constant moment region of 16 ft (L_M) was maintained between supports for all beams. This allowed all lap splices (L_S) to be located entirely within this region. The length of the shear region was selected to be 4 ft (L_V) away from the supports. To prevent the possibility of a shear failure during testing, twelve No. 4 Grade 60 stirrups were spaced at 4-1/4 in. between the support and the ends of the beam. A 1 ft overhang (L_O) was included to ensure anchorage of the reinforcement. Overall, the selected dimensions produced a total length of 26 ft (L_T) for all confined and unconfined beam specimens. The beam test configuration is shown in Figure 4.4.

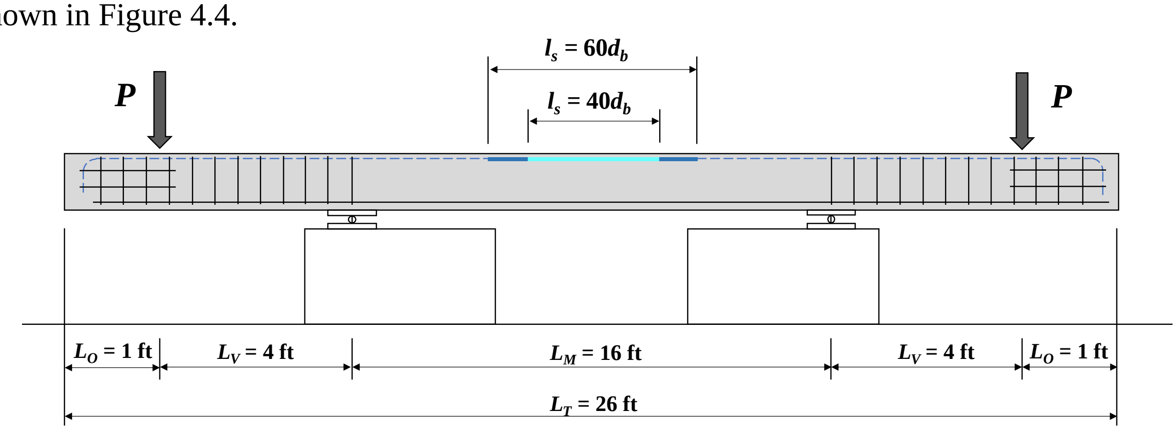

Figure 4.4: Typical Beam Test Specimen

4.2.3 Beam Testing Matrix

Table 4.2 and Table 4.3 provide the testing matrix for the unconfined and confined specimens, respectively. The splice length, concrete strength, and amount of confinement were investigated while the bar size, bar spacing, and concrete cover remained constant for each matrix. All stirrups placed within the constant moment region of the confined specimens were centered at midspan of the beam. Therefore, all beams with an even number of stirrups within the constant moment region did not have a stirrup at midspan. The full stirrup configurations for all confined beams in Series VI and VII can be found in Figure 4.5 and Figure 4.6, respectively.

Table 4.2: Unconfined Beam Testing Matrix

Series	Specimen ID	Splice Length (l_s)		Longitudinal Bar Size (No.)	Target Concrete Strength (f'_c)	c_{si}	c_{so}	c_b
		d_b	in.		ksi	in.	in.	in.
VI	U-40-10	40	40	8	10	1	1.875	1.875
	U-60-10	60	60	8	10	1	1.875	1.875
	U-40-5-X	40	40	8	5	1	1.875	1.875
	U-60-5-X	60	60	8	5	1	1.875	1.875
	U-50-5	50	50	8	5	1	1.875	1.875

Table 4.3: Confined Beam Testing Matrix

Series	Specimen ID	Splice Length (l_s)		Long. Bar Size (No.)	Target Concrete Strength (f'_c)	c_{si}	c_{so}	c_b	Nominal Pressure (p_c)	Stirrup Spacing[1] (s)	Total No. Stirrups		
		d_b	in.		ksi	in.	in.	in.	psi	in.	Splice Region	Constant Moment Region[2]	Shear Regions
VI	C3/60/2-40-10-50	40	40	8	10	1	1.5	1.5	50	19	2	10	24
	C3/60/3-40-10-50	40	40	8	10	1	1.5	1.5	50	19	3	9	24
	C3/60/2-40-10-25	40	40	8	10	1	1.5	1.5	25	38	2	4	24
VII	C3/60-40-5-150	40	40	8	5	1	1.5	1.5	150	6.375	6	12	24
	C3/60-40-5-200	40	40	8	5	1	1.5	1.5	200	4.75	8	14	24
	C3/60-50-5-150	50	50	8	5	1	1.5	1.5	150	6.375	8	14	24
	C3/60-50-5-200	50	50	8	5	1	1.5	1.5	200	4.75	10	16	24

[1] *Spacing for stirrups within constant moment region.*
[2] *Stirrups within the splice region.*

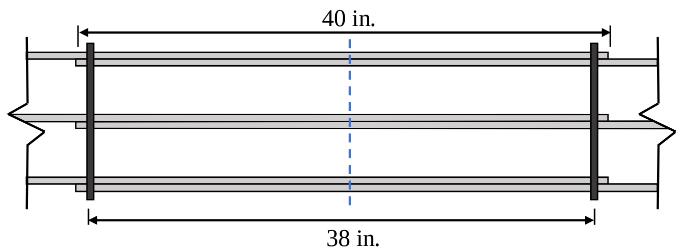

a) C3/60/2-40-10-25

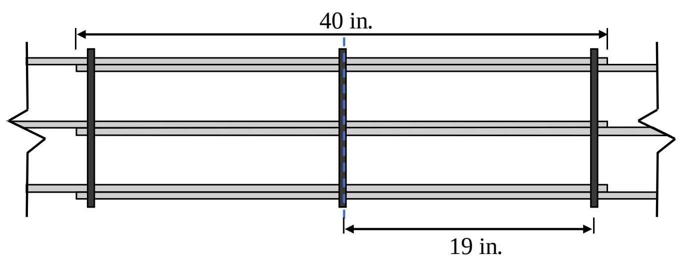

b) C3/60/3-40-10-50

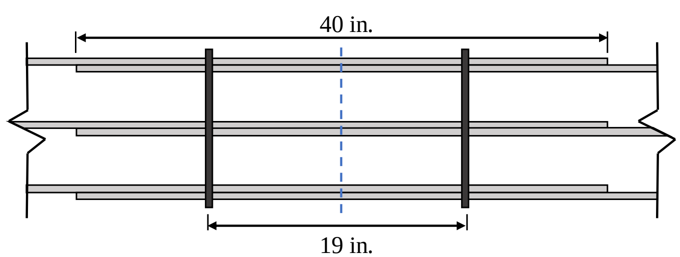

c) C3/60/2-40-10-50

Figure 4.5: Series VI Stirrup Configurations

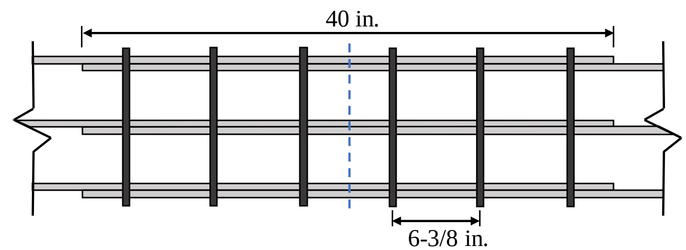

a) C3/60-40-5-150

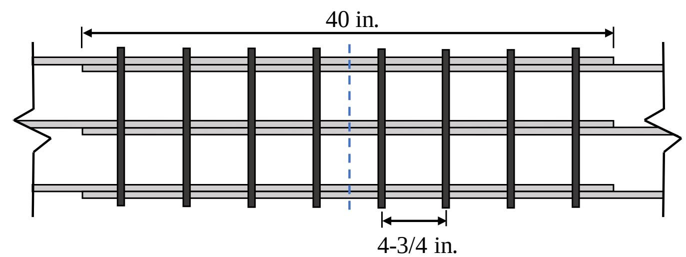

b) C3/60-40-5-200

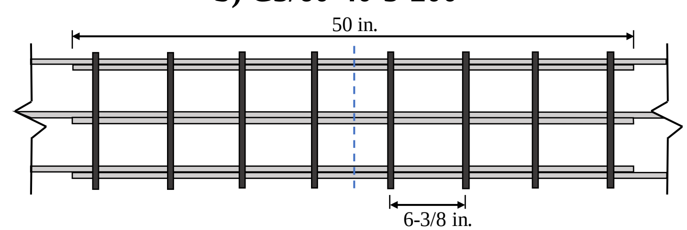

c) C3/60-50-5-150

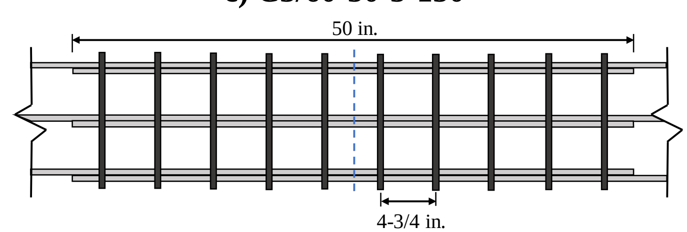

d) C3/60-50-5-200

Figure 4.6: Series VII Stirrup Configurations

4.3 Materials

4.3.1 Concrete

Concrete for Series VI and VII was provided by Irving Materials, Inc. (IMI). All test specimens were constructed and cast in the Bowen Laboratory for Large-Scale Civil Engineering Research in West Lafayette, Indiana.

The concrete mixture design selected for three specimens in Series VI and all of Series VII was consistent with Series I through IV of this project. The concrete had a target compressive strength of 5000 psi and a target slump of 6 in. A breakdown of general casting information for both series, indicating the division of specimens by truck, is given in Table 4.4. The mix design for the normal-strength mix is provided in Table 4.5 with the batched quantities in Series VI and VII.

Table 4.4: General Beam Casting Information

Casting Quantities	Series VI			Series VII
Cast Date	9/18/2018			12/18/2018
Truck No.	1	2	3	1
Load Size (yd^3)	7	5	7	8.5
Specimens	U-60-10 C3/60/3-40-10-50 C3/60/2-40-10-50 -	U-40-10 C3/60/2-40-10-25 - -	U-40-5-X U-60-5-X U-50-5 -	C3/60-40-5-150 C3/60-40-5-200 C3/60-50-5-150 C3/60-50-5-200

Table 4.5: Normal-Strength Concrete – Mix Design Summary

Material	Type	Mix Design 4101CC	Batched	
			Series VI Truck 3	Series VII
Cement	ASTM C150 - Type I (lb/yd^3)	517	512	514
Coarse Aggregate	#8 Limestone (lb/yd^3)	1875	1866	1875
Fine Aggregate	#23 Natural Sand (lb/yd^3)	1475	1523	1522
Water-Reducing Admixture (oz/yd^3)	MasterGlenium 7511 (oz/yd^3)	20.7	20.2	20.6
Water (lb/yd^3)		250	248	251
Water/Cement Ratio		0.483	0.485	0.471
Slump (in.)		6.0	6.0	5.5

For Series VI, five of the eight beams required a mix design to achieve a target compressive strength of 10,000 psi. The selection of cementitious material, coarse aggregate, and fine aggregate was consistent with the previous mix design selected for normal-strength concrete; however, slag and silica fume were also included. The mix design for the high-strength concrete beams in Series VI is provided in Table 4.6 along with the batched quantities.

Table 4.6: High-Strength Concrete – Mix Design Summary

Material	Type	Mix Design 7820CM	Batched	
			Series VI Truck 1	Series VI Truck 2
Cement	ASTM C150 - Type I (lb/yd^3)	705	703	702
	ASTM C989 - Slag (lb/yd^3)	200	202	198
	ASTM C1240 - Silica Fume (lb/yd^3)	25	25	25
Coarse Aggregate	#8 Limestone (lb/yd^3)	1700	1691	1692
Fine Aggregate	#23 Natural Sand (lb/yd^3)	1203	1243	1244
Water-Reducing Admixture	MasterGlenium 7511 (oz/yd^3)	65.1	62.9	63.2
Water (lb/yd^3)		275	269	268
Water/Cement Ratio		0.304	0.297	0.298
Slump (in.)		6.0	5.0	5.5

4.3.1.1 Concrete Testing

In Series VI and VII, mechanical properties of the concrete were determined using an ASTM C193 standard cylinder size of 6 x 12 in. for each truck. Before cylinder testing began, each cylinder was marked with a label indicating series, truck number, designated test, and cylinder number for that test. Figure 4.7 shows an example of the identification label.

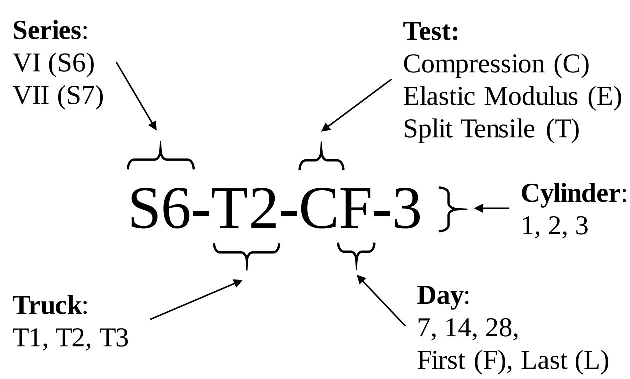

Figure 4.7: Cylinder Testing Identification

4.3.1.2 Compression Testing

To determine the increase in compressive strength of the concrete as it cured, several cylinders were tested to failure following the "Standard Test Method for Compressive Strength of Cylindrical Concrete Specimens" in ASTM C39 (2018).

Steel caps lined with a neoprene elastomeric pad were installed on the top and bottom faces of the cylinder to ensure uniform distribution of the compression load and to reduce the chances of edge spalling. Two standard 60-durometer pads were selected for Truck 3 of Series VI and all cylinders in Series VII consistent with the target compressive strength of the concrete mix. Two 70-durometer pads were selected for Truck 1 and Truck 2 in Series VI because of the use of high-strength concrete. Compressive strengths were recorded and averaged in Table 4.7 through Table 4.10. A typical compression cylinder test setup before and after failure is shown in Figure 4.8(a) and Figure 4.8(b), respectively. Average concrete compressive strength, f_c, over time is also plotted in Figure 4.9. The compressive strength gain for Series V is included for comparison.

Table 4.7: Series VI Truck 1 Compression and Tension Properties

Time (days)	**Compressive Strength, f_c (psi)**				**Fracture Pattern (ASTM C39)**			**Split Tensile Strength, f_t (psi)**			
	Cylinders			Avg.	Cylinders			Cylinders			Avg.
	1	2	3		1	2	3	1	2	3	
7	8630	8490	8430	**8520**	6	4	6	-	-	-	-
14	9190	9140	8990	**9110**	3	5	6	-	-	-	-
28[1]	8960	9820	10,000	**9590**	6	5	5	680	660	525	**622**
35[2]	10,200	10,300	9790	**10,100**	4	5	6	580	665	755	**667**

[1] *First Day of Testing*
[2] *Last Day of Testing*

Table 4.8: Series VI Truck 2 Compression and Tension Properties

Time (days)	**Compressive Strength, f_c (psi)**				**Fracture Pattern (ASTM C39)**			**Split Tensile Strength, f_t (psi)**			
	Cylinders			Avg.	Cylinders			Cylinders			Avg.
	1	2	3		1	2	3	1	2	3	
28	9680	10,100	9480	**9750**	4	5	5	505	755	815	**692**
37[1]	10,400	10,000	9780	**10,100**	3	2	6	625	685	725	**678**
58[2]	10,100	9000	10,500	**9870**	6	6	3	-	-	-	**-**

[1] *First Day of Testing*
[2] *Last Day of Testing*

Table 4.9: Series VI Truck 3 Compression and Tension Properties

Time (days)	Compressive Strength, f_c (psi)				Fracture Pattern (ASTM C39)			Split Tensile Strength, f_t (psi)			
	Cylinders			Avg.	Cylinders			Cylinders			Avg.
	1	2	3		1	2	3	1	2	3	
7	4340	4210	4180	**4240**	6	5	2	-	-	-	**-**
14	4620	4870	4800	**4760**	2	2	5	-	-	-	**-**
28	5180	5120	5320	**5210**	5	6	3	395	560	485	**480**
43[1]	5320	5260	5350	**5310**	5	6	5	495	560	595	**550**
69[2]	5680	5840	5500	**5670**	2	2	2	465	555	580	**533**

[1] *First Day of Testing*

[2] *Last Day of Testing*

Table 4.10: Series VII Compression and Tension Properties

Time (days)	Compressive Strength, f_c (psi)				Fracture Pattern (ASTM C39)			Split Tensile Strength, f_t (psi)			
	Cylinders			Avg.	Cylinders			Cylinders			Avg.
	1	2	3		1	2	3	1	2	3	
21	5700	6090	-	**5900**	2	2	-	-	-	-	-
28[1]	6160	6320	6160	**6210**	5	6	5	520	620	540	**560**
42[2]	6540	6670	6710	**6640**	5	6	5	545	510	495	**517**

[1] *First Day of Testing*

[2] *Last Day of Testing*

a) Before Failure

b) After Failure

Figure 4.8: Typical Compression Cylinder Failure

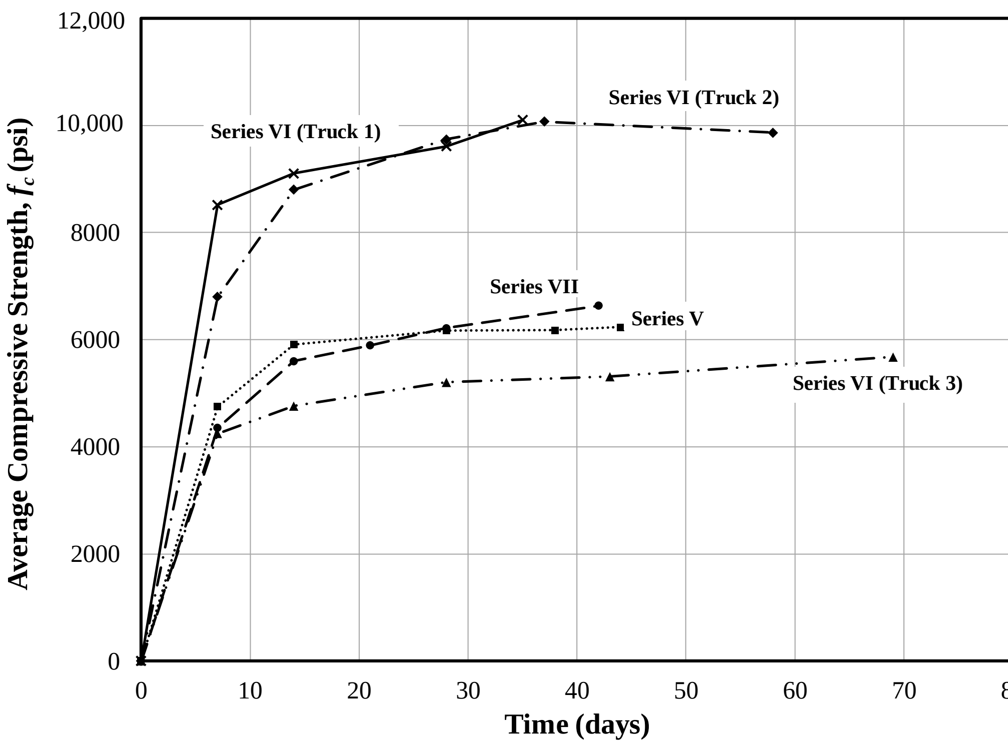

Figure 4.9: Concrete Compressive Strength Variation Over Time

4.3.1.3 Split Cylinder Testing

Split cylinder testing was conducted in accordance with ASTM C496 (2017). Tensile strengths were recorded and averaged in Table 4.6 through Table 4.9. A typical splitting tensile test setup before and after failure is shown in Figure 4.10(a) and Figure 4.10(b), respectively.

a) Before Failure **b) After Failure**

Figure 4.10: Series VI Splitting Tensile Cylinder Failure

4.3.1.4 Elastic Modulus and Poisson's Ratio

The method for determining Young's modulus and Poisson's ratio followed the same procedure as Series V and was in accordance with ASTM C469 (2014). Average compressive load from previous testing was used to specify a 40% upper bound for modulus testing (ASTM C469) conducted over three loading cycles. Average values for Young's Modulus and Poisson's Ratio were calculated and provided in Table 4.11 through Table 4.14.

Table 4.11: Series VI Truck 1 Stress-Strain Properties

Time (days)	**Young's Modulus, *E* (ksi)**			**Poisson's Ratio, *v***		
	Cylinders		Avg.	Cylinders		Avg.
	1	2		1	2	
28[1]	5470	5570	**5520**	0.27	0.27	**0.27**
35[2]	5620	5910	**5770**	0.27	0.27	**0.27**

[1] *First Day of Testing*
[2] *Last Day of Testing*

Table 4.12: Series VI Truck 2 Stress-Strain Properties

Time (days)	Young's Modulus, *E* (ksi)			Poisson's Ratio, *ν*		
	Cylinders		Avg.	Cylinders		Avg.
	1	2		1	2	
37[1]	5540	5530	**5540**	0.28	0.26	**0.27**

[1] *First Day of Testing*

Table 4.13: Series VI Truck 3 Stress-Strain Properties

Time (days)	Young's Modulus, *E* (ksi)			Poisson's Ratio, *ν*		
	Cylinders		Avg.	Cylinders		Avg.
	1	2		1	2	
43[1]	5150	5010	**5080**	0.48	0.24	**0.36**
69[2]	5130	4910	**5020**	0.29	0.22	**0.26**

[1] *First Day of Testing*
[2] *Last Day of Testing*

Table 4.14: Series VII Stress-Strain Properties

Time (days)	Young's Modulus, *E* (ksi)			Poisson's Ratio, *ν*		
	Cylinders		Avg.	Cylinders		Avg.
	1	2		1	2	
28[1]	5800	5570	**5690**	0.24	0.20	**0.22**
42[2]	5620	5620	**5620**	0.25	0.26	**0.26**

[1] *First Day of Testing*
[2] *Last Day of Testing*

4.3.2 Reinforcing Steel

Reinforcing steel in Series VI and VII was supplied by Nucor Steel, Kankakee, Illinois, and fabricated by Harris Rebar (Series VI) and Circle City Rebar (Series VII). Longitudinal and transverse reinforcing bars were used in Series VI and VII. Table 4.15 provides information for the reinforcing steel used in these two series. All bars designated as Grade 100 were rolled from the same heat while Grade 60 bars of different sizes were rolled from different heats.

Table 4.15: Reinforcing Steel Bar Information

Series	Material	Type	Supplier	Fabricator	Grade	Size (No.)	Purpose
VI	ASTM A615	Black	Nucor[1]	Harris Rebar[2]	60	3	Vertical Stirrups
							Longitudinal Compression
						4	Vertical Stirrups
							Horizontal Stirrups
					100	8	Longitudinal
	ASTM A1035	MMFX[3]	Cascade[4]	Harris Rebar	100	8	Longitudinal
VII	ASTM A615	Black	Nucor	Circle City Rebar[5]	60	3	Vertical Stirrups
							Longitudinal Compression
						4	Vertical Stirrups
							Horizontal Stirrups
				Harris Rebar	100	8	Longitudinal

[1] *Nucor Steel-Kankakee, IL*
[2] *Harris Rebar-Mooresville, IN*
[3] *MMFX, a Commercial Metals Company-Irving, TX*
[4] *Cascade Steel Rolling Mills, Inc.-McMinnville, OR*
[5] *Circle City Rebar, LLC-Indianapolis, IN*

4.3.2.1 ASTM A615

Bar strength testing was conducted in a 220-kip MTS universal testing machine for all longitudinal bars and a 120-kip Baldwin universal testing machine for smaller transverse reinforcement. Stress was calculated by dividing applied load by the nominal bar area. A 2-in. extensometer was installed on each bar to measure strain during testing. A typical stress-strain response for the A615 No. 8 bars is provided in Figure 4.11, while the stress-strain responses for all steel used in Series VI and VII is provided in Appendix B. From the linear-elastic region of the response, the linear-elastic limit was estimated by determining the point where the linear slope begins to decrease. The 0.2% offset method, as specified in ASTM E8-04 (2016), was selected to determine the yield strength of the steel in Series VI and VII. The ultimate strength of the steel occurred just before fracture. Material properties are documented in Table 4.16.

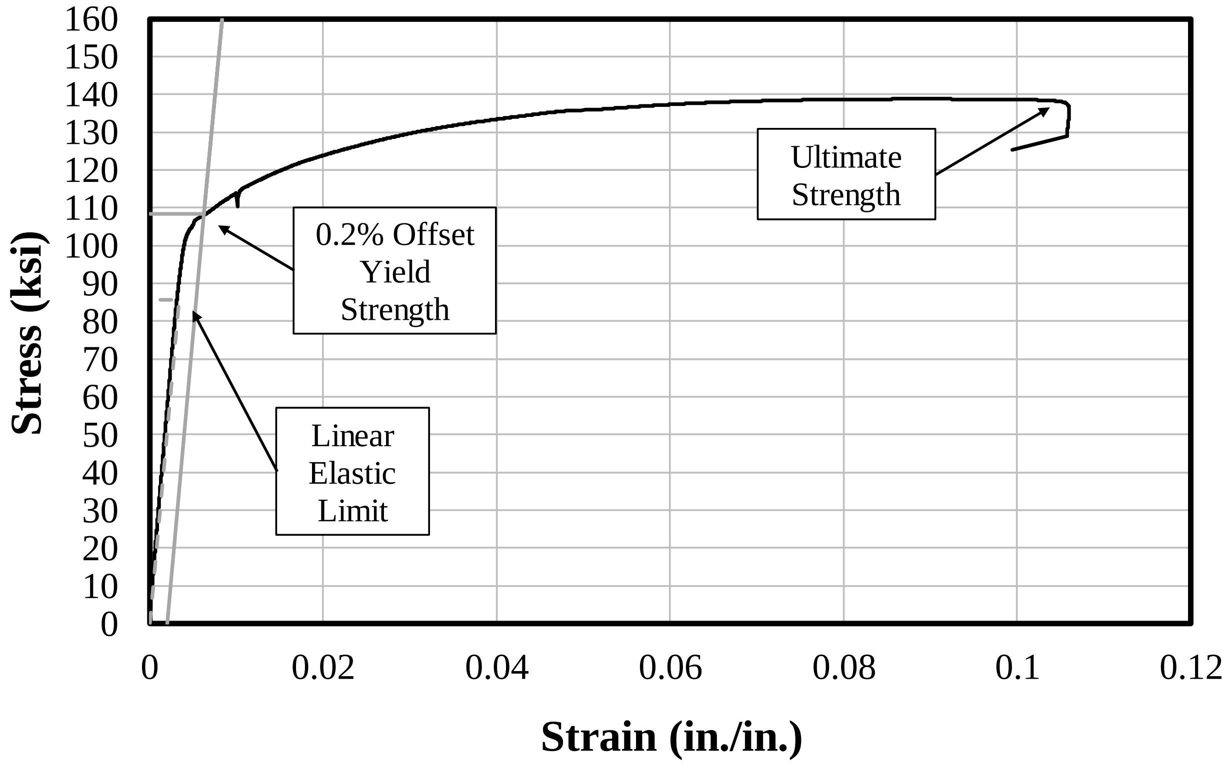

Figure 4.11: Typical Stress-Strain Response for A615 Gr. 100 No. 8 Bars

Table 4.16: ASTM A615 Material Properties

Series	ASTM	Bar Size (No.)	Grade	Elastic Limit Stress (ksi)	Yield Stress 0.2% Offset (ksi)	Ultimate Strength (ksi)
VI	A615	3	60	62	79	101
VII				58	64	98
VI, VII	A615	4[1]	60	-	-	-
VI, VII		8[2]	100	87	108	140

[1] *No. 4 bars in Series VI and VII were not included in the test region*
[2] *No. 8 bars originated from same roll and heat as Series I through IV No. 8 bars*

For Series VI and VII beam construction, additional high-strength steel bars were required. These additional bars came from the same heat and were rolled at the same time as the initial steel shipment from Series I through IV; however, these bars were stored outside and accumulated rust along the surface. Abrams (1913) suggested that the formation of rust on the bar surface helps to increase bond strength. To prevent the iron oxide from significantly affecting bond strength, the bars were wire-brushed within the splice region and approximately 12 in. outside of the splice region for all beams constructed with this steel is Series VI and VII. A comparison between the original bar shipment, the new shipment before wire brushing, and the new shipment after wire brushing is provided in Figure 4.12. Wire brushing was conducted in accordance with ACI 318-14 (Section 26.6.1.2).

Figure 4.12: Comparison of Grade 100 Bar Surfaces

4.3.2.2 MMFX

Conforming to ASTM A1035, MMFX steel (Martensitic Microcomposite Formable Steel) is a low-carbon, high chromium alloy, high-strength steel. Tests were conducted in Series VI of this research program to investigate bond capacity in members constructed using MMFX longitudinal reinforcement.

This steel was used in two specimens in Series VI and was supplied by Cascade Steel Rolling Mills, Inc. in McMinnville, Oregon. In this program, the ChromX 9000 series of steel bars with a minimum specified yield strength of 100 ksi were tested, formerly known as MMFX II. A typical stress-strain response for the A1035 No. 8 bars is provided in Figure 4.13, while material properties are documented in Table 4.17.

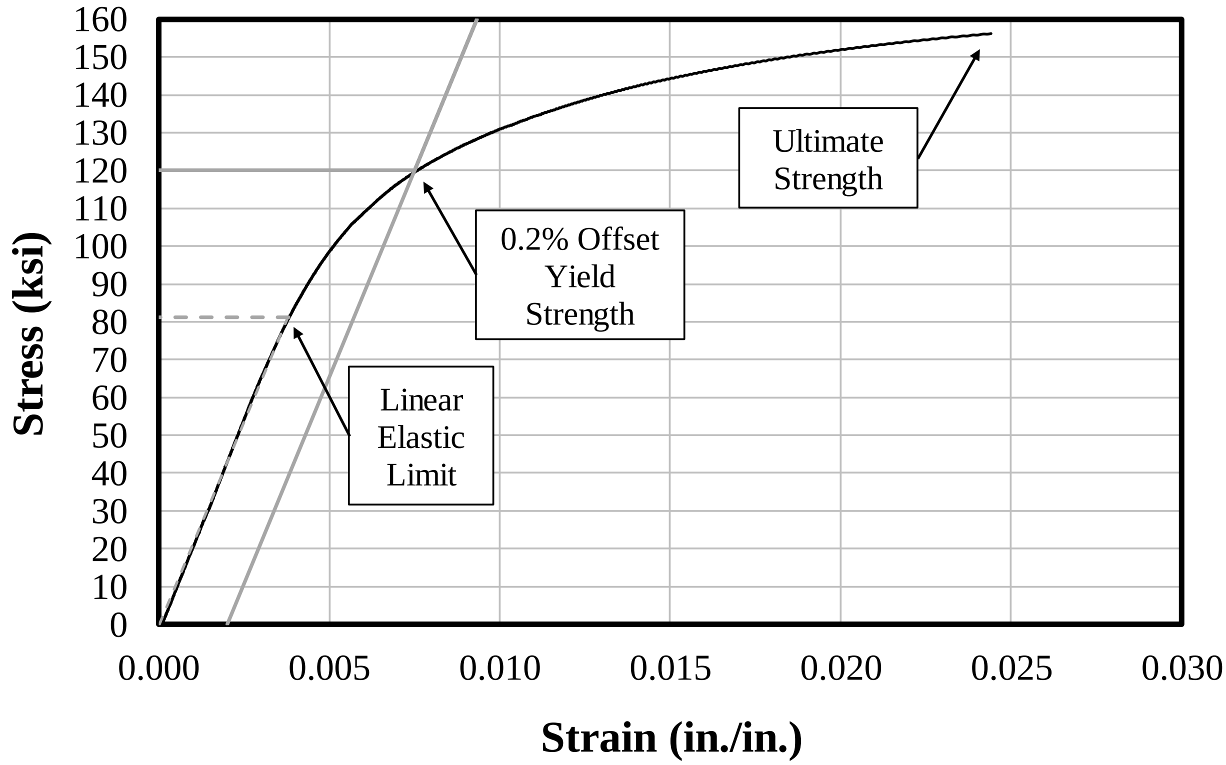

Figure 4.13: Typical Stress-Strain Response for A1035 Gr. 100 No. 8 Bars

Table 4.17: ASTM A1035 Material Properties

Series	ASTM	Bar Size (No.)	Grade	Elastic Limit Stress (ksi)	Yield Stress 0.2% Offset (ksi)	Ultimate Strength (ksi)
VI	A1035	8	100	81	120	156

4.4 Specimen Construction

Twelve (12) beam specimens were constructed by first arranging and securing the appropriate formwork. Once formwork construction was completed, the necessary steel was placed and tied within the forms before casting.

4.4.1 Formwork Assembly

For specimens cast in Series VI and VII, the same four platforms from Series V were used. A 20-in. vertical center form was secured along the bottom face with lag screws to divide each of the four platforms into 2 halves. This center form was constructed on 2 x 4-in. lumber. Typical 2 x 4-in. wood bracing studs were installed vertically at a 16-in. spacing along the length. With the center form complete, a 20-in. wide sheet of HDO plyform with a thickness of 3/4 in. was attached on one side using 3/8-in. diameter wood screws. Finally, another plyform sheet was attached to the other side, enclosing and completing the center form. The components of the formwork are shown in (Figure 4.14).

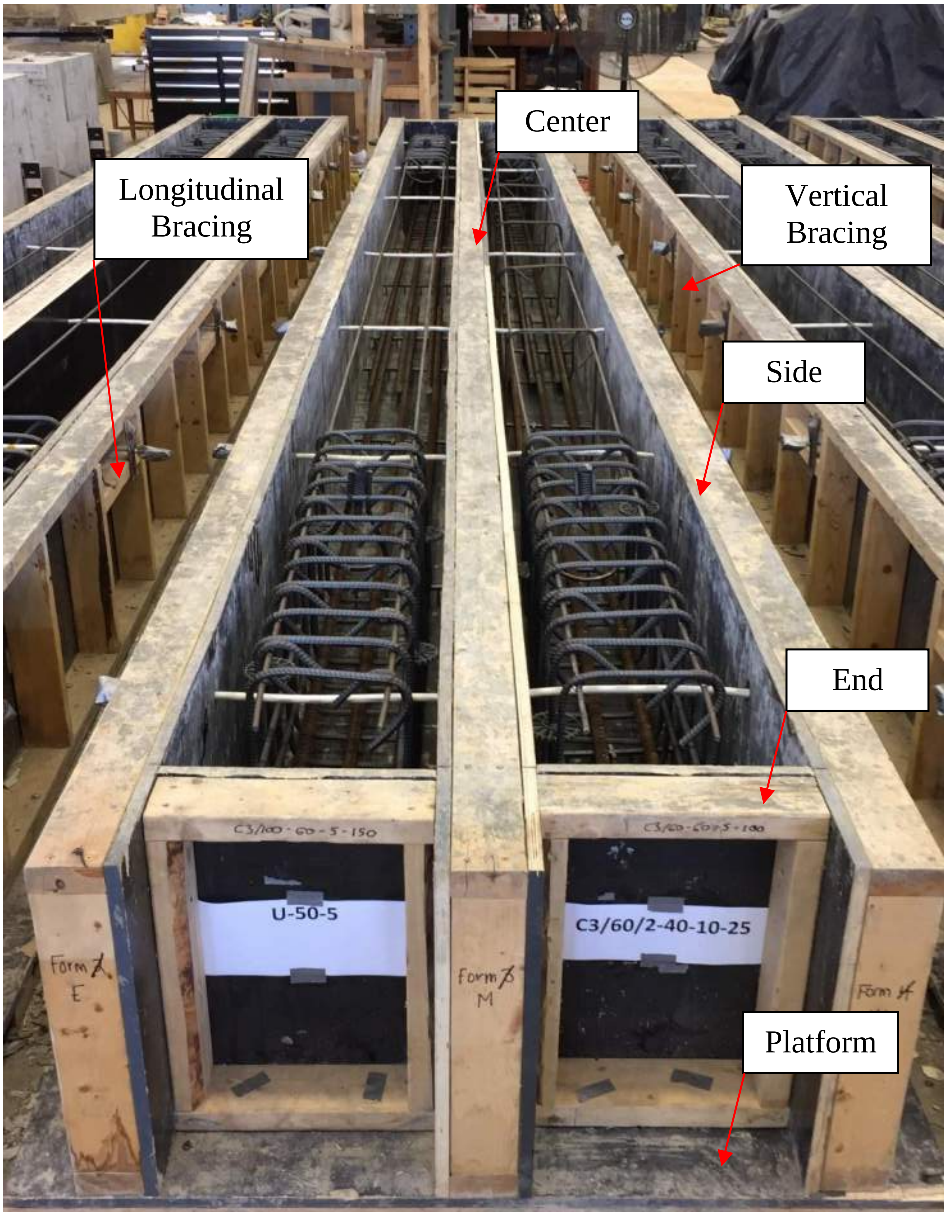

Figure 4.14: Series VI and VII Formwork Components

The side forms for each platform were constructed in the same manner as the center form, but only one side sheet of HDO plyform was required for each. Supplemental stability was provided by adding longitudinal bracing throughout the side forms (Figure 4.14). This also provided a bracing point for the end plates of the form tie installations.

The end forms were constructed identically to the side forms but with an overall length of 13-3/4 in. to match the specified width of the beam specimens. The locations of all formwork components were first marked on the platforms with chalk lines before being secured with 1/4-in. lag screws and washers. The completed formwork construction for Series VI is shown in Figure 4.15(a), while the completed formwork construction for Series VII is shown in Figure 4.15(b).

a) Series VI

b) Series VII

Figure 4.15: Beam Specimen Formwork Space

Any remaining concrete from previous casts was removed from all plyform surfaces to ensure a flat and clean surface for Series VI casting. Any seams, joints, or noticeable damage on the plyform surfaces were repaired with silicone caulk and smoothed. All end forms were labeled with the appropriate beam identification label in Series VI and VII before cage construction began. Series VII required the construction of new end and side forms as a result of poor formwork surface conditions. Center forms and platforms were repaired as needed and oiled before casting.

4.4.2 Steel Cage Construction

The longitudinal steel for all cages was placed near the bottom of the forms so that the reinforcement was in the bottom cast position. Seven blocks of 4 x 6-in. lumber were placed above each beam's formwork to support the hanging steel cage during construction (Figure 4.16). Two No. 3 mild steel bars were marked with the location of stirrups and the midpoint for each beam, extending from the shear region on one end of the beam to the shear region on the other. The No. 3 mild steel bars were mounted on the 4 x 6-in. wood blocks above each form void to be cast in the compression zone of the beams.

Figure 4.16: Series VII Cage Support Blocks

Because Series VI contained confined and unconfined specimens, different stirrup layouts were used. For unconfined beams, stirrups were necessary in both end shear regions (Figure 4.17(a)). For those beams with confining steel, stirrups were placed along the length of the member in the constant moment region (Figure 4.17(b)) and both shear regions. For confined beams in Series VI, stirrups were included along the entire length of the constant moment region. For confined beams in Series VII with transverse steel in the constant moment region, stirrups were included over the entire splice and three stirrups were included past both ends of the splice. This had no effect on experimental results and allowed the construction process to be expedited. All stirrups were attached to the No. 3 mild steel bars using 9-in. annealed steel ties.

a) Shear Region **b) Splice Region**

Figure 4.17: Typical Beam Cage Construction Details

Longitudinal reinforcement was laid out, marked, and cut to the appropriate length for the splice lengths selected. By leaving the end forms unsecured from each beam, longitudinal steel was placed within the beam from the end, bearing directly on the hanging stirrups. The six bars in each beam were aligned with a plumb bob to achieve the correct lap splice configuration and bar spacing within the splice region. For confined specimens, the lap splice was configured within the constant moment region using 9-in. steel ties to engage the longitudinal reinforcing and the stirrups (Figure 4.17(b)); however, because the unconfined splice had no stirrups for support in the constant moment region, wood cribbing was placed in the middle of the beam beneath the splice region to keep the center of the longitudinal bars level with the ends while tying. Two horizontal stirrups were placed at the ends of each beam and tied to the vertical stirrups (Figure 4.18) to provide confinement and prevent splitting at the ends of the hooks.

Figure 4.18: Beam Shear Region and Cage Lifting

Once tying was complete, an overhead crane was used to lift the cages up, allowing the 4 x 6-in. support blocks to be removed and the form bases to be cleaned. Plastic chairs (2 in.) were cut and grinded to a specified height of 1-7/8 in. before being spaced within the form at regular intervals of 3 ft. To avoid altering the propagation of stresses that develop within the splice region, a single chair was placed at the middle of the region where bond stress was considered to be the smallest to provide stability in cage construction and to maintain the bar spacing, top cover, and side cover. Care was taken to prevent chairs from being placed at the ends of the splice region where bond stress is maximum. Chairs were instead placed just outside the splice region to avoid altering the distribution of tensile stresses along the length of the splice. Cages were lowered back into the forms onto the chairs and adjusted to align the center of the splice with the center of the form for all confined (Figure 4.19(a)) and unconfined (Figure 4.19(b)) beams.

a) Confined Specimen **b) Unconfined Specimen**

Figure 4.19: Typical Beam Cage Configurations

Steel coil loop lifting-inserts were greased and attached to the end stirrups 42 in. from each end of the beam using 9-in. steel ties. Threaded bars (1/4-in. diameter) were guided through the formwork and secured at the ends using wheeler plates and nuts to prevent the formwork sides from bowing out when the concrete was later cast. Polyvinyl chloride tubing surrounded the threaded bars within the steel cage to prevent bonding with the concrete and to permit easy removal during moist curing. Plastic spacer wheels were placed at the ends of each beam along the sides of the stirrups to achieve proper alignment of the steel cage with respect to the formwork. Figure 4.20 shows the final construction details. All end forms were secured, and all cages were straightened and cleaned before casting.

Figure 4.20: Final Beam Construction Details

4.5 Casting, Curing, and Storage

4.5.1 Cylinders

The interior face of all plastic 6 x 12-in. cylinder molds was lined with a thin layer of form oil to aid in the demolding process after curing. Slump tests were performed before casting cylinders (Figure 4.21(a)). Molds were filled halfway before using a low frequency internal vibrator to consolidate the concrete. The mold was then filled to the top and vibrated a second time, ensuring that the steel-head vibrator penetrated the bottom layer of concrete approximately 1 in. to consolidate the concrete (Figure 4.21(b)). The top surface was finished before sealing the mold with a domed plastic lid to prevent moisture loss and maintain shape during curing.

All concrete cylinders were cured in the same location as the specimens to prevent any differences in humidity or temperature. Each cylinder was moist cured for seven days. On Day 7, all cylinders were relocated for storage, and all plastic molds were removed. The cylinders were labeled with the appropriate series, truck, and test number (Figure 4.7) before being stored.

a) Slump Test **b) Cylinder Casting Space**

Figure 4.21: Series VI Cylinders

4.5.2 Casting

4.5.2.1 Series VI

All specimens in Series VI were cast at the same time from the same delivery of concrete. Series VI required the use of three trucks of concrete due to the number of specimens tested and the requirement of two different target compressive strengths. All three slump tests achieved an appropriate measure of slump on the first test. The beams in Series VI were filled using two equal lifts along the beam length due to the increased member depth required for consolidation. Because each platform housed formwork for two beams, half of one beam was filled followed by filling the neighboring beam halfway to prevent bowing of the formwork (Figure 4.22(a)). Concrete was then placed to the top of each beam.

a) Half-Beam Casting

b) Casting In Progress

Figure 4.22: Series VI Casting Process

Concrete was delivered to the specimens using a concrete bucket. Care was taken to ensure that the steel cages stayed in place while concrete was placed. Two external mechanical vibrators operating at 3600 cycles per minute (60 Hz) were inserted following concrete shoveling to maximize consolidation. Concrete from a given truck was maintained in one specimen; therefore, it was not possible to balance side-by-side beams in all cases (Figure 4.22(b)). To prevent the neighboring voided form from bowing out during the wait for the following truck of concrete, metal rods were used to brace the formwork to the correct nominal width of 13-3/4 in. (Figure 4.23). This resulted in Specimens U-60-10 and C3/60/2-40-10-25 needing bracing. Because the high-strength concrete mix set very fast due to the warm temperature of the day, the top compression surface of these two beams was not finished perfectly level. This variation was not considered a problem as this was the compression face of the member during testing.

Figure 4.23: Series VI Form Bracing

Once all the concrete had been cast and vibrated within each test specimen, the top surface was screeded with 2 x 4-in. lumber and finished by hand with a float. Figure 4.24 shows the final state of all eight beams after casting was completed.

Figure 4.24: Series VI Cast Complete

4.5.2.2 Series VII

The concrete casting process for Series VII was conducted similar to Series VI. Because only one truck was required with one target compressive strength, no center form bracing with external steel bars was required. The half-beam cast method from Series VI was implemented when placing concrete to maintain stability. Once all the concrete had been cast, consolidation was provided by vibrating each test specimen along the entire length (Figure 4.25(a)). All beams were screeded with 2 x 4-in. lumber (Figure 4.25(b)) and finished by hand with a float. The casting process and completed specimens are shown in Figure 4.26 and Figure 4.27, respectively.

a) Consolidation Process

b) Screeding Process

Figure 4.25: Series VII Casting Procedure

Figure 4.26: Series VII Cast In Progress

Figure 4.27: Series VII Cast Complete

4.5.3 Curing and Storage

Once all test specimens were finished and cured for approximately one hour, a final finish was performed with a magnesium float to smooth out any noticeable irregularities in specimen height. To initiate moist curing, all specimens were covered with burlap sheets and watered evenly (Figure 4.28). Plastic sheathing was then placed over the specimens to maintain moisture and promote hydration (Figure 4.29). The burlap was watered each day for the following five days, with the final watering period occurring on Day 6. On Day 7, the burlap was not watered and three compression cylinder tests were performed to evaluate strength gain of the concrete.

Figure 4.28: Series VI Moist Curing – Burlap Cover

Figure 4.29: Series VI Moist Curing – Plastic Cover

Once the concrete had adequate strength on Day 7, the side formwork and threaded bars were completely removed from all beams. The beams were then flipped (Figure 4.30) about their longitudinal axis using the crane to orient the lap splice on the top face of each member. All beams were stacked in a staging area before being moved to the test setup.

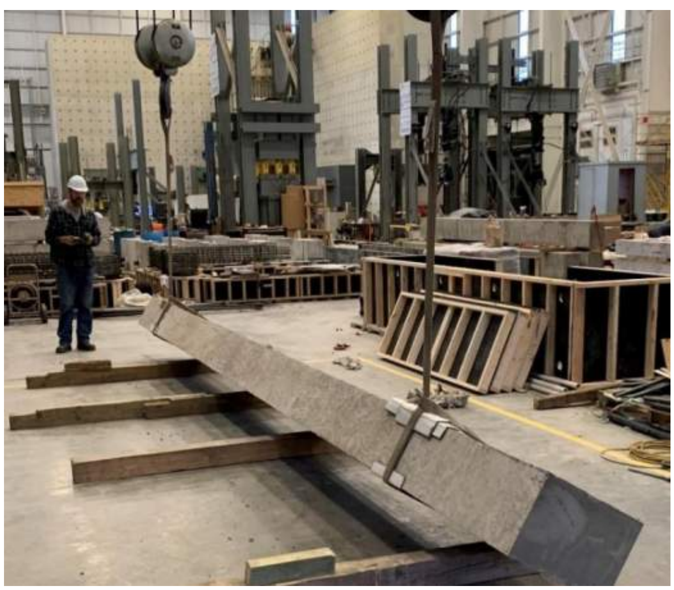

Figure 4.30: Series VII Beam Flipping Process

4.6 <u>Test Setup</u>

4.6.1 Schematic

All specimens in Series VI and VII were tested in four-point bending using an identical test setup shown in Figure 4.31. Roller supports were selected to support the specimens during testing. Due to the larger moment of inertia compared to the slab specimens and lower expected deflections, a 1-in. steel rod was selected for the roller supports. The rod was placed between two 1/2-in. thick steel plates measuring 6 x 24 in. to distribute bearing stresses uniformly (Figure 4.32(a)). The supports under all beams were constructed on two 4 x 4 x 2-1/2 ft concrete bearing blocks. Hydrostone was used to secure these components to the bearing blocks and the specimens. Wood cribbing was placed below the test specimens in the middle and near the ends to protect string potentiometers (Figure 4.32(b)) and provide a safer testing environment when failure was reached.

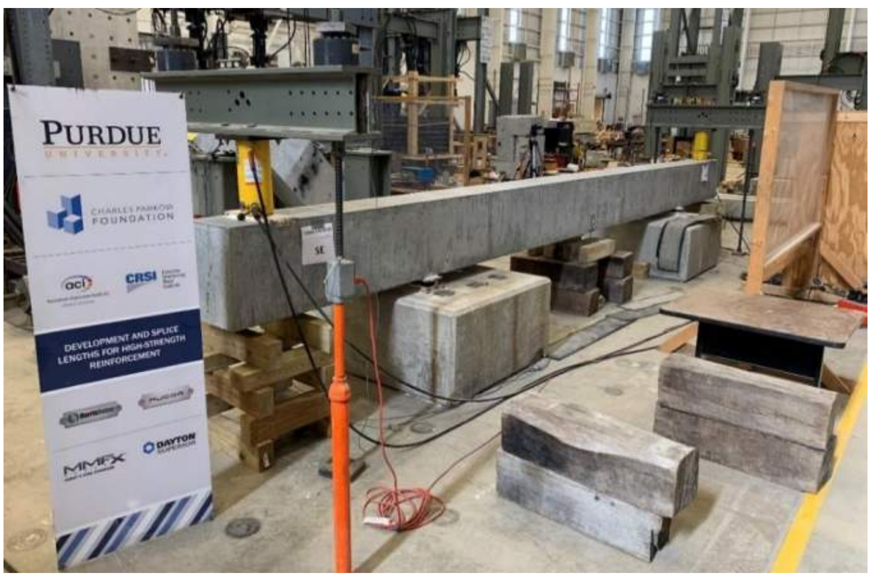

Figure 4.31: Series VI and VII Test Setup

a) Roller Support **b) Middle Cribbing**

Figure 4.32: Series VI and VII Testing Details

Once the beams were placed and secured with hydrostone to the roller supports, two bearing plates were positioned on the top face to align with the loading rams. Two (2) 100-ton double-acting hydraulic rams, each with a maximum stroke of 9.8 in. were secured to the bottom face of a crossbeam built-up from a double channel steel section using 3/8-in. bolts (Figure 4.33). The crossbeam was threaded through two 1-1/4-in. diameter DYWIDAG bars that were secured to the strong floor. Center-hole load cells were secured above the crossbeam before being threaded through the supporting DYWIDAG bars. Once the hydraulic rams were lowered and centered on the bearing plates, the crossbeam was leveled. Figure 4.34 shows an elevation of the test setup implemented for Series VI and VII while Figure 4.35 shows various plan sections of the test setup.

Figure 4.33: Typical Crossbeam Setup

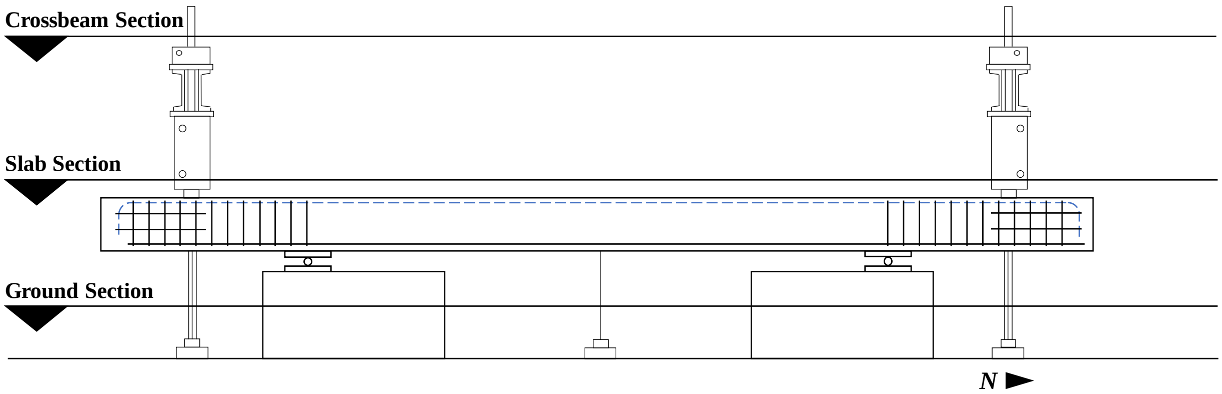

Figure 4.34: Series VI and VII Test Setup – East Elevation

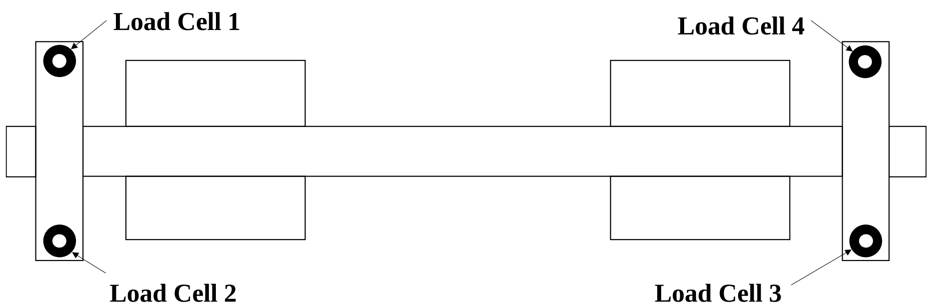

a) Crossbeam Section

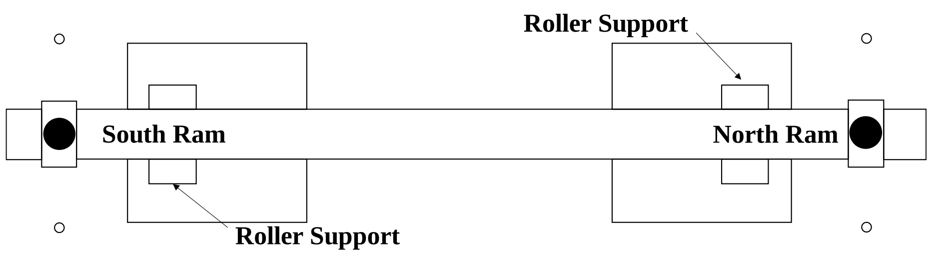

b) Beam Section

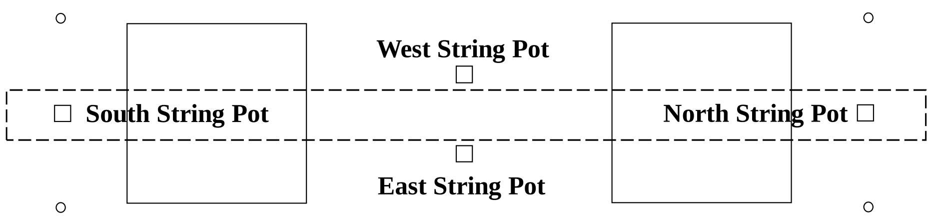

c) Ground Section

Figure 4.35: Series VI and VII Test Setup Schematic Plans

4.6.2 Instrumentation and Equipment

Details of the test setup used in Series VI and VII follow in accordance with the test setup used in Series I through IV.

4.6.3 General Testing Procedure

The testing procedure was nearly identical for all beams, regardless of confinement. The top surface of all beams was first inspected for any minor cracks caused by flipping or transporting the specimen to the test setup space. No perceptible cracks were present on the five unconfined specimens or the seven confined specimens in Series VI and VII before testing began. The pressure reading was recorded at the beginning of each test. Load was applied to the beams until cracking moment was reached between 11 and 15 kips, depending on the concrete strength.

Cracks were then mapped across the tension face and sides of each specimen (Figure 4.36). Load was applied throughout testing in 5-kip intervals and cracks widths were measured up until failure of the specimen. For unconfined specimens, flexural cracking was mapped on the specimens in 10-kip intervals up to failure, starting at 15 kips. For confined specimens, flexural cracks were mapped on the beams in 15-kip intervals up to failure, starting at 15 kips. This larger mapping interval was selected to maintain a consistent testing timeframe due to the higher loads required to fail all confined specimens. Video footage was captured for each load step and any notable specimen deformations were documented. This process was repeated throughout testing until failure was reached. As-built dimensions were measured after failure within the splice region to document cover and bar spacing dimensions from constructed. These measurements are provided for all Series VI and VII beams in Appendix I.

Figure 4.36: General Beam Test – Crack Mapping (C3/60/2-40-10-50)

4.7 Results Introduction

The experimental results of each test in Series VI and VII are presented to evaluate the effects of splice length, concrete strength, high-strength steel type, and confinement on bond strength. Series VI and VII consisted of twelve beams total. The test results are summarized in Table 4.18. Eleven (11) beams reached failure of the splice while one beam failed in flexure over the support.

4.8 Experimental Results

The applied load at failure, P_{ult}, was determined by averaging the load applied to the north and south end of each beam. This load was measured through the use of two load cells at each end. Load cell measurements varied for all test specimens with an average approximate difference of 1% between load cells. The ultimate moment at failure, M_{ult}, was calculated by multiplying the failure load, P_{ult}, by the shear span for each beam. The increased moment due to self-weight was neglected.

The stress achieved in the longitudinal reinforcing bars, f_b, was calculated using moment-curvature analysis and the failure load reached for each beam. All cross-sectional dimensions used in this calculation were design values. The tensile capacity of the concrete was neglected. Any influence from the compression steel was also neglected. The stress-strain relationship for the longitudinal steel was determined from experimental lab testing of the material, while the stress-strain relationship for the concrete was represented using the Hognestad (1951) model.

As included in Table 4.18, the test age was recorded for all specimens, with test dates ranging from 28 days to 69 days. Concrete compressive strength, f_c, was calculated by linear interpolation of the first and last day of testing.

Table 4.18: Beam Test Results

Series	Specimen	Test Age (days)	f_c (psi)	l_s (in.)	P_{ult} (kip)	M_{ult} (ft-kip)	f_b (ksi)	Failure Mode
VI	U-40-5-X	69	5600	40	55.0	220	71.0[1]	Bond
	U-60-5-X	43	5300	60	61.4	245.6	80.8[1]	Bond
	U-50-5	49	5400	50	55.5	222	73.2	Bond
	U-40-10	58	9800	40	65.0	260	83.6	Bond
	U-60-10	30	9700	60	73.2	292.8	94.2[2]	Bond
	C3/60/2-40-10-25	37	10,000	40	69.5	278	89.4[2]	Bond
	C3/60/2-40-10-50	28	9600	40	68.8	275.2	88.4[2]	Bond
	C3/60/3-40-10-50	35	10,100	40	68.7	274.8	88.2	Bond
VII	C3/60-40-5-150	28	6200	40	69.9	279.6	90.4[2]	Bond
	C3/60-40-5-200	30	6300	40	74.5	298	96.8[2]	Bond
	C3/60-50-5-150	40	6600	50	80.1	320.4	104.6[2]	Bond
	C3/60-50-5-200	42	6600	50	85.2	340.8	111.3[3]	Flexure

[1] *Within the linear-elastic limit of the A1035 response (81 ksi)*
[2] *Beyond linear-elastic limit of A615 response (87 ksi)*
[3] *Beyond yield strength of A615 response (108 ksi)*

4.8.1 Self-Weight

As previously discussed for the slab specimens, self-weight is a small percentage of the applied loading. The moment diagrams for the beam loading configuration are shown in Figure 4.37 and Figure 4.38.

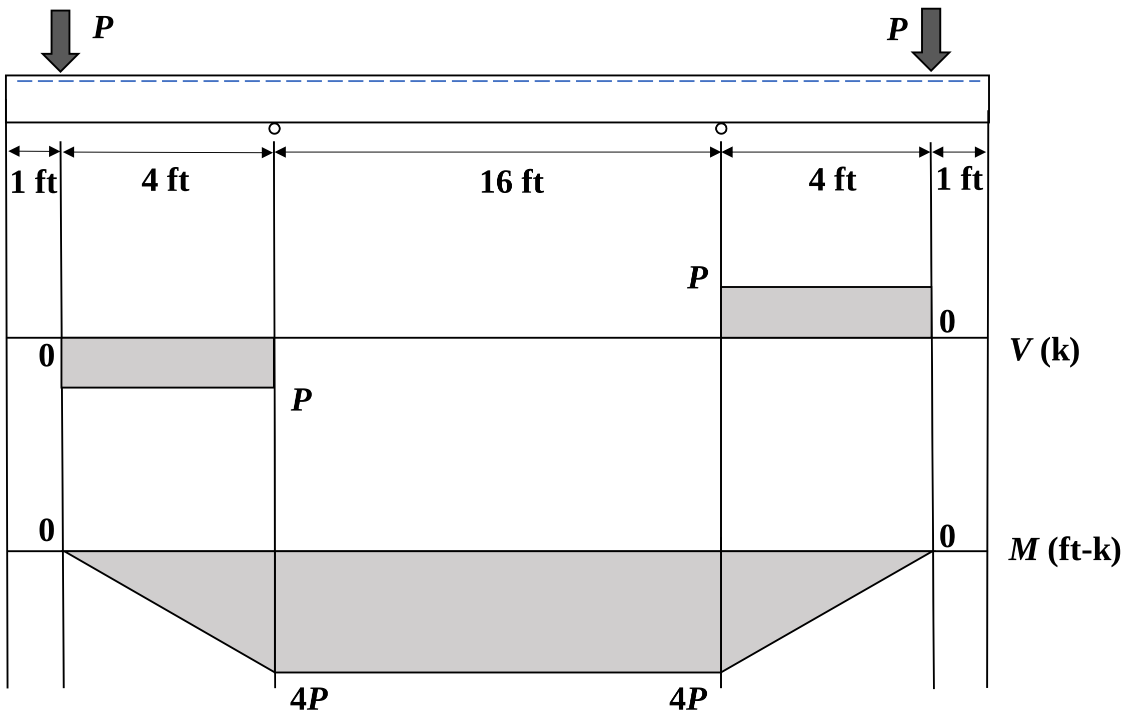

Figure 4.37: Shear and Moment Diagrams for Beams from Loading

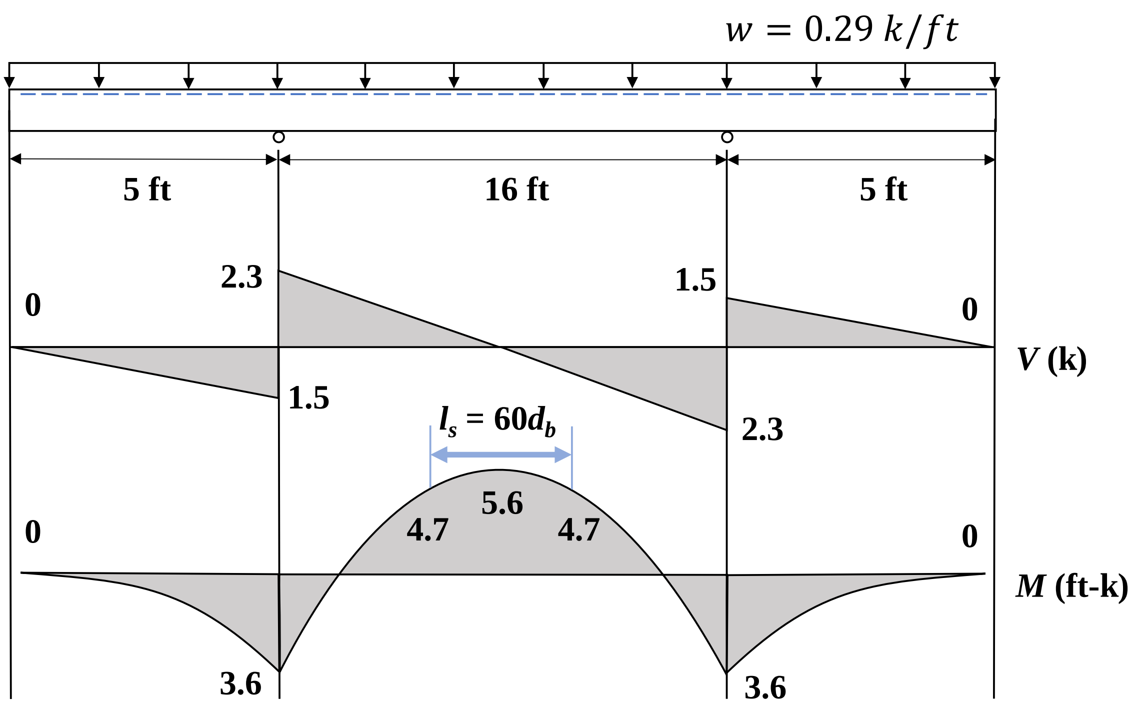

Figure 4.38: Shear and Moment Diagram for Beam Self-Weight

Because a maximum constant negative moment from the applied load occurs between the supports while the maximum negative moment due to the beam's self-weight peaks at each support, the overall ultimate moment occurs at the supports. The largest variation in moment across the splice is 0.9 ft-k for the 60d_b specimens resulting from the self-weight positive moment in the center of 5.6 ft-k and 4.7 ft-k at the end of the splice.

Considering the applied loads, the greatest influence on self-weight is for Specimen U-40-5-X for which the self-weight provides a 1.6% increase in the ultimate moment. This difference is considered negligible; therefore, the self-weight is ignored for all beams.

4.8.2 Specimen Observations

The unconfined beams experienced minimal amounts of end and middle deflection compared to the slab specimens; therefore, more wood cribbing was required at the ends to support the end of the beam after failure and to decrease the severity of concrete spalling around the splice. General spacing of cracking patterns varied slightly within the splice region between the unconfined (Figure 4.39) and the confined (Figure 4.40) beam specimens.

Figure 4.39: Typical Flexural Cracking within Unconfined Splice Region (U-60-10)

Figure 4.40: Typical Flexural Cracking within Confined Splice Region (C3/60-40-5-200)

4.9 Load-Deflection Response

Load-deflection behavior was monitored for all beam specimens. Although each curve was unique to a specific test, the underlying mechanics and regions within the responses were similar in Series VI and VII. Before reaching the cracking moment for each beam, the stiffness of the specimen was primarily governed by the concrete as shown in Region 1 of Figure 4.41. Once cracking occurred, the stiffness of the member immediately decreased as evident in Region 2 where the overall response is linear due to the elastic response of the steel. The final region (Region 3) demonstrates yielding of the longitudinal bars. Region 3 only occurred in specimens where the splice strength exceeded the yield strength of the steel. This region provides the lowest member stiffness observed during testing.

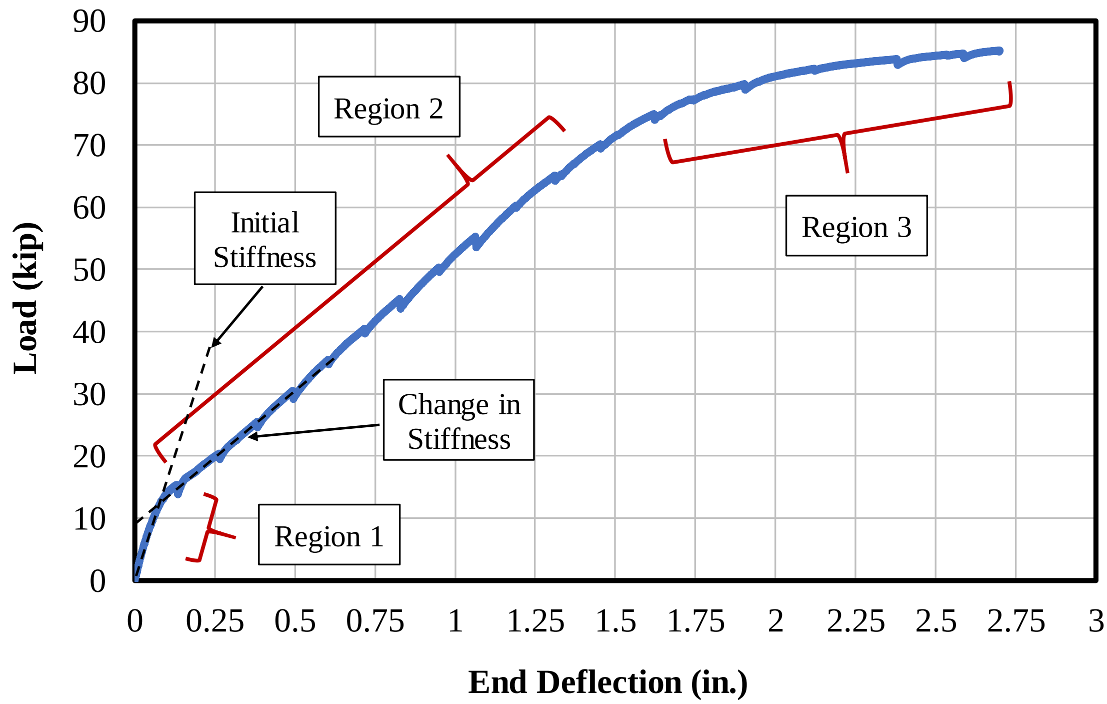

Figure 4.41: General Load-Deflection Behavior (C3/60-50-5-200)

In Series VI, five of the eight beams remained within the linear-elastic region of the response while three exceeded this limit but remained below the yield strength of the bars. In Series VII, all four beams achieved a bar stress above the linear-elastic limit. One beam surpassed the yield strength (greater than 0.2% offset) of the longitudinal reinforcement by approximately 3 ksi. This specimen (C3/60-50-5-200) developed sufficient bond strength and ultimately failed in flexure initiated by crushing of the concrete in the compression zone.

A comparison of all unconfined beams is provided in Figure 4.42 while a comparison of all confined beams is shown in Figure 4.43. Beams cast with high-strength concrete are represented by blue dashed lines and beams with MMFX spliced bars are represented by solid green lines. Load-deflection response for all specimens is provided in Appendix J.

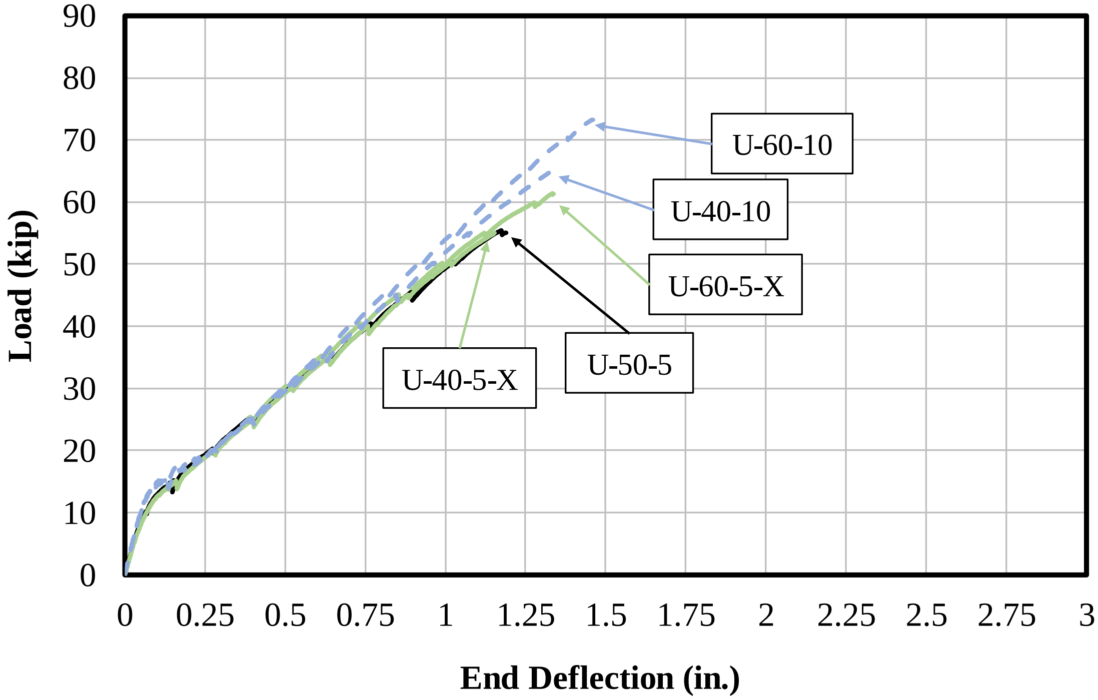

Figure 4.42: Unconfined Load-Deflection Responses

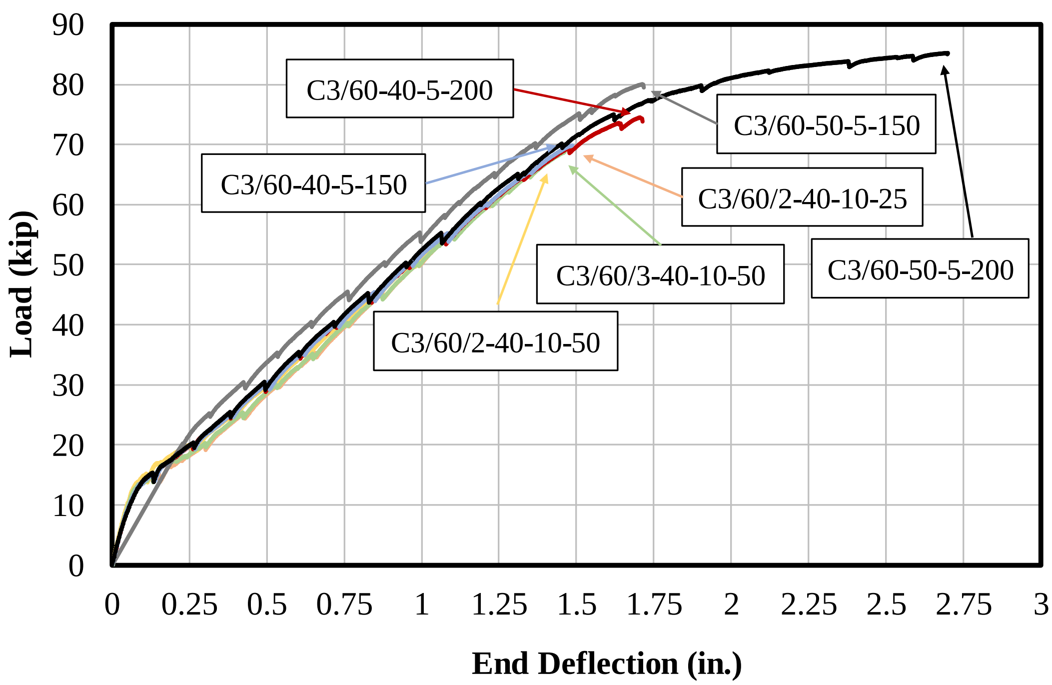

Figure 4.43: Confined Load-Deflection Responses

4.10 Concrete Crack Behavior

Four cracks were selected in the constant moment region, two past the north end of the splice region and two past the south end. Crack widths were monitored at each load step and recorded. The growth of these flexural crack widths as bar stress increased is provided in Appendix K for all specimens.

Throughout testing within the linear range of the reinforcing steel, crack widths consistently increased linearly as applied load increased for the unconfined and the confined beam specimens. Average and maximum crack width measurements for all beams are provided in Figure 4.44. Cracking initiated early during testing at a spacing between 4 in. and 15 in. with most cracks occurring in intervals of 10 in. (Figure 4.45) and continuing throughout the constant moment region but not the shear span. Transverse flexural cracking propagated at a wider spacing in the splice region with concentrated regions of flexural cracking developing near the ends of the splice.

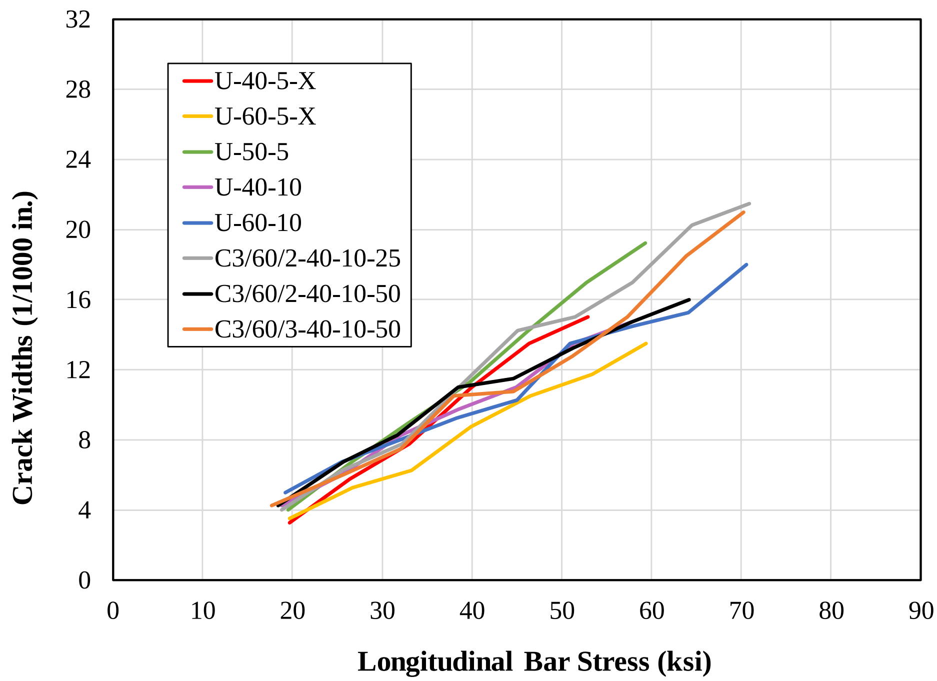

a) Average Crack Widths

Figure 4.44: Series VI and VII Crack Width Measurements

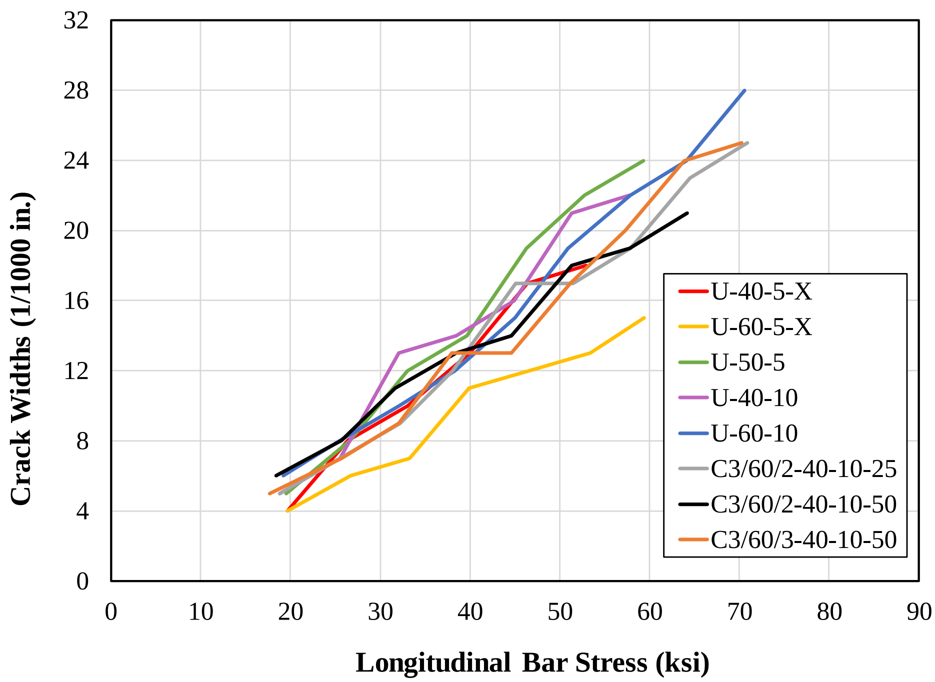

b) Maximum Crack Widths

Figure 4.44: Series VI and VII Crack Width Measurements - Continued

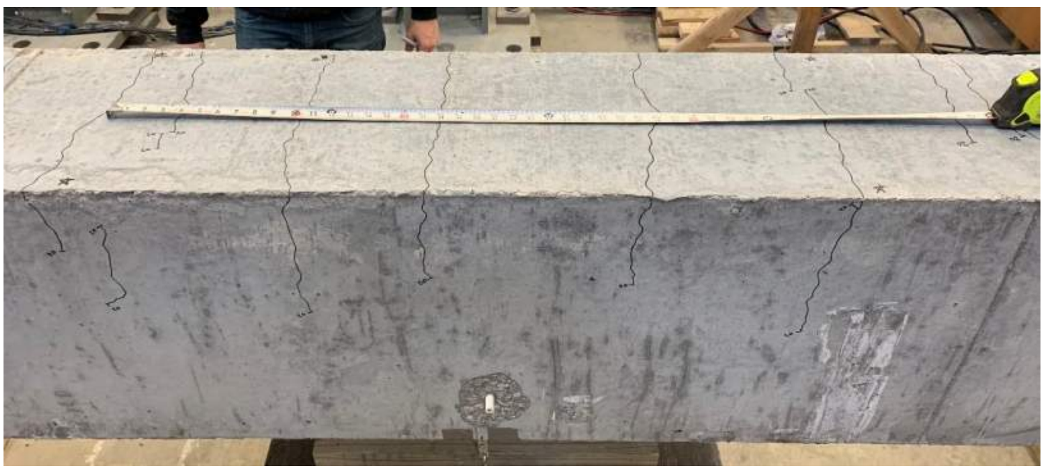

Figure 4.45: Transverse Flexural Cracking within Splice Region (C3/60/2-40-10-50)

After the cracking moment was exceeded, side cracking propagated down toward the compression region by approximately half the depth of the beams and is shown in Figure 4.46, regardless of confinement and concrete strength. This depth was indicative of the neutral axis location of the cross-section as load was applied.

a) West Elevation (U-40-5-X) b) West Elevation (C3/60/2-40-10-25)

Figure 4.46: Initiation of Flexural Side Cracking

Flexural cracking was not initially present in the shear span of the beam specimens (Figure 4.47). Most cracks along the tension face and the beam sides were only present between supports immediately after surpassing the cracking moment. As the applied load increased, transverse flexural cracks began to develop in the shear span and slowly progressed from above the support toward the point of applied load. Crack spacing was noticeably larger in this region than in the constant moment region. Diagonal cracking was observed across the member depth in the shear span for all specimens in Series VI and VII as the applied load increased (Figure 4.48).

Figure 4.47: Shear Span – Early Testing (C3/60-40-5-200)

Figure 4.48: Shear Span – Late Testing (C3/60-40-5-200)

Longitudinal cracking initiated near the ends of the splice on the tension face for all beam specimens. For most beams, longitudinal cracking was not observed until approximately 30 kips, regardless of confinement. For confined beams in Series II through IV, it was found that primary transverse flexural cracks within the splice region typically formed at or near the underlying stirrups. This finding was also present during confined beam testing, as evidenced by Figure 4.49(a). Cracks formed above most stirrups in the splice region, however, cracking also occurred where stirrups were not present depending on stirrup spacing. Furthermore, cracking typically formed at the end of the splice due to the cross-section discontinuity (blue in Figure 4.49(b)).

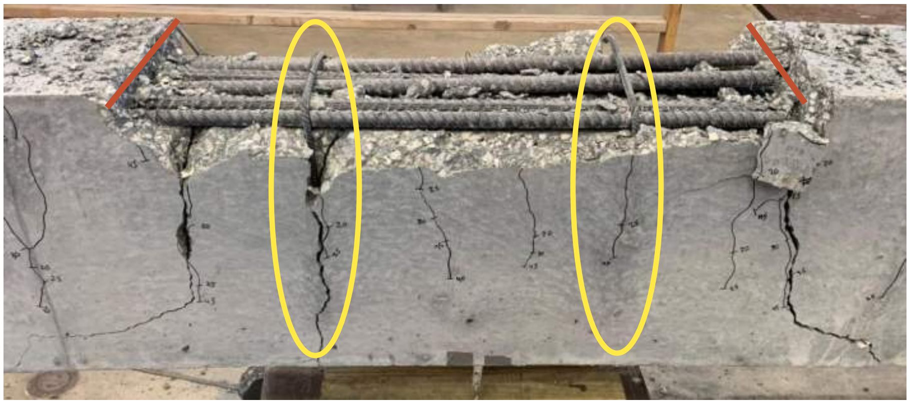

a) C3/60/2-40-10-50

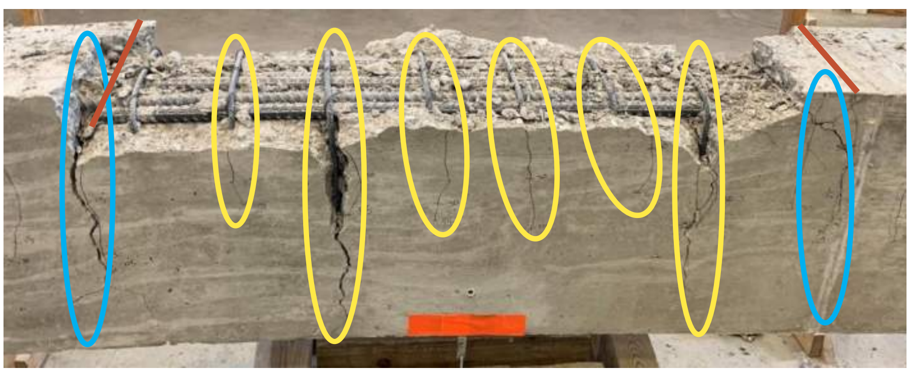

b) C3/60-50-5-150

Figure 4.49: Flexural Cracking at Stirrup Locations

Longitudinal cracking was present in all beam specimens, regardless of confinement and failure mode. As load increased, longitudinal cracks slowly propagated toward the middle of the specimen from the ends of the splice and did not necessarily occur over all three bar splices. Many beam specimens experienced longitudinal cracking along the outer two splices as shown in Figure 4.50(a). Some specimens exhibited longitudinal cracking that branched from one lap splice to another as load increased (Figure 4.50(b)). Although Specimen C3/60-50-5-200 failed in flexure at the north support, longitudinal cracking was present over the splice (Figure 4.51).

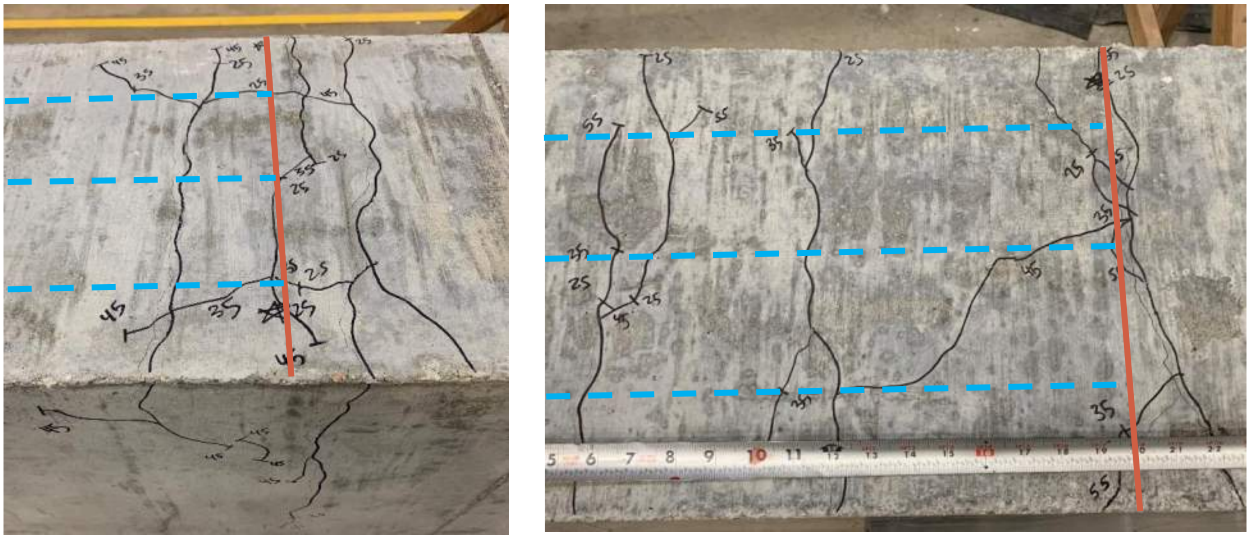

a) Edge Splitting Cracks (U-40-10) **b) Branching Crack (C3/60/2-40-10-25)**

Figure 4.50: Longitudinal Crack Propagation in Splice Region Failure

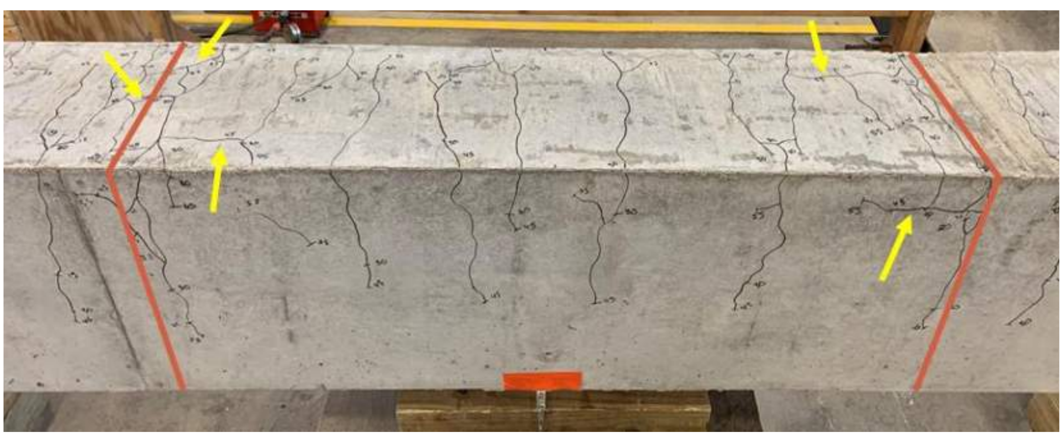

Figure 4.51: Longitudinal and Branch Cracking Before Flexural Failure (C3/60-50-5-200)

4.11 <u>Failure</u>

4.11.1 Unconfined Specimens

All five unconfined beams failed in splitting. Table 4.19 provides the results for each unconfined specimen at the end of testing.

Table 4.19: Test Results for Unconfined Beams

Specimen	Load (kip)	Avg. End Deflection (in.)	Avg. Midspan Deflection (in.)	Bar Stress (ksi)	Failure Mode
U-40-5-X	55.0	1.2	0.9	71.0	Splitting
U-60-5-X	61.4	1.3	1.1	79.6	Splitting
U-50-5	55.5	1.2	1.0	71.8	Splitting
U-40-10	65.0	1.3	1.0	82.3	Splitting
U-60-10	73.2	1.5	0.9	92.9	Splitting

Failure was brittle and explosive. Instead of releasing energy gradually, release occurred suddenly and without warning. The propagation of crack branching and longitudinal cracking along the sides and tension face, however, provided evidence that failure was imminent. Longitudinal cracks began at the ends of the splice and slowly extended toward the middle.

It was observed upon reaching failure that a full-depth crack opened at the ends of the splice and propagated entirely to the compression face of all unconfined beams. Typically, these larger cracks extended down part of the depth before extending out longitudinally approximately a distance d away from the end of the splice as shown in Figure 4.52 and Figure 4.53.

a) U-40-10

b) U-60-5-X

Figure 4.52: Typical Splice Side Cracking at Failure

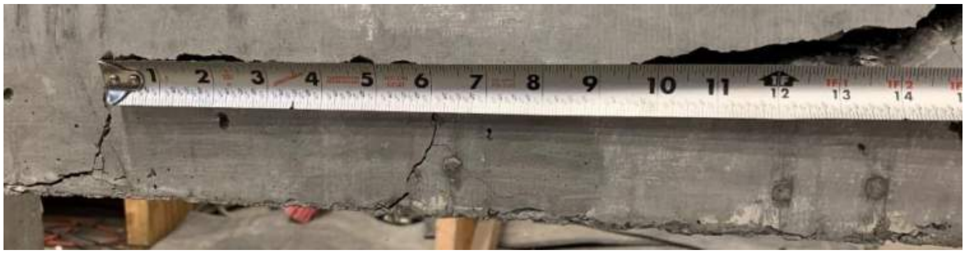

a) U-40-10

b) U-60-5-X

Figure 4.53: Typical Failure Side Crack Extensions

Upon reaching failure, the beam remained intact only due to the No. 3 mild steel bars within the compression region. Two unconfined beams in Series VI were cast with a target concrete compressive strength of 10,000 psi. The failures of these beams appeared to be more brittle, louder, and more explosive than the normal-strength concrete beams. All other observations at failure remained consistent with beams cast with a target concrete compressive strength of 5000 psi.

4.11.2 Confined Specimens

Table 4.20 provides the results for each confined specimen at the end of testing. Three of the seven confined beam specimens were cast using a high-strength concrete mix with a target compressive strength of 10,000 psi. No difference in specimen behavior during testing and at failure relative to normal-strength concrete specimens was observed.

Table 4.20: Test Results for Confined Beams

Specimen	Load (kip)	Avg. End Deflection (in.)	Avg. Midspan Deflection (in.)	Bar Stress (ksi)
C3/60/2-40-10-25	69.5	1.5	1.1	88.1
C3/60/2-40-10-50	68.8	1.5	1.1	87.1
C3/60/3-40-10-50	68.7	1.5	1.1	86.8
C3/60-40-5-150	69.9	1.5	1.1	90.4
C3/60-40-5-200	74.5	1.7	1.4	96.8
C3/60-50-5-150	80.1	1.7	1.3	104.6
C3/60-50-5-200	85.2	2.7	2.0	111.3

Due to the presence of transverse reinforcement, the ductility of the confined beams was higher than the unconfined specimens. In addition, greater tensile strains were achieved in the longitudinal reinforcement, allowing for more curvature and vertical deformation at the ends of the beam and at midspan. The greater ductility and vertical deflection also allowed splitting failure of the specimens to be slightly more predictable. Longitudinal cracking throughout the splice region also provided indication that failure was approaching, similar to the unconfined specimens.

Confined beams that failed in splitting behaved similarly to the unconfined beams. Concrete immediately spalled from the splice region; however, confining stirrups prevented the longitudinal bars from moving vertically. This mechanism helped contain the failure more than the unconfined beams and decreased the amount and distance of concrete blowout upon failure of the splice.

The final crack pattern at the ends of the splice after failure was slightly less severe than the unconfined beams as shown in Figure 4.54 for Specimen C3/60/3-40-10-50. The presence of transverse steel did not prevent the longitudinal crack in the compression zone from propagating along the beam length, but crack widths were noticeably smaller. The concrete in this region was held together and confined by the stirrups and the No. 3 bars in the compression zone.

a) Full Splice at Failure

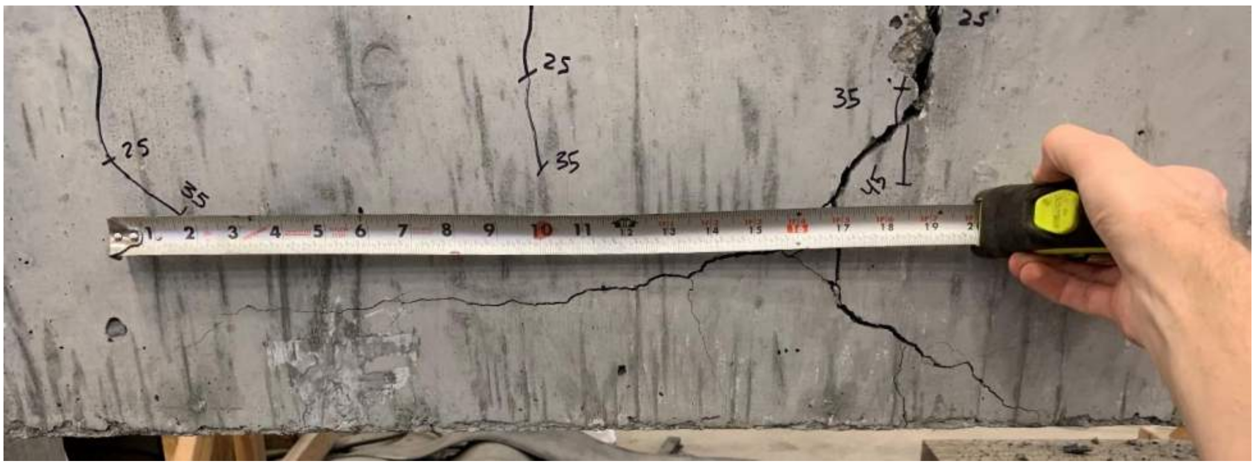

b) Side Crack Extension and Attenuation

Figure 4.54: Specimen C3/60/3-40-10-50 Side Cracking

After failure, the spalled concrete was collected to verify that cracks occurred at stirrup locations. These pieces were reconstructed to assemble the splice planes of the C3/60/2-40-10-50 and C3/60/3-40-10-50 specimens. These specimens had identical design parameters with the exception of the stirrup locations (Figure 4.5). It was observed that some of the cracks that developed along the splice formed directly above or next to the specified stirrup locations (Figure 4.55), indicating that the stirrup locations clearly influence crack locations.

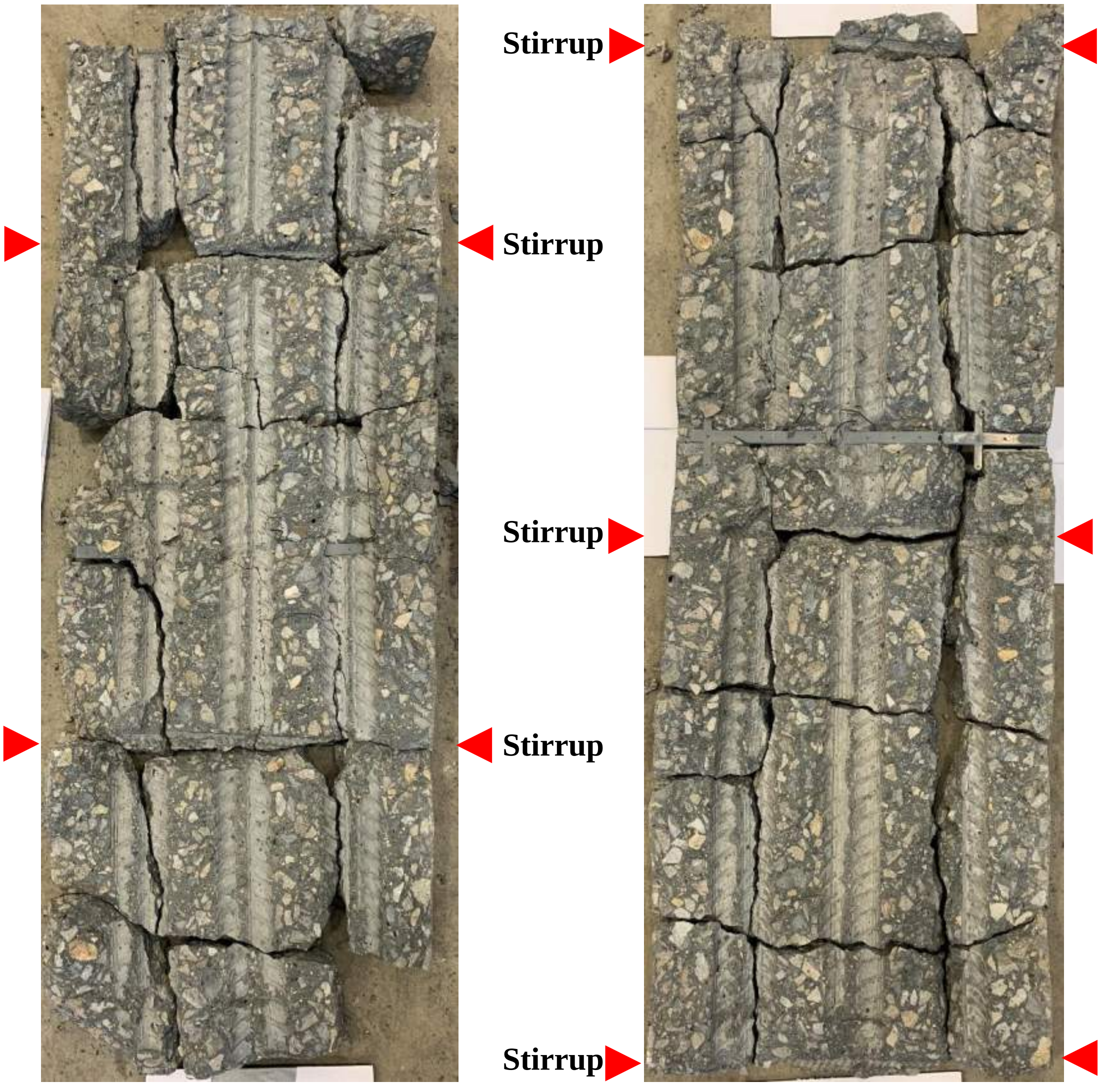

a) C3/60/2-40-10-50 **b) C3/60/3-40-10-50**

Figure 4.55: Reconstructed Confined Splice Planes

4.11.2.1 25-psi Specimen

The C3/60/2-40-10-25 specimen contained two stirrups, each located at the ends of the splice. It was observed after failure that all three of the longitudinal reinforcing bars had slipped out from under the confining stirrups (Figure 4.56). It is unclear whether the bars slipped out of the confining steel before failure was achieved when deformations were large or immediately after failure occurred when the longitudinal bars were pulled outward. It is assumed due to the lack of a singular large crack at this location that the slip followed failure. The correct spacing and placement of these two stirrups within the beam was verified after failure.

Figure 4.56: Bar Slip on Specimen C3/60/2-40-10-25

4.11.2.2 50-psi Specimens

Upon inspection of the C3/60/3-40-10-50 specimen after failure, the outer two splices remained well-confined; however, the inner splice was pulled out from under the confining stirrup (Figure 4.57). At both ends of the splice, it was observed that the stirrup was pushed away from its original location, indicating that the inner splice was confined for the entirety of testing up until failure. When failure occurred and the beam reacted upward, the bars slipped and bent the stirrup upon reaching a rest position.

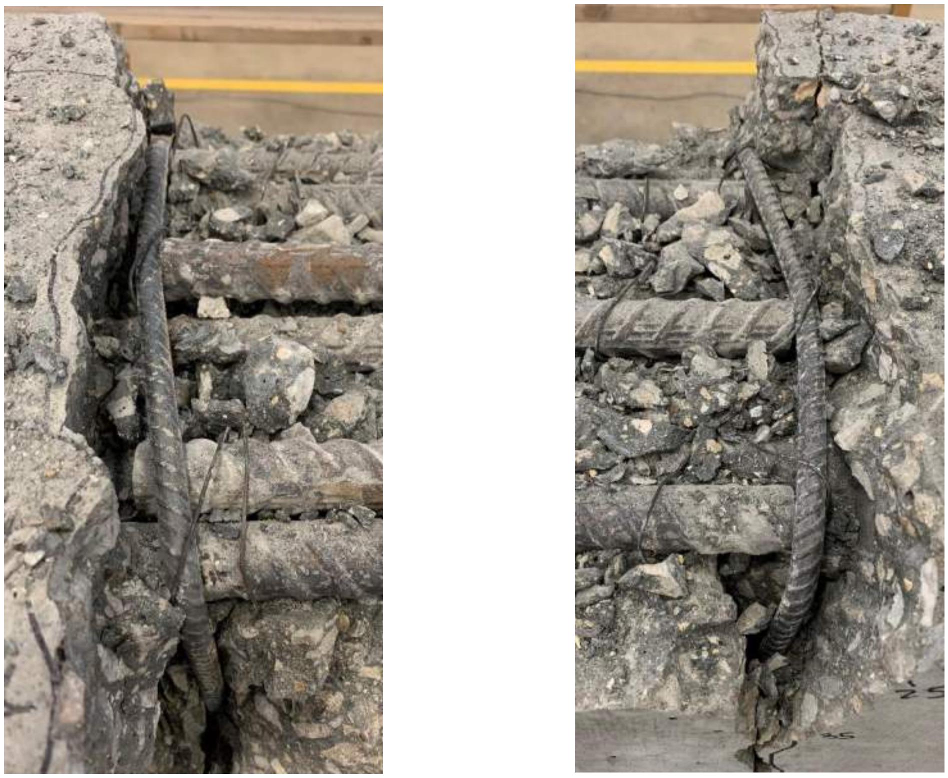

a) South End of Splice **b) North End of Splice**

Figure 4.57: Bent Stirrup on Specimen C3/60/3-40-10-50

For the C3/60/2-40-10-50 specimen, one of the two stirrups in the splice region exceeded its yield strength and ruptured at failure as shown in Figure 4.58. The failure of this stirrup may have initiated the failure of the entire splice itself. Similar failure results were observed by Azizinamini et al. (1999) when it was observed that confining stirrups near the ends of the splice could experience very high strains and exceed the yield strength of the material.

Figure 4.58: Ruptured Stirrup on Specimen C3/60/2-40-10-50

4.11.2.3 200-psi Specimen

Specimen C3/60-50-5-200 experienced a flexural failure at both supports. Longitudinal branch cracking was present at the ends of the splice in this specimen (Figure 4.59). Longitudinal bars reached yield and experienced large axial strains resulting in increased member deformations at the ends of the beam and at midspan. A flexural failure ultimately occurred at the north and south supports (Figure 4.60) evidenced by the initiation of concrete crushing within the compression zone.

Figure 4.59: Longitudinal Crack Branching (C3/60-50-5-200)

a) North Support

b) South Support

Figure 4.60: Flexural Failure of Specimen C3/60-50-5-200

CHAPTER 5. ANALYSIS OF TEST RESULTS

5.1 Influence of Investigated Parameters

In this testing program, 30 specimens failed in bond and eight failed in flexure. Series I through IV investigated the influence of splice length (l_s), bar spacing ($2c_{si}$), transverse reinforcement spacing (s), and transverse reinforcement yield strength (f_{yt}). In Series V through VII, the variables investigated included splice length (l_s), concrete compressive strength (f_c'), and the influence of transverse reinforcement parameters. The combined results for all seven series of splice specimen testing are documented in Table 5.1. These combined testing results were used for the investigation of several parameters and their influence on bond strength in this chapter.

5.1.1 Summary of Test Results

The U-40-5 and U-60-5 specimens in Series I were neglected in any forthcoming analyses due to problems experienced during testing, resulting in low bar stresses achieved at failure. Duplicate specimens in Series IV, U-40-5a and U-60-5a, achieved more appropriate results at failure. This provided a total of 28 specimens that failed in bond and eight specimens that failed in flexure. Of these 36 specimens, 18 contained transverse reinforcement (confined) while 18 did not (unconfined). All specimens in Series I through Series VII use the same specimen label identification. Additionally, three specimens in Series I were constructed using the minimum spliced bar spacing allowed by ACI and therefore had a slightly decreased width in the cross-section. These specimen labels contain an additional “M” in Table 5.1 to indicate this difference.

Table 5.1: Experimental Results Summary

Series	Specimen	f_c (psi)	l_s (in.)	P_{ult} (kip)	M_{ult} (ft-k)	f_b (ksi)	f_{norm}[4] (ksi)
I	U-40-5	4740	40	44.9	180	58.2	59.0
	U-60-5	4740	60	52.7	211	68.4	69.3
	U-80-5	4740	80	77.6	310	102.2[1]	103.6
	U-100-5	4740	100	78.7	315	103.7[1]	105.1
	U-120-5	4740	120	78.6	314	103.6[1]	105.0
	U-80-5-M	4740	80	73.3	293	97.7[1]	99.0
	U-100-5-M	4740	100	73.2	293	97.5[1]	98.8
	U-120-5-M	4740	120	71.8	287	95.6[1]	96.9
II	C3/60-60-5-50	7360	60	80.4	322	103.3[1]	93.8
	C3/60-60-5-100	7360	60	85.9	344	110.5[2][3]	100.3
	C3/60-60-5-150	7360	60	85.1	340	109.4[2][3]	99.3
	C4/60-60-5-100	7360	60	84.7	339	108.9[2][3]	98.9
	C3/100-60-5-100	7360	60	86.3	345	111.0[2][3]	100.8
III	C3/60-80-5-50	6310	80	79.4	318	101.9[1][3]	96.1
IV	U-40-5a	6260	40	54.6	218	69.8	66.0
	U-60-5a	6260	60	69.3	277	88.9[1]	84.0
	U-70-5	6260	70	73.8	295	94.9[1]	89.7
	C3/60/2-40-5-50	6260	40	63.9	256	81.8	77.3
	C3/60/3-40-5-50	6260	40	70.0	280	89.8[1]	84.9
	C3/100/3-40-5-50	6260	40	66.4	266	85.0	80.4
	C3/60-40-5-100	6260	40	71.4	286	91.7[1]	86.7
	C3/100-40-5-100	6260	40	72.5	290	93.1[1]	88.0
V	S-40-5	6240	25	11.1	44.4	97.9[1]	92.6
	S-60-5	6200	37.5	13.6	54.4	121.0[2]	114.7
	S-80-5	6180	50	13.4	53.6	119.2[2][3]	113.1
	S-100-5	6490	62.5	13.2	52.8	117.0[2][3]	109.6
VI	U-40-5-X	5670	40	55.0	220	71.0	68.8
	U-60-5-X	5310	60	61.4	245.6	80.8	79.6
	U-50-5	5400	50	55.5	222	73.2	71.8
	U-40-10	9870	40	65.0	260	83.6	70.5
	U-60-10	9700	60	73.2	292.8	94.2[1]	79.8
	C3/60/2-40-10-25	10,100	40	69.5	278	89.4[1]	75.0
	C3/60/2-40-10-50	9590	40	68.8	275.2	88.4[1]	75.1
	C3/60/3-40-10-50	10,100	40	68.7	274.8	88.2	74.0
VII	C3/60-40-5-150	6200	40	69.9	279.6	90.4[1]	85.7
	C3/60-40-5-200	6300	40	74.5	298	96.8[1]	91.4
	C3/60-50-5-150	6600	50	80.1	320.4	104.6[1]	97.6
	C3/60-50-5-200	6600	50	85.2	340.8	111.3[2][3]	103.8

[1] *Beyond linear-elastic limit of corresponding longitudinal bar steel*
[2] *Beyond yield stress of corresponding longitudinal bar steel*
[3] *Failed in flexure*
[4] *Bar stresses normalized to 5000 psi with the quarter root*

5.2 Splice Length

The effect of splice length on bond strength was investigated in this program. The general trend was a nonlinear increase in bar stress, f_b, as the splice length, l_s, increased. As the splice length increased, the effectiveness per unit length decreased. There was scatter even among specimens that had the same properties.

5.2.1 Unconfined

5.2.1.1 Slabs

Due to different member cross-sections, slabs and beams were separated when reviewing the test results. Figure 5.1 shows the increase in bar stress achieved in slabs as the splice length increases from 25 in. to 62.5 in. To account for the effect of variations in concrete strength among tested specimens, bar stresses normalized to a compressive strength of 5000 psi are also provided (all normalizations use the quarter root of compressive strengths). By increasing the splice length from 40d_b to 60d_b, a significant increase in bar stress was achieved. While the steel reached yield, a splice failure still resulted. Once the splice length increased to 80d_b, a flexure failure was achieved. Once a flexural failure was achieved, increasing splice length was not beneficial as the flexure capacity was fully achieved.

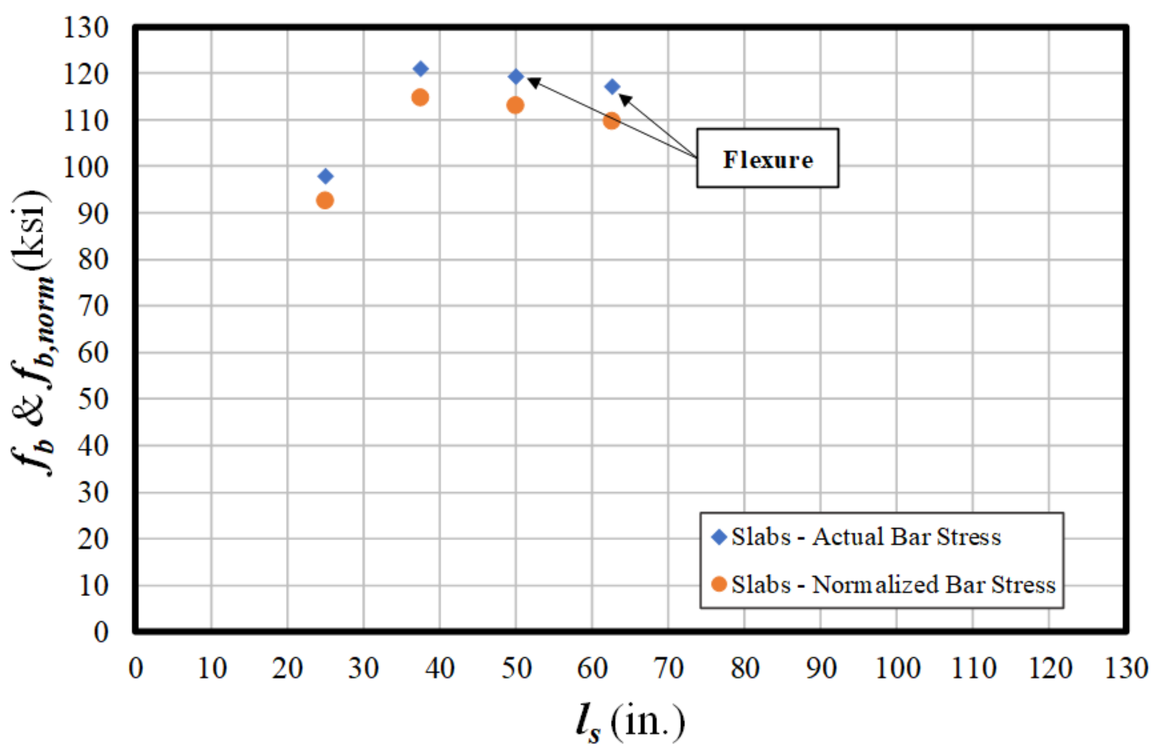

a) l_s

Figure 5.1: Effect of Splice Length on Bar Stress (Slabs)

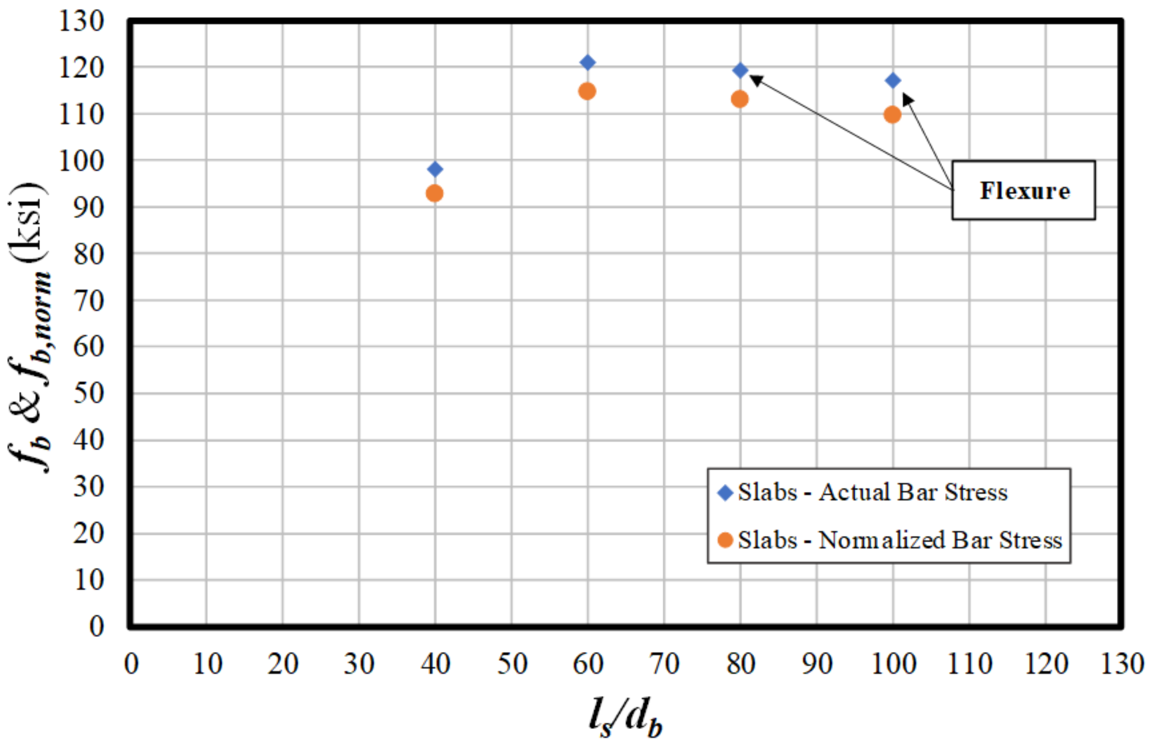

b) l_s/d_b

Figure 5.1: Effect of Splice Length on Bar Stress (Slabs) - Continued

5.2.1.2 Beams

Figure 5.2 shows the relationship between splice length and bond strength for beams. In Figure 5.2, all specimens, except for U-40-5a, exceeded their elastic limits during testing. The bars that reached the elastic limit are noted because of the round house stress-strain curve that is representative of Grade 100 steel (Figure 2.8). As shown in Appendix D, unconfined specimens cannot endure as much bar strain as confined specimens. Because all longitudinal bars in this experimental program are No. 8 bars with a diameter of 1 in., the splice length represented in Figure 5.2(a) is equivalent to the splice length in terms of bar diameter. Figure 5.2(b) shows that with an increase in splice length, there is additional strength added to the splice length up until the longitudinal bars progress beyond their elastic yield. As shown, the behavior is non-linear. The increase in splice strength can be represented by a power or piece-wise function. A trendline with the 0.5 power is plotted in Figure 5.2(b).

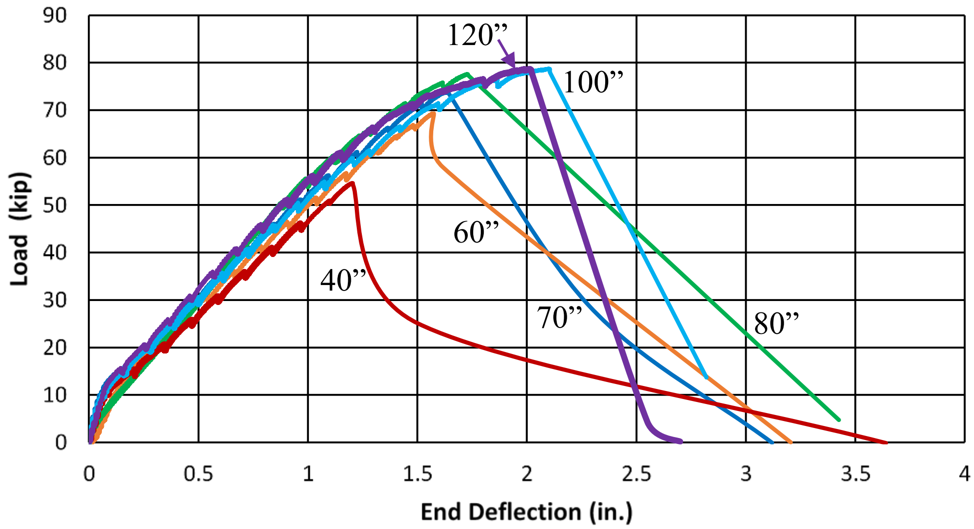

a) Load-Deflection Response

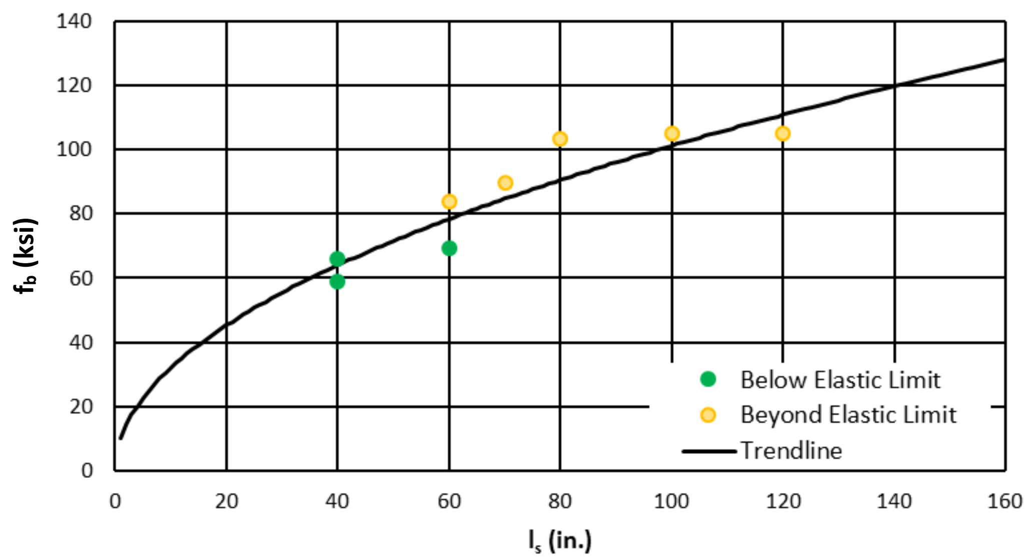

b) Bar Stress

Figure 5.2: Effect of Splice Length on Bond Strength in Unconfined Specimens

All unconfined beams are provided in Figure 5.3 for various splice lengths. Note that if Figure 5.3 is plotted against l_s/d_b, the plots are unchanged because all unconfined beams contained No. 8 spliced bars (d_b = 1 in.). Note that all MMFX, high-strength concrete, and minimum width beams are labeled. An increase in bar stress is observed for splices less than or equal to 80 in.; however, for larger splice lengths, as the embedded length increases, no additional bar stress is achieved. For the minimum width beams with large splice lengths, the bar stress appears to remain unchanged or decrease slightly as the splice length increases.

Figure 5.3(b) compares the unconfined specimen splice lengths to their failure stresses normalized to a concrete compressive strength of 5000 psi. Results from specimens with splice lengths less than 80 in. are condensed, including the high-strength concrete and MMFX specimens. This clearly shows that the quarter root normalization represents the concrete strength well. Furthermore, the MMFX specimens performed no differently than the similar A615 splice beams at splice lengths of 40d_b and 60d_b.

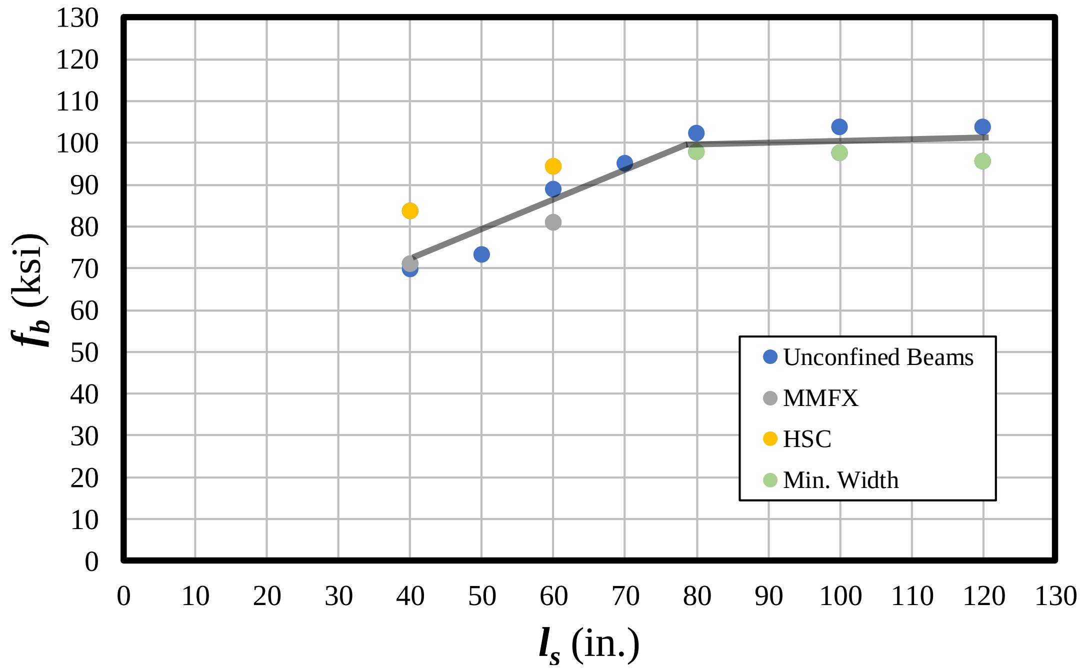

a) Actual Bar Stress

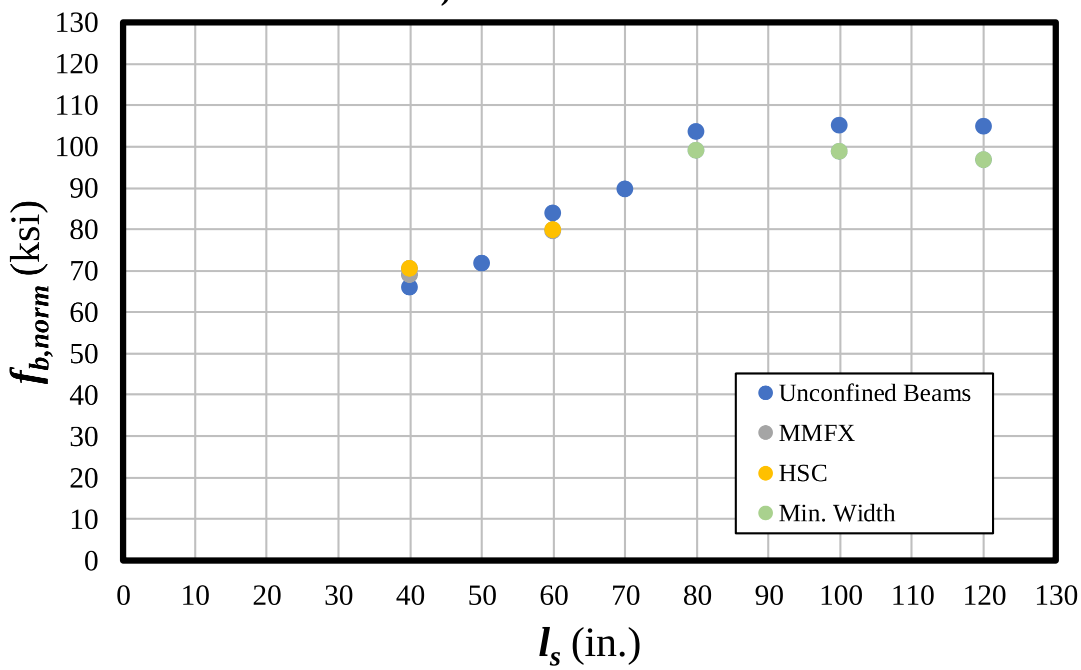

b) Normalized Bar Stress

Figure 5.3: Effect of Splice Length on Bar Stress (Unconfined)

5.2.2 Confined

5.2.2.1 Beams

Figure 5.4 shows a similar relationship as Figure 5.2. With an increase in splice length, there is also an increase in bond strength. All specimens plotted have a nominal pressure of 50 psi so that the effect of splice length can be observed. Specimen C3/60-80-5-50 failed in flexure. As both specimens C3/60-60-5-50 and C3/60-80-5-50 moved past the elastic limit of the longitudinal bars, the difference in splice strength was minimal.

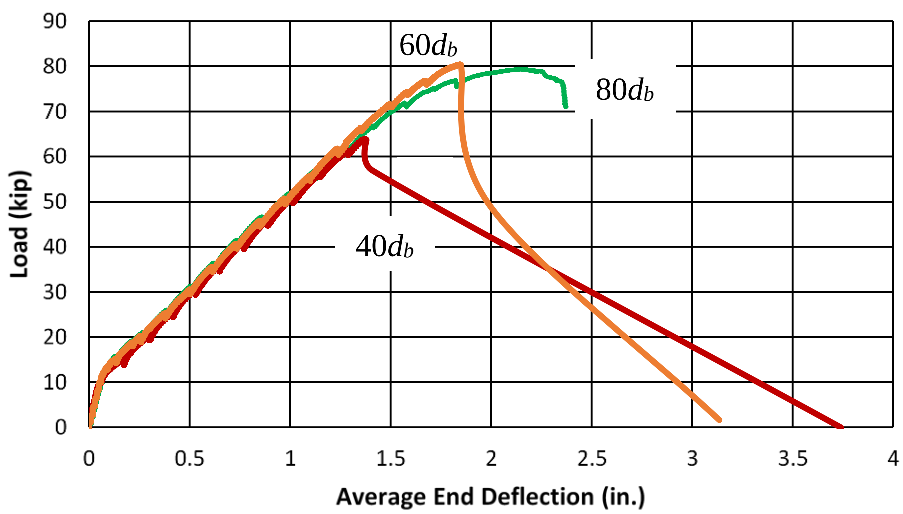

a) Load-Deflection

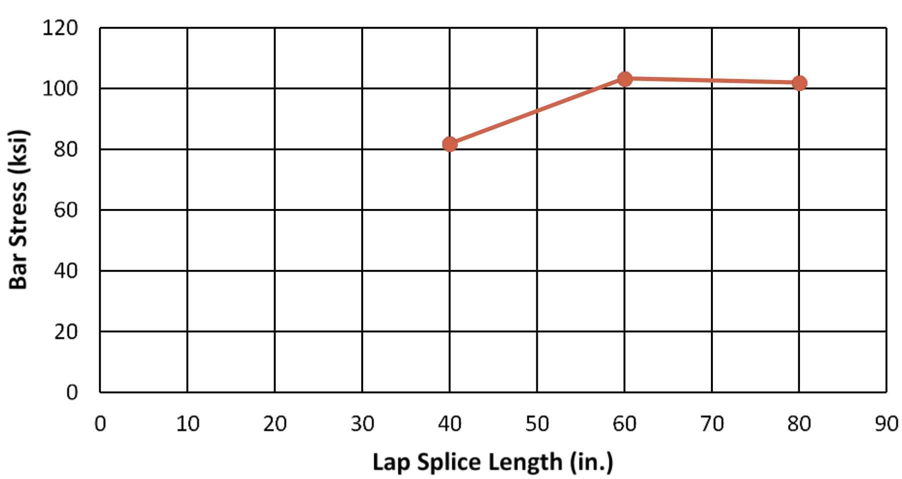

b) Bar Stress

Figure 5.4: Effect of Splice Length on Bond Strength in Confined Specimens (50 psi)

Correlations between splice length and bar stress for confined beams when multiple different confinement pressures are plotted are not evident due to the variation in confinement (Figure 5.5). However, by isolating the confined beams constructed with 50 psi of nominal pressure along the splice, a correlation is observed between splice length and bar stress (Figure 5.6). For 50-psi confined beams with a splice length of $40d_b$, failures occurred within a range of 10 ksi (some variation of concrete strength). As splice length was increased to $60d_b$ and $80d_b$, bar stress increased and the failure mode ultimately changed from splitting to flexure.

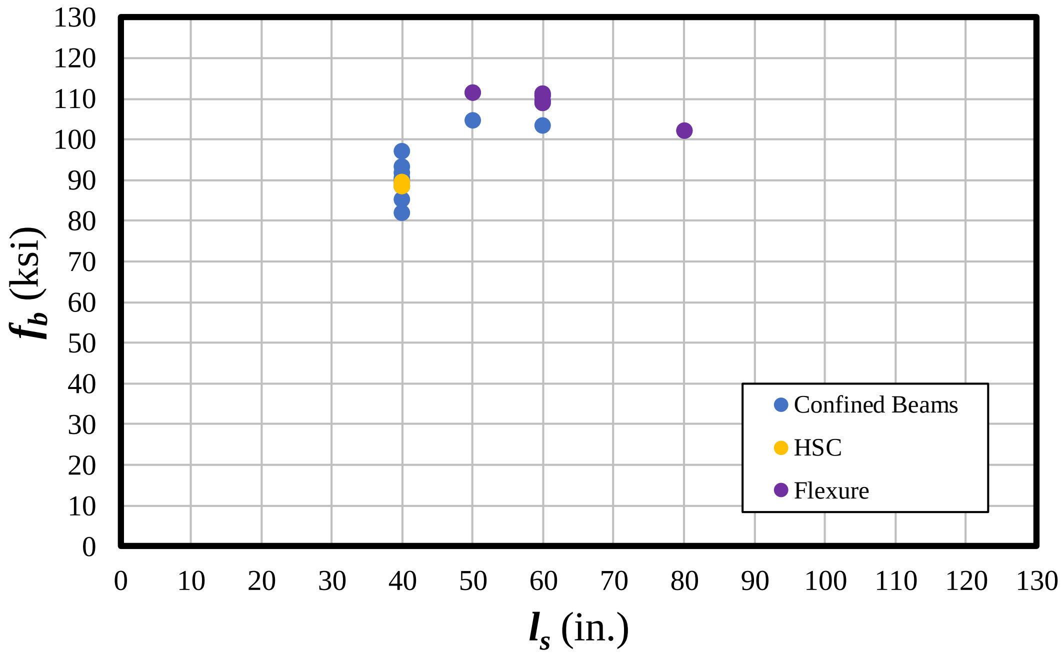

Figure 5.5: Effect of Splice Length on Actual Bar Stress

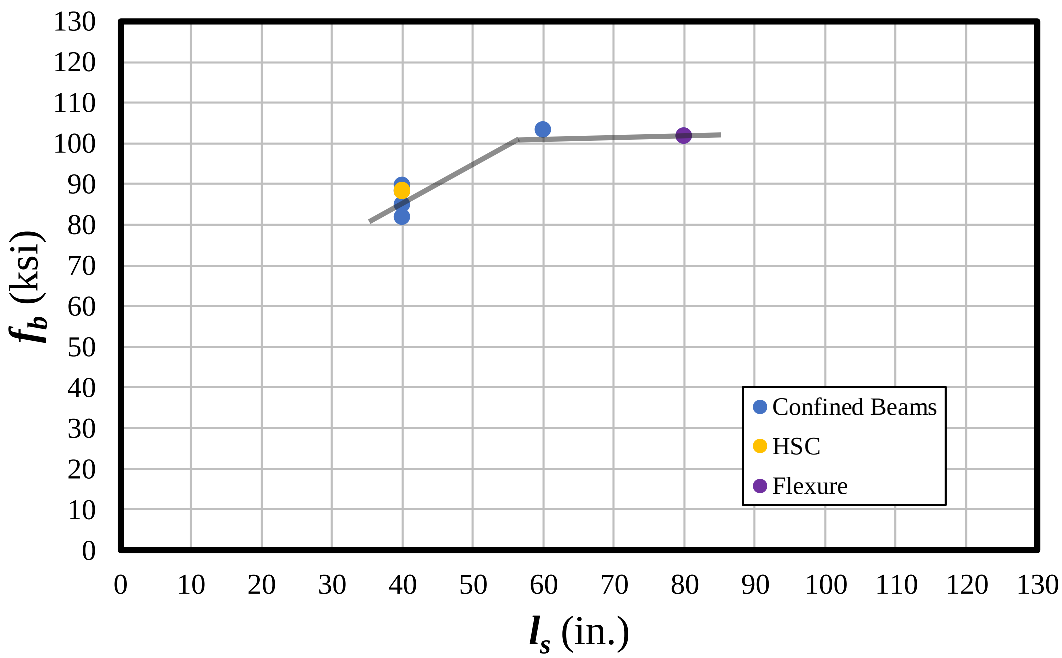

Figure 5.6: Effect of Splice Length on Actual Bar Stress (Confined 50-psi Beams)

5.3 Bar Clear Spacing

The bar spacing was selected based on common design practices for this testing program. Three specimens were also designed with the minimum bar spacing, d_b, specified in ACI 318-14. Because all three minimum unconfined specimens exceeded the elastic limit of the longitudinal bars (U-80-5-M, U-100-5-M, and U-120-5-M), the impact of bar spacing is difficult to observe (Figure 5.7). The slight increase in bar stress could be a trend observed or typical scatter in the test results.

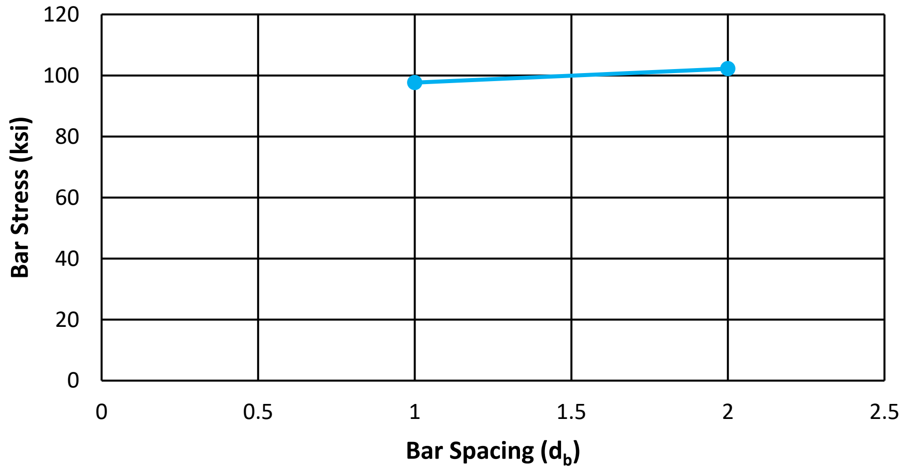

a) 80d_b Splice Length

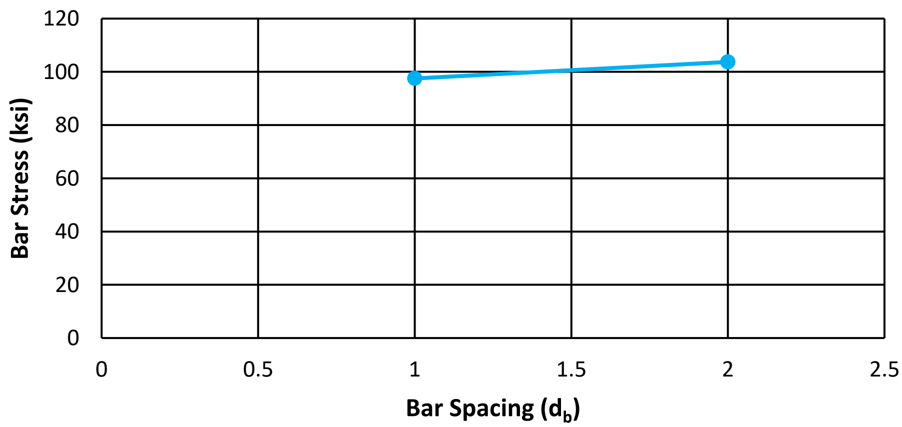

b) 100d_b Splice Length

Figure 5.7: Effect of Bar Spacing on Bond Strength

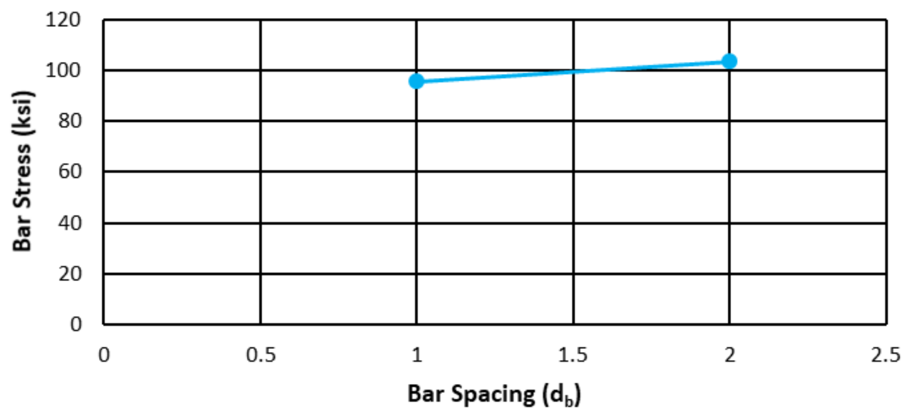

c) 120d_b Splice Length

Figure 5.7: Effect of Bar Spacing on Bond Strength - Continued

5.4 Concrete Compressive Strength

5.4.1 Unconfined Specimens

The range of concrete strengths tested on unconfined beams ranged from 4740 psi to 9870 psi. Figure 5.8 shows this range and indicates which specimens contained MMFX bars, high-strength concrete, and the minimum bar spacing. No clear correlation between concrete compressive strength and bar stress is observed in this plot.

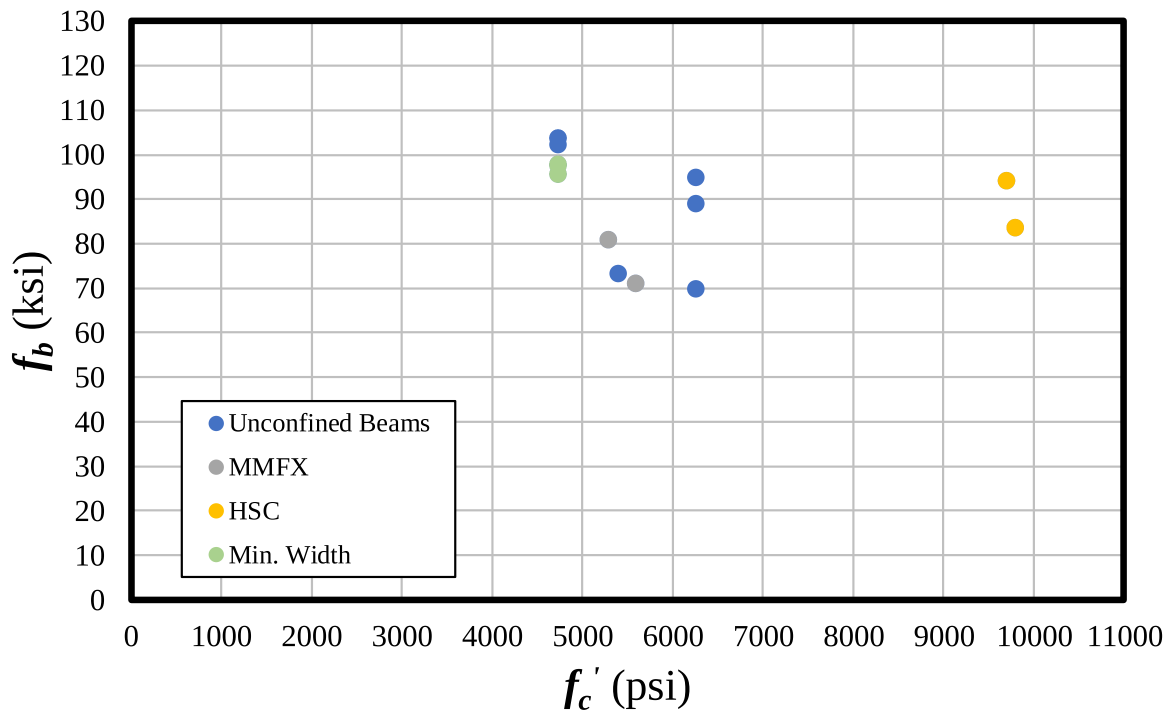

Figure 5.8: Effect of Concrete Strength on Actual Bar Stress (Unconfined)

Figure 5.9(a) provides a comparison between the concrete compressive strength and the bar stress for all unconfined beams. Slabs were not included because Series V was for a different cross-section. All specimens in Figure 5.9(a) are grouped by identical splice length, with lengths of 40d_b and 60d_b having the most specimens. There is an observed increase in bar stress as concrete compressive strength increases for a constant splice length. For the 60d_b unconfined beams, the relationship between compressive strength and bar stress appears to be nonlinear. Note that the cluster of beams with concrete compressive strength of 4740 psi contains the greatest splice lengths and three beams with minimum bar spacing. Figure 5.9(b) shows the effect on bar stress normalized to 5000 psi (using the quarter root), which shifts the high-strength concrete beams downward. The flat trend in the normalization supports the use of the quarter root to represent the influence of concrete compressive strength.

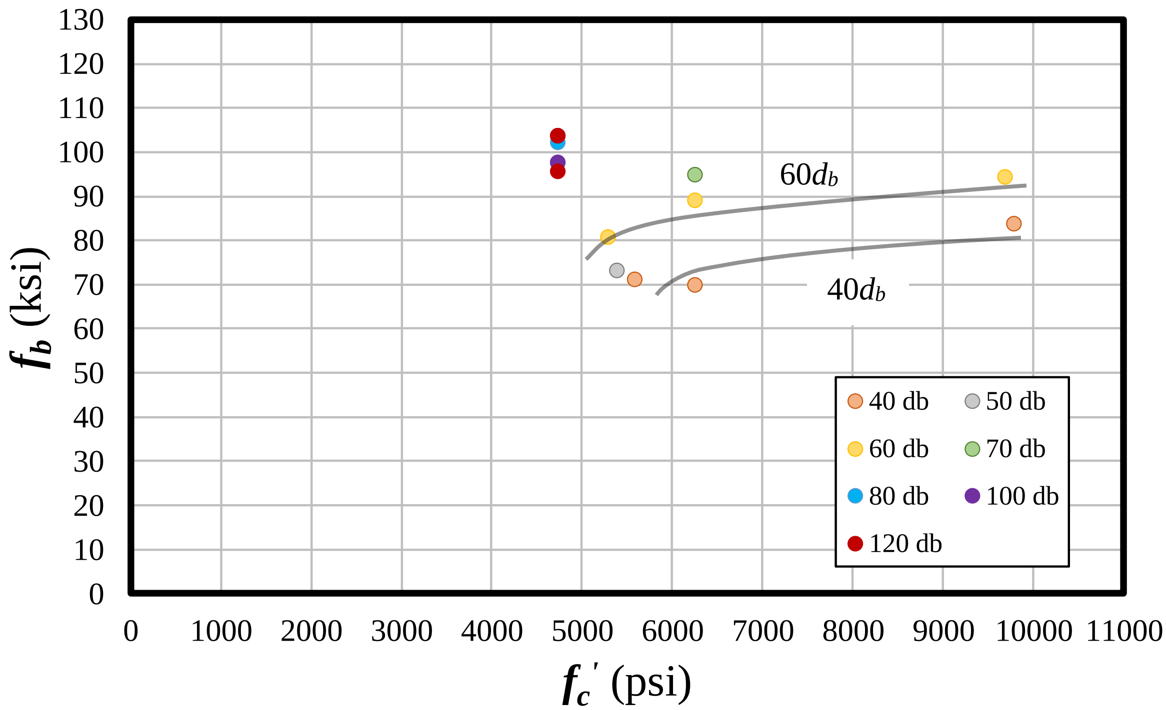

a) Actual Bar Stress

Figure 5.9: Effect of Concrete Strength on Bar Stress by Splice Length – Unconfined

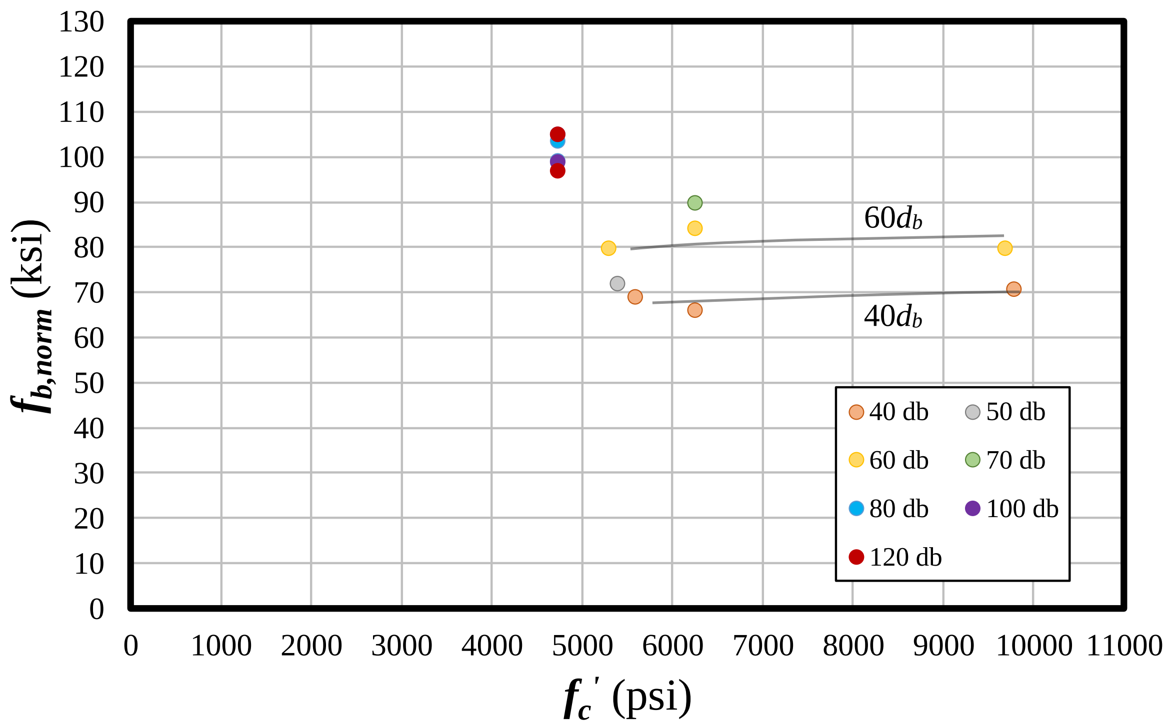

b) Normalized Bar Stress

Figure 5.9: Effect of Concrete Strength on Bar Stress by Splice Length (Unconfined) - Continued

The change in bar stress between specimens cast with normal-strength concrete and high-strength concrete is provided in Table 5.2 for 40d_b and 60d_b specimens. The two beams from Series VI containing MMFX reinforcing bars are included in this comparison because the behavior during testing and at failure was identical to the beams reinforced with A615 longitudinal bars. Additionally, a comparison between representing the concrete strength by the square root and the quarter root is provided. For the 60d_b specimens, the quarter root of the difference in concrete strengths provides a better representation when compared to the use of the square root. For splice lengths of 40d_b, the quarter root is more accurate for Specimen U-40-5-X; however, this is untrue for Specimen U-40-5a where the square root is slightly closer in representing the change in concrete strength.

Table 5.2: Effect of High-Strength Concrete for 40d_b and 60d_b Specimens

Specimens		f_c (psi)	f_b (ksi)	f_b Increase	$\sqrt{f'_{c,HSC}/f'_{c,NSC}}$	$\sqrt[4]{f'_{c,HSC}/f'_{c,NSC}}$
40d_b	U-40-5a	6260	69.8	20%	25%	12%
	U-40-5-X	5600	71.0	18%	32%	15%
	U-40-10	9800	83.6	-	-	-
60d_b	U-60-5a	6260	88.9	6%	24%	12%
	U-60-5-X	5300	80.8	17%	35%	16%
	U-60-10	9700	94.2	-	-	-

5.4.2 Confined Specimens

The range of concrete strengths tested on confined beams ranged from 6200 psi to 10,100 psi. Figure 5.10 shows this range and indicates which specimens contained high-strength concrete, minimum bar spacing, or failed in flexure. No clear correlation between concrete compressive strength and bar stress is observed in this plot.

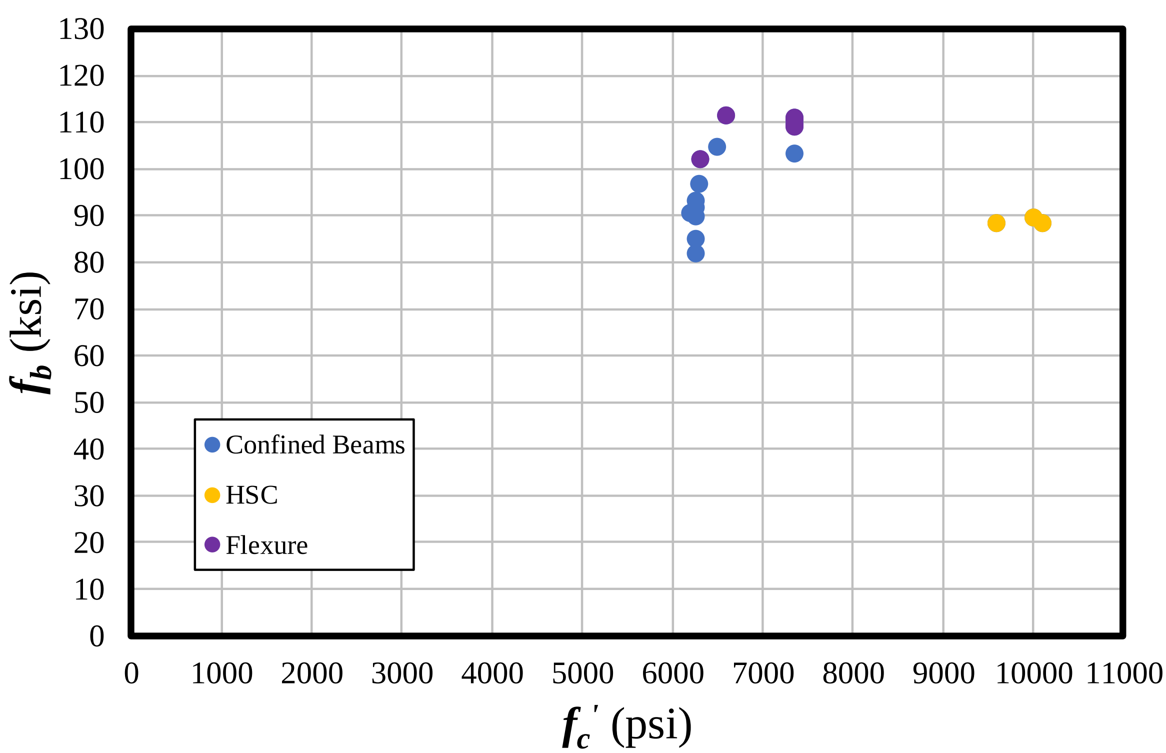

Figure 5.10: Effect of Concrete Strength on Bar Stress (Confined)

Additional parameters were isolated to observe trends among compressive strength and bar stress. Figure 5.11(a) groups confined beams that failed in splitting (no flexure) by splice length for 40d_b, 50d_b, 60d_b, and 80d_b specimens. Only the 40d_b specimens contained a large range of concrete compressive strengths. In addition, the most common confinement pressure used in this testing program was 50 psi of transverse reinforcement; therefore, all 40d_b confined beams with 50 psi of transverse reinforcement were isolated in Figure 5.11(b). A slight positive correlation between concrete strength and bar stress was found for confined specimens; however, this may be attributed to typical scatter of the data.

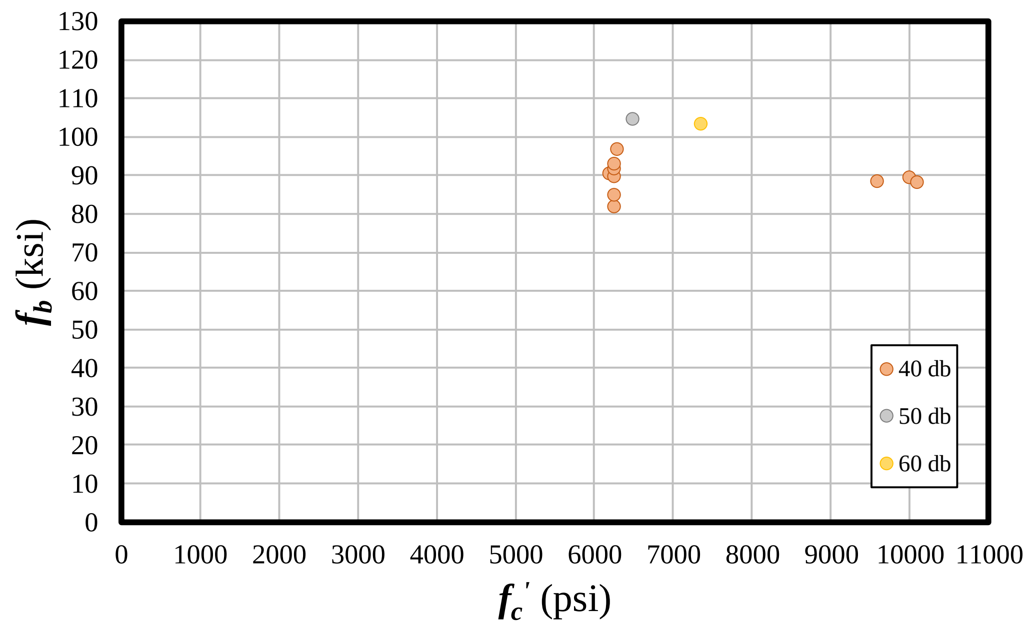

a) All Splice Lengths

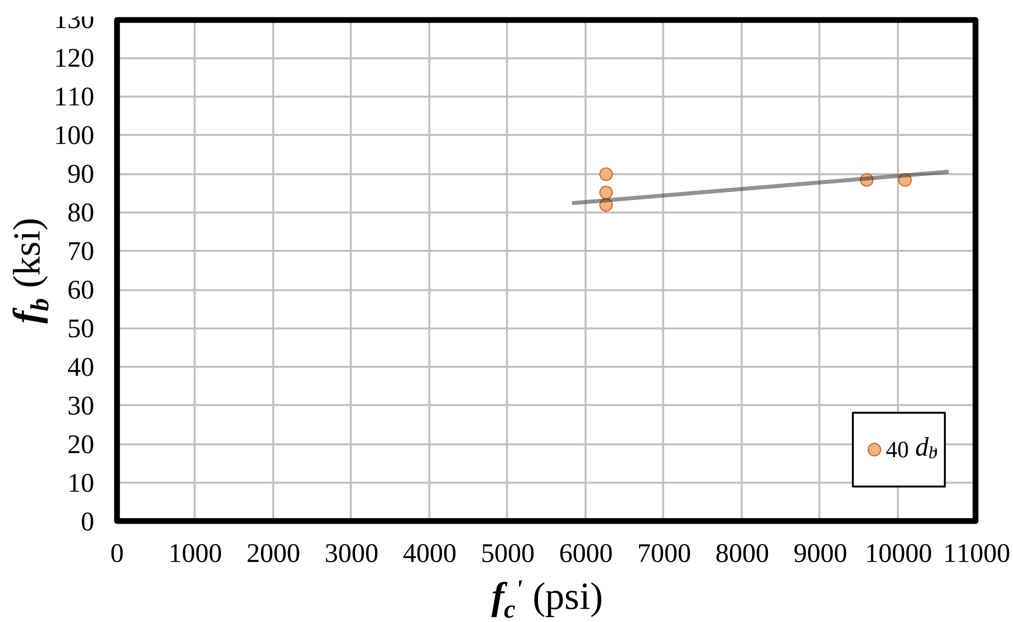

b) 40d_b Specimens with 50-psi Confinement Pressure

Figure 5.11: Effect of Concrete Strength on Bar Stress (Confined)

5.5 <u>Transverse Reinforcement</u>

To better understand the influence of transverse reinforcement on bond strength, six parameters were believed to have a strong influence on the confinement contribution to bar stress. The variables of interest are the confinement level (related to the confinement pressure), distributed transverse reinforcement ratio (ρ_t), confinement pressure (p_c), average transverse reinforcement ratio (ρ_{avg}), stirrup location, and transverse reinforcement grade (f_{yt}).

5.5.1 Confinement Level

Various transverse reinforcement spacings corresponding to different nominal transverse pressures were investigated. In Figure 5.12, Specimen C3/60/2-40-5-50 (red) was compared with Specimen C3/60-40-5-100 (blue). The only difference in specimens was that Specimen C3/60/2-40-5-50 had a 19-in. center-to-center spacing of transverse reinforcement (50 psi), while Specimen C3/60-40-5-100 had a 9-1/2-in. center-to-center spacing (100 psi). A 12% increase in strength was observed in the 40d_b specimens (Figure 5.12(b)). The same trends are also observed in the 60d_b specimens (Figure 5.13). The increase cannot be quantified in the case of the 60d_b specimens because the specimens with 100 psi and 150 psi of nominal pressure failed in flexure, indicating that the splice strength was sufficient. It is interesting, however, that the increase in bar stress with increasing nominal pressure from 50 psi to 100 psi is approximately the same (10 ksi), regardless of splice length (Figure 5.13(b)).

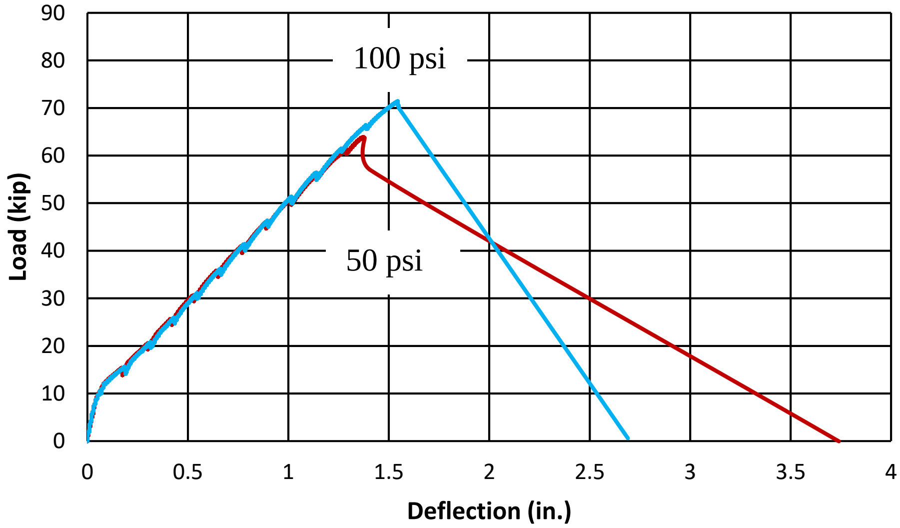

a) Load-Deflection

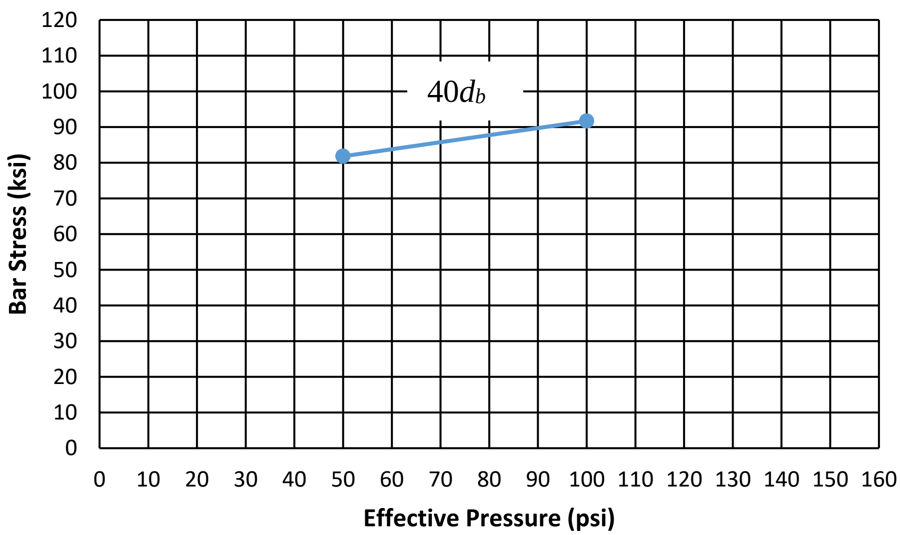

b) Bar Stress

Figure 5.12: Effect of Confinement Level on Bond Strength ($40d_b$ Specimens)

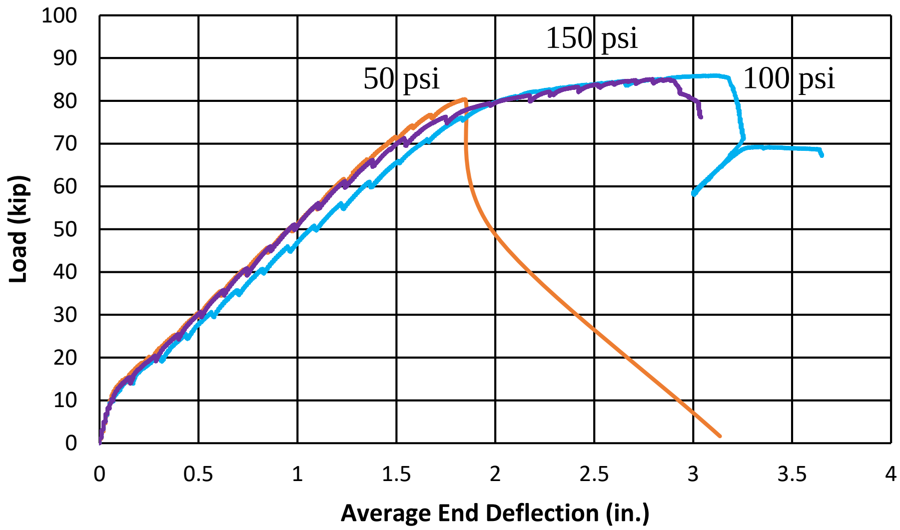

a) Load-Deflection

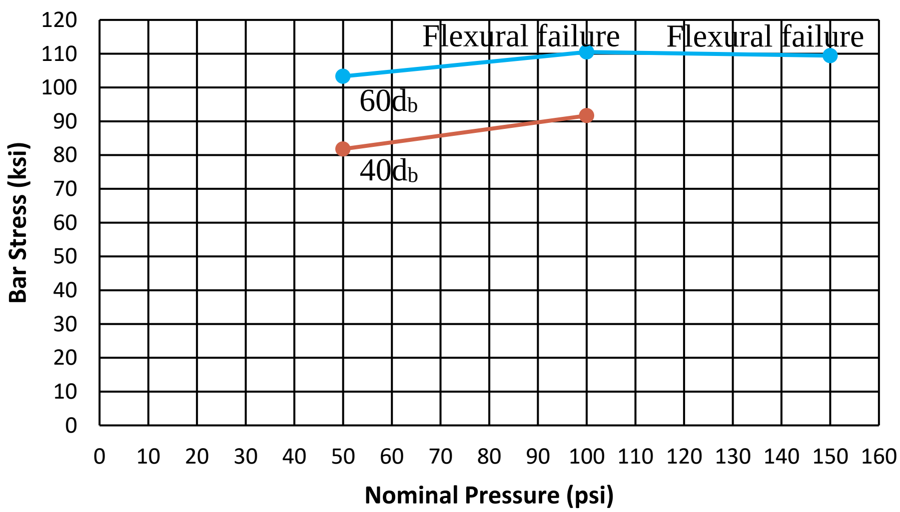

b) Bar Stress

Figure 5.13: Effect of Confinement Level on Bond Strength (60d_b Specimens)

5.5.2 Distributed Transverse Reinforcement Ratio

While Glucksman 2018 found a positive correlation between the confinement contribution to bar stress and the total area of transverse reinforcement present, several important confinement variables such as stirrup spacing and effective area of the stirrup in the splice plane may better describe the effect of transverse reinforcement.

The fundamental mechanics that initiate bond failure occur when tensile strength of the concrete is exceeded by the stresses developed over the lap splice. The tensile load that accumulates is resisted primarily by the concrete until cracking initiates. As bar stresses continue to increase, the transverse steel becomes responsible for resisting this stress entirely without contribution from the surrounding cracked concrete. The resisting stress or pressure occurs over the entire plane of splitting.

The distributed transverse reinforcement ratio, ρ_t, is a term used by ACI 318-14 in determining reinforcement requirements for wall and diaphragm design. The term takes the transverse reinforcement area of one confining element and compares it to the gross area of concrete over which it is confining. This ratio is helpful in describing the amount of transverse reinforcement within a region and is independent of the yield strength of the material. Figure 5.4 provides a graphic of Equation 5-1.

$$\rho_t = \frac{A_v}{A_g} = \frac{N_l A_t}{b_w s} \qquad (5\text{-}1)$$

where:

A_g = *gross area of concrete in splitting plane within stirrup spacing s (in.^{2})*

A_t = *area of one leg of a closed stirrup, hoop, or tie within spacing s (in.^{2})*

A_v = *area of shear reinforcement within spacing s (in.^{2})*

b_w = *beam width (in.)*

N_l = *number of legs on a given stirrup*

s = *stirrup spacing (in.)*

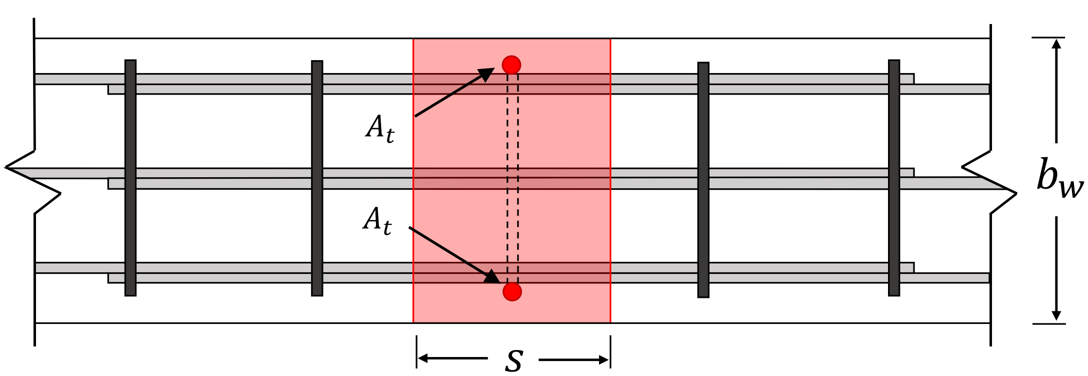

Figure 5.14: Representation of ρ_t

All confined specimens are plotted in Figure 5.15(a). Beams cast with high-strength concrete and beams that experienced a flexural failure at large stresses are noted. Values for ρ_t range from 0.04% to 0.34% within the splice. There is a slight increasing trend in bar stress as ρ_t increases. To further evaluate, beams experiencing a flexure failure were removed and all confined beams were grouped by splice length (Figure 5.15(b)). The 40d_b and 60d_b specimens provide the most data across a large range of ρ_t values. General observed trends are noted for these two lengths of specimens. Note that a ρ_t value of zero indicates an unconfined beam of the specified splice length.

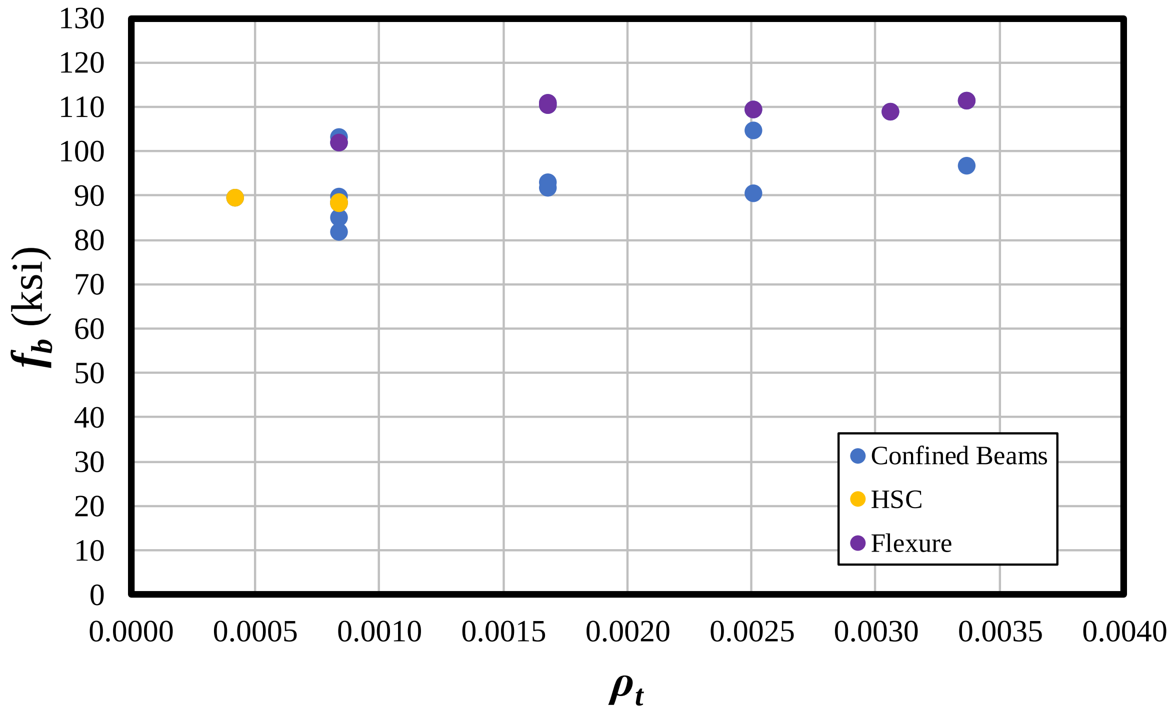

a) All Confined Beams

Figure 5.15: Effect of Transverse Reinforcement Ratio on Actual Bar Stress

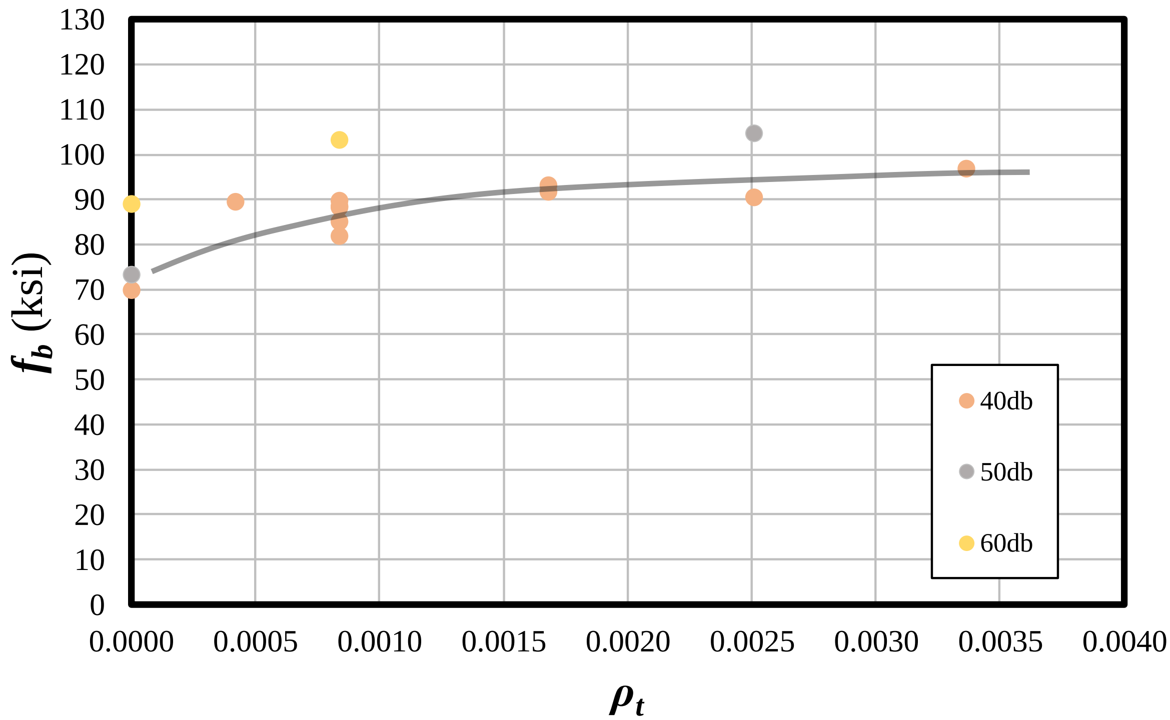

b) Grouped by Splice Length

Figure 5.15: Effect of Transverse Reinforcement Ratio on Actual Bar Stress - Continued

Figure 5.16(a) provides results when failure bar stresses are normalized to a concrete strength of 5000 psi. Unconfined reference values are provided in Figure 5.16(b) as well as specimens grouped by splice lengths and possible trend lines. Specimens with lower ρ_t values were observed to experience increased bar stresses with small increases in ρ_t; however, as ρ_t increased above approximately 0.1%, a smaller increase in bond stress was observed. The region of larger stirrup spacing and lower ρ_t values exhibits more variability in bar stress contribution due to the large range of possible stirrup locations.

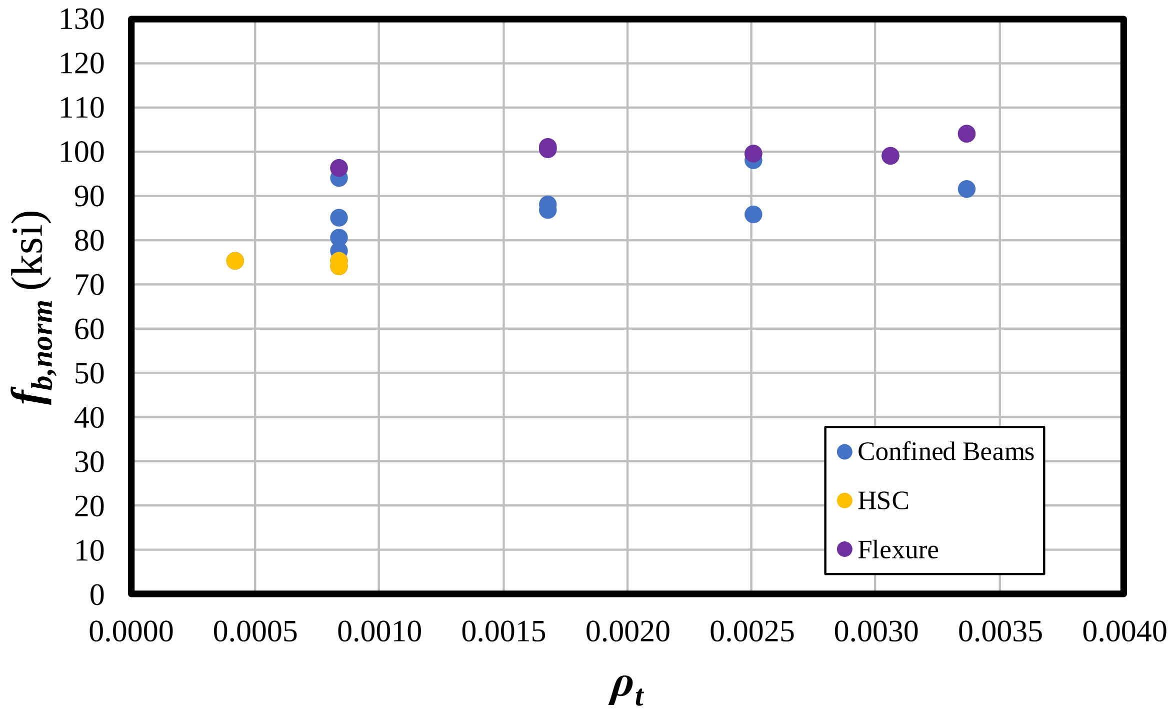

a) All Confined Beams

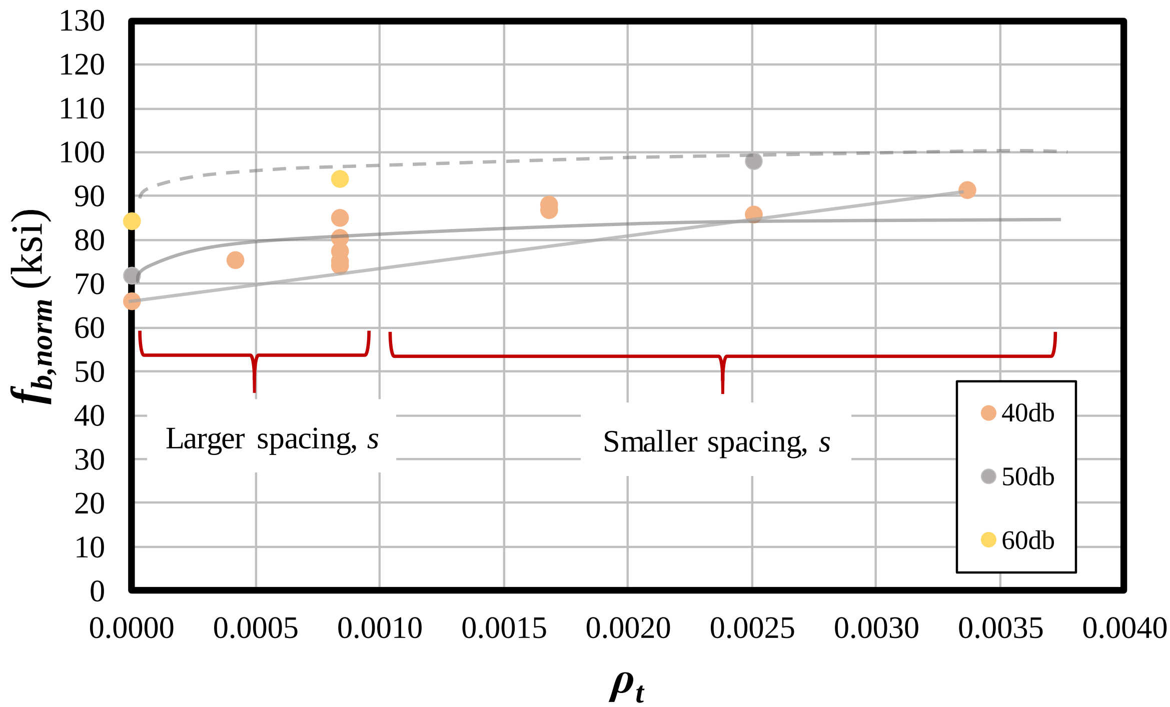

b) Grouped by Splice Length

Figure 5.16: Effect of Transverse Reinforcement Ratio on Normalized Bar Stress

By subtracting the bar stress provided by the concrete (unconfined case for each confined beam, f_{bc}) from the failure bar stress of each confined beam (f_b), a value is obtained for the contribution to total bar stress provided by the transverse reinforcement (f_{bs}). Figure 5.17(a) provides f_{bs} values for all confined beams in this testing program. Specimens cast with high-strength concrete and beams that failed in flexure are indicated. When splice lengths are isolated (Figure 5.17(b)), trends are observed with the 40d_b and 50d_b specimens. The four beams tested in Series VII show nearly identical increases in bar stress contribution from confinement as ρ_t increases between the 40d_b and 50d_b beams. Note that specimens experiencing a flexural failure are included in Figure 5.17(b) to show a trend in Series VII.

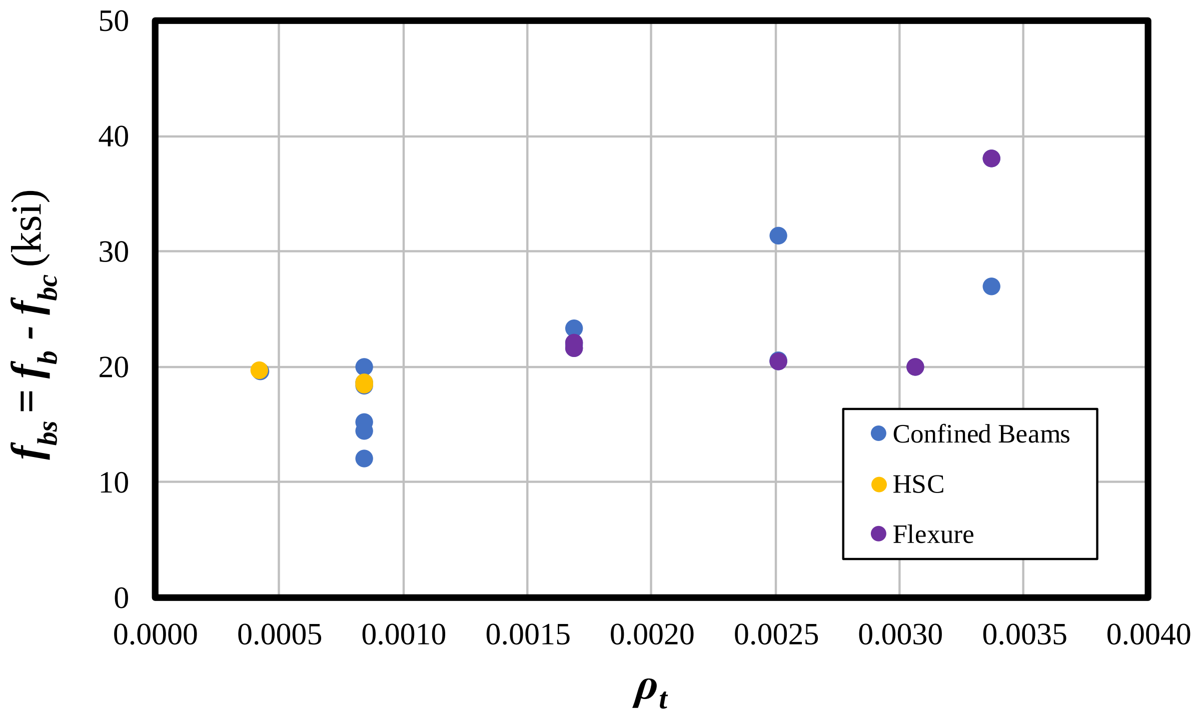

a) All Confined Beams

Figure 5.17: Effect of Transverse Reinforcement Ratio on Steel Contribution to Bar Stress

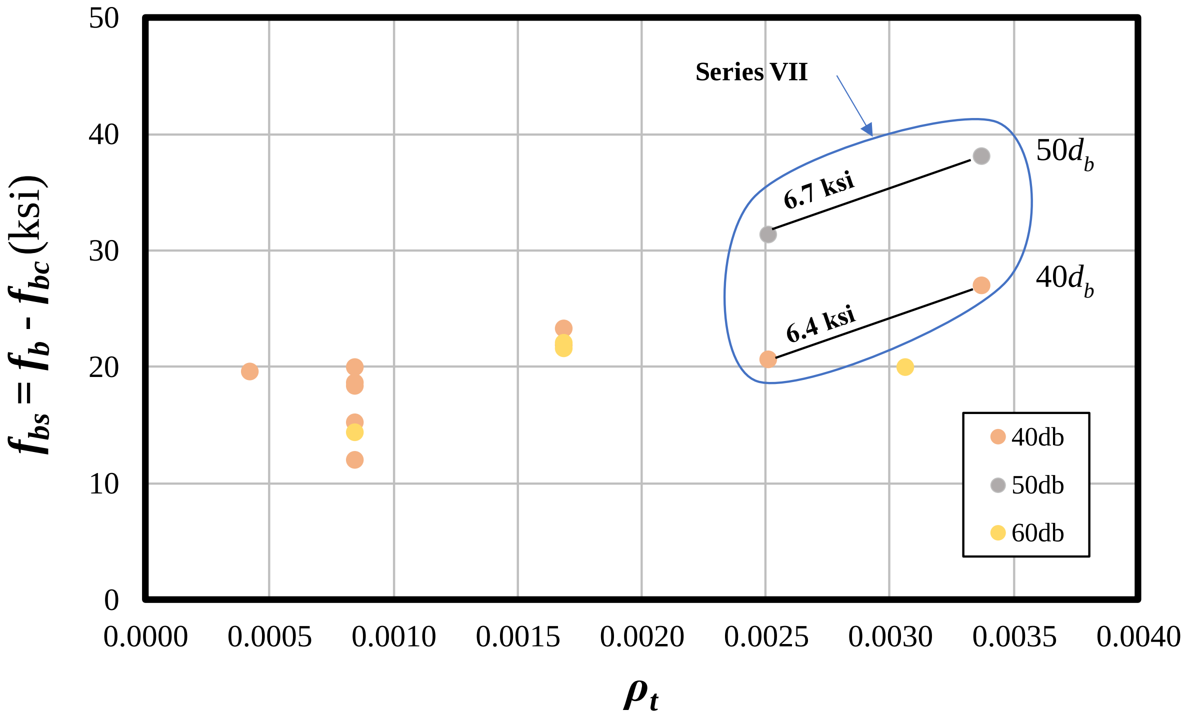

b) Grouped by Splice Length

Figure 5.17: Effect of Transverse Reinforcement Ratio on Steel Contribution to Bar Stress - Continued

Finally, bar stress contributions (f_{bs}) were adjusted to account for differences in concrete strength. Actual failure stresses for confined beams were implemented while the unconfined counterpart beam stresses were normalized to a concrete strength of 5000 psi. Figure 5.18(a) plots the results for the confined beams. Figure 5.18(b) isolates the effect of splice length and shows that when flexure is neglected, f_{bs} increases as ρ_t increases.

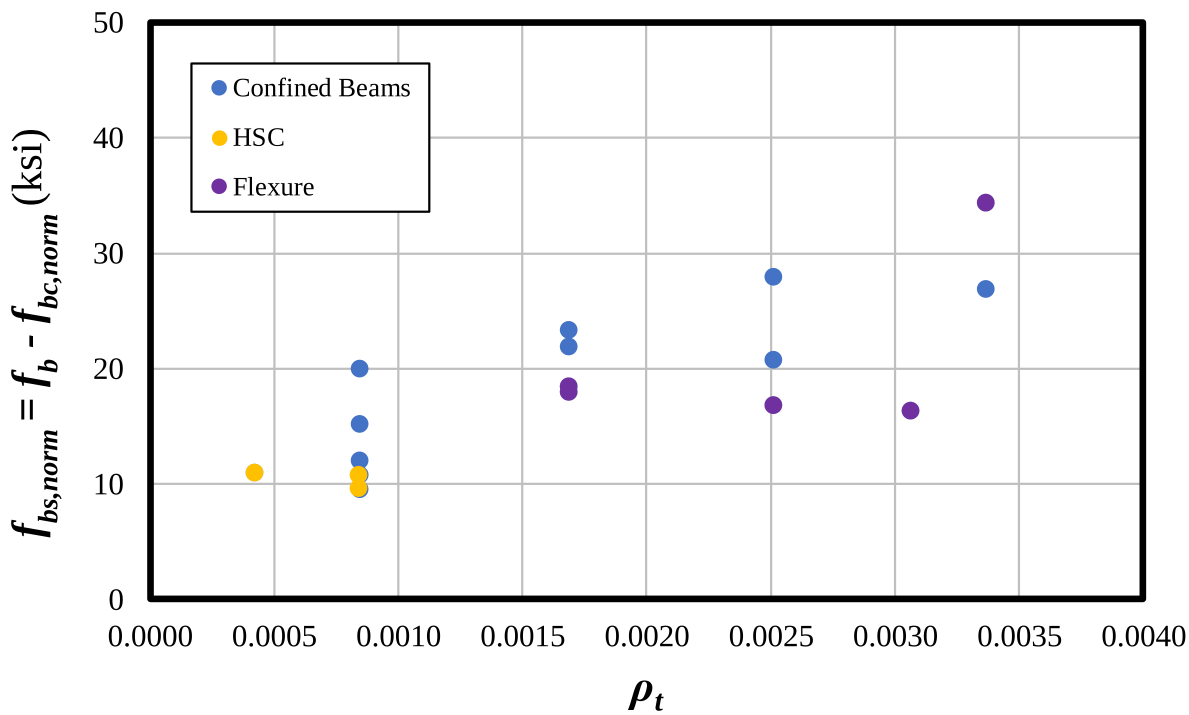

a) All Confined Beams

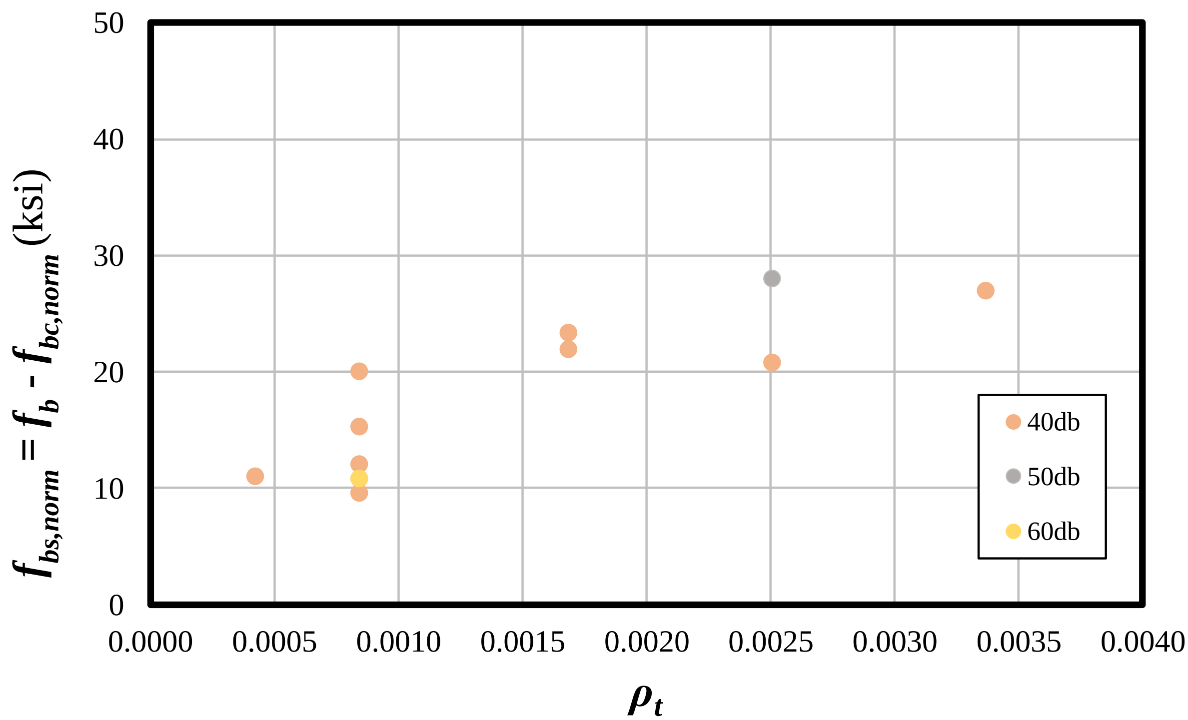

b) Grouped by Splice Length

Figure 5.18: Effect of Transverse Reinforcement Ratio on Normalized Steel Contribution to Bar Stress

5.5.3 Confinement Pressure

The confinement pressure (p_c) for each stirrup can be calculated from the specified yield strength of the stirrup and the distributed transverse reinforcement ratio:

$$p_c = f_{yt}\rho_t \tag{5-2}$$

where:

f_{yt} = *actual yield strength of transverse reinforcement (psi)*

p_c = *confining pressure developed by transverse reinforcing (psi)*

ρ_t = *distributed transverse reinforcement ratio*

$$= \frac{A_v}{A_g} = \frac{N_l A_t}{b_w s}$$

Various confinement pressures are plotted against the failure bar stress in Figure 5.19(a). Note that this confinement bar stress is different than the nominal confinement pressure selected to design the confined specimens. The nominal value is an estimate based on general stirrup spacing and neglects the yield strength variation in the transverse reinforcement. High-strength stirrups are noted, as well as high-strength concrete beams and flexure-failed specimens. All pressures are calculated using the actual yield strength of the transverse reinforcement; therefore, specimens noted as having Grade 100 stirrups have an f_{yt} value of 102 ksi. Figure 5.19(b) isolates each specimen by splice length and shows general trends for the $40d_b$ and $60d_b$ specimens.

Although there is a clear positive correlation between confinement pressure p_c and bar stress, this correlation is believed to be primarily influenced by ρ_t in the p_c equation, not f_{yt}.

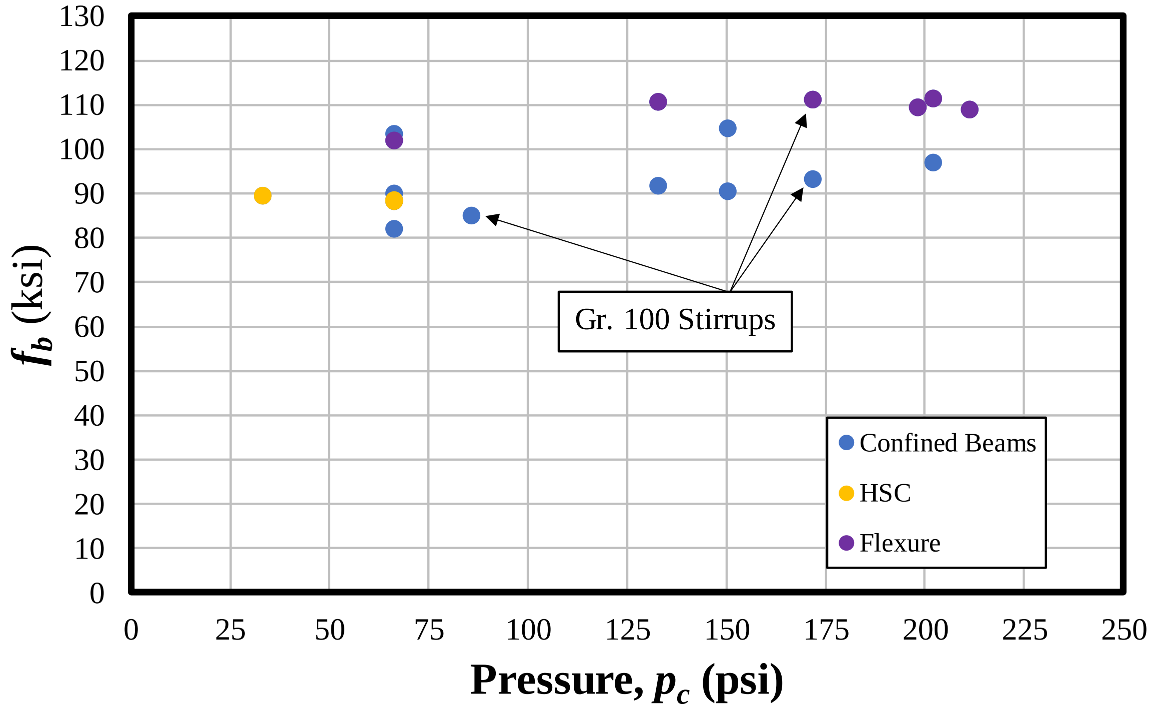

a) All Confined Beams

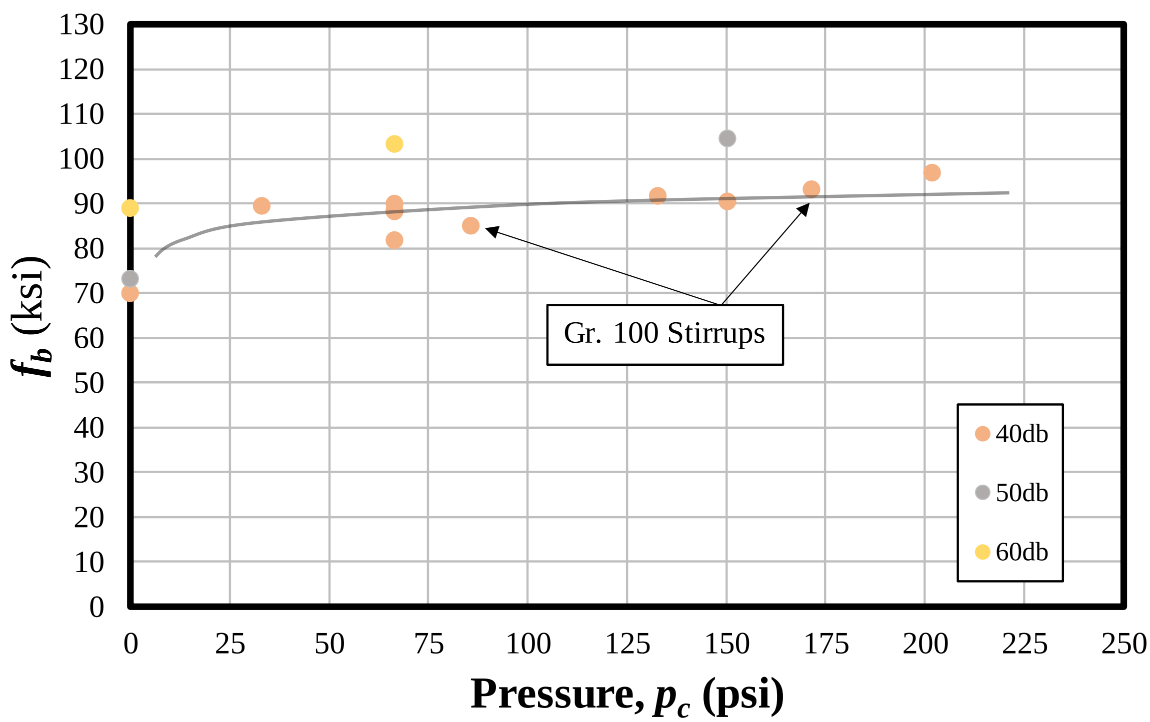

b) Grouped by Splice Length

Figure 5.19: Effect of Confinement Pressure on Actual Bar Stress

When bar stress is normalized to a 5000-psi concrete compressive strength, test results with respect to confinement pressure are slightly compressed. In general, as the confining pressure around the splice increases, the bar stress increases. This normalized bar stress comparison for all confined specimens is provided in Figure 5.20(a) with beams identified that contained high-strength concrete and that experienced flexural failures. Figure 5.20(b) isolates the effect of splice length for all confined beams.

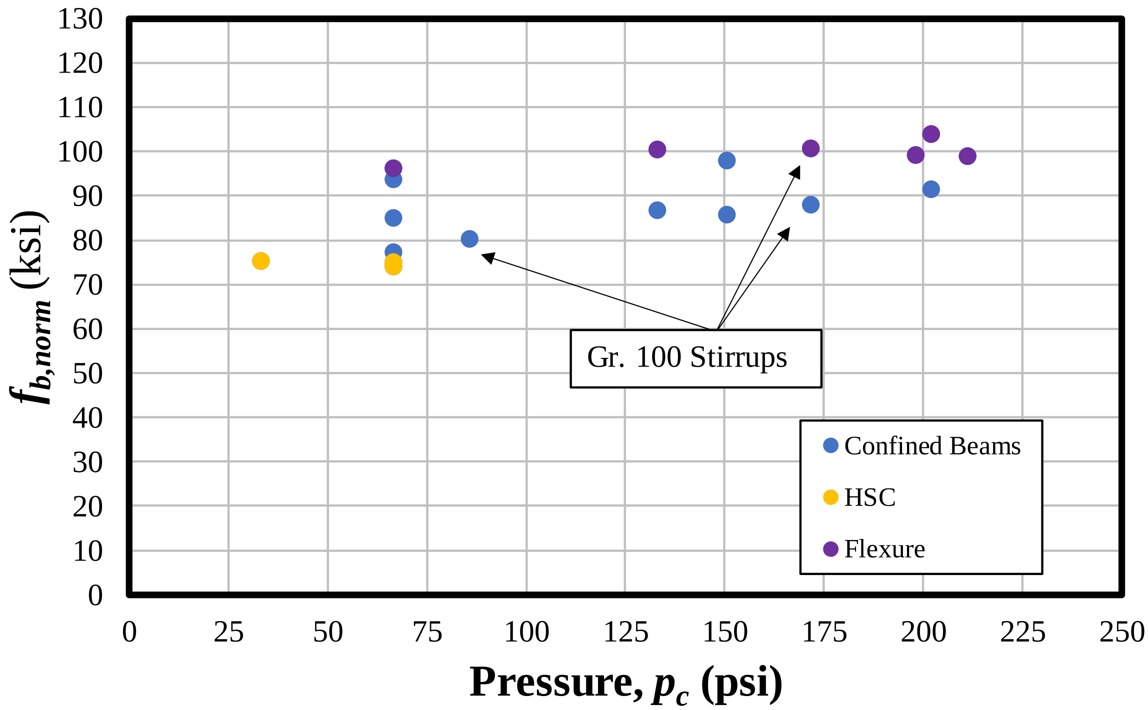

a) All Confined Beams

Figure 5.20: Effect of Confinement Pressure on Normalized Bar Stress

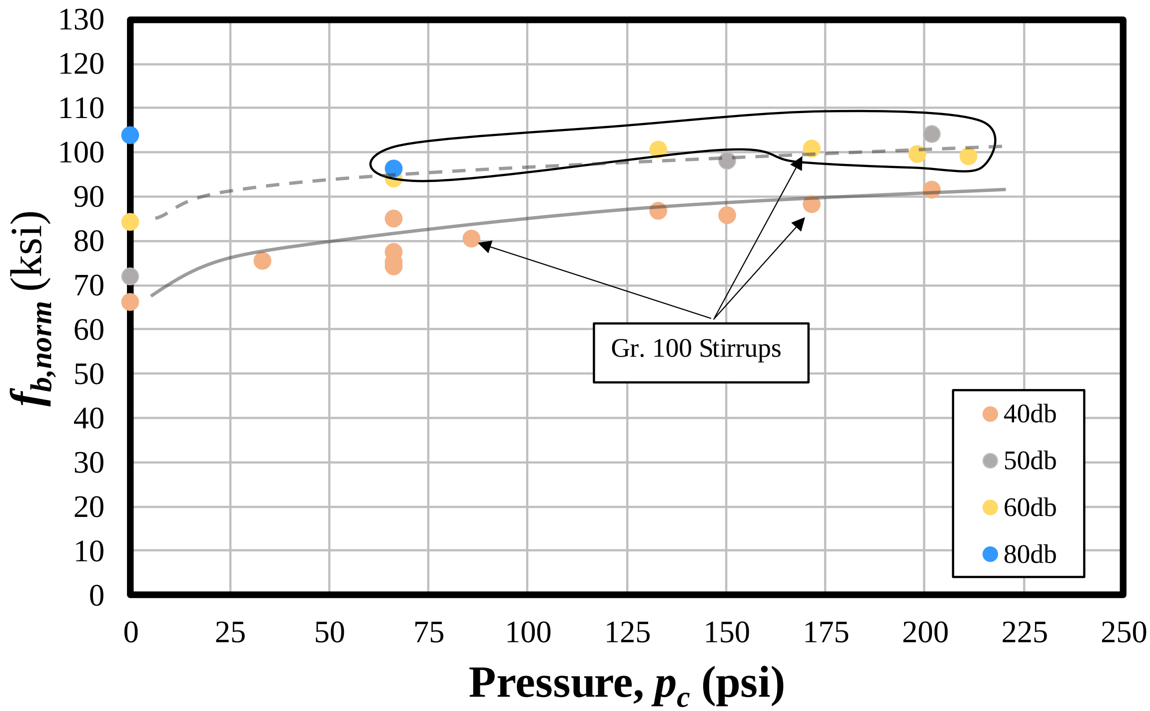

b) Grouped by Splice Length

Figure 5.20: Effect of Confinement Pressure on Normalized Bar Stress - Continued

5.5.4 Average Transverse Reinforcement Ratio

The distributed transverse reinforcement ratio (ρ_t) accounts for the area of concrete being confined by each stirrup; however, the configuration of the stirrups across the entire length of the splice may change this value for end stirrups. An average can be calculated if all stirrups within the splitting plane are considered:

$$\rho_{avg} = \frac{A_{tr}}{A_{sp}} = \frac{N_s N_l A_t}{b_w l_s} \quad (5\text{-}3)$$

where:

A_{sp} = *area of the splitting plane within the splice region (in.^{2})*

A_{tr} = *total cross-sectional area of all transverse reinforcement within spacing s that crosses the potential plane of splitting through the reinforcement being developed (in.^{2})*

l_s = *splice length (in.)*

N_s = *number of stirrups along the length of splice*

Consequently, the average confinement pressure for the entire splice region can be calculated in a similar manner by replacing the distributed transverse reinforcement ratio with ρ_{avg}; however, after analyzing the effect of ρ_t and f_{yt} on bond strength in this study, stirrup yield strength was found to contribute little to the contribution of transverse reinforcement. For a general analysis in this study, total confinement pressure was not explored as a parameter of interest.

Figure 5.21(a) provides a comparison between bar stress and average transverse reinforcement ratio, ρ_{avg}. Although some values are translated, the overall trends remain unchanged when compared to ρ_t. Figure 5.21(b) compares the average transverse reinforcement ratio to a failure bar stress normalized to a concrete compressive strength of 5000 psi. A clear positive correlation is observed for the 40d_b specimens. A similar finding can be observed for the 60d_b specimens.

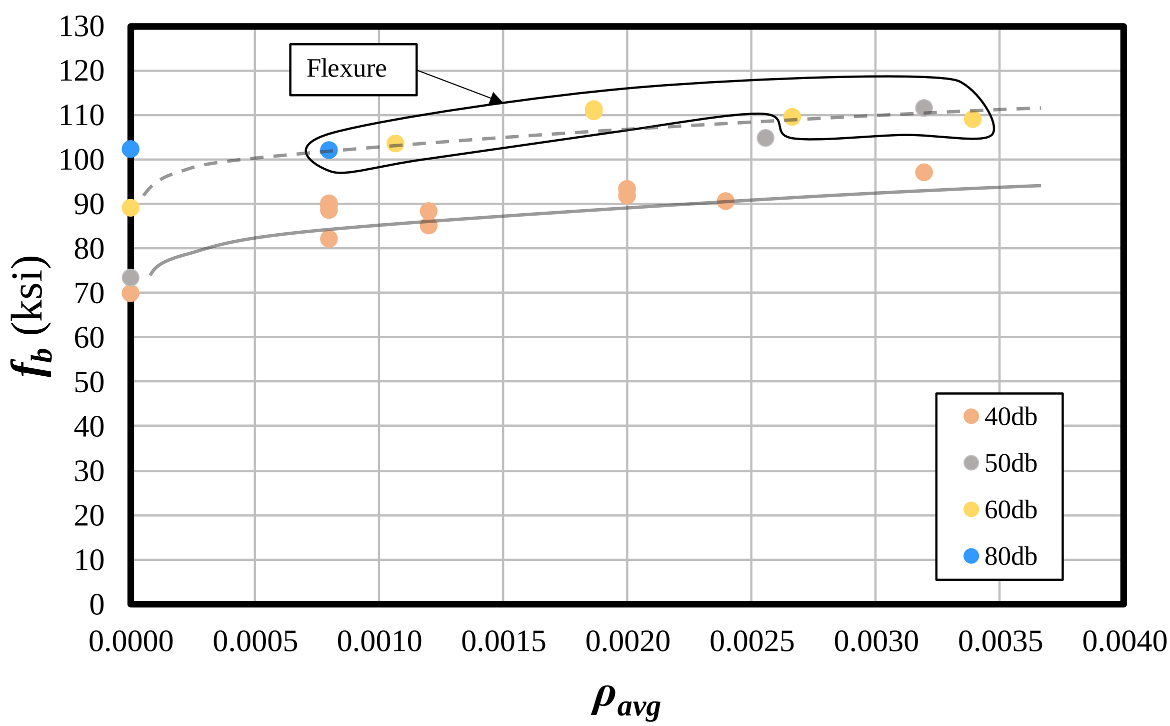

a) Actual Bar Stress

Figure 5.21: Effect of Total Transverse Reinforcement Ratio on Bar Stress, Grouped by Splice Length

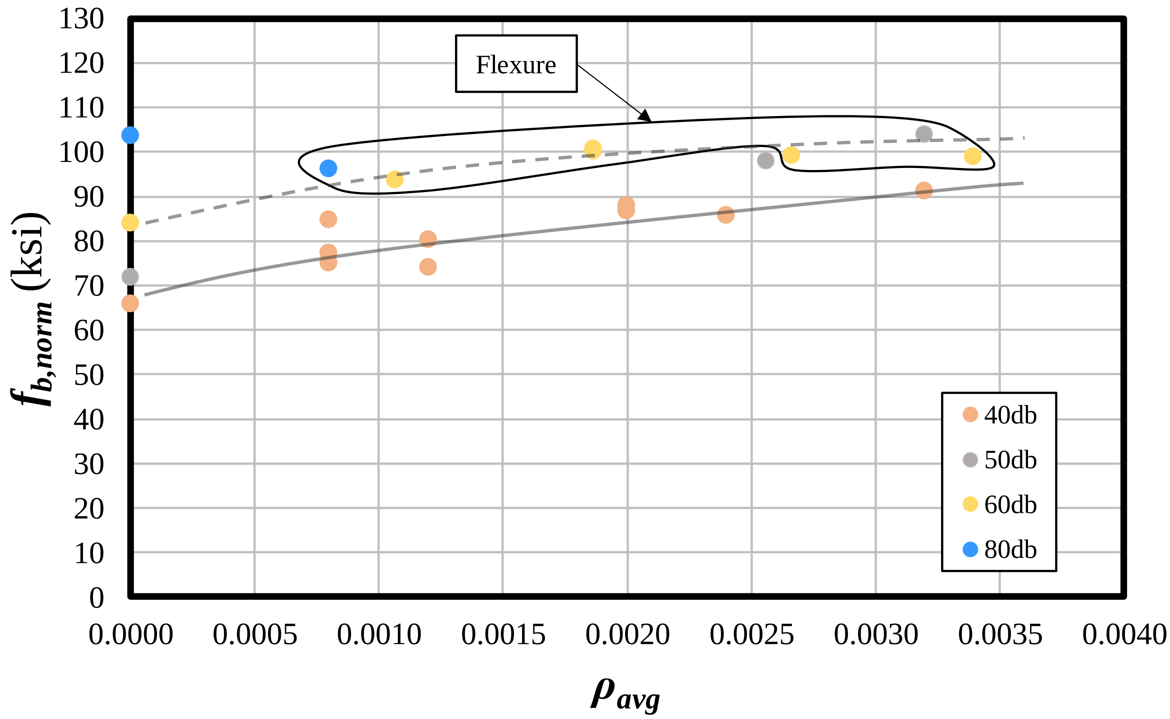

b) Normalized Bar Stress

Figure 5.21: Effect of Total Transverse Reinforcement Ratio on Bar Stress, Grouped by Splice Length - Continued

5.5.5 Location of Transverse Reinforcement

Figure 5.22 compares Specimen C3/60/2-40-5-50 (red) to Specimen C3/60/3-40-5-50 (blue). Sim (2014) concluded that stirrups placed closer to the ends of the splice were more effective. Therefore, two identical specimens having the same confinement stress were constructed, except one specimen had two stirrups in the splice region (Specimen C3/60/2-40-5-50) and the other specimen had three (Specimen C3/60/3-40-5-50). The specimen with three stirrups in the splice region (Specimen C3/60/3-40-5-50) performed better than the one with two stirrups (Specimen C3/60/2-40-5-50). Based on Sim's (2014) conclusions, this behavior occurred because the stirrups are placed closer to the end of the splice rather than because of the additional stirrup within the splice region. Elevation views for each of the confined 40d_b specimens are shown in Figure 5.23.

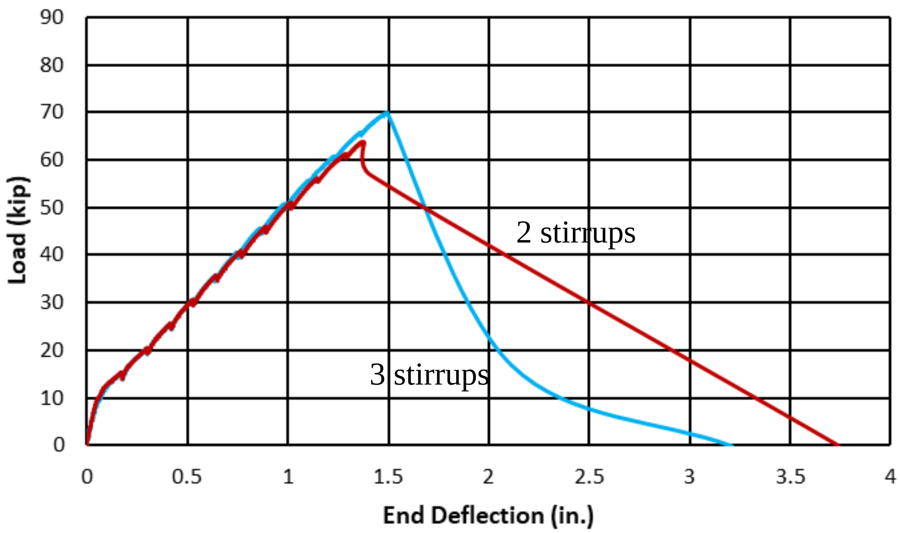

a) Load-Deflection

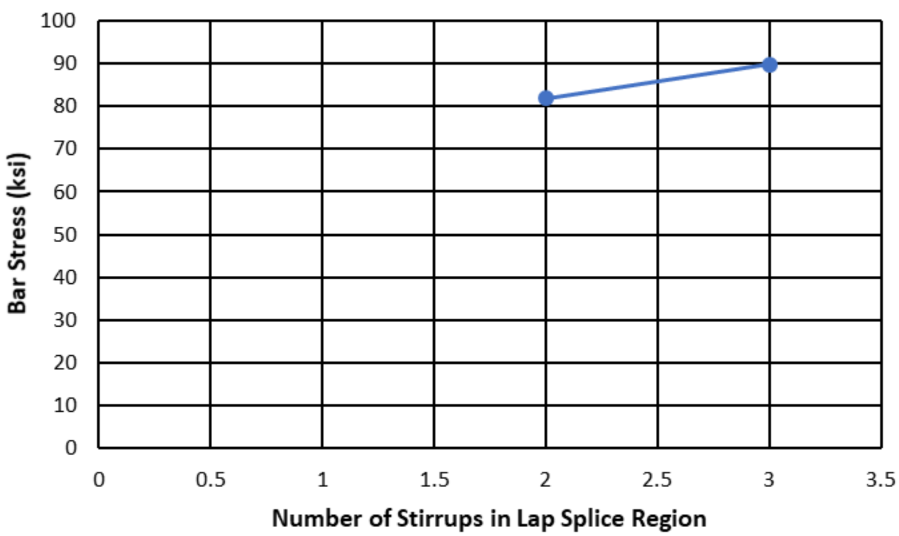

b) Bar Stress

Figure 5.22: Effect of Stirrup Location on Bond Strength

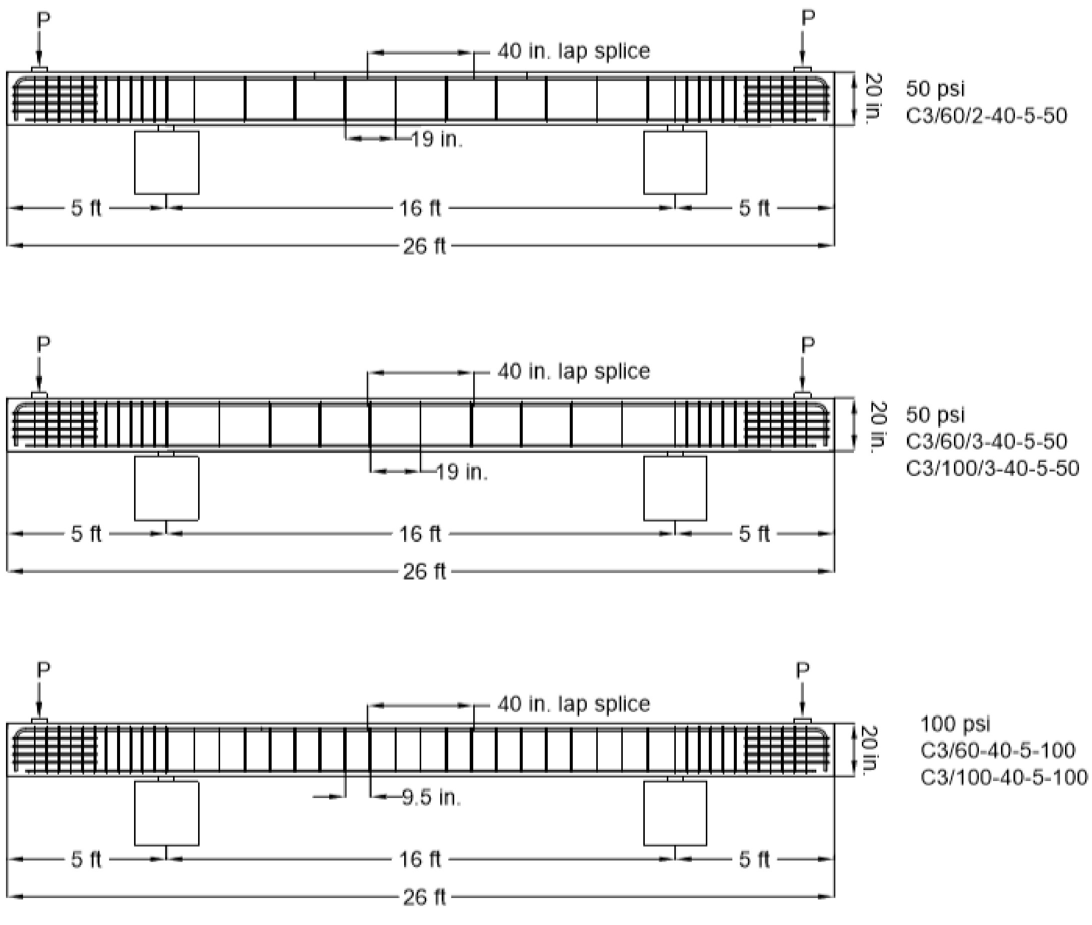

Figure 5.23: Elevations of 40d_b Confined Specimens

Three specimens in Series VI contained various stirrup locations to determine a correlation between stirrup placement and its contribution to bar stress. Figure 5.24(a) provides one configuration with stirrups being placed at a 38-in. spacing and two configurations with stirrups spaced at 19-in. on-center and being arranged in different ways (Figure 5.24(b) and Figure 5.24(c)).

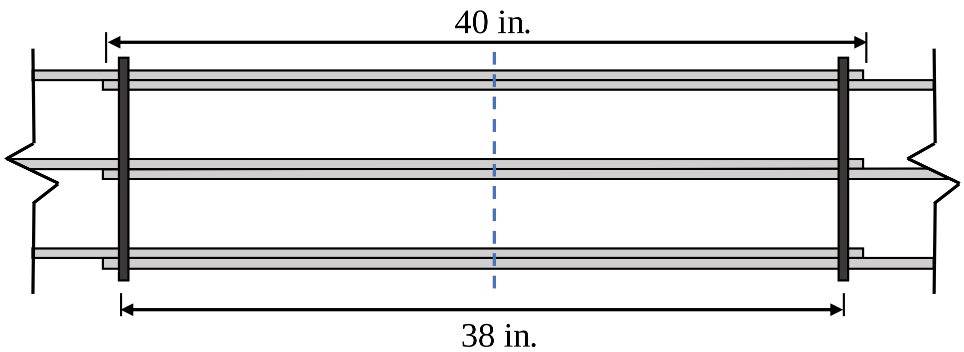

a) C3/60/2-40-10-25

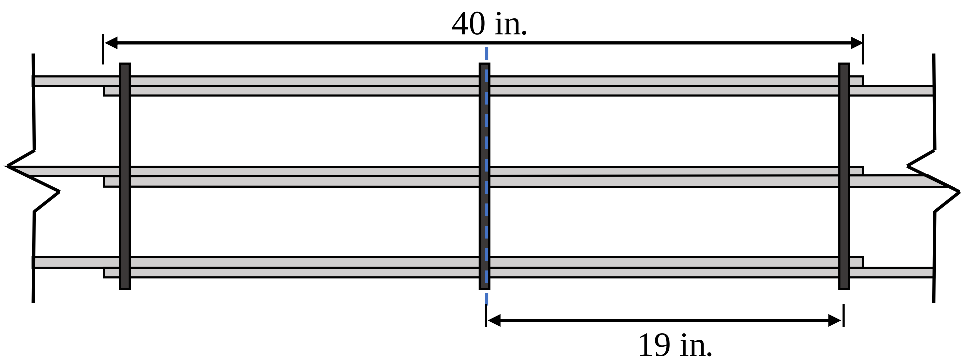

b) C3/60/2-40-10-50

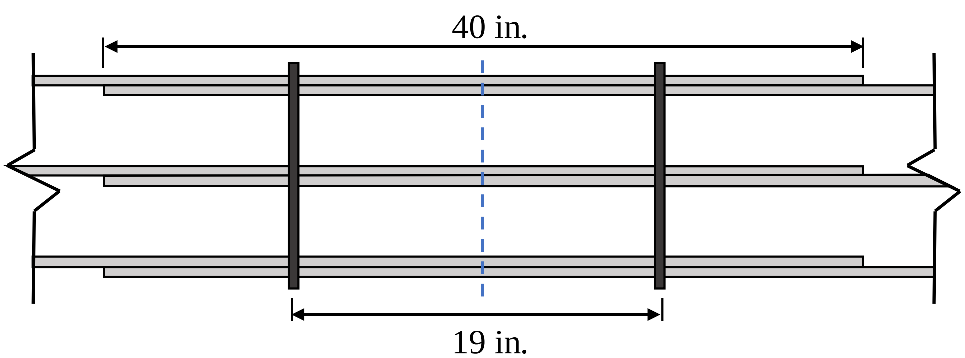

c) C3/60/3-40-10-50

Figure 5.24: Series VI Stirrup Configurations

A comparison of failure bar stress is provided in Figure 5.25 with indicated ρ_t values. The findings from this comparison indicate that the middle stirrup is ineffective in providing additional bond strength. Additionally, when only two stirrups are placed at the ends of the splice, this configuration tends toward a higher increase in bond strength when compared to a layout where two stirrups are located closer to the middle of the splice. Similar results were found by studies conducted by Sim (2014).

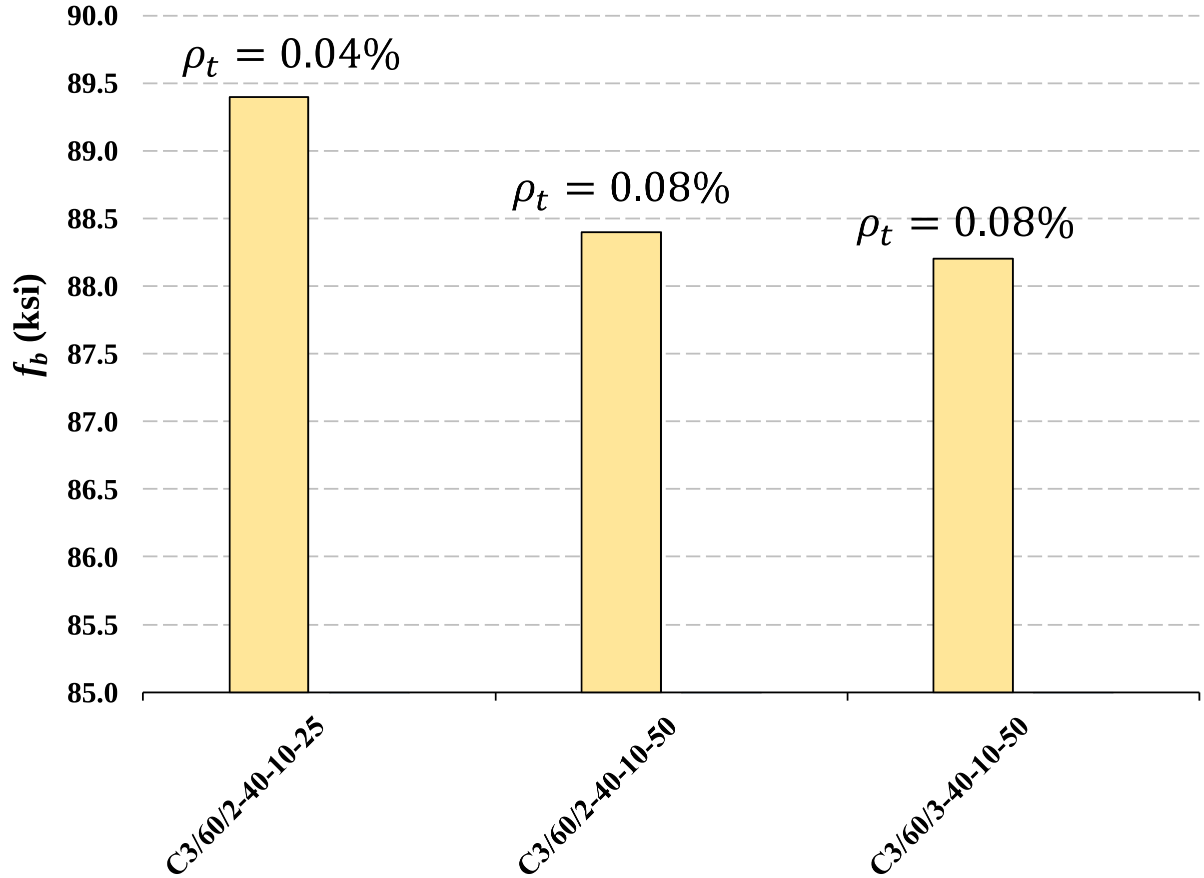

Figure 5.25: Effect of Stirrup Configuration on Bar Stress

5.5.6 Confinement Grade

The effect of Grade 100 transverse reinforcement was also investigated. According to older studies conducted by Maeda et al. (1991), Sakurada et al. (1993), and Azizinamini et al. (1993), transverse reinforcement rarely yields during a bond failure. More recent studies by Azizinamini et al. (1999) showed that the strain in stirrups, specifically stirrups located at the ends of the splice region, can reach their yield strength.

This experimental program attempted to determine if using Grade 100 transverse reinforcement would be useful. Grade 100 stirrups were used in 40d_b (Figure 5.26) and 60d_b (Figure 5.27) specimens. As shown in Figure 5.26(b), for both 50-psi and 100-psi confinement levels, the longitudinal bar stresses achieved were independent of the transverse reinforcement grade. The 60d_b specimens yielded before experiencing a flexural failure. Even in this case, the longitudinal bar stress achieved remained the same, which was expected for this failure mode (Figure 5.27(b)). The results from tests in this study show that the use of Grade 100 transverse reinforcement provides no increase in bond strength compared with the use of Grade 60 transverse reinforcement.

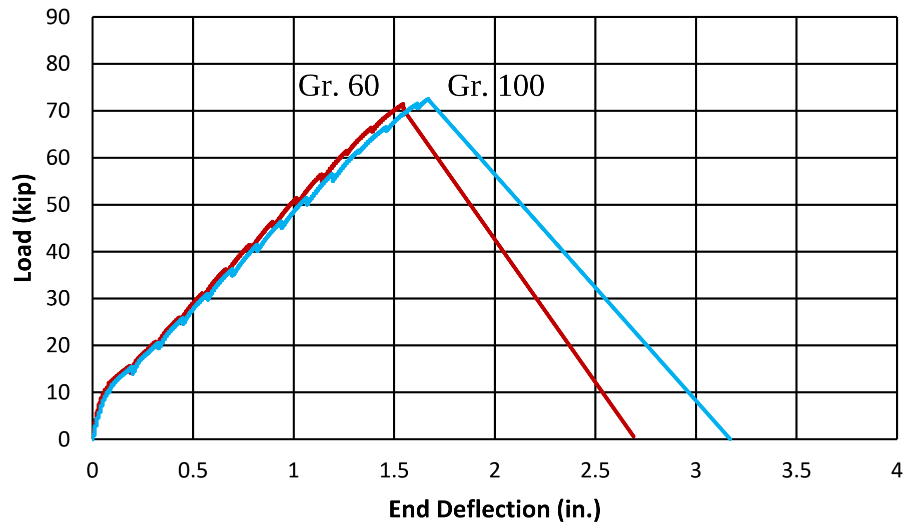

a) Load-Deflection

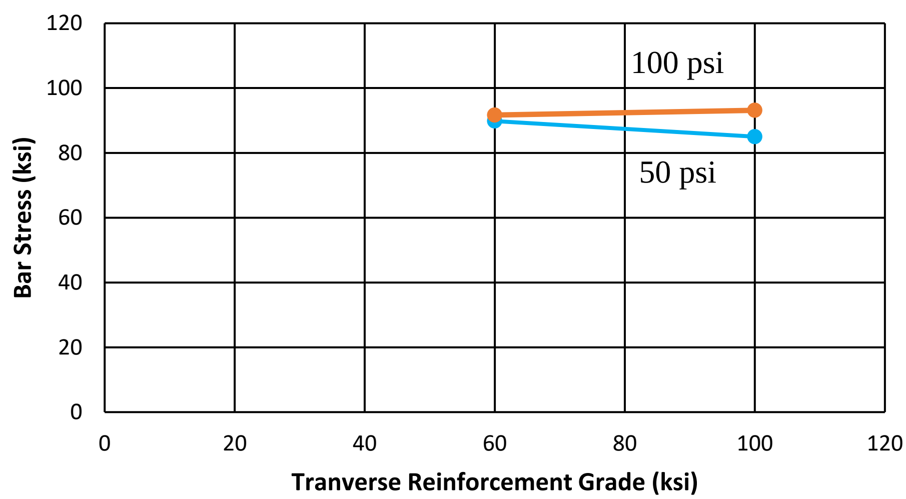

b) Bar Stress

Figure 5.26: Effect of Transverse Reinforcement Grade on Bond Strength (40d_b Specimens)

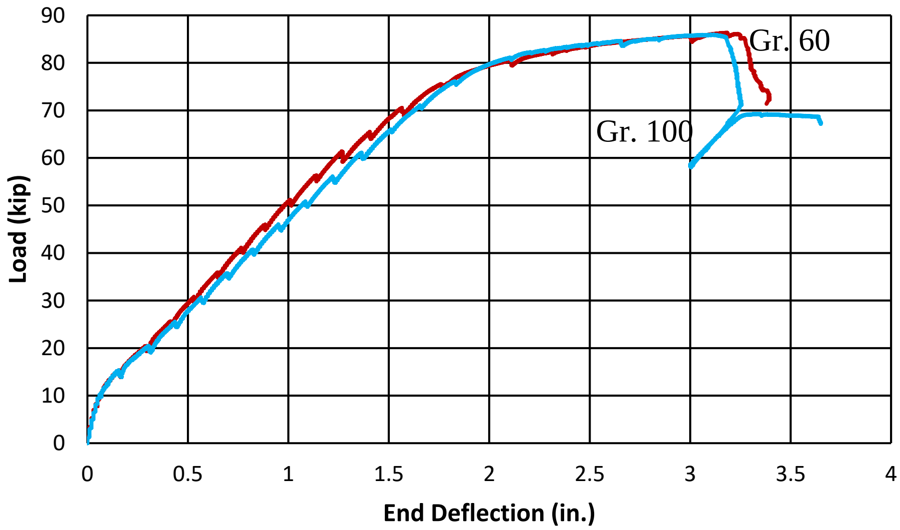

a) Load-Deflection

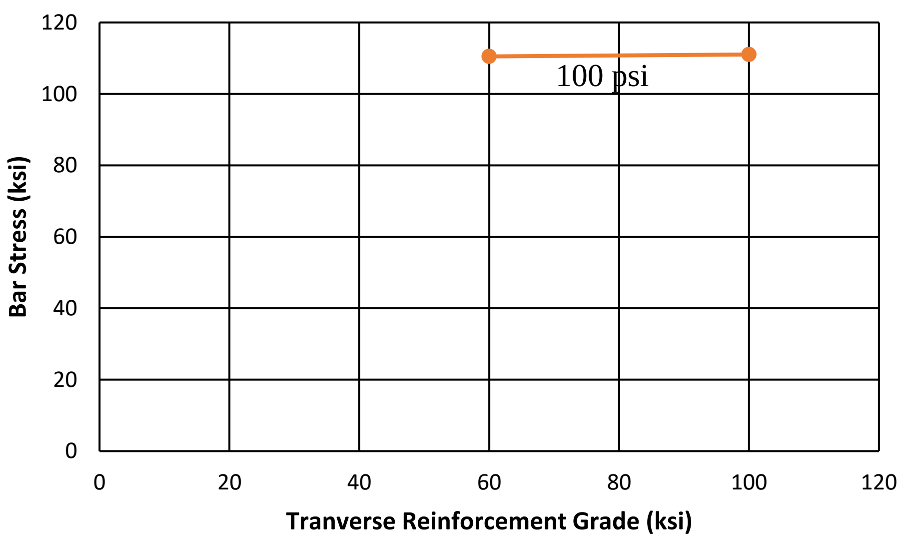

b) Bar Stress

Figure 5.27: Effect of Transverse Reinforcement Grade on Bond Strength (60d_b Specimens)

CHAPTER 6. BOND MODELING

6.1 Introduction

To develop a general expression for the bond strength of concrete members spliced with high-strength reinforcing steel bars, two databases of previous unconfined and confined beam testing were compiled and analyzed to determine the best models.

6.2 Unconfined Database

For the unconfined database in this study, 132 beams were selected from the 192 unconfined, bottom cast, uncoated beams in the ACI 408 Database 10-2001. All beams that exceeded the yield strength of the spliced bars were neglected from the original database, as well as beams with concrete strengths less than 2500 psi and splice lengths less than 12 in. An additional 75 unconfined splice specimens were included from research testing on bond strength that took place after the ACI 408 Database was compiled, including the five unconfined beams from this study. Two (2) slabs from this study were included that did not experience a flexural failure; however, one slab experienced yielding of the bars. This resulted in a total of 209 unconfined specimens. Of these tests, 167 were reinforced with conventional black steel longitudinal bars while 42 contained ASTM A1035 MMFX steel reinforcing bars.

Appendix L (Table L.1) lists the specimens contained within the unconfined database. The table indicates the testing program, number of tests, splice length, bar size, ratio of splice length to bar diameter, ratio of side cover to bar diameter, and concrete compressive strength.

6.2.1 Frequency Distribution of Database Parameters

Several parameters of interest are included in the unconfined database. The frequency distribution for the 209 unconfined specimens is provided. Figure 6.1 shows the frequency distribution of concrete strength for the unconfined specimens. Approximately 62% of the unconfined specimens exhibit concrete compressive strengths between 3000 psi and 6000 psi. The largest quantity within a given distribution is 56 specimens (27%) with concrete compressive strengths between 5000 psi and 6000 psi.

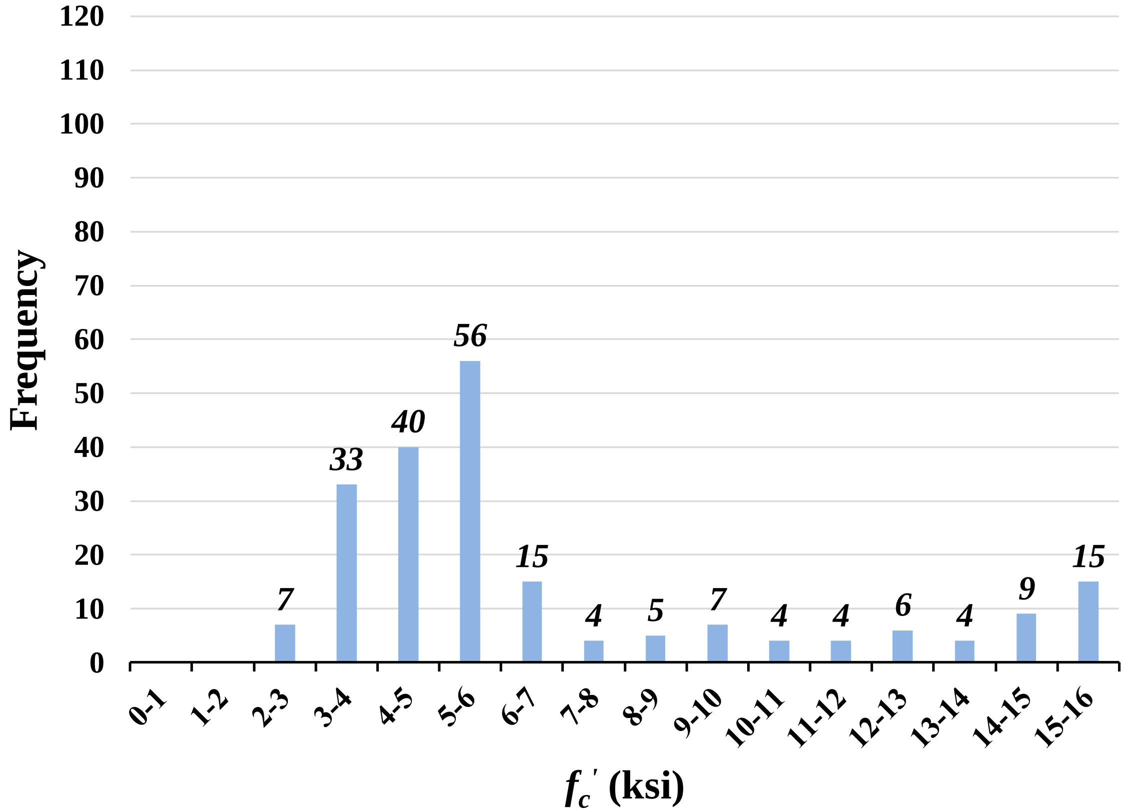

Figure 6.1: Distribution of Concrete Compressive Strength for Unconfined Database

Figure 6.2 shows the frequency distribution of bar sizes for the unconfined database. Approximately 88% of the unconfined specimens contain either No. 6, No. 8, or No. 11 spliced bars. The largest quantity within a given distribution is 106 specimens (51%) containing No. 8 longitudinal spliced bars.

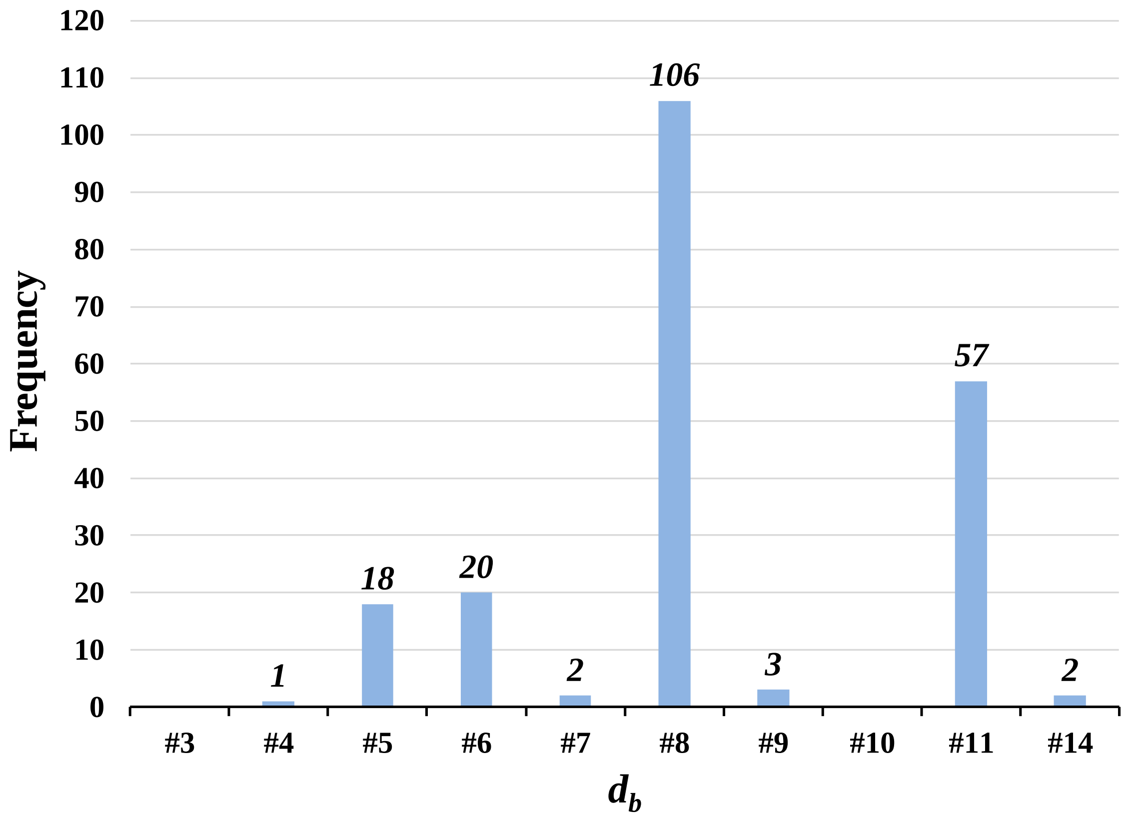

Figure 6.2: Distribution of Bar Size for Unconfined Database

Figure 6.3 shows the frequency distribution of splice lengths for the unconfined database. Approximately 74% of the unconfined specimens contain lapped splice lengths between 10 in. and 40 in. The largest quantity within a given distribution is 62 specimens (30%) containing splices between 10 in. and 20 in.

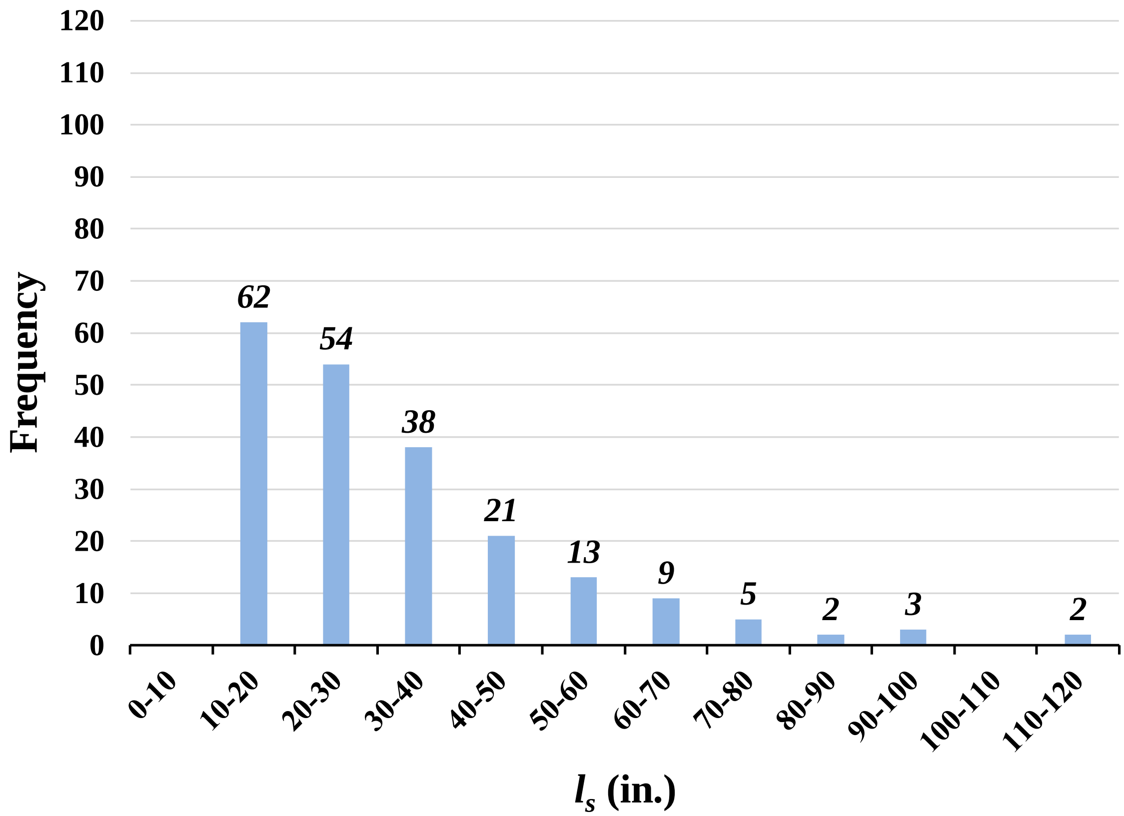

Figure 6.3: Distribution of Splice Length for Unconfined Database

Figure 6.4 shows the frequency distribution of splice length to bar diameter ratios for the unconfined database. Approximately 79% of the unconfined specimens contain ratios of splice length to bar diameter between 10 and 40. The largest quantity within a given distribution is 67 specimens (32%) containing ratios of splice length to bar diameter between 20 and 30.

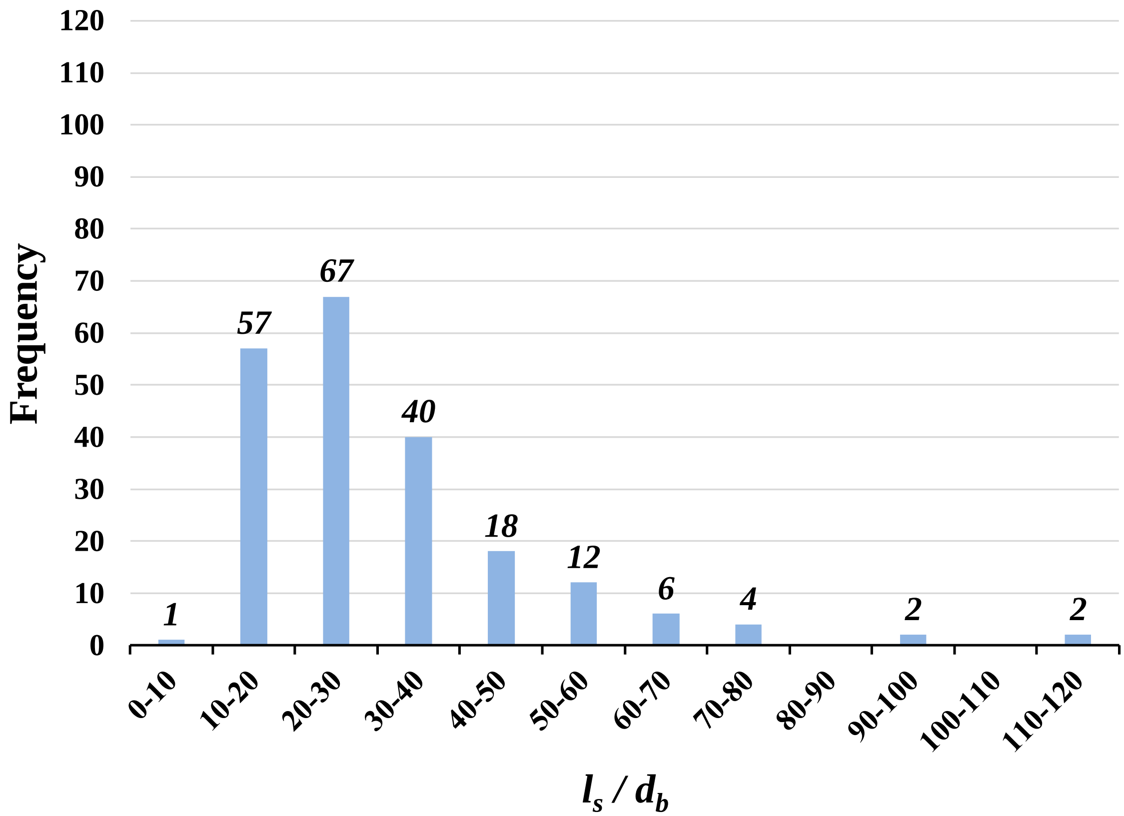

Figure 6.4: Distribution of Splice-Length-to-Bar-Diameter Ratio for Unconfined Database

Figure 6.5 shows the frequency distribution of side cover to bar diameter ratios for the unconfined database. Approximately 69% of the unconfined specimens contain ratios of side cover to bar diameter between 1.0 and 2.5. The largest quantity within a given distribution is 59 specimens (29%) containing ratios of side cover to bar diameter between 1.5 and 2.0. Note that two specimens did not have recorded side cover values and were neglected from this frequency distribution histogram.

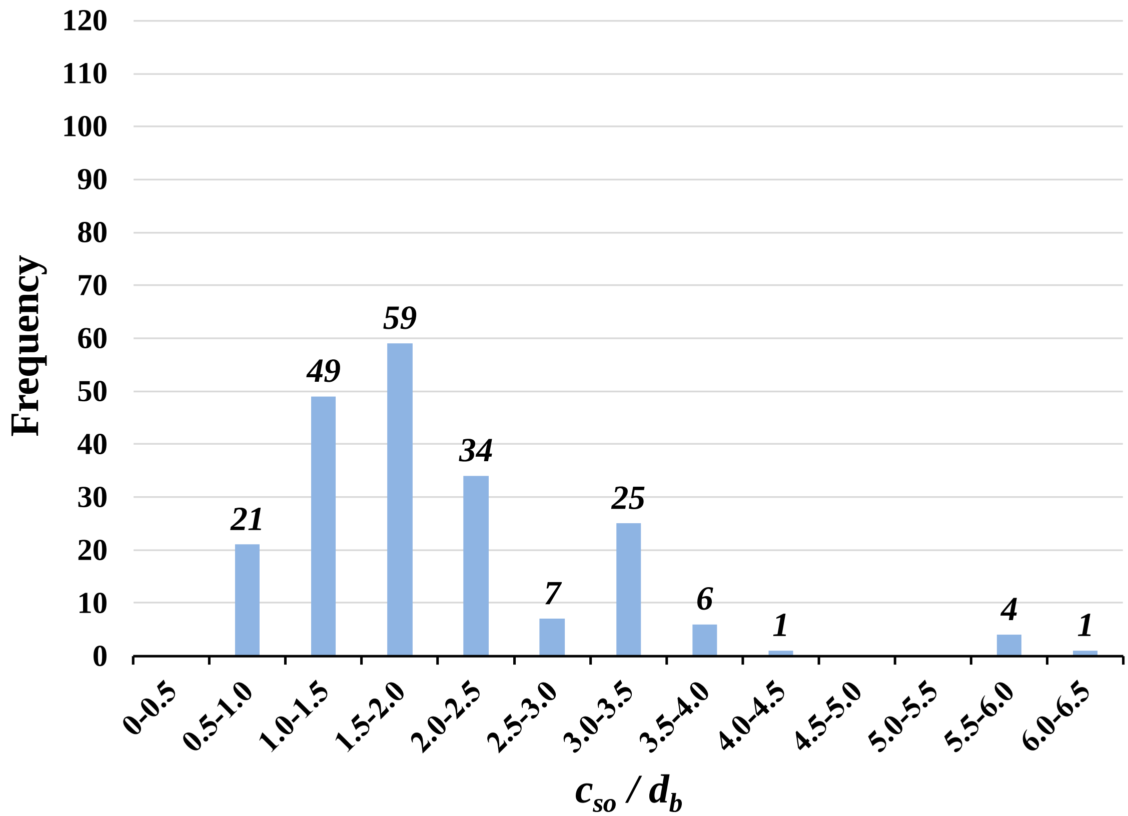

Figure 6.5: Distribution of Side-Cover-to-Bar-Diameter Ratio for Unconfined Database

6.3 Unconfined Model

An investigation was conducted to develop an equation for unconfined beams to represent the concrete contribution to total bar stress. This equation is based on trends observed over the full database of unconfined specimens and two slab specimens from this study. By comparing three previous equations for bar stress (Pay 2005, Sim 2014, Glucksman 2018), three general terms were identified to be consistent in all equations: concrete compressive strength, splice length, and a cover modifier.

6.3.1 Equation Components

Concrete compressive strength, splice length, and cover were all found to have a significant influence on the overall bar stress achieved at failure:

1. The influence of concrete compressive strength on bar stress has been best represented with the quarter root by analyses in several research programs (Darwin et al. 1996, Zuo and Darwin 2000, Canbay and Frosch 2005, Pay 2005, Sim 2014).
2. Canbay and Frosch, Pay, and Sim observed that the ratio of splice length to bar diameter has a nonlinear correlation to bar stress.

3. Cover has been considered differently in various research studies. Because there are three different concrete dimensions surrounding spliced bars that can be analyzed in the database, different conclusions have been provided. Findings by Orangun, Jirsa, and Breen (1977) suggest that the ratio of a cover term to the bar diameter has a stronger correlation to the bar stress than a cover term alone. Observations on the linearity of this term have also been approached differently in research programs with some recommending a linear correlation (Pay 2005) and others recommending a nonlinear representation (Sim 2014).

An investigation was performed to evaluate an appropriate cover modification term for a general unconfined bar stress equation.

6.3.2 Cover Investigation

The unconfined database was evaluated specifically for the effect of cover and bar spacing on bar stress. Powers for the compressive strength and splice length were selected to be 0.25 and 0.50, respectively, based on previous research. The cover modification and its power were changed to explore the influence on bar stress. A total of eight possible cover modification terms were evaluated and raised to a power to account for a potential nonlinear relationship. Table 6.1 provides the eight cover terms used in this study. Equation 6-1 was calculated for each specimen in the unconfined database with Series V slabs to determine f_{trial} values for all eight cover modifiers.

Table 6.1: Cover Modification Terms

(1) $c_{mod,1}$	$\frac{c_{so}}{d_b}$	(5) $c_{mod,5}$	$\frac{\min(c_{si}, c_b)}{d_b}$
(2) $c_{mod,2}$	$\frac{c_{si}}{d_b}$	(6) $c_{mod,6}$	$\frac{\min(c_{so}, c_b)}{d_b}$
(3) $c_{mod,3}$	$\frac{2c_{si}}{d_b}$	(7) $c_{mod,7}$	$\frac{\min(c_{so}, c_{si})}{d_b}$
(4) $c_{mod,4}$	$\frac{c_{si}}{2d_b}$	(8) $c_{mod,8}$	$\frac{\min(c_{so}, c_{si}, c_b)}{d_b}$

$$f_{trial} = (C_1)^{1.0}(f_c')^{0.25}\left(\frac{l_s}{d_b}\right)^{0.5}(c_{mod})^{z} \qquad \text{(6-1)}$$

where:

c_b = *bottom clear cover of spliced bars (in.)*

c_{mod} = *cover modification term*

c_{si} = *half the clear spacing between spliced bars (in.)*

c_{so} = *side clear cover of spliced bars (in.)*

C_1 = *constant selected to be 1*

d_b = *longitudinal bar diameter (in.)*

f'_c = *concrete compressive strength (psi)*

f_{trial} = *trial bar stress for cover modification investigation (ksi)*

l_s = *splice or development length (in.)*

z = *power constant*

To isolate the term of best fit for the data, f_{trial} was calculated for all eight equations and used to calculate f_{test}/f_{trial} for each specimen in the unconfined database. The coefficient of variation (COV) was then calculated for each modifier for z powers ranging from zero to one. Figure 6.6 shows the change in COV for all eight equations. Specimens that did not have recorded values for terms in the modifier were excluded in the COV calculation for that equation.

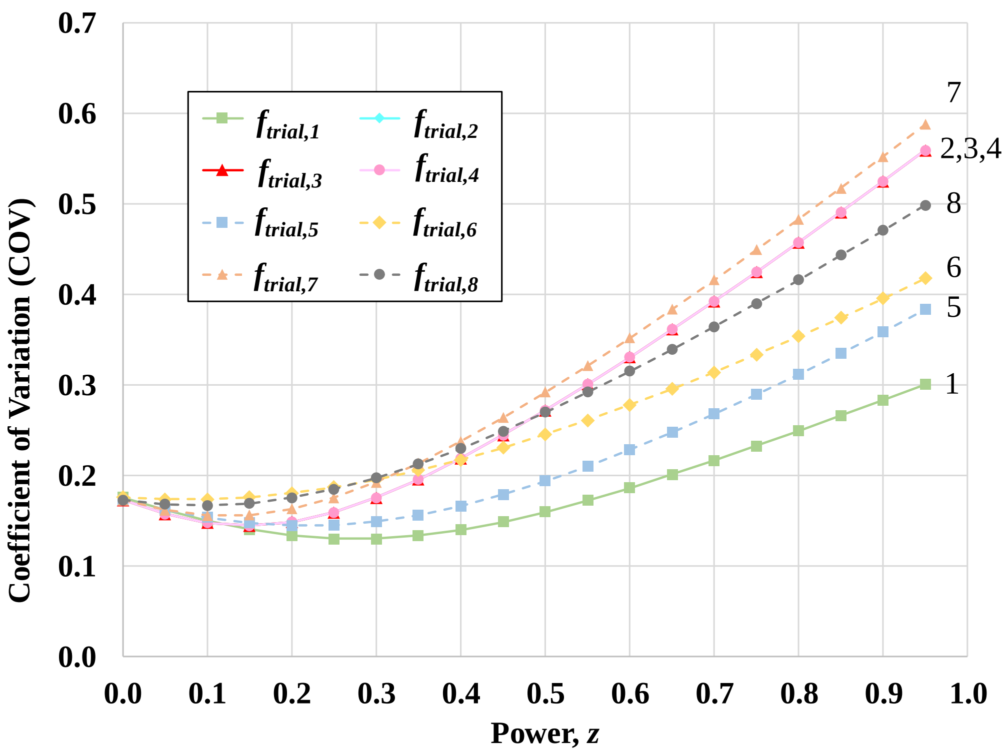

Figure 6.6: Comparison of Cover Modification Terms c_{mod}

Equations 2, 3, and 4 all result in the same COV for changing powers because the cover modifiers for these equations only differ by a constant. Equation 1 appears to fit the unconfined specimen data with the least amount of variation for all powers between zero and one. Because the COV for this equation reaches a minimum of 0.130 at a power of approximately 0.3 instead of 1, the influence of this term is assumed to be nonlinear.

When the power $z = 0.30$ and is placed on the cover term in Equation 6-1, a statistical analysis can be performed on all eight equations to further validate that side cover has the strongest influence on bond strength. Each of the eight cover modifier terms is substituted into Equation 7-1 for the comparison provided in Table 6.2.

Table 6.2: Statistical Analysis of f_{test}/f_{trial} in Cover Modifier Equations

	Eq. 1	**Eq. 2**	**Eq. 3**	**Eq. 4**	**Eq. 5**	**Eq. 6**	**Eq. 7**	**Eq. 8**
Max.	1.61	1.79	1.45	2.20	1.79	2.02	1.92	1.92
Min.	0.77	0.65	0.52	0.79	0.80	2.02	0.72	0.72
Mean ($\bar{x}$)	1.09	1.15	0.93	1.41	1.24	1.18	1.18	1.25
Standard Deviation (σ)	0.14	0.20	0.16	0.25	0.18	0.23	0.23	0.25
COV	0.13	0.18	0.18	0.18	0.15	0.20	0.19	0.20
r^2	0.85	0.62	0.62	0.62	0.61	0.65	0.60	0.54

The use of the ratio between side cover and bar diameter results in the lowest coefficient of variation and the highest correlation coefficient (r^2) among the eight cover modification terms. This study finds that the ratio of side cover to bar diameter has more influence on bond strength than inner bar spacing and bottom cover; therefore c_{so}/d_b will be considered for the cover modifier in the general bar stress equation.

6.3.3 Nonlinear Regression Analysis

Based on the recommended cover modification term, the unconfined bar stress can be expressed as follows:

$$f_{bc} = (C_1)(f_c')^x \left(\frac{l_s}{d_b}\right)^y \left(\frac{c_{so}}{d_b}\right)^z \tag{6-2}$$

where:

c_{so} = *side clear cover of spliced bars (in.)*

C_1	=	*constant*
d_b	=	*longitudinal bar diameter (in.)*
f_{bc}	=	*contribution to bond stress provided by concrete (ksi)*
f_c'	=	*concrete compressive strength (psi)*
l_s	=	*splice or development length (in.)*
x, y, z	=	*constants to be determined by nonlinear regression analysis*

Although previous power values have been estimated based on past bond strength research, a nonlinear regression analysis was performed to independently evaluate the powers for each variable. By applying the natural logarithmic function to the entire equation, Equation 6-2 can be written in a more suitable way for regression analysis:

$$\ln(f_{bc}) = \ln(C_1) + x\ln(f_c') + y\ln\left(\frac{l_s}{d_b}\right) + z\ln\left(\frac{c_{so}}{d_b}\right) \quad (6\text{-}3)$$

Nonlinear regression analysis was performed on the 207 specimens from the unconfined database in addition to two slab specimens from Series V. A correlation coefficient of 0.92 was generated by this analysis with a 95% confidence interval. Coefficients were rounded for convenience. All constants were determined as follows:

$C_1 = 0.90$ $x = 0.28$ $y = 0.48$ $z = 0.29$

By substituting these values for the constants in Equation 6-3, Equation 6-4 takes the following form:

$$f_{bc} = 0.9(f_c')^{0.28}\left(\frac{l_s}{d_b}\right)^{0.48}\left(\frac{c_{so}}{d_b}\right)^{0.29} \quad (6\text{-}4)$$

To simplify this equation for easier use, all power constants were adjusted to multiples of the quarter root. Additionally, the coefficient was adjusted to one to maintain an average f_{test}/f_{calc} value for the analyzed unconfined database beams. The expression for concrete contribution to bar stress is given by Equation 6-5:

$$f_{bc} = 1.0(f_c')^{0.25}\left(\frac{l_s}{d_b}\right)^{0.5}\left(\frac{c_{so}}{d_b}\right)^{0.25} \quad (6\text{-}5)$$

Equation 6-5 was applied to all 209 beams in the unconfined database and compared with the results using the ACI 318-14 design expression provided in Equation 6-6:

$$f_b = \frac{40\lambda\sqrt{f'_c}}{3\psi_t\psi_e\psi_s}\left(\frac{l_d}{d_b}\right)\left(\frac{c_b + K_{tr}}{d_b}\right) \tag{6-6}$$

where:

A_{tr}	=	*total cross-sectional area of transverse reinforcement within the spacing s that crosses the plane of splitting through the developed reinforcement (in.^{2})*
c_b	=	*minimum of (a) the concrete side cover measured to the center of the bar, (b) the bottom concrete cover measured to the center of the bar, and (c) half the center-to-center spacing of the bars (in.)*
d_b	=	*bar diameter of lap-spliced longitudinal bar (in.)*
f_b	=	*stress achieved in lap-spliced longitudinal bar (psi)*
f'_c	=	*compressive strength of concrete (psi)*
K_{tr}	=	*transverse reinforcement index (in.)*
	=	$\frac{40A_{tr}}{sn}$
l_d	=	*development length in tension of deformed bar (in.)*
n	=	*number of bars or wires being developed or lap spliced*
s	=	*spacing of transverse reinforcement, center-to-center (in.)*
λ	=	*lightweight modification factor (ranging from 0.75 to 1.0)*
ψ_t	=	*casting position modification factor (ranging from 1.0 to 1.3)*
ψ_e	=	*epoxy coating modification factor (ranging from 1.0 to 1.5)*
ψ_s	=	*reinforcement size modification factor (ranging from 0.8 to 1.0)*

Table 6.3 provides a statistical comparison of the results. Graphic comparisons between ACI 318-14 and the proposed unconfined equation are provided in Figure 6.7 through Figure 6.14 for different variables of interest.

Table 6.3: Statistical Analysis Comparison of f_{test}/f_{calc} for Unconfined Beams

	ACI 318-14	Proposed Equation (7-5)
Max.	2.61	1.52
Min.	0.59	0.65
Mean ($\bar{x}$)	1.23	1.00
Standard Deviation (σ)	0.405	0.155
COV	0.328	0.155

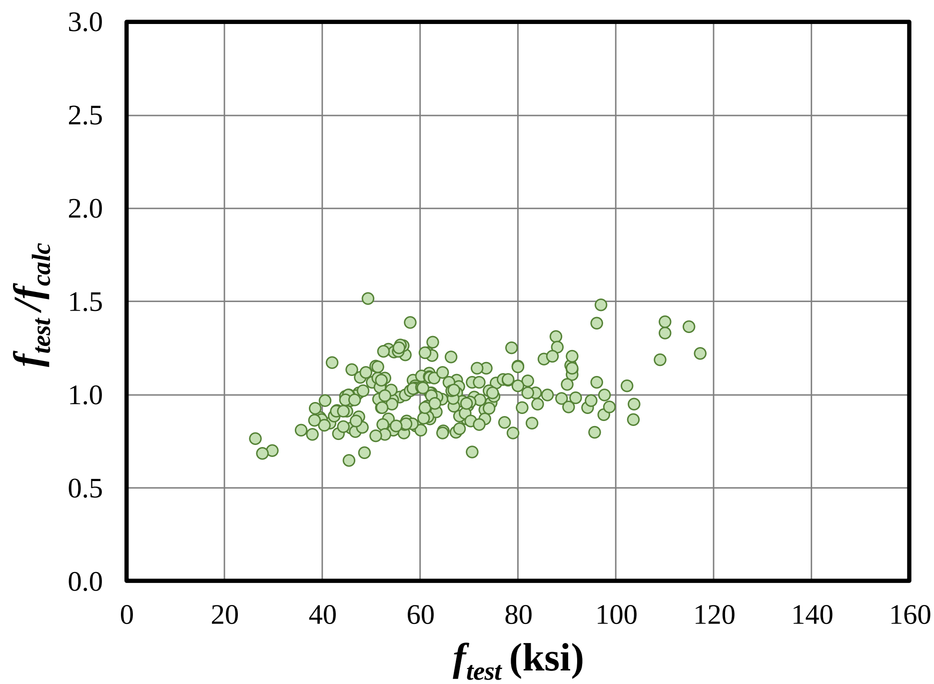

a) Equation 6-5

Figure 6.7: Equation Comparison for Bar Stress at Failure (Unconfined)

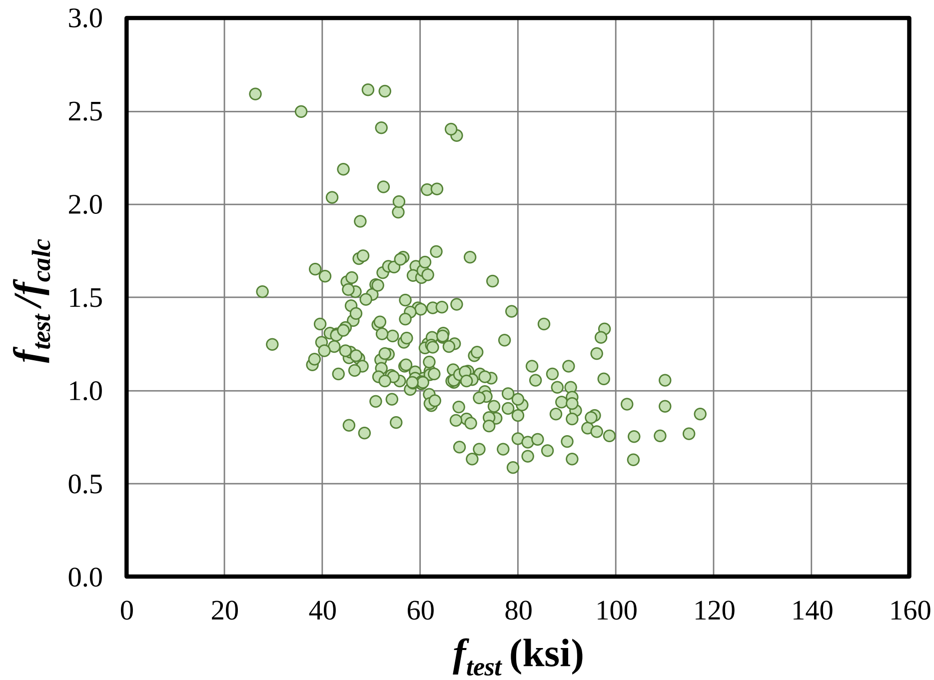

b) ACI 318-14

Figure 6.7: Equation Comparison for Bar Stress at Failure (Unconfined) - Continued

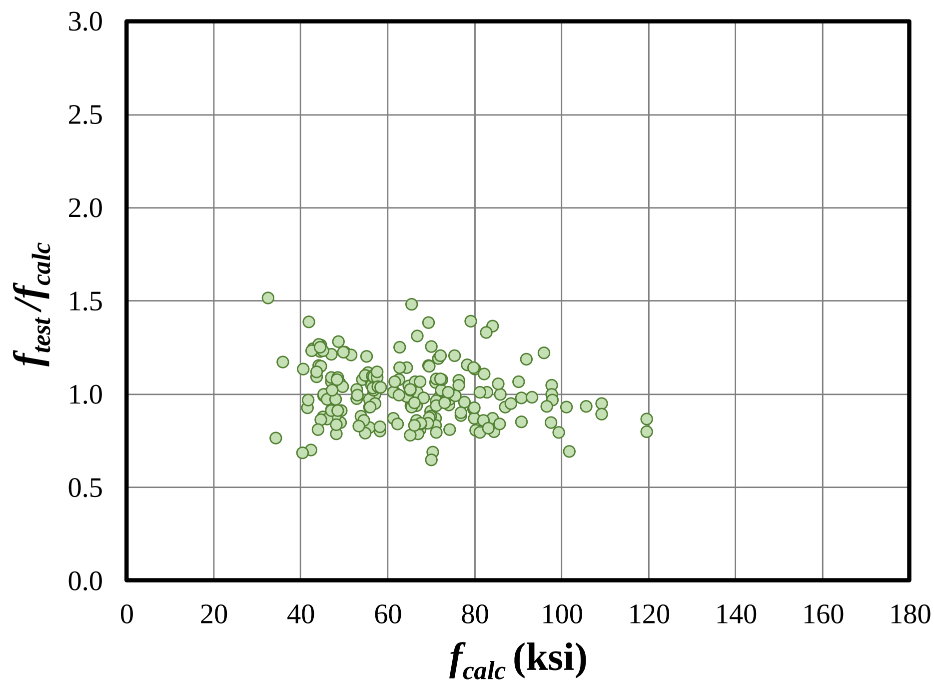

a) Equation 6-5

Figure 6.8: Equation Comparison for Calculated Bar Stress (Unconfined)

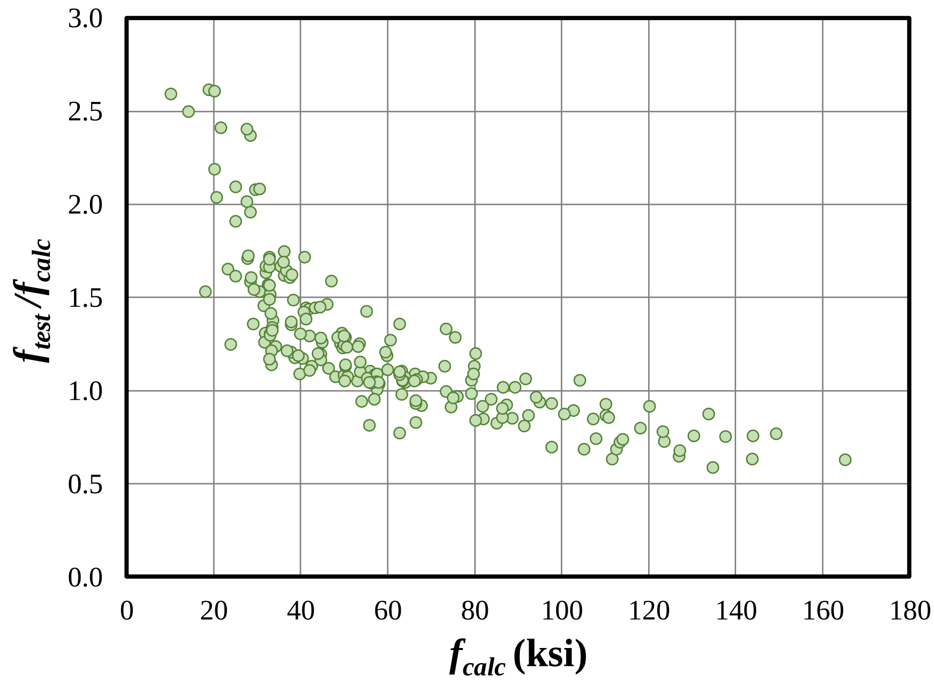

b) ACI 318-14

Figure 6.8: Equation Comparison for Calculated Bar Stress (Unconfined) – Continued

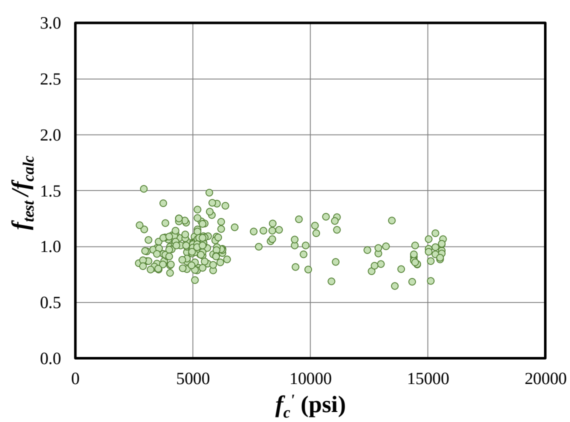

a) Equation 6-5

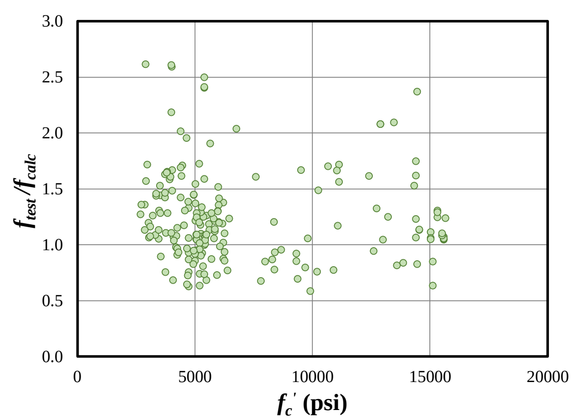

b) ACI 318-14

Figure 6.9: Equation Comparison for Concrete Strength (Unconfined)

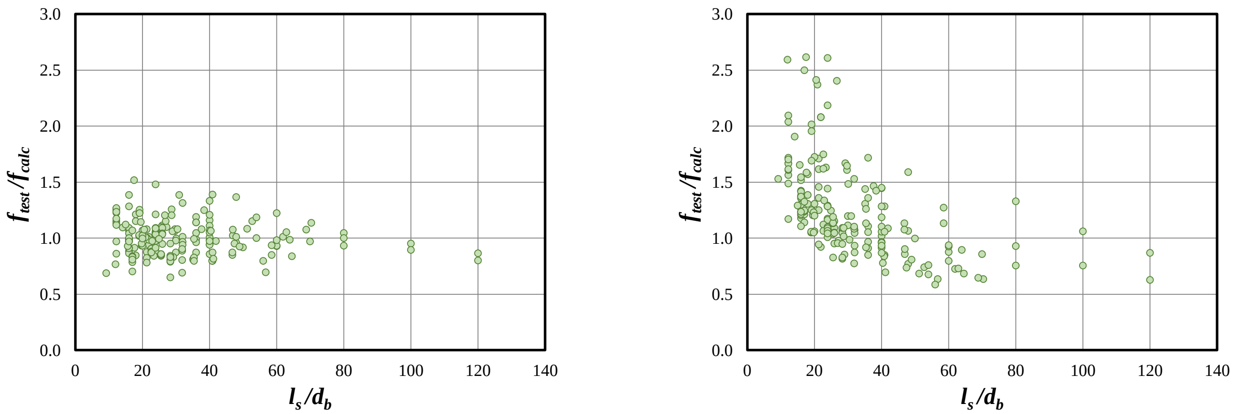

a) Equation 6-5 **b) ACI 318-14**

Figure 6.10: Equation Comparison for Splice Length over Bar Diameter (Unconfined)

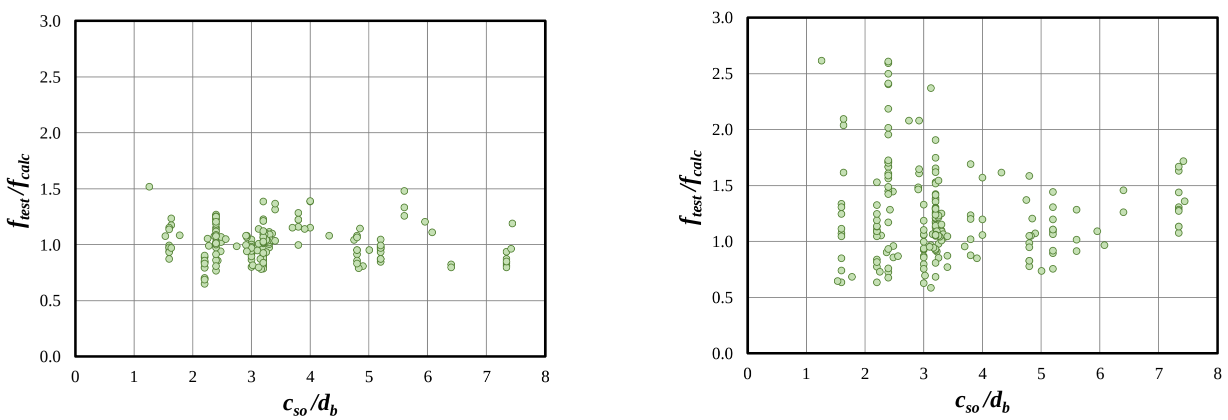

a) Equation 6-5 **b) ACI 318-14**

Figure 6.11: Equation Comparison for Side Cover over Bar Diameter (Unconfined)

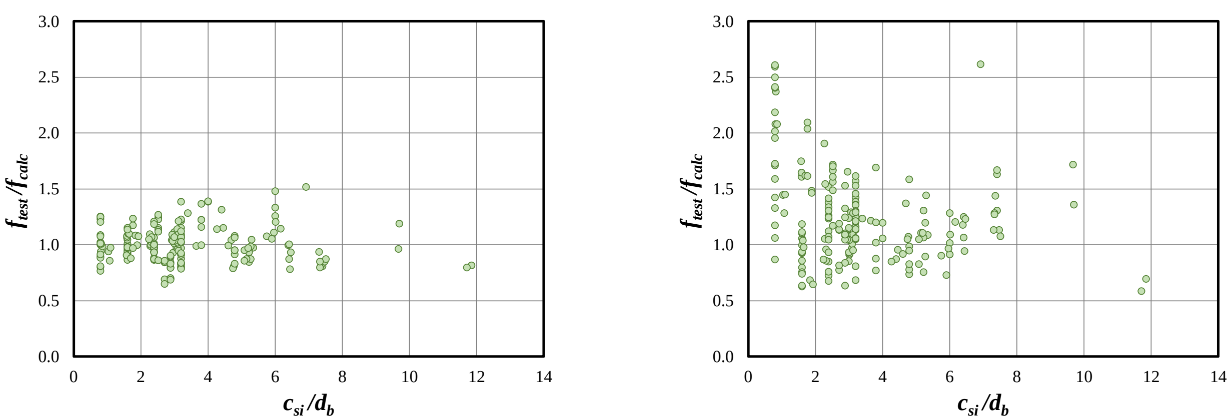

a) Equation 6-5 **b) ACI 318-14**

Figure 6.12: Equation Comparison for Half Bar Spacing over Bar Diameter (Unconfined)

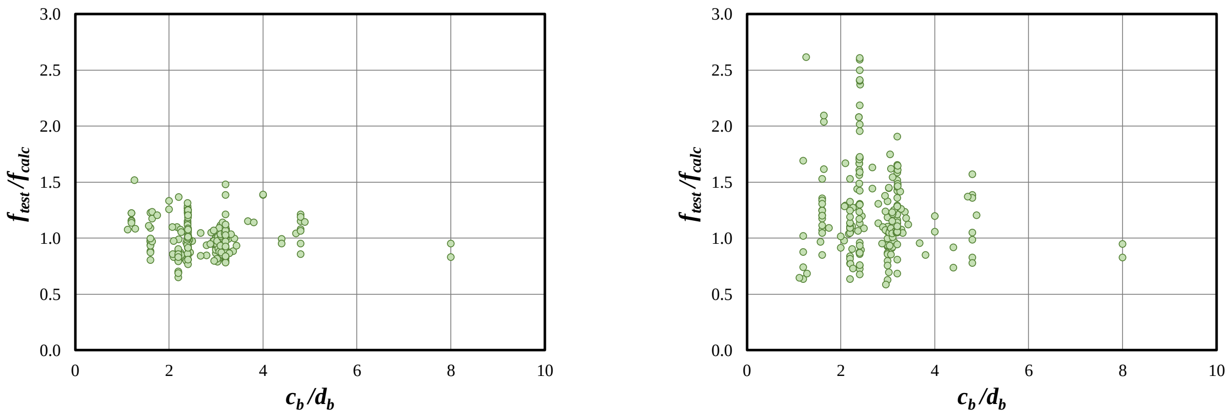

a) Equation 6-5

b) ACI 318-14

Figure 6.13: Equation Comparison for Bottom Cover over Bar Diameter (Unconfined)

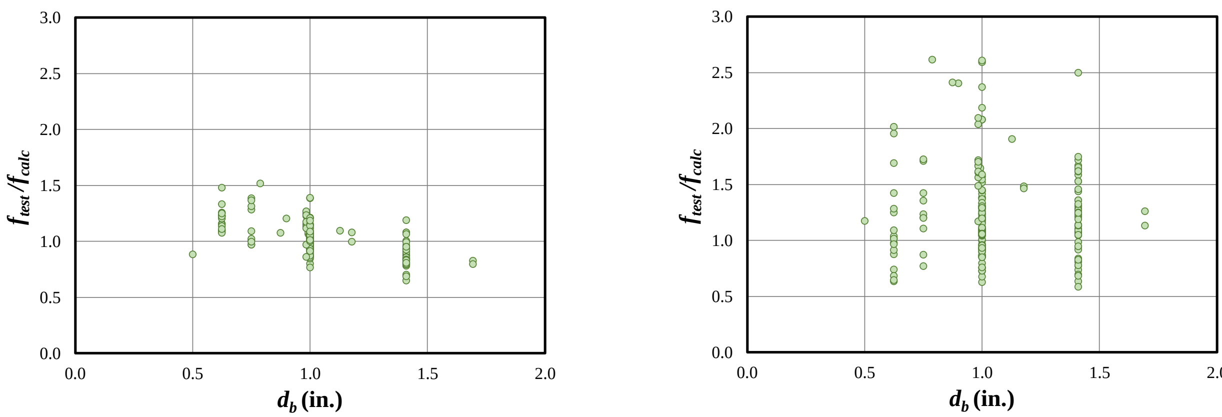

a) Equation 6-5

b) ACI 318-14

Figure 6.14: Equation Comparison for Bar Diameter (Unconfined)

For all results from Figure 6.7 through Figure 6.14, scatter is reduced when Equation 6-5 is used compared to use of the design expression in ACI 318-14.

6.4 Confined Database

The database for confined specimens used in this study contains the 286 confined, bottom cast, uncoated beams from the original ACI 408 Database 10-2001. An additional 70 confined beams were included from research testing on bond strength that took place after the ACI 408 Database was compiled, including the six confined beams that failed in splitting from this study. From this total, exclusion criteria were selected and implemented, removing all beams with a splice length less than 12 in. and concrete strengths less than 2500 psi. Furthermore, specimens with only one stirrup within the splice region and specimens consisting of only one splice were excluded. Therefore, the total number of specimens selected in the database was 322 confined beams. Of these tests, 85 specimens reached yielding of the longitudinal bars before failure, 281 specimens were reinforced with conventional black steel longitudinal bars, and 41 contained ASTM A1035 MMFX reinforcing bars.

Appendix L (Table L.2) lists the specimens contained within the confined database and indicates the testing program, number of tests, splice length, bar size, ratio of splice length to bar diameter, ratio of side cover to bar diameter, and concrete compressive strength. Additionally, beam pairs were selected from various tests that contained a confined beam with an identical unconfined specimen. A total of 101 beam pairs were used in this study.

6.4.1 Frequency Distribution of Database Parameters

Several parameters of interest are included in the confined database. The frequency distribution for all 322 confined specimens was evaluated. Figure 6.15 shows the frequency distribution of concrete compressive strengths for the confined database. Approximately 58% of the confined specimens exhibit concrete compressive strengths between 3000 psi and 6000 psi. The largest quantity within a given distribution is 85 specimens (26%) with concrete compressive strengths between 4000 psi and 5000 psi.

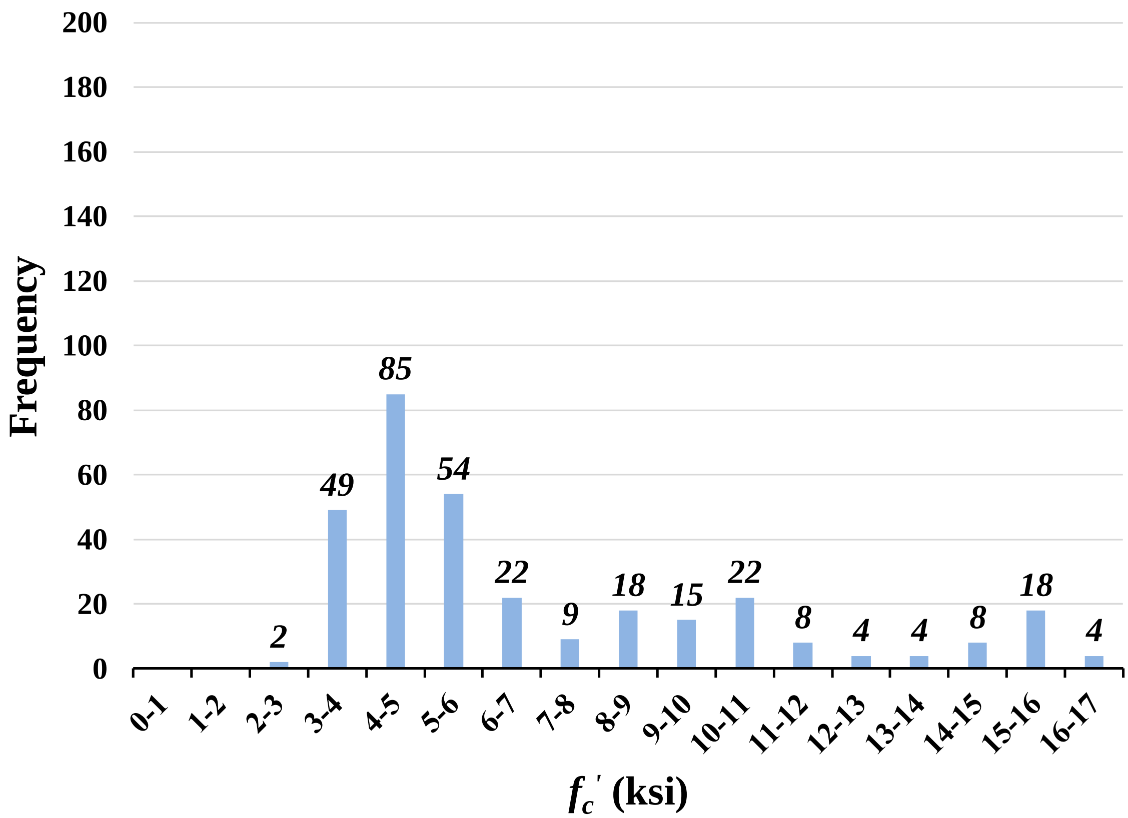

Figure 6.15: Distribution of Concrete Compressive Strength for Confined Database

Figure 6.16 shows the frequency distribution of spliced bar sizes for the confined database. Approximately 94% of the confined specimens contain either No. 6, No. 8, or No. 11 bars. The largest quantity within a given distribution is 193 specimens (60%) containing No. 8 longitudinal bars.

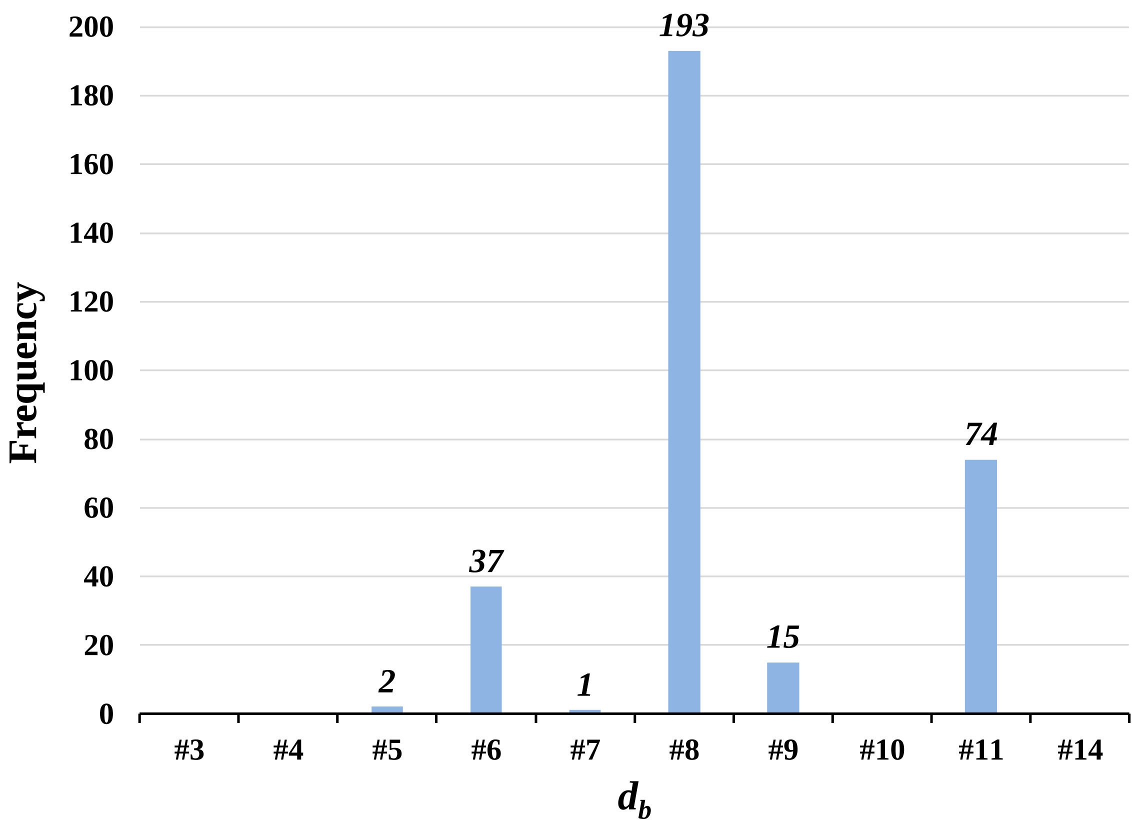

Figure 6.16: Distribution of Bar Size for Confined Database

Figure 6.17 shows the frequency distribution of longitudinal lapped splice lengths in the confined database. Approximately 89% of the confined specimens contain lapped splice lengths between 10 in. and 40 in. The largest quantity within a given distribution is 136 specimens (42%) containing splices between 20 in. and 30 in.

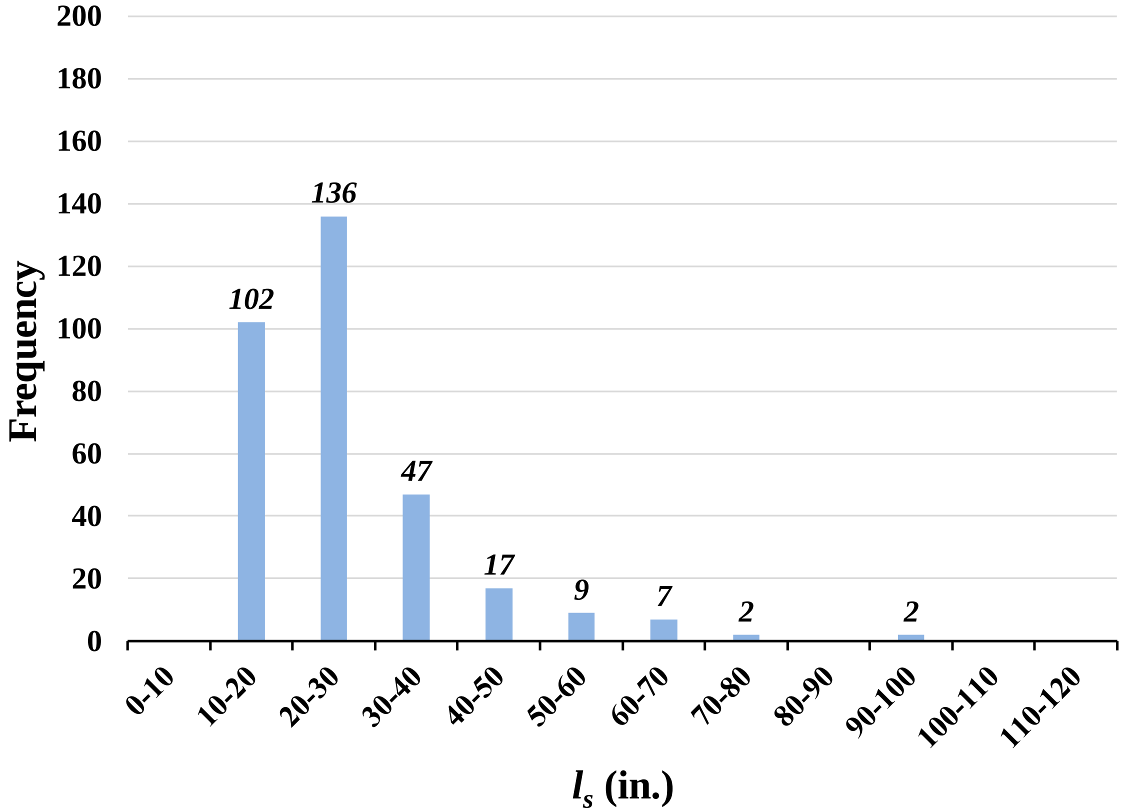

Figure 6.17: Distribution of Splice Length for Confined Database

Figure 6.18 shows the frequency distribution of splice-length-to-bar-diameter ratios in the confined database. Approximately 91% of the confined specimens contain ratios of splice length to bar diameter between 10 and 40. The largest quantity within a distribution is 130 specimens (40%) containing ratios of splice length to bar diameter between 10 and 20.

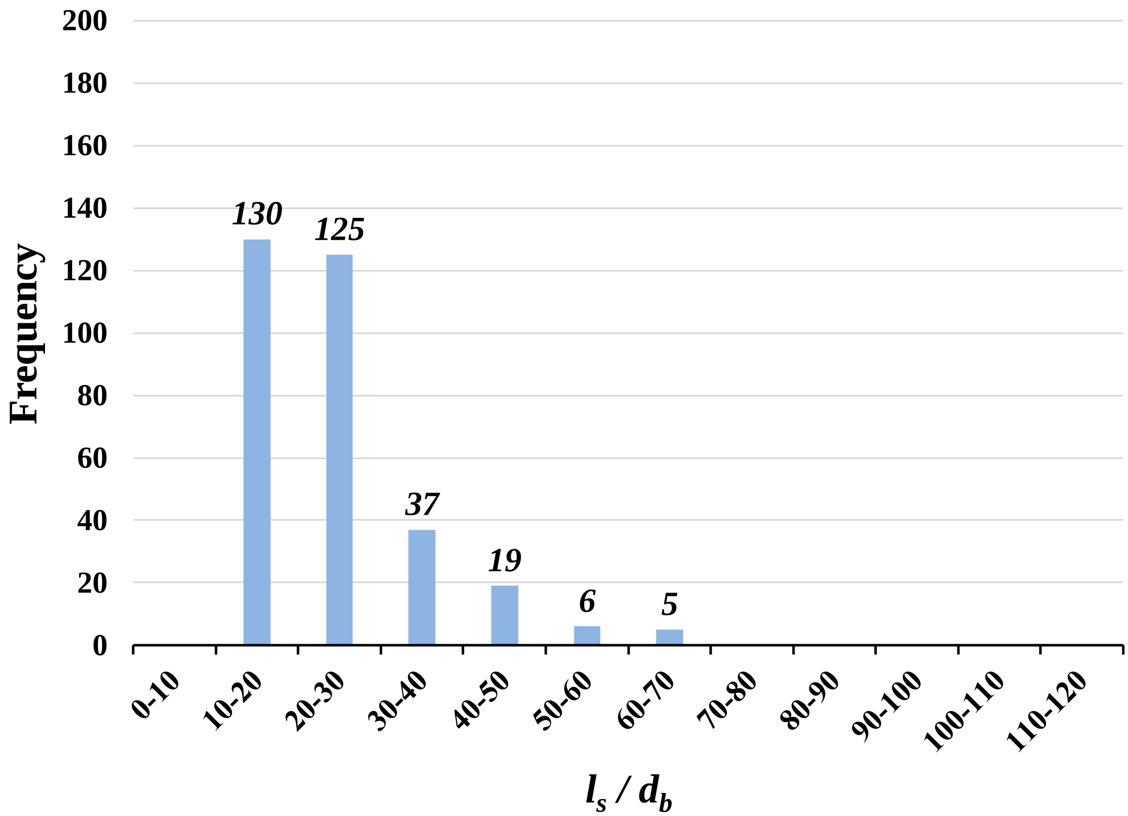

Figure 6.18: Distribution of Splice-Length-to-Bar-Diameter Ratio for Confined Database

Figure 6.19 shows the frequency distribution of side-cover-to-bar-diameter ratios in the confined database. Approximately 87% of the confined specimens contain ratios of side cover to bar diameter between 1.0 and 2.5. The largest quantity within a given distribution is 102 specimens (32%) containing ratios of side cover to bar diameter between 1.5 and 2.0.

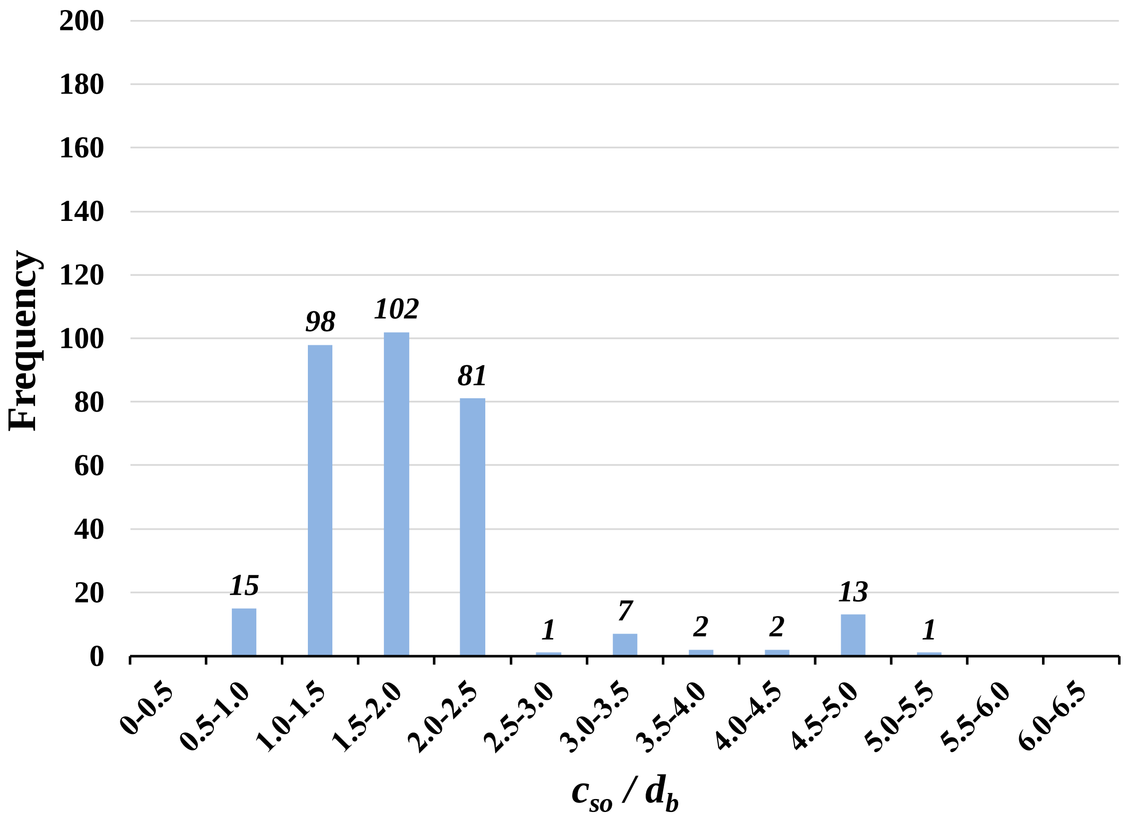

Figure 6.19: Distribution of Side-Cover-to-Bar-Diameter Ratio for Confined Database

Figure 6.20 shows the frequency distribution of total transverse reinforcement areas across the splitting plane for the confined database. Approximately 77% of the confined specimens contain total areas of transverse reinforcement between 0.35 in.^{2} and 2.0 in.^{2}. The largest quantity within a given distribution is 104 specimens (32%) containing total areas of transverse reinforcement between 0.5 in.^{2} and 1.0 in.^{2}.

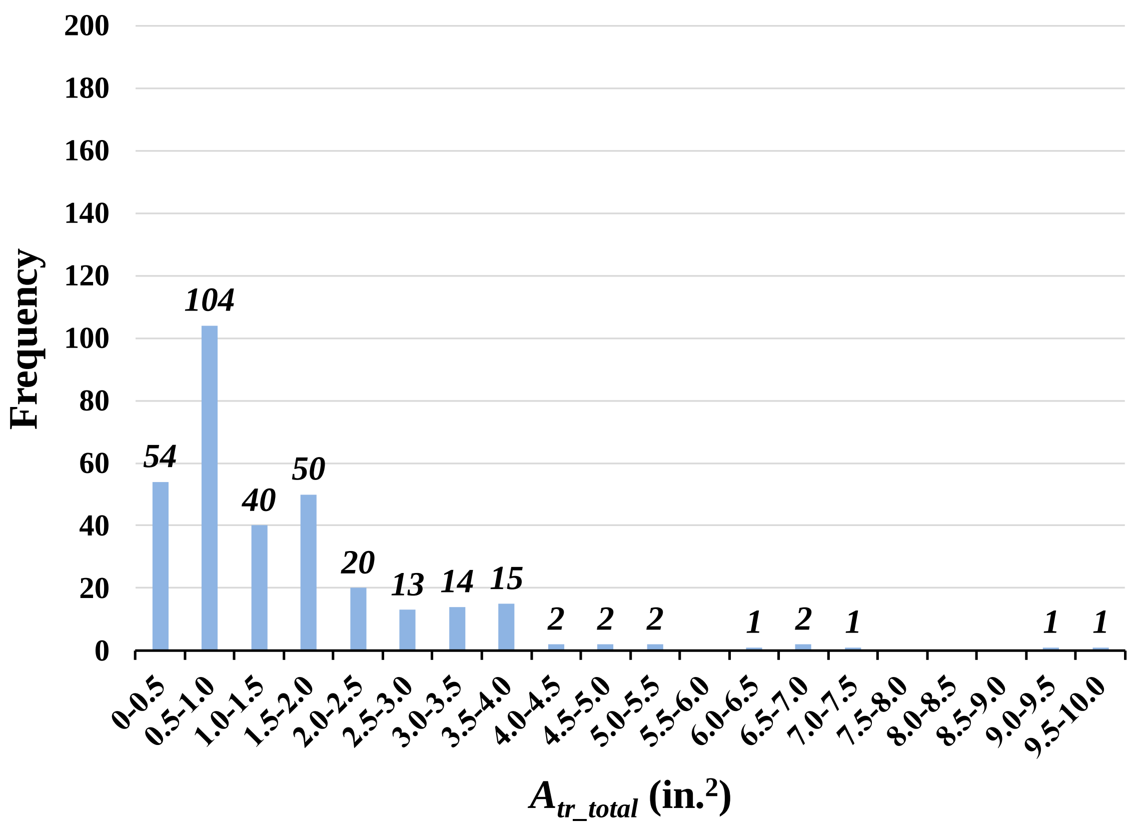

Figure 6.20: Distribution of Total Transverse Reinforcement Area for Confined Database

Figure 6.21 shows the frequency distribution of distributed transverse reinforcement ratios for the confined database. Approximately 66% of the confined specimens contain distributed transverse reinforcement ratios between 0.1% and 0.5%. The largest quantity within a given distribution is 67 specimens (21%) containing distributed transverse reinforcement ratios between 0.1% and 0.2%.

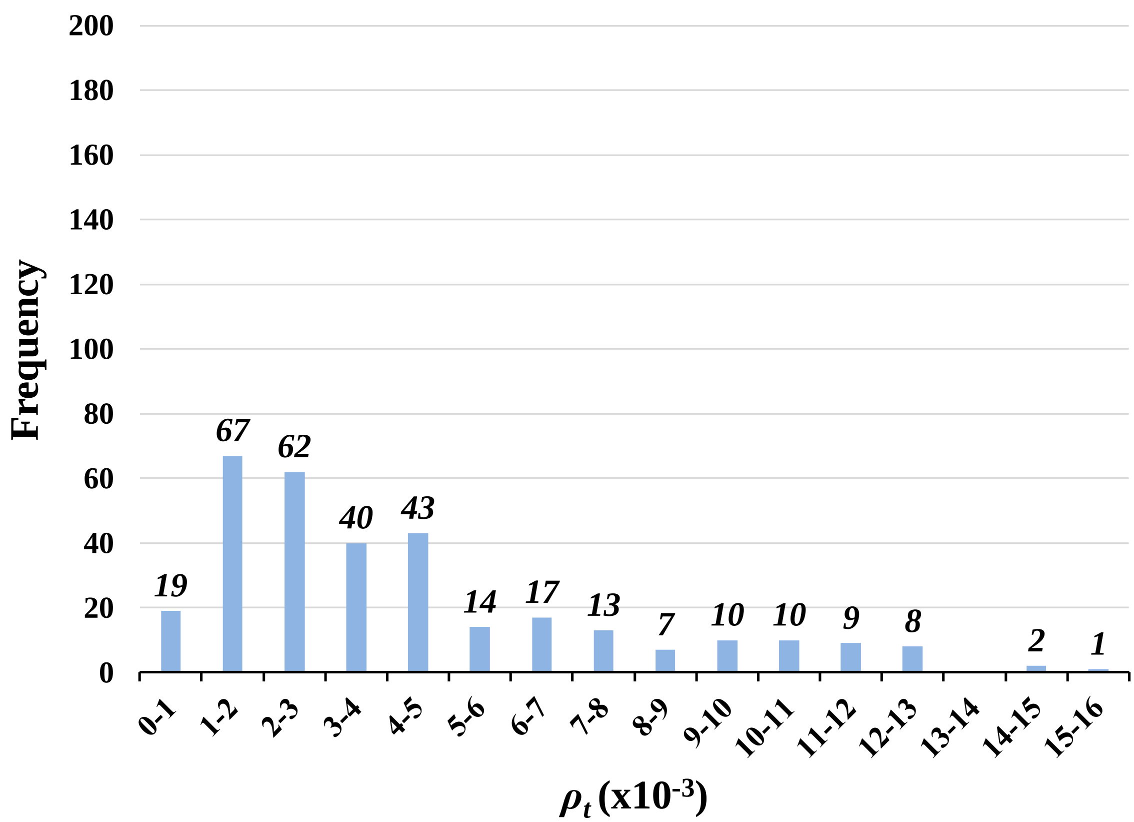

Figure 6.21: Distribution of ρ_t for Confined Database

6.5 Confinement Model

6.5.1 Model

A model was developed that explores the effect of transverse reinforcement location on bond strength of confined concrete members. This transverse reinforcement location model is based on the understanding that bond stress distribution across a splice is nonlinear (Thompson et al. 1975, Azizinamini et al. 1999, Canbay and Frosch 2005, Sim 2014). Because stresses are not constant across the splice, stirrups in different locations may experience different amounts of tensile resisting stress. Figure 6.22 (from Canbay and Frosch (2005)) illustrates how this concept applies to shorter splices and how it changes as the splice length increases.

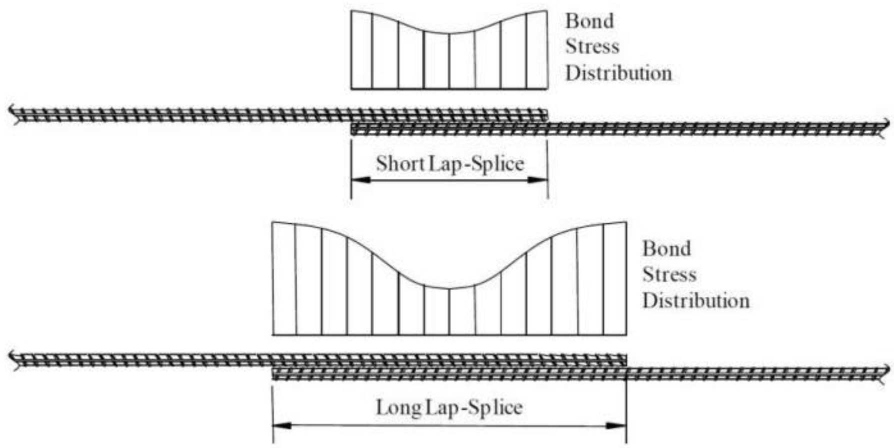

Figure 6.22: Nonlinear Bond Stress Distribution (Canbay and Frosch, 2005)

Further research by Sim (2014) found that when the total area of transverse reinforcement in the splitting plane is constant, stirrups placed at the ends of the splice experience greater strains than stirrups located directly in the middle of the splice. Differences in bar stress at failure were observed including no increase in longitudinal bar stress provided by stirrups located mid-splice and a 30% increase when only end stirrups were provided rather than being distributed. These results align closely with Series VI testing in this research program.

Based on this behavior, a model needs to consider bond stress distribution and stirrup location. The location of a stirrup along the splice determines its effectiveness in resisting tensile stress. Assumptions made to develop this Effective Confinement (EC) model include:

1. Stirrups are limited by their yield strength.

2. The splice zone may be discretized into five (5) regions: two regions of full effectiveness from confinement at the ends, one region of no effectiveness from confinement in the middle, and two regions of partial effectiveness in between.

A typical EC model with six stirrups distributed along the splice is provided in Figure 6.23 and shows the location of each region. Note that the red lines indicate the percent contribution value of each stirrup based on its location along the splice.

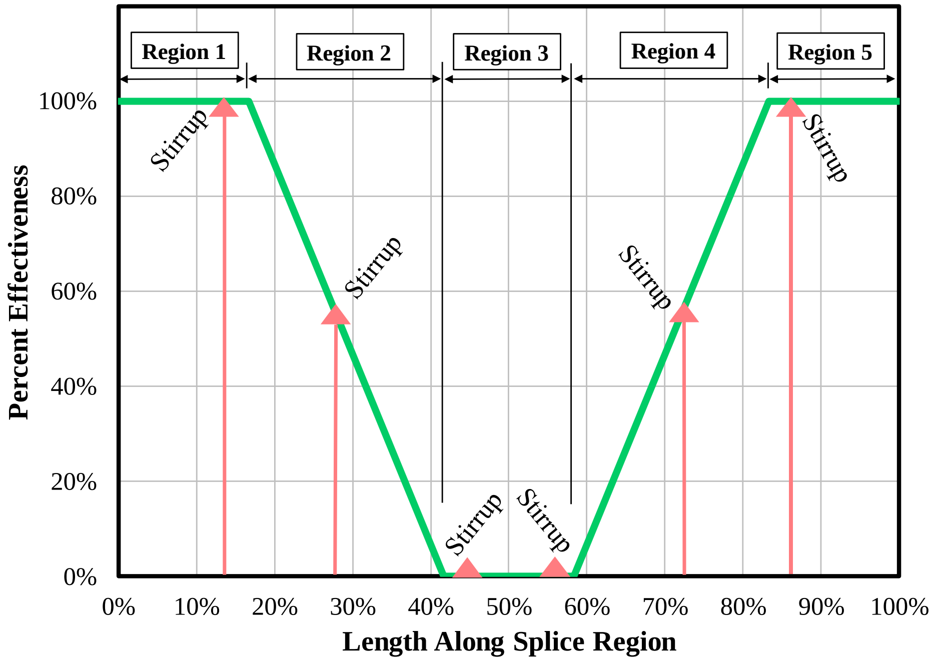

Figure 6.23: Typical Model Regions

Four models were generated in this study, each with different region lengths across the splice. All models are symmetric about the midpoint of the splice to reflect the symmetrical distribution of bond stresses across a symmetrically-loaded beam. The differences between these models are described in Table 6.4 followed by graphical configurations for all four models in Figure 6.24.

Table 6.4: Trial Model Region Dimensions

Potential Models	Lengths of Model Regions				
	Region 1	Region 2	Region 3	Region 4	Region 5
A	$l_s/6$	$l_s/3$	0	$l_s/3$	$l_s/6$
B	$0.15l_s$	$l_s/5$	$0.3l_s$	$l_s/5$	$0.15l_s$
C	$l_s/6$	$l_s/4$	$l_s/6$	$l_s/4$	$l_s/6$
D	$l_s/6$	$l_s/6$	$l_s/3$	$l_s/6$	$l_s/6$

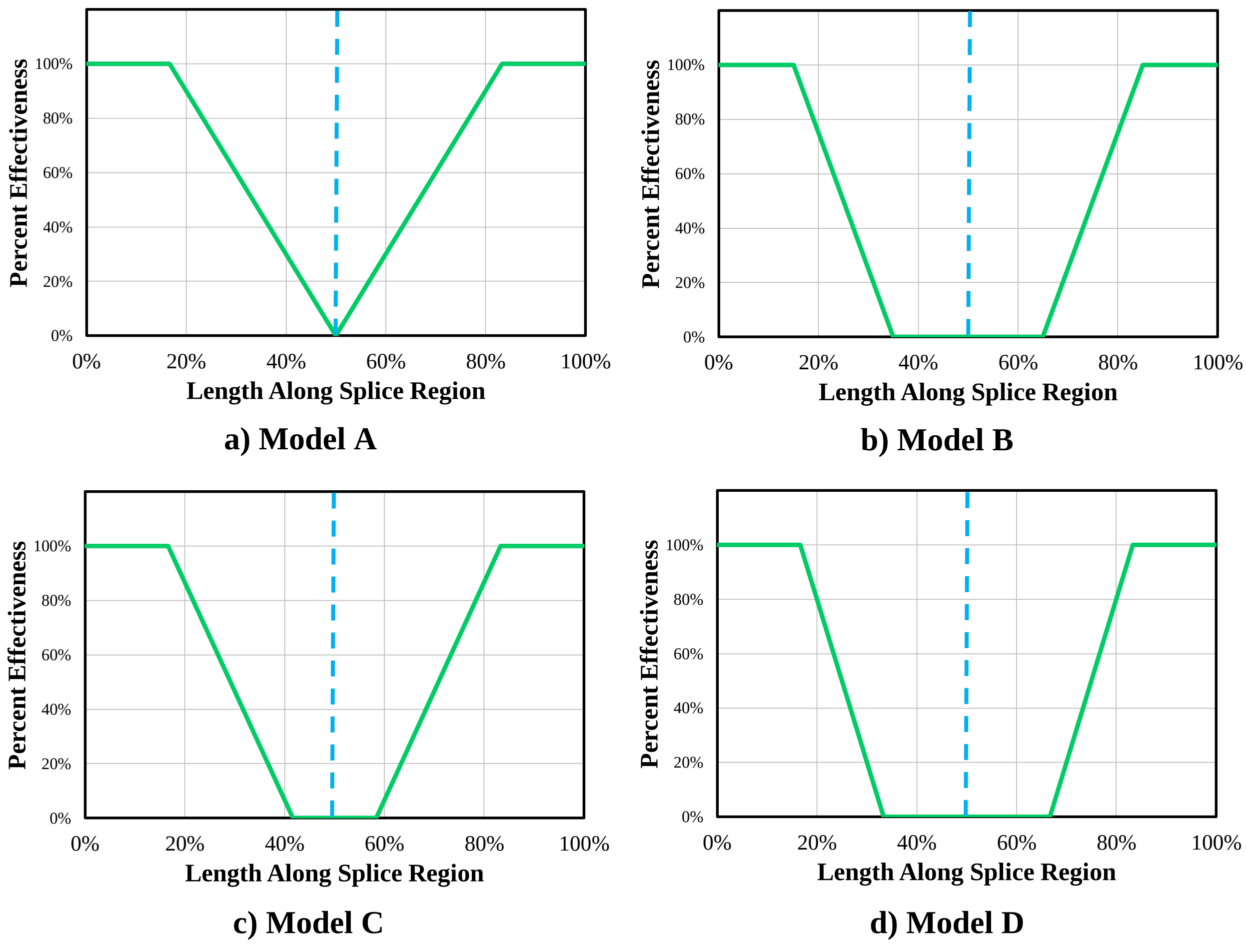

Figure 6.24: Potential Effective Confinement Models

To determine the effectiveness of a stirrup along the splice length, all four models require knowing the location of that stirrup. The total number of effective stirrups ($N_{s,eff}$) along the splice is calculated by summing all percent contributions. For example, given a splice length of 50 in. with three stirrups spaced at quarter points, all four models indicate that the middle stirrup provides no additional tensile resistance (0%). However, the other two stirrups are located within the linear interpolation range and can be either 50% (Model B and D), 67% (Model C), or 75% (Model A) effective, depending on the model. Model A outputs the most stirrup efficiency with $N_{s,eff} = 0 + 0.75 + 0.75 = 1.5$ effective stirrups while Models B and D output $N_{s,eff} = 0 + 0.5 + 0.5 = 1$ effective stirrup for this case.

6.5.2 Model Application

The number of effective stirrups within the splice region $N_{s,eff}$ can be determined by equating the effective stress developed in the transverse reinforcement to the additional stress in the longitudinal bars.

$$N_l A_t f_{yt} N_{s,eff} = N_b\, A_b (f_b - f_{bc}) \tag{6-7}$$

where:

A_b = *area of one longitudinal reinforcing bar (in.^{2})*

A_t = *area of one stirrup leg (in.^{2})*

f_b = *total bar stress at failure of confined specimen (ksi)*

f_{bc} = *bar stress at failure of identical unconfined specimen; concrete contribution to bar stress (ksi)*

f_{yt} = *yield strength of transverse reinforcement (ksi)*

N_b = *number of longitudinal reinforcing bars*

N_l = *number of legs of transverse reinforcement crossing the splice plane*

Note that the term $(f_b - f_{bc})$ represents the additional stress (f_{bs}) gained from the presence of confinement steel within the splice. The stress obtained from an unconfined specimen is subtracted from the total bar stress of each confined specimen where design parameters between the two specimens are identical, except the presence of confinement. This equation is also a measure of equilibrium between the force crossing the splitting plane and the force transferred from the transverse reinforcement to the longitudinal reinforcement. The final rearranged equation takes the following form:

$$N_{s,eff} = \frac{N_b\, A_b (f_b - f_{bc})}{N_l A_t f_{yt}} \tag{6-8}$$

Confined beam tests in Series VI and VII were conducted to isolate the additional bond strength provided from the transverse reinforcement. These tests allow for comparing beams with varying amounts of confinement steel to an identical beam with no transverse reinforcement. By running each of these beams through all four models, the ratio (Equation 6-9) of the number of effective stirrups $N_{s,eff}$ to the number of actual stirrups present N_s could be investigated. This ratio k represents the percent contribution of transverse reinforcement toward increasing bond strength. This value should always be less than or equal to one.

$$k = \frac{N_{s,eff}}{N_s} \tag{6-9}$$

where:

k = *percent contribution of transverse reinforcement in splice region*

$N_{s,eff}$ = *number of effective stirrups within the splice region*

N_s = *number of stirrups within the splice region*

To visualize how the value of *k* changes as the number of stirrups is increased within the splice, a spectrum of possible spacings was determined for a range of N_s values from 1 to 15, resulting in an upper and lower bound for possible model results. Additionally, an average stirrup spacing was implemented to determine an average k_{calc} value. Note that all stirrups are assumed to be evenly spaced and symmetric about the center of the splice. Table 6.5 shows the possible spacings and *k* values for each model. Spacing limits were determined from the following:

$$s_{min} = \frac{l_s}{N_s + 1} \qquad s_{avg} = \frac{l_s}{N_s} \qquad s_{max} = \frac{l_s}{N_s - 1}$$

Table 6.5: Model Boundaries

N_s	Possible Spacings (s)			k_{calc}											
				A			B			C			D		
	Min	Avg	Max	Min	Avg	Max	Min	Avg	Max	Min	Avg	Max	Min	Avg	Max
1	-	-	-	-	0	-	-	0	-	-	0	-	-	0	-
2	$l_s/3$	$l_s/2$	l_s	0.50	0.75	1.0	0.08	0.50	1.0	0.33	0.67	1.0	0	0.50	1.0
3	$l_s/4$	$l_s/3$	$l_s/2$	0.50	0.67	0.67	0.33	0.61	0.67	0.44	0.67	0.67	0.33	0.67	0.67
4	$l_s/5$	$l_s/4$	$l_s/3$	0.60	0.69	0.75	0.38	0.50	0.54	0.47	0.58	0.67	0.40	0.50	0.50
5	$l_s/6$	$l_s/5$	$l_s/4$	0.60	0.64	0.70	0.40	0.50	0.60	0.53	0.59	0.67	0.40	0.48	0.60
6	$l_s/7$	$l_s/6$	$l_s/5$	0.62	0.67	0.73	0.44	0.50	0.58	0.51	0.56	0.64	0.43	0.50	0.60
7	$l_s/8$	$l_s/7$	$l_s/6$	0.61	0.65	0.71	0.43	0.48	0.57	0.52	0.59	0.67	0.43	0.49	0.57
8	$l_s/9$	$l_s/8$	$l_s/7$	0.62	0.67	0.71	0.43	0.50	0.58	0.52	0.58	0.63	0.41	0.50	0.57
9	$l_s/10$	$l_s/9$	$l_s/8$	0.62	0.67	0.69	0.44	0.51	0.56	0.53	0.59	0.63	0.44	0.52	0.56
10	$l_s/11$	$l_s/10$	$l_s/9$	0.64	0.67	0.70	0.44	0.50	0.54	0.54	0.59	0.62	0.45	0.50	0.53
11	$l_s/12$	$l_s/11$	$l_s/10$	0.64	0.66	0.69	0.45	0.50	0.55	0.54	0.58	0.62	0.45	0.50	0.55
12	$l_s/13$	$l_s/12$	$l_s/11$	0.64	0.67	0.70	0.47	0.50	0.54	0.55	0.58	0.62	0.46	0.50	0.54
13	$l_s/14$	$l_s/13$	$l_s/12$	0.64	0.66	0.69	0.46	0.49	0.54	0.55	0.58	0.61	0.46	0.50	0.54
14	$l_s/15$	$l_s/14$	$l_s/13$	0.64	0.67	0.69	0.46	0.50	0.54	0.55	0.59	0.61	0.46	0.50	0.54
15	$l_s/16$	$l_s/15$	$l_s/14$	0.64	0.67	0.69	0.47	0.50	0.53	0.56	0.59	0.61	0.47	0.51	0.53

The k_{calc} values vs. N_s for each model are shown in Figure 6.25. Note that for a particular number of specified stirrups within the splice region, each model provides a range of possible percent contributions with an upper bound and a lower bound based on stirrup spacing. For lower values of N_s, the possible values of k_{calc} that each model can predict is large. As more stirrups are included within the splice region, this range of k_{calc} values converges upon one distinct constant in all four models. The large amount of initial scatter in the model is a result of the range of possible stirrup locations along the anchorage length. Spacing variability permits stirrups to be placed in regions of varying effectiveness, lending to a large range of k_{calc} values. It should also be noted that regardless of model accuracy, all four models approached a distinct value after approximately four stirrups were placed within the splice region.

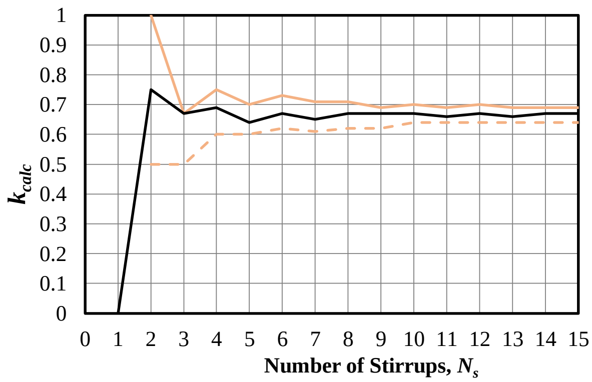

a) Model A

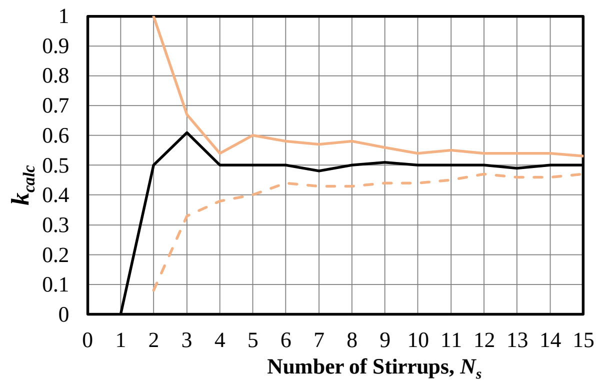

b) Model B

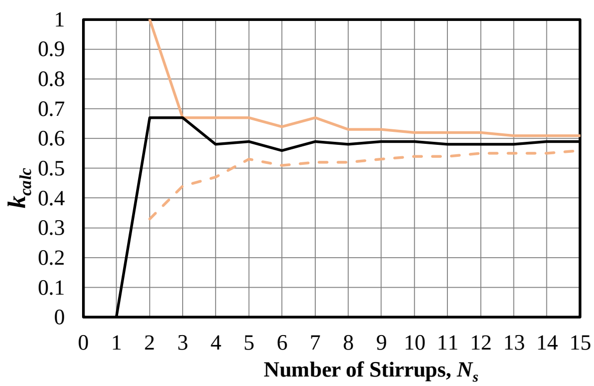

c) Model C

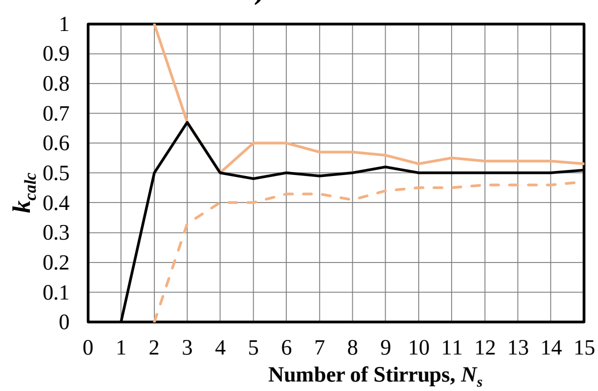

d) Model D

Figure 6.25: Potential Ranges of k_{calc}

Values of k_{test} were calculated in two trials for several beams from this testing program, as well as from Sim (2014). The specimens from this testing program were grouped into two phases, with Phase I consisting of specimens from the first four series of testing, while Phase II contained specimens from Series V through VII. The value of k_{test} was calculated by substituting Equation 6-8 into Equation 6-9 to produce the following equation:

$$k_{test} = \frac{N_b\, A_b(f_b - f_{bc})}{N_s N_l A_t f_{yt}} \qquad (6\text{-}10)$$

For Trial 1, measured values of f_{yt} were used to obtain initial k_{test} percentages for comparison. Nominal confined bar stress at failure and unconfined bar stress at failure were used; therefore, any differences in concrete strength between the confined and unconfined specimens were not included. The results of Trial 1 are provided in Table 6.6.

Table 6.6: Effective Confinement Test Specimens

Program	Specimen	l_s (in.)	f_c' (psi)	f_{test} (ksi)	N_s	Trial 1		Trial 2		
						$N_{s,eff}$	k_{test}	f_{norm}[1] (ksi)	$N_{s,eff}$	k_{test}
Phase I: Series I - IV	U-40-5a	40	6260	69.8	-	-	-	-	-	-
	C3/60/2-40-5-50	40	6260	81.8	2	1.64	0.82	70.8	1.98	0.99
	C3/60/3-40-5-50	40	6260	89.8	3	2.73	0.91	70.8	3.41	1.14[2]
	C3/100/3-40-5-50	40	6260	85.0	3	1.61	0.54	70.8	2.55	0.85
	C3/60-40-5-100	40	6260	91.7	5	2.99	0.60	70.8	3.75	0.75
	C3/100-40-5-100	40	6260	93.1	5	2.46	0.49	70.8	4.00	0.80
Phase II: Series V-VII	C3/60-40-5-150	40	6200	90.4	6	3.47	0.58	70.7	3.54	0.59
	C3/60-40-5-200	40	6300	96.8	8	4.54	0.57	71.0	4.63	0.58
	U-50-5	50	5400	73.2	-	-	-	-	-	-
	C3/60-50-5-150	50	6600	104.6	8	5.29	0.66	76.7	5.01	0.63
Sim (2014)	B-8-S-24	24	4400	44.2	-	-	-	-	-	-
	B-8-S-24-C1	24	4400	51.5	2	1.31	0.66	44.2	1.31	0.66
	B-8-S-24-C2	24	4400	48.7	2	0.81	0.40	44.2	0.81	0.40
	B-8-S-24-C3	24	4400	54.3	3	1.81	0.60	44.2	1.81	0.60
	M-8-S-48	48	5400	74.7	-	-	-	-	-	-
	M-8-S-48-C1	48	5400	97.1	2	2.21	1.11[2]	74.7	2.21	1.11[2]
	M-8-S-48-C2	48	5400	76.6	2	0.19	0.09	74.7	0.19	0.09
	M-8-S-48-C3	48	5400	97.0	3	2.20	0.73	74.7	2.20	0.73

[1] *Values reflect the unconfined concrete strength, normalized to the concrete strength of the confined beam*
[2] *Experimental test performed better than model prediction*

Trial 1 k_{test} values are plotted in Figure 6.26. Three specimens from Phase II are shown as yellow squares, five specimens from Phase I are shown as blue circles, and six specimens by Sim (2014) are shown as green triangles.

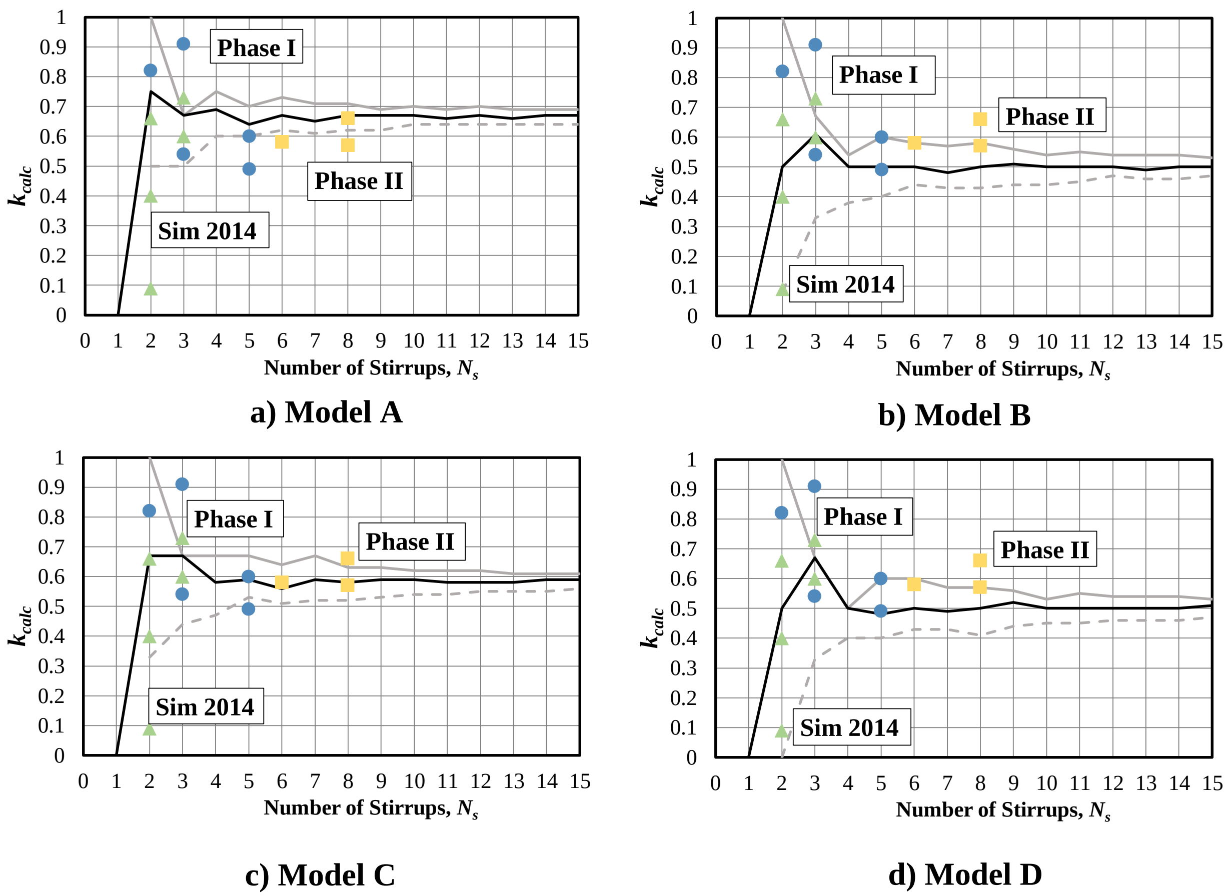

Figure 6.26: Trial 1 k_{test} vs. k_{calc}

Note that one specimen from Sim (2014) exceeded $k = 1$ in Trial 1 and is not included in Figure 6.26. Additionally, one specimen from Sim (2014) resulted in a k_{test} value of only 9%. This beam was constructed with two No. 4 Grade 60 stirrups place in the middle of a 48-in. lap splice. It was concluded in this test that the addition of transverse reinforcement had essentially no effect on bond strength. Another beam achieved a k_{test} of 40% that contained two No. 3 Grade 60 stirrups in the middle of a 24-in. lap splice and slightly contributed to a higher bond strength. Figure 6.26 supports these findings.

In Trial 2, yield strength and variability in concrete strength were handled differently. Based on findings from this testing program, yield strength of the transverse reinforcement is negligible in determining the additional bond strength contribution. Therefore, yield strength f_{yt} in Equation 6-10 was taken to be a lower bound of 60 ksi for all beams, regardless of grade.

To account for the variation in concrete strength between the confined beam and its unconfined counterpart, a general normalization function was implemented. It has been previously supported that the representation of concrete strength in a spliced member without transverse reinforcement is best described by a power of 0.25 (Darwin et al. 1996, Zuo and Darwin 2000, Canbay and Frosch 2005, Pay 2005, Sim 2014). The failure stresses of all baseline unconfined beams were normalized to the concrete strength of the confined specimen of interest. Equation 6-11 was used to normalize the longitudinal failure stress (f_{orig}) that reflects the difference in concrete strength between the unconfined beam and the confined beam.

$$f_{norm} = f_{orig} \sqrt[4]{\frac{f_{target}}{f_c'}} \tag{6-11}$$

where:

f_c'	=	*concrete cylinder strength (psi)*
f_{norm}	=	*new normalized longitudinal bar stress at failure (ksi)*
f_{orig}	=	*original longitudinal bar stress at failure (ksi)*
f_{target}	=	*normalization target strength (psi)*

Table 6.6 presents the calculated f_{norm} and k_{test} values for Trial 2. A comparison between k_{test} and k_{calc} is plotted for all four models in Figure 6.27.

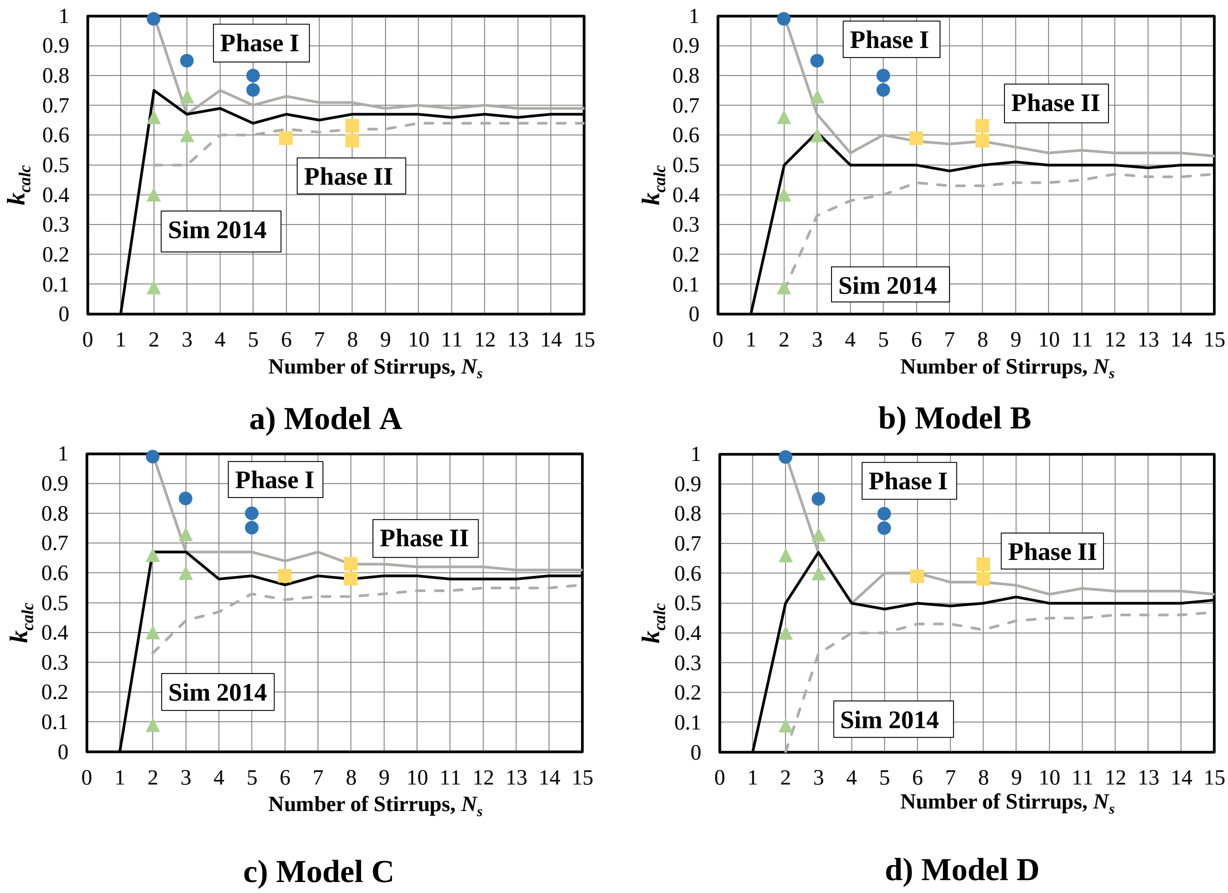

Figure 6.27: Trial 2 k_{test} vs. k_{calc}

Note that one beam from Phase I of this study and Sim (2014) produced k_{test} values of 1.14 and 1.11, respectively, due to the high contribution from the transverse reinforcement when three stirrups were placed along the splice. These tests are not shown in Figure 6.27.

Each model from both trials was compared to determine a best fit. Model A shows that many k_{test} values were below the k_{calc} convergence average of 67%, indicating that more stirrups were effective in the model than observed from the test. In addition, the lower bound for k_{calc} minimizes at 0.50 (2 or 3 stirrups) and does not capture values below this minimum. Model C fits the test data slightly better and results in a convergence k_{calc} value of 59%; however, the model is unable to accommodate lower k_{test} values because the lower bound reaches a minimum of 33%.

Models B and D closely fit the test data and provide reasonable bounds for the k_{calc} term. Both converge on a value of 50%, suggesting that when a reasonable distribution of transverse reinforcement is provided in the splice region, only half of those stirrups fully contribute to any additional bond strength. In other words, over the splice length, half of the stirrups are considered fully effective. For simplicity purposes, Model D was selected based on the ease in calculating the five region lengths as 1/3-regions (Fully effective regions sum to l_s/3, interpolated regions sum to l_s/3, and region of no effectiveness is l_s/3).

6.5.3 Steel Contribution Term, f_{bs}

Equation 6-7 relates the vertical force resisted by the transverse reinforcement and the horizontal force resisted by the longitudinal reinforcement. By rearranging the equation to solve for the transverse steel contribution, Equation 6-12 results. Note that the amount of force transferred from the vertical stirrups to the longitudinal bars (p) is assumed to be 100% of the vertical tension resisting force:

$$f_{bs} = \frac{F_{horiz}}{A_b N_b} = \frac{pF_{vert}}{A_b N_b} \tag{6-12}$$

where:

A_b = *area of one longitudinal reinforcing bar (in.^{2})*

f_{bs} = *bar stress contribution from the presence of transverse steel (ksi)*

F_{horiz} = *horizontal force transferred to the longitudinal reinforcement by the transverse reinforcement (kip)*

F_{vert} = *vertical force provided by transverse reinforcement (kip)*

N_b = *number of longitudinal reinforcing bars*

p = *transfer factor between vertical and horizontal force; Assumed to be 1*

The force developed in the vertical transverse steel is limited by the yield strength of each stirrup; therefore, the product of stirrup force resistance and the total number of effective stirrups results in the vertical contribution force (Equation 6-13).

$$F_{vert} = N_{s,eff} R_s \tag{6-13}$$

where:

A_t = *area of one stirrup leg (in.²)*

f_{yt} = *yield strength of transverse reinforcement (ksi)*

k = *percent contribution of transverse reinforcement in splice region*

N_l = *number of legs of transverse reinforcement that cross the splitting plane*

N_l = *number of stirrups along the splice*

$N_{s,eff}$ = *number of effective stirrups within the splice region*

= kN_s

R_s = *resistance force provided by one stirrup (kip)*

= $N_l A_t f_{yt}$

Substituting Equation 6-13 in Equation 6-12 results in the following:

$$f_{bs} = \frac{pkN_s N_l A_t f_{yt}}{A_b N_b} \tag{6-14}$$

The value of p is taken to be one because it is assumed that the entire vertical force in the stirrups is transferred to the longitudinal steel. As previously discussed, in the model study *k* was found to converge to a value between 0.4 and 0.6. To further explore the value of *k*, the normalized steel contribution stress (f_{bs}) from each specimen in the confined pair database was plotted against Equation 7-13 for different values of k ranging from 40% to 65%. A linear trend is included, and its slope should approach a value of one as *k* approaches the correct value. Figure 6.28(c) indicates that a contribution of 50% is most appropriate for the bar stress equation. This value is also consistent with findings by Sim (2014). Note that the normalized steel contribution stress is equal to the failure stress less the contribution from the concrete ($f_{bs,norm} = f_b - f_{bc,norm}$).

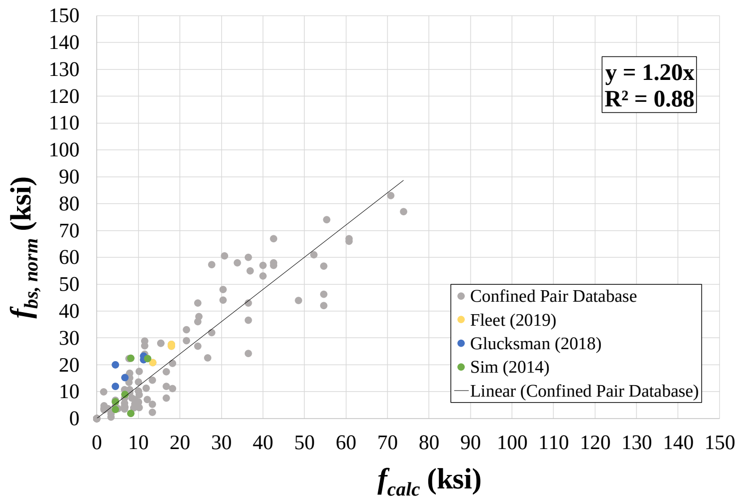

a) k = 40%

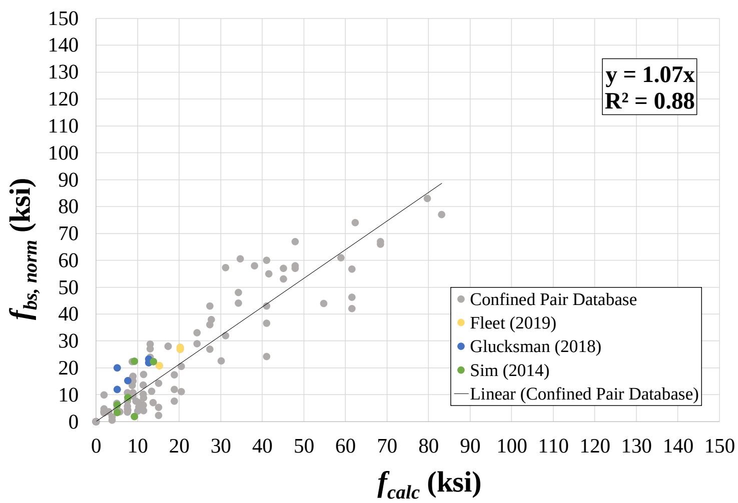

b) k = 45%

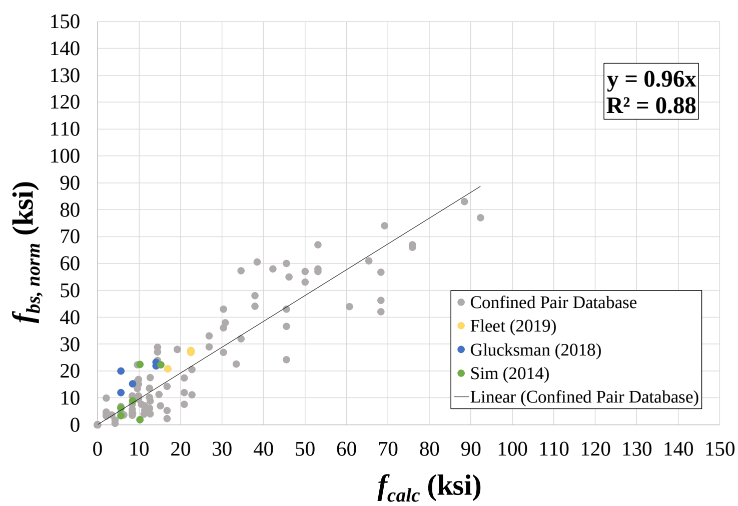

c) k = 50%

Figure 6.28: Normalized Steel Contribution to Bar Stress vs. Proposed Equation

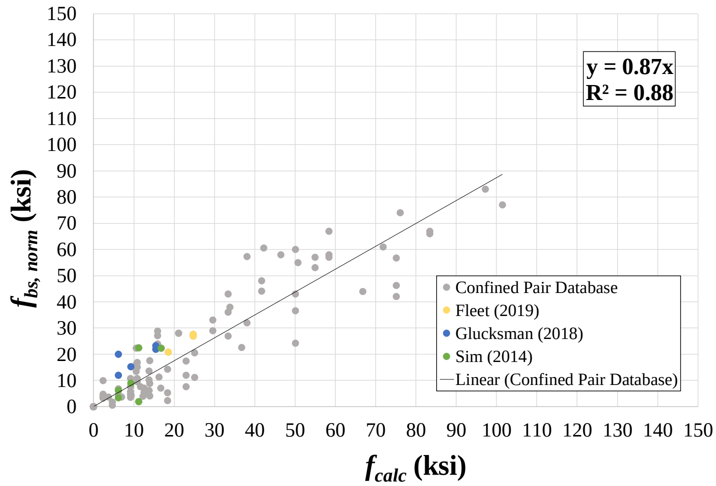

d) k = 55%

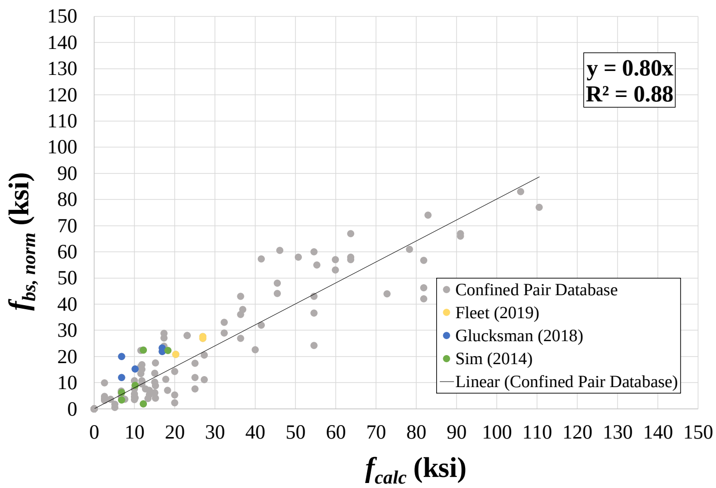

e) k = 60%

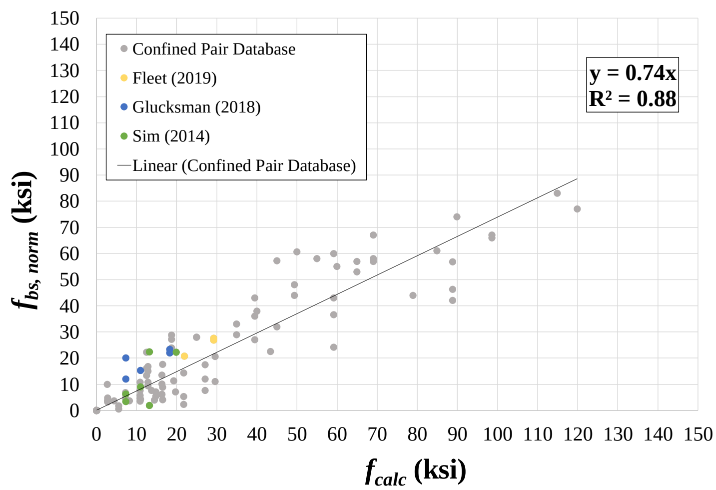

f) k = 65%

Figure 6.28: Normalized Steel Contribution to Bar Stress vs. Proposed Equation - Continued

By substituting a value of 0.5 for k, the final equation for the stress contribution from transverse reinforcement results in Equation 6-15. As shown in Figure 6.28(c), the test results fit very well with the model.

$$f_{bs} = \frac{f_{yt} N_s N_l A_t}{2 N_b A_b} \tag{6-15}$$

6.6 Bond Model

The total bar stress at failure can be considered the sum of the concrete contribution and the added contribution of any transverse reinforcement within the lap splice (Equation 6-16):

$$f_b = f_{bc} + f_{bs} \tag{6-16}$$

where:

f_b = *total bond strength (ksi)*

f_{bc} = *contribution to bond strength provided by concrete (ksi)*

f_{bs} = *contribution to bond strength provided by transverse steel (ksi)*

By substituting Equations 6-5 and 6-15 into Equation 6-16, the final expression for bar stress takes the following form:

$$f_b = (f_c')^{0.25} \left(\frac{l_s}{d_b}\right)^{0.5} \left(\frac{c_{so}}{d_b}\right)^{0.25} + \frac{N_s N_l A_t f_{yt}}{2 N_b A_b} \tag{6-17}$$

This expression is applicable for the development of unconfined and confined beams containing bars of all steel grades. Equation 6-17 was applied to the 322 beams in the confined database to evaluate its performance. For comparative purposes, the results provided by the ACI 318-14 design expression (Equation 6-6) are also included.

Table 6.7 provides a statistical comparison of the results. Graphic comparisons between ACI 318-14 and proposed expression (Equation 6-17) are provided in Figure 6.29 through Figure 6.37 for different variables of interest.

Table 6.7: Statistical Analysis Comparison of f_{test}/f_{calc} for Confined Beams

	ACI 318-14	Proposed Equation (7-16)
Max.	2.21	1.30
Min.	0.63	0.64
Mean ($\bar{x}$)	1.30	0.94
Standard Deviation (σ)	0.300	0.129
COV	0.230	0.136

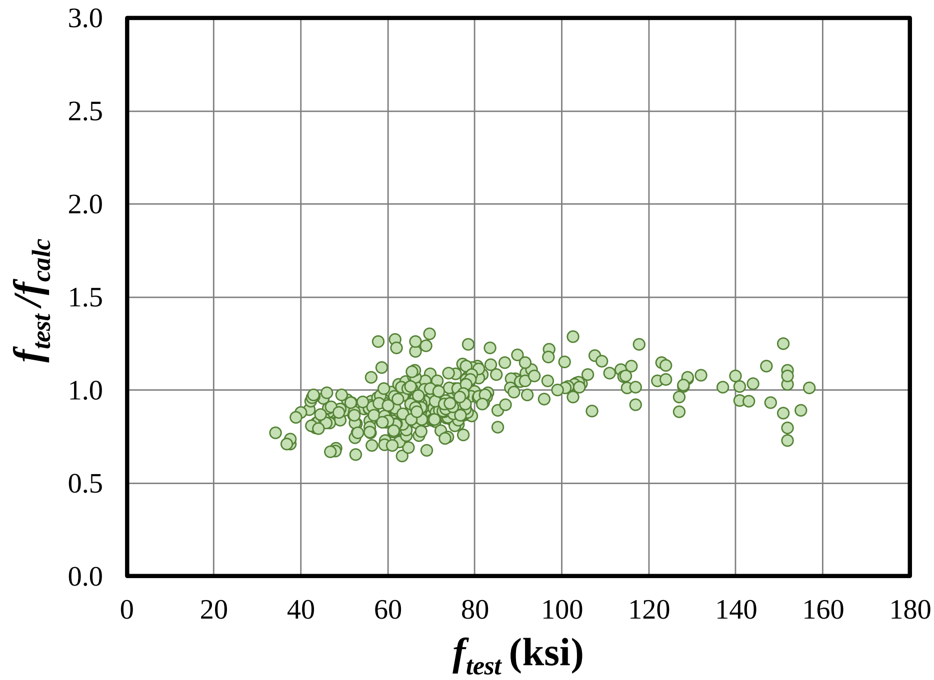

a) Equation 6-17

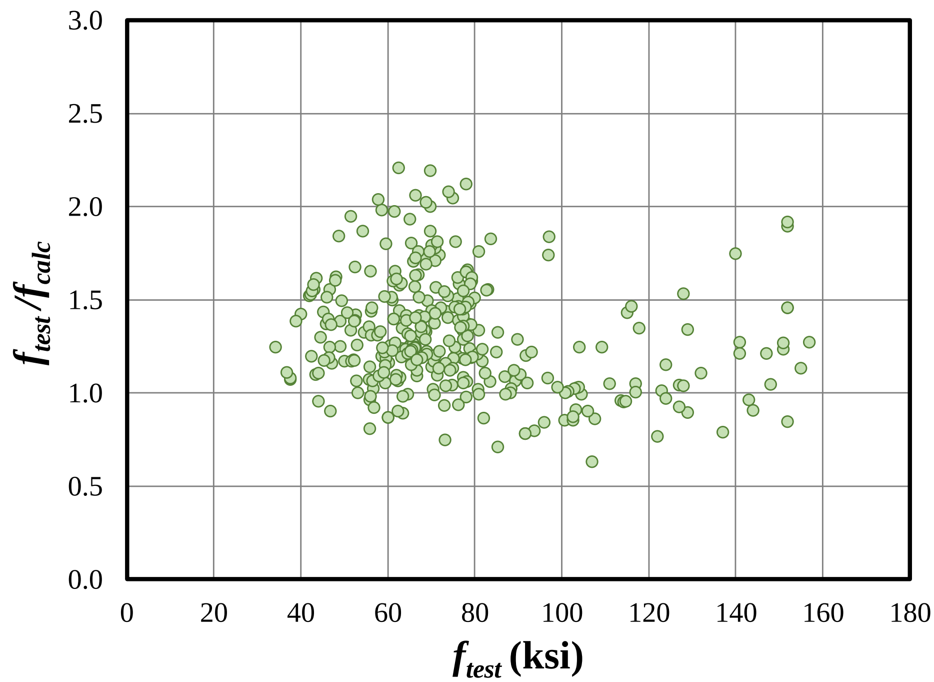

b) ACI 318-14

Figure 6.29: Equation Comparison for Bar Stress at Failure (Confined)

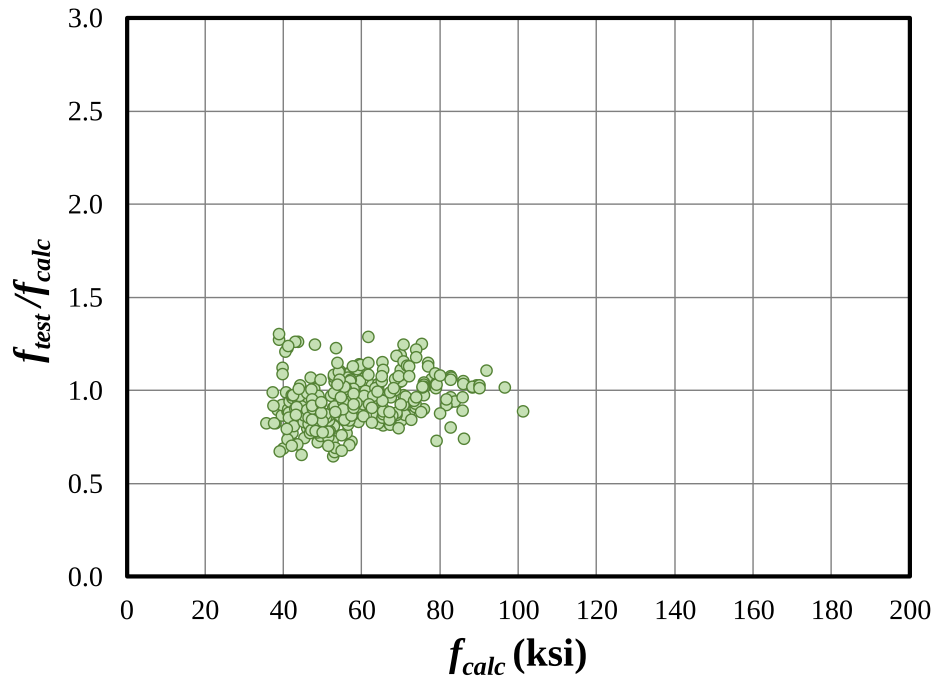

a) Equation 6-17

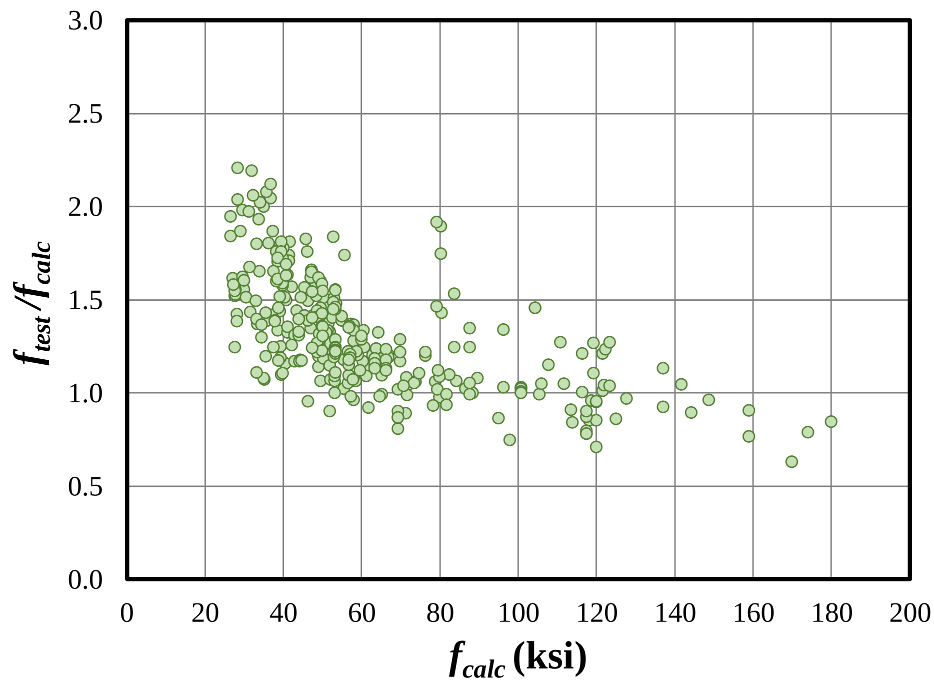

b) ACI 318-14

Figure 6.30: Equation Comparison for Calculated Bar Stress (Confined)

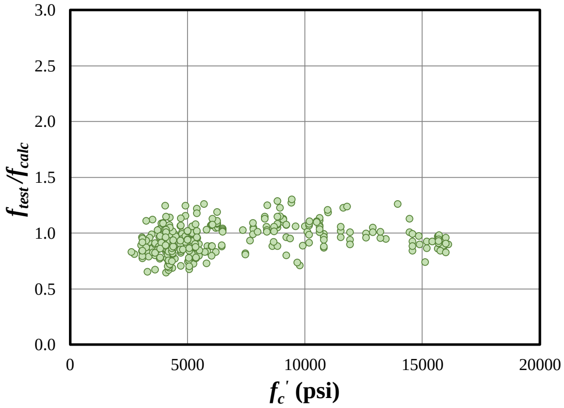

a) Equation 6-17

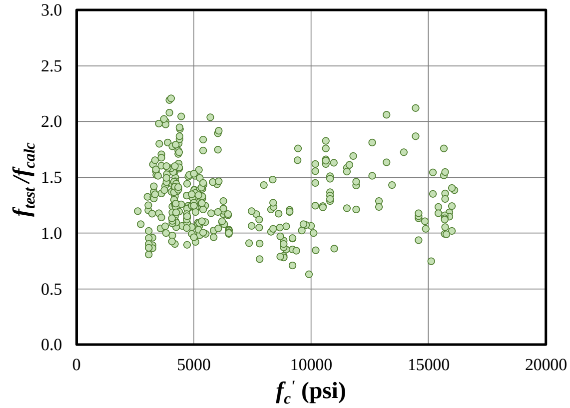

b) ACI 318-14

Figure 6.31: Equation Comparison for Concrete Strength (Confined)

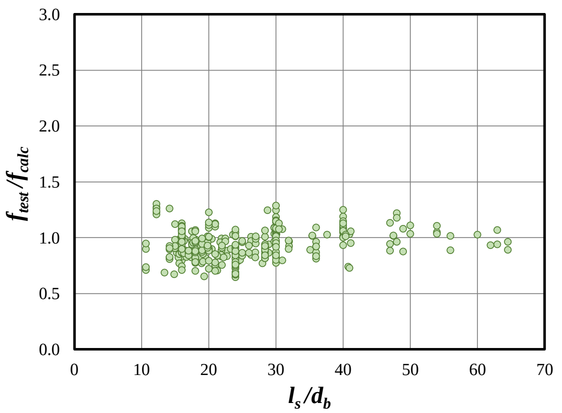

a) Equation 6-17

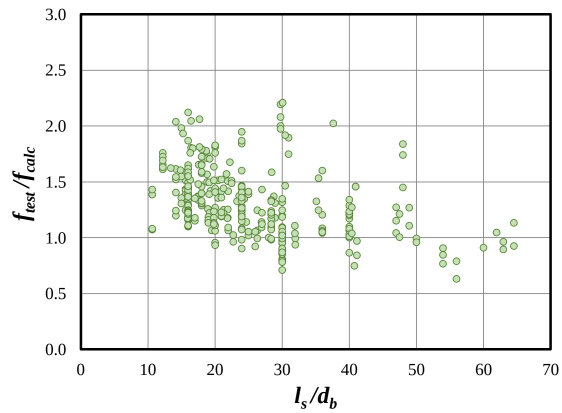

b) ACI 318-14

Figure 6.32: Equation Comparison for Splice Length over Bar Diameter (Confined)

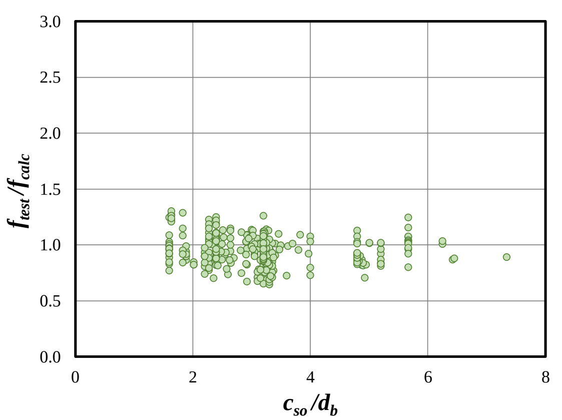

a) Equation 6-17

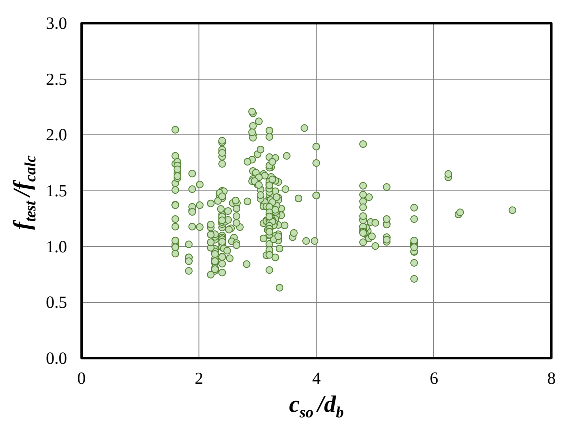

b) ACI 318-14

Figure 6.33: Equation Comparison for Side Cover over Bar Diameter (Confined)

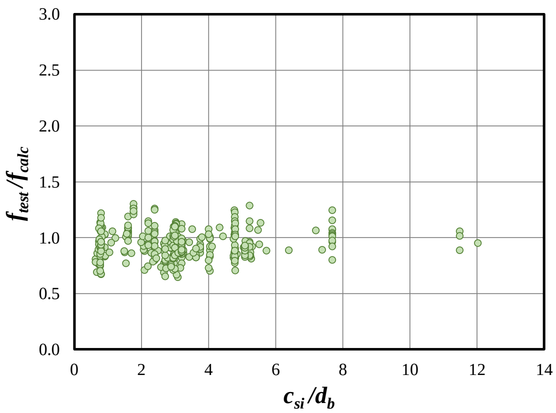

a) Equation 6-17

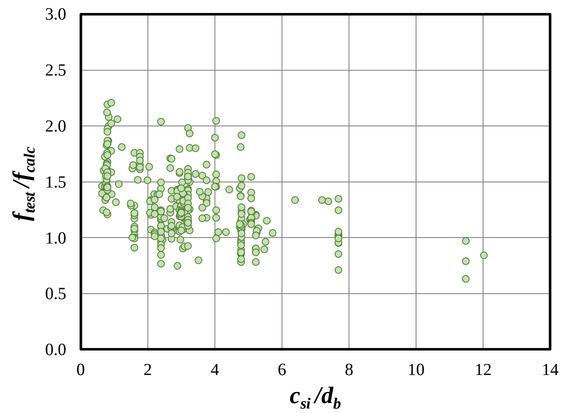

b) ACI 318-14

Figure 6.34: Equation Comparison for Half Bar Spacing over Bar Diameter (Confined)

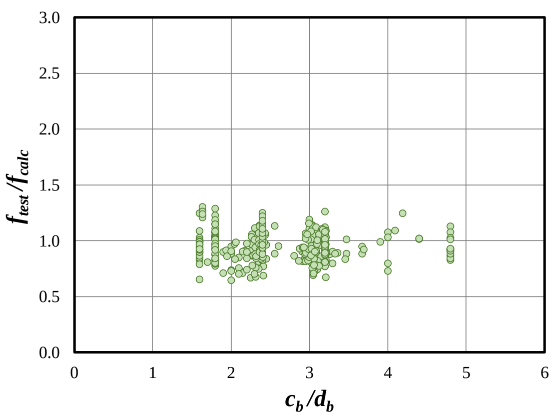

a) Equation 6-17

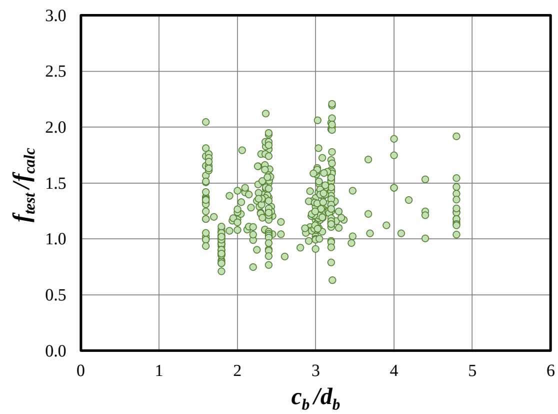

b) ACI 318-14

Figure 6.35: Equation Comparison for Bottom Cover over Bar Diameter (Confined)

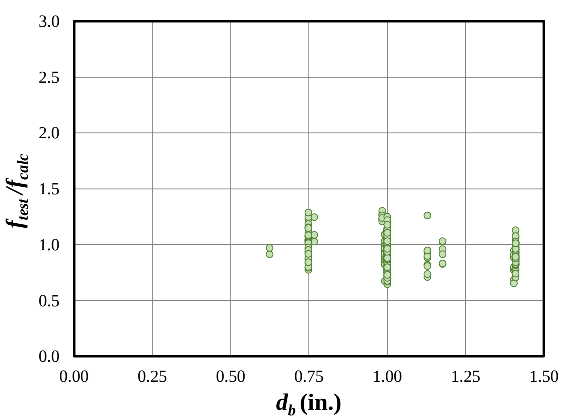

a) Equation 6-17

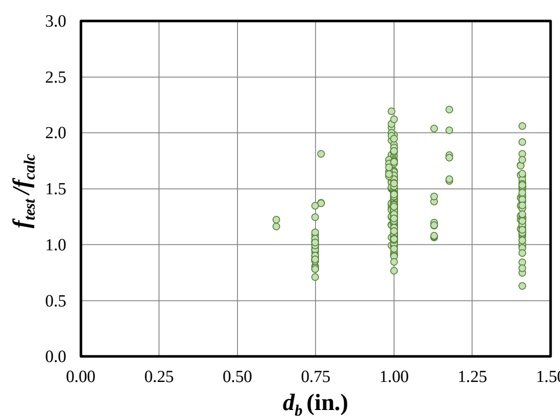

b) ACI 318-14

Figure 6.36: Equation Comparison for Bar Diameter (Confined)

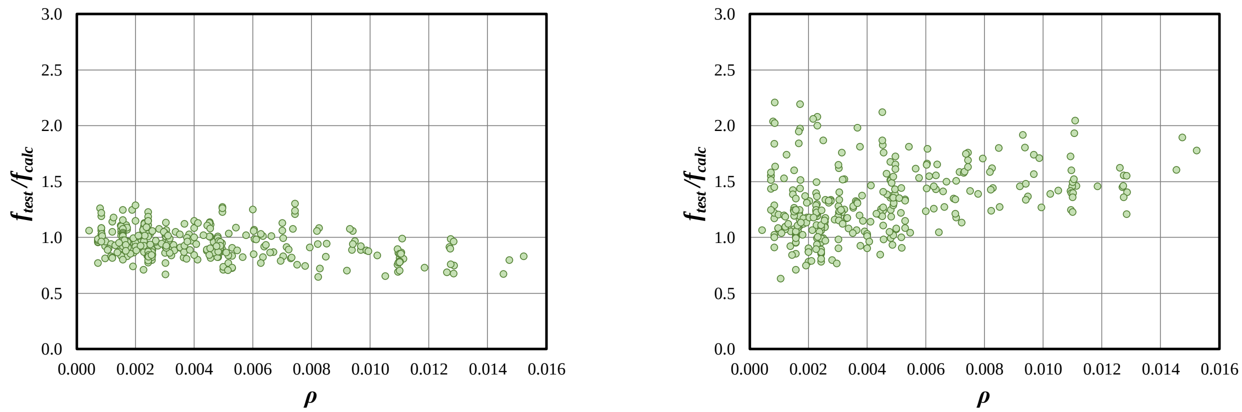

a) Equation 6-17 **b) ACI 318-14**

Figure 6.37: Equation Comparison for Transverse Reinforcement Ratio (Confined)

For all results from Figure 6.29 through Figure 6.37, scatter is reduced when Equation 6-17 is implemented compared to the design expression in ACI 318-14.

6.7 <u>Recommendations</u>

The following expression is proposed for the development and splicing of reinforcing steel:

$$f_b = (f_c')^{0.25}\left(\frac{l_s}{d_b}\right)^{0.5}\left(\frac{c_{so}}{d_b}\right)^{0.25} + \frac{N_s N_l A_t f_{yt}}{2 N_b A_b} \qquad (6\text{-}18)$$

where:

A_b = *area of one longitudinal reinforcing bar (in.^{2})*

A_t = *area of one stirrup leg (in.^{2})*

c_{so} = *side clear cover of spliced bars (in.)*

d_b = *longitudinal bar diameter (in.)*

f_b = *total bond strength (ksi)*

f_c' = *concrete compressive strength (psi)*

f_{yt} = *yield strength of transverse reinforcement = 60 ksi*

l_s = *splice or development length (in.)*

N_b = *number of longitudinal reinforcing bars*

N_l = *number of legs of transverse reinforcement crossing the splice plane*

N_s = *number of stirrups in the splice region*

The value recommended for f_{yt} is 60 ksi after findings from this study indicate that transverse reinforcement with a yield strength of 100 ksi has no additional effect on bond strength when compared to transverse reinforcement having a yield strength of 60 ksi.

For design purposes, Equation 6-18 can be rearranged and solved for the splice length in terms of bar diameter in order to achieve the design stress f_y.

$$\left(\frac{l_s}{d_b}\right)^{0.5} = \frac{(f_y - f_{bs})}{(f_c')^{0.25}}\left(\frac{d_b}{c_{so}}\right)^{0.25} \tag{6-19}$$

where:

$$f_{bs} = \left(\frac{f_{yt}}{2}\right)\left(\frac{N_s N_l A_t}{N_b A_b}\right)N_s$$

Solving for l_s/d_b results in Equation 6-20:

$$\frac{l_s}{d_b} = \frac{(f_y - f_{bs})^2}{\sqrt{f_c'}}\sqrt{\frac{d_b}{c_{so}}} \tag{6-20}$$

Note that the cover modifier can be conservatively taken as one for typical beams (Equation 6-21). For slabs which provide large bar spacings, use of the cover modifier has a significant effect and should be considered. For slabs, c_{so} should be calculated as half the inner bar spacing, c_{si}.

$$\frac{l_s}{d_b} = \frac{(f_y - f_{bs})^2}{\sqrt{f_c'}} \tag{6-21}$$

CHAPTER 7. CONCLUSIONS

7.1 Summary

For the implementation of high-strength reinforcement in practice, it is essential that the stresses required by use of these bars be properly developed. Therefore, the objective of this study was to evaluate the development of high-strength reinforcing steel and establish a design expression for the development and splicing of this steel. An experimental investigation was conducted testing 38 beams and slabs across seven testing series investigating the following:

1. Influence of splice length on bond strength
2. Influence of transverse reinforcement on bond strength
3. Effectiveness of high-strength (100 ksi) transverse reinforcement on bond strength
4. Bar development in slabs
5. Influence of high-strength concrete (10,000 psi) on bond strength
6. Effect of different stress-strain relationships of the high-strength steel (ASTM A615 vs. ASTM A1035) on bond strength
7. Influence of transverse reinforcement location on bond strength

Considering the results of the experimental study, an analytical investigation was also conducted using results of a large database of splice beam tests resulting in the development of a bond model for both unconfined and confined beams.

7.2 Experimental Findings

7.2.1 Slabs

Four reinforced concrete slabs with splice lengths ranging from $40d_b$ to $100d_b$ were tested in this program. For shorter splice lengths ($\leq 60d_b$), bond failures occurred by splitting of the side and top cover around the splice. As splice length increased, the failure mode transitioned to flexure at the supports evidenced by crushing of the concrete in the compression zone. For these specimens with No. 5 bars spaced at 6 in., it was possible to develop the full strength of the ASTM A615 Grade 100 reinforcement with a splice length of at least $80d_b$.

7.2.2 Unconfined Beams

A total of 16 unconfined reinforced concrete beams were tested to explore the influence of splice length, concrete compressive strength, and bar type on the bond strength of members spliced with high-strength reinforcement. Based on testing, the following findings are provided:

1. As the splice length increases, the unit length effectiveness decreases. The relationship between bar stress and splice length can be fit to a nonlinear power equation ($l_s^{0.5}$).

2. Only bond failures were observed for unconfined specimens, even when the splice length was increased from 40d_b up to 120d_b. It was not possible to provide enough embedment length to initiate a flexure failure.

3. Failure of the unconfined beams was brittle and explosive, regardless of splice length, and was typically preceded by extensive amounts of longitudinal cracking at the ends of the splice.

4. The use of high-strength concrete allowed for an increase in bond strength of approximately 18% to 20% for unconfined 40d_b beams when compared to similar specimens cast with normal-strength concrete. Unconfined 60d_b beams experienced increases in bond strength of 6% and 17% when high-strength concrete was implemented. The quarter root provides a more accurate representation of the effect of concrete compressive strength on bond strength for normal-strength and high-strength concrete when compared to the square root.

5. Beams containing ASTM A1035 spliced bars behaved similarly to beams spliced with ASTM A615 Grade 100 bars. For all tests conducted in this testing program, failure occurred within the linear-elastic region of the steel response.

7.2.3 Confined Beams

A total of 18 confined reinforced concrete beams were tested to explore the influence of splice length, transverse reinforcement grade and location, and concrete compressive strength on the bond strength of members spliced with high-strength reinforcement. Based on testing, the following findings are provided:

1. For confined beams, primary flexural cracks formed directly above the transverse reinforcement at all stirrup locations with the exception of stirrups placed close to the end of the splice. In this case, the primary flexural crack formed at the end of the splice.

2. The presence of transverse reinforcement did not prevent propagation of longitudinal cracks but did contain the growth of these cracks.

3. Failure of confined beams was generally less explosive than splitting failures in unconfined beams.

4. When stirrups were placed at the end of a given splice, the potential for the longitudinal bars to slip out from this confinement under increased loading was high. It appears that the bars slipped out after failure, but due to the brittle nature of the failure, this could not be confirmed.

5. Stirrup location has a significant impact on bond strength. Transverse reinforcement near the middle of the splice provides a negligible increase in bond strength; however, bond strength significantly increased when stirrups were placed near the ends of the splice.

6. In general, an increase in bond strength was observed for confined beams as the transverse reinforcement ratio ρ_t increased. A larger increase in bar stress was observed for small values of ρ_t when compared to an unconfined specimen.

7. Grade 100 transverse reinforcement does not provide an additional increase to the bond strength of a specimen beyond that provided by Grade 60 transverse reinforcement.

8. Confinement is required within the splice length to eliminate bond splitting failure so that the full strength of the splice can be achieved. The addition of confinement steel within the splice can transition the failure mode from bond to flexure. Table 7.1 provides the pressures required for each splice length to achieve the full strength of the longitudinal bars. The full bar strength of the $40d_b$ specimens could not be achieved with the maximum confinement pressure tested of 200 psi.

Table 7.1: Confinement Pressures Required to Transition to Flexure Failure

Splice Length (d_b)	Required Pressure (psi)
40	-[1]
50	200
60	100
80	50

[1] *Flexure failure not achieved with pressures up to 200 psi*

7.3 <u>Bond Modeling</u>

The total bar stress achieved in a specimen was considered as the sum of the individual contributions from the concrete and the transverse steel (Equation 7-1). This theory has been supported by several previous findings and proposed models (ACI 408 2003, Canbay and Frosch

2005, Sim 2014). Various bond models were explored using existing data to develop the components of this general design expression.

$$f_b = f_{bc} + f_{bs} \tag{7-1}$$

where:

f_b = *total bond strength (ksi)*

f_{bc} = *contribution to bond strength provided by concrete (ksi)*

f_{bs} = *contribution to bond strength provided by transverse steel (ksi)*

7.3.1 Unconfined

A comparison of bar stress equation recommendations from previous studies indicates three parameters in common that have a significant influence on bond strength. Concrete compressive strength, splice length, and cover were investigated using a database of bottom-cast specimens without transverse reinforcement to determine this influence. The ratio of side cover to bar diameter was selected for a cover modifier due to its minimum coefficient of variation and high coefficient of correlation across multiple powers. By performing a nonlinear regression analysis, Equation 7-2 was found to be the best fit for the concrete contribution to bar stress:

$$f_{bc} = 0.9(f_c')^{0.28}\left(\frac{l_s}{d_b}\right)^{0.48}\left(\frac{c_{so}}{d_b}\right)^{0.29} \tag{7-2}$$

where:

c_{so} = *side clear cover of spliced bars (in.)*

d_b = *longitudinal bar diameter (in.)*

f_c' = *concrete compressive strength (psi)*

l_s = *splice or development length (in.)*

This equation was simplified for design by rounding the power constants and adjusting the coefficients, resulting in Equation 7-3.

$$f_{bc} = (f_c')^{0.25}\left(\frac{l_s}{d_b}\right)^{0.5}\left(\frac{c_{so}}{d_b}\right)^{0.25} \tag{7-3}$$

This equation which was independently developed supports the findings by Sim (2014) for an expression that determines the expected bar stress for an unconfined reinforced concrete specimen. In fact, the same equation is provided.

7.3.2 Confined

By analyzing the difference in bar stress between pairs of unconfined and confined beams with identical details, the contribution to steel bar stress was isolated. Through this analysis, a physical model for evaluating the effectiveness of stirrups within the splice region based on stirrup location was developed, as shown in Figure 7.1.

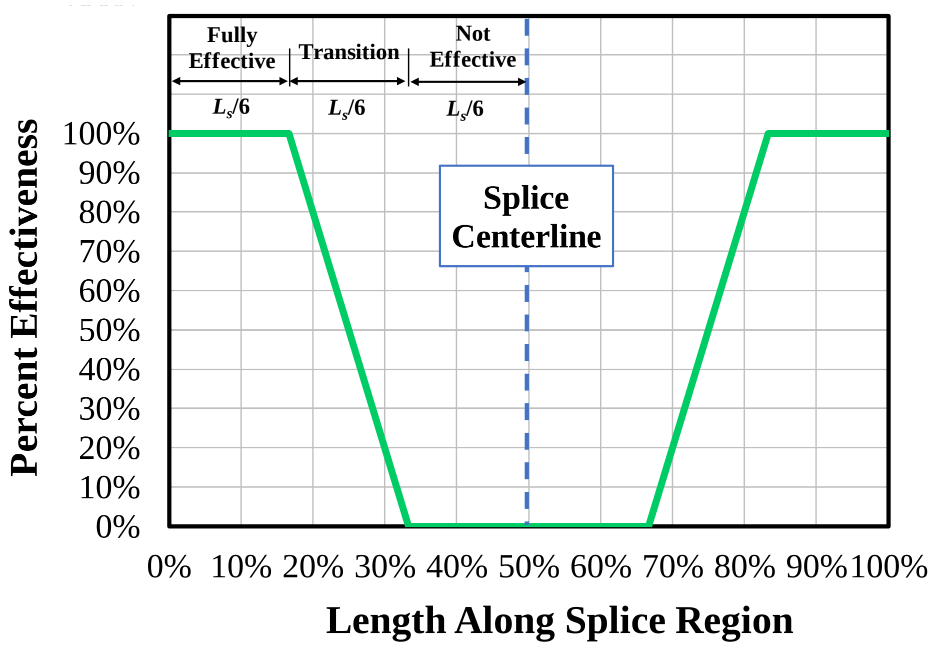

Figure 7.1: Proposed Effective Confinement Model

The percent contribution of transverse reinforcement was calculated for a selection of beam specimens tested by Sim (2014) and this study. The exact location of these stirrups was known and percent contributions were compared to the selected model for comparison. The proposed model represents the test results well.

A parametric study indicates that the proposed model converges on an average of 50% of the stirrups across the splice being effective once four or more stirrups are provided using a consistent spacing. The increase in bar force developed in the spliced bars (F_{long}) was found to be equivalent to the vertical force provided by the effective transverse reinforcement (F_{trans}). This relationship is displayed in Figure 7.2.

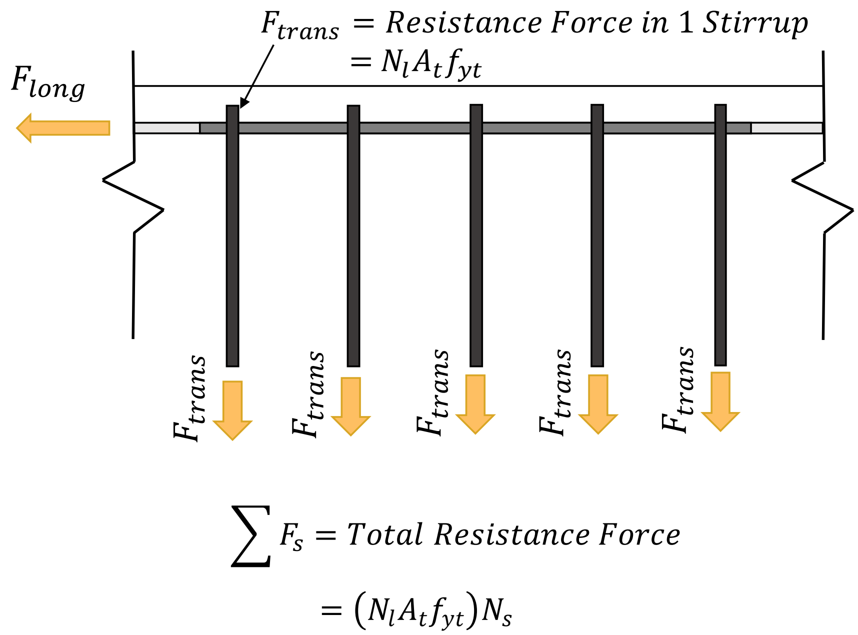

Figure 7.2: Total Effective Force from Transverse Reinforcement

By equating the longitudinal force with the transverse force, an expression for the transverse steel contribution can be derived in Equation 7-4:

$$F_{long} = F_{trans}$$

$$(A_b f_{bs}) N_b = (N_l A_t f_{yt})(k N_s) \tag{7-4}$$

By substituting a value of 0.5 for the percent contribution term k, the number of effective stirrups is included in the equation. Therefore, the stress contribution from the transverse steel to bar stress developed can be expressed according to Equation 7-5.

$$f_{bs} = \frac{(N_l A_t f_{yt})}{N_b A_b} \left(\frac{N_s}{2} \right) \tag{7-5}$$

where:

A_b = *area of one longitudinal reinforcing bar (in.^{2})*

A_t = *area of one stirrup leg (in.^{2})*

f_{yt} = *yield strength of transverse reinforcement (ksi)*

N_b = *number of longitudinal reinforcing bars*

N_l = *number of legs of transverse reinforcement crossing the splice plane*

N_s = *number of stirrups in the splice region*

While the percent contribution factor (50%) was determined using the model illustrated in Figure 7.1, Equation 7-5 supports findings by Sim (2014) for an expression that determines the additional bar stress provided by transverse reinforcement for confined reinforced concrete specimens. Again, this evaluation independently results in the same expression. Additionally, the transverse steel yield strength, f_{yt}, is fixed at 60 ksi for this expression based on findings from this study indicating that transverse reinforcement with a yield strength of 100 ksi has no additional effect on bond strength when compared to transverse reinforcement having a yield strength of 60 ksi; therefore, a simplified expression takes the following form where f_{bs} is in ksi:

$$f_{bs} = \frac{30N_s(N_l A_t)}{N_b A_b} \tag{7-6}$$

where:

A_b = *area of one longitudinal reinforcing bar (in.^{2})*

A_t = *area of one stirrup leg (in.^{2})*

N_b = *number of longitudinal reinforcing bars*

N_l = *number of legs of transverse reinforcement crossing the splice plane*

N_s = *number of stirrups in the splice region*

7.3.3 Design Recommendations

Based on the results from comparing various models to describe the contributions of concrete and steel to the overall bar stress, the following analytical expression was developed for reinforced concrete members:

$$f_b = f_{bc} + f_{bs}$$

$$f_b = (f_c')^{0.25}\left(\frac{l_s}{d_b}\right)^{0.5}\left(\frac{c_{so}}{d_b}\right)^{0.25} + \frac{30N_s(N_l A_t)}{N_b A_b} \tag{7-7}$$

where:

A_b = *area of one longitudinal reinforcing bar (in.^{2})*

A_t = *area of one stirrup leg (in.²)*

c_{so} = *bar cover modifier term*

for beams = side clear cover (in.)

for slabs = 1/2 clear bar spacing (in.)

d_b = *longitudinal bar diameter (in.)*

f_b = *total bond strength (ksi)*

f_c' = *concrete compressive strength (psi)*

l_s = *splice length (in.)*

N_b = *number of longitudinal reinforcing bars*

N_l = *number of legs of transverse reinforcement crossing the splice plane*

N_s = *number of stirrups in the splice region*

For design, Equation 7-7 can be rearranged to solve for the required development length in terms of bar diameter given a required stress, f_b. In design, the yield strength, f_y replaces f_b.

$$\frac{l_s}{d_b} = \frac{\left(f_y - f_{bs}\right)^2}{\sqrt{f_c'}}\sqrt{\frac{d_b}{c_{so}}} \tag{7-8}$$

If desired, the cover factor $\sqrt{d_b/c_{so}}$ can be conservatively taken to 1.0 for beams and slabs. This provides some conservatism for beams but may be too conservative for slabs depending on bar size and spacing. It is strongly recommended in beams that transverse reinforcement always be provided. Test results indicate that regardless of splice length, splitting failures occur when confinement is absent. Because of the importance of transverse reinforcement location on bond strength, a minimum of four stirrups should be provided across the splice at equal bar spacings. It is also recommended that the end stirrup be placed at a minimum of 2 in. from the end of the splice to avoid the potential for longitudinal bar slip.

7.4 Further Research

To better understand the behavior and development of high-strength steel in spliced reinforced concrete members, it is suggested that further research be conducted on the development of high-strength reinforcing steel with an emphasis on the following topics:

1. Stirrup Concentration: Conduct testing on splice beams that have transverse reinforcement concentrations within $l_s/6$ from the splice ends (varying the length of the fully effective region).

2. $40d_b$ Flexure Failure Transition Point: Conduct beam testing on $40d_b$ specimens containing confinement pressures greater than 200 psi to determine the point at which the initiation of flexure failure precludes a splitting failure.

3. Continuous Nonlinear Confinement Model: Develop an alternate confinement model that more closely reflects the distribution of bond stresses across the splice to determine the effectiveness of stirrup location.

4. Nonlinear Response of ASTM A1035 Steel: Conduct beam testing using ASTM A1035 longitudinal steel to produce bond failures in the nonlinear region of the stress-strain curve.

REFERENCES

Abrams, D. A. (1913), "Tests of Bond between Concrete and Steel," *University of Illinois Bulletin*, No. 71, The University of Illinois, Urbana-Champaign, IL., 238 pp.

ACI Committee 234 (2000), *Guide for the Use of Silica Fume in Concrete*, ACI 234R-96, American Concrete Institute, Farmington Hills, MI., 51 pp.

ACI Committee 318 (2014), *Building Code Requirements for Structural Concrete and Commentary*, ACI 318-14, American Concrete Institute, Farmington Hills, MI., 519 pp.

ACI Committee 318, Subcommittee B (2018), "Development Length for Deformed Bars and Deformed Wires in Tension (CB 603)," *Ballot LB18-03*, American Concrete Institute, Farmington Hills, MI.

ACI Committee 408 (2003), "Suggested Development, Splice, and Standard Hook Provisions for Deformed Bars in Tension," (ACI 408.1R-03), American Concrete Institute, Farmington Hills, MI., 49 pp.

Ansley, M. H. (2002), "Investigation into the Structural Performance of MMFX Reinforcing," Florida Department of Transportation.

ASTM A1035 (2016), "Standard Specification for Deformed and Plain, Low-Carbon, Chromium, Steel Bars for Concrete Reinforcement," American Society of Testing and Materials International, West Conshohocken, PA., 8 pp.

ASTM A370 (2018), "Standard Test Methods and Definitions for Mechanical Testing of Steel Products," American Society of Testing and Materials International, West Conshohocken, PA., 50 pp.

ASTM A615 (2016), "Standard Specification for Deformed and Plain Carbon-Steel Bars for Concrete Reinforcement," American Society for Testing and Materials, West Conshohocken, PA., 8 pp.

ASTM C1231 (2015), "Standard Practice for Use of Unbonded Caps in Determination of Compressive Strength of Hardened Cylindrical Concrete Specimens," American Society of Testing and Materials International, West Conshohocken, PA., 5 pp.

ASTM C1240 (2015), "Standard Specification for Silica Fume Used in Cementitious Mixtures," American Society of Testing and Materials International, West Conshohocken, PA., 7 pp.

ASTM C143 (2015), "Standard Test Method for Slump of Hydraulic-Cement Concrete," American Society of Testing and Materials International, West Conshohocken, PA., 4 pp.

ASTM C150 (2018), "Standard Specification for Portland Cement," American Society of Testing and Materials International, West Conshohocken, PA., 9 pp.

ASTM C192 (2016), "Standard Practice for Making and Curing Concrete Test Specimens in the Laboratory," American Society for Testing and Materials, West Conshohocken, PA., 8 pp.

ASTM C31 (2018), "Standard Practice for Making and Curing Concrete Test Specimens in the Field," American Society of Testing and Materials International, West Conshohocken, PA., 6 pp.

ASTM C39 (2017), "Standard Test Method for Compressive Strength of Cylindrical Concrete Specimens," American Society for Testing and Materials, West Conshohocken, PA., 8 pp.

ASTM C469 (2014), "Standard Test Method for Static Modulus of Elasticity and Poisson's Ratio of Concrete in Compression," American Society of Testing and Materials International, West Conshohocken, PA., 5 pp.

ASTM C470 (2015), "Standard Specification for Molds for Forming Concrete Test Cylinders Vertically," American Society of Testing and Materials International, West Conshohocken, PA., 5 pp.

ASTM C496 (2017), "Standard Test Method for Splitting Tensile Strength of Cylindrical Concrete Specimens," American Society of Testing and Materials International, West Conshohocken, PA., 5 pp.

ASTM C989 (2018), "Standard Specification for Slag Cement for Use in Concrete and Mortars," American Society of Testing and Materials International, West Conshohocken, PA., 7 pp.

ASTM E8 (2016), "Standard Test Methods for Tension Testing of Metallic Materials," American Society of Testing and Materials International, West Conshohocken, PA., 30 pp.

ATC-115 (2014), "Roadmap for the Use of High-Strength Reinforcement in Reinforced Concrete Design," Applied Technology Council, Redwood City, CA., 197 pp.

Azizinamini, A., Pavel, R., Hatfield, E., and Ghosh, S. K. (1999), "Behavior of Spliced Reinforcing Bars Embedded in High-Strength Concrete," *ACI Structural Journal*, Vol. 96, No. 5, pp. 826-835.

Azizinamini, A., Stark, M., Roller, J. J., and Ghosh, S. K. (1993), "Bond Performance of Reinforcing Bars Embedded in High-Strength Concrete," *ACI Structural Journal*, Vol. 90, No. 5, pp. 554-561.

Briggs, M. G. (2008), "Bond Strength of ASTM A1035 Grade 100 Reinforcing Steel," *M.S. Thesis*, School of Civil Engineering, University of Kansas, Lawrence, KS.

Canbay, E., and Frosch, R. J. (2005), "Bond Strength of Lap-Spliced Bars," *ACI Structural Journal*, Vol. 102, No. 4, July-Aug., pp. 605-614.

Chamberlin, S. J. (1956), "Spacing of Reinforcement in Beams," ACI Journal, *Proceedings*, Vol. 53, No. 1, pp. 113-134.

Chamberlin, S. J. (1958), "Spacing of Spliced Bars in Beams," ACI Journal, *Proceedings*, Vol. 54, No. 8, Feb., pp. 689-697.

Chinn, J., Ferguson, P. M., and Thompson, J. N. (1955), "Lapped Splices in Reinforced Concrete Beams," ACI Journal, *Proceedings*, Vol. 52, No. 10, Oct., pp. 201-213

Clemeña, G. G., and Virmani, Y. P. (2004), "Comparing the Chloride Resistance of Reinforcing Bars," *Concrete International*, Vol. 25, No. 11, pp. 39-49.

Darwin, D., Browning, J. P., Nguyen, T. V., Locke, C. E. (2002), "Mechanical and Corrosion Properties of a High-Strength, High Chromium Reinforcing Steel for Concrete," *SM Report* No. 66, University of Kansas Center for Research, Lawrence, KS., Mar., 169 pp.

Darwin, D., McCabe, S. L., Idun, E, K., and Schoenekase, S. P. (1992), "Development Length Criteria: Bars Not Confined by Transverse Reinforcement," *ACI Structural Journal*, Vol. 89, No. 6, Nov.-Dec., pp. 709-720.

Darwin, D., and Zuo, J. (2002), "Discussion of Proposed Changed to ACI 318 in ACI 318-02 Discussion and Closure," *Concrete International*, Vol. 24, No. 1, Jan., pp. 91-101.

Darwin, D., Zuo, J., Tholen, M. L., and Idun, E. K. (1996), "Development Length Criteria for Conventional and High Relative Rib Area Reinforcing Bars," *ACI Structural Journal*, Vol. 93, No. 3, May-June, pp. 347-359.

El-Hacha, R., El-Agroudy, H., and Rizkalla, S. H. (2006), "Bond Characteristics of High-Strength Steel Reinforcement." *ACI Structural Journal*, Vol. 103, No. 6, pp. 771-782.

Eligehausen, R., Popov, E. P., and Bertero, V. V. (1983), "Local Bond Stress-Slip Relationships of Deformed Bars Under Generalized Excitations," *Report* No. UCB/EERC-82/23, Earthquake Engineering Research Center, University of California at Berkeley, CA., 169 pp.

Esfahani, M. R., and Rangan, B. V. (1998), "Bond between Normal Strength and High-Strength Concrete (HSC) and Reinforcing Bars in Splices in Beams." *ACI Structural Journal*, Vol. 102, No. 1, pp. 22-30.

Ferguson, P. M., and Breen, J. E. (1965), “Lapped Splices for High-Strength Reinforcing Bars,” ACI Journal, *Proceedings*, Vol. 62, No. 9, Sept., pp. 1063-1078.

Ferguson, P. M., and Krishnaswamy, C. N. (1971), “Tensile Lap Splices Part 2: Design Recommendations for Retaining Wall Splices and Large Bar Splices,” *Rep. No. 113-3*. TX: The Texas Highway Department.

Ferguson, P. M., and Thompson, J. N. (1965), “Development Length for Large High Strength Reinforcing Bars,” ACI Journal, *Proceedings*, Vol. 62, No. 1, Jan., pp. 71-94.

Fleet, E. T. (2019), “Effective Confinement and Bond Strength of Grade 100 Reinforcement,” Master’s Thesis, Lyles School of Civil Engineering, Purdue University, West Lafayette, IN., 319 pp.

Glucksman, R. (2018), “Bond Strength of ASTM A615 Grade 100 Reinforcement for Beams,” Master’s Thesis, Lyles School of Civil Engineering, Purdue University, West Lafayette, IN., 226 pp.

Goto, Y. (1971), “Cracks Formed in Concrete Around Deformed Tension Bars,” ACI Journal, Vol. 68, No. 26, April, pp. 244-251.

Hadje-Ghaffari, H., Choi, O. C., Darwin, D., and McCabe, S. L. (1994), “Bond of Epoxy-Coated Reinforcement: Cover, Casting Position, Slump, and Consolidation.” *ACI Structural Journal,* Vol. 91, No. 1, pp. 59-68.

Hognestad, E. (1951), “A Study of Combined Bending and Axial Load in Reinforced Concrete Members,” *University of Illinois Bulletin Series,* No. 399, The University of Illinois, Urbana-Champaign, IL., 128 pp.

Hognestad, E. (1962), “High-Strength Bars as Concrete Reinforcement - Part 2: Flexural Cracking,” *Journal, PCA Research and Development Laboratories*, Vol. 4, No. 1, pp. 46-63.

Hosny, A., Seliem, H. M., Rizkalla, S. H., and Zia, P. (2012), “Development Length of Unconfined Conventional and High-Strength Steel Reinforcing Bars,” *ACI Structural Journal,* Vol. 109, No. 5, Sept.-Oct., pp. 655-664.

Hwang, H., Park, H., and Yi, W. (2017). “Nonuniform Bond Stress Distribution Model for Evaluation of Bar Development Length.” *ACI Structural Journal,* Vol. 114, No. 4, pp. 839-849.

Jirsa, J. O., and Breen, J. E. (1981), “Influence of Casting Position and Shear on Development and Splice Length - Design Recommendation,” *Research Report* No. 242-3F, Center for Transportation Research, The University of Texas at Austin, Austin, TX., 51 pp.

Johnston, D. W., and Zia, P. (1982), "Bond Characteristics of Epoxy-Coated Reinforcing Bars," *Report* No. FHWA/NC/82-002, Department of Civil Engineering, North Carolina State University, Raleigh, NC., Aug., 176 pp.

Kluge, R. W., and Tuma, E. C. (1945), "Lapped Bar Splices in Concrete Beams," ACI Journal, *Proceedings*, Vol. 42, Sept., pp. 13-33.

Kosmatka, S. H., Kerkhoff B., and Panarese, W. C. (2017), "Design and Control of Concrete Mixtures," 14th Ed., EB001, Portland Cement Association, Skokie, IL., 358 pp.

Lutz, L. A., and Gergely, P. (1967), "Mechanics of Bond and Slip of Deformed Bars in Concrete," ACI Journal, *Proceedings*, Vol. 64, No. 11, Nov., pp. 711-721.

Maeda, M., Otani, S., and Aoyama H., "Bond Splitting Strength in Reinforced Concrete Members," *Transactions*, Japan Concrete Institute, Vol. 13 (1991), pp. 581-588.

Mathey, R., and Watstein, D. (1961), "Investigation of Bond in Beam and Pull-Out Specimens with High-Yield-Strength Deformed Bars," ACI Journal, *Proceedings*, Vol. 57, No. 3, Mar., pp. 1071-1090.

McCormac, J. C., and Brown, R. H. (2016), "Design of Reinforced Concrete," 10th Ed., *Wiley*, Hoboken, NJ., 672 pp.

Miller, Mark A. (2012), "Section 900 - Materials Details," *Standard Specifications*, Indiana Department of Transportation, Indianapolis, IN., pp. 784-1039.

Morita, S., and Fujii, S. (1982), "Bond Capacity of Deformed Bars Due to Splitting of Surrounding Concrete," *Proceedings of the International Conference on Bond in Concrete*, Scotland, June 14-16., Applied Science Publishers, London, U.K., pp. 331-341.

NIST (2014), "Use of High-Strength Reinforcement in Earthquake-Resistant Concrete Structures," *Research Report NIST GCR 14-917-30*, NEHRP Consultants, Red City, CA.

Orangun, C. O., Jirsa, J. O., and Breen, J. E. (1975), "The Strength of Anchored Bars: A Reevaluation of Test Data on Development Length and Splices," *Research Report No. 154-3F*, Center for Highway Research, The University of Texas, Austin, TX, Jan.

Orangun, C. O., Jirsa, J. O., and Breen, J. E. (1977), "Reevaluation of Test Data on Development Length and Splices," *ACI Journal*, Proceedings, Vol. 74, No. 3, pp. 114-122.

Pay, A. C. (2005), "Bond Behavior of Unconfined Steel and Fiber Reinforced Polymer (FRP) Bar Splices in Concrete Beams," *Ph.D. Dissertation*, Lyles School of Civil Engineering, Purdue University, West Lafayette, IN., 313 pp.

Pay, A. C., Canbay, E., and Frosch, R. J. (2014), "Bond Strength of Spliced Fiber-Reinforced Polymer Reinforcement." *ACI Structural Journal*, Vol. 111, No. 2, Mar.-April.

Rezansoff, T., Konkankar, U. S., and Fu, Y. C. (1992), "Confinement Limits for Tension Lap Splices under Static Loading," *Canadian Journal of Civil Engineering*, Vol. 19, No. 3, pp. 447-453.

Richter, B. P. (2012), "A New Perspective on the Tensile Strength of Lap Splices in Reinforced Concrete Members," Master's Thesis, Lyle's School of Civil Engineering, Purdue University, West Lafayette, IN., 165 pp.

Sakurada, T., Morohashi, N. and Tanaka, R. (1993), "Effect of Transverse Reinforcement on Bond Splitting Strength of Lap Splices." *Transactions*, Japan Concrete Institute, Vol. 15, pp. 572-580.

Seliem, H. M., Hosny, A., Rizkalla, S., Zia, P., Briggs, M., Miller, S., Darwin, D., Browning, J., Glass, G. M., Hoyt, K., Donnelly, K., and Jirsa, J. O. (2009), "Bond Characteristics of ASTM A1035 Steel Reinforcing Bars," *ACI Structural Journal*, V. 106, No. 4, July-Aug., pp. 530-539.

Sim, C. (2014), "Structural and Corrosion Performance of Concrete Bridge Decks Reinforced with Corrosion-Resistant Reinforcing Steel," *Ph.D. Dissertation*, School of Civil Engineering, Purdue University, West Lafayette, IN., 563 pp.

Tepfers, R. (1973), "A Theory of Bond Applied to Overlapping Tensile Reinforcement Splices for Deformed Bars," *Publication* 73:2, Division of Concrete Structures, Chalmers University of Technology, Goteborg, Sweden, 328 pp.

Tepfers, R. (2009), "Bond Characteristics of ASTM A1035 Steel Reinforcing Bars," *ACI Structural Journal*, V. 106, No. 4, July-Aug., pp. 530-539.

Thompson, M. A., Jirsa, J. O., Breen, J. E., and Meinheit, D. F. (1975), "The Behavior of Multiple Lap Splices in Wide Sections," *Research Report No. 154-1*, Center for Highway Research, The University of Texas, Austin, TX., Feb., 75 pp.

Treece, R. A., and Jirsa, J. O. (1989), "Bond Strength of Epoxy-Coated Reinforcing Bars," *ACI Materials Journal*, Vol. 86, No. 2, Mar.-Apr., pp. 167-174.

Trejo, D., Monteiro, P. J., Thomas, G., and Wang, X. (1994), "Mechanical Properties and Corrosion Susceptibility of Dual-Phase Steel in Concrete," *Cement and Concrete Research*, Vol. 24, No. 7, pp. 1245-1254.

Zekany, A. J., Neumann, S., Jirsa, J. O., and Breen, J. E. (1981), "The Influence of Shear on Lapped Splices in Reinforced Concrete," *Tech. No. FHWA/TX-81/20+242-2*. Austin, TX:

Texas State Department of Highways and Public Transportation; Transportation Planning Division.

Zsutty, T. C. (1968), "Beam Shear Strength Prediction by Analysis of Existing Data," ACI Journal, Proceedings, Vol. 65, No. 11, Nov., pp. 943-951.

Zuo, J., and Darwin, D. (1998), "Bond Strength of High Relative Rib Area Reinforcing Bars," *SM Report* No. 46, University of Kansas Center for Research, Lawrence, KS., 350 pp.

Zuo, J., and Darwin, D. (2000), "Splice Strength of Conventional and High Relative Rib Area Bars in Normal and High-Strength Concrete," *ACI Structural Journal,* Vol. 97, No. 4, July-Aug., pp. 630-641.

APPENDIX A: AS-BUILT DIMENSIONS (SERIES I-IV)

Dimensions were measured for all beams after failure at the locations shown in Figure A.1. The total beam width b_w accounts for three (3) splices of No. 8 bars, or 6 in. Bottom cover is measured along the middle splice for the south, middle, and north longitudinal locations.

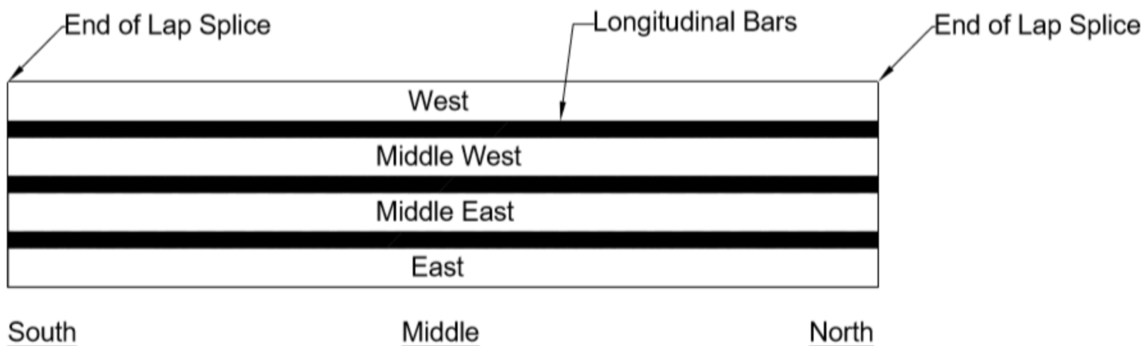

Figure A.1: Nomenclature for As-Built Dimensions

Table A.1: U-40-5

	South (in.)	Middle (in.)	North (in.)
West	1.7630	1.9000	2.0220
Middle West	2.0870	2.1870	2.2205
Middle East	1.7520	1.8870	2.0620
East	1.8940	1.9885	2.2115
Total	13.4960	13.9625	14.5160

Table A.2: **U-40-5a**

	South (in.)	Middle (in.)	North (in.)
West	2.3140	2.2860	2.1140
Middle West	1.7940	1.9930	2.0800
Middle East	1.9440	1.7420	1.6840
East	2.2120	2.1050	2.1640
Total	14.2640	14.1260	14.0420

Table A.3: U-60-5

	South (in.)	Middle (in.)	North (in.)
West	2.0800	1.9740	1.8180
Middle West	2.4200	2.2040	2.2910
Middle East	1.8890	1.8730	2.1530
East	1.7260	1.7830	1.8430
Total	14.1150	13.8340	14.1050

Table A.4: U-60-5a

	South (in.)	Middle (in.)	North (in.)
West	2.3960	2.1210	2.1230
Middle West	1.7990	1.7850	1.6020
Middle East	1.8410	1.8670	1.7850
East	1.8660	2.1600	2.4380
Total	13.9020	13.9330	13.9480

Table A.5: U-70-5

	South (in.)	Middle (in.)	North (in.)
West	2.3010	1.8580	1.7855
Middle West	1.8450	1.8875	1.8980
Middle East	1.8700	1.8365	1.9985
East	2.0280	2.1405	2.2685
Total	14.0440	13.7225	13.9505

Table A.6: U-80-5

	South (in.)	Middle (in.)	North (in.)
West	2.0020	1.7270	1.8020
Middle West	2.1400	2.1690	2.1280
Middle East	1.8720	1.8420	1.8890
East	1.8240	1.9070	1.9440
Total	13.8380	13.6450	13.7630

Table A.7: U-100-5

	South (in.)	Middle (in.)	North (in.)
West	1.9640	2.0080	2.0140
Middle West	1.7760	2.0900	1.9660
Middle East	1.8590	1.9390	1.8790
East	1.9370	1.7680	1.9910
Total	13.5360	13.8050	13.8500

Table A.8: U-120-5

	South (in.)	Middle (in.)	North (in.)
West	2.0290	1.8690	2.1280
Middle West	2.1110	1.8710	1.6480
Middle East	1.5600	1.7000	1.5880
East	1.8640	2.1870	2.5140
Total	13.5640	13.6270	13.8780

Table A.9: U-80-5-M

	South (in.)	Middle (in.)	North (in.)
West	2.3390	2.2620	2.2730
Middle West	0.7350	0.7170	0.6150
Middle East	0.9320	1.1030	1.1040
East	1.9065	1.9280	1.9530
Total	11.9125	12.0100	11.9450

Table A.10: U-100-5-M

	South (in.)	Middle (in.)	North (in.)
West	2.2210	2.1805	1.9430
Middle West	0.9735	0.9860	1.0700
Middle East	0.8925	0.8820	0.7400
East	1.5020	1.6445	1.9105
Total	11.5890	11.6930	11.6635

Table A.11: U-120-5-M

	South (in.)	Middle (in.)	North (in.)
West	2.0020	1.9830	2.2310
Middle West	0.8970	0.9590	0.7420
Middle East	0.7140	0.9240	0.8390
East	2.1130	2.1460	2.0780
Total	11.7260	12.0120	11.8900

Table A.12: C3/60/2-40-5-50

	South (in.)	Middle (in.)	North (in.)
West	2.7430	2.6350	2.7270
Middle West	1.5290	1.3410	1.2320
Middle East	1.2860	1.3270	1.4760
East	2.4100	2.5880	2.6420
Total	13.9680	13.8910	14.0770

Table A.13: C3/60/3-40-5-50

	South (in.)	Middle (in.)	North (in.)
West	2.6720	2.5980	2.5220
Middle West	1.7110	1.8470	1.8760
Middle East	1.1040	1.0800	1.1400
East	2.2960	2.4800	2.4880
Total	13.7830	14.0050	14.0260

Table A.14: C3/100/3-40-5-50

	South (in.)	Middle (in.)	North (in.)
West	2.0985	2.1240	2.1505
Middle West	1.8445	1.6340	1.6215
Middle East	1.3540	1.4360	1.4825
East	2.4065	2.6055	2.5585
Total	13.7035	13.7995	13.8130

Table A.15: C3/60-40-5-100

	South (in.)	Middle (in.)	North (in.)
West	2.3285	2.2900	2.0955
Middle West	1.5185	1.5510	1.2825
Middle East	1.6755	1.7025	1.8225
East	2.2985	2.4935	2.5620
Total	13.8210	14.0370	13.7625

Table A.16: C3/100-40-5-100

	South (in.)	Middle (in.)	North (in.)
West	2.4020	2.1890	1.9970
Middle West	1.4700	1.5490	1.5110
Middle East	1.8440	1.7990	1.8420
East	2.2680	2.3630	2.5770
Total	13.9840	13.9000	13.9270

Table A.17: C3/60-60-5-50

	South (in.)	Middle (in.)	North (in.)
West	1.9805	2.1025	2.1365
Middle West	2.0155	1.9635	1.9810
Middle East	1.7935	1.8090	1.7955
East	2.1390	2.1345	2.1295
Total	13.9285	14.0095	14.0425

Table A.18: C3/60-60-5-100

	South (in.)	Middle (in.)	North (in.)
West	2.0050	2.1370	2.1865
Middle West	1.9170	2.0180	2.1670
Middle East	1.6885	1.5430	1.4960
East	2.0805	2.1770	2.0235
Total	13.6910	13.8750	13.8730

Table A.19: C3/60-60-5-150

	South (in.)	Middle (in.)	North (in.)
West	2.3095	2.1850	2.0905
Middle West	1.8305	1.8160	1.8280
Middle East	1.8345	1.8225	1.8165
East	2.0965	2.0165	2.0985
Total	14.0710	13.8400	13.8335

Table A.20: C4/60-60-5-100

	South (in.)	Middle (in.)	North (in.)
West	2.3605	1.9935	2.1650
Middle West	1.5035	1.6470	1.6025
Middle East	1.5880	1.5890	1.5940
East	2.4230	2.3490	2.3905
Total	13.8750	13.5785	13.7520

Table A.21: C3/100-60-5-100

	South (in.)	Middle (in.)	North (in.)
West	2.3805	2.3070	2.0835
Middle West	1.6000	1.8490	2.0770
Middle East	1.3860	1.3510	1.2225
East	2.4475	2.3770	2.4140
Total	13.8140	13.8840	13.7970

Table A.22: C3/60-80-5-50

	South (in.)	Middle (in.)	North (in.)
West	1.7800	2.0265	2.1805
Middle West	1.7365	1.6475	1.7965
Middle East	1.3550	1.3130	1.3610
East	2.8740	2.8305	2.6305
Total	13.7455	13.8175	13.9685

APPENDIX B: STEEL STRESS-STRAIN CURVES

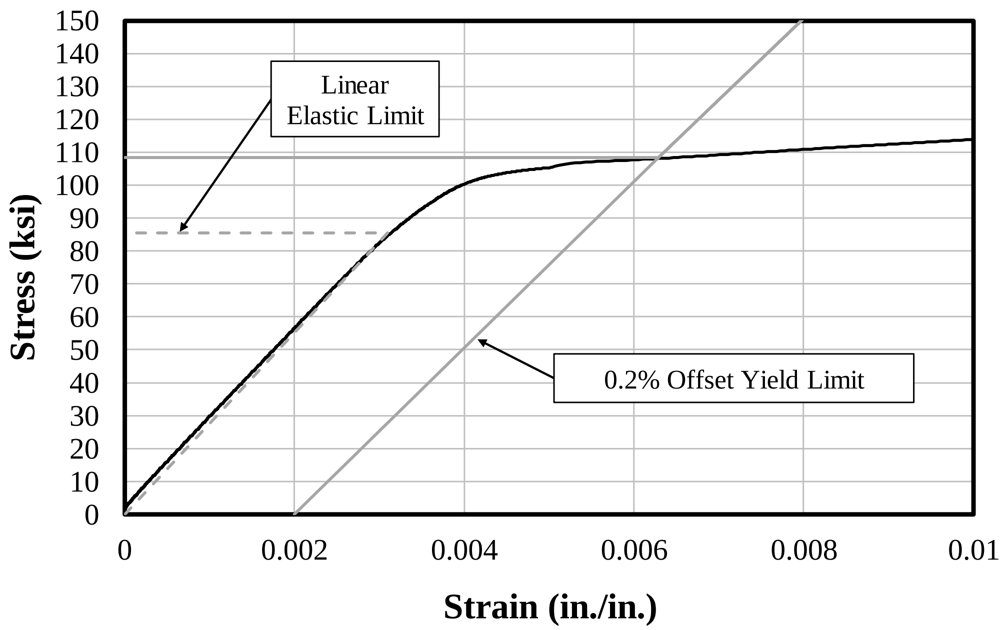

a) Initial Behavior Limits

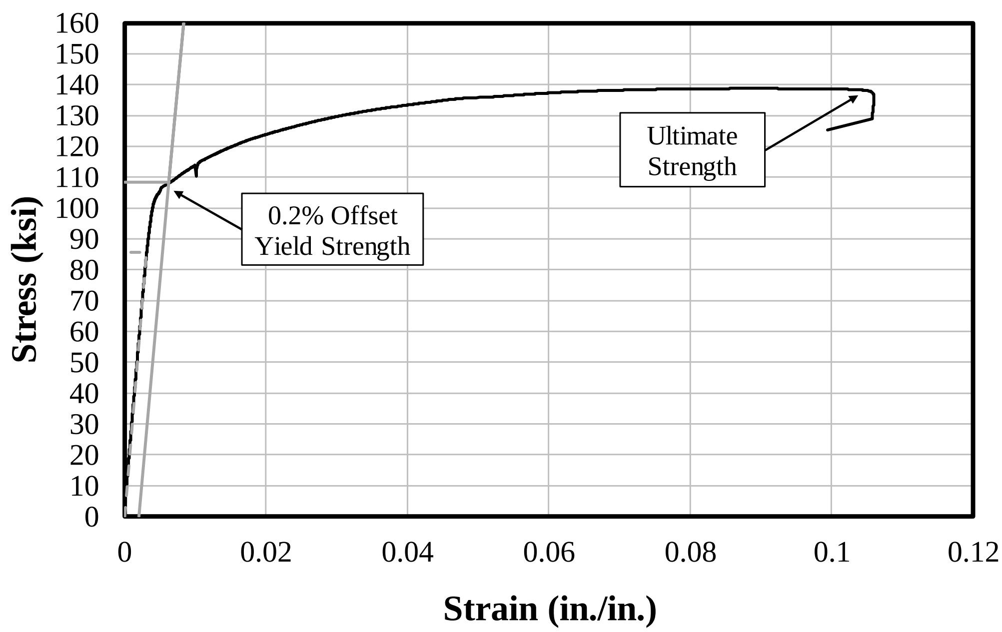

b) Full Behavior

Figure B.1: A615 Gr. 100 No. 8 Longitudinal Bar - Stress Strain Curve

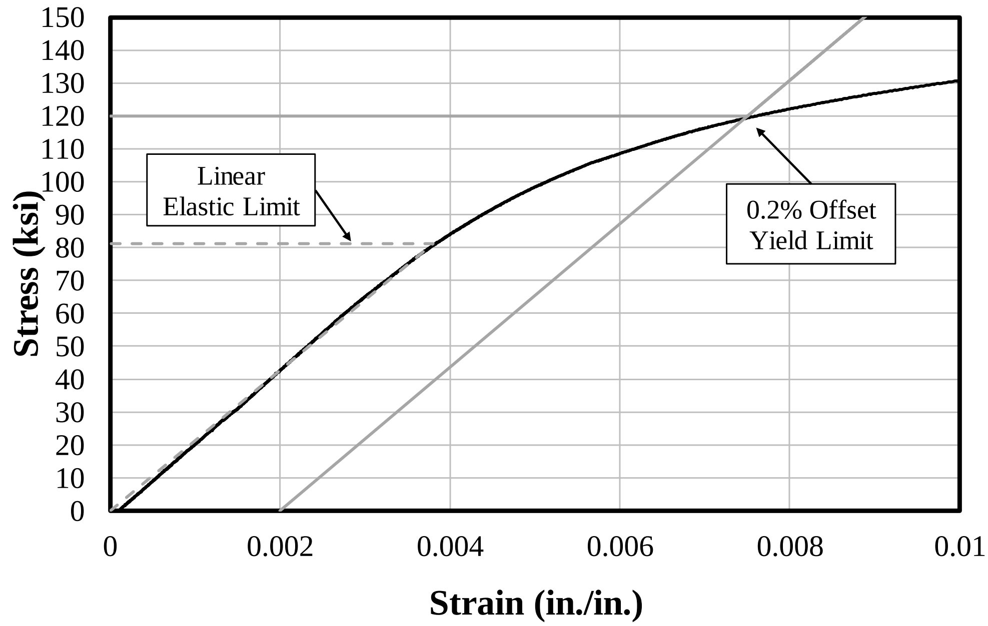

a) Initial Behavior Limits

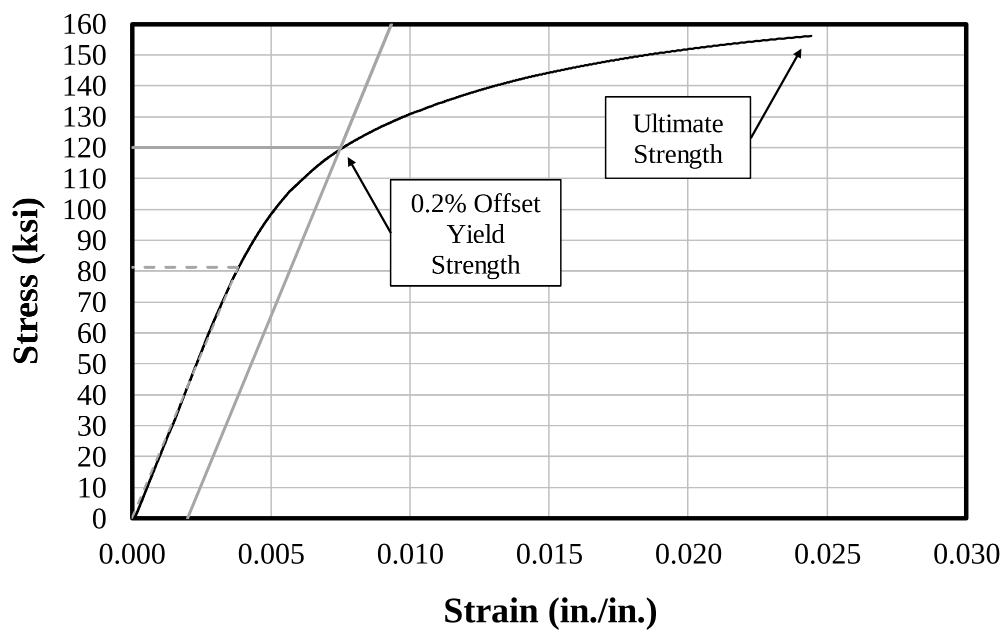

b) Full Behavior

Figure B.2: A1035 Gr. 100 No. 8 Longitudinal Bar (MMFX) Stress Strain Curve

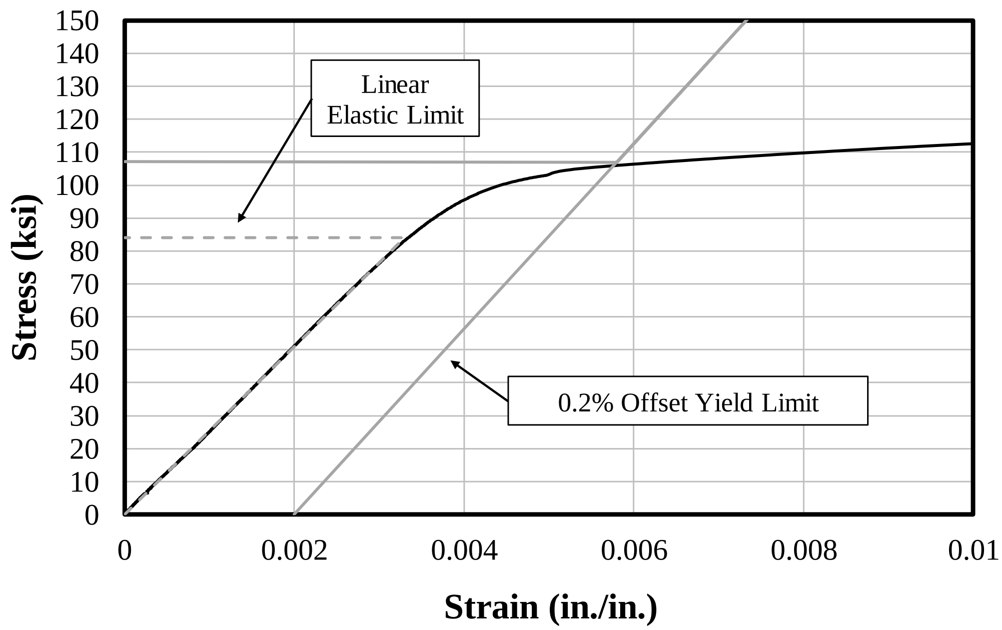

a) Initial Behavior Limits

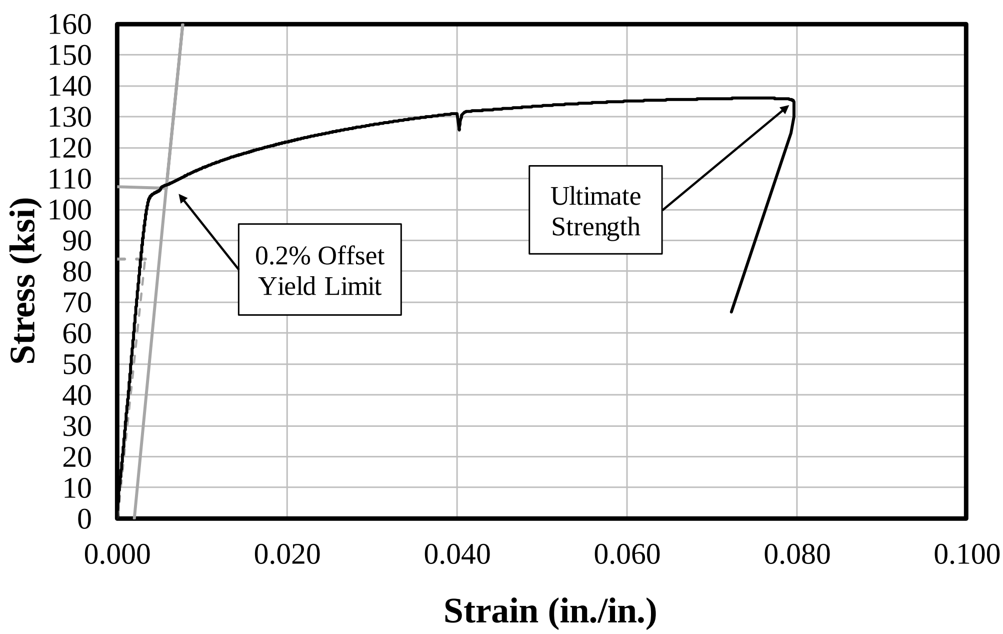

b) Full Behavior

Figure B.3: A615 Gr. 100 No. 5 Longitudinal Bar - Stress Strain Curve

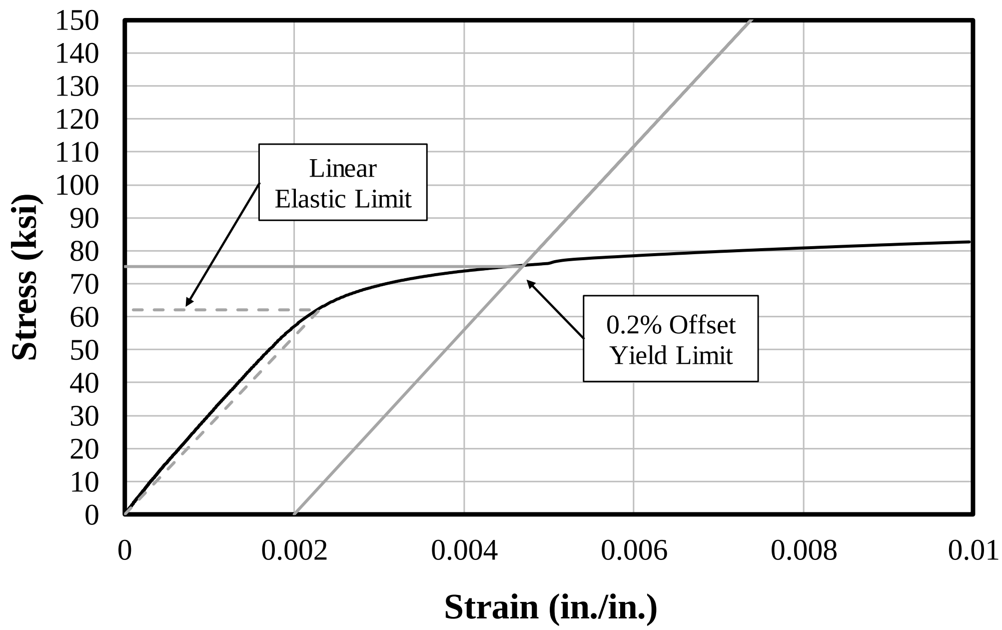

a) Initial Behavior Limits

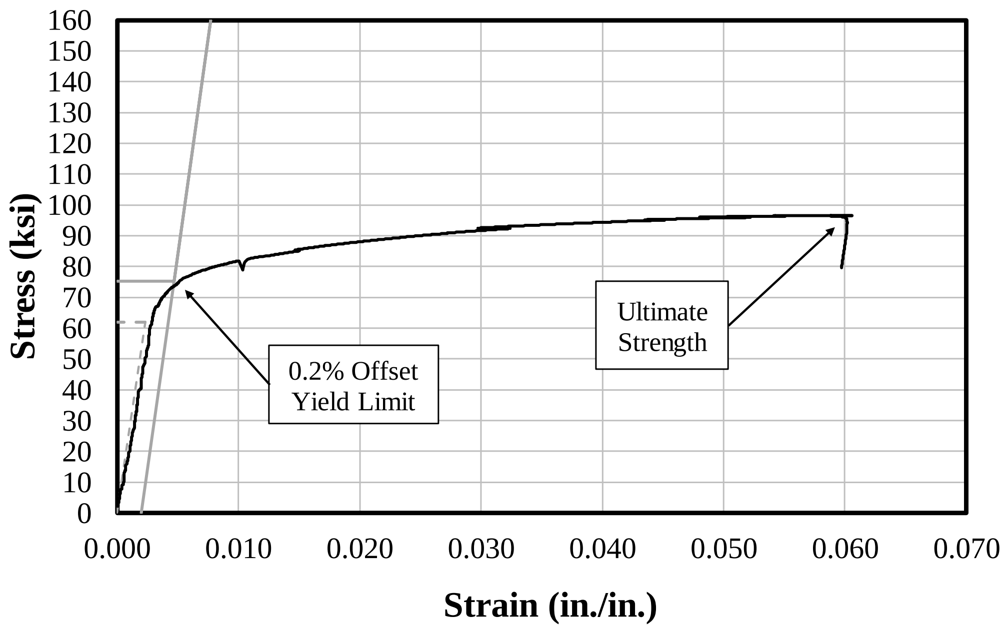

b) Full Behavior

Figure B.4: A615 Gr. 60 No. 3 Transverse Bar (Series I - VI) - Stress Strain Curve

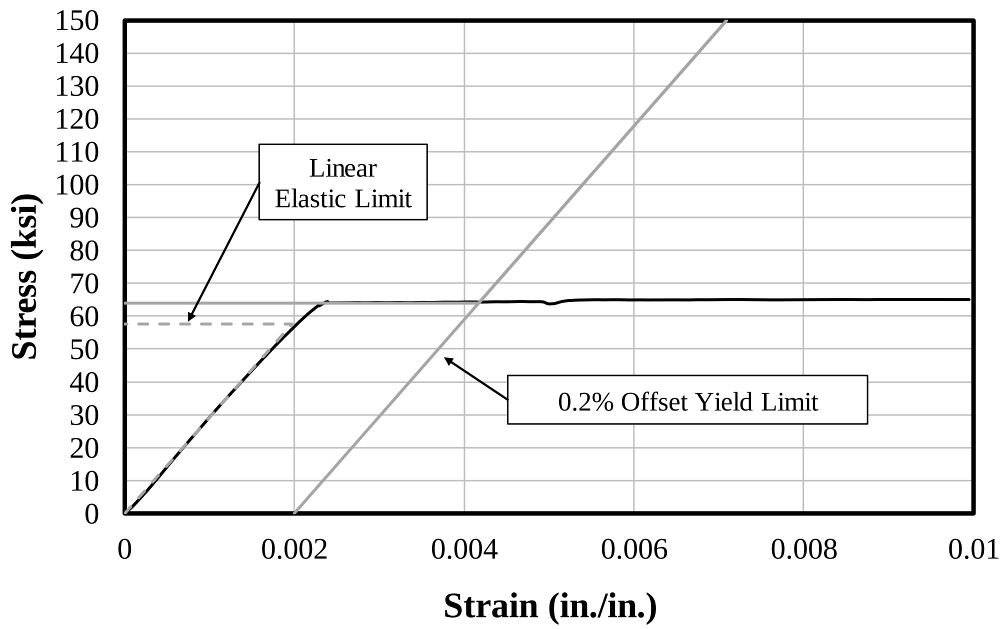

Figure B.5: A615 Gr. 60 No. 3 Transverse Bar (Series VII) - Stress Strain Curve

Note: Full stress-strain behavior was not measured due to a broken break-away extensometer during coupon testing. Post-processed data indicates an ultimate strength of 98 ksi after typical stress-strain behavior up to failure, similar to Figure B.4(b).

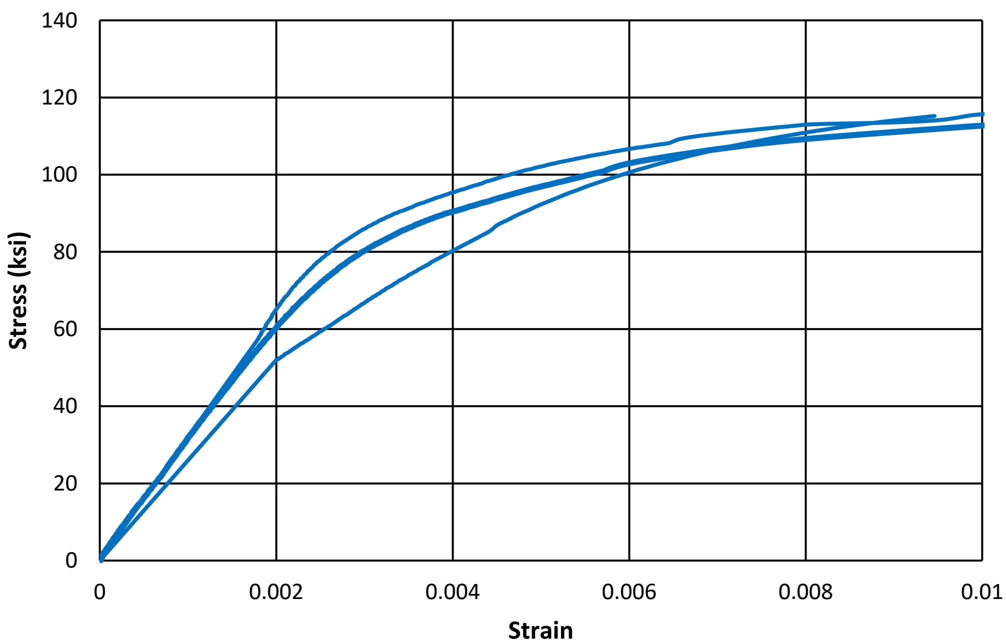

a) Partial Curve

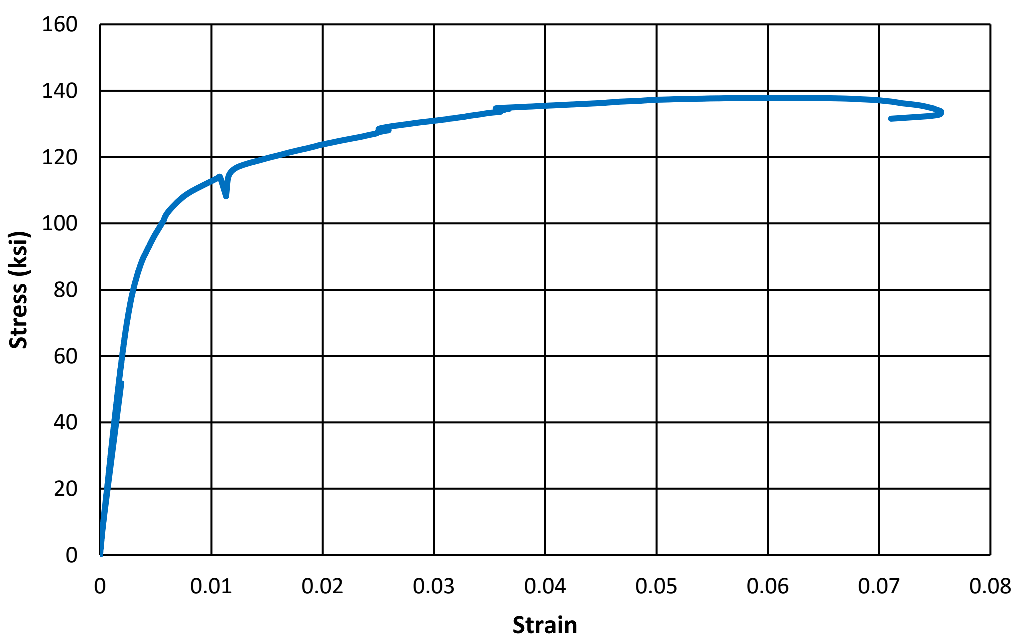

b) Complete Curve

Figure B.6: Complete Stress-Strain Curve for #3 Grade 100 Stirrups

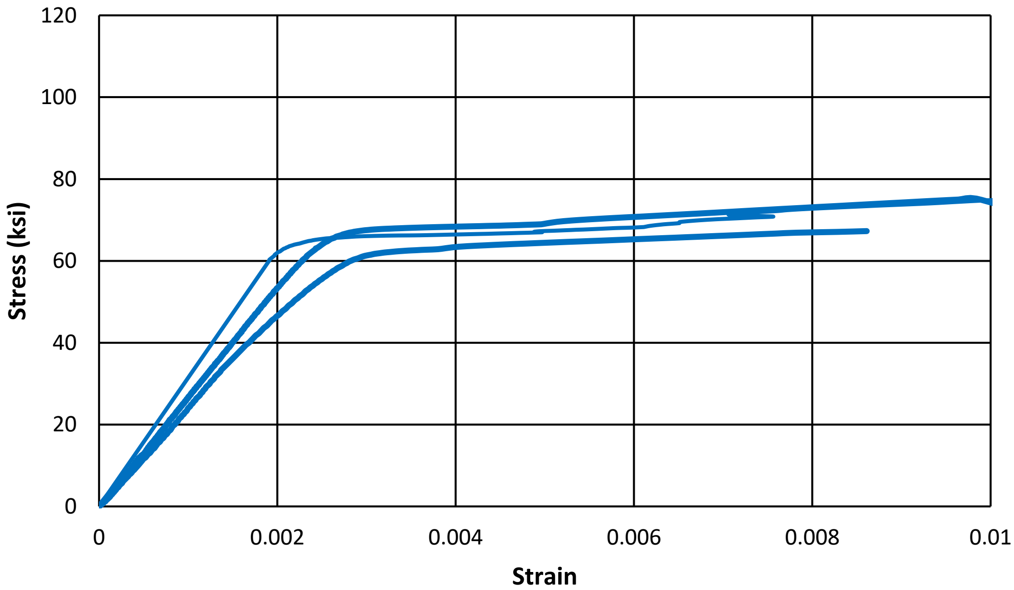

a) Partial Curve

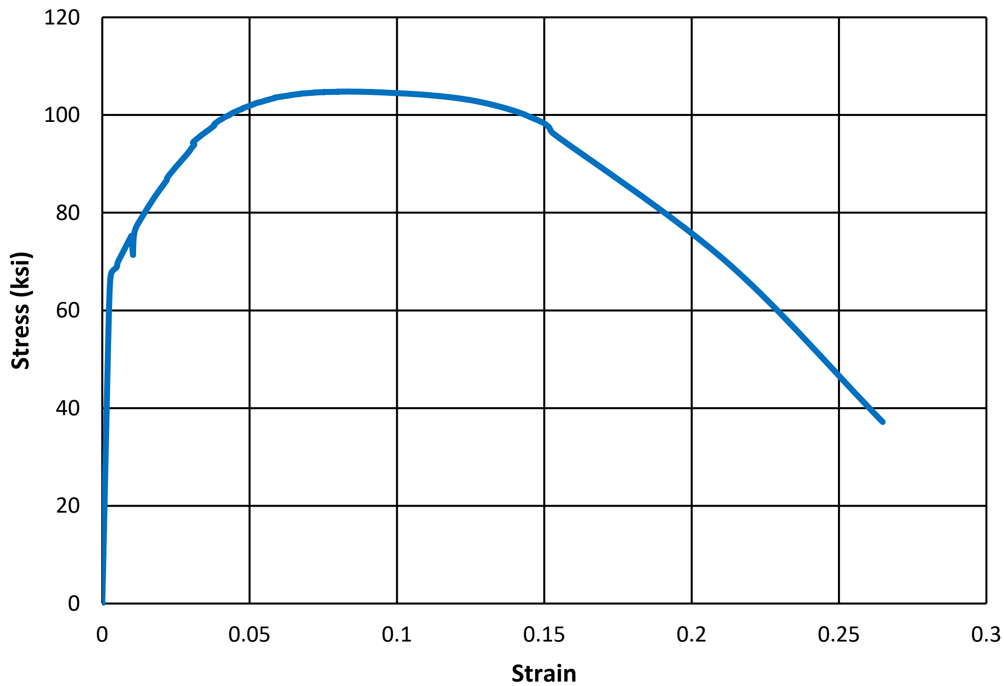

b) Complete Curve

Figure B.7: Complete Stress-Strain Curve for #4 Grade 60 Stirrups

APPENDIX C: CONCRETE MIX INFORMATION (SERIES I-IV)

Table C.1: Concrete Mixes as Supplied

Series	1		2		3		4	
Truck	1	2	1	2	1	2	1	2
Mix Code	4101CC		4601CC		4101CC		4101CC	
Nominal Strength (psi)	4000		4500		4000		4000	
Type I Cement (lb/yd^3)	515.3	519.4	561.7	561.7	518.4	515.3	515.3	520
#8 Limestone (lb/yd^3)	1865.8	1861.8	1841.8	1846.3	1872.4	1864.1	1868.2	1865.8
Fine Aggregate (lb/yd^3)	1471.1	1471.3	1444.8	1447.0	1472.4	1471.3	1470.3	1468.8
Water (lb/yd^3)	242.3	243.3	243.3	243.3	249.3	257.4	234.2	232.2
Water Added (lb/yd^3)	11.1	4.9	4.6	-	4.4	-	4.4	11.1
Mid-Range Water Reducer (oz/yd^3)	20.8	20.6	11.2	11.2	20.7	20.6	20.5	20.7
Slump (in.)	7.5	6	4	6	7	6.5	5.5	6.5

Table C.2: Concrete Truck Distribution for Each Series

Series	Specimen	Truck
I	U-40-5	2
	U-60-5	
	U-80-5	
	U-100-5	
	U-120-5	1
	U-80-5-M	
	U-100-5-M	
	U-120-5-M	
II	C3/60-60-5-50	1
	C3/60-60-5-100	
	C3/60-60-5-150	
	C3/60-60-5-200	
	C4/60-60-5-100	2
	C4/60-60-5-150	
	C3/100-60-5-100	
	C3/100-60-5-150	
III	C3/60-80-5-50	1
	C3/60-80-5-100	
	C3/60-80-5-150	
	C3/60-80-5-200	
	C4/60-80-5-100	2
	C4/60-80-5-150	
	C3/100-80-5-100	
	C3/100-80-5-150	
IV	U-40-5a	1
	U-60-5a	
	U-70-5	
	C3/60/2-40-5-50	
	C3/60/3-40-5-50	
	C3/100/3-40-5-50	2
	C3/60-40-5-100	
	C3/100-40-5-100	

APPENDIX D: LOAD-DEFLECTION RESPONSE (SERIES I-IV)

Load-deflection responses are constructed from end load and end deflection data for all specimens in this testing program. All load and deflection values are averages of the north and south ends, unless noted otherwise. The stress-strain response for the longitudinal steel in each specimen is provided to give an indication of longitudinal steel behavior at failure.

Accurate deflection measurements could not be exported.

a) Load-Deflection

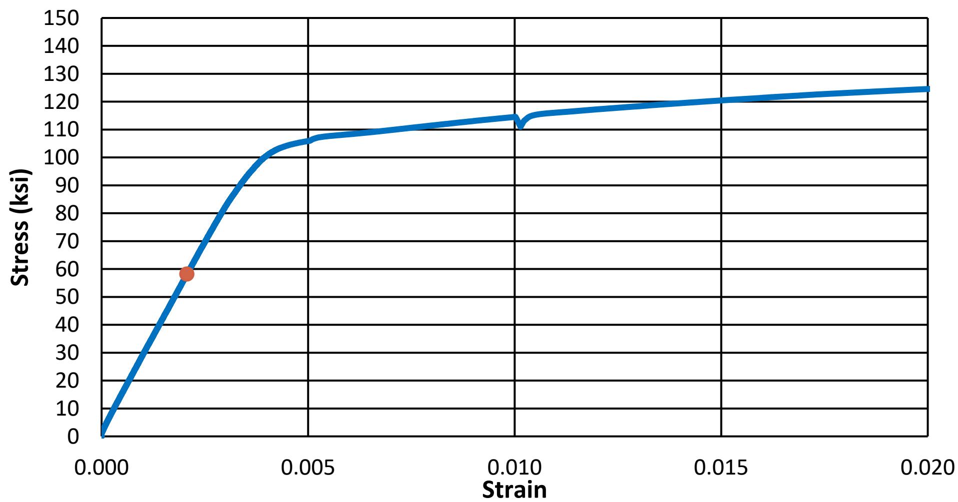

b) Stress-Strain

Figure D.1: U-40-5

Accurate deflection measurements could not be exported.

a) Load-Deflection

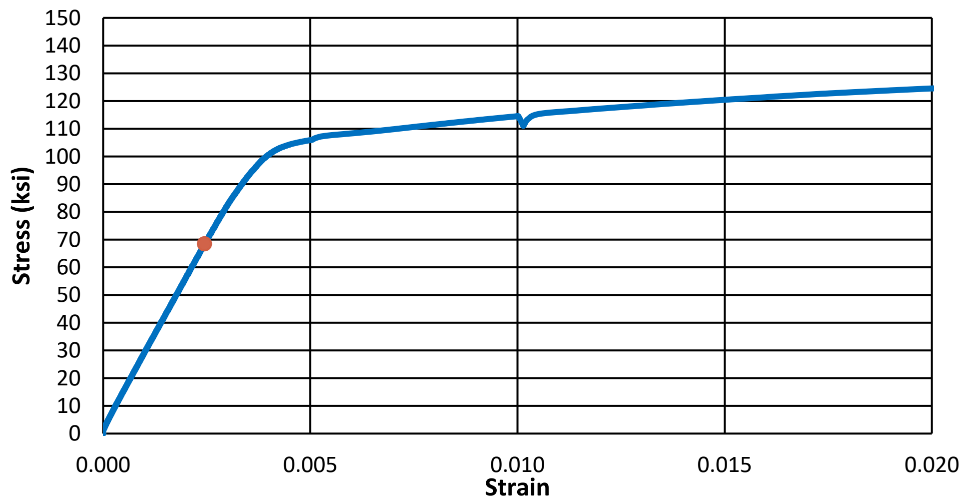

b) Stress-Strain

Figure D.2: U-60-5

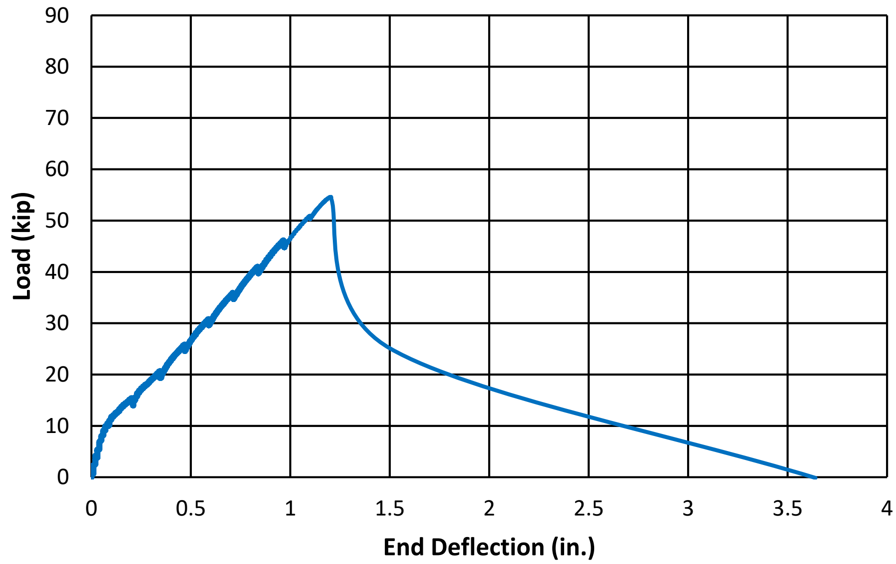

a) Load-Deflection

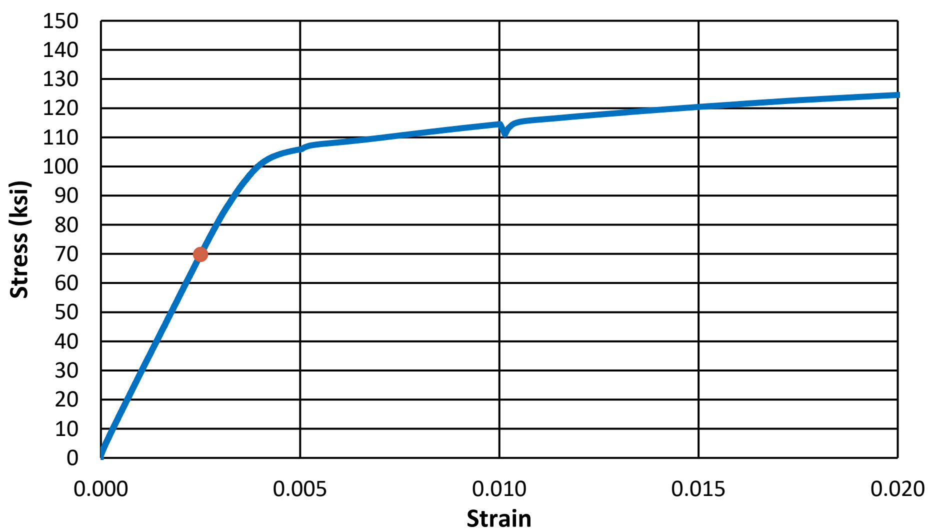

b) Stress-Strain

Figure D.3: U-40-5a

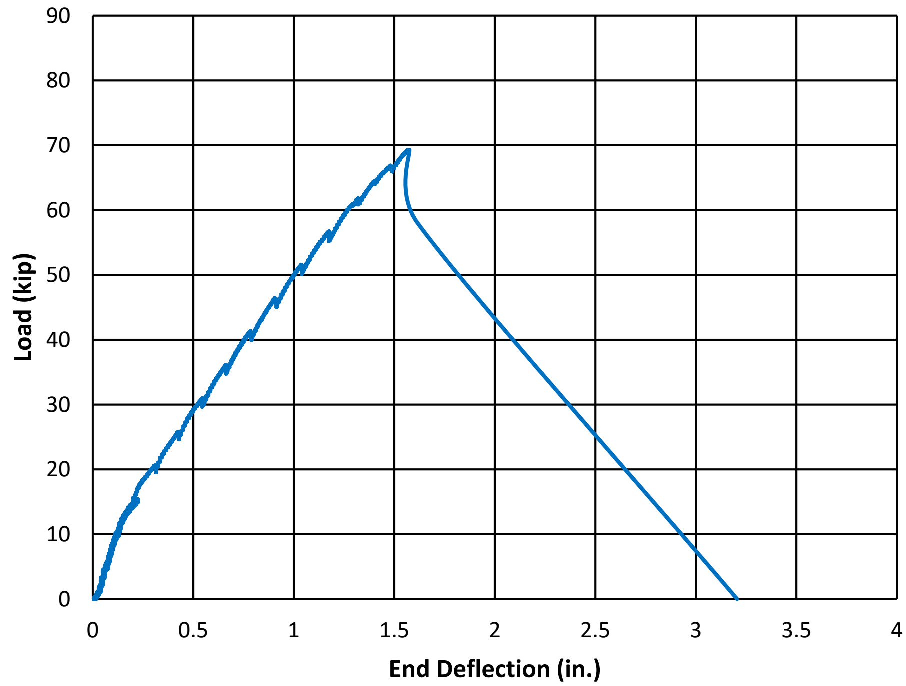

a) Load-Deflection

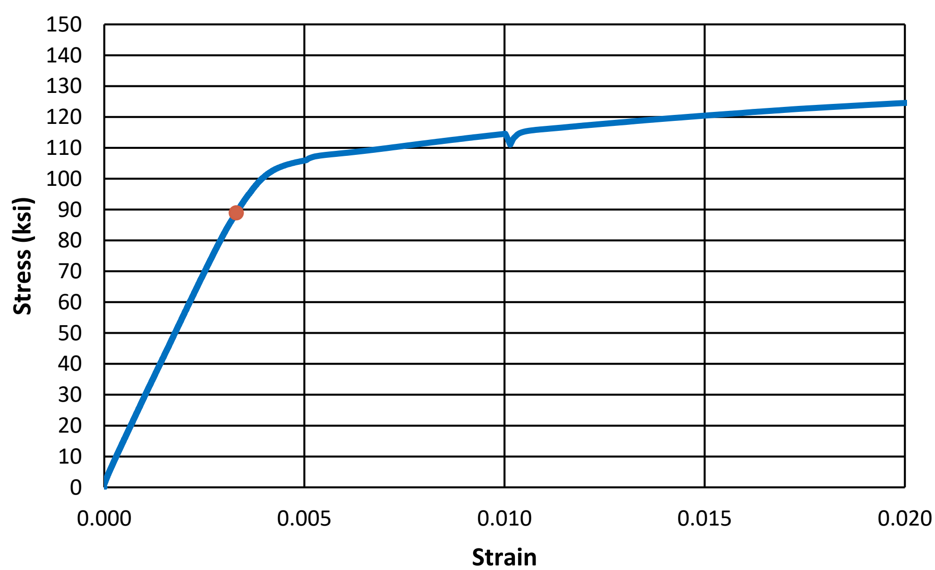

b) Stress-Strain

Figure D.4: U-60-5a

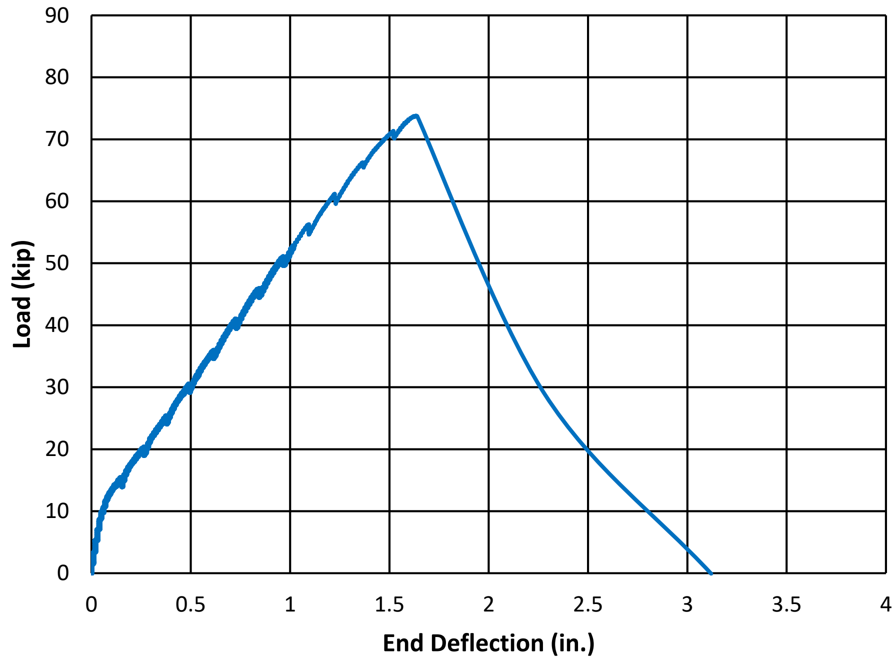

a) Load-Deflection

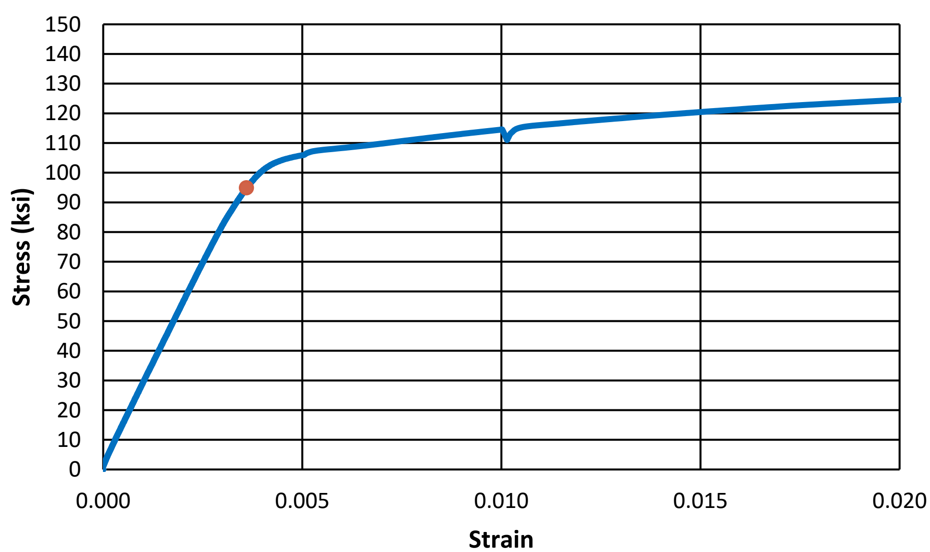

b) Stress-Strain

Figure D.5: U-70-5

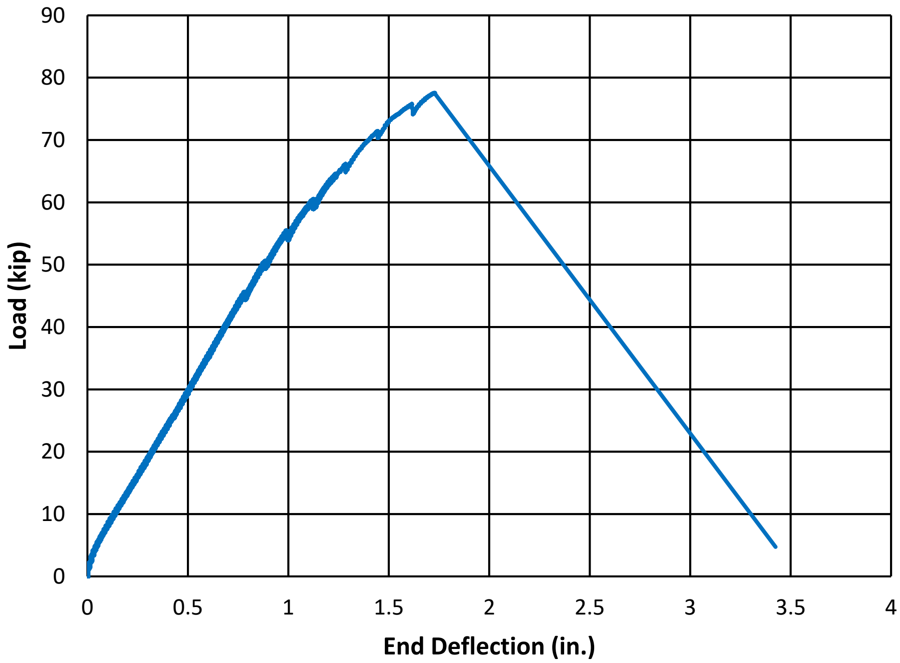

a) Load-Deflection

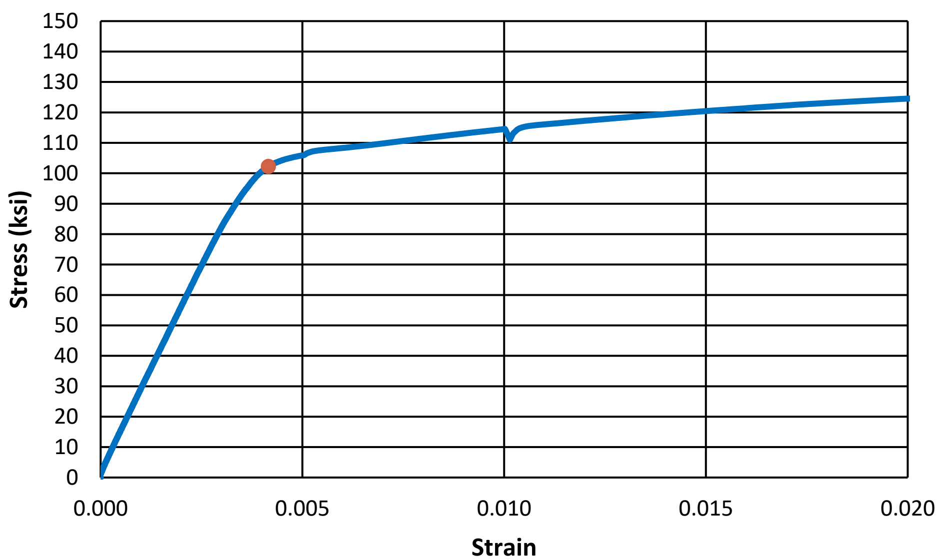

Stress-Strain

Figure D.6: U-80-5

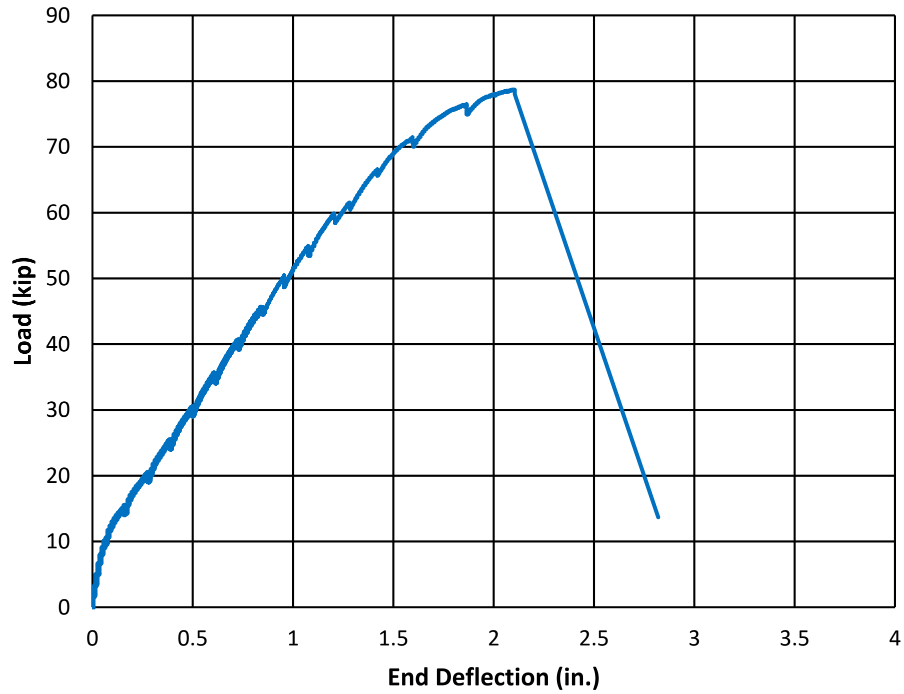

a) Load-Deflection

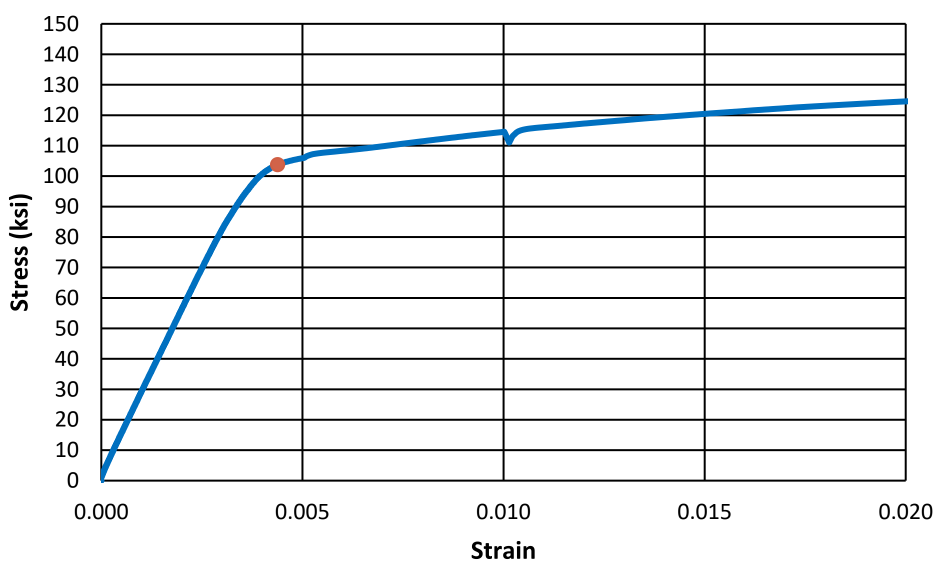

b) Stress-Strain

Figure D.7: U-100-5

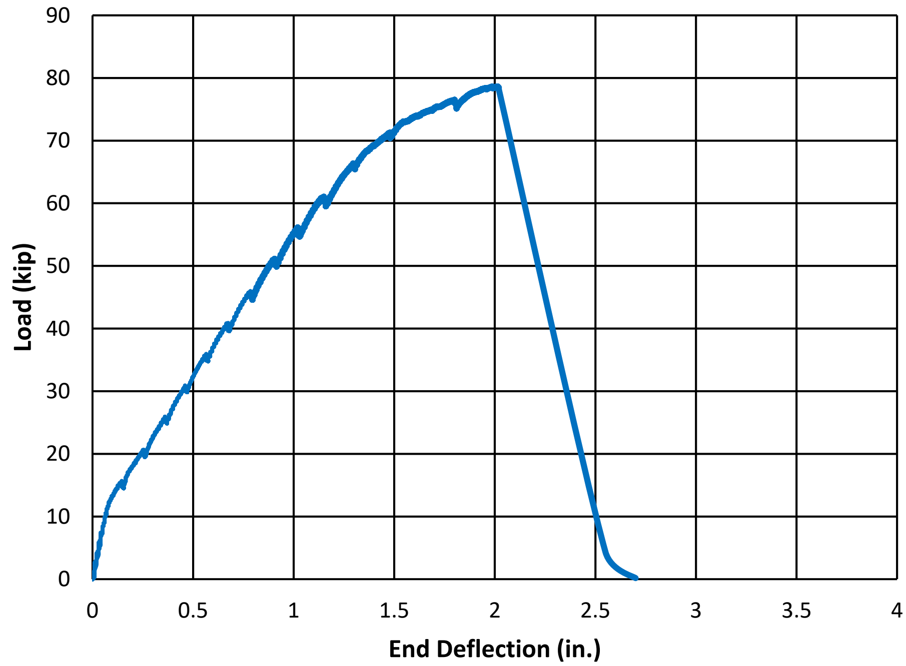

a) Load-Deflection

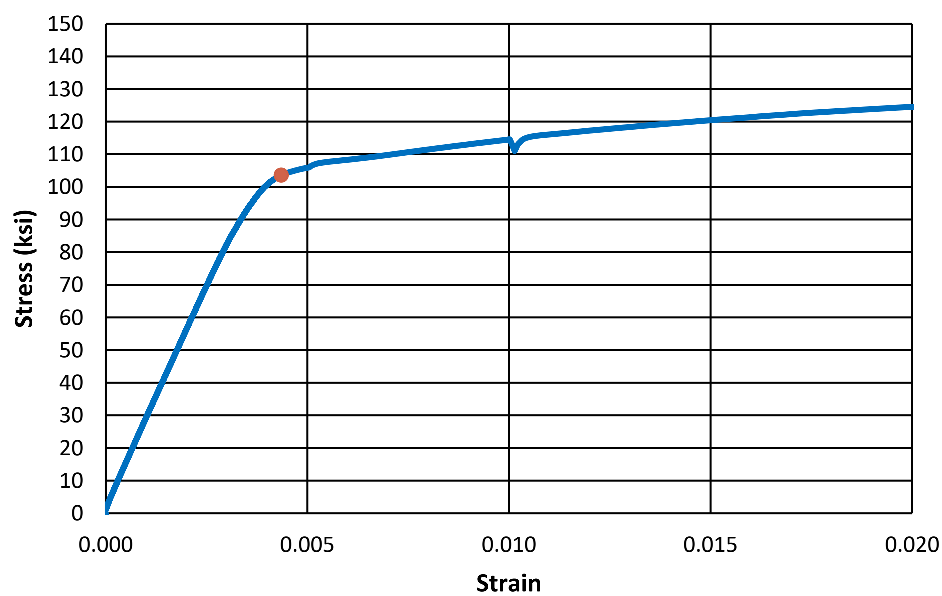

b) Stress-Strain

Figure D.8: U-120-5

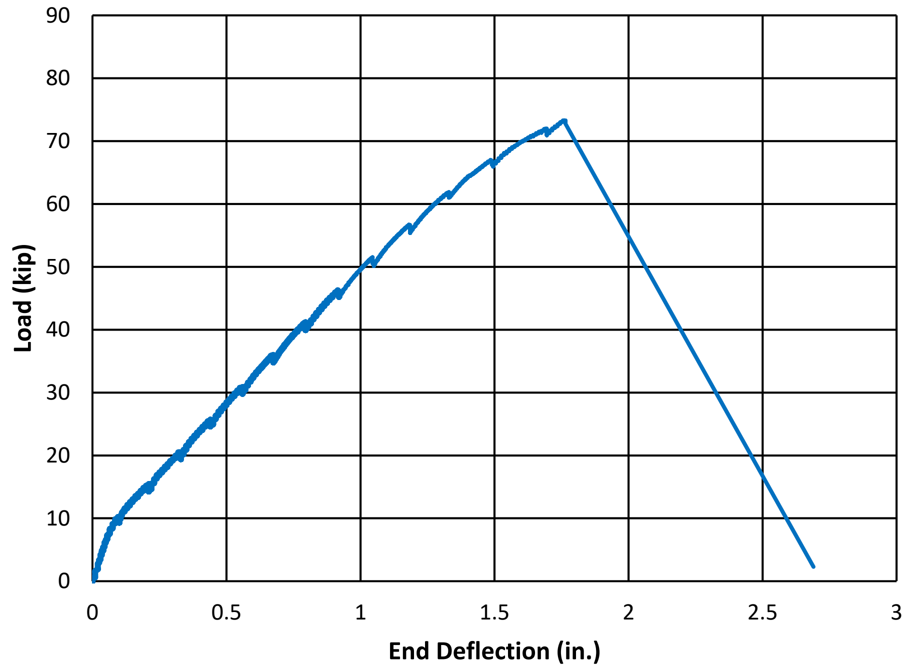

a) Load-Deflection

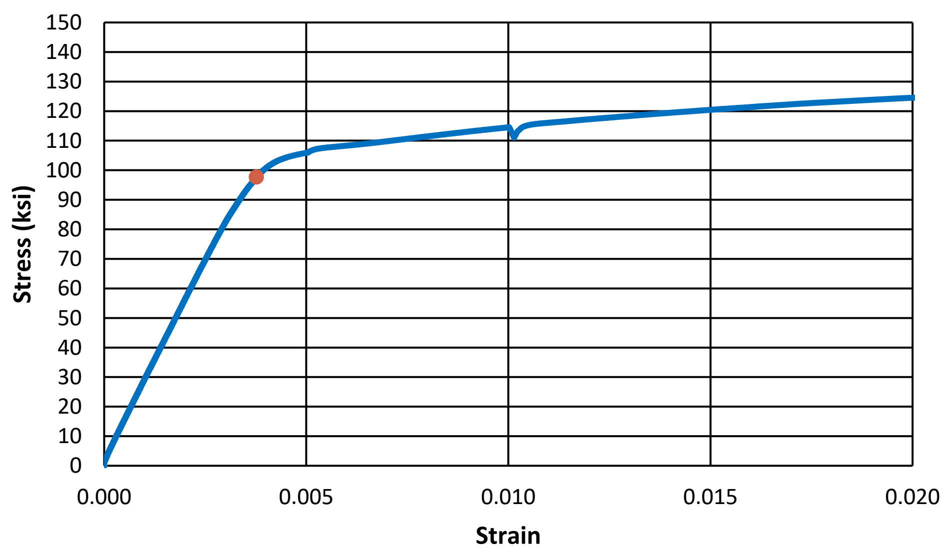

b) Stress-Strain

Figure D.9: U-80-5-M

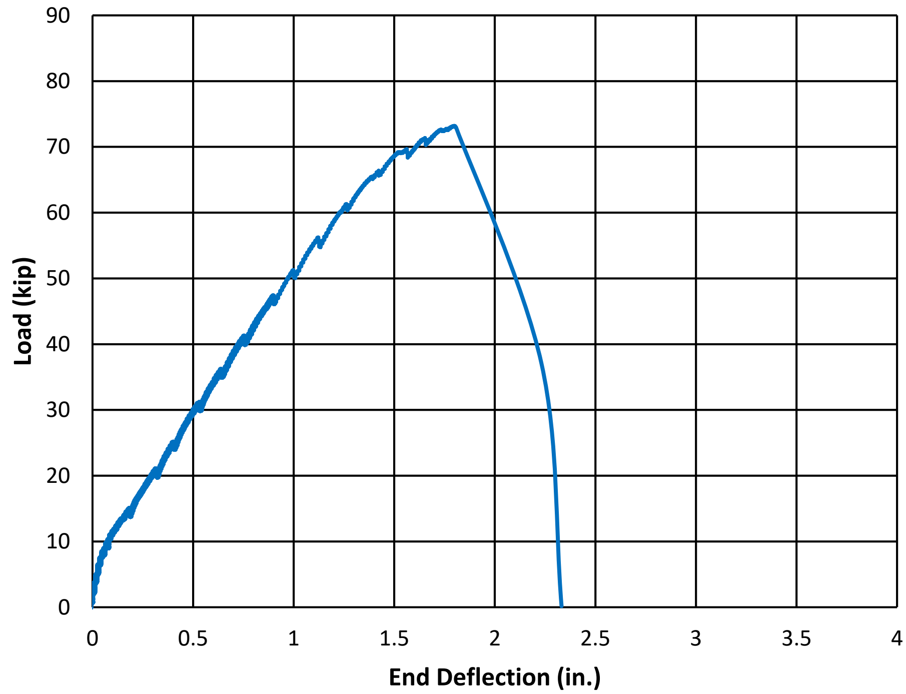

a) Load-Deflection

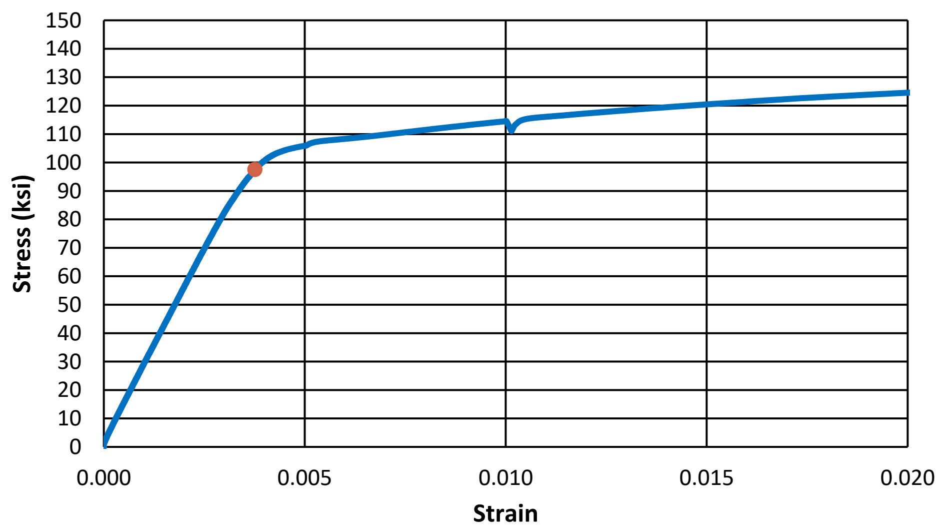

b) Stress-Strain

Figure D.10: U-100-5-M

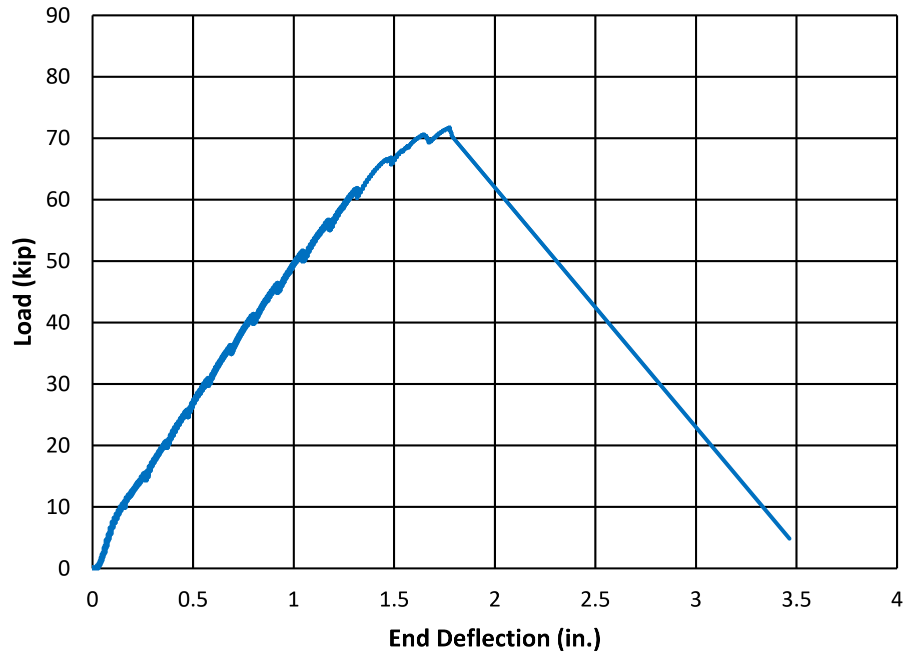

a) Load-Deflection

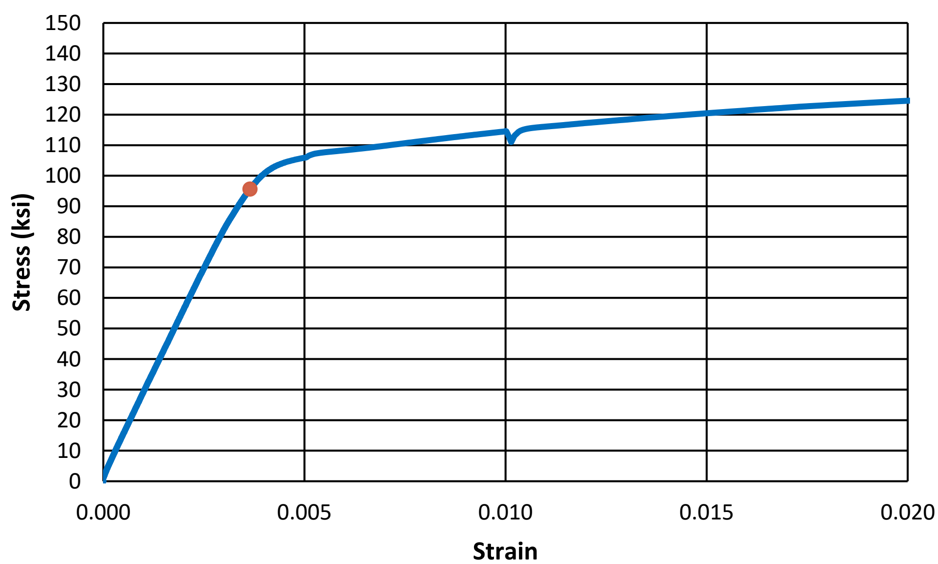

b) Stress-Strain

Figure D.11: U-120-5-M

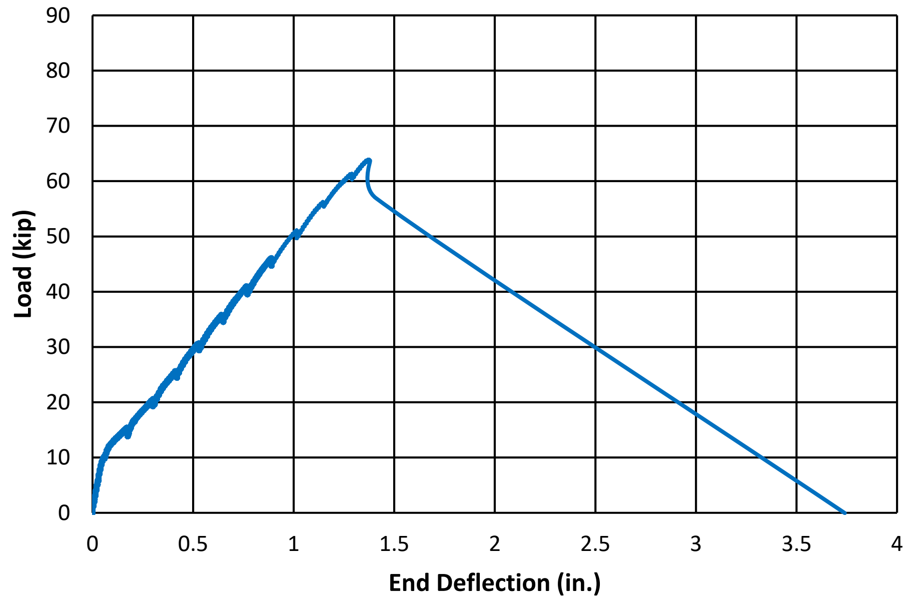

a) Load-Deflection

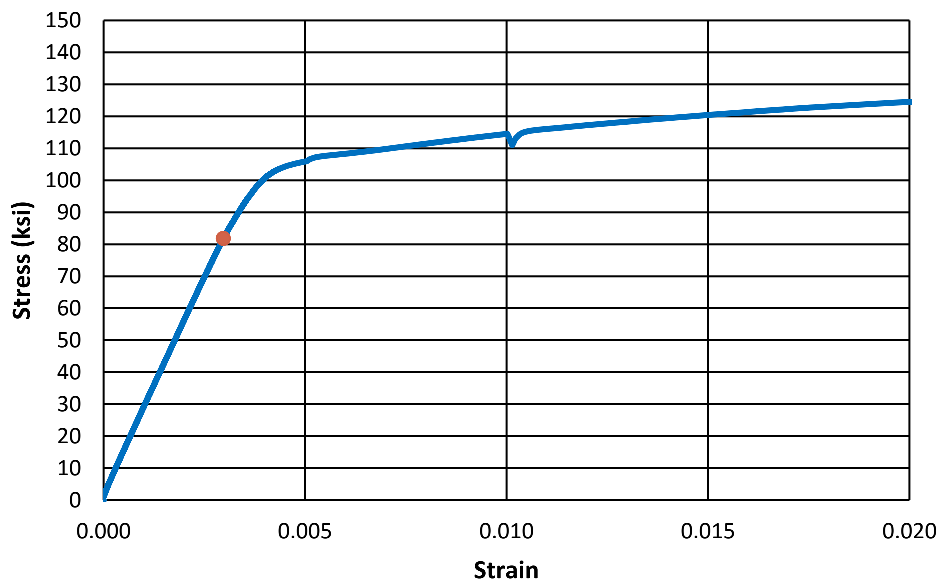

b) Stress-Strain

Figure D.12: C3/60/2-40-5-50

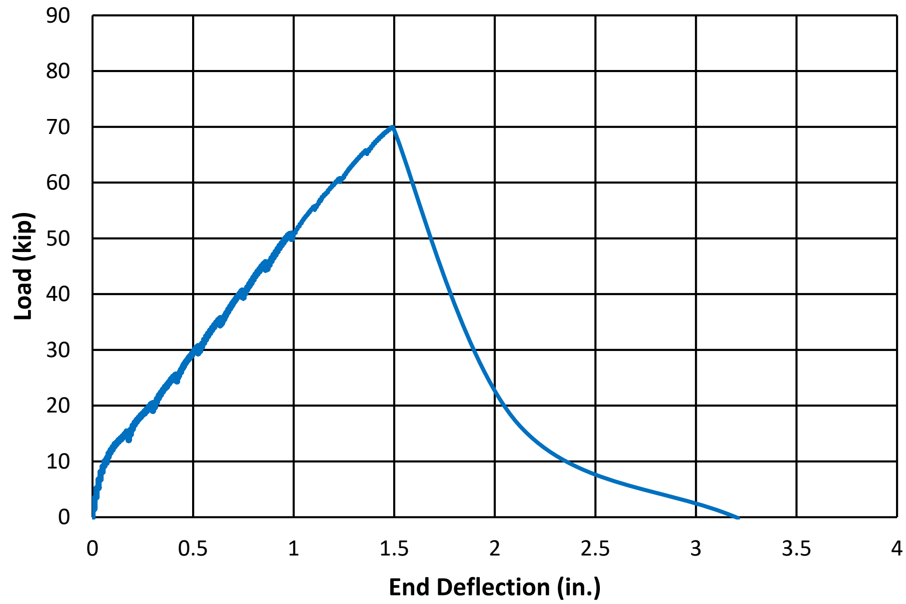

a) Load-Deflection

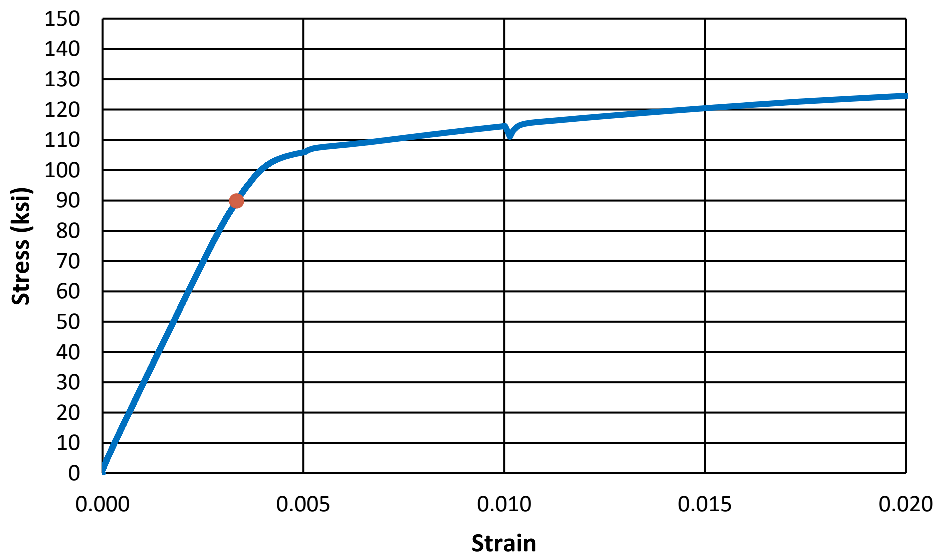

b) Stress-Strain

Figure D.13: C3/60/3-40-5-50

Accurate deflection measurements could not be exported.

a) Load-Deflection

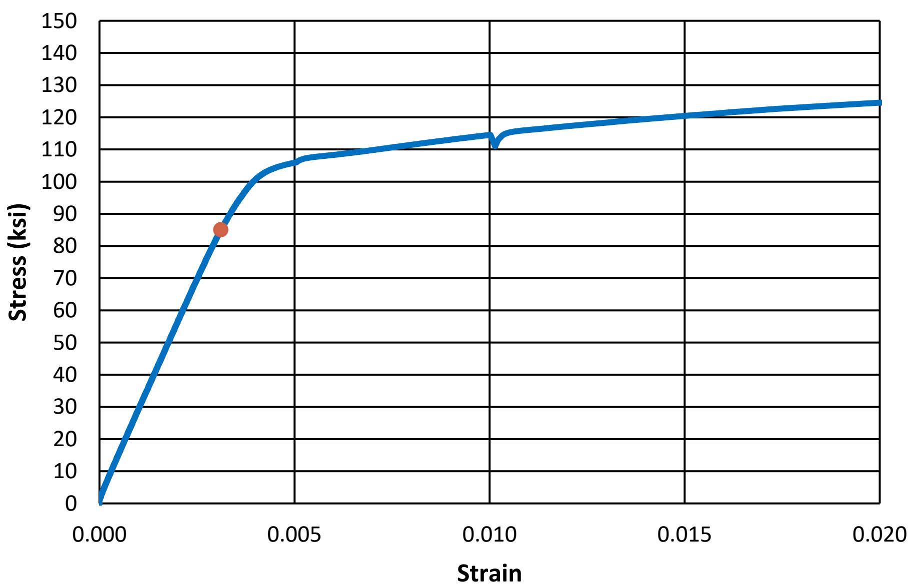

b) Stress-Strain

Figure D.14: C3/100/3-40-5-50

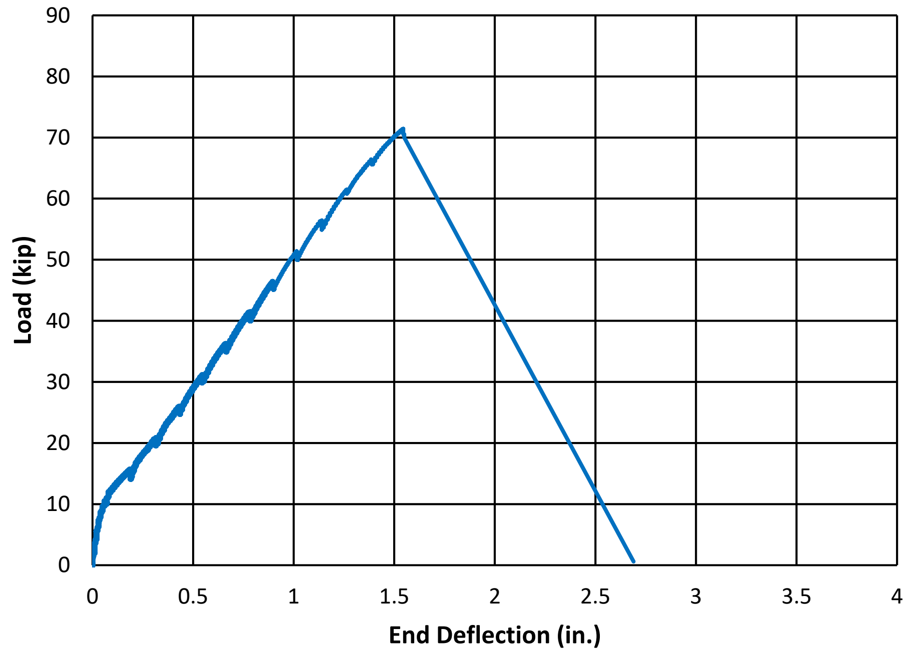

a) Load-Deflection

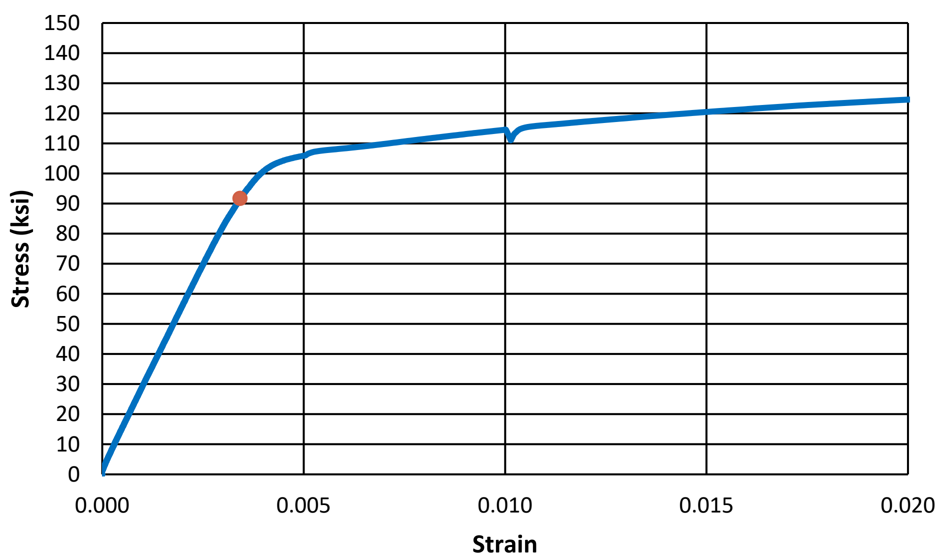

b) Stress-Strain

Figure D.15: C3/60-40-5-100

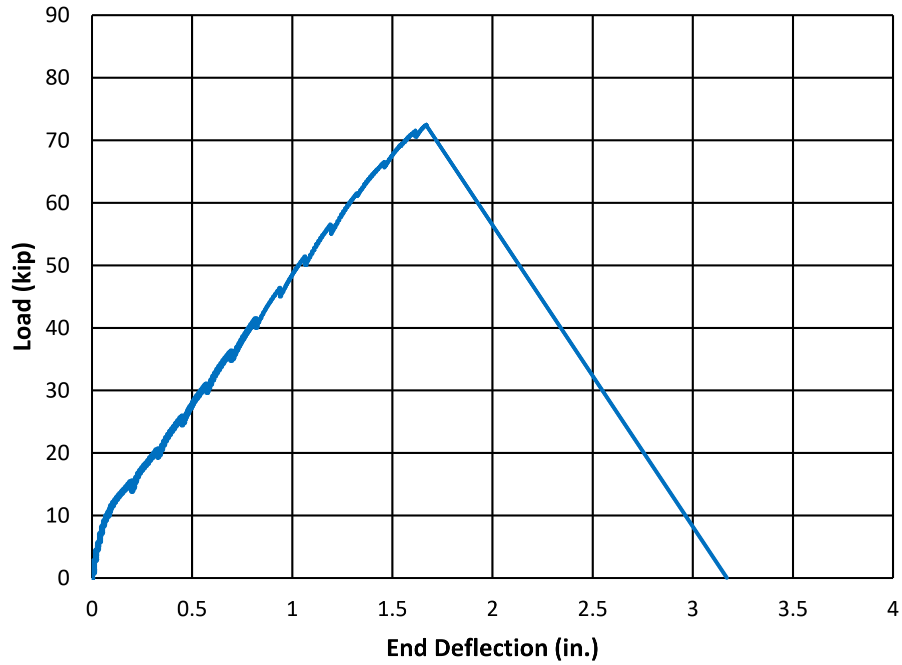

a) Load-Deflection

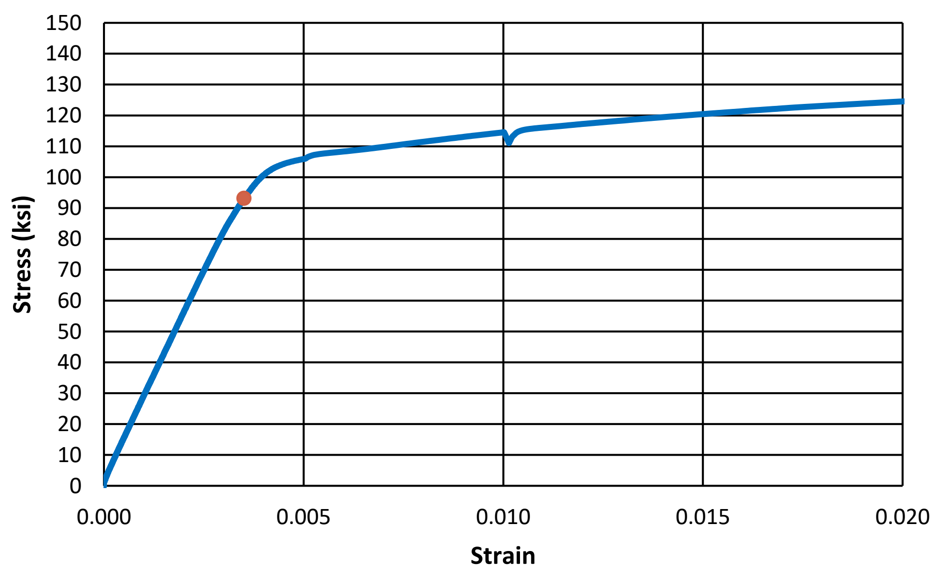

b) Stress-Strain

Figure D.16: C3/100-40-5-100

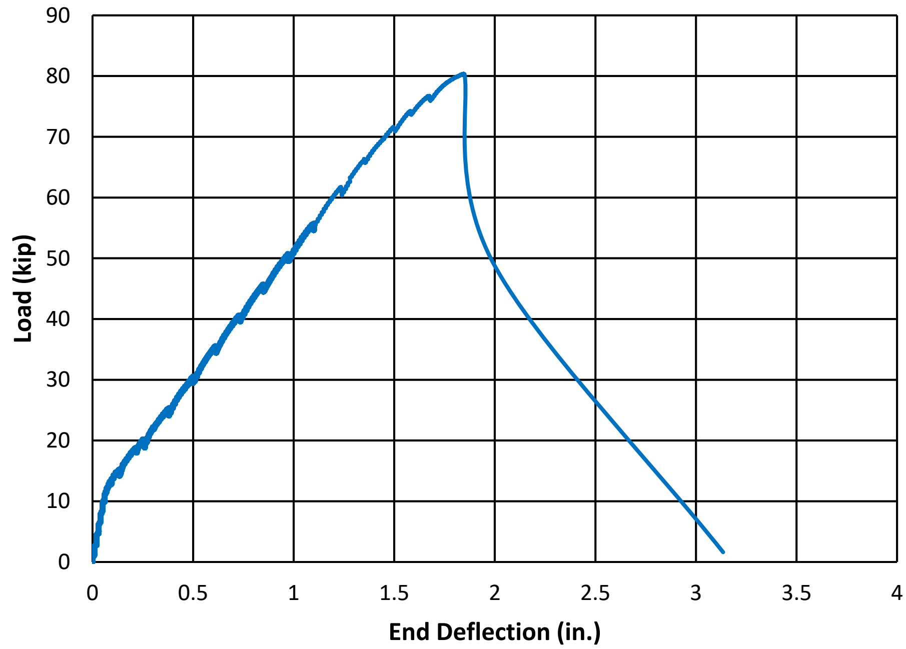

a) Load-Deflection

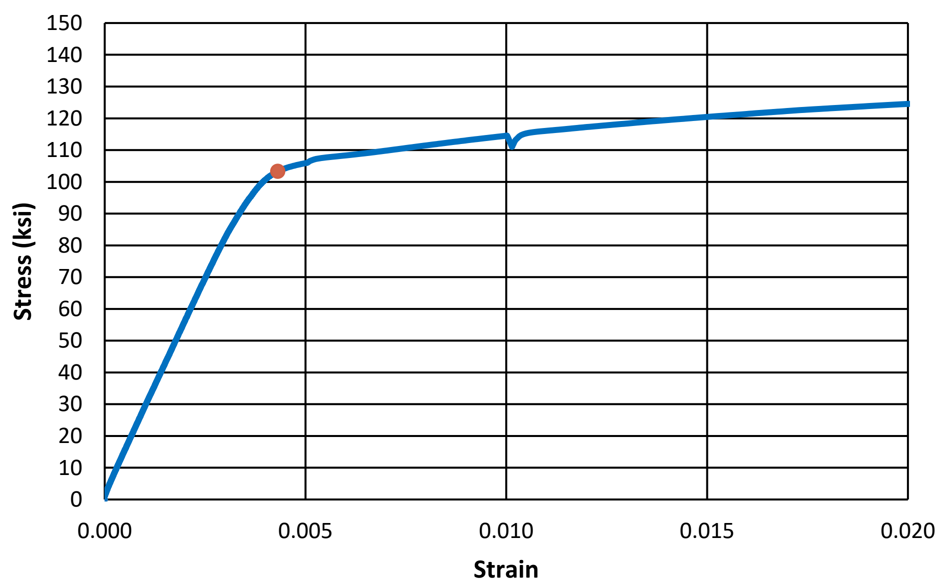

b) Stress-Strain

Figure D.17: C3/60-60-5-50

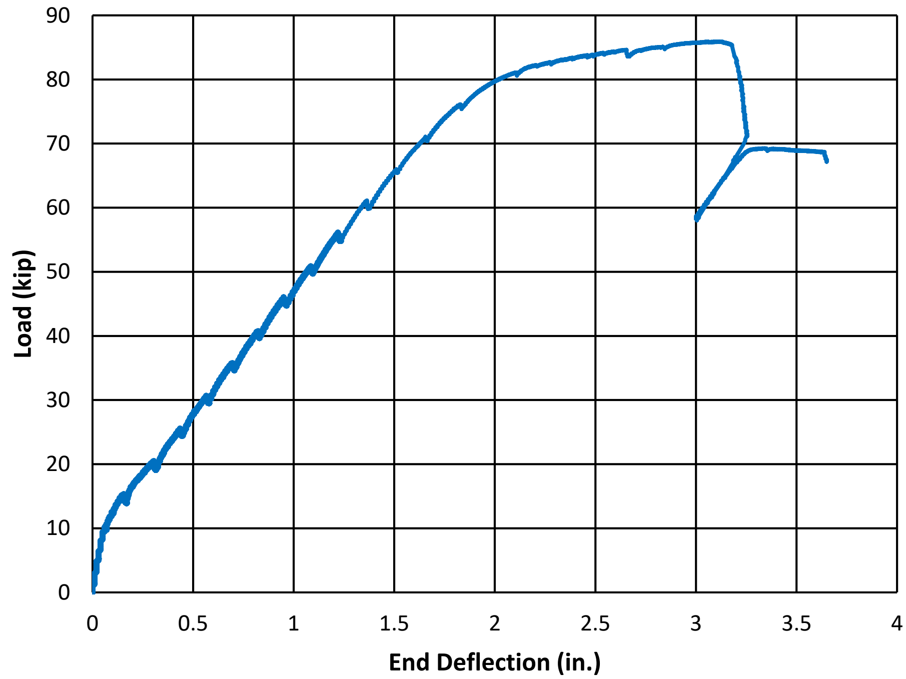

a) Load-Deflection

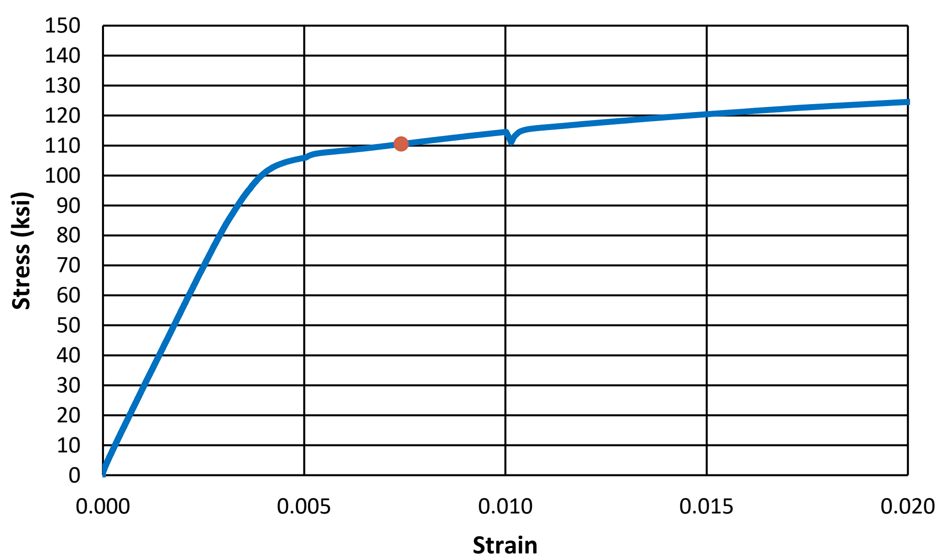

b) Stress-Strain

Figure D.18: C3/60-60-5-100

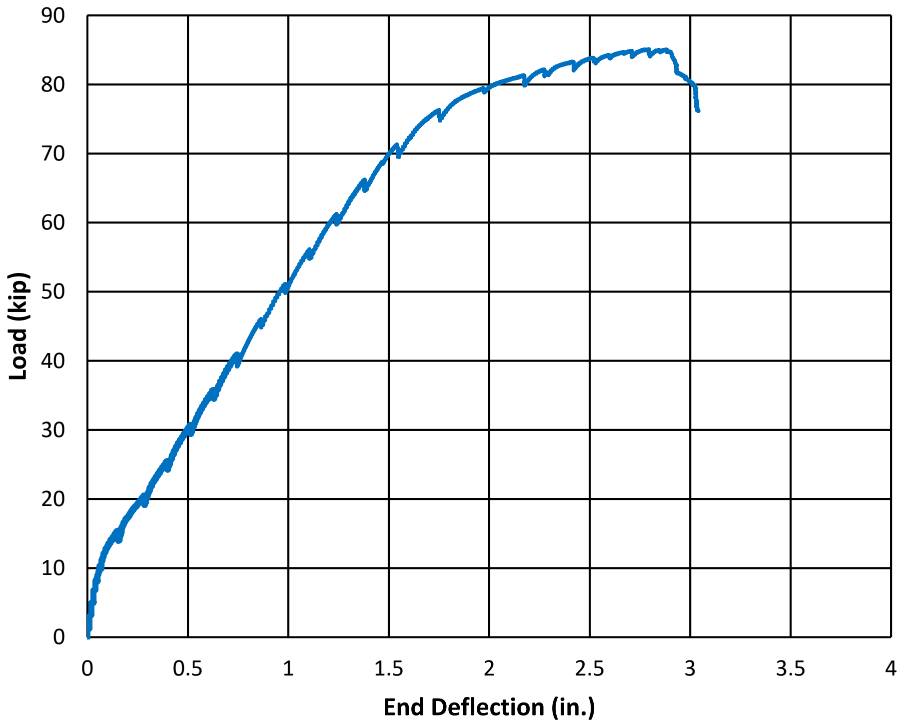

a) Load-Deflection

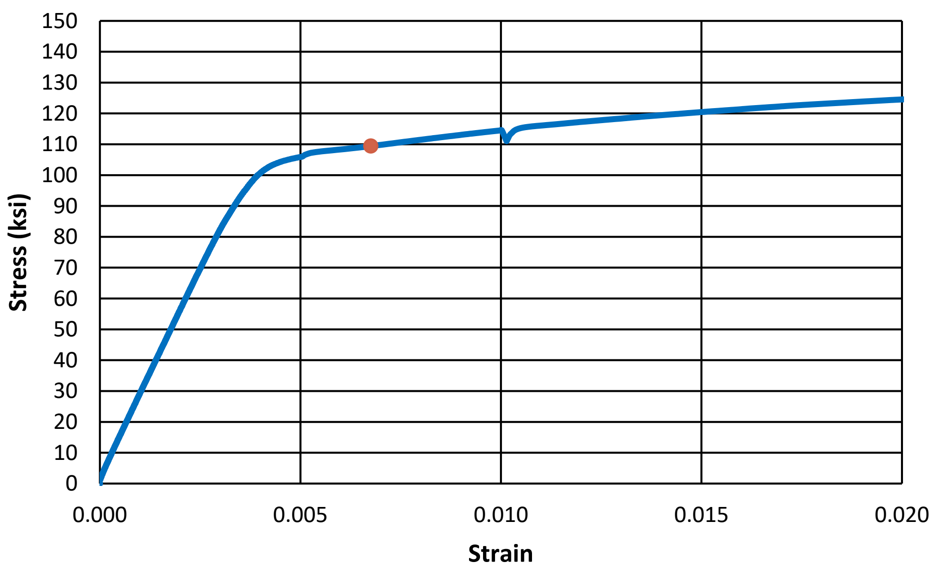

b) Stress-Strain

Figure D.19: C3/60-60-5-150

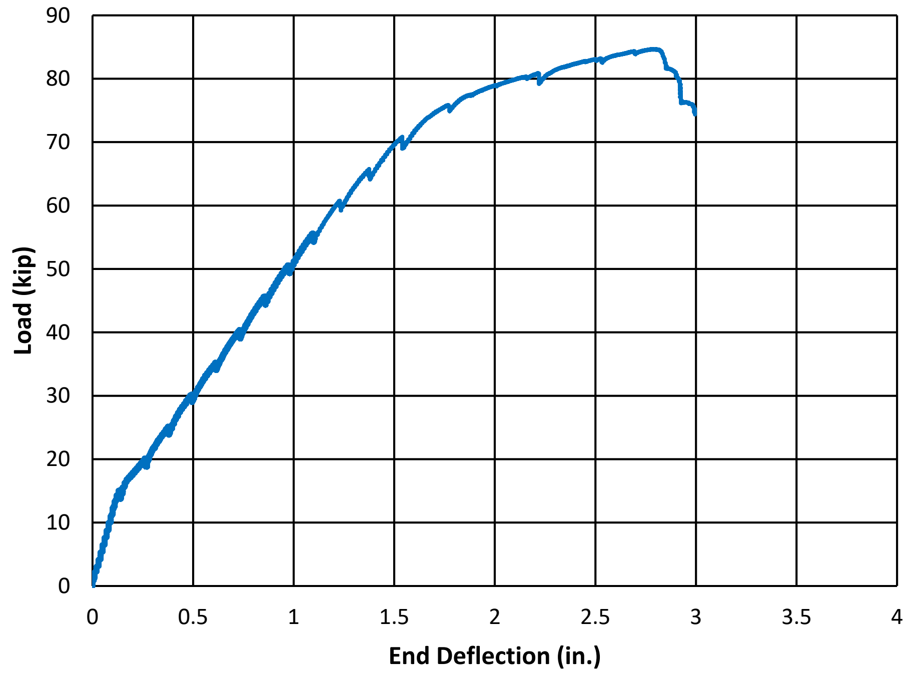

a) Load-Deflection

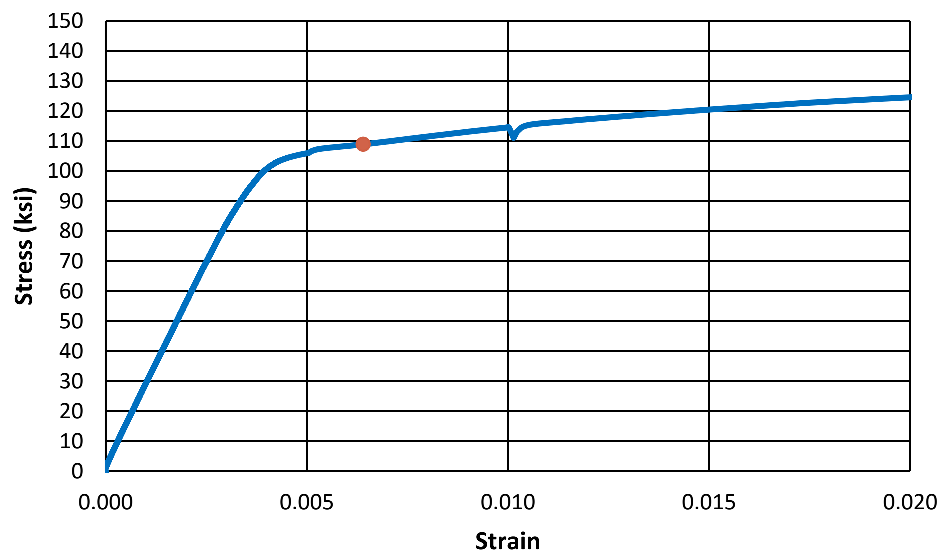

b) Stress-Strain

Figure D.20: C4/60-60-5-100

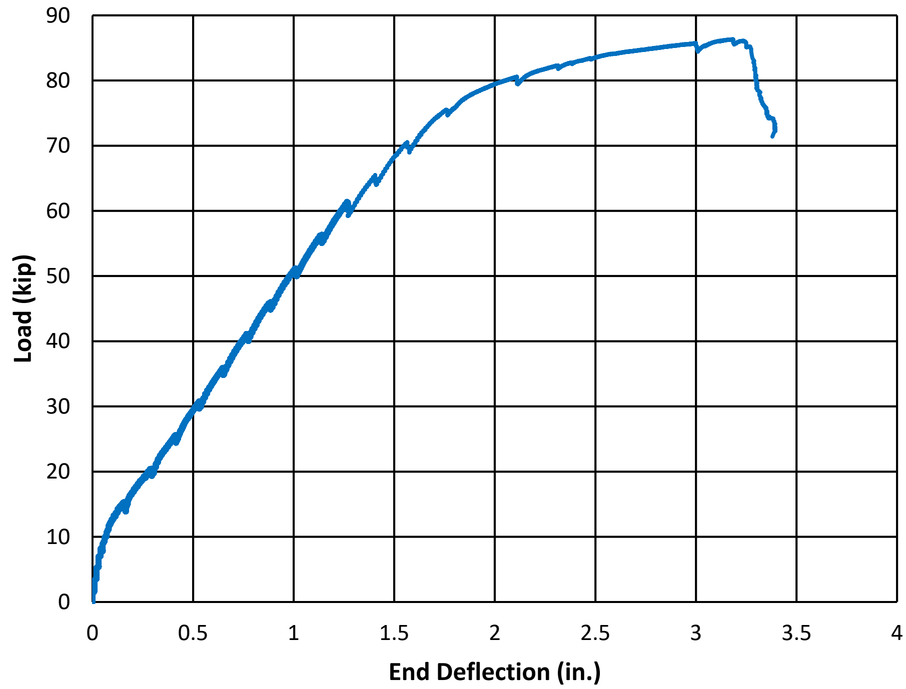

a) Load-Deflection

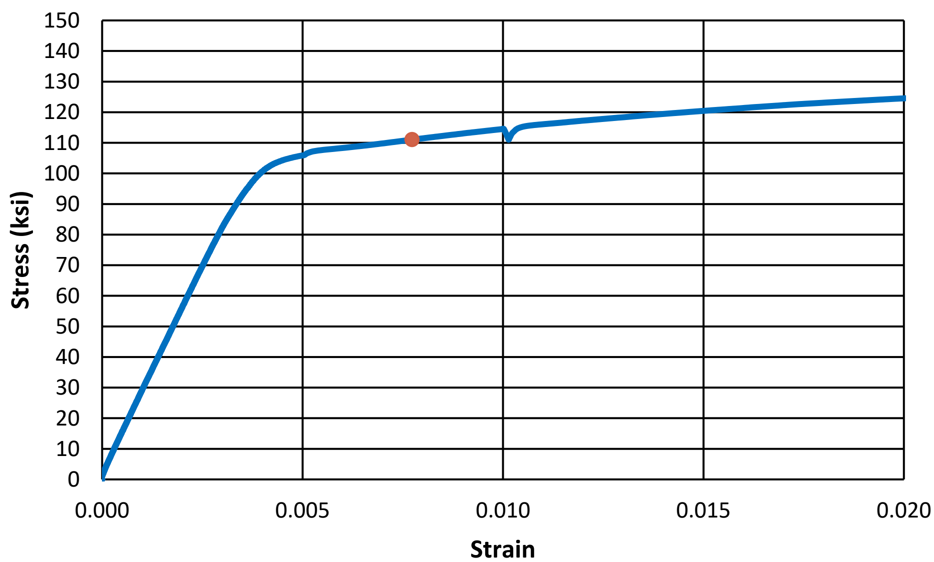

b) Stress-Strain

Figure D.21: C3/100-60-5-100

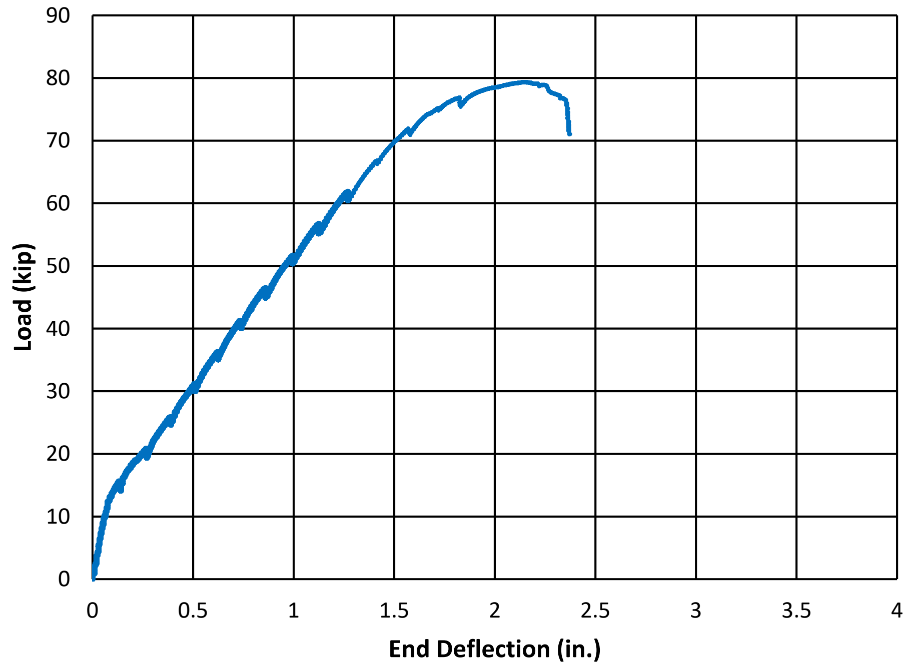

a) Load-Deflection

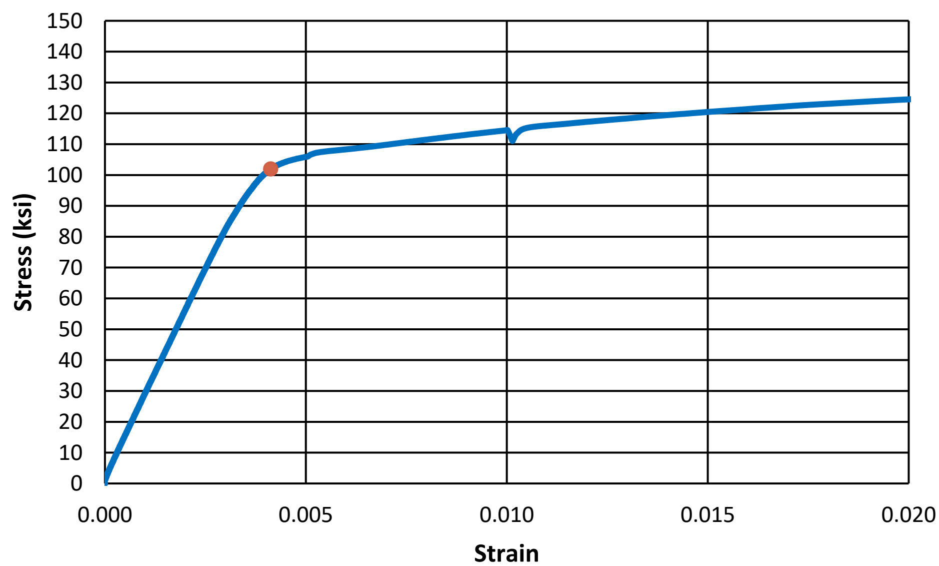

b) Stress-Strain

Figure D.22: C3/60-80-5-50

APPENDIX E: CRACK WIDTH MEASUREMENTS (SERIES I-IV)

All cracks are measured from specimen centerline and remain within the constant moment region. Four (4) cracks were monitored in each test. The average crack width growth was plotted for each test specimen. A typical test specimen showing any regions of interest and locations of these cracks is provided in Figure E.1.

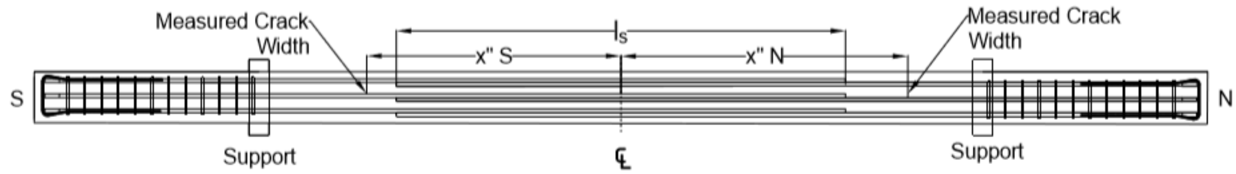

Figure E.1: Description of Nomenclature

Crack widths were not recorded for Specimens U-40-5 and C3/100/3-40-5-50.

Table E.1: U-40-5a

Load (kip)	Bar Stress (ksi)	Crack Widths (in.)				
		56.5" N	26.5" N	36" S	53" S	Average
15	19.0	0.004	0.003	0.003	0.003	0.0033
20	25.3	0.008	0.005	0.005	0.005	0.0058
25	31.7	0.009	0.007	0.006	0.007	0.0073
30	38.1	0.011	0.009	0.007	0.009	0.0090
35	44.5	0.011	0.012	0.009	0.011	0.0108
40	50.9	0.012	0.014	0.010	0.013	0.0123
45	57.3	0.012	0.016	0.013	0.015	0.0140

Table E.2: U-60-5

Load (kip)	Bar Stress (ksi)	Crack Widths (in.)*				
		Crack 1	Crack 2	Crack 3	Crack 4	Average
20	25.7	0.005	0.010	0.005	0.005	0.0063
25	32.1	0.005	0.010	0.005	0.005	0.0063
30	38.6	0.010	0.020	0.010	0.010	0.0125
35	45.1	0.015	0.025	0.010	0.020	0.0175
40	51.6	0.020	0.025	0.010	0.020	0.0188
45	58.2	0.020	0.030	0.015	0.020	0.0213
50	64.8	0.020	0.030	0.015	0.025	0.0225

***Crack location not measured**

Table E.3: U-60-5a

Load (kip)	Bar Stress (ksi)	Crack Widths (in.)				
		77" N	53" N	44" S	59" S	Average
15	19.0	0.002	0.002	0.003	0.002	0.0023
20	25.3	0.006	0.003	0.003	0.004	0.0040
25	31.7	0.008	0.005	0.006	0.006	0.0063
30	38.1	0.013	0.007	0.008	0.007	0.0088
35	44.5	0.015	0.009	0.011	0.009	0.0110
40	50.9	0.018	0.011	0.014	0.012	0.0138
45	57.3	0.021	0.013	0.016	0.013	0.0158
50	63.7	0.021	0.014	0.021	0.016	0.0180
55	70.2	0.025	0.016	0.022	0.018	0.0203

Table E.4: U-70-5

Load (kip)	Bar Stress (ksi)	Crack Widths (in.)				
		63.5" N	43" N	47" S	63.5" S	Average
15	19.0	0.002	0.002	0.002	0.002	0.0020
20	25.3	0.003	0.004	0.003	0.002	0.0030
25	31.7	0.004	0.006	0.003	0.003	0.0040
30	38.1	0.006	0.006	0.004	0.004	0.0050
35	44.5	0.007	0.009	0.006	0.005	0.0068
40	50.9	0.009	0.009	0.008	0.009	0.0088
45	57.3	0.010	0.012	0.009	0.010	0.0103
50	63.7	0.012	0.017	0.009	0.012	0.0125
55	70.2	0.014	0.018	0.011	0.013	0.0140
60	76.7	0.019	0.021	0.012	0.019	0.0178

Table E.5: U-80-5

Load (kip)	Bar Stress (ksi)	Crack Widths (in.)*				
		Crack 1	Crack 2	Crack 3	Crack 4	Average
15	19.2	0.004	0.006	0.004	0.005	0.0048
20	25.7	0.004	0.007	0.005	0.005	0.0053
25	32.1	0.005	0.009	0.005	0.005	0.0060
30	38.6	0.007	0.010	0.006	0.011	0.0085
35	45.1	0.011	0.012	0.013	0.013	0.0123
40	51.6	0.014	0.013	0.014	0.013	0.0135
45	58.2	0.012	0.011	0.014	0.016	0.0133
50	64.8	0.013	0.013	0.016	0.020	0.0155
55	71.4	0.015	0.013	0.018	0.020	0.0165
60	78.1	0.017	0.013	0.019	0.022	0.0178

*****Crack location not measured

Table E.6: U-100-5

Load (kip)	Bar Stress (ksi)	Crack Widths (in.)				
		74" N	66" N	64" S	85" S	Average
15	19.2	0.002	0.004	0.003	0.003	0.0030
20	25.7	0.005	0.007	0.004	0.005	0.0053
25	32.1	0.005	0.008	0.004	0.006	0.0058
30	38.6	0.007	0.009	0.004	0.011	0.0078
35	45.1	0.008	0.014	0.005	0.016	0.0108
40	51.6	0.010	0.017	0.008	0.017	0.0130
45	58.2	0.010	0.020	0.010	0.017	0.0143
50	64.8	0.012	0.023	0.010	0.019	0.0160
55	71.4	0.015	0.023	0.012	0.025	0.0188
60	78.1	0.016	0.030	0.012	0.028	0.0215

Table E.7: U-120-5

Load (kip)	Bar Stress (ksi)	Crack Widths (in.)				
		90" N	78" N	70" S	79" S	Average
20	25.7	0.005	0.006	0.007	0.007	0.0063
25	32.1	0.007	0.009	0.007	0.017	0.0100
30	38.6	0.009	0.011	0.009	0.019	0.0120
35	45.1	0.010	0.011	0.009	0.024	0.0135
40	51.6	0.013	0.015	0.010	0.024	0.0155
45	58.2	0.014	0.018	0.012	0.025	0.0173
50	64.8	0.016	0.018	0.018	0.025	0.0193
55	71.4	0.016	0.019	0.018	0.030	0.0208
60	78.1	0.019	0.025	0.018	0.035	0.0243

Table E.8: U-80-5-M

Load (kip)	Bar Stress (ksi)	Crack Widths (in.)				
		78.5" N	48.5" N	56.5" S	68" S	Average
15	19.4	0.005	0.004	0.004	0.003	0.0040
20	25.9	0.007	0.006	0.006	0.005	0.0060
25	32.4	0.010	0.011	0.008	0.007	0.0090
30	39.0	0.012	0.012	0.010	0.007	0.0103
35	45.5	0.013	0.012	0.013	0.008	0.0115
40	52.2	0.016	0.015	0.014	0.011	0.0140
45	58.8	0.018	0.017	0.015	0.011	0.0153
50	65.5	0.021	0.024	0.018	0.012	0.0188

Table E.9: U-100-5-M

Load (kip)	Bar Stress (ksi)	Crack Widths (in.)				
		87.5" N	72" N	66.5" S	72.5" S	Average
20	25.9	0.006	0.007	0.006	0.005	0.0060
25	32.4	0.007	0.009	0.010	0.007	0.0083
30	39.0	0.015	0.012	0.011	0.011	0.0123
35	45.5	0.017	0.013	0.014	0.014	0.0145
40	52.2	0.019	0.020	0.015	0.015	0.0173
45	58.8	0.021	0.022	0.018	0.017	0.0195
50	65.5	0.022	0.025	0.022	0.017	0.0215
55	72.3	0.028	0.025	0.027	0.021	0.0253

Table E.10: U-120-5-M

Load (kip)	Bar Stress (ksi)	Crack Widths (in.)				
		80" N	71" N	64" S	78" S	Average
15	19.4	0.003	0.004	0.004	0.006	0.0043
20	25.9	0.008	0.007	0.007	0.009	0.0078
25	32.4	0.011	0.010	0.014	0.010	0.0113
30	39.0	0.015	0.011	0.015	0.013	0.0135
35	45.5	0.016	0.013	0.018	0.014	0.0153
40	52.2	0.019	0.014	0.022	0.014	0.0173
45	58.8	0.024	0.015	0.025	0.015	0.0198
50	65.5	0.029	0.019	0.027	0.015	0.0225
55	72.3	0.031	0.021	0.028	0.015	0.0238
60	79.1	0.033	0.025	0.028	0.016	0.0255

Table E.11: C3/60/2-40-5-50

Load (kip)	Bar Stress (ksi)	Crack Widths (in.)				
		68" N	29" N	28" S	55" S	Average
15	19.0	0.005	0.005	0.003	0.004	0.0043
20	25.3	0.007	0.007	0.005	0.006	0.0063
25	31.7	0.010	0.010	0.006	0.008	0.0085
30	38.1	0.012	0.013	0.007	0.011	0.0108
35	44.5	0.013	0.014	0.010	0.015	0.0130
40	50.9	0.016	0.015	0.010	0.017	0.0145
45	57.3	0.018	0.015	0.013	0.019	0.0163
50	63.7	0.019	0.016	0.014	0.019	0.0170

Table E.12: C3/60/3-40-5-50

Load (kip)	Bar Stress (ksi)	Crack Widths (in.)				
		37" N	27" N	37" S	56" S	Average
15	19.0	0.003	0.002	0.003	0.003	0.0028
20	25.3	0.004	0.003	0.006	0.004	0.0043
25	31.7	0.008	0.005	0.006	0.006	0.0063
30	38.1	0.010	0.006	0.007	0.010	0.0083
35	44.5	0.012	0.006	0.009	0.011	0.0095
40	50.9	0.013	0.007	0.010	0.013	0.0108
45	57.3	0.014	0.007	0.011	0.015	0.0118
50	63.7	0.014	0.010	0.015	0.017	0.0140

Table E.13: C3/60-40-5-100

Load (kip)	Bar Stress (ksi)	Crack Widths (in.)				
		73" N	29" N	37" S	56" S	Average
15	19.0	0.003	0.003	0.004	0.002	0.0030
20	25.3	0.003	0.006	0.005	0.005	0.0048
25	31.7	0.003	0.007	0.009	0.007	0.0065
30	38.1	0.004	0.007	0.010	0.009	0.0075
35	44.5	0.004	0.010	0.012	0.011	0.0093
40	50.9	0.006	0.014	0.014	0.012	0.0115
45	57.3	0.006	0.015	0.015	0.014	0.0125
50	63.7	0.009	0.017	0.016	0.017	0.0148
55	70.2	0.009	0.018	0.020	0.019	0.0165

Table E.14: C3/100-40-5-100

Load (kip)	Bar Stress (ksi)	Crack Widths (in.)				
		73" N	29" N	37" S	56" S	Average
15	19.0	0.004	0.005	0.003	0.005	0.0043
20	25.3	0.005	0.006	0.006	0.005	0.0055
25	31.7	0.008	0.006	0.007	0.007	0.0070
30	38.1	0.010	0.006	0.009	0.009	0.0085
35	44.5	0.011	0.013	0.011	0.009	0.0110
40	50.9	0.013	0.014	0.014	0.012	0.0133
45	57.3	0.017	0.017	0.016	0.013	0.0158
50	63.7	0.019	0.020	0.017	0.015	0.0178
55	70.2	0.024	0.023	0.019	0.017	0.0208

Table E.15: C3/60-60-5-50

Load (kip)	Bar Stress (ksi)	Crack Widths (in.)				
		70" N	49" N	71" S	87" S	Average
20	25.4	0.006	0.004	0.008	0.006	0.0060
25	31.7	0.010	0.005	0.011	0.009	0.0088
30	38.1	0.012	0.007	0.014	0.012	0.0113
35	44.5	0.013	0.009	0.016	0.013	0.0128
40	50.9	0.017	0.013	0.019	0.017	0.0165
45	57.3	0.020	0.015	0.021	0.018	0.0185
50	63.7	0.020	0.017	0.025	0.022	0.0210
55	70.2	0.025	0.021	0.027	0.022	0.0238
60	76.7	0.030	0.022	0.031	0.026	0.0273

Table E.16: C3/60-60-5-100

Load (kip)	Bar Stress (ksi)	Crack Widths (in.)				
		71" N	55.5" N	41" S	57" S	Average
15	19.0	0.004	0.005	0.003	0.003	0.0038
20	25.4	0.005	0.006	0.005	0.004	0.0050
25	31.7	0.010	0.011	0.008	0.005	0.0085
30	38.1	0.011	0.014	0.011	0.006	0.0105
35	44.5	0.014	0.016	0.014	0.009	0.0133
40	50.9	0.016	0.021	0.017	0.009	0.0158
45	57.3	0.018	0.022	0.018	0.009	0.0168
50	63.7	0.020	0.024	0.021	0.011	0.0190
55	70.2	0.025	0.027	0.023	0.012	0.0218
60	76.7	0.026	0.032	0.025	0.012	0.0238

Table E.17: C3/60-60-5-150

Load (kip)	Bar Stress (ksi)	Crack Widths (in.)				
		54.5" N	42.5" N	40.25" S	65" S	Average
15	19.0	0.003	0.002	0.002	0.003	0.0025
20	25.4	0.004	0.004	0.008	0.006	0.0055
25	31.7	0.005	0.005	0.013	0.006	0.0073
30	38.1	0.008	0.006	0.014	0.009	0.0093
35	44.5	0.009	0.007	0.015	0.012	0.0108
40	50.9	0.010	0.010	0.020	0.012	0.0130
45	57.3	0.010	0.010	0.020	0.016	0.0140
50	63.7	0.015	0.010	0.022	0.017	0.0160
55	70.2	0.016	0.010	0.030	0.019	0.0188
60	76.7	0.016	0.014	0.030	0.019	0.0198
65	83.1	0.016	0.014	0.032	0.020	0.0205
70	89.6	0.016	0.018	0.033	0.021	0.0220

Table E.18: C3/100-60-5-100

Load (kip)	Bar Stress (ksi)	Crack Widths (in.)				
		80.25" N	55.25" N	55.25" S	74.75" S	Average
15	19.0	0.005	0.004	0.003	0.005	0.0043
20	25.4	0.007	0.007	0.006	0.009	0.0073
25	31.7	0.010	0.009	0.007	0.010	0.0090
30	38.1	0.010	0.009	0.011	0.011	0.0103
35	44.5	0.012	0.010	0.012	0.018	0.0130
40	50.9	0.014	0.011	0.018	0.020	0.0158
45	57.3	0.019	0.013	0.018	0.020	0.0175
50	63.7	0.019	0.014	0.019	0.028	0.0200
55	70.2	0.019	0.018	0.021	0.028	0.0215
60	76.7	0.023	0.020	0.025	0.032	0.0250
65	83.1	0.029	0.023	0.025	0.033	0.0275
70	89.6	0.029	0.024	0.031	0.036	0.0300

Table E.19: C4/60-60-5-100

Load (kip)	Bar Stress (ksi)	Crack Widths (in.)				
		85" N	60.5" N	58" S	81" S	Average
15	19.0	0.005	0.005	0.004	0.006	0.0050
20	25.4	0.007	0.005	0.006	0.007	0.0063
25	31.7	0.010	0.006	0.011	0.011	0.0095
30	38.1	0.010	0.007	0.011	0.012	0.0100
35	44.5	0.012	0.009	0.013	0.013	0.0118
40	50.9	0.014	0.011	0.017	0.017	0.0148
45	57.3	0.015	0.011	0.018	0.019	0.0158
50	63.7	0.018	0.013	0.019	0.023	0.0183
55	70.2	0.018	0.015	0.023	0.026	0.0205
60	76.7	0.020	0.017	0.026	0.029	0.0230
65	83.1	0.025	0.018	0.028	0.030	0.0253
70	89.6	0.026	0.020	0.030	0.034	0.0275

Table E.20: C3/60-80-5-50

Load (kip)	Bar Stress (ksi)	Crack Widths (in.)				
		73" N	46" N	46" S	67" S	Average
20	25.2	0.007	0.005	0.006	0.005	0.0058
25	31.6	0.010	0.008	0.006	0.006	0.0075
30	37.9	0.014	0.009	0.009	0.010	0.0105
35	44.3	0.015	0.009	0.010	0.012	0.0115
40	50.7	0.017	0.010	0.011	0.015	0.0133
45	57.1	0.021	0.012	0.014	0.014	0.0153
50	63.5	0.022	0.015	0.015	0.020	0.0180
55	70.0	0.024	0.016	0.018	0.020	0.0195
60	76.4	0.029	0.016	0.019	0.025	0.0223

APPENDIX F: AS-BUILT DIMENSIONS (SERIES V)

Dimensions were measured for all slabs after failure at the locations shown in Figure F.1. The total slab width b_w accounts for four (4) splices of No. 5 bars, or 5 in. Bottom cover is measured between the two inner splices for the south, middle, and north locations. Percent error values indicate comparisons between the measured values and the original design values specified in Table F.1.

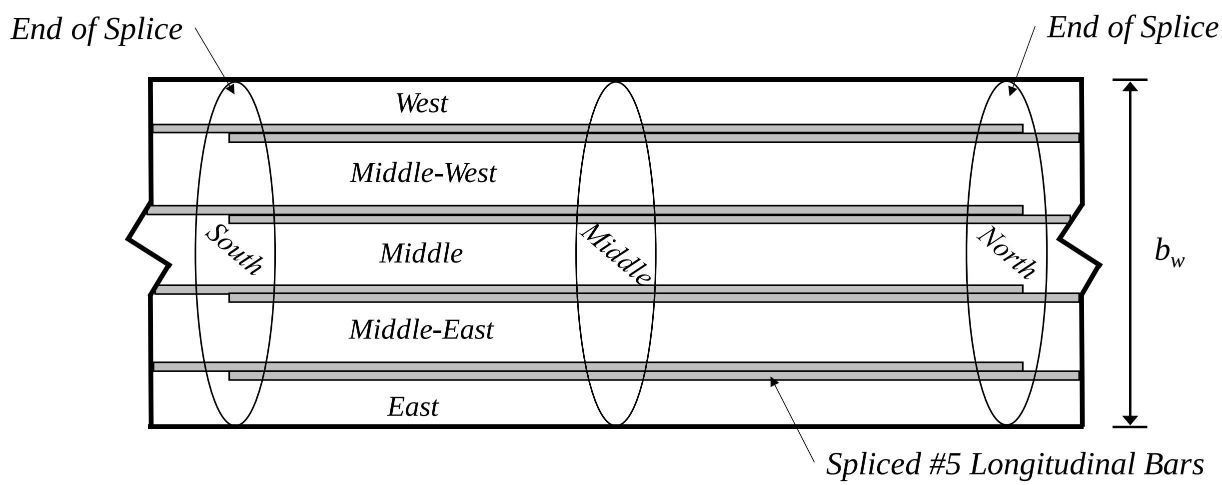

Figure F.1: Slab Splice Region Layout for As-Built Dimensions

Table F.1: Slab Design Dimensions

Location Along Width	Design Value (in.)
West	2-3/8
Middle-West	4-3/4
Middle	4-3/4
Middle-East	4-3/4
East	2-3/8
Total (b_w)	24
Bottom Cover (c_b)	3/4

Table F.2: S-40-5

Transverse Location	Longitudinal Location					
	South (in.)	% Error	Middle (in.)	% Error	North (in.)	% Error
West	2.464	3.7%	1.872	-21.2%	1.875	-21.1%
Middle-West	5.829	22.7%	5.106	7.5%	5.553	16.9%
Middle	6.423	35.2%	5.838	22.9%	6.813	43.4%
Middle-East	4.958	4.4%	4.263	-10.3%	4.628	-2.6%
East	1.969	-17.1%	2.177	-8.3%	2.935	23.6%
Total	26.643	11.0%	24.256	1.1%	26.804	11.7%
Bottom Cover	0.789	5.2%	0.786	4.8%	0.824	9.9%

Table F.3: S-60-5

Transverse Location	Longitudinal Location					
	South (in.)	% Error	Middle (in.)	% Error	North (in.)	% Error
West	2.115	-10.9%	2.078	-12.5%	2.026	-14.7%
Middle-West	4.759	0.2%	4.985	4.9%	5.210	9.7%
Middle	5.481	15.4%	5.156	8.5%	4.863	2.4%
Middle-East	4.867	2.5%	4.841	1.9%	4.731	-0.4%
East	2.011	-15.3%	1.989	-16.3%	2.434	2.5%
Total	24.233	1.0%	24.049	0.2%	24.264	1.1%
Bottom Cover	0.759	1.2%	.777	3.6%	.893	19.1%

Table F.4: S-80-5

Transverse Location	Longitudinal Location					
	South (in.)	% Error	Middle (in.)	% Error	North (in.)	% Error
West	2.370	-0.2%	2.344	-1.3%	2.715	14.3%
Middle-West	4.917	3.5%	4.927	3.7%	5.076	6.9%
Middle	4.762	0.2%	4.904	3.2%	5.098	7.3%
Middle-East	5.014	5.5%	4.768	0.4%	4.651	-2.1%
East	1.998	-15.9%	1.783	-24.9%	1.834	-22.8%
Total	24.059	0.2%	23.724	-1.2%	24.373	1.6%
Bottom Cover	0.744	-0.8%	0.804	7.1%	0.787	4.9%

Table F.5: S-100-5

Transverse Location	Longitudinal Location					
	South (in.)	% Error	Middle (in.)	% Error	North (in.)	% Error
West	0.916	-61.4%	1.840	-22.5%	2.395	0.8%
Middle-West	4.921	3.6%	4.659	-1.9%	4.424	-6.9%
Middle	4.933	3.9%	5.234	10.2%	5.470	15.2%
Middle-East	5.284	11.2%	4.998	5.2%	4.573	-3.7%
East	2.719	14.5%	2.261	-4.8%	2.112	-11.1%
Total	23.773	-0.9%	23.992	0.0%	23.973	-0.1%
Bottom Cover	0.732	-2.4%	0.767	2.3%	0.790	5.3%

APPENDIX G: LOAD-DEFLECTION RESPONSE (SERIES V)

Load-deflection responses are constructed from end load and end deflection data for all specimens in this testing program. All load and deflection values are averages of the north and south ends, unless noted otherwise. The stress-strain response for the longitudinal steel in each specimen is provided to give an indication of longitudinal steel behavior at failure. Maximum load, maximum midspan deflection, maximum end deflection, and bar stress at failure are also provided for each specimen.

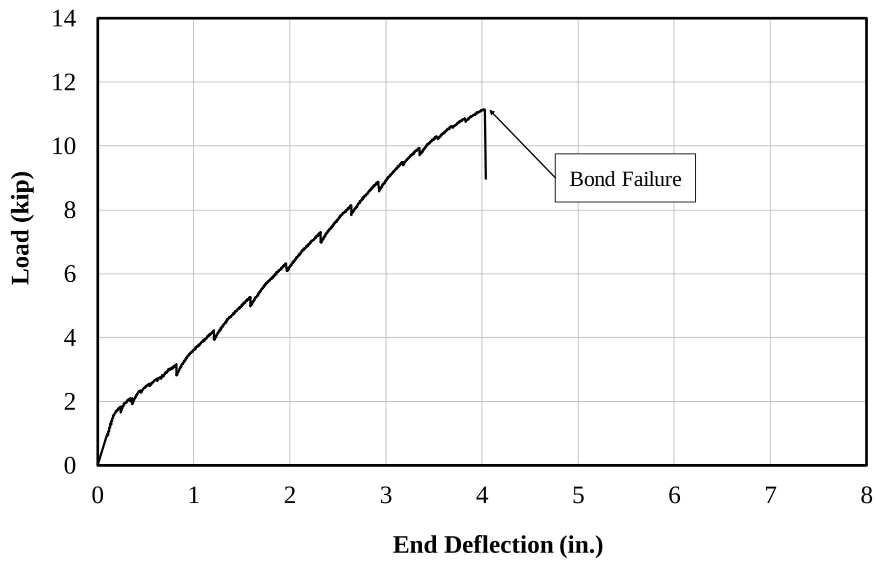

a) Load-Deflection*

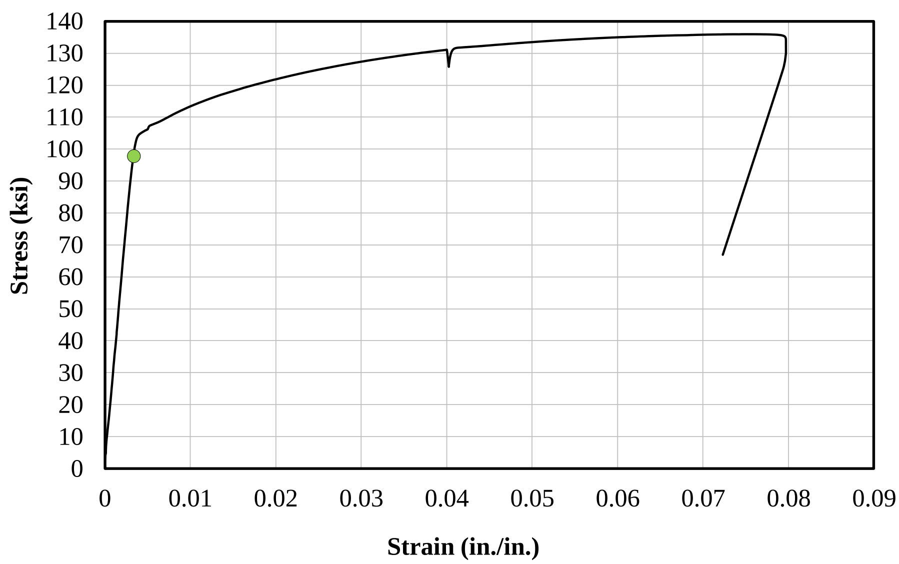

b) Stress-Strain (A615 Gr. 100 No. 5)

Figure G.1: S-40-5

*Response reflects the south end deflection and twice the southeast load cell reading.

Table G.1: S-40-5 Maximum Testing Values

Load (kip)	Avg. End Deflection (in.)	Avg. Midspan Deflection (in.)	Bar Stress (ksi)
11.1	4.0	2.2	97.9

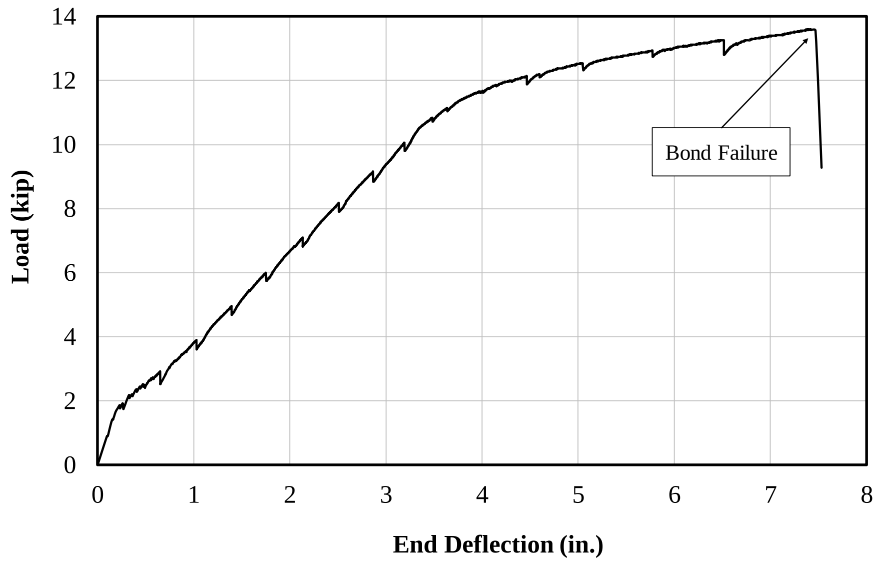

a) Load-Deflection*

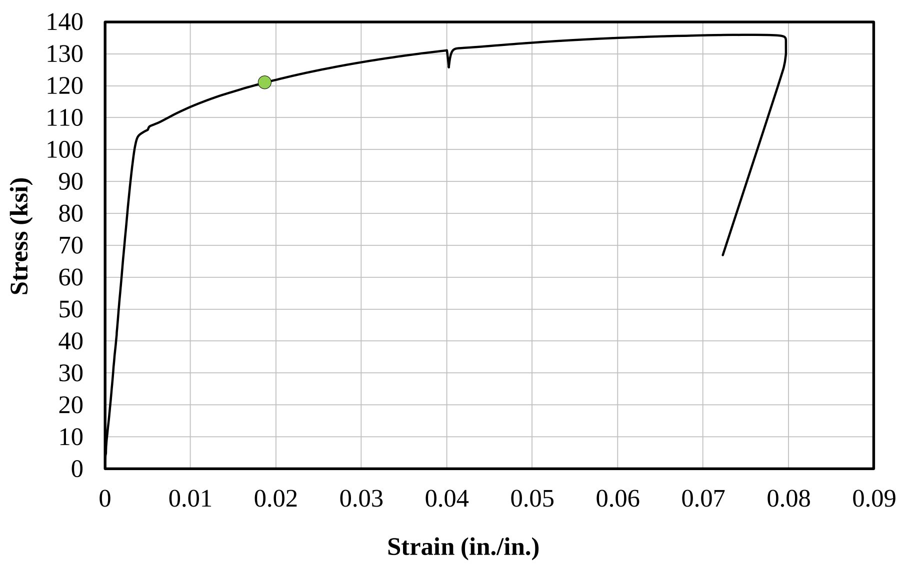

b) Stress-Strain (A615 Gr. 100 No. 5)

Figure G.2: S-60-5

*Response reflects the north end deflection and twice the northwest load cell reading.

Table G.2: S-60-5 Maximum Testing Values

Load (kip)	Avg. End Deflection (in.)	Avg. Midspan Deflection (in.)	Bar Stress (ksi)
13.6	7.5	3.7	121.0

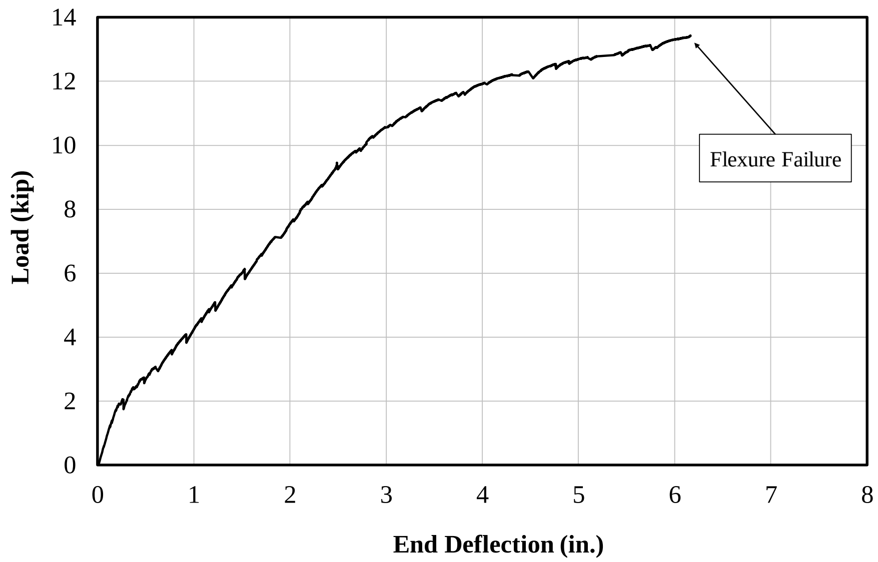

a) Load-Deflection*

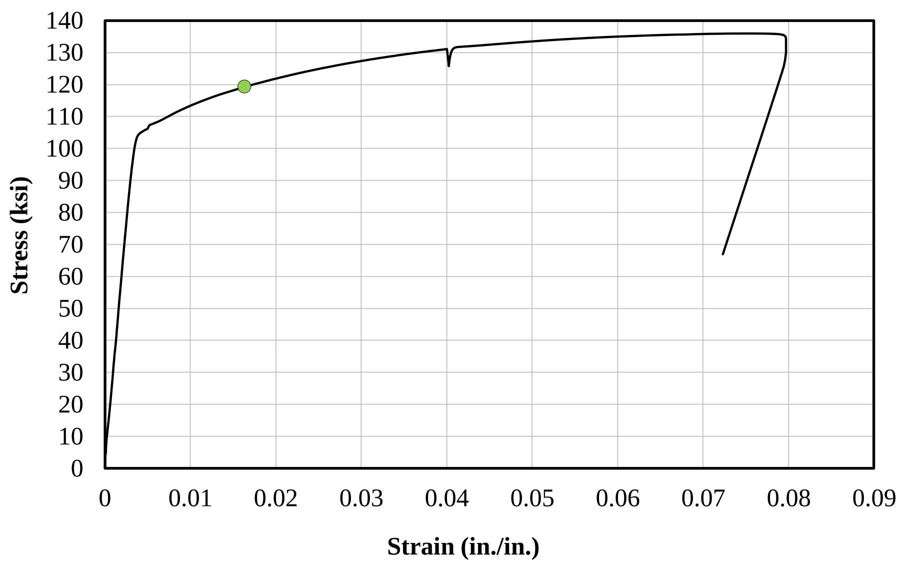

b) Stress-Strain (A615 Gr. 100 No. 5)

Figure G.3: S-80-5

*Response reflects the south end deflection and twice the southwest load cell reading.

Table G.3: S-80-5 Maximum Testing Values

Load (kip)	Avg. End Deflection (in.)	Avg. Midspan Deflection (in.)	Bar Stress (ksi)
13.4	6.2	2.9	119.2

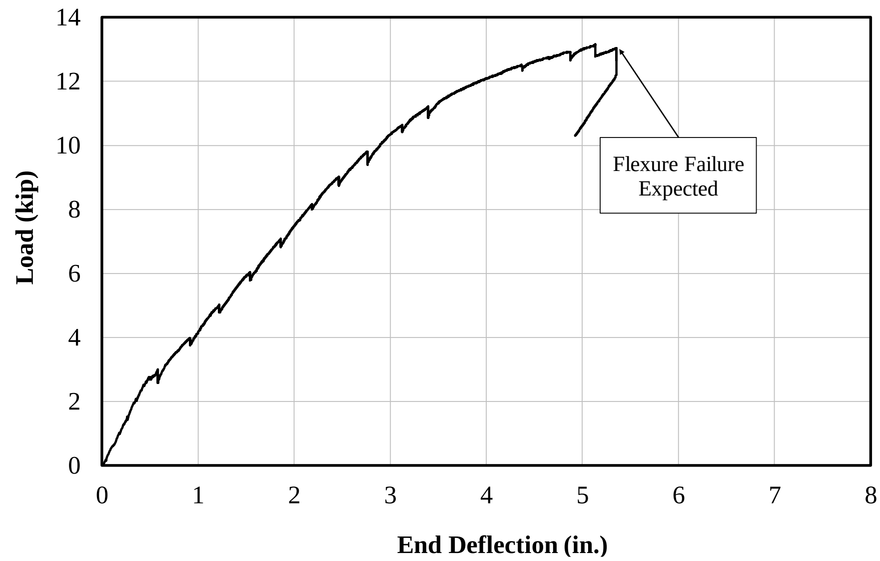

a) Load-Deflection*

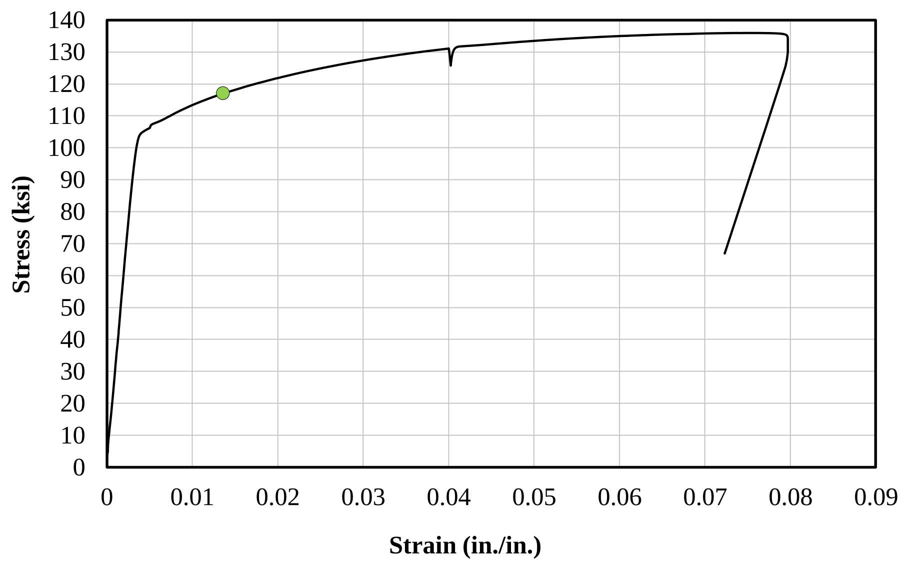

b) Stress-Strain (A615 Gr. 100 No. 5)

Figure G.4: S-100-5

*Response reflects the south end deflection and twice the southwest load cell reading.

Table G.4: S-100-5 Maximum Testing Values

Load (kip)	Avg. End Deflection (in.)	Avg. Midspan Deflection (in.)	Bar Stress (ksi)
13.2	5.4	2.2	117.0

APPENDIX H: CRACK WIDTH MEASUREMENTS (SERIES V)

All cracks are measured from specimen centerline and remain within the constant moment region. Four (4) cracks were monitored in each test. The average crack width growth was plotted for each test specimen. A typical test specimen showing any regions of interest and locations of these cracks is provided in Figure H.1.

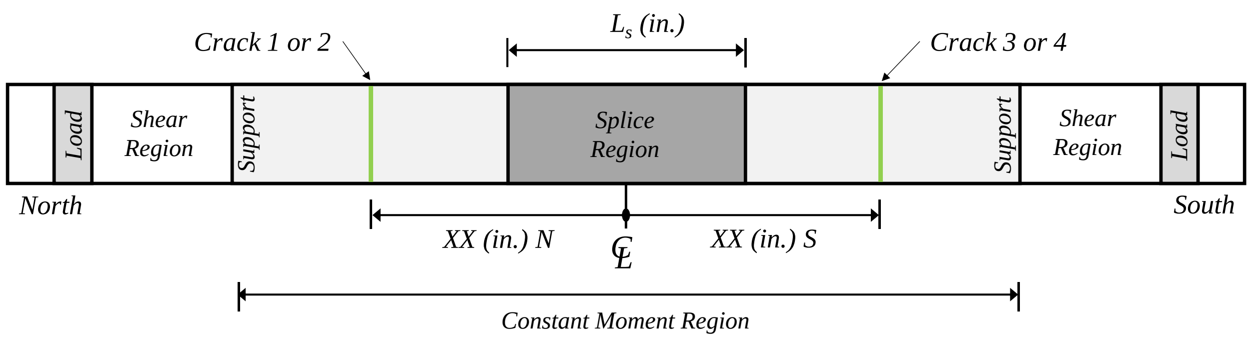

Figure H.1: Typical Specimen Crack Monitoring Diagram

Table H.1: S-40-5 Crack Width Summary

Load (kip)	Moment (ft-kip)	Bar Stress (ksi)	Crack Widths (1/1000 in.)					
			Crack 1 33” N	Crack 2 20” N	Crack 3 19.5” S	Crack 4 30” S	Max.	Avg.
2.0	8.0	17.6	3	6	3	3	6	4
3.0	12.0	26.3	4	9	4	5	9	6
4.0	16.0	35.1	7	10	5	6	10	7
5.0	20.0	43.8	9	11	7	8	11	9
6.0	24.0	52.5	10	13	9	10	13	11
7.0	28.0	61.3	11	15	9	14	15	12
8.0	32.0	70.1	14	15	12	16	16	14

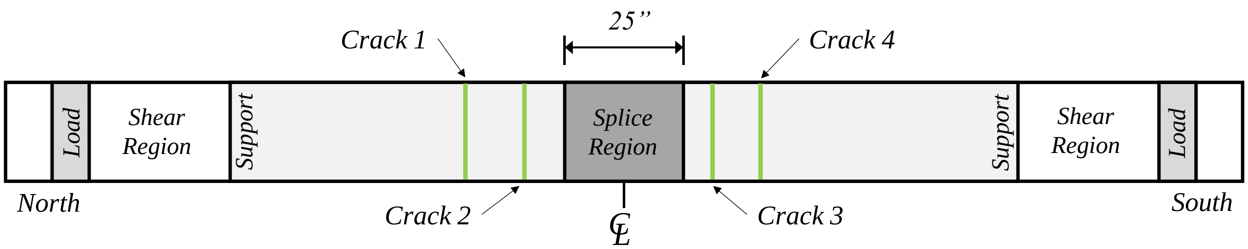

a) Crack Locations

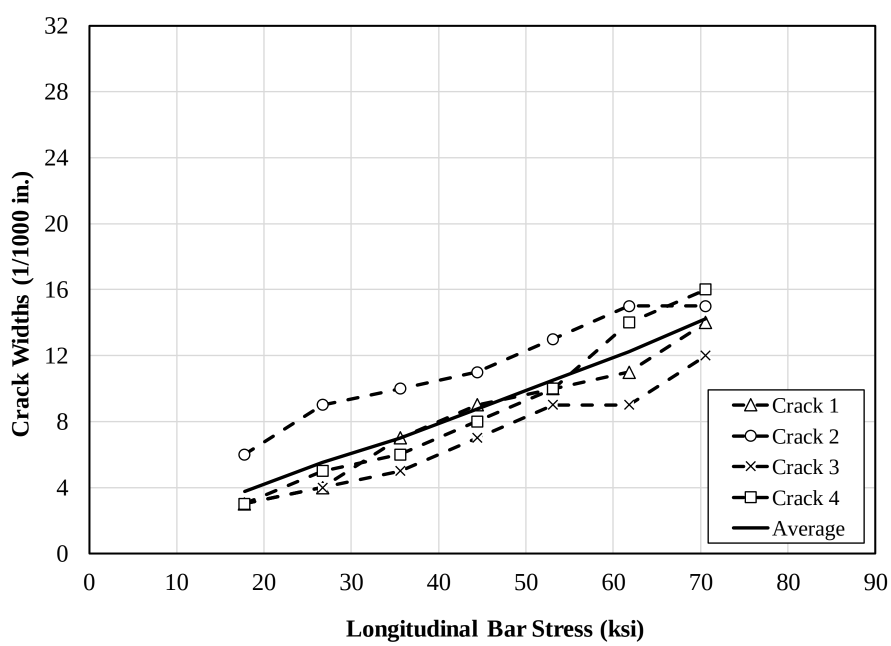

b) Crack Widths

Figure H.2: S-40-5

Table H.2: S-60-5 Crack Width Summary

Load (kip)	Moment (ft-kip)	Bar Stress (ksi)	Crack Widths (1/1000 in.)					
			Crack 1 48" N	Crack 2 37" N	Crack 3 23.5" S	Crack 4 39.5" S	Max.	Avg.
2.0	8.1	17.8	2	2	3	3	3	3
3.0	12.0	26.7	4	5	5	4	5	5
4.0	16.0	35.6	8	5	6	6	8	6
5.0	20.0	44.4	11	8	10	8	11	9
6.0	24.0	53.1	23	8	10	11	23	13
7.0	28.0	61.8	27	11	12	14	27	16
8.0	32.0	70.6	29	12	16	16	29	18
9.0	36.0	79.3	31	13	18	18	31	20

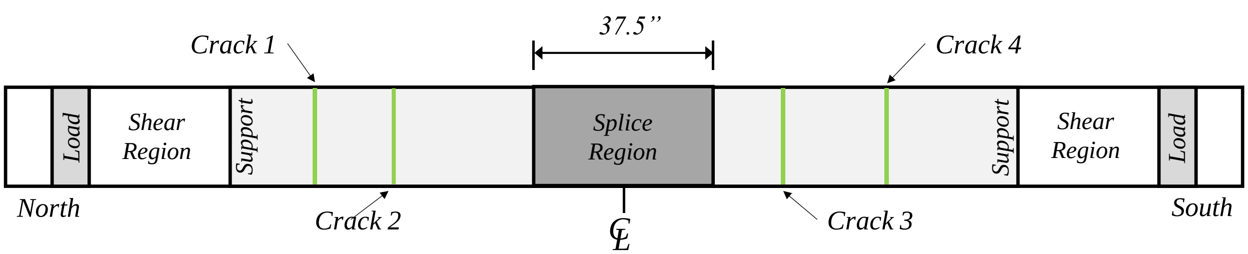

a) Crack Locations

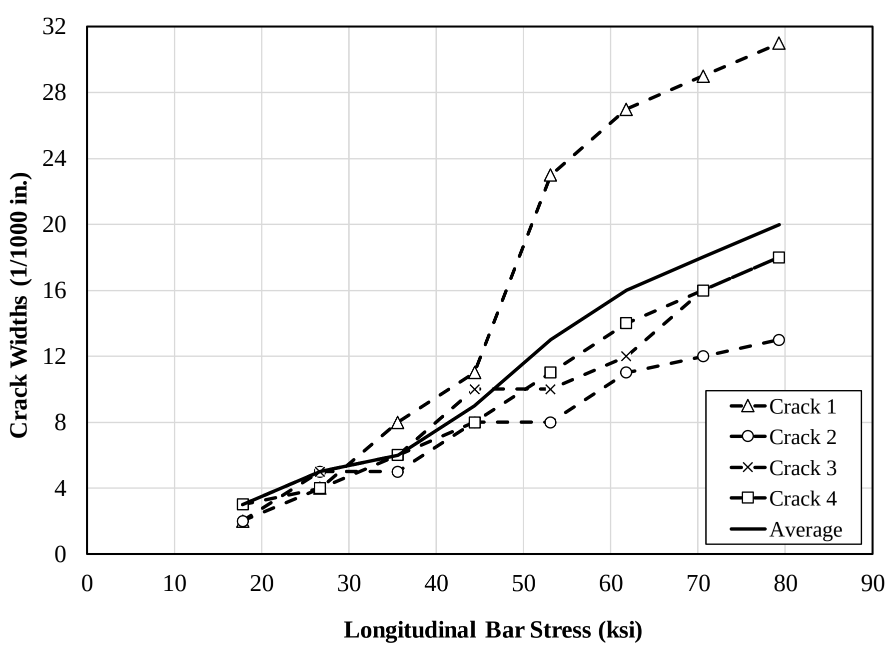

b) Crack Widths

Figure H.3: S-60-5

Table H.3: S-80-5 Crack Width Summary

Load (kip)	Moment (ft-kip)	Bar Stress (ksi)	Crack Widths (1/1000 in.)					
			Crack 1 50" N	Crack 2 31" N	Crack 3 30.5" S	Crack 4 46" S	Max.	Avg.
2.0	8.0	17.8	4	3	2	3	4	3
3.0	12.0	26.7	5	4	2	4	5	4
4.0	16.0	35.6	6	5	2	6	6	5
5.0	20.0	44.4	10	8	3	9	10	8
6.0	24.0	53.1	10	10	3	10	10	8
7.0	28.0	61.8	13	13	5	11	13	11

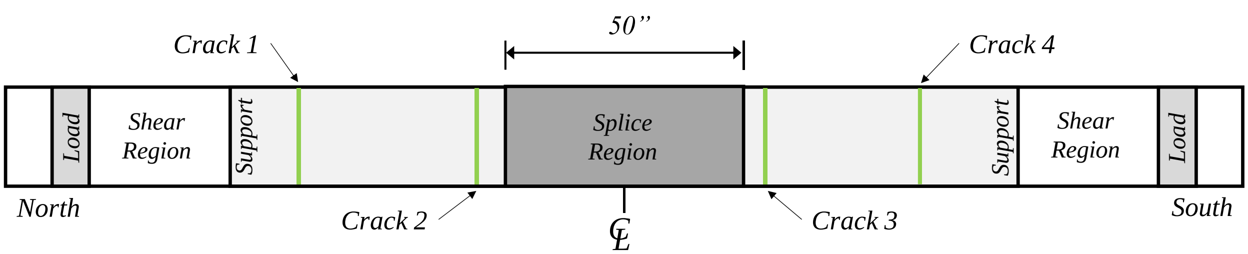

a) Crack Locations

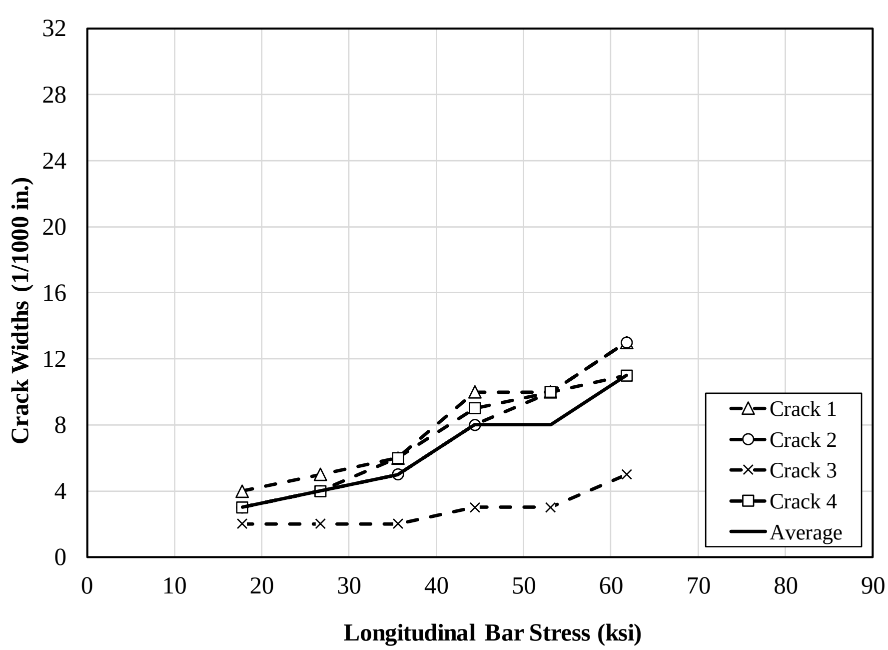

b) Crack Widths

Figure H.4: S-80-5

Table H.4: S-100-5 Crack Width Summary

Load (kip)	Moment (ft-kip)	Bar Stress (ksi)	Crack Widths (1/1000 in.)					
			Crack 1 56” N	Crack 2 41” N	Crack 3 34” S	Crack 4 46” S	Max.	Avg.
2.7	11.0	24.0	5	4	4	8	8	5
3.9	15.7	34.6	9	8	7	9	9	8
5.0	20.0	44.3	10	9	9	13	13	10
6.0	23.9	52.9	12	11	11	17	17	13
7.0	28.0	61.7	14	16	12	18	18	15
8.0	31.8	70.5	20	18	17	23	23	20
10.0	40.0	88.1	21	22	17	26	26	22

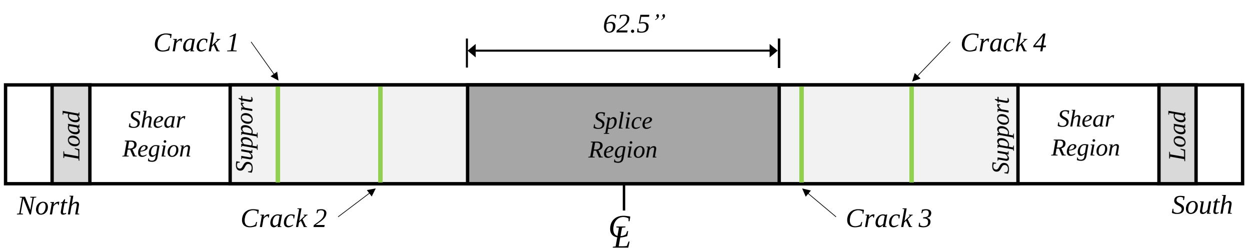

a) Crack Locations

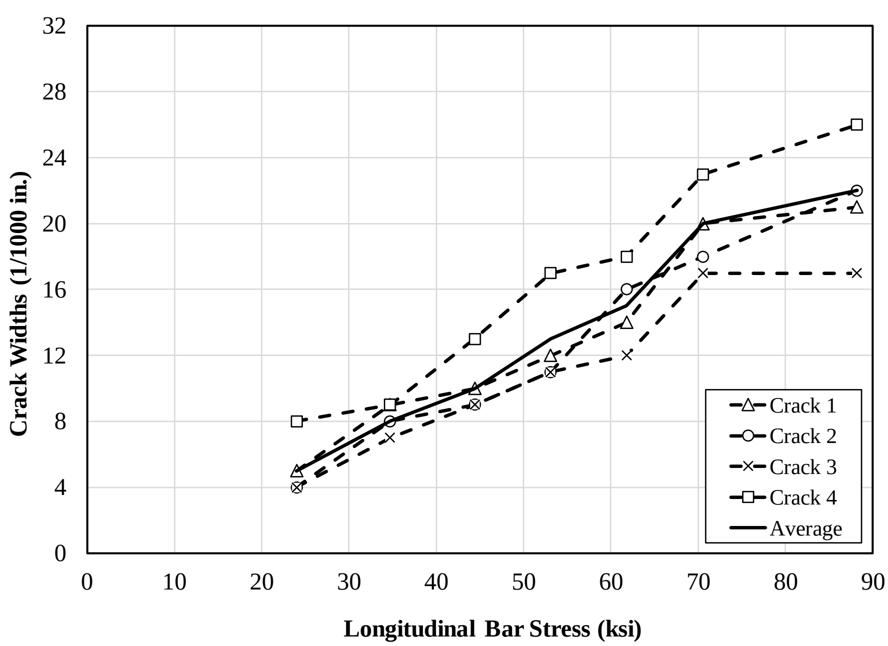

b) Crack Widths

Figure H.5: S-100-5

APPENDIX I: AS-BUILT DIMENSIONS (SERIES VI-VII)

Dimensions were measured for all beams after failure at the locations shown in Figure I.1. The total beam width b_w accounts for three (3) splices of No. 8 bars, or 6 in. Bottom cover is measured along the middle splice for the south, middle, and north longitudinal locations. Percent error values indicate comparisons between the measured values and the original design values specified in Table I.1.

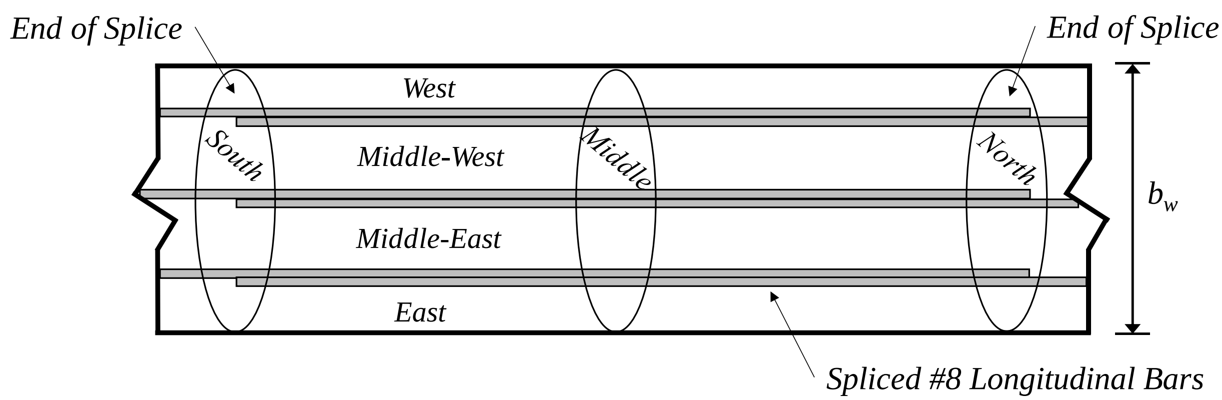

Figure I.1: Beam Splice Region Layout for As-Built Dimensions

Table I.1: Beam Design Dimensions

Location Along Width	Design Value (in.)
West	1-7/8
Middle-West	2
Middle-East	2
East	1-7/8
Total (b_w)	13-3/4
Bottom Cover (c_b)	1-7/8

Table I.2: U-40-5-X

Transverse Location	Longitudinal Location					
	South (in.)	% Error	Middle (in.)	% Error	North (in.)	% Error
West	1.668	-11.0%	1.697	-9.5%	1.738	-7.3%
Middle-West	1.981	-0.9%	1.904	-4.8%	1.717	-14.2%
Middle-East	1.993	-0.3%	2.024	1.2%	2.088	4.4%
East	2.111	12.6%	1.878	0.2%	1.781	-5.0%
Total	13.753	0.0%	13.503	-1.8%	13.324	-3.1%
Bottom Cover	2.081	11.0%	2.039	8.7%	1.823	-2.8%

Table I.3: U-60-5-X

Transverse Location	Longitudinal Location					
	South (in.)	% Error	Middle (in.)	% Error	North (in.)	% Error
West	1.919	2.3%	2.120	13.0%	2.041	8.8%
Middle-West	2.016	0.8%	1.856	-7.2%	1.868	-6.6%
Middle-East	1.652	-17.4%	1.817	-9.2%	2.024	1.2%
East	2.193	16.9%	1.904	1.5%	1.660	-11.5%
Total	13.779	0.2%	13.696	-0.4%	13.592	-1.2%
Bottom Cover	1.871	-0.2%	1.917	2.2%	1.908	1.8%

Table I.4: U-50-5

Transverse Location	Longitudinal Location					
	South (in.)	% Error	Middle (in.)	% Error	North (in.)	% Error
West	1.931	3.0%	1.848	-1.4%	1.682	-10.3%
Middle-West	1.763	-11.9%	1.805	-9.8%	2.124	6.2%
Middle-East	2.137	6.9%	2.187	9.3%	2.207	10.4%
East	1.949	3.9%	2.075	10.7%	1.900	1.3%
Total	13.780	0.2%	13.915	1.2%	13.913	1.2%
Bottom Cover	1.857	-1.0%	1.847	-1.5%	1.815	-3.2%

Table I.5: U-40-10

Transverse Location	Longitudinal Location					
	South (in.)	% Error	Middle (in.)	% Error	North (in.)	% Error
West	2.009	7.1%	1.822	-2.8%	1.674	-10.7%
Middle-West	1.783	-10.9%	1.794	-10.3%	1.853	-7.4%
Middle-East	1.663	-16.9%	1.846	-7.7%	2.201	10.1%
East	2.070	10.4%	2.000	6.7%	2.088	11.4%
Total	13.525	-1.6%	13.462	-2.1%	13.816	0.5%
Bottom Cover	1.893	1.0%	1.916	2.2%	1.888	0.7%

Table I.6: U-60-10

Transverse Location	Longitudinal Location					
	South (in.)	% Error	Middle (in.)	% Error	North (in.)	% Error
West	2.086	11.3%	2.160	15.2%	1.814	-3.3%
Middle-West	2.143	7.1%	2.188	9.4%	2.021	1.1%
Middle-East	1.663	-16.9%	1.893	-5.4%	1.872	-6.4%
East	2.001	6.7%	2.159	15.1%	2.345	25.1%
Total	13.893	1.0%	14.400	4.7%	14.052	2.2%
Bottom Cover	1.952	4.1%	1.982	5.7%	1.934	3.1%

Table I.7: C3/60/2-40-10-25

Transverse Location	Longitudinal Location					
	South (in.)	% Error	Middle (in.)	% Error	North (in.)	% Error
West	1.993	6.3%	2.030	8.2%	2.275	21.3%
Middle-West	1.569	-21.6%	1.802	-9.9%	1.849	-7.6%
Middle-East	1.668	-16.6%	1.756	-12.2%	1.547	-22.7%
East	2.224	18.6%	2.178	16.2%	1.953	4.1%
Total	13.453	-2.2%	13.766	0.1%	13.623	-0.9%
Bottom Cover	2.013	7.3%	2.009	7.1%	1.924	2.6%

Table I.8: C3/60/2-40-10-50

Transverse Location	Longitudinal Location					
	South (in.)	% Error	Middle (in.)	% Error	North (in.)	% Error
West	1.741	-7.1%	1.935	3.2%	2.007	7.0%
Middle-West	1.663	-16.9%	1.922	-3.9%	1.885	-5.8%
Middle-East	1.677	-16.2%	1.563	-21.9%	1.431	-28.5%
East	2.393	27.6%	2.395	27.7%	2.235	19.2%
Total	13.474	-2.0%	13.815	0.5%	13.558	-1.4%
Bottom Cover	2.104	12.2%	1.926	2.7%	1.800	-4.0%

Table I.9: C3/60/3-40-10-50

Transverse Location	Longitudinal Location					
	South (in.)	% Error	Middle (in.)	% Error	North (in.)	% Error
West	2.073	10.5%	2.234	19.1%	2.292	22.2%
Middle-West	1.452	-27.4%	1.574	-21.3%	1.665	-16.8%
Middle-East	1.702	-14.9%	1.633	-18.4%	1.566	-21.7%
East	2.11	12.5%	2.123	13.2%	2.035	8.5%
Total	13.336	-3.0%	13.564	-1.4%	13.557	-1.4%
Bottom Cover	1.795	-4.3%	1.910	1.8%	1.865	-0.5%

Table I.10: C3/60-40-5-150

Transverse Location	Longitudinal Location					
	South (in.)	% Error	Middle (in.)	% Error	North (in.)	% Error
West	2.060	9.9%	1.808	-3.6%	1.722	-8.2%
Middle-West	1.840	-8.0%	1.792	-10.4%	1.831	-8.5%
Middle-East	2.011	0.6%	1.883	-5.9%	1.832	-8.4%
East	2.060	9.9%	2.247	19.8%	2.421	29.1%
Total	13.971	1.6%	13.730	-0.1%	13.806	0.4%
Bottom Cover	1.882	0.4%	1.845	-1.6%	1.910	1.9%

Table I.11: C3/60-40-5-200

Transverse Location	Longitudinal Location					
	South (in.)	% Error	Middle (in.)	% Error	North (in.)	% Error
West	2.478	32.1%	2.369	26.4%	2.069	10.3%
Middle-West	1.768	-11.6%	1.839	-8.1%	2.010	0.5%
Middle-East	1.901	-5.0%	1.857	-7.2%	1.853	-7.4%
East	1.820	-2.9%	2.004	6.9%	2.045	9.0%
Total	13.967	1.6%	14.069	2.3%	13.977	1.6%
Bottom Cover	1.878	0.2%	1.836	-2.1%	1.717	-8.4%

Table I.12: C3/60-50-5-150

Transverse Location	Longitudinal Location					
	South (in.)	% Error	Middle (in.)	% Error	North (in.)	% Error
West	2.117	12.9%	2.113	12.7%	2.072	10.5%
Middle-West	1.680	-16.0%	1.622	-18.9%	1.711	-14.5%
Middle-East	1.798	-10.1%	1.661	-17.0%	1.638	-18.1%
East	2.078	10.8%	2.427	29.4%	2.241	19.5%
Total	13.673	-0.6%	13.823	0.5%	13.662	-0.6%
Bottom Cover	1.824	-2.7%	1.980	5.6%	1.818	-3.0%

Table I.13: C3/60-50-5-200

Transverse Location	Longitudinal Location					
	South (in.)	% Error	Middle (in.)	% Error	North (in.)	% Error
West	1.991	6.2%	1.691	-9.8%	1.743	-7.0%
Middle-West	2.044	2.2%	1.908	-4.6%	1.800	-10.0%
Middle-East	2.074	3.7%	1.969	-1.6%	1.888	-5.6%
East	2.243	19.6%	2.363	26.0%	2.486	32.6%
Total	14.352	4.4%	13.932	1.3%	13.917	1.2%
Bottom Cover	1.815	-3.2%	1.911	1.9%	1.958	4.4%

APPENDIX J: LOAD-DEFLECTION RESPONSE (SERIES VI-VII)

Load-deflection responses are constructed from end load and end deflection data for all specimens in this testing program. All load and deflection values are averages of the north and south ends, unless noted otherwise. The stress-strain response for the longitudinal steel in each specimen is provided to give an indication of longitudinal steel behavior at failure. Maximum load, maximum midspan deflection, maximum end deflection, and bar stress at failure are also provided for each specimen.

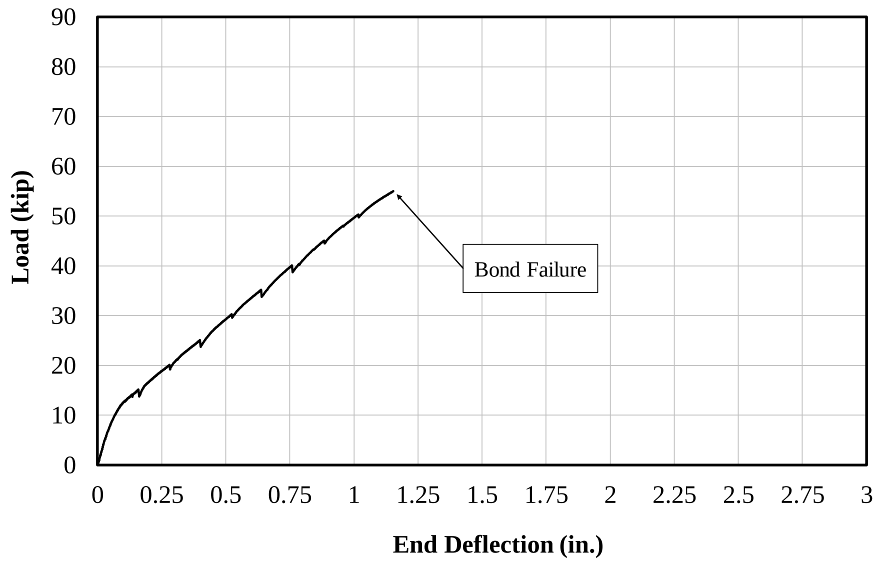

a) Load-Deflection

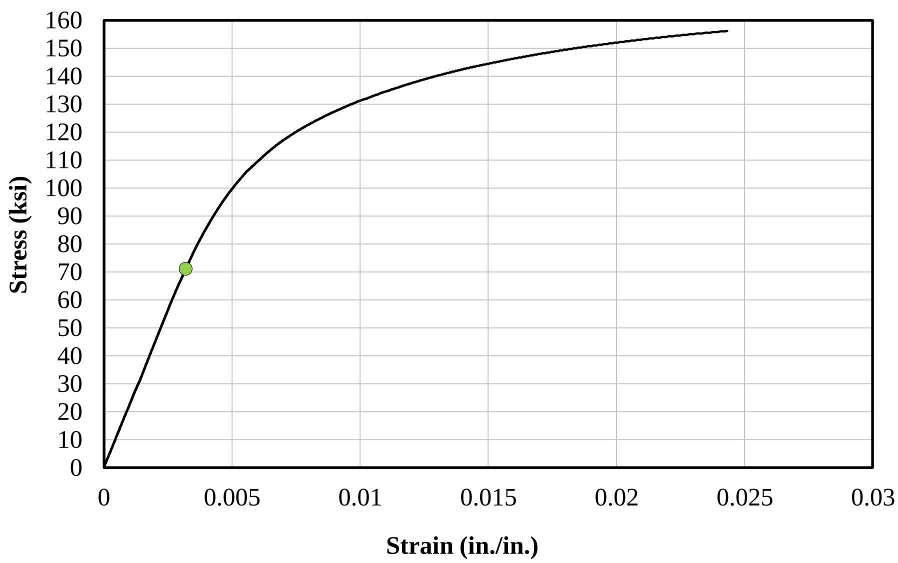

b) Stress-Strain (A1035 Gr. 100 No. 8)

Figure J.1: U-40-5-X

Table J.1: U-40-5-X Maximum Testing Values

Load (kip)	Avg. End Deflection (in.)	Avg. Midspan Deflection (in.)	Bar Stress (ksi)
55.0	1.2	0.9	71.0

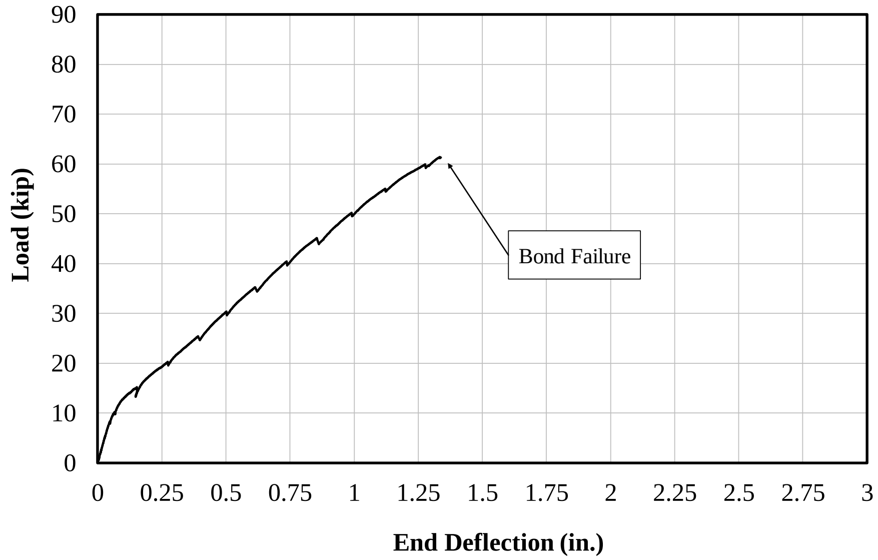

a) Load-Deflection

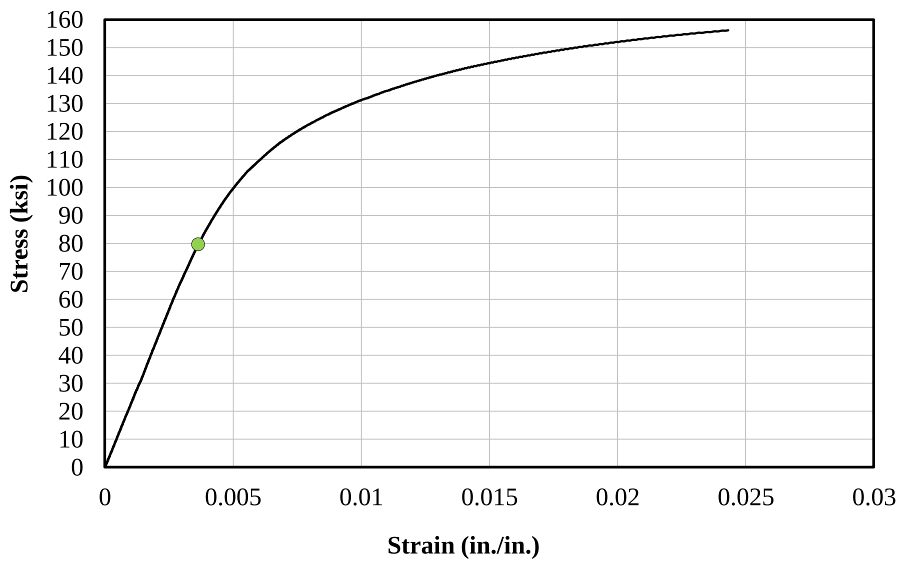

b) Stress-Strain (A1035 Gr. 100 No. 8)

Figure J.2: U-60-5-X

Table J.2: U-60-5-X Maximum Testing Values

Load (kip)	Avg. End Deflection (in.)	Avg. Midspan Deflection (in.)	Bar Stress (ksi)
61.4	1.3	1.1	80.8

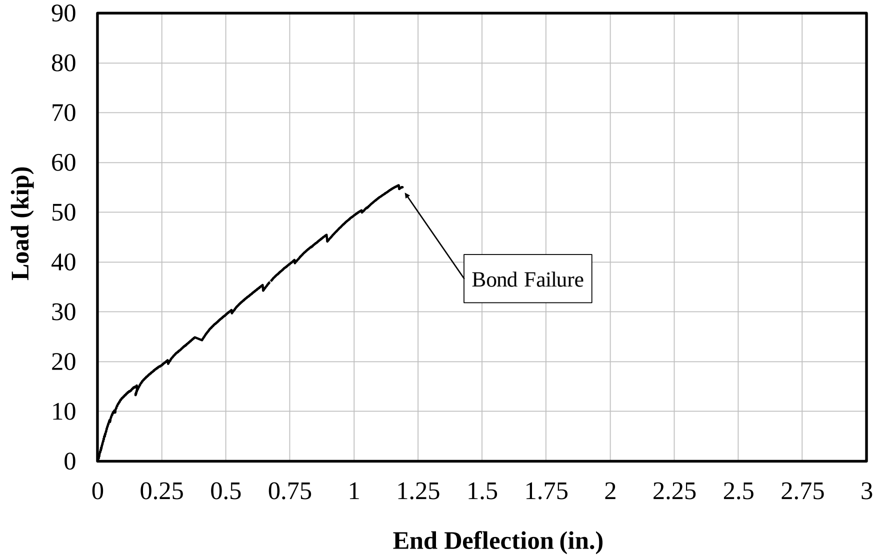

a) Load-Deflection

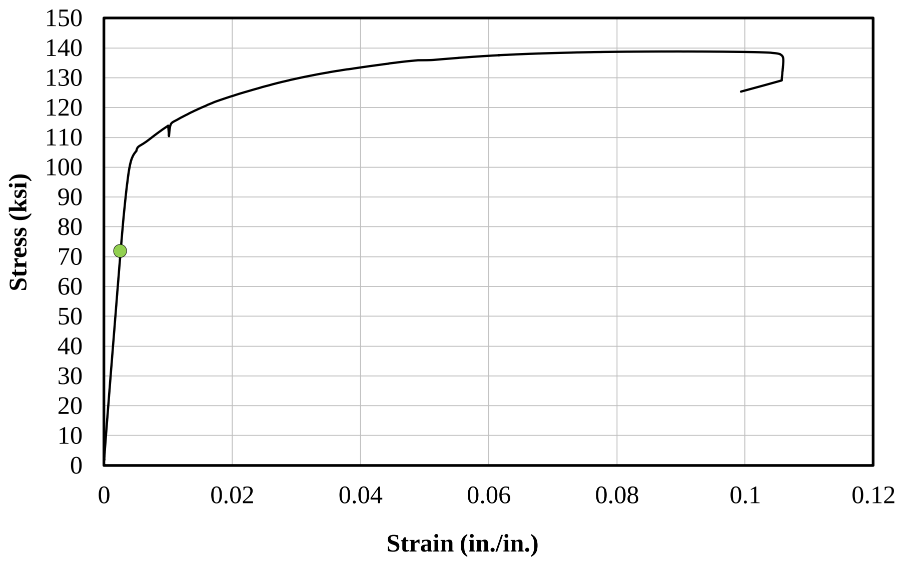

b) Stress-Strain (A615 Gr. 100 No. 8)

Figure J.3: U-50-5

Table J.3: U-50-5 Maximum Testing Values

Load (kip)	Avg. End Deflection (in.)	Avg. Midspan Deflection (in.)	Bar Stress (ksi)
55.5	1.2	1.0	73.2

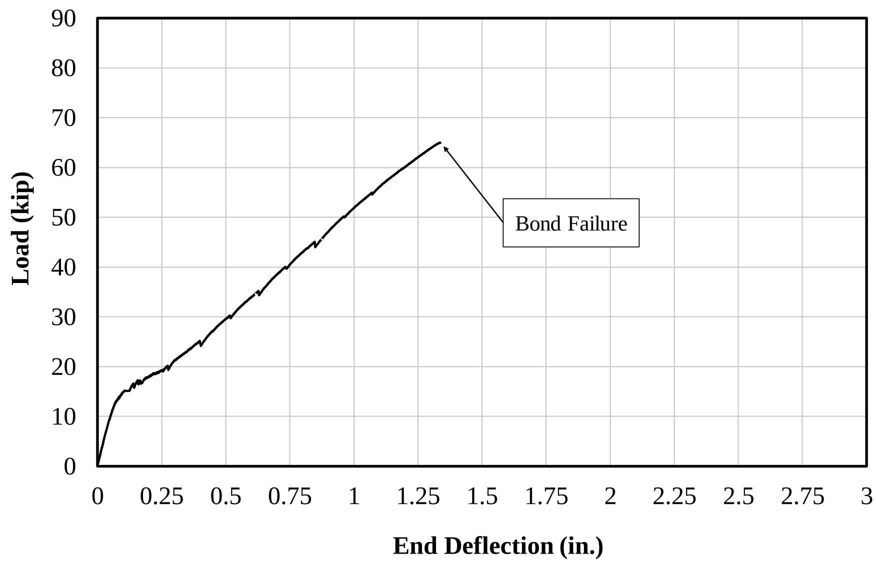

a) Load-Deflection

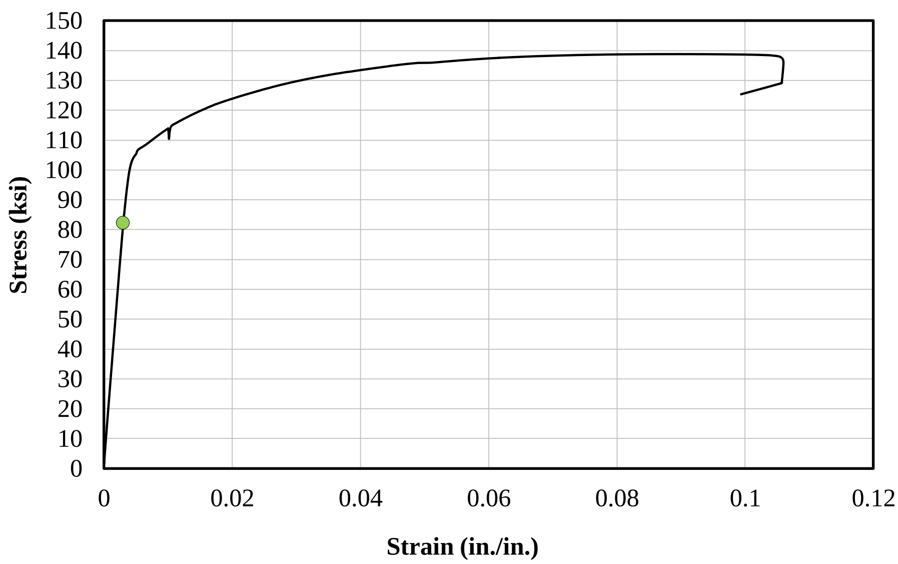

b) Stress-Strain (A615 Gr. 100 No. 8)

Figure J.4: U-40-10

Table J.4: U-40-10 Maximum Testing Values

Load (kip)	Avg. End Deflection (in.)	Avg. Midspan Deflection (in.)	Bar Stress (ksi)
65.0	1.3	1.0	83.6

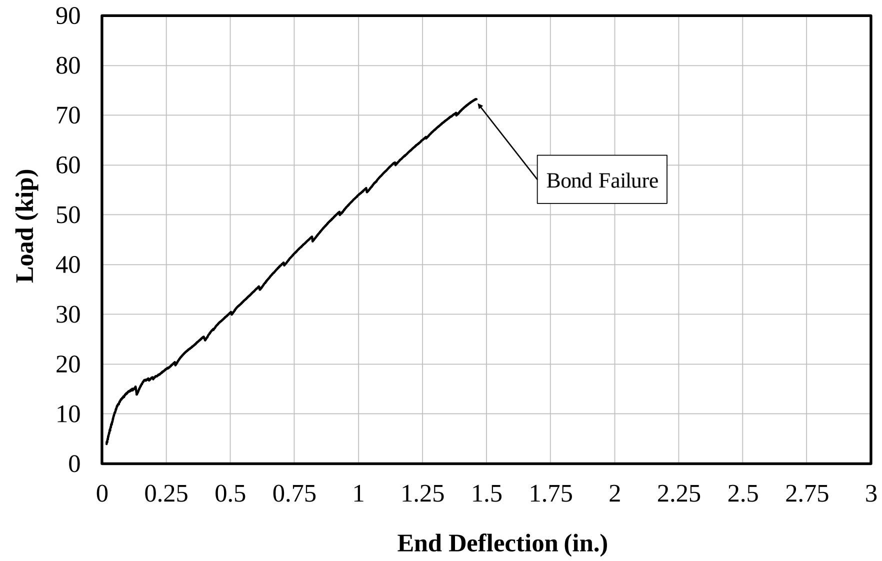

a) Load-Deflection

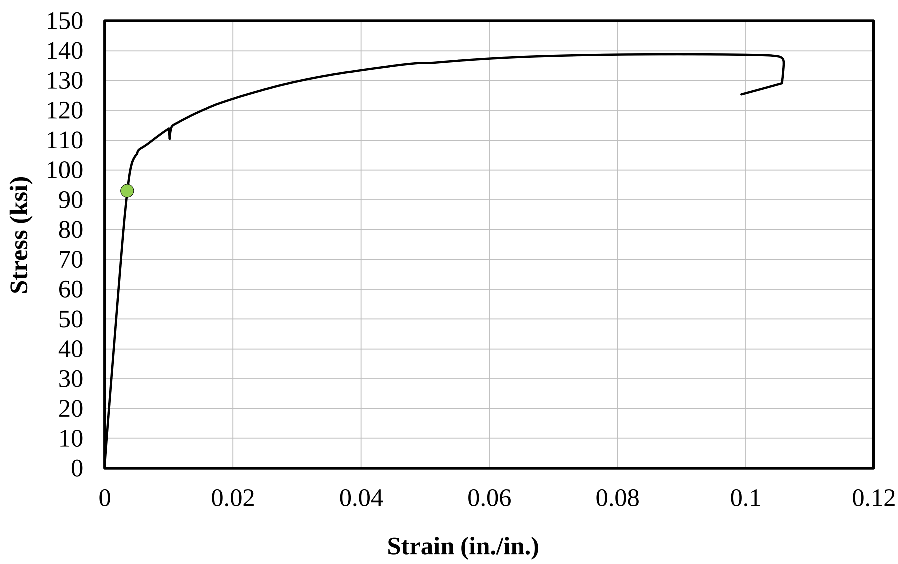

b) Stress-Strain (A615 Gr. 100 No. 8)

Figure J.5: U-60-10

Table J.5: U-60-10 Maximum Testing Values

Load (kip)	Avg. End Deflection (in.)	Avg. Midspan Deflection (in.)	Bar Stress (ksi)
73.2	1.5	0.9	94.2

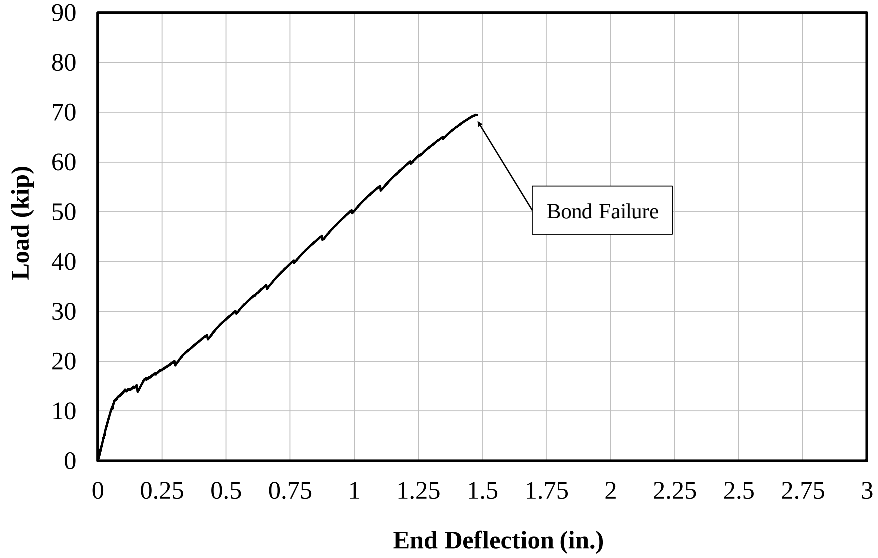

a) Load-Deflection

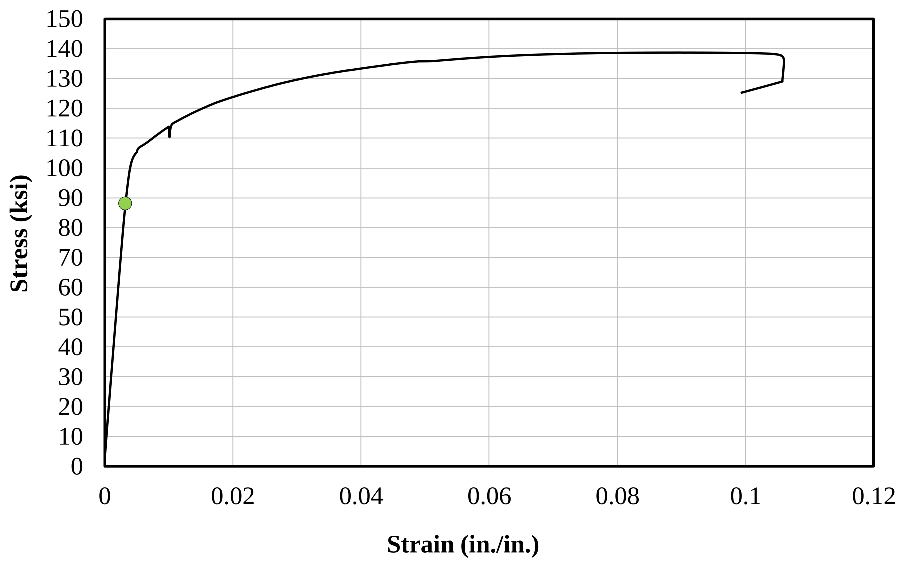

b) Stress-Strain (A615 Gr. 100 No. 8)

Figure J.6: C3/60/2-40-10-25

Table J.6: C3/60/2-40-10-25 Maximum Testing Values

Load (kip)	Avg. End Deflection (in.)	Avg. Midspan Deflection (in.)	Bar Stress (ksi)
69.5	1.5	1.1	89.4

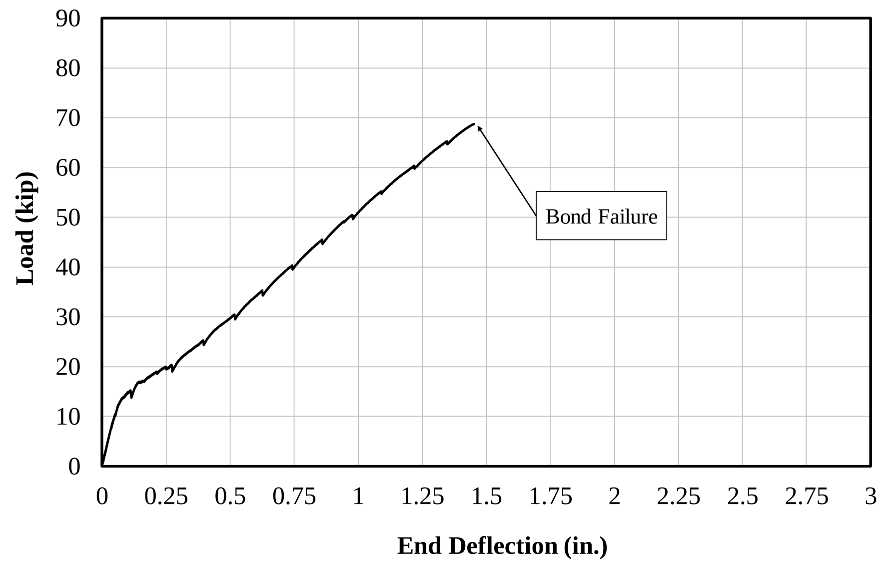

a) Load-Deflection

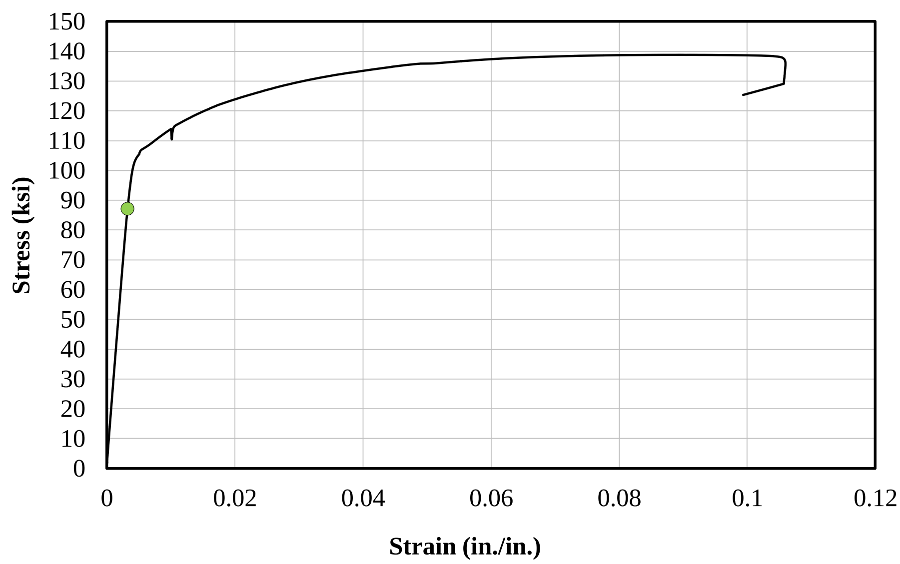

b) Stress-Strain (A615 Gr. 100 No. 8)

Figure J.7: C3/60/2-40-10-50

Table J.7: C3/60/2-40-10-50 Maximum Testing Values

Load (kip)	Avg. End Deflection (in.)	Avg. Midspan Deflection (in.)	Bar Stress (ksi)
68.8	1.5	1.1	88.4

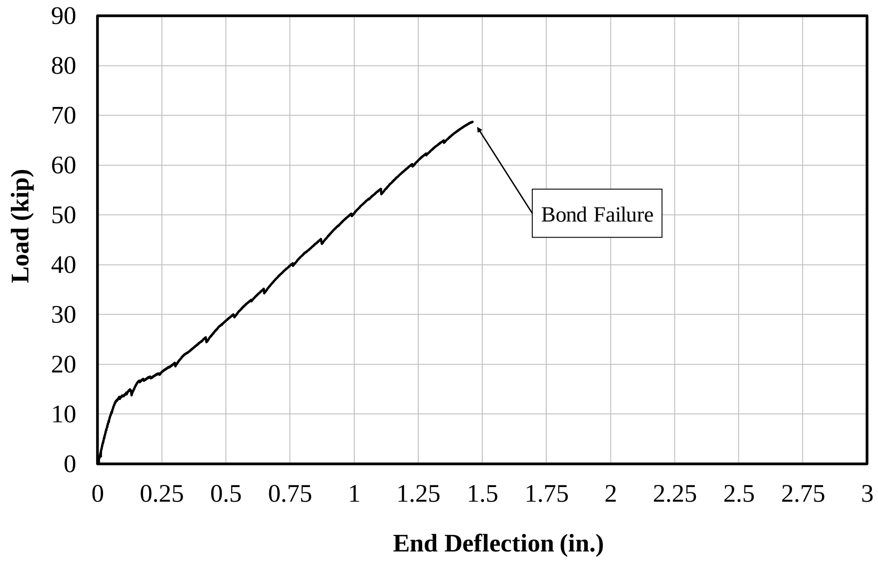

a) Load-Deflection

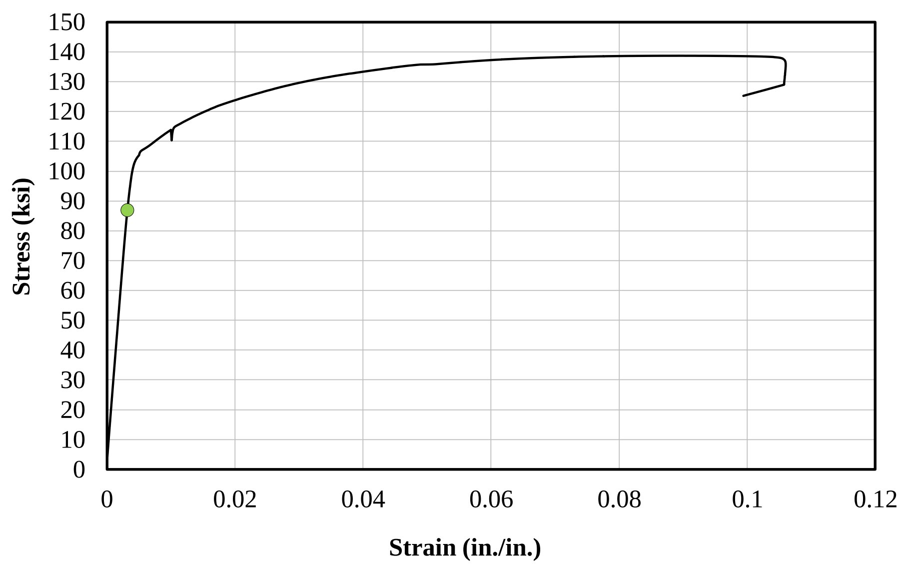

b) Stress-Strain (A615 Gr. 100 No. 8)

Figure J.8: C3/60/3-40-10-50

Table J.8: C3/60/3-40-10-50 Maximum Testing Values

Load (kip)	Avg. End Deflection (in.)	Avg. Midspan Deflection (in.)	Bar Stress (ksi)
68.7	1.5	1.1	88.2

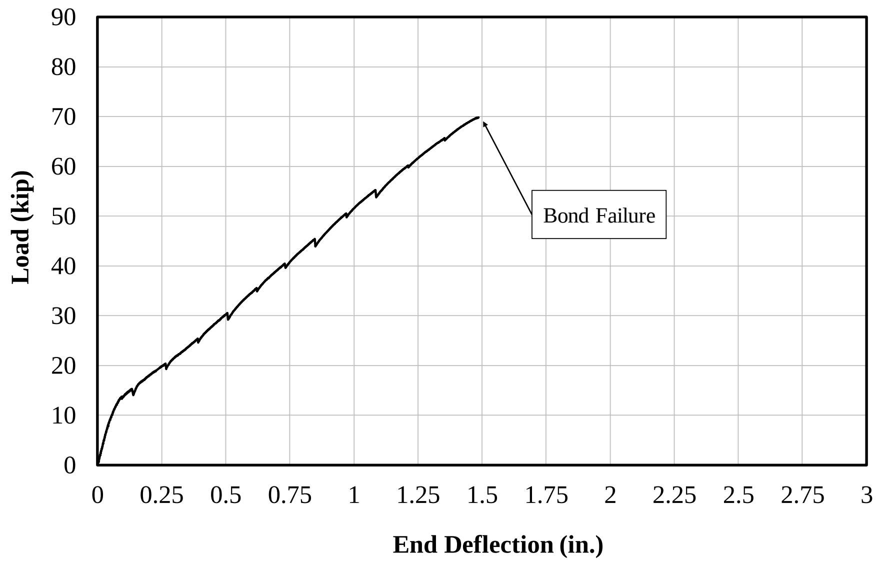

a) Load-Deflection

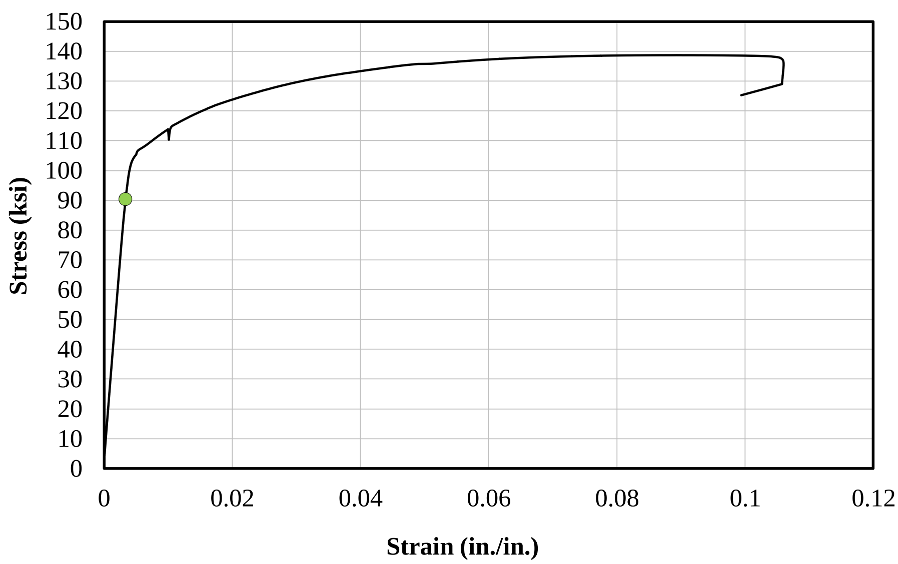

b) Stress-Strain (A615 Gr. 100 No. 8)

Figure J.9: C3/60-40-5-150

Table J.9: C3/60-40-5-150 Maximum Testing Values

Load (kip)	Avg. End Deflection (in.)	Avg. Midspan Deflection (in.)	Bar Stress (ksi)
69.9	1.5	1.1	90.4

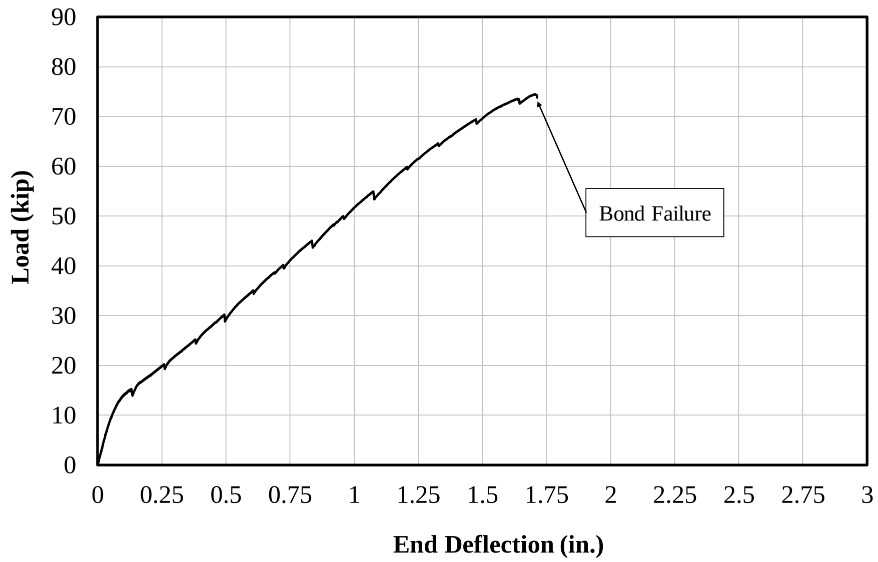

a) Load-Deflection

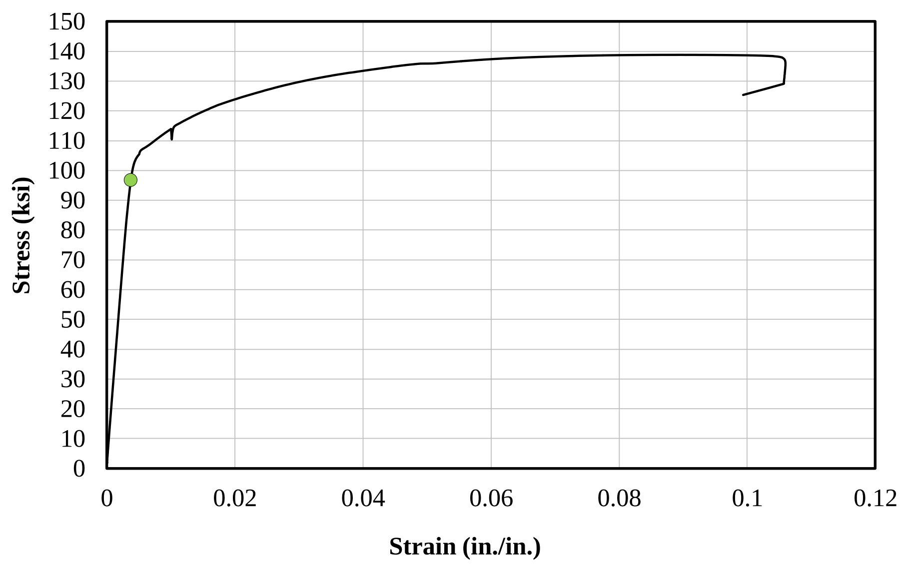

b) Stress-Strain (A615 Gr. 100 No. 8)

Figure J.10: C3/60-40-5-200

Table J.10: C3/60-40-5-200 Maximum Testing Values

Load (kip)	Avg. End Deflection (in.)	Avg. Midspan Deflection (in.)	Bar Stress (ksi)
74.5	1.7	1.4	96.8

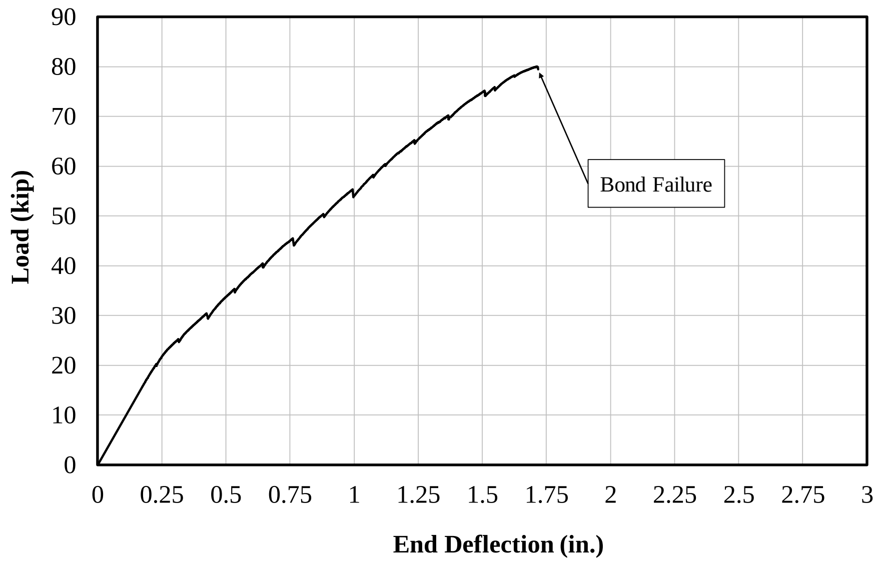

a) Load-Deflection

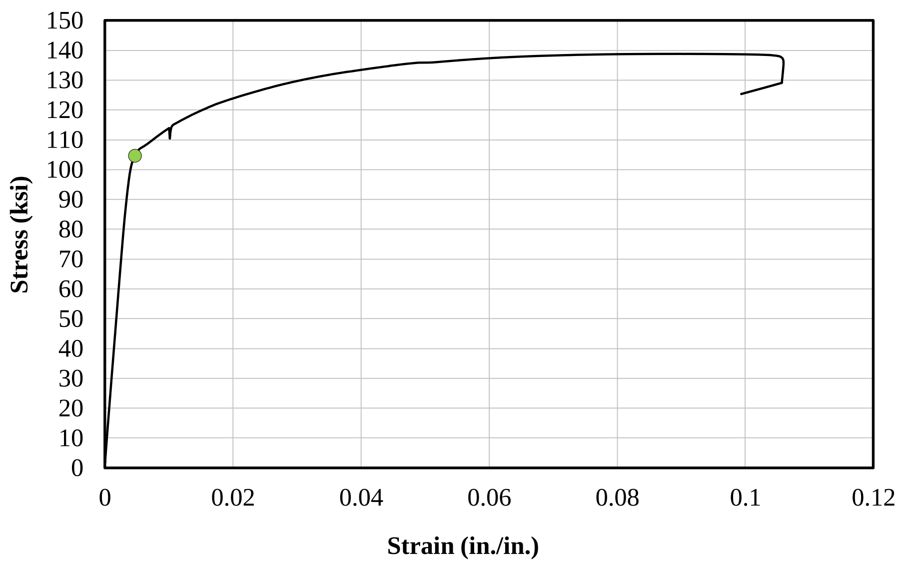

b) Stress-Strain (A615 Gr. 100 No. 8)

Figure J.11: C3/60-50-5-150

Table J.11: C3/60-50-5-150 Maximum Testing Values

Load (kip)	Avg. End Deflection (in.)	Avg. Midspan Deflection (in.)	Bar Stress (ksi)
80.1	1.7	1.3	104.6

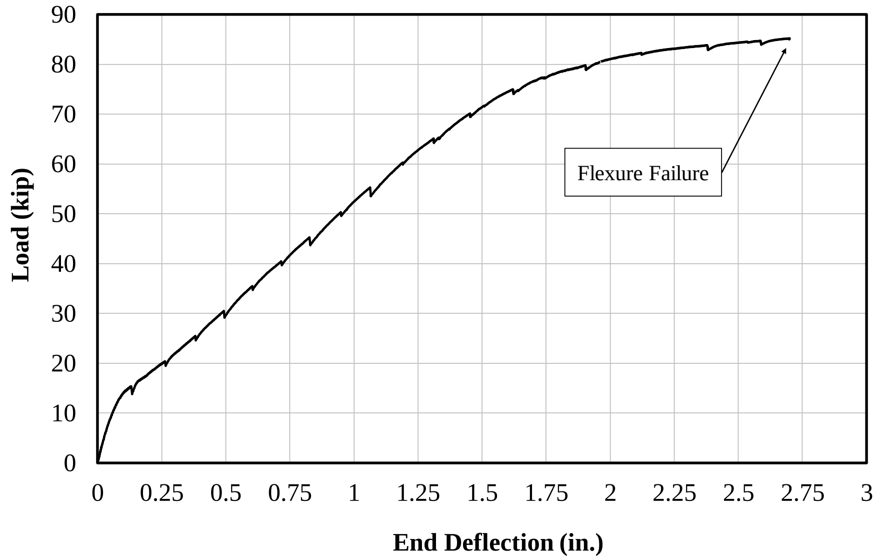

a) Load-Deflection

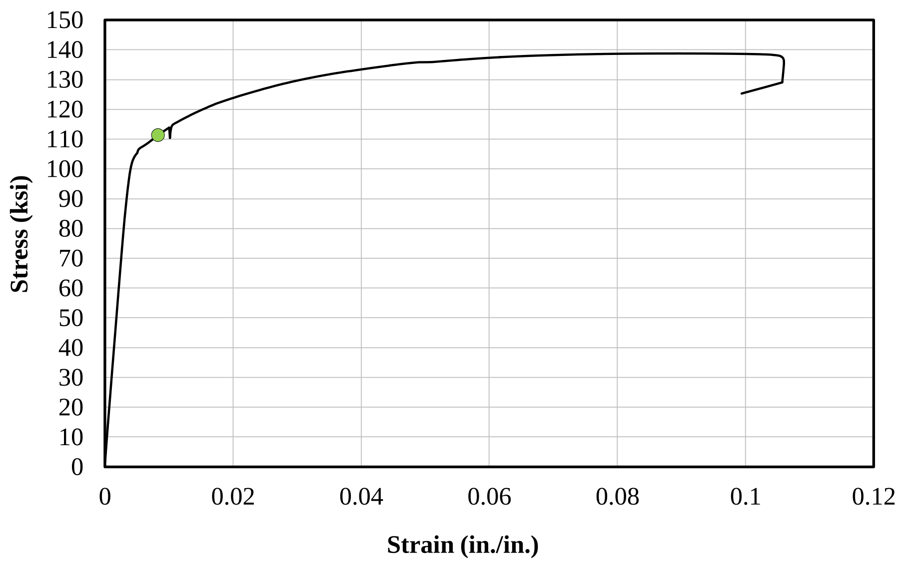

b) Stress-Strain (A615 Gr. 100 No. 8)

Figure J.12: C3/60-50-5-200

Table J.12: C3/60-50-5-200 Maximum Testing Values

Load (kip)	Avg. End Deflection (in.)	Avg. Midspan Deflection (in.)	Bar Stress (ksi)
85.2	2.7	2.0	111.3

APPENDIX K: CRACK WIDTH MEASUREMENTS (SERIES VI-VII)

All cracks are measured from specimen centerline and remain within the constant moment region. Four (4) cracks were monitored in each test. The average crack width growth was plotted for each test specimen. A typical test specimen showing any regions of interest and locations of these cracks is provided in Figure K.1.

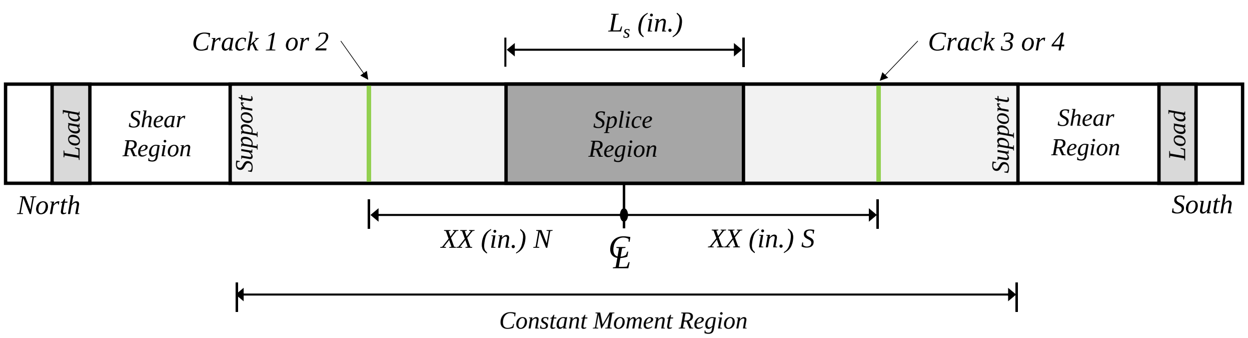

Figure K.1: Typical Specimen Crack Monitoring Diagram

Table K.1: U-40-5-X Crack Width Summary

Load (kip)	Moment (ft-kip)	Bar Stress (ksi)	Crack Widths (1/1000 in.)					
			Crack 1	Crack 2	Crack 3	Crack 4	Max.	Avg.
			83” N	45” N	48” S	65” S		
15.0	60.1	19.7	3	4	2	4	4	3
20.2	80.7	26.4	5	6	4	8	8	6
25.2	100.7	33.0	7	9	5	10	10	8
30.4	121.6	40.0	12	13	6	13	13	11
35.3	141.1	46.4	14	17	8	15	17	14
40.2	160.9	52.9	15	17	10	18	18	15

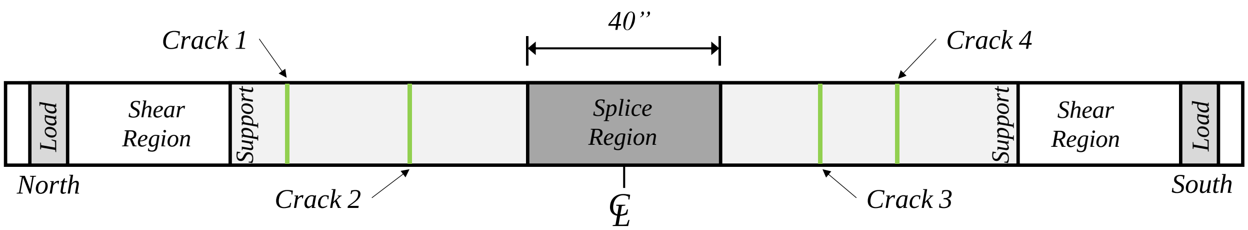

a) Crack Locations

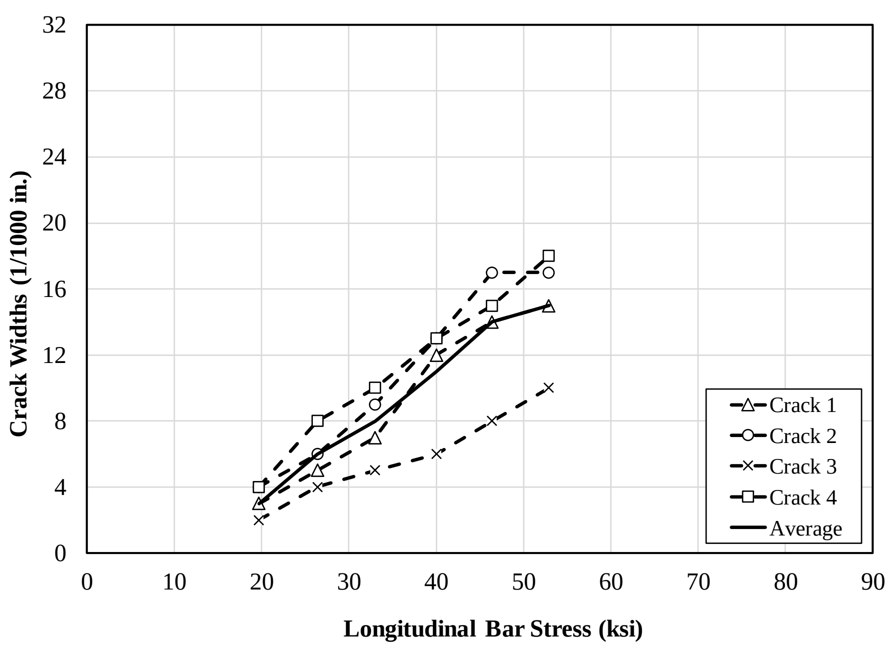

b) Crack Widths

Figure K.2: U-40-5-X

Table K.2: U-60-5-X Crack Width Summary

Load (kip)	Moment (ft-kip)	Bar Stress (ksi)	Crack Widths (1/1000 in.)					
			Crack 1 65” N	Crack 2 51” N	Crack 3 54” S	Crack 4 70” S	Max.	Avg.
15.0	59.8	19.7	3	4	4	3	4	4
20.2	80.8	26.7	4	6	5	6	6	5
25.2	101.0	33.3	5	7	6	7	7	6
30.2	120.6	39.9	5	10	11	9	11	9
35.1	140.3	46.5	7	12	12	11	12	11
40.4	161.6	53.4	10	12	13	12	13	12
45.1	180.4	59.4	12	15	13	14	15	14

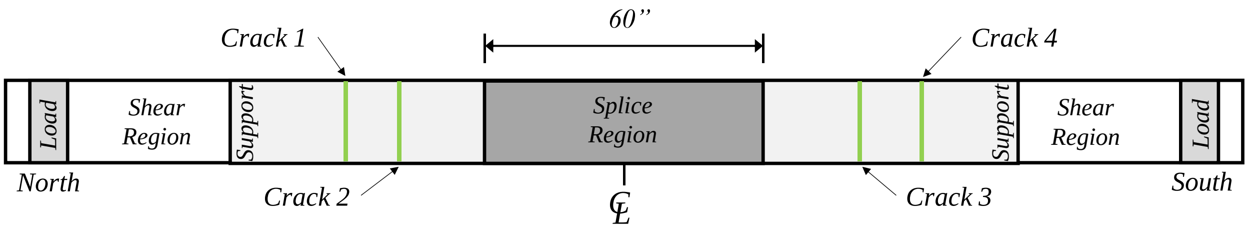

a) Crack Locations

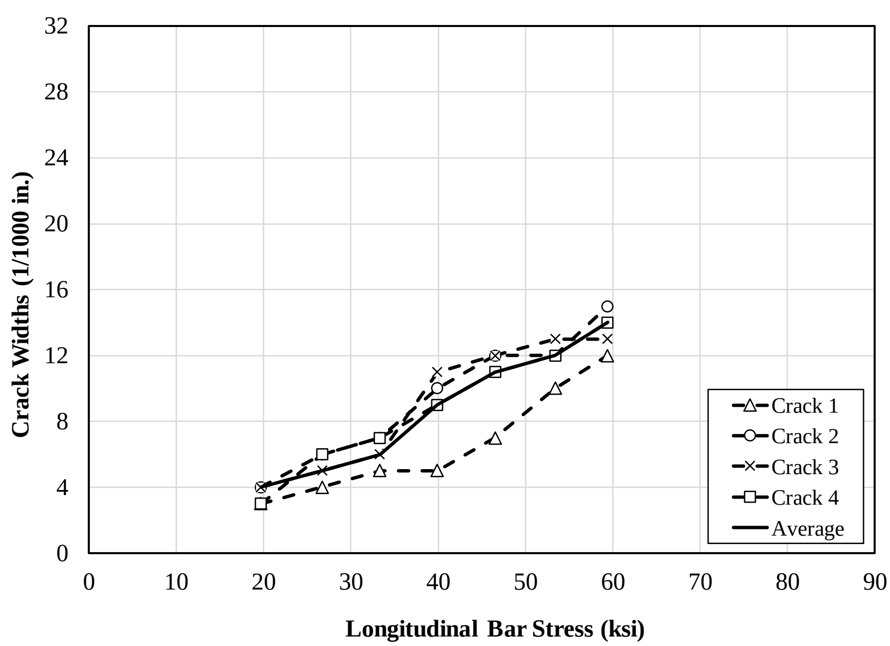

b) Crack Widths

Figure K.3: U-60-5-X

Table K.3: U-50-5 Crack Width Summary

Load (kip)	Moment (ft-kip)	Bar Stress (ksi)	Crack Widths (1/1000 in.)					
			Crack 1 68" N	Crack 2 47" N	Crack 3 47" S	Crack 4 84" S	Max.	Avg.
14.8	59.2	19.5	4	4	5	3	5	4
20.2	80.6	26.6	7	6	6	8	8	7
25.0	100.1	33.0	7	12	8	9	12	9
30.1	120.2	39.7	9	14	12	10	14	11
35.0	140.1	46.3	11	19	16	11	19	14
40.0	160.1	52.8	14	22	18	14	22	17
45.1	180.4	59.3	18	24	20	15	24	19

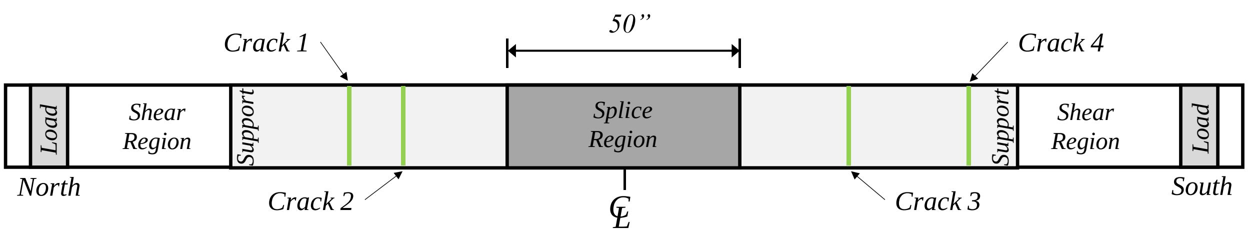

a) Crack Locations

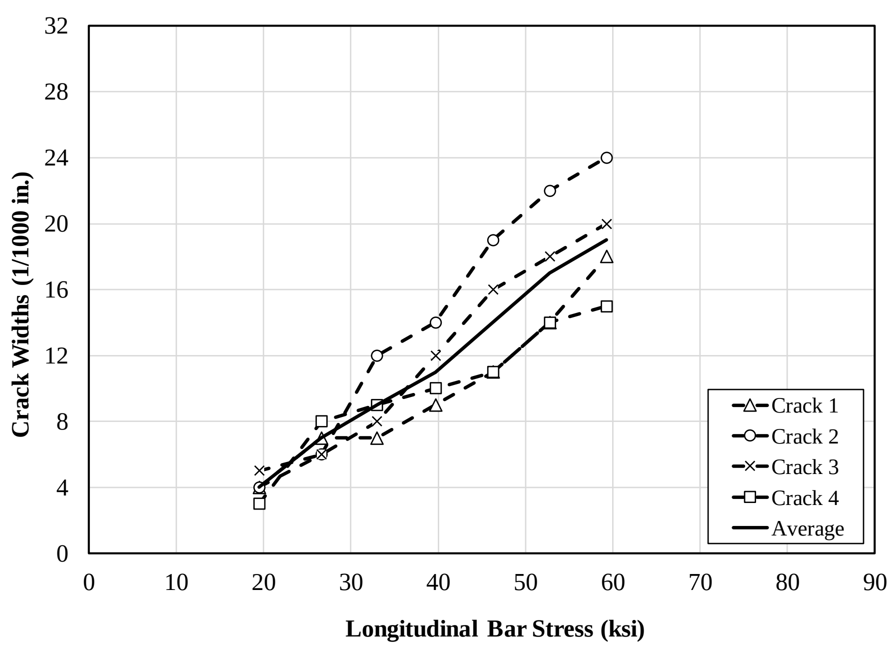

b) Crack Widths

Figure K.4: U-50-5

Table K.4: U-40-10 Crack Width Summary

Load (kip)	Moment (ft-kip)	Bar Stress (ksi)	Crack Widths (1/1000 in.)					
			Crack 1 76” N	Crack 2 46” N	Crack 3 35” S	Crack 4 60” S	Max.	Avg.
14.8	59.1	18.8	5	5	4	3	5	4
20.0	79.9	25.5	7	7	7	3	7	6
25.2	100.7	32.1	9	7	13	4	13	8
30.2	120.8	38.5	12	9	14	4	14	10
35.2	140.6	44.9	16	9	16	3	16	11
40.1	160.2	51.3	20	9	21	4	21	14
45.1	180.4	57.8	22	11	22	4	22	15

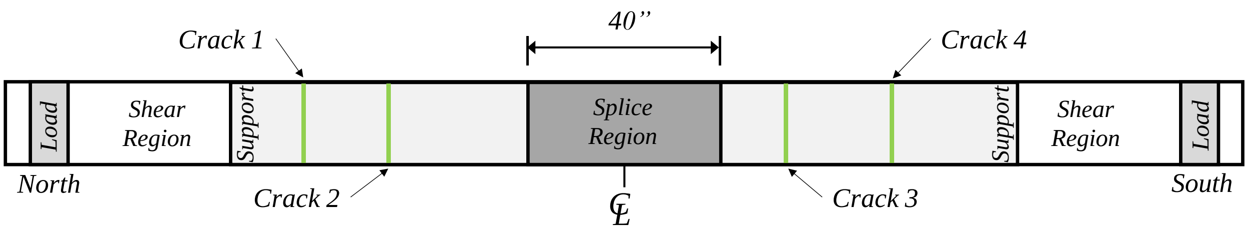

a) Crack Locations

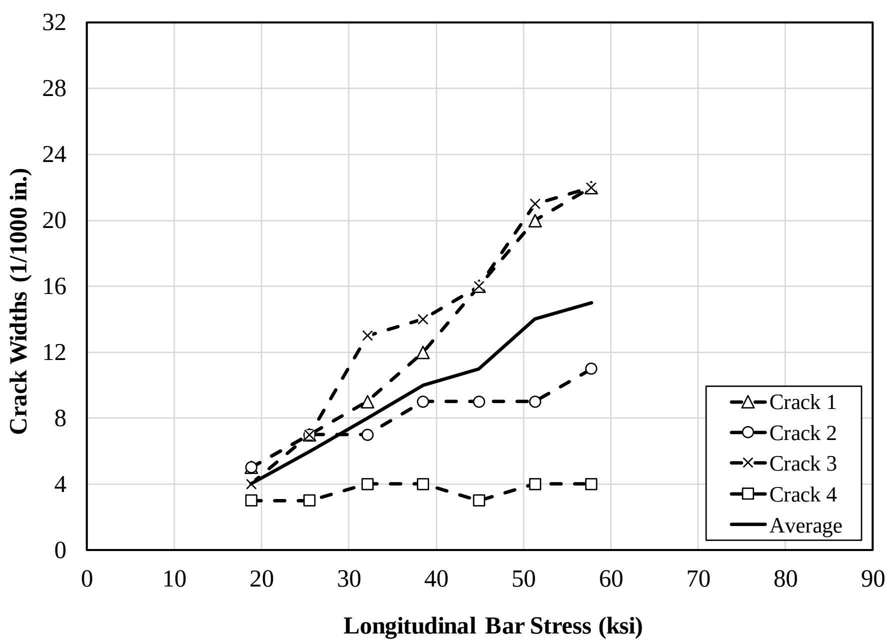

b) Crack Widths

Figure K.5: U-40-10

Note: Crack 4 did not grow larger for U-40-10 due to the presence of a nearby primary crack.

Table K.5: U-60-10 Crack Width Summary

Load (kip)	Moment (ft-kip)	Bar Stress (ksi)	Crack Widths (1/1000 in.)					
			Crack 1 90" N	Crack 2 43" N	Crack 3 44" S	Crack 4 84" S	Max.	Avg.
15.1	60.3	19.2	6	5	5	4	6	5
20.0	80.0	25.5	7	8	8	4	8	7
25.2	100.7	32.1	8	10	9	5	10	8
30.1	120.3	38.3	9	12	11	5	12	9
35.2	140.8	45.0	10	15	11	5	15	10
39.8	159.0	50.9	14	19	12	9	19	14
45.2	180.9	57.9	15	22	12	9	22	15
50.0	200.2	64.1	15	24	13	9	24	15
55.1	220.2	70.6	21	28	13	10	28	18

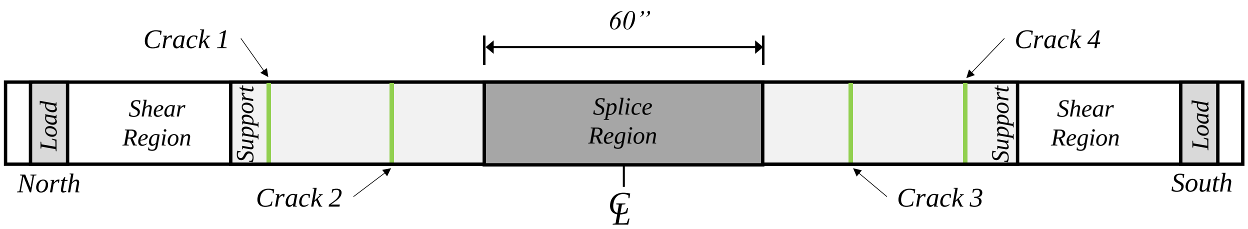

a) Crack Locations

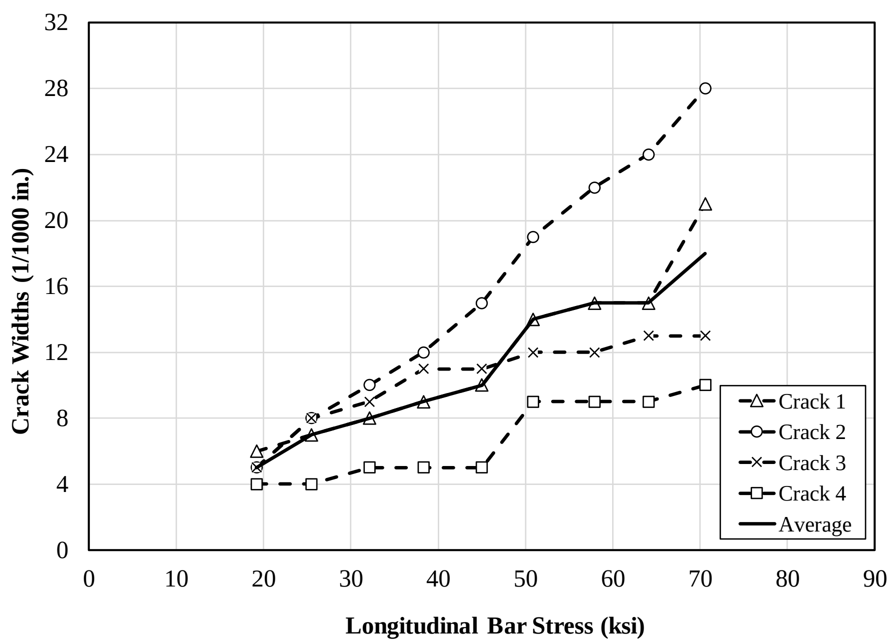

b) Crack Widths

Figure K.6: U-60-10

Table K.6: C3/60/2-40-10-25 Crack Width Summary

Load (kip)	Moment (ft-kip)	Bar Stress (ksi)	Crack Widths (1/1000 in.)					
			Crack 1 53” N	Crack 2 40” N	Crack 3 38” S	Crack 4 53” S	Max.	Avg.
14.8	59.0	18.8	4	3	5	4	5	4
20.0	80.0	25.5	7	6	6	6	7	6
25.3	101.1	32.2	9	8	8	6	9	8
29.9	119.8	38.1	12	10	11	10	12	11
35.3	141.2	45.1	17	12	15	13	17	14
40.3	161.0	51.5	17	14	15	14	17	15
45.2	180.9	57.9	19	15	18	16	19	17
50.4	201.5	64.5	23	17	21	20	23	20
55.2	221.0	70.9	25	19	22	20	25	22

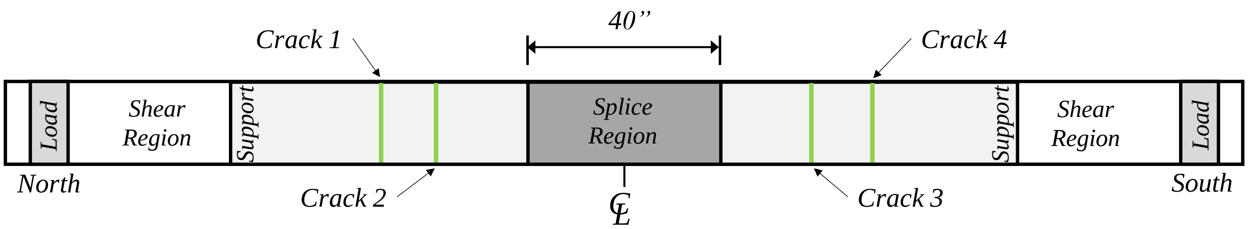

a) Crack Locations

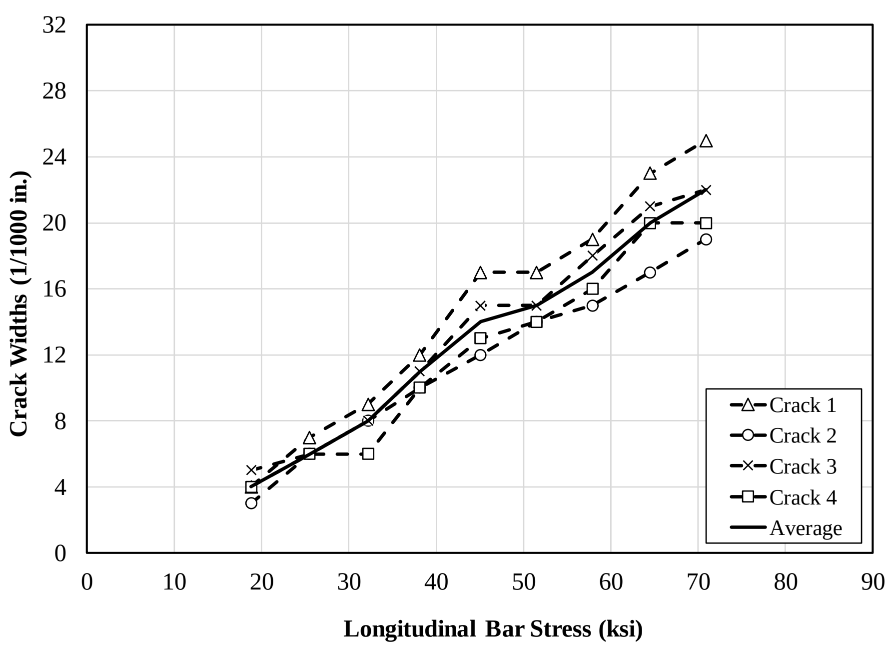

b) Crack Widths

Figure K.7: C3/60/2-40-10-25

Table K.7: C3/60/2-40-10-50 Crack Width Summary

Load (kip)	Moment (ft-kip)	Bar Stress (ksi)	Crack Widths (1/1000 in.)					
			Crack 1 74” N	Crack 2 53” N	Crack 3 62” S	Crack 4 80” S	Max.	Avg.
14.5	58.1	18.4	3	3	5	6	6	4
20.2	81.0	25.7	5	7	8	7	8	7
25.0	100.0	31.7	6	8	11	8	11	8
30.4	121.4	38.5	9	12	13	10	13	11
35.1	140.3	44.6	9	12	14	11	14	12
40.3	161.0	51.3	12	12	18	11	18	13
45.3	181.3	57.8	14	13	19	13	19	15
50.3	201.2	64.2	14	13	21	16	21	16

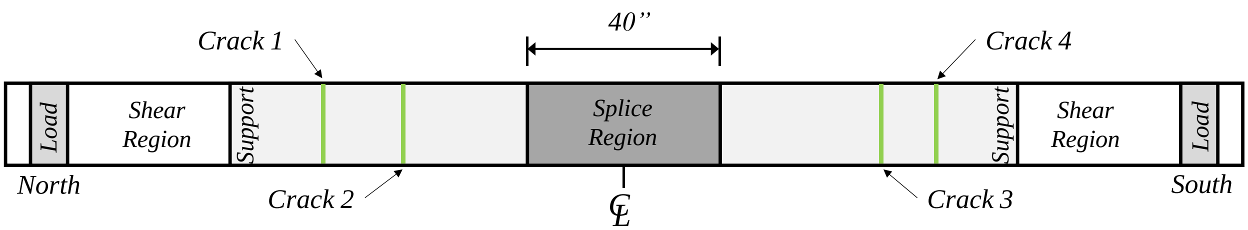

a) Crack Locations

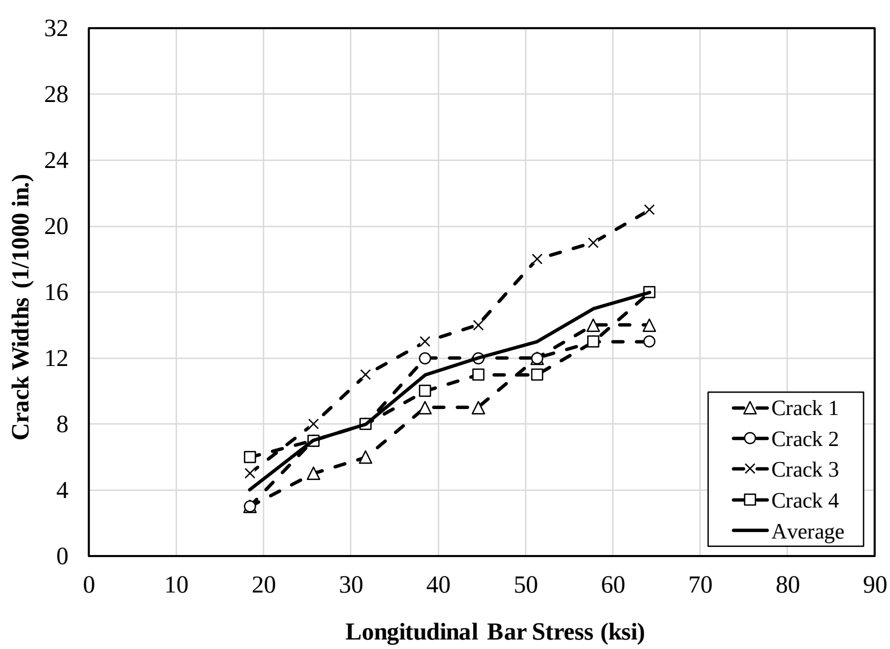

b) Crack Widths

Figure K.8: C3/60/2-40-10-50

Table K.8: C3/60/3-40-10-50 Crack Width Summary

Load (kip)	Moment (ft-kip)	Bar Stress (ksi)	Crack Widths (1/1000 in.)					
			Crack 1 76" N	Crack 2 46" N	Crack 3 44" S	Crack 4 77" S	Max.	Avg.
14.0	56.1	17.7	5	3	5	4	5	4
20.3	81.3	25.7	6	5	6	7	7	6
25.4	101.6	32.1	6	7	9	8	9	8
30.1	120.3	38.0	9	8	13	12	13	11
35.2	140.6	44.6	9	8	13	13	13	11
40.3	161.3	51.2	10	8	17	16	16	13
45.1	180.3	57.3	12	10	18	20	20	15
50.2	200.8	63.9	15	14	21	24	24	19
55.1	220.4	70.3	16	20	23	25	25	21

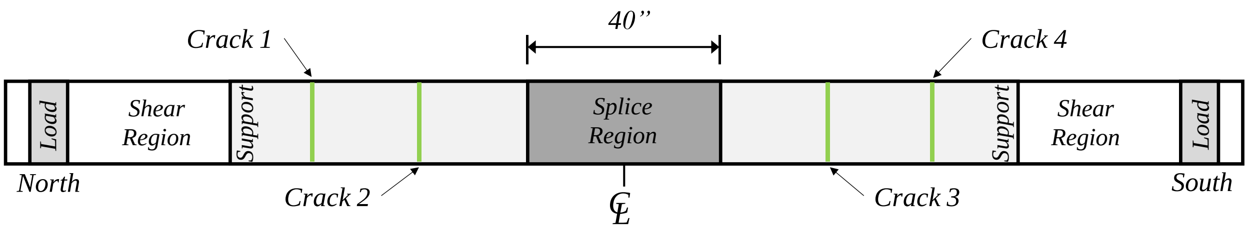

a) Crack Locations

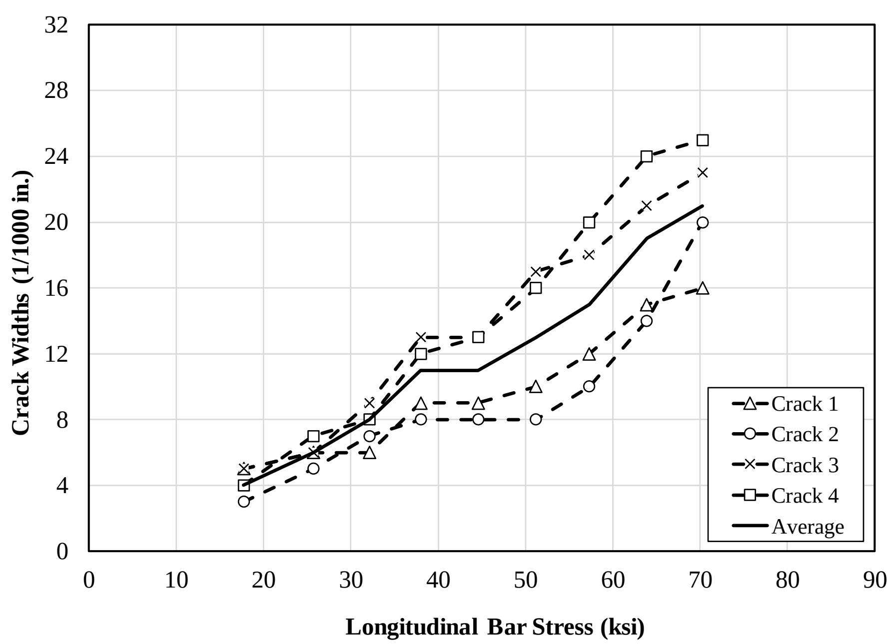

b) Crack Widths

Figure K.9: C3/60/3-40-10-50

Table K.9: C3/60-40-5-150 Crack Width Summary

Load (kip)	Moment (ft-kip)	Bar Stress (ksi)	Crack Widths (1/1000 in.)					
			Crack 1 92" N	Crack 2 26" N	Crack 3 36" S	Crack 4 56" S	Max.	Avg.
14.8	59.2	18.9	4	5	3	3	5	4
20.2	80.8	25.7	6	8	6	5	8	6
25.2	100.8	32.1	7	10	10	7	10	9
30.4	121.6	38.7	9	11	11	8	11	10
35.4	141.6	45.2	10	13	12	9	13	11
40.3	161.2	51.5	11	15	12	13	15	13
45.2	181.0	57.9	12	17	13	15	17	14
50.4	201.7	64.6	14	20	13	16	20	16
55.1	220.5	70.9	14	24	13	16	24	17

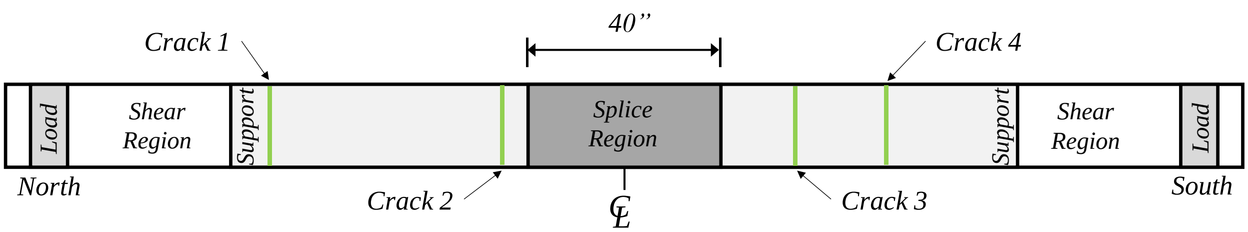

a) Crack Locations

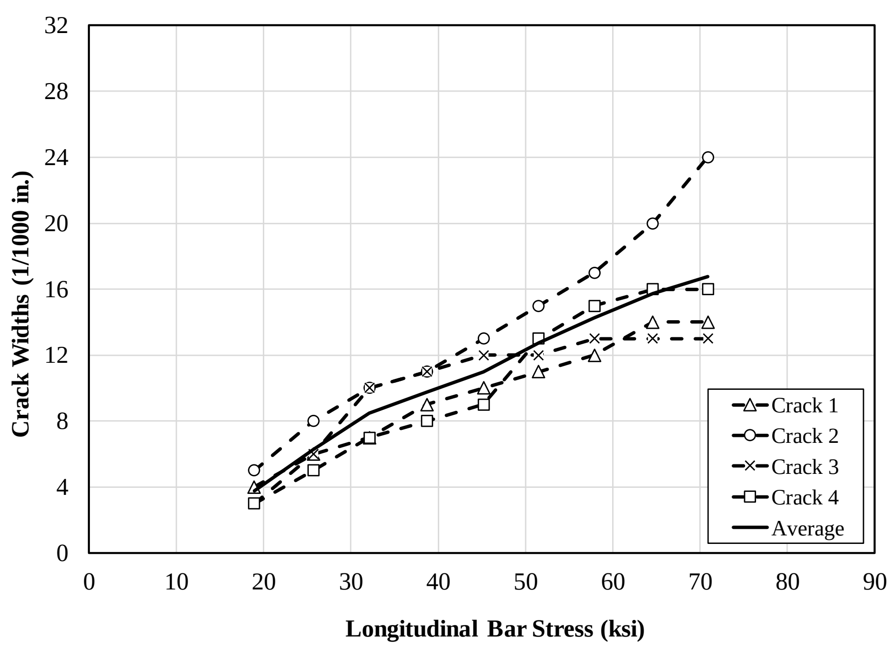

b) Crack Widths

Figure K.10: C3/60-40-5-150

Table K.10: C3/60-40-5-200 Crack Width Summary

Load (kip)	Moment (ft-kip)	Bar Stress (ksi)	Crack Widths (1/1000 in.)					
			Crack 1 75” N	Crack 2 23” N	Crack 3 43” S	Crack 4 83” S	Max.	Avg.
15.3	61.3	19.5	3	3	3	4	4	3
20.8	83.1	26.4	5	6	6	7	7	6
25.3	101.4	32.3	9	11	8	10	11	10
30.4	121.6	38.7	11	15	12	13	15	13
35.3	141.1	45.0	15	16	12	18	18	15
40.3	161.4	51.6	17	16	14	21	21	17
45.4	181.4	58.0	19	17	14	23	23	18
50.3	201.2	64.4	21	18	17	25	25	20
55.4	221.4	71.2	23	20	20	28	28	23

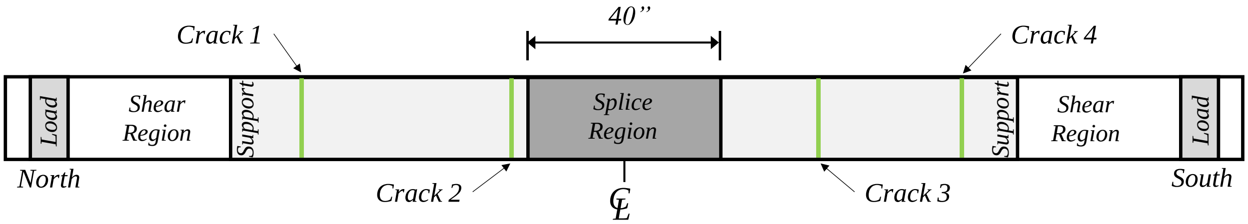

a) Crack Locations

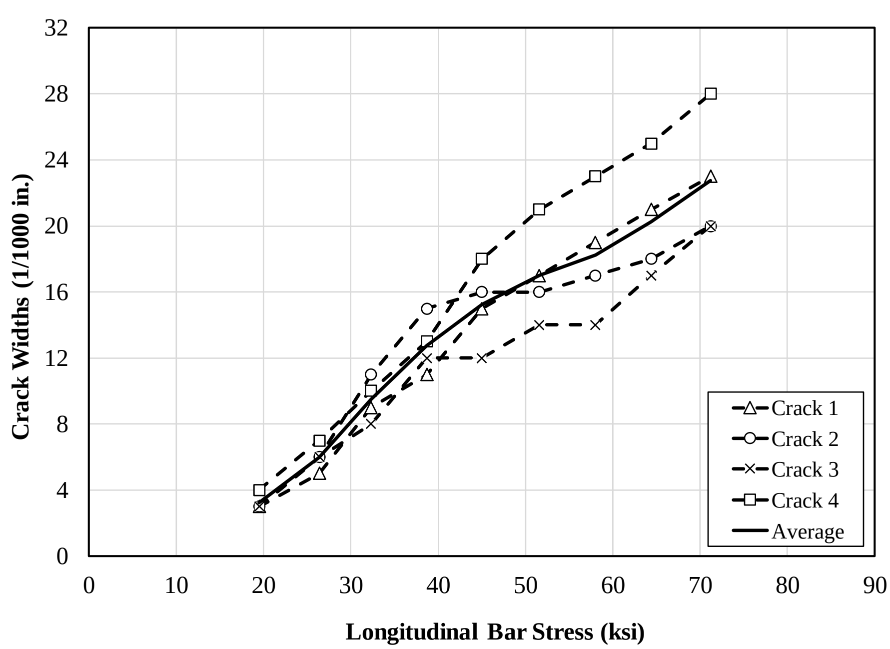

b) Crack Widths

Figure K.11: C3/60-40-5-200

Table K.11: C3/60-50-5-150 Crack Width Summary

Load (kip)	Moment (ft-kip)	Bar Stress (ksi)	Crack Widths (1/1000 in.)					
			Crack 1 82” N	Crack 2 42” N	Crack 3 41” S	Crack 4 75” S	Max.	Avg.
15.4	61.6	19.6	4	5	3	4	5	4
20.2	80.8	25.7	6	7	4	6	7	6
25.2	100.8	32.0	7	9	6	7	9	7
30.3	121.2	38.5	11	10	7	9	11	9
35.2	140.8	44.9	12	13	8	11	13	11
40.3	161.2	51.5	13	13	8	14	14	12
45.4	181.6	58.1	15	14	9	15	15	13
50.3	201.2	64.4	17	16	10	17	17	15
55.3	221.2	71.1	18	16	12	20	20	17

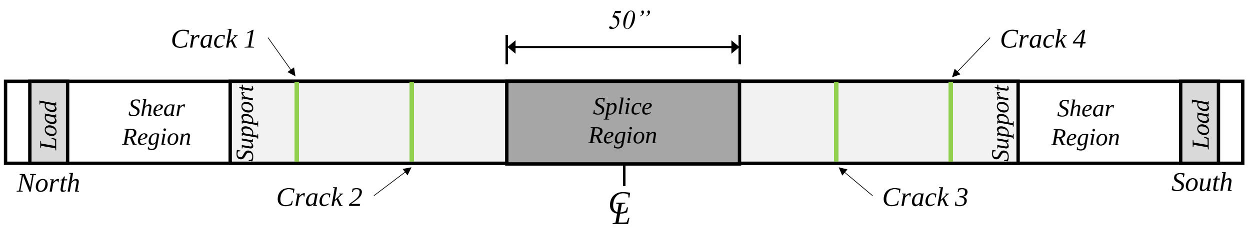

a) Crack Locations

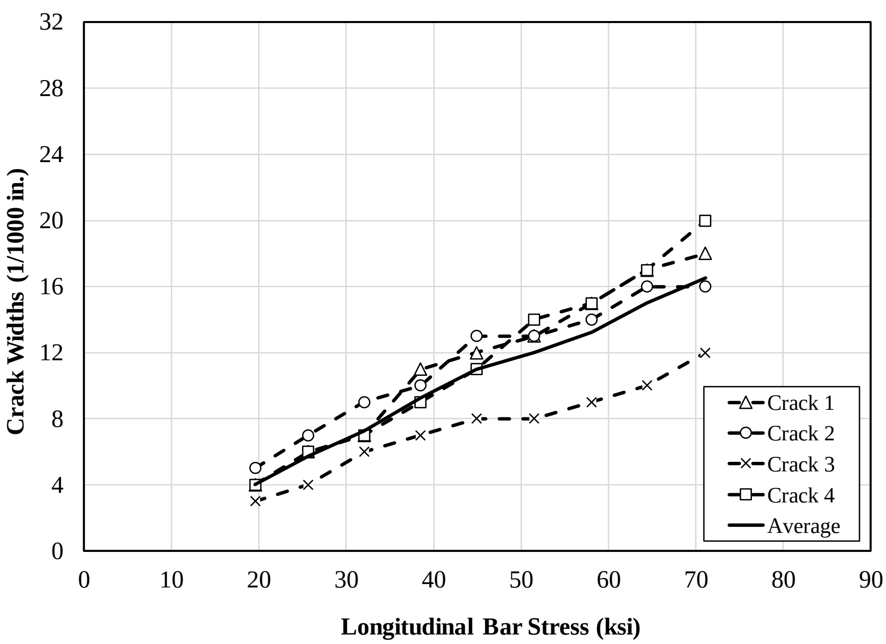

b) Crack Widths

Figure K.12: C3/60-50-5-150

Table K.12: C3/60-50-5-200 Crack Width Summary

Load (kip)	Moment (ft-kip)	Bar Stress (ksi)	Crack Widths (1/1000 in.)					
			Crack 1 83" N	Crack 2 62" N	Crack 3 45" S	Crack 4 60" S	Max.	Avg.
15.3	61.2	19.4	3	2	3	2	3	3
20.3	81.2	25.8	5	5	4	3	5	4
25.4	101.4	32.2	6	5	9	4	9	6
30.3	121.3	38.5	7	7	9	7	9	8
35.4	141.6	45.1	7	9	11	9	11	9
40.4	161.5	51.6	7	11	14	11	14	11
45.2	180.9	57.8	7	12	17	11	17	12
50.3	201.2	64.3	9	13	20	14	20	14
55.2	220.8	70.9	10	15	21	15	21	15

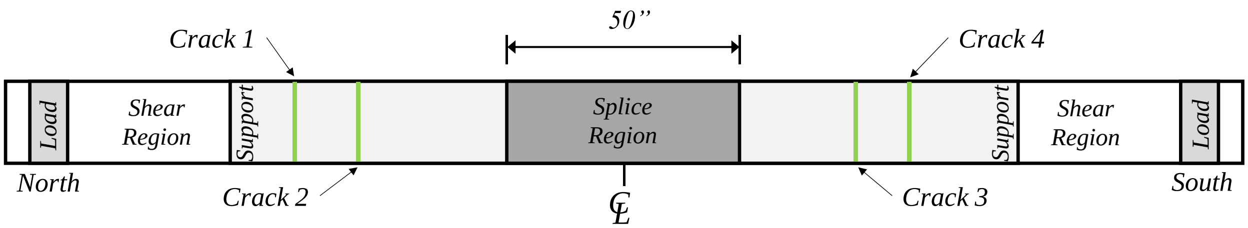

a) Crack Locations

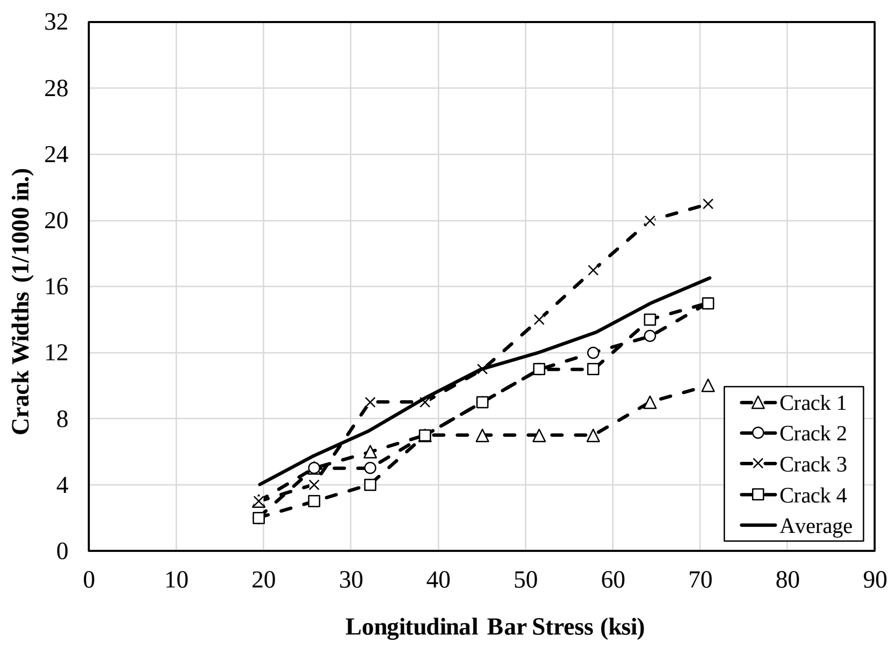

b) Crack Widths

Figure K.13: C3/60-50-5-200

APPENDIX L: STEEL DATABASE

Table L.1: Summary of Unconfined Lap-Splice Specimen Database

Reference	No. of Tests	l_s (in.)	d_b (No.)	l_s/d_b	c_{so}/d_b	f_c' (psi)
Azizinamini, Pavel, Hatfield and Ghosh; 1997	27	13-80	8, 11	9.2-56.7	0.98-2.13	5080-15,591
Chamberlin; 1956	1	12	4	24	4.00	4540
Chinn, Ferguson, and Thompson; 1955	11	12.5-24.0	6, 11	14.4-32.0	1.41-3.92	3580-7480
Choi, Hadje-Ghaffari, Darwin, and McCabe; 1990, 1991	7	12-24	5, 6, 8, 11	16.0-19.2	1.42-3.20	5360-6010
Cleary, Ramirez; 1991	1	12	6	16.0	4.33	3990
Darwin, Tholen, Idun, and Zuo; 1995	13	16-40	5, 8, 11	16.0-28.3	2.00-3.35	3830-5250
El-Hacha, Hossam El-Agroudy, and Sami H. Rizkalla; 2006	3	12-36	6	16-48	2.84-3.17	5713-6380
Ferguson and Breen; 1965	18	18.0-82.5	8, 11	18-80	1.42-3.26	2690-5620
Ferguson and Thompson; 1965	4	49.4-63.3	11	35.0-44.9	3.30[1]	2730-3410
Fleet and Frosch; 2019	7	25-60	5, 8	40-60	1.88-3.80	5300-9800
Glucksman and Frosch; 2018	9	40-120	8	40-120	1.88	4740-6260
Hamad, Itani; 1998	8	12	8	12	1.50	7585-11,124
Hamad, Machaka; 1999	3	12	8	12	1.02	6772-13,459
Hamad, Mansour; 1996	1	13.8	6	18.4	1.05	2900
Hester, Salamizavaregh, Darwin, and McCabe; 1991, 1993	7	16.0-22.8	8	16.0-22.8	2.00	5240-6450
Pay and Frosch; 2005	1	12	8	12	1.50	4020
Rezansoff, Akanni, and Sparling; 1993	4	29.5-44.3	8, 9	29.5-39.3	1.60-1.80	3726-4031
Richter, Pujol, Sozen, and McCain; 2012	2	40	11	28.4	2.10	4940-4950
Seliem, Hosny, Rizkalla, Zia, Briggs, Miller, Darwin, Browning, Glass, Hoyt, Donnelly, and Jirsa; 2009	30	15-91	5, 8, 11	24.0-70.4	1.34-6.08	4060-10,200
Sim and Frosch; 2014	12	12-48	5, 6, 7, 8, 11	17-48	1.06-3.80	3990-5400
Thompson, Jirsa, Breen, and Meinheit; 1975	11	12-60	6, 8, 11, 14	16.0-35.4	1.18-2.84	2865-4710
Zekany, Neumann, Jirsa, and Breen; 1981	2	16-22	9, 11	14.2-15.6	1.42-1.77	3825-5650
Zuo and Darwin; 1998	27	17-40	8, 11	17-40	1.40-3.03	4250-15,650
Total	**209**					

[1] *Side cover data not recorded for two specimens in testing program*

Table L.2: Summary of Confined Lap-Splice Specimen Database

Reference	No. of Tests	No. of Pairs within Tests	l_s (in.)	d_b (No.)	l_s/d_b	c_{so}/d_b	f_c' (psi)
Azizinamini, Pavel, Hatfield and Ghosh; 1997	25	16	15.0-57.5	8, 11	14.2-40.8	0.98-2.13	14,578-16,003
Darwin, Tholen, Idun, and Zuo; 1995	54	4	12-40	5, 8, 11	16-36	1.00-2.55	3810-5250
DeVries, Moehle, and Hester; 1991	8	0	12-22	9	10.6-19.5	1.22-1.72	7460-16,100
Ferguson and Breen; 1965	7	2	30.0-49.5	8, 11	30-36	3.25	2610-4170
Fleet and Frosch; 2019	6	3	40-50	8	40-50	1.50	6200-10,100
Glucksman and Frosch; 2018	6	5	40-60	8	40-60	1.50	6260-7360
Hamad, Machaka; 1999	6	6	12	8	12	1.02	9427-13,952
Hasan, Cleary, and Ramirez; 1996	1	0	12	7	13.7	5.29	3900
Hester, Salamizavaregh, Darwin, and McCabe; 1991, 1993	10	10	16.0-22.8	8	16.0-22.8	2.00	5240-6450
Kadoriku; 1994	34	0	14.9-37.4	6	19.9-49.9	1.52-4.72	3072-10,980
Rezansoff, Akanni, and Sparling; 1993	10	0	14.8-44.3	8, 9	14.8-39.3	1.61-1.83	3625-4089
Rezansoff, Konkankar and Fu; 1991	34	0	15.1-38.0	6, 8, 9, 11	13.4-29.5	1.00-1.77	3219-5742
Seliem, Hosny, Rizkalla, Zia, Briggs, Miller, Darwin, Browning, Glass, Hoyt, Donnelly, and Jirsa; 2009	38	38	27-91	8, 11	27.0-64.4	1.25-2.50	4060-10,200
Sim and Frosch; 2014	6	6	24-48	8	24-48	1.50	4400-5400
Thompson, Jirsa, Breen, and Meinheit; 1975	4	1	15-30	8, 11	14.2-21.3	1.42-2.00	3063-3507
Zekany, Neumann, Jirsa, and Breen; 1981	10	10	16-22	9, 11	14.2-15.6	1.42-1.77	3750-5700
Zuo and Darwin; 1998	63	0	16-40	8, 11	16-30	1.39-4.03	4250-15,650
Total	**322**	**101**					